TECHNISCHE UNIVERSITÄT MÜNCHEN
Department Chemie
Institute for Advanced Study

Biochemical and NMR Spectroscopic Investigations on the Hsp90 Chaperone System

Stephan Lagleder

Vollständiger Abdruck der von der Fakultät für Chemie der Technischen Universität München zur Erlangung des akademischen Grades eines

Doktors der Naturwissenschaften

genehmigten Dissertation.

Vorsitzende:	Univ.-Prof. Dr. S. Weinkauf
Prüfer der Dissertation:	1. Univ.-Prof. Dr. Dr. h.c. H. Kessler
	2. Univ.-Prof. Dr. J. Buchner
	3. Univ.-Prof. Dr. Th. Kiefhaber

Die Dissertation wurde am 03.04.2012 bei der Technischen Universität München eingereicht und durch die Fakultät für Chemie am 30.05.2012 angenommen.

Meinen Eltern

Vorliegende Arbeit wurde von Oktober 2006 bis März 2012 unter Leitung von Prof. Dr. Horst Kessler am Department Chemie der Technischen Universität München angefertigt.

Acknowledgment

An erster Stelle gebührt mein Dank Herrn Prof. Dr. Horst Kessler für die Möglichkeit, an spannenden Projekten biochemisch und NMR spektroskopisch arbeiten zu können sowie die exzellenten Arbeitsbedingungen und die große wissenschaftliche Freiheit, die ich erfahren durfte. Durch sein stetiges Interesse am Fortgang der Projekte und seine motivierende Art hat er maßgeblich zum Gelingen der Arbeit beigetragen.

Genauso möchte ich auch Herrn Prof. Dr. Johannes Buchner danken für die hervorragende Kollaboration, die es mir erlaubte, an vielfältigen und interessanten Fragestellungen im Zusammenhang mit dem Hsp90 Chaperon System zu arbeiten. Dank seines großen Wissens in allen Fragen der Biochemie und des Hsp90 Bereichs sowie wertvoller Diskussionen konnte er mir immer wieder neue wichtige Anregungen vermitteln.

Mein herzlicher Dank gilt natürlich auch den zahlreichen anderen Personen, die durch ihre Arbeit und Kollegialität überhaupt erst eine Promotion möglich machen:

- Dr. Rainer Häßner, der bei allen Problemen mit Computern und NMR - Spektrometern immer Hilfe bot, selbst im Urlaub, und stets eine Lösung wußte.

- Dr. Gerd (“Gustav”) Gemmecker, der mit seinem exzellenten Wissen häufig zur Klärung von Fragen im Bereich der NMR - Spektroskopie beigetragen hat sowie bei diversen Topsin software bugs

umgehend zur Stelle war, um die Messzeit zu retten, auch spät abends noch!

- Meinen Kollegen im Labor und Büro, Johannes Beck, Dr. Franz Hagn, Dr. Oliver Demmer und Dr. Udaya Kiran Marelli für die angenehme Arbeitsatmosphäre und interessante Dikussionen

- Meinen Kollegen Johannes Beck und Dr. Franz Hagn für tolle Erlebnisse auf unseren gemeinsamen Konferenzreisen (*Dancing Dingo* etc.!)

- Den Mitarbeitern aus der Arbeitsgruppe von Prof. Dr. Johannes Buchner, Dr. Klaus Richter, Dr. Julia Rohrberg, Lars Mitschke, Alexandra Rehn, Dr. Martin Hessling, Dr. Sebastian Wandinger, Dr. Andreas Schmid und Alina Röhl für hervorragende Zusammenarbeit auf diversen Hsp90 Projekten sowie die Bereitstellung einzelner Plasmide oder Proteine

- Dr. Fabio Falsone für die Bereitstellung von α - Synuclein Proben

- Dr. Oliver Demmer für die Synthese zahlreicher Peptide

- Meinen Praktikantinnen Sarah Port und Maria Hillreiner für ihre engagierte Mitarbeit im Labor

- Den Sekretärinnen Frau Fill, Fau Nietsch und Frau Bruckmaier für Hilfe in allen Fragen von Verwaltungsangelegenheiten

- Prof. Dr. Michael Sattler, Dr. Peijian Zou und Alexander Frenzl für the gemeinsame Organisation und Nutzung des Biochemie Labors

- Den technischen Assistentinnen Gülden Demiraslan und Stefanie Lichtnow für ihre Arbeit bei der Organisation des Biochemie Labors

- Allen anderen Kollegen, die das Arbeiten in der Gruppe so angenehm gemacht haben

Ganz besonderer Dank gilt aber meinen Eltern, auf deren Unterstützung ich mich seit jeher immer verlassen durfte bei allem was ich tue und die mir fortwährend den Rücken freihielten, um mir diese Arbeit zu ermöglichen.

Herzlichen Dank!

Parts of this work have been published in:

Hagn, F., Lagleder, S., Retzlaff, M., Rohrberg, J., Demmer, O., Richter, K., Buchner, J., Kessler, H., Structural analysis of the interaction between Hsp90 and the tumor suppressor protein p53. *Nat Struct Mol Biol* **18** (2011), 1086-1093.

Schmid, A. B., Lagleder, S., Gräwert, M. A., Röhl, A., Hagn, F., Wandinger, S. K., Cox, M. B., Demmer, O., Richter, K., Groll, M., Kessler, H., Buchner, J., The architecture of functional modules in the Hsp90 co-chaperone Sti1/Hop. *EMBO J* **31** (2012), 1506-1517.

Further publications:

Retzlaff M., Stahl M., Eberl H.C., Lagleder S., Beck J., Kessler H., Buchner J., Hsp90 is regulated by a switch point in the C-terminal domain. *EMBO Rep*, **10** (2009), 1147-1153.

Retzlaff, M., Rohrberg J., Küpper, N.J., Lagleder, S., Bepperling, A., Manzenrieder, F., Kessler, H., Buchner, J., The regulatory domain stabilizes the p53 tetramer by intersubunit contacts with the DNA binding domain. *Submitted to PNAS*.

Table of Contents

List of Figures

List of Tables

Abbreviations and Symbols

δ	Chemical shift
ϵ	Molar extinction coefficient
μM	Micromolar
17 - AAG	17 - N - allylamino - 17 - demethoxygeldanamycin
1D	One - dimensional
2D	Two - dimensional
3D	Three - dimensional
5' - FOA	5' - fluor orotic acid
Å	Ångstrøm
$[\Theta]$	Molar ellipticity
A	Absorption
a.u.	Arbitrary units
ADP	Adenosine diphosphate
Aha1	Activator of Hsp90 ATPase 1
AIRs	Ambiguous interaction restraints

AMP - PNP ..... Adenosine 5' - (β,γ - imido)triphosphate

APS ..... Ammoniumpersulfate

ATP ..... Adenosine triphosphate

aUC ..... Analytical ultracentrifugation

Bp ..... Base pairs

CD ..... Circular dichroism

CFTR ..... Cystic fibrosis transmembrane conductance regulator

CHAPS ..... 3 - [(3 - cholamidopropyl)dimethylammonio] - 1 - propanesulfonate

CIP ..... Calf intestinal phosphatase

cm ..... Centimeter

COSY ..... Correlated spectroscopy

CSI ..... Chemical shift index

CSP ..... Chemical shift perturbation

CV ..... Column volume

Cyp40 ..... Cyclophilin 40

D ..... Diffusion coefficient

DBD ..... DNA binding domain

deg ..... Degree

dmol ..... Decimole

DMSO ..... Dimethyl sulfoxide

DOC ..... Deoxycorticosterone

DOSY ..... Diffusion ordered spectroscopy

DP ..... Aspartate proline rich

E. coli ..... Escherichia coli

EDC ..... 1 - ethyl - 3 - (3 - dimethylaminopropyl) - carbodi - imide

EDTA ..... Ethylenediaminetetraacetate

ER ..... Endoplasmic reticulum

FAM - SE ..... 5' - 6' - carboxyfluorescein succinimidyl ester

FKBP ..... FK506 binding protein

FPLC ..... Fast protein liquid chromatography

G ..... Gauss

g ..... Standard gravity

GA ..... Geldanamycin

GHKL ..... Gyrase, Hsp90, kinase, MutL

GR ..... Glucocorticoid receptor

Grp ..... Glucose regulated protein

GST ..... Glutathione S - transferase

h ..... Hour

Hch1 ..... High copy suppressor of Hsp90 1

HEPES	4 - (2 - hydroxyethyl) - 1 - piperazineethanesul - fonic acid
Hip	Hsc70 - interacting protein
Hop	Hsp70/Hsp90 organizing protein
Hsc70	Constitutively expressed form of Hsp70 in eukaryotic cells
Hsp	Heat shock protein
Hsp90	Heat shock protein of 90 kDa
HSQC	Heteronuclear single quantum coherence
HtpG	High temperature protein G
HTS	High - throughput screening
Hz	Hertz
IMAC	Immobilized metal ion affinity chromatography
IPTG	Isopropyl - β - D - thiogalactopyranosid
ITC	Isothermal titration calorimetry
J	Scalar coupling constant
K	Kelvin
K_a	Association constant
K_d	Dissociation constant
kDa	Kilodalton
L	Liter

LDH ..... Lactic dehydrogenasae

mAU ..... Milliabsorbance units

MHz ..... Megahertz

min ..... Minute

mM ..... Millimolar

MRW ..... Mean residue weight

NADH ..... Nicotinamide adenine dinucleotide

NHS ..... N - hydroxysuccinimide

nM ..... Nanomolar

NMR ..... Nuclear magnetic resonance

NMWL ..... Nominal Molecular Weight Limit

NOE ..... Nuclear Overhauser effect

ns ..... Nanosecond

OD_{600} ..... Optical density at 600 nm

ONPG ..... o - nitrophenyl - β - D - galactopyranosid

P ..... Polarization

PAGE ..... Polyacrylamide gel electrophoresis

PCR ..... Polymerase chain reaction

PDB ..... Protein data bank

PEP ..... Phosphoenol pyruvate

pI ..... Isoelectric point

PK ..... Pyruvate kinase

PPIase ..... Peptidylprolyl isomerase

ppm ..... Parts per million

PR ..... Progesterone receptor

PROXYL ..... 2,2,5,5 - tetramethyl - 1 - pyrrolidinyloxy

ps ..... Picosecond

RDC ..... Residual dipolar coupling

RMSD ..... Root mean square deviation

rpm ..... Rotations per minute

RU ..... Response unit

S ..... Svedberg constant

s ..... Second

S. cerevisiae ..... Saccharomyces cerevisiae

SAXS ..... Small angle X - ray scattering

Sba1 ..... Sensitive to benzoquinoid ansamycins

SD ..... Standard deviation

SDS ..... Sodium dodecyl sulfate

SHR ..... Steroid hormone receptor

SPR ..... Surface plasmon resonance

Src ..... Sarcoma

Ssa1 ..... Stress seventy - related a; cytosolic Hsp70 member in

Saccharomyces cerevisiae

Sti1 ..... Stress inducible protein 1

T_M ..... Thermal melting point

TCEP ..... Tris - (2 - carboxyethyl)phosphine hydrochloride

TEMED ..... N,N,N',N' - tetramethylethylendiamine

TFE ..... Trifluoroethanol

TOCSY ..... Total correlation spectroscopy

TPR ..... Tetratricopeptide repeat

Trap1 ..... Tumor necrosis factor receptor - associated protein 1

Tris ..... 2 - amino - 2 - hydroxymethyl - propane - 1,3 - diol

TROSY ..... Transverse relaxation optimized spectroscopy

TX - 100 ..... Triton X - 100

UV ..... Ultraviolet

VS ..... Virtual screening

YDJ1 ..... Hsp40 family member in yeast cells

Scope of this Work

The highly conserved Hsp90 chaperone system represents one of the most complex protein folding machineries found in cells with an incredibly large interaction network that is still constantly extended. Given the numerous different proteins that are dependent on its function, it is not surprising that Hsp90 is an essential protein in nearly all higher organisms.

In the past years, many biochemical and structural studies have enormously contributed to the understanding of Hsp90. In particular, mechanistic aspects of the Hsp90 ATPase activity have been addressed in detail that led to profound insights into the large conformational rearrangements in the molecule that accompany the Hsp90 nucleotide hydrolysis reaction. Concomitantly, the regulation of the Hsp90 chaperone cycle by several different associated proteins, so called cochaperones, was elucidated.

Not all of the currently ~ 20 known Hsp90 cochaperones have been amenable to crystallographic studies so far, potentially due to their complex structures, inherent flexibility or their rather weak interaction with Hsp90. Among these is the cochaperone Sti1/Hop that was previously found to serve as an adapter molecule connecting the two important Hsp70 and Hsp90 chaperone systems. Although well known to be an inhibitor of the Hsp90 nucleotide hydrolysis, it remains still elusive by which mechanism it causes Hsp90 ATPase arrest. This issue should be an-

alyzed in more detail here using different biophysical methods to identify Sti1/Hop binding sites on Hsp90 and obtain a model for its interaction with the chaperone.

Besides its function as an Hsp90 inhibitor protein and providing a physical linkage between Hsp70 and Hsp90, Sti1/Hop contains two so called DP domains. These were found to be absolutely essential in the activation of steroid hormone receptors, which have been implicated as Hsp90 dependent client proteins. Despite their high importance, the Sti1/Hop DP domains remain structurally nearly uncharacterized. Therefore, a further aim in the context of the Sti1/Hop project was to determine the fold of the Sti1 DP domains by NMR (nuclear magnetic resonance) spectroscopy, which might potentially contribute to an understanding of fundamental processes in steroid hormone signaling in cells.

Another Hsp90 cochaperone that has been poorly characterized with respect to its structural properties is Hch1, which shares high homology with Aha1 and is only found in fungal organisms. Strikingly, this protein coexists together with Aha1 in yeast cells. This raises the question to which extent Hch1 and Aha1 have overlapping function. Hch1 should be analyzed in this work in more detail to reveal potential differences in its mode of action with respect to Hsp90 regulation compared to Aha1.

p23/Sba1 was implicated in earlier studies as Hsp90 ATPase inhibiting protein. This cochaperone has an interesting structural feature, a presumably intrinsically unfolded C-terminal domain besides a conserved N-terminal β-sandwich domain that has been characterized previously. The unfolded nature of the C-terminal part in p23/Sba1 makes it a candidate for being studied with NMR spectroscopy since crystallographic studies are usually largely hampered by such flexible systems. Thus, this work here aimed at analyzing the structural properties in particular of the p23/Sba1 C-domain and its role in the interaction with Hsp90.

Part I

Introduction

Chapter 1

The Hsp90 Molecular Chaperone

1.1 Conservation of the Hsp90 Chaperone System

Protein folding is one of the basic cellular processes. To fulfill their specific tasks, most proteins have to a adopt a well defined three dimensional structure. This is, according to Anfinsen's theorem [1,2], a spontaneous process under physiological conditions, which is determined only by the amino acid sequence of the protein and thermodynamics. However, many factors can contribute to the misfolding or aggregation of a protein like elevated temperatures or the extremely high protein concentrations found in the cytosol of cells, which is often referred to as "molecular crowding" [3]. This would lead to the accumulation of unfunctional and potentially toxic protein species and indeed many diseases were found to be connected to protein folding defects [4,5]. To stabilize otherwise labile proteins that are prone to aggregation and to assist nascent polypeptide chains in folding into their native states, each cell maintains a special-

ized machinery of so called “molecular chaperones”. These are a set of structurally and functionally different proteins that serve to maintain proteostasis in a cell. Since it was found that such protective proteins are upregulated in response to elevated temperatures, the term “heat shock protein” (Hsp) was coined.

Among the known chaperones, Hsp90 (heat shock protein of 90 kDa) likely represents one of the most complex systems due to its huge interaction network. On the one hand, it is regulated by a large cohort of associated factors, so called cochaperones (see section 2) that influence its own activity. On the other hand, numerous (on the order of hundreds) substrate proteins or “clients” that are completely unrelated in structure and function essentially depend on the action of Hsp90 to achieve their biologically active state. Therefore, not surprising, the Hsp90 chaperone systems of different organisms are highly conserved.

Hsp90 is an abundant protein that is found in all bacterial and eukaryotic cells but seems to be absent in archaeal organisms[6–8]. Despite the term “heat shock protein”, Hsp90 is found in a high amount even in unstressed cells, representing ~ 1 to 2 % of total soluble protein[9,10]. This supports the important cellular functions Hsp90 fullfills also under normal growth conditions. Indeed, in eukaryotes cytoplasmic Hsp90 was demonstrated to be absolutely essential for cell viability[11,12]. In contrast, the bacterial Hsp90 homologue HtpG (high temperature protein G) seems to be largely dispensable, however, more specifically required at elevated temperatures and nutrient starvation stress[13–15].

Most organism produce two different forms of cytosolic Hsp90: In the yeast *Saccharomyces cerevisiae* the genes *HSP82* and *HSC82* code for the Hsp90 isoforms hsp82 and hsc82, respectively, which are to 97 % identical. Hsc82 is expressed at high levels at normal growth conditions and upregulated only slightly ($\sim$ twofold) under heat shock. In contrast, hsp82

is found only in low amount at normal temperature but is therefore highly induced by heat shock (~ 20 - fold) [11]. Similarly, in mammals cytosolic Hsp90 exists as Hsp90α and Hsp90β [16,17]. The sequence identity between the two proteins here is $\sim 85\,\%$ and it is the expresssion of the α - variant that is induced in response to stress conditons.

Besides the constitutively expressed and inducible Hsp90 cytosolic isoforms, additionally organelle specific Hsp90 members exist in higher eukaryotes. Grp94 (glucose regulated protein of 94 kDa), which is also called endoplasmin [18,19], is localized to the ER (endoplasmic reticulum) and therefore predominantly involved in secretory processes connected to this cell compartment [20–28]. Furthermore, also mitochondria harbor their own specific Hsp90 variant called Trap1 (tumor necrosis factor receptor - associated protein 1)/Hsp75, whose function is less characterized but seems to have a role in the protection of cells from apoptosis [29–32]. Not surprising, also chloroplasts of plant cells contain an Hsp90 paralogue that obviously has functions in the biogenesis of this organelle [33,34]. A novel member in the Hsp90 family is Hsp90N which lacks the conserved N - terminal domain typical for all other Hsp90 proteins. It was shown to interact with the Raf kinase and has a role in the transformation of cells [35].

A genomic study analyzing the degree of relationship between the different Hsp90 family members suggested a nomenclature system according to the phylogeny of the proteins with overall five classes: A bacterial group with the different HtpG variants and four eukaryotic lineages comprising cytosolic Hsp90A, endoplasmic Hsp90B, chloroplast Hsp90C and mitochondrial Trap that all developed out of an ancestral HtpG [7]. Among the eukaryotic Hsp90 variants, Trap has the highest similarity to the HtpG proteins [29,36]. Interestingly, the cytosolic Hsp90A and the chloroplast Hsp90C obviously arose from independent gene duplication

of endoplasmic Hsp90B, and some fungi appear to have lost the Hsp90B variant[7].

Additional to the organelle specific paralogues, it has been found that Hsp90 can also be directed to the cell nucleus upon certain stimuli[37–40], and since Hsp90 lacks a nuclear localization sequence, this translocation seems to be a co-transport with other proteins[8]. Hsp90 was even reported to occur in the extracellular matrix[41].

In general, the homology between Hsp90 members from different organisms is high. On the amino acid sequence level, cytosolic yeast Hsp90 variants are to $\sim 60\,\%$[16] and bacterial HtpG to $\sim 40\,\%$[42] identical to human Hsp90α. Consequently, also the strucuters of the respecitve Hsp90 variants show high similarity (section 1.2).

1.2 Hsp90 Structure

The Hsp90 variants from different organisms share high structural homology with a similar domain organization comprising an N-, M- and C-domain as shown in figure 1.1. As an exception, in the recently dis-

Figure 1.1: Domain structure of Hsp90. Hsp90 homologues from different organisms share an overall similar domain structure as shown. A longer linker region, however, seems to exist only in Hsp90 of higher organisms. Domain boundaries are for Hsp90 from the yeast *Saccharomyces cerevisiae* that was studied in this work.

covered Hsp90N form the conserved N domain is replaced by a shorter hydrophobic sequence [35]. In the Hsp90 proteins from higher organisms, an extended and highly charged linker region connects the N-domain flexibly to the rest of the protein. In the bacterial HtpG variants and also eukaryotic Trap1 that shares the highest homology to the prokaryotic HtpG, this region is shorter and seems to be dispensable to a certain extent [43]. However, nearly full deletion of this segment causes obviously a lethal phenotype in yeast cells and furthermore, cochaperone regulation of Hsp90 and client protein activation by Hsp90 were found to be dependent on the linker region [44]. A certain role for this part of the protein in the basic chaperoning function of Hsp90 was also reported recently [45]. The organelle specific Hsp90 variants additionally carry an N-terminal localization sequence to be directed to their specific compartments.

Several crystal structures mainly of isolated Hsp90 domains [46–50] but also of the full-length proteins from prokaryotic [51] and eukaryotic organisms [52,53] have been obtained so far. Hsp90 forms an extended dimer,

as shown in figure 1.2, upper panel, in the crystal structure for the yeast variant [52], and dimerization was demonstrated to be essential for its function [43,54–57].

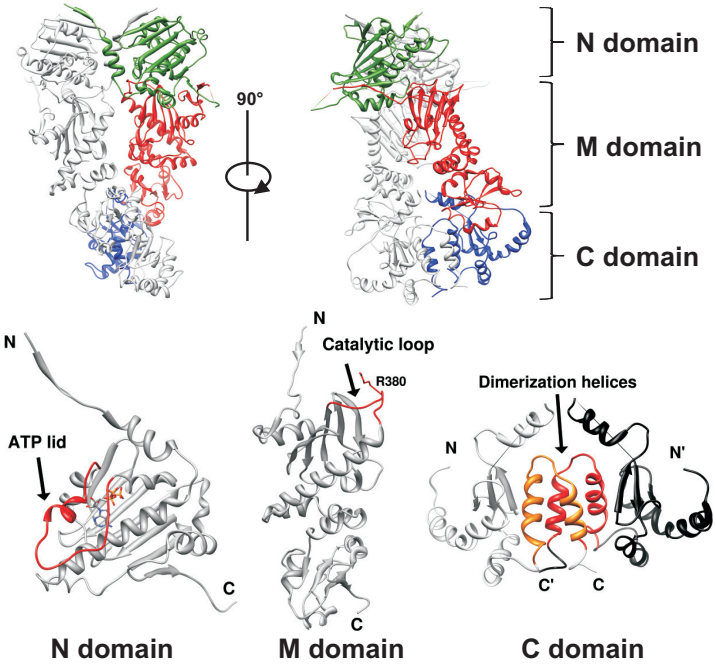

Figure 1.2: Crystal structure (PDB: 2CG9) of full-length yeast Hsp90 in the nucleotide bound closed state. Upper panel: Hsp90 is a constitutive dimer consisting of an N (green), M (red) and C (blue) domain. The second protomer of the dimer is colored uniformly gray for clarity. Lower panel: Single domains of Hsp90 highlighting important structure elements of the molecule.

The N domain of Hsp90 contains the nucleotide binding site of the molecule [46,47]. It has rather globular shape and is composed of a large

β-sheet with eight strands building the bottom of the ligand pocket, whereas surrounding α-helices make up the walls (figure 1.2, lower panel). The N domain of Hsp90 has strong similarity with other ATP (adenosine triphosphate) binding proteins like bacterial DNA gyrase B, MutL DNA-mismatch repair enzymes or histidine kinases, sharing the typical Bergerat ATP binding fold with them [58]. Therefore, it represents a member of the so called GHKL (gyrase, Hsp90, kinase, MutL) class of ATP binding proteins [59]. An important structural element that plays a role for the ATP hydrolysis by Hsp90 is the ATP-lid (residues 95 to 120) that closes over the ligand pocket when nucleotide is bound (see section 1.3) [52,60].

The large Hsp90 M domain has a very elongated shape and consists of two $\alpha\beta\alpha$-motives that are connected by a small helical coil element (figure 1.2, lower panel) [48]. Compared to the structures of other GHKL class members, the Hsp90 M domain shows higher divergence of corresponding regions, and in particular the second smaller $\alpha\beta\alpha$-motive represents an independent fold not found in other GHKL proteins. Amino acids 375 to 388 form the conserved catalytic loop within the Hsp90 M domain, harboring the arginine 380 residue that is essential for ATP hydrolysis as it contacts the γ-phosphate of the ATP ligand (see section 1.3) [48]. The Hsp90 M domain was reported to be likely involved in the binding of client proteins [48,61–63] which – given its large surface – seems reasonable. Indeed, especially a mutation of W300 that is part of a hydrophobic spot within the Hsp90 M domain was demonstrated to have severe *in vivo* effects.

As mentioned, Hsp90 is a constitutive dimer and the dimerization interface is provided by its C domain [49,54,55]. The association between the Hsp90 protomers is on the order of $K_d \sim 60\,\mathrm{nM}$ [55] and thus comparatively strong. The Hsp90 C domain consists of a mixed structure with a

small β-sheet comprising three strands and five α-helices (figure 1.2, lower panel). The helices four and five within each subunit of the C domain dimer undergo tight packing contacts with the respective counterpart from the other subunit in a four-helix bundle, mediating high affinity oligomerization. The residues $\sim$680 to 709 in the C domain of yeast Hsp90 were not resolved in the crystal structure of yeast Hsp90 [52] and appear to be unfolded. Nevertheless, at the very C-terminal end of this stretch in the protein a highly conserved MEEVD peptide motive is located that serves as binding site for TPR (tetratricopeptide repeat) domain cochaperones [64–72]. The C domain is not involved directly in the ATP hydrolysis reaction of Hsp90 but it essentially contributes to this function by mediating the dimeric state: Cysteine bridged NM mutants of Hsp90 comprising only the N and M domain had ATPase activity similar to the wild-type protein whereas the monomeric NM variants had barely detectable ATP hydrolyis [56]. However, the Hsp90 C domain serves as regulation site that has influence on the ATPase activity by post-translational modifications. For example, a cysteine residue within the Hsp90 C domain is targeted for S-nitrosylation which decreases its ATPase function [73–75].

1.3 Hsp90 ATPase Activity and Chaperone Cycle

Like other members of the GHKL class of proteins, Hsp90 is an ATPase that hydrolyzes ATP, and as mentioned in the previous section, the N domain contains the ligand binding pocket [46]. The ATPase activity of Hsp90 seems to be absolutely essential for its function since Hsp90 mutants defective in this respect do not support cell viability [76,77]. ATP hydrolysis is a conserved feature of bacterial and eukaryotic Hsp90 variants [77–79]. In general, the ATP hydrolysis by Hsp90 is slow, with a turnover number of $\sim$0.5 min^{-1} for yeast Hsp90 and HtpG [77,80,81] and only 0.09 min^{-1} for human Hsp90 [78]. The affinity of Hsp90 for nucleotide is rather weak with a K_d (dissociation constant) on the order of $\sim 100\,\mu$M [46,56,77,81].

Crystallographic studies demonstrated that ATP is bound in an unusual way to the Hsp90 N domain with a kinked conformation [46]. Whereas the adenosine and ribose moieties of ATP are shielded from the solvent when bound in the nucleotide pocket, its γ - phosphate is pointing out to the solvent. Such a binding mode is also found for other GHKL class members. In these proteins, hydrolysis of ATP is achieved by interaction of parts from a domain different from the nucleotide binding domain with the γ - phosphate of ATP [59]. The homology to related GHKL proteins suggested a similar ATPase mechanism for Hsp90. Indeed, although the Hsp90 N domain contains the full nucleotide binding site, its ATPase activity in isolation is barely detectable [55,82]. Since the dimeric state of Hsp90 was clearly found to be essential for its function [43,54,55], this could be assumed to be due to the N domain being monomeric. However, even artificially dimerized N domains were shown to be unable to efficiently hydrolyze ATP whereas dimers of a fragment comprising the N and M domain had wild - type ATPase activity [56]. This clearly pointed at an essential involvement of the M domain in the ATP hydrolysis reaction. Additionally, also

the kinetic analysis of Hsp90 ATP hydrolysis suggested a participation of parts outside the N domain in the ATPase reaction [81]. Crystal structures obtained for M domain of Hsp90 and biochemical studies further supported this assumption. Hsp90 was found to be a "split" ATPase [48] that achieves ATP hydrolysis in a concerted action of the N and M domain [52].

The slow ATP hydrolysis by Hsp90 pointed at larger conformational changes occurring prior to ATP hydrolysis that represent the rate limiting step in the reaction [60,83–87]. In particular, N domain dimerization represents a key step [81,82] that traps the nucleotide in the binding pocket and commits it to hydrolysis [55,81]. In this process, the N - terminal residues of the Hsp90 N domain were found to be important [52,60,86].

Hsp90 seems to be conformationally highly flexible, cycling between different states which is driven by nucleotide binding and hydrolysis. A comparison of the crystal structures for nucleotide free HtpG from *E. coli* (PDB: 1IOQ) [51] and nucleotide bound Hsp90 from *S. cerevisiae* (PDB: 2CG9) [52] reveals largely different overall conformations (figure 1.3, upper panel). In particular, the crystal structure of the yeast full - length Hsp90 confirmed the substantial nucleotide dependent structural changes in the molecule in the N and also M domain that were proposed in earlier biochemical studies (figure 1.3).

Upon ATP binding, the so called ATP - lid closes over the ligand pocket, trapping the nucleotide inside (figure 1.3, lower panel) [60]. Concomitantly, the first β - strand from each N domain is released, rendering it available for pairing to the β - sheet from the other N domain. This strand - swapping stabilizes the "closed" conformation of Hsp90 with transiently dimerized N domains. However, for ATP hydrolysis additional M domain rearrangements are required that lead to an intermolecular docking between the N and M domain within the same protomer. Overall, the M domains approach each other by ~ 40 Å, resulting finally in a twisted

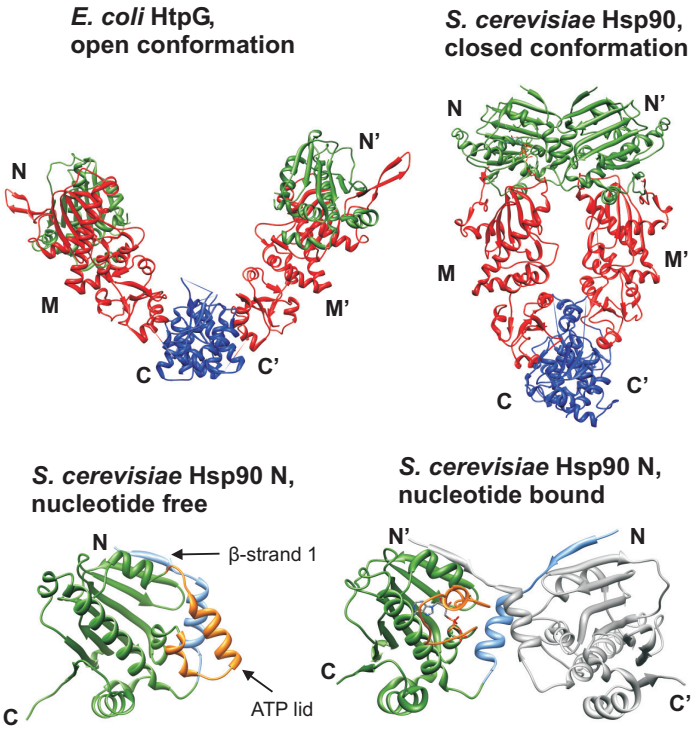

Figure 1.3: Conformational flexibility of Hsp90. Upper panel: HtpG from *E. coli* (left, PDB: 2IOQ) in its open conformation and Hsp90 from *S. cerevisiae* (right, PDB: 2CG9) in its nucleotide bound closed conformation. Lower panel: Isolated Hsp90 N domain (left, PDB: 1AM1) and in its nucleotide bound dimerized state (right, PDB: 2CG9).

ring - like structure with N and C domains associated, previously termed as a "molecular clamp"[52,82]. This particular conformation positions the loop projecting out from the M domain (compare figure 1.2, lower panel)

in a way that allows for the catalytically important R380 to contact the γ-phosphate of the ATP bound to the N domain. This helps to polarize the β-γ-phosphodiester bond in the nucleotide to enable a reasonably fast hydrolysis reaction [52]. After nucleotide hydrolysis, ADP (adenosine diphosphate) is released from the N domains, accompanied by their dissociation and returning of Hsp90 to the open conformation. The structure rearrangements described are the rate limiting step of the Hsp90 ATP hydrolysis and are much slower than the hydrolysis reaction itself [88]. They are commonly termed as the Hsp90 "chaperone cycle" or "ATPase cycle" as shown in figure 1.4.

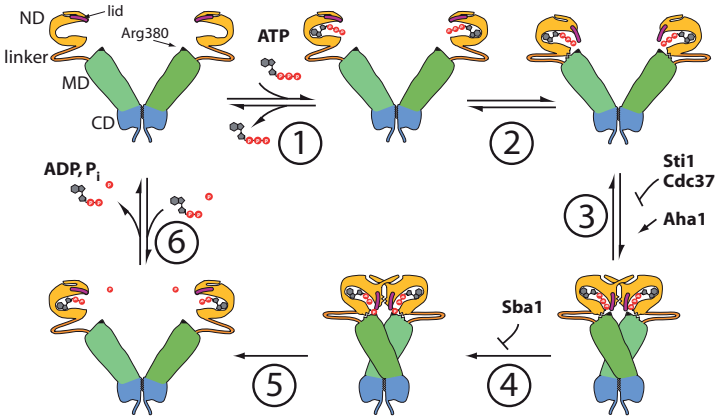

Figure 1.4: The Hsp90 ATPase cycle. Hsp90 ATP hydrolysis is achieved by a series of large conformational changes in the molecule, termed the Hsp90 "chaperone cycle" or "ATPase cycle". Graphic is taken from Wandinger *et al.*, 2008.

Interestingly, another crystal structure of the endoplasmic Grp94 paralogue from *Canis familiaris* [53] showed a significantly different domain

orientation for the nucleotide bound state of the molecule compared to the structure obtained for the yeast variant, with the N domains not dimerized. This raises the question to which extent the conformational rearrangements are conserved between the individual Hsp90 proteins. Due to the inherent flexibility of Hsp90, the structures for full-length yeast Hsp90 and the *Canis familiaris* Grp94 were both obtained on engineered molecules that were lacking the linker regions. In case of yeast Hsp90, additionally the A107N mutation favoring ATP-lid closure and therefore the closed state was introduced and furthermore, the molecule was co-crystallized with the cochaperone Sba1 that stabilizes the dimerized conformation. These experimental differences might account for the discrepancies observed, but also crystal packing might play a role. Alternatively, species specific differences might potentially exist.

Recently, it has also been suggested that the mentioned crystal structures might possibly represent only different snapshots of transient conformational states during the course of an indeed conserved chaperone cycle [8]. This seems plausible and is supported by electron microscopy studies that indicated Hsp90 to exist in a conformational equilibrium with multiple states of the molecule present at the same time [89]. The binding of nucleotides would thereby only shift the equilibrium more in favor of the closed state without locking all molecules in a similar conformation, and the preferred conformational state in dependence of nucleotide might potentially be species specific.

As mentioned, the Hsp90 ATP hydrolysis is essential for its cellular function [76,77] and is further subjected to a complex regulation network. Additional proteins associated with Hsp90, so called cochaperones, have partially impact on its ATPase cycle by increasing or slowing down ATP turnover. Currently, more than 20 cochaperones have been identified, some of which are summarized in table 1.1. However, not for all of them

Table 1.1: Hsp90 associated cochaperones. Several of the Hsp90 associated cochaperones influence its ATPase activity and have additional specific functions in the activation of Hsp90 client proteins. PPIase, peptidylprolyl isomerase; FKBP, FK506 binding protein; Cyp40, Cyclophilin 40. Table is adapted from Wandinger *et al.*, 2008.

	Hsp90 ATPase	Function
TPR domain		
Hop (Sti1)*	↓	Hsp70/Hsp90 adapter, client maturation
Sgt1 (Sgt1)	/	Client protein adapter
FKBP51/52 (/)	/	PPIase, chaperone, client maturation
PP5 (Ppt1)	/	Hsp90 phosphatase
Cyp40 (Cpr6,Cpr7)	/	PPIase, chaperone, client maturation
TTC4 (Cns1)	/	Essential for yeast cell viability
non TPR domain		
Aha1 (Aha1/Hch1)	↑	ATPase activator
p23 (Sba1)	↓	Chaperone, client maturation
Cdc37 (Cdc37)	↓	Chaperone, kinase specific cochaperone

*Names in brackets are for the yeast Hsp90 system

the mechanistic details about how they influence the Hsp90 ATP hydrolysis are understood so far. Many of the Hsp90 cochaperones serve additionally highly specific functions besides regulating the Hsp90 ATPase activity, in some cases they even seem to essentially participate in the maturation of a particular subset of Hsp90 dependent client proteins. Due to their specificity, the Hsp90 cochaperones are conserved to a varying extent in different species. Despite being termed “cochaperones”, not all of these proteins have a real chaperone activity on their own. A large group among them are the TPR domain containing cochaperones. TPR domains in general are interaction modules mediating complex formation between proteins, which will be discussed further in section 2.1.3. Details about

the role of three particular Hsp90 cochaperones, Hop/Sti1, p23/Sba1 and Aha1/Hch1 will be addressed in chapter 2.

The Hsp90 ATPase activity can also be modulated by small molecules binding to the ATP pocket of Hsp90. Several compounds of fungal origin have surprisingly high affinity for Hsp90 and can inhibit its ATP hydrolysis. Geldanamycin (GA) and Herbimycin A are a class of ansamycin antibiotics that have antitumor activity [90]. Their effect was originally thought to be a direct binding to kinases involved in tumorigenesis [91–93]. However, it turned out that these compounds bind to Hsp90 [47,84,94,95], which leads to a reduced interaction of kinase clients often upregulated in tumor cells with the chaperone [96–98], ultimately causing their degradation via the proteasom [97,99–101].

The binding of GA to the Hsp90 N domain is with a K_d of $\sim 1\,\mu$M significantly stronger than that of ATP (more than two orders of magnitude) [94], thus GA and related compounds are highly competitive inhibitors of the Hsp90 nucleotide binding. Another compound, Radicicol, also from a fungal organism, is a macrolactone structurally different from GA, but has an affinity for the Hsp90 N domain even higher compared to GA. The K_d in this case was found to be in the nM - range [94]. Despite their structural difference to the natural ligand, both compounds seem to mimic the unusual kinked conformation of the nucleotide when bound to the ligand pocket of the Hsp90 N domain (figure 1.5).

Exploiting the fact that tumor cells often require increased levels of cell signaling molecules like kinases for proliferation and that these are strongly dependent on Hsp90 function, the inhibition of Hsp90 by compounds derived from template structures like GA and Radiciol turned out to be a promising strategy in the treatment of cancer. Indeed, clinical studies were initiated in the past years targeting Hsp90 for inhibition with compounds like 17 - AAG (17 - allylamino,17 - demethoxgeldanamy-

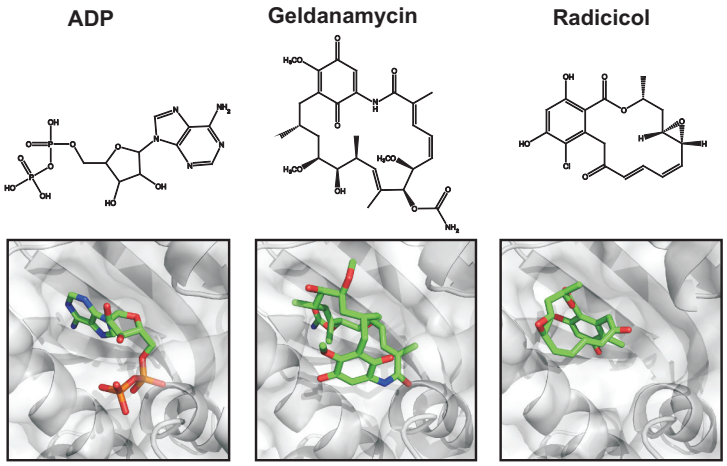

Figure 1.5: Hsp90 N domain inhibitors. Upper panel: Structures of the competitive Hsp90 nucleotide binding inhibitors Geldanamycin and Radicicol in comparison to ADP. Lower panel: Binding modes of ADP (PDB: 1AM1), Geldanamycin (PDB: 1YET) and Radicicol (PDB: 1BGQ) as found in crystal structures of the Hsp90 N domain in complex with the respective ligand.

cin) [102–104]. Libraries of compounds were created on basis of the natural template structures of GA and Radicicol to further improve their affinity and selectivity as well as new classes of ligands designed that could potentially display better pharmacological behavior [105–109].

1.4 Hsp90 Chaperone Activity

Despite large progress in the understanding of its ATPase function and regulation by different cochaperones, the role of Hsp90 in the stabilization and maturation of its substrate proteins or "clients" is still poorly understood so far and just at the beginning to be elucidated. Clearly, Hsp90 has functions as a chaperone in the classical sense: Initially, it was discovered to be upregulated under cellular stress conditions, as typical for a heat shock protein [110,111]. Also, *in vitro* experiments confirmed the ability of Hsp90 to suppress an aggregation process of model proteins under elevated temperatures [45,112] that is independent of ATP [112–114]. However, this seems to be only one specific aspect of Hsp90's function.

As already mentioned, Hsp90 is found in high concentrations even in unstressed cells and is indispensable in most organisms also under physiological conditions (compare section 1.1). This clearly indicates an involvement of Hsp90 in fundamental biological processes. Indeed, the number of proteins found to be interacting with Hsp90 is rapidly increasing [115–117]. Among these, transcription factors and kinases represent two major groups, indicating that Hsp90 function might largely impact on cell signaling [118] (table 1.2).

But Hsp90 seems to influence also many other aspects of cell biology like viral infection, protein trafficking, innate immune response, cell motility or even evolution [119,120] by interacting with key proteins involved those processes [8]. Currently, it is estimated that overall Hsp90 from yeast *S. cerevisiae* physically or genetically interacts with more than 1000 different proteins [121,122], which accounts for $\sim 20\,\%$ of the yeast proteins [8]. However, it is not clear to which extent all proteins found to pyhsically interact with Hsp90 are really depedent on its action for adopting their functional states, and cell - type specific differences or par-

Table 1.2: Hsp90 client proteins. Two major classes of proteins found to interact with Hsp90 are kinases and transcription factors. Therefore, Hsp90 action has indirectly large influence on cellular signaling processes. Table adapted from `http://www.picard.ch/downloads/Hsp90interactors.pdf`.

Kinases	**Transcriptions factors**	**Others**
Bcr-Abl	CAR	α_{2c} adrenergic receptor
Cdk2, Cdk4, Cdk6, Cdk9, Cdk11	HSF-1	Apaf-1
eEF-2 kinase	IRF3	Argonaute-1
HER3	Mal63	Bcl-2
Insulin receptor	p53	Bcl-xL
Integrin-linked kinase	Stat3	calmodulin
IRAK-1	Stat5	Diphtheria toxin
JAK1	GR, MR, ER, PR, AR	DNA polymerase α
MAPK6	TonEBP/OREBP	F1F0-ATP synthase
pp60v-src, c-src	Ure2	Mdm2
Raf-1, B-Raf	VDR	telomerase
VEGFR1, VEGFR2	WT1	ZEITLUPE

ticular cell environmental conditions may cause a different requirement of Hsp90.

The seemingly "random" binding of proteins completely unrelated in function and structure by Hsp90 raises the question about the specificity of theses interactions and the precise role Hsp90 plays with respect to substrate protein folding. Up to date, still comparatively little knowledge exists about the details of Hsp90 - client protein complexes, and their structural analysis could by far not keep up with the number of newly discovered Hsp90 interactors. The promiscuous, presumably weak and highly dynamic binding between client proteins and Hsp90 which is often additionally modulated by cochaperones might have hampered a more in depth structural characterization so far.

In contrast to other chaperons like Hsp70 that recognize partially unfolded proteins exposing hydrophobic parts, Hsp90 seems to preferen-

tially act on highly structured nearly native - like substrate proteins [112]. A recent study for example could show that Hsp90 specifically bound only to the structured region of a staphylococcal nuclease fragment that was otherwise largely unfolded [63].

Also, in case of the steroid hormone receptors that have been implicated as Hsp90 client proteins for a rather long time [123,124] and essentially depend on Hsp90 to acquire hormone binding activity, Hsp90 does likely not promote the folding of a denatured form of the receptor. Here, Hsp90 seems to be involved in the late step maturation of the client, interacting with the hydrophobic ligand binding cleft to allow for access of the hormone [125–128]. Thus, Hsp90 serves a highly specific task in this example, however, only in essential association with cochaperones [118]. Potentially, the large interaction network of Hsp90 is partially also based on the modulating effects of cochaperones which contributes to a certain specificity in the complex formation between Hsp90 and clients. Indeed, Hsp90 was initially isolated as part of large heterocomplexes with several additional components by immunoprecipitation, as for example in case of the steroid hormone receptors. This shows that Hsp90 exerts its function mostly in conjunction with other proteins.

In general, the role of Hsp90 seems to be likely a stabilization of a specific labile conformation of the client but not to promote its *de novo* folding [129]. The conformational state of a protein might be a more important determinant for rendering it a candidate suited for Hsp90 binding than a particular well defined binding motive. This could give an explanation for structurally completely different proteins being Hsp90 clients. This assumption is supported by observations made on the oncogenic Src (sarcoma) kinase client protein: The cellular variant of this protein, c - Src, is to a large extent independent from Hsp90 function. The viral variant, v - Src [130], although to $\sim 95\,\%$ identical to c - Src [131], essentially requires

Hsp90 interaction [131–133].

So far, the determination of the client protein binding site on Hsp90 has likely been hampered to a large extent by the weakness and transient nature of these interactions and the potential requirement of additional factors to mediate complex formation. Therefore, a high resolution structure of an Hsp90 - client complex has not been obtained up to date. Several reports implicated presumably the N and M domain of the chaperone as client binding sites. An electron microscopy study yielded a low resolution structure of an Hsp90 - Cdk4 complex in association with Cdc37 [134], a kinase specific cochaperone [135]. Interestingly, the Cdk4 kinase and Cdc37 were bound asymmetrically to Hsp90 with only one molecule of the client as well as Cdc37 per Hsp90 dimer. Cdk4 interacted with the N and M domain of the same Hsp90 protomer whereas Cdc37 was positioned between the Hsp90 N domains.

In another recent report likewise the N and M domain of HtpG from *E. coli* were suggested to be involved in binding of a nuclease fragment, based on the results from SAXS (small angle X - ray scattering) measurements [63]. Obviously, HtpG seemed to adopt a more compact conformation in this case, partially closing around the client protein. This observation seems to be consistent with the aforementioned report about the Hsp90 - Cdk4 - Cdc37 complex.

The M domain of Hsp90 was also implicated as interaction site for p53 [62,136] and seems to play a role for the activation of substrates like v - Src and the glucocorticoid receptor [137]. Severe *in vivo* defects upon mutation of residues from a presumable client protein binding site within the Hsp90 M further support its potential role in this respect [48]. But also the C domain of Hsp90 was suggested to be involved in its chaperone function [45,49,138,139] and found to provide an interaction site for the glucocorticoid receptor [140].

The nucleotide dependence of the Hsp90 chaperone function seems to be different for particular cellular tasks. *In vitro*, the suppression of protein aggregation by Hsp90 did not require ATP[112,139]. This might be in particular of importance for a general passive chaperoning to stabilize proteins as under heat shock conditions. However, for more specific tasks as for example the conformational maturation of clients like the steroid hormone receptors, nucleotide binding obviously plays an essential role[118,139]. Indeed, Hsp90 lacking ATPase activity does not support cell viability[48,76,77].

The effect of ATP binding and hydrolysis on Hsp90 client protein binding is not yet fully understood. Recently, in case of *E. coli* HtpG an increased affinity for a model substrate protein, a staphylococcal nuclease fragment, was reported in the nucleotide bound state of the chaperone and furthermore, a stimulation of the ATP turnover occurred[63]. The same effect was observed for the human Hsp90 ATPase activity that was strongly increased (200 - fold) in presence of the glucocorticoid receptor ligand binding domain[78]. By altering the conformational state of Hsp90, nucleotide binding might lead to an exposure of specific client protein binding sites not available in the open conformation of Hsp90. The ATPase stimulation by client protein binding suggests a certain influence of the conformational transitions of Hsp90 during the chaperone cycle.

In vivo, also the binding of highly conformation sensitive cochaperones like p23/Sba1 to Hsp90 might play a role for client protein maturation as it is the case for steroid hormone receptors[118]. For p53 as a substrate protein, an ATP dependent disruption of its interaction with Hsp90 was observed[141]. Consistent with an important role of nucleotide binding/hydrolysis, a competitive inhibition of the Hsp90 ATP binding by small molecule inhibitors like GA or Radicicol results in a reduced interaction of cell signaling proteins like kinases or steroid hormone receptors

with Hsp90, which are in this case targeted for degradation [99,100,142–144] (compare section 1.3). In particular, tumor cells are strongly dependent on these proteins for proliferation harbor increased levels of them, rendering them sensitive to an Hsp90 inhibition. This led to the idea of Hsp90 being a druggable protein in cancer treatment. Overall, the nucleotide binding seems to have very differential effects on Hsp90's complex formation with client proteins, strongly depending on the client protein to be chaperoned.

Given its extraordinary importance for fundamental cellular processes, further work will be required to understand the Hsp90 function in the context of client protein activation. Although challenging, especially further structural studies might contribute to elucidate key factors governing complex formation between Hsp90 and client proteins. Despite a remarkably profound knowledge about the mechanisms underlying the ATPase regulation of Hsp90 by cochaperones, their specific roles with respect to modulating the chaperoning of client proteins by Hsp90 will also have to be addressed in more detail in the future.

Chapter 2

Hsp90 Cochaperones

2.1 Sti1/Hop

2.1.1 Functions of Sti1/Hop in the Hsp70 - Hsp90 System

The Hsp90 cochaperone Sti1 (stress inducible protein 1) from yeast was initially identified as a protein of about 66 kDa related to cellular stress conditions. It was found to be up - regulated up to tenfold under elevated temperatures and other stress factors in yeast cells. A knockout of Sti1 did not affect cell viability of yeast cells at normal temperatures but led to impaired growth at lower or higher temperatures [145]. However, a deletion of Sti1 combined with mutations in Hsp90 or its cochaperones reduced or eliminated growth even at normal temperatures [146,147]. This indicates that Sti1 and Hsp90 function are closely linked together.

Sti1 was shown to share high homology with a human protein of 62.6 kDa [148]. Later, the human protein and homologous proteins from other

systems previously known as p60 were then named“Hop” (Hsp70/Hsp90 organizing protein) [64]. Although termed “cochaperone”, Sti1/Hop does not have chaperone activity on its own *in vitro* [149,150].

In affinity pull downs with different tissue extracts Sti1/Hop was found as a component of larger protein complexes co - purifying with the Hsp70 and Hsp90 chaperones [151,152]. Distinct parts of Sti1/Hop could subsequently be assigned to be involved in either Hsp70 or Hsp90 binding (see 2.1.3) [64,68]. Thus, one main function of Sti1/Hop was concluded to be a physical bridging of Hsp70 and Hsp90 to assist in the formation of multi-chaperone complexes.

Sti1/Hop seems to have essential functions in the assembly of hetero-complexes with the Hsp70/Hsp90 chaperones and steroid hormone receptors as for example the glucocorticoid (GR) and the progesterone receptor (PR) [64,66,153,154]. It is assumed that association of the GR with Hsp90 keeps the receptor in a conformation competent of ligand binding [155,156]. An *in vitro* - reconstitution of a functional GR - Hsp70 - Hsp90 heterocomplex was only possible when a fraction containing Sti1/Hop was added to the system [154]. Together with Hsp40, Hsp70, Hsp90 and p23, Hop/Sti1 makes up the minimal chaperone system that has refolding activity with respect to the PR and GR *in vitro* [157–159]. *In vivo*, the activity of the human GR expressed in yeast cells was significantly reduced when Sti1 was deleted [146]. An involvement of Sti1/Hop in the maturation of another Hsp90 substrate, the oncogenic protein v - Src could also be demonstrated. Since v - Src shares no structural or functional similarity with the steroid hormone receptors, it seems likely that Sti1/Hop plays a general role for the maturation of Hsp90 dependent client proteins [146].

Sti1 obviously acts at an intermediate stage of the maturation process in the substrate - Hsp70 - Hsp90 heterocomplexes [146,153]. It is thought that client proteins first interact with Hsp40 and Hsp70 [160]. After this ini-

tial step, Sti1/Hop mediates interaction of the client loaded Hsp70 with Hsp90 to allow for a transfer of the client to Hsp90, releasing Hsp70 out of the complex[6,161,162]. However, this substrate transfer from Hsp70 to Hsp90 is poorly understood so far. In a later step, Sti1/Hop is replaced in the heterocomplex by conformational changes that lead to additional binding of p23/Sba1[142,163].

The function Sti1/Hop in the Hsp70 - Hsp90 complexes is not only restricted to a mere adapter protein physically linking the two chaperone systems. It was reported that in yeast cells Sti1 should act as a potent stimulator of the Hsp70 ATPase activity[164], although this stimulation could not be found for the mammalian system with Hop[164,165]. This might possibly reflect species specific differences in the action of Sti1/Hop proteins. On the other hand, it was shown that yeast Sti1 has an inhibitory effect on the ATPase activity of Hsp90[166,167]. The inhibition by Sti1 is non - competitive since Sti1 does not block access of ATP to the nucleotide binding pocket in the N - terminal domain of Hsp90[167]. The mechanism of inhibition seems to be rather on the level of influencing conformational changes within Hsp90 that were shown to be necessary for ATP hydrolysis, in particular blocking of its N - terminal dimerization[52,168]. For the human system, in contrast, it was found that Hop had little influence on the basal ATPase activity of Hsp90 but could significantly inhibit the client protein stimulated ATPase rate[78].

2.1.2 Domain Structure of Sti1/Hop

Sti1/Hop is a multi - domain cochaperone of Hsp90 consisting of five different domains. It comprises three tetratricopeptide repeat (TPR) containing domains that have very similar structures, TPR1, TPR2A, and TPR2B and two aspartate proline rich (DP) domains [66,68,70,148,151,169–172]

(figure 2.1). In some cases, homologues of Sti1/Hop from other organisms however have slightly different domain structure: For example Hop from *Drosophila melanogaster* lacks the DP1 domain [173] and Hop from *Caenorhabditis elegans* lacks both TPR1 and DP1 [147,174]. Using bioinformatical approaches it was suggested that the Sti1/Hop domain arrangement might result from a successive recombination of an ancestral TPR - DP module as a functional unit [147,173,175]. There seems to be some evidence that – contrary to the general opinion Sti1/Hop proteins would only be found in eukaryotic systems – Hop - like proteins also might exist in bacteria [175].

Figure 2.1: Domain structure of the Hsp90 cochaperone Sti1. Sti1 consists of three TPR modules and two DP domains.

2.1.3 Sti1/Hop Tetratricopeptide Repeat (TPR) Domains

The tetratricopeptide repeat (TPR) motive is a common structural module that mediates specific protein - protein interactions and serves in the assembly of multi - protein complexes. It can be found in numerous proteins unrelated in their functions [176]. Initially, the TPR fold was discovered in proteins involved in cell - cycle control in yeast [177,178], but subsequently many other proteins were identified that also contain TPR mod-

ules. Among these are proteins implicated in processes like splicing, transcription, protein transport, protein folding and signal transduction [176].

The TPR motive is a loosely conserved 34 amino acid stretch forming two anti - parallel helices named A and B (figure 2.2). It can be found as isolated structure element in proteins but usually several TPR modules are arranged in tandem arrays to form larger protein domains. The number of TPR modules grouped together can vary ranging from three up to sixteen.

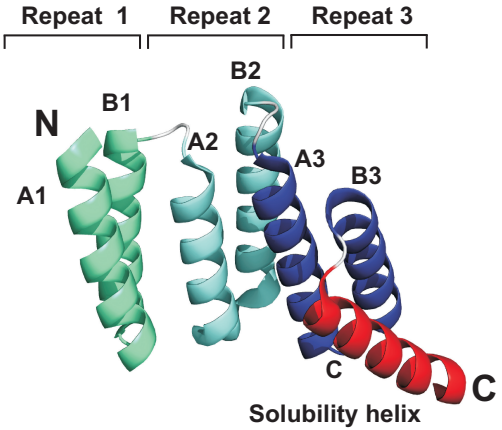

Figure 2.2: TPR domain structure. Crystal structure of the TPR2A domain from human Hop (PDB: 1ELR) [68]. A typical TPR domain found in Sti1/Hop proteins consists of three repeat motives each comprising two helices (named A and B) with 34 amino acids. The additional helix seven (named C) usually contains a high number of charged residues to increase the solubility of the domain.

The conservation of amino acids within the TPR motive is more on the level of conserved properties of residues like size or hydrophobicity at certain positions. Overall, eight positions of the TPR motive show par-

ticular conservation generating a consensus, amino acids 4 (W/L/F), 7 (L/I/M), 8 (G/A/S), 11 (Y/L/F), 20 (A/S/E), 24 (F/Y/L), 27 (A/S/L) and 32 (P/K/E) [176,178,179]. The sequence between these positions shows high variability, resulting in TPR motives with very different properties. This explains the wide-spread occurrence of TPR domains and their involvement in quite different biological processes. However, conservation can also be found outside these eight positions when TPR domains are compared that have related functions, for example TPR domains binding Hsp90 [176].

The helices of the TPR motives have usually amphipathic character. Hydrophobic contacts with an aromatic residue phenylalanin from helix B fitting into a hydrophobic pocket in helix A pack the helices together. This is also known as "knob and hole" model [177]. Residues located at the outside of TPR module are often charged like glutamine, glutamate or lysine.

The first crystal structure obtained on a TPR domain protein was the structure of PP5, which gave detailed information about the overall fold of TPR containing proteins [65]. The typical fold of PP5 was later also found for many other TPR domain proteins: The parallel arrangement of several helix-turn-helix elements of the TPR units creates a right-handed shape in a TPR domain, with contacts formed between two helices A from consecutive TPR motives. Thus, a concave and a convex surface are generated in a TPR domain. Additional to the three TPR units, PP5 had a seventh helix (named C) and nearly all TPR domain structures that were solved so far also have this helix (figure 2.2). It is an integral part of the structure as it packs against the adjacent TPR motive, similar as the TPR motives among each other. It usually contains several charged residues to increase the stability of the domain and is called capping or solubility helix.

Many biochemical data indicated that TPR domains mediate protein-protein interactions, however, details about how TPR domains recognize binding partners were not available. From the PP5 structure it was speculated that TPR domains might bind ordered structure elements like helices as the groove formed by the arrangement of the TPR modules could in principle accommodate a helical peptide[65]. However, later it turned out that this is not the case for most TPR domains.

As outlined in 2.1.2, Sti1/Hop contains three TPR domains, each composed of three TPR motifs and the additional solubility helix. Using deletion mutants, it was found that the N-terminal TPR1 domain of Hop was involved in binding of the Hsp70 C-terminal region and the centrally located TPR2 block (i.e. TPR2A + TPR2B) was responsible for the interaction with Hsp90[64,180,181]. Within Hsp90, the C-terminal domain was identified as binding site for Hop[67,182] and a mutation of the conserved terminal EEVD motive of Hsp90 led to a reduced binding of Hop[183].

A basic question about the function of Sti1/Hop is how specific binding of either Hsp70 or Hsp90 is achieved by its different TPR domains to organize the Hsp70-Hsp90 complexes. All eukaryotic Hsp70 and Hsp90 family members terminate with a highly conserved EEVD peptide motive. Therefore, a high degree of selectivity must be obtained for residues recognized by TPR domains adjacent to this motive. The TPR1 and TPR2A domains of human Hop could be co-crystallized with their ligands, and these structures revealed important details about the interaction of TPR domains with binding partners in general and the interaction of Hop TPR domains with Hsp70 and Hsp90 in particular (figure 2.3[68]. TPR1 bound a heptameric peptide corresponding to the C-terminus of Hsp70 whereas TPR2A bound a pentameric peptide corresponding to the Hsp90 C-terminus. Both peptides were bound in an extended conformation to the respective TPR domain. TPR1 an TPR2A are highly selective in pep-

tide binding as could be demonstrated by calorimetric data. TPR1 bound the Hsp70 peptide more than tenfold tighter than the Hsp90 peptide and vice versa [68]. This is surprising given the fact that both Hsp70 and Hsp90 share the same conserved C-terminal sequence EEVD. Figure 2.3 shows the crystal structure of the TPR2A domain in complex with the MEEVD peptide. The binding between the TPR domain and the peptide has a significant electrostatic contribution. Within the binding groove of the protein a strong positive potential can be found (figure 2.3, left). This is also the case for the TPR1 domain.

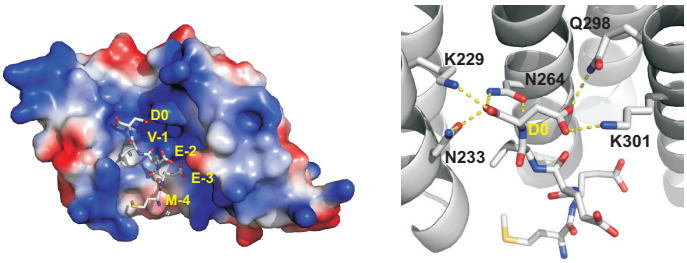

Figure 2.3: Binding of the Hsp90 peptide to the TPR2A domain of human Hop. Crystal structure of the TPR2A domain from human Hop in complex with the Hsp90 peptide MEEVD (PDB: 1ELR) [68]. Left: Electrostatics of the binding groove of TPR2A. Blue color indicates positive, red color negative potential. Binding of the MEEVD peptide is strongly mediated by electrostatics with highly positive potential within the peptide binding site. Residues of the peptide ligand are indicated in yellow. The numbering for residues of the peptide ligand is 0 for the last C-terminal residue, residues upstream/N-terminally are numbered accordingly -1,-2 etc. The electrostatic potential was generated using PyMOL. Right: Details of the two-carboxylate clamp of the TPR2A domain showing how Hsp70/Hsp90 binding TPR domain cochaperones interact with the conserved EEVD motive. Conserved residues contacting the terminal D0 residue of the ligand via hydrogen bonds are indicated.

The peptide is bound via contacts only to the sidechains of the protein. Interactions between the protein and the ligand involve unspecific hydrogen - bonding to the backbone of the peptide and specific bonds to the peptide side - chains, conferring selectivity to the binding. A basic contribution to the peptide binding of TPR proteins recognizing Hsp70/Hsp90 comes from the so called "two - carboxylate clamp"[68]. The terminal Asp residue, named D0, of the peptide ligand is hydrogen - bonded by the sidechains of a set of highly conserved residues from the TPR domain. In the Hop TPR2A domain, residues K229/N233 (helix A1) and N264 (helix A2) contact the main chain carboxylate moiety of D0, Q298 and K301 (helix A3) its side - chain carboxylate (figure 2.3, right). These binding interactions mediate a basic anchoring of the peptide in the TPR ligand binding groove. Alignment of sequences from other TPR proteins binding Hsp70/Hsp90 show that the same residues can be found also within the binding sites of these proteins, suggesting a similar mode of peptide binding[68].

Besides electrostatic contributions to the peptide binding, the discrimination between the Hsp70 and Hsp90 ligand is mainly achieved via the additional hydrophobic contacts to residues upstream of the common EEVD motif. The length of the peptide ligand recognized by the TPR domain is an important factor for selectivity and binding affinity. For the Hop TPR2A domain, the Hsp90 pentapeptide MEEVD gave the maximum binding affinity, for TPR1, in contrast, an Hsp70 heptapeptide PTIEEVD was required to obtain full binding in interaction studies[68].

The extended conformation of the bound peptides also contributes to increase the specificity. In this way, the peptide presents its maximum possible surface, ensuring reasonable selectivity in binding of such rather small ligands. The affinities for TPR1 binding the Hsp70 peptide and TPR2A binding the Hsp90 peptide were both found to be around

10 μM [68].

With the details of the crystal structures available, subsequently many mutational studies were carried out on the TPR domains of Sti1/Hop. As expected, mutations of human Hop TPR2A carboxylate clamp residues selectively abolished Hsp90 binding and mutations of TPR1 carboxylate clamp residues the Hsp70 binding, thus well confirming the findings from the crystallographic studies [171]. These results could also be confirmed by experiments using truncation mutants of yeast Sti1: A deletion of TPR1 significantly reduced Hsp70 binding and a mutant lacking TPR2A was no more able to bind Hsp90 [147]. Therefore, as expected, the selectivities of human and yeast TPR1 and TPR2A domains seem to be similar. More surprising was an observation that also TPR2A carboxylate clamp mutations somehow reduced Hsp70 binding of human Hop in a more complex system with reticulocyte lysates [171], but the relevance of this finding is not clear so far.

Data on the binding selectivity of the third TPR domain of Sti1/Hop, TPR2B, are somehow controversial. As alignments show, TPR2B has the typical residues required to form the two - carboxylate clamp. Nevertheless, for the Hop TPR2B domain only a weak peptide binding activity was reported, with affinities of 130 μM for binding an Hsp70 peptide and 290 μM for the binding of an Hsp90 peptide [184]. Mutational studies were carried out changing residues from the two - carboxylate clamp of TPR2B. These mutations did not affect the ability of human Hop to bind Hsp90, however, Hsp70 binding to Hop was lost [171]. In a second report, mutations in yeast Sti1 TPR2B led to impaired regulation of Hsp90 in an *in vivo* system and therefore it was suggested that TPR2B might be a potential binding site for Hsp90 [185]. These differences might be due to different functions of the TPR2B domain in human and yeast systems. In yet another work it was concluded that Sti1 TPR2B is involved in binding

both Hsp70 and Hsp90: Here it was found that neither TPR2A nor TPR2B alone could stably interact with Hsp90. Only Sti1 fragments combining both TPR domains tightly bound Hsp90. On the other hand, a carboxylate clamp mutation in TPR1 was not sufficient to disrupt Hsp70 binding to Sti1, but upon additional mutation of TPR2B Hsp70 binding was significantly impaired [147]. Therefore, overall the precise role of the TPR2B domain remains elusive so far.

In general, the requirement of the TPR domains with respect to Hsp70 binding seems to be different for human Hop and yeast Sti1. Deletion mutants of Hsp70 lacking the conserved terminal EEVD motive still could bind to human Hop [171] while for the yeast system the respective Hsp70 deletion mutant nearly lost binding to Sti1 [147]. This argues for additional Hsp70 binding sites within human Hop, independent from the TPR domains, and indeed the DP2 domain was found to be also implicated in Hsp70 interactions [171] (see 2.1.4).

The existence of three different TPR domains within Sti1/Hop raises the question how much each of these domains contributes to the general cellular functions of the protein. As described under 2.1.1, a knockout of Sti1 in yeast cells was found not to be lethal [145], but when combined with an additional knockout of YDJ1 (an Hsp40 family member), cells get inviable [186]. In such a genetical background, viability can be restored by introducing a plasmid into the cells expressing Sti1 (or YDJ1). Therefore, this system has been used to investigate basic functions of Sti1. Individual carboxylate clamp mutants of TPR1, TPR2A or TPR2B did not affect the rescuing capability of a Sti1 plasmid in a yeast Sti1/YDJ1 deletion strain. Also, a combination of carboxylate clamp mutations in TPR1 + TPR2A or TPR2A + TPR2B supported viability of the cells. But a combined mutation of TPR1 and TPR2B carboxylate clamp residues turned out to be lethal [187]. Therefore, TPR1 and TPR2B seem to have somehow overlap-

ping *in vivo* functions and might possibly both serve as a Hsp70 binding site.

Furthermore additional studies were carried out on the specific role of the individual Sti1/Hop TPR domains in the activation process of Hsp90 dependent client proteins. Sti1/Hop was found to be important for the maturation of steroid hormone receptors as described under 2.1.1. As it was shown, the human GR can be expressed heterologously in yeast cells, retaining its hormone binding ability and transcriptional activity. A deletion of Sti1 in GR expressing cells reduces the activity of the receptor to activate transcription, without GR protein levels being affected. GR activity can be restored to wild-type level by transforming cells with a plasmid expressing Sti1 [146]. In such a system, Sti1 TPR domain mutants were tested for their ability to support GR activity. Single point mutations of TPR1, TPR2A or TPR2B carboxylate clamp residues reduced the GR activity to ~ 50-60 % of the wild-type level. Combined muations of carboxylate clamp residues in TPR1 + TPR2A or TPR2A + TPR2B led to an additional decrease of GR activity, but combining TPR1 and TPR2B mutations resulted only in background level activity of the receptor [187]. Again, as described above, TPR1 and TPR2B turned out to have partially overlapping functions.

2.1.4 Sti1/Hop DP Domains

The DP domains (see also 2.1.2) were identified as separate folded domains in Sti1/Hop proteins by proteolytic digestion experiments [188,189]. They are characterized by the presence of a conserved dipeptide motive aspartate - proline (DP). DP domains share a significant homology with parts of another Hsp70 binding protein called Hip (Hsc70 - interacting protein, Hsc70 is the constitutively expressed form of Hsp70 in eukaryotic cells) [169,170,189,190]. The C - terminal region of Hip has 42% identity with yeast Sti1 and 30% identity with human Hop [190].

In contrast to the TPR domains (see 2.1.3), the DP domains are structurally poorly characterized so far. Mutation of the human Hop DP motive obviously results in an altered conformation [66] and concomitantly increased sensitivity to proteolytic digestion [189]. It was furthermore speculated that the C - terminal DP domain of human Hop may also influence the conformation of other parts within Hop [189]. However, a detailed structural analysis of DP domains is not yet available.

In yeast Sti1, the DP2 domain appears to be essential for the general *in vivo* functions of the protein. As described under 2.1.3, a combined knockout of Sti1 and YDJ1 in yeast leads to a lethal phenotype that can be reversed by introducing a plasmid into the cells expressing Sti1 [186]. In this system, a plasmid encoding Sti1 with a deletion of DP1 could rescue cells from lethality, similar to a plasmid with wild - type Sti1, however, a deletion mutant lacking the DP2 domain did not support viability [147,187]. This clearly shows that at least some of the basic cellular functions of Sti1 are mediated by the DP2 domain.

The DP2 domain of human Hop seems to be implicated also in the binding of Hsp70. Mutations of the conserved DP motive in DP2 reduced complex formation between Hop and the chaperone, but analogous mu-

tations in DP1 did not have such effect [66,171]. Furthermore, DP domains might also play a role *in vivo* in the assembly of PR - Hsp70 - Hsp90 heterocomplexes: Hop with DP motive mutations within DP2 failed to bind to the PR and did not support association of Hsp90 with the PR [66]. Similar to mutation of the DP motive, a C - terminal truncation of 11 residues from the human Hop C - terminal DP2 domain led to reduced Hsp70 binding and recruitment of Hop into PR - Hsp70 - Hsp90 heterocomplexes [189]. In contrast to human Hop, the function of the DP domains in the yeast homologue Sti1 seem to be slightly different: Here the DP domains obviously have no importance for the binding of Hsp70 or Hsp90 [147].

DP2 plays a significant role in the activation of Hsp90 dependent client proteins. As described in 2.1.1, Sti1/Hop is an important component in the maturation process of the steroid hormone receptors. The transcriptional activity of heterologously expressed human GR in yeast cells was shown to be strictly dependent on the presence of Sti1 (see 2.1.3) [146]. Human Hop could functionally replace Sti1 in a yeast GR expression system [171], but Drosophila Hop could not, although the Drosophila protein was able to rescue growth defects of yeast cells at elevated temperatures that were associated with the absence of yeast endogenous Sti1 [173]. The main difference between yeast Sti1, human Hop and Drosophila Hop is the lack of the DP1 domain in the Drosophila protein, besides the expected sequence differences (see also 2.1.2). However, surprisingly it was found that it was not the missing DP1 domain that was responsible for the defects of Drosophila Hop in GR activation, because a chimeric Drosophila Hop with a human Hop DP1 domain inserted between TPR1 and TPR2A was likewise unable to function in GR activation [173]. In fact, the failure of Drosophila Hop to activate the GR in the yeast system could be assigned to the DP2 domain: A chimeric human Hop protein with a Drosophila Hop DP2 domain could not support GR transcriptional activ-

ity in the yeast testing system, although the chimeric Hop protein had full Hsp70 and Hsp90 binding. This means, although it was shown that DP2 might have functions in Hsp70 binding, the contribution of DP2 to GR maturation here must be something different as the chimeric protein in this case retained full Hsp70 binding [173].

Further studies were carried out on the system with heterologously expressed GR in yeast cells and consistent with the experiments using chimeric Hop constructs, it was found that also all mutations affecting the DP2 domain of yeast Sti1 (deletion, truncation and even point mutation) led to a loss of the GR activity [187]. These findings demonstrate the importance of the Sti1/Hop DP2 domains, on the one hand for the general cellular function of Sti1/Hop and on the other hand for its specific role in the activation of steroid hormone receptors. It appears that the role of Sti1/Hop is not only restricted to a mere adapter protein physically bridging Hsp70 and Hsp90 as previously thought. Rather, Sti1/Hop has additional possibly regulatory functions that are connected to the DP2 domains. Overall, so far the DP2 domain seems to be more important for Sti1 functions than DP1, and the role of DP1 remains even more elusive compared to DP2.

2.2 Aha1/Hch1

The Aha1/Hch1 family of Hsp90 cochaperones was initially identified in a genetic screen for suppressors of a temperature sensitive phenotype in yeast cells caused by an Hsp90 E381K loss-of-function mutation [191]. Yeast cells harboring the Hsp90 E381K variant do not grow well even at normal and not at all at elevated temperatures [192]. In such a background, Hch1 was found to suppress the cellular growth defects and restore the wild-type phenotype when overexpressed. Therefore, the protein was termed "high copy Hsp90 suppressor 1", Hch1.

Interestingly, the 153 residues of Hch1 show high homology to another protein from yeast, Aha1 [193], sharing 37 % sequence identity with its N-terminal half [191] (figure 2.4). In contrast to Hch1, Aha1 possesses an

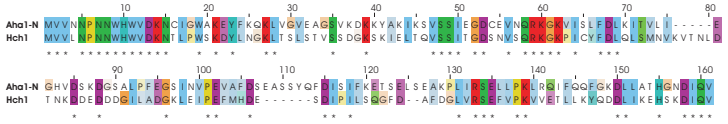

Figure 2.4: Amino acid sequence alignment of the yeast Aha1 N-domain and Hch1. UniProt reference codes of the sequences used for the alignment are 12449 for Aha1 and P53834 for Hch1. The alignment was generated using T-Coffee [194] and visualized with Jalview [195]. The coloring scheme is according to amino acid properties and the degree of conservation of a particular position, with more intense color indicating higher conservation.

additional C-domain of 197 residues. Whereas shorter Hch1-like proteins seem to exist only in other fungal organism as for example the yeast *Candida albicans*, Aha1 is conserved throughout all higher organisms [196]. Both, Hch1 and Aha1, were found to directly interact with Hsp90, *in vivo* and *in vitro* [193]. Obviously, no other interactors for Hch1/Aha1 seem to exist besides Hsp90 [196].

Hch1 and Aha1 have a stimulatory effect on the Hsp90 ATPase activity, however, to a different extent. Due to this function, the name for the Hch1 - like protein “Aha1”, “activator of Hsp90 ATPase 1”, was derived [193]. Aha1 accelerates the Hsp90 ATP turnover up to ~ 12 - fold. The isolated Aha1 N - terminal fragment, which corresponds to the Hch1 full - length protein, still shows a ~ 3.5 - fold ATPase stimulation, its C - terminal fragment, however, has no effect. Hch1 was shown to stimulate the Hsp90 ATPase activity to a similar extent as Aha1 N, but in this case, higher concentrations of the cochaperone were required to obtain the same ATPase acceleration. Given their overlapping functions with respect to Hsp90 ATPase activation, it is surprising that yeast cells contain Hch1 and Aha1 at the same time, whereas in higher organisms only Aha1 can be found.

Crystallographic and biochemical studies identified the major binding site for the Aha1 N domain within the M domain of Hsp90 [196,197] and pointed at the mechanism that underlies the ATPase stimulatory effect (figure 2.5). Aha1 induces conformational rearrangements within the catalytic loop region (compare figure 1.2) of the Hsp90 M domain that reorient the important Arg380 in a way that allows for contact formation with the nucleotide bound to the N domain, thus promoting efficient ATP hydrolysis [197]. The Aha1 C domain was shown to further contribute to the ATPase stimulation by providing additional binding contacts with the N domains of Hsp90, which stabilizes its closed dimerized conformation capable of ATP hydrolysis [198,199]. Interestingly, Aha1 binds in an asymmetric fashion to Hsp90, one molecule of the cochaperone per Hsp90 dimer is sufficient for full ATPase stimulation, leaving in principle the possibility of a simultaneous client protein binding to an Hsp90 - Aha1 complex.

Conflicting reports exist about the coexistence of the cochaperones

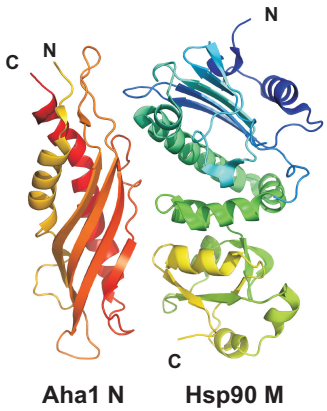

Figure 2.5: Complex between the Aha1 N and Hsp90 M domain. Crystal structure of the N-terminal domain of Aha1 (residues 1 to 153) bound the Hsp90 M domain (PDB: 1USV).

Aha1 and Sti1 in complexes with Hsp90: One report concluded a simultaneous binding of Aha1 and Sti1 to Hsp90 [193] while another found it to be competitive [196], which would point at (partially) overlapping binding sites for the two cochaperones on Hsp90.

A knockout of Hch1 in yeast cells did not result in an obvious growth defect, suggesting that its function might be intimately connected only with rather specific Hsp90 actions [191,193,196]. Likewise, cells lacking Aha1 were nearly unaffected in growth [193,196]. However, when Hsp90 levels were depleted in cells, a double knockout of Hch1 and Aha1 led to a reduced thermotolerance [196]. Also, under other stress conditions Aha1 or Hch1 knockout strains showed a restricted growth at elevated temperatures, which was more pronounced when both cochaperones were absent [193].

Hch1 was demonstrated to have substantial influence on the maturation of a strictly Hsp90 dependent client protein, v-Src kinase [131]. Yeast cells expressing an Hsp90 E381K mutant show only low v-Src activation [192] that is however strongly increased by overexpression of Hch1. A deletion of Aha1 in cells expressing wild-type Hsp90 caused a reduced activation of v-Src, which was completely abolished when additionally also Hch1 was missing [193]. This indicates that Hch1 can to some extent compensate for Aha1 functions and that both cochaperones obviously impact on Hsp90 client protein activation. This is further supported by other studies: A knock-down of Aha1 led to a rescued cell surface presentation of the CFTR (cystic fibrosis transmembrane conductance regulator) ΔF508 mutant that is normally trapped in the endoplasmic reticulum [199,200] and the cellular levels of Aha1 were found to influence the phosphorylation/activation status of different Hsp90 client proteins [201]. Thus, for the Hch1/Aha1 cochaperones their rather unique property in that they accelerate the Hsp90 ATPase function seems to be connected with the activation of certain Hsp90 client proteins, supporting the assumption that cochaperones might importantly contribute to the client specificity of the Hsp90 machinery.

2.3 p23/Sba1

p23 is a small acidic protein present in all tissues that was identified initially as a component of Hsp90 - Hsp70 - steroid hormone receptor heterocomplexes [202–204]. However, it was demonstrated to be associated also with other Hsp90 - client protein complexes containing for example Fes tyrosine kinase, the transcription factor Hsf1, the Ah receptor [205], the heme - regulated kinase HRI [206], telomerase [207] or hepadnavirus reverse transcriptase [208]. p23 is essentially required for the maturation of steroid receptors [209]. In a minimal system with Hsp90, Hsp70, Hsp40 and Hop, p23 can active different Hsp90 client proteins *in vitro* [118,168,210]. It seems to be specifically incorporated in the late steps during the steroid hormone receptor assembly process [142,211,212].

p23 is a well conserved component of the Hsp90 machinery and exists in all higher organisms from yeast to mammals and plants [213]. The respective homologue from yeast was named "Sba1" [214]. It shares 24 % amino acid identity with the human p23 and is by 5.4 kDa larger (24.1 versus 18.7 kDa). In particular, the C - terminal portion of the vertebrate and yeast p23 variants show differences, and the yeast protein comprises additional hydrophobic residues here as well as a five times repeated motive GGA. In contrast, the acidic nature of the C - terminal regions in p23 and Sba1 is conserved (compare figure 6.21). A knockout of Sba1 in yeast cells caused only mild effects with a moderately reduced growth at higher but also lower temperatures. Thus, in yeast Sba1 is not an essential protein [214]. However, a p23 kockout in mice causes perinatal death with skin defects and underdeveloped lungs due to a defective glucocortocoid response [215].

p23/Sba1 consists of two distinct domains, an N - terminal conserved β - sheet portion and a presumably unfolded C - terminal part [216]. For

isolated human p23 lacking the C-terminus, a crystal structure was obtained [217]. The protein comprises an eight-stranded β-sandwich and formed a disulphide-linked dimer in the crystal which likely does not reflect the physiological active state since the protein seems to be largely monomeric in solution. The overall structure of the p23 N-domain resembles the immunoglobulin fold and has high similarity also with small heat shock proteins MjHsp16.5 from *Methanococcus jannischii* [218] and Hsp16.9B from wheat [219], although the sequences do not indicate a major relationship between the proteins (figure 2.6). Thus, here obviously a

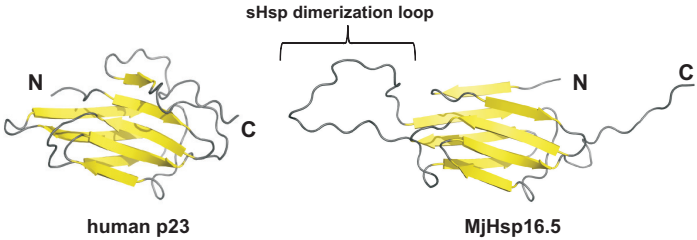

Figure 2.6: Similarity between the Hsp90 cochaperone p23 and small heat shock proteins. Crystal structures of the N-terminal domain of human p23 (residues 1 to 110, left, PDB: 1EJF) and the small heat shock protein 16.5 from *Methanococcus janaschii* (right, PDB: 1SHS).

common protein fold was adapted for rather different functions. In contrast to the small heat shock proteins, however, p23 lacks an extensive loop region found in these proteins that mediates dimerization.

Different to some other protein factors associated with Hsp90 and termed “cochaperone”, p23/Sba1 has a real chaperone activity on its own by passively preventing the aggregation of other proteins under heat shock conditions [149,150]. This chaperone activity is connected its unfolded C-terminal domain [216]. Interestingly, also a function of this region in the

protein was reported for the activation of the Hsp90 dependent glucocorticoid receptor client [217]. The charged residues might here be of particular importance, as in case of the small heat shock proteins for which their C-terminal unfolded extensions were found to have a role in increasing solubility when in complex with denatured substrate proteins [220].

p23/Sba1 were found to directly bind to Hsp90, and this complex formation is strongly enhanced by ATP [85,211,214]. The name of the yeast variant "Sba1", sensitive to benzoquinoid ansamycins 1 [214] , was derived since the interaction of Hsp90 and p23/Sba1 is disrupted by Geldanamycin [84,142,211,214]. For the binding of Hsp90, the C-terminal unfolded portion of p23/Sba1 is obviously not required [216,217]. Sba1/p23 seems to be highly specific for the closed conformation of Hsp90 that is induced by nucleotide binding and furthermore, p23/Sba1 inhibits the Hsp90 ATPase activity [87].

A crystal structure was obtained that could explain the mechanism underlying the nucleotide dependent interaction of Sba1 and Hsp90: Sba1 undergoes significant binding contacts with the backside of the ATP-lid in the N domain of Hsp90 which is only accessible upon ATP binding to Hsp90 and concomitant structural rearrangements leading to lid closure and exposure of the Sba1 interaction surface [52]. By trapping the N-terminally dimerized state, Sba1 slows down the conformational transitions of Hsp90 that are necessary to achieve ATP hydrolysis. Consistent with earlier biochemical studies [87], two molecules of Sba1 were bound symmetrically to the Hsp90 dimer in the crystal. Obviously, post-translational modifications of Hsp90 also have influence on the binding of p23, hyperacetylation led to a disruption of the interaction between p23 and the chaperone [221,222]. Sba1 can form ternary complexes with Hsp90 and the cochaperone Cpr6, however, competes with Sti1 [87,163] and Aha1 [223] for binding, clearly demonstrating p23/Sba1 being rather

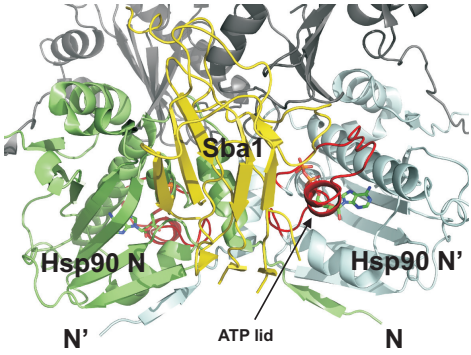

Figure 2.7: Conformation specific interaction of Sba1 and Hsp90. Crystal structure of Hsp90 in complex with Sba1 (PDB: 2CG9). Forming the full binding interface on Hsp90 for the interaction with Sba1 requires ATP binding to its N domains and lid closure.

part of late Hsp90 - client protein heterocomplexes.

Besides its role as a component in the Hsp90 chaperone machinery, human p23 was also proposed to have a prostaglandin E2 synthase activity [224]. And furthermore, recently a role of p23/Sba1 in secretion/golgi function, DNA repair, ribosome biogenesis and nuclear processes was found [225]. This indicates that p23/Sba1 is involved in a large variety of cellular tasks that might partially be even independent from Hsp90 action.

Part II

Results

Chapter 3

Analysis of Hsp90 – Client Protein Complexes

3.1 Binding Affinities of Isolated Hsp90 Domains and p53 DBD

p53 has been shown to be among the large cohort of proteins found associated with Hsp90 [62,226–229] and likely represents one of the most prominent examples of a substrate dependent on Hsp90 function. Surprisingly, little knowledge exists about the details of Hsp90 - client protein interactions in general and the Hsp90 - p53 interactions in particular, despite a huge number of p53 related publications available in literature. The inherently weak and dynamic nature of complexes between Hsp90 and its clients required to enable the transient and promiscuous binding of numerous (currently more than 100) different substrate proteins might have hampered a more in - depth structural analysis so far. However, for

such systems NMR seems to be a well suited method as also rather flexible parts of a protein and even very weak complexes can be studied. On the other hand, there are limitations with respect to the size of the proteins that are amenable to an NMR analysis which currently restricts its application to systems with a molecular size not beyond ~ 100 kDa. One aim of this work here was to characterize the interaction of the model substrate p53 with Hsp90 in more detail using NMR and other biophysical methods. This could potentially provide basic insights into the mechanism of client protein chaperoning by Hsp90 and contribute to the understanding of molecular chaperones in general.

Earlier reports have demonstrated that the binding between Hsp90 and the tumor suppressor protein p53 is mediated by its DNA binding domain (DBD, core domain). Furthermore, specifically the M and C domains of yeast Hsp90 seem to serve as interaction sites for p53 [62]. Using NMR spectroscopy, Dr. Franz Hagn (Institute for Advanced Study, TUM) could indeed confirm the p53 DBD – Hsp90 M complex formation in work carried out previously and additionally identified a very weak binding of p53 DBD also to the Hsp90 N domain. Thus, obviously multiple domains of Hsp90 contribute to the interaction with p53. The potential C - terminal binding site for p53 on Hsp90 has not yet been characterized so far and should therefore be subjected a closer analysis here. To this end the isolated Hsp90 C domain (residues 528 to 709) was cloned into a pET28a vector with an N - terminal His - tag and expressed in *E. coli*. The protein was well soluble and could be purified by standard methods with yields of ~ 20 mg per liter of cell culture. A rough structural characterization of the domain by CD (circular dichroism) spectroscopy indicated a well folded, predominantly α - helical protein that was highly stable and appeared to be well suited for further studies (figure 3.1).

To characterize the relative contribution of the individual Hsp90 do-

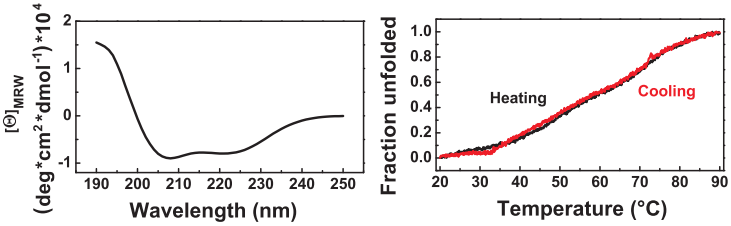

Figure 3.1: CD spectroscopic characterization of the Hsp90 C domain. Left: CD spectrum of the Hsp90 C domain construct (residues 528 to 709) recorded at 20°C. Right: Thermally induced unfolding of the Hsp90 C domain monitored by CD spectroscopy at a wavelength of 222 nm. The Hsp90 C domain is highly stable and unfolds reversibly. The protein was measured in a buffer of 10 mM potassium phosphate, 1 mM TCEP, pH 7.5.

mains to the interaction with p53, fluorescence polarization experiments were performed. Constructs for the isolated Hsp90 N (residues 1 to 210) and M domain (residues 273 to 527) as well as for the full-length protein and p53 DBD were already available for expression and purification. A construct for the Hsp90 C domain was prepared in this work, as mentioned above. The p53 core domain (p53 DBD) was labeled with carboxyfluoresecein and then titrated with full-length Hsp90 and individual domains thereof. Upon adding the full-length Hsp90 protein to p53 DBD a significant change in the polarization was observable and a typical binding curve could be obtained (figure 3.2). The shape of the curve indicated non-cooperative binding and data fitting applying a one-site binding model yielded an affinity of $K_d \sim 1.9\,\mu$M for the interaction of full-length Hsp90 and p53 DBD.

With the Hsp90 N and M domain no significant binding could be detected under the conditions used, which however can not exclude a weak complex formation. Titration of the Hsp90 C domain to p53 DBD fi-

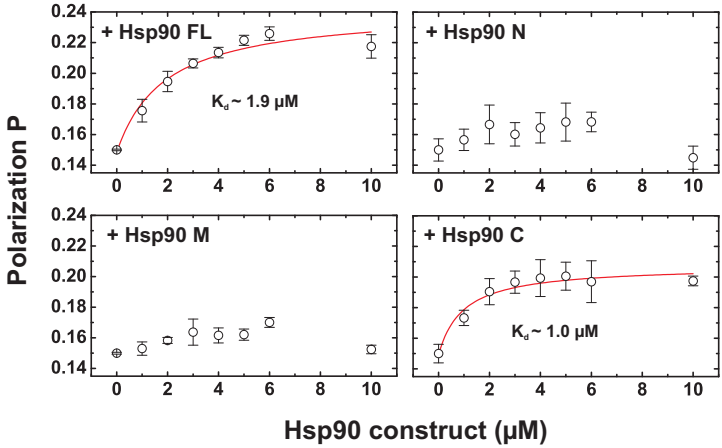

Figure 3.2: Binding of Hsp90 or domains thereof to p53 DBD monitored by fluorescence polarization. p53 DBD was labeled with carboxyfluorescein and titrated with full-length (FL) Hsp90 or isolated domains thereof. Only with Hp90 FL and Hsp90 C significant binding was detectable under the conditions used. Measurements were done in a buffer of 10 mM potassium phosphate, 1 mM TCEP, pH 7.5 at 20°C. Hsp90 constructs were added in increasing concentration to 500 nM of labeled p53 DBD.

nally gave a binding curve comparable to the experiment with full-length Hsp90. Consistent with the much lower molecular weight of the Hsp90 C domain compared to the full-length protein (40 kDa versus 164 kDa), the overall change in the polarization P was lower here. Fitting the data a K_d of $\sim 1.0\,\mu$M was found for the interaction, which is nearly identical to the affinity observed for binding of full-length Hsp90 to p53 DBD. In general, the K_d-values determined here in the low μM range can be regarded as intermediate affinities that are typical for protein-protein interactions. Overall the data demonstrate that a dominating contribution

to the complex formation between Hsp90 and p53 DBD comes from the C domain of Hsp90 which therefore seems to be the main binding site of p53 DBD on Hsp90.

Since previous data obtained Dr. Franz Hagn (Institute for Advanced Study, TUM) indicated presumably much weaker p53 DBD interaction sites also within the Hsp90 N and M domains, as mentioned, further binding experiments were performed to determine the respective complex affinities. It turned out that a direct titration of the labeled p53 DBD even with very high amounts of Hsp90 N and M did not yield any acceptable binding curve. In addition to the rather weak binding, likely the difference in molecular size between the free labeled p53 DBD and in complex with Hsp90 N or M was not large enough to result in a detectable change in the polarization. Therefore, in order to estimate the affinity of p53 DBD for Hsp90 N and M, in this case a displacement titration was done instead of a direct titration. The respective Hsp90 domain was added in increasing concentration to a preformed complex of full-length Hsp90 and carboxyfluorescein labeled p53 DBD and the decrease in the polarization was monitored (figure 3.3). The midpoints of these titration curves were around $\sim 150\,\mu$M for Hsp90 N and $\sim 70\,\mu$M for Hsp90 M, respectively. Thus, the interaction of p53 DBD with these two Hsp90 domains is roughly on the order of a magnitude weaker than its interaction with Hsp90 C. In summary, the fluorescence binding experiments demonstrate that Hsp90 provides multiple binding sites for the interaction with p53 that have largely different affinities.

As the C domain turned out to be the major binding site for p53 DBD on Hsp90, its interaction with p53 DBD should be characterized in more detail using NMR. However, due to a comparatively high molecular weight (~ 40 kDa as a dimer) it seemed reasonable to first attempt to optimize the Hsp90 C domain construct prior to an NMR analysis. In the crys-

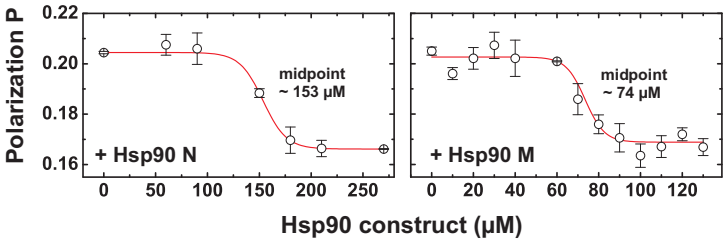

Figure 3.3: Binding of Hsp90 N (left) and M (right) to p53 DBD monitored by fluorescence polarization. A preformed complex of carboxyfluorescein labeled p53 DBD and full-length Hsp90 was titrated with the Hsp90 N and M domain. p53 DBD binds significantly weaker to Hsp90 N and M than to Hsp90 C (compare figure 3.2). Measurements were done in a buffer of 10 mM potassium phosphate, 1 mM TCEP, pH 6.8 at 20°C. Hsp90 constructs were added in increasing concentration to 500 nM of labeled p53 DBD and 5 μM full-length Hsp90.

tal structure of the full-length Hsp90 the very C-terminal region of the Hsp90 C domain comprising residues 680 to 709 is not resolved and appears to be unstructured [52]. In particular, such unfolded elements negatively impact the behavior of proteins in NMR experiments as they significantly increase their hydrodynamic radius. This leads to slower molecular tumbling and therefore broad NMR signals. A deletion of the respective residues would presumably not affect the overall structure of the domain, but since the Hsp90 C domain is a constitutive dimer even only 10 or 20 amino acids removed from the individual protomers would significantly reduce its size and favorably influence NMR relaxation properties. Therefore, consecutive truncations of 10, 20 and 30 residues were introduced into the Hsp90 C domain (Hsp90 CΔX variants) to determine the optimal construct size.

The CD spectra of the Hsp90 C domain mutants created showed in principle identical secondary structure content as the wild-type protein

(figure 3.4). This shows that the deleted residues were indeed unfolded.

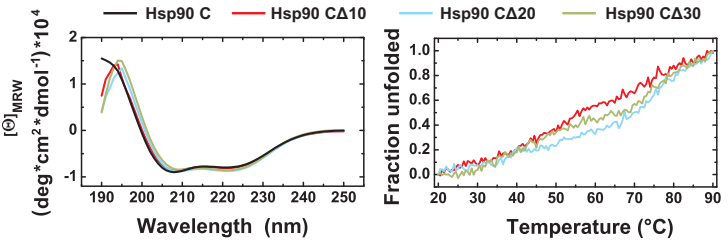

Figure 3.4: CD spectroscopic characterization of Hsp90 C domain truncation mutants lacking 10 (CΔ10), 20 (CΔ20) and 30 (CΔ30) residues from the C-terminus. Left: CD spectra of Hsp90 C domain truncation mutants in comparison to the wild-type domain recorded at 20°C. No major impact of the deletions on the secondary structure of the domain is visible. Right: Thermally induced unfolding of Hsp90 C domain truncation mutants monitored by CD spectroscopy at a wavelength of 222 nm. The mutants have similar stability as the wild-type domain (compare figure 3.1). The proteins were measured in a buffer of 10 mM potassium phosphate, 1 mM TCEP, pH 7.5.

Also, the thermal stability of Hsp90 C seemed to be unaffected by the truncations and all proteins unfolded reversibly under heat denaturation (data not shown).

The Hsp90 C deletion mutants were then assessed for interaction with p53 DBD using again fluorescence polarization assays as before. The Δ10 variant showed a slightly decreased but still significant binding of p53 DBD ($K_d \sim 3.1\,\mu$M, figure 3.5). Hsp90 CΔ20 likewise bound p53 DBD with an affinity that was nearly comparable to the wild-type domain ($K_d \sim 1.9\,\mu$M). However, in contrast to the other mutants, a deletion of 30 residues as in the Hsp90 CΔ30 variant unexpectedly caused a significant reduction or potentially complete loss in binding between the Hsp90 C domain and p53 DBD. In this case no binding curve could be obtained anymore under the conditions used. Thus, obviously an important p53 DBD

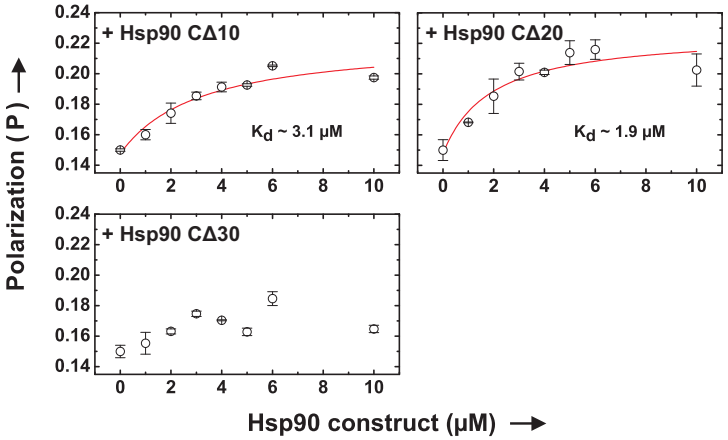

Figure 3.5: Binding of Hsp90 C truncation mutants to p53 DBD monitored by fluorescence polarization. p53 DBD was labeled with carboxyfluorescein and titrated with Hsp90 C domain truncation mutants lacking 10 (CΔ10), 20 (CΔ20) or 30 (CΔ30) residues from its C - terminus. For the Hsp90 CΔ30 variant no significant binding is observed anymore. Measurements were done in a buffer of 10 mM potassium phosphate, 1 mM TCEP, pH 7.5 at 20°C. Hsp90 constructs were added in increasing concentration to 500 nM of labeled p53 DBD.

binding motive seems to reside within a stretch of unfolded amino acids comprising residues 679 to 689 of the Hsp90 C domain.

For comparison, the binding between p53 DBD and Hsp90 was also assessed using analytical ultracentrifugation (aUC) as another method besides fluorescence polarization. These experiments were carried out in collaboration with Dr. Klaus Richter (Lehrstuhl für Biotechnologie, TUM). A fluorescein label was attached to p53 DBD (p53 DBD*) to monitor its sedimentation behavior in absence or presence of different Hsp90 constructs in a fluorescence detected aUC setup. p53 DBD* alone had a sedimentation coefficient S of ~ 2.7 (figure 3.6). When Hsp90 FL was added

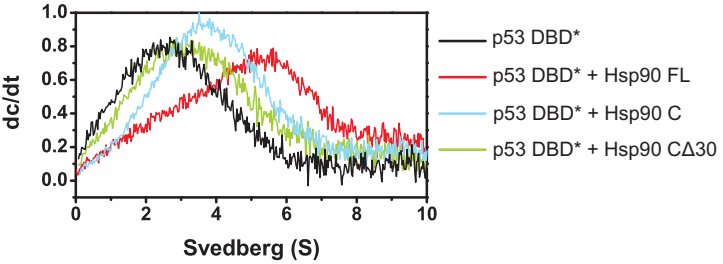

Figure 3.6: Complex formation between p53 DBD and Hsp90 or domains thereof studied with analytical ultracentrifugation. Fluorescently labeled p53 DBD (p53 DBD*) was monitored for complex formation with full-length (FL) Hsp90, Hsp90 C and Hsp90 CΔ30. In presence of Hsp90 CΔ30 nearly no peak shift is observed anymore, indicating a significantly impaired complex formation of this variant with p53 DBD. For the measurements 4 μM of labeled p53 DBD were used. Hsp90 FL was added in a 2.5-fold and Hsp90 C domain constructs in a 10-fold molar excess over p53 DBD. Measurements were done in 10 mM potassium phosphate, 1 mM TCEP, pH 6.8 at 20°C.

to p53 DBD*, a significant peak shift to a higher S-value of $\sim$5.5 S was observed, indicating complex formation as expected. Similarly, in presence of isolated Hsp90 C a peak shift to $\sim$3.5 S confirmed the binding between p53 DBD and this Hsp90 fragment. With the Hsp90 CΔ30 variant, in contrast, the maximum of the sedimentation curve for p53 DBD* was nearly unaffected, pointing at a strongly impaired interaction here. The slight shift to $\sim$2.9 S might reflect a very weak remaining but most likely severalfold decreased binding in this case. In conclusion, the results from the aUC experiments are well consistent with the previous findings obtained using fluorescence polarization.

In general, the fluorescence polarization experiments seemed to be well suited to determine the binding affinities between Hsp90 (or its domains) and p53 DBD. But a question that is rather difficult to answer with this

method regards the exact binding stoichiometry of a protein - protein interaction. However, this issue can perfectly be addressed with isothermal titration calorimetry (ITC). To estimate the stoichiometry of the Hsp90 – p53 DBD complex therefore also ITC measurements were performed here. Due to the inherently low stability of p53 DBD it was difficult to obtain reliable binding curves. Probably mechanical stress caused by the sample stirring required for the ITC measurements additionally favored an aggregation of the protein. Using rather low temperatures, finally a binding transition for the titration of p53 DBD with full - length Hsp90 could be observed (figure 3.7). Fitting the integrated binding heats gave a K_d of

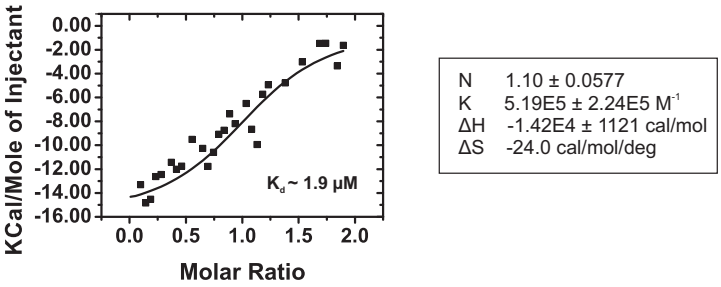

Figure 3.7: Binding of full - length Hsp90 to p53 DBD monitored by ITC. A binding transition can be observed for the titration of p53 DBD with full - length Hsp90. Data fitting yields an affinity of $K_d \sim 1.9\,\mu$M for the interaction which is in good agreement with the fluorescence polarization data (compare figure 3.2). Notably, the stoichiometry obtained indicates the binding of 1 molecule p53 DBD to each subunit of the Hsp90 dimer. 20 μM of p53 DBD in the measurement cell of the instrument was titrated with a 200 μM solution of full - length Hsp90 at 10°C in a buffer of 10 mM potassium phosphate, 1 mM TCEP, pH 6.8.

$\sim 1.9\,\mu$M for the interaction which is in very good agreement with the fluorescence polarization data (compare figure 3.2). Thus, obviously indeed a specific binding was observed in these initial experiments.

Interestingly, the binding stoichiometry N found in with ITC is around one. This means that each protomer of an Hsp90 dimer can associate with one molecule p53 DBD. The additional binding sites for p53 DBD on Hsp90 N and M are likely not significantly reflected in the observed ITC stoichiometries due to their low affinities compared to the dominating preferred interaction of p53 DBD with Hsp90 C.

3.2 NMR Backbone Assignment of the Hsp90 CΔ20 Mutant

The previous binding experiments using fluorescence polarization clearly showed that the Hsp90 C domain is the dominating binding site for p53 on Hsp90. Furthermore, a deletion of as many as 20 residues from the C-terminus in the Hsp90 C domain had no impact on p53 DBD binding whereas a deletion of another 10 more residues abolished complex formation. Thus, the Hsp90 CΔ20 mutant represents the minimal C domain construct capable of high affinity p53 DBD binding. For a detailed analysis of the interaction with p53 DBD using NMR a backbone resonance assignment of this variant had to be obtained.

However, due to the size of the protein (37.4 kDa as a dimer) the spectral quality of even the 2D spectra turned out to be low for Hsp90 CΔ20 (figure 3.8). Though the protein appeared to be partially folded and predominantly α-helical, as expected, a severe signal overlap in the middle of the ^{15}N-HSQC spectrum also indicated a significant portion of random coil present. Additionally, the line width of the signals was unfavorably high. For comparison, a spectrum of the Hsp90 CΔ30 variant was recorded under the same conditions which was overall by 20 residues smaller compared to Hsp90 CΔ20 and thus could potentially show better spectral quality. But also in this case the central region in the ^{15}N-HSQC was found to be extremely crowded. This indicated that it were not only the additional 10 more unfolded C-terminal residues of the Hsp90 CΔ20 variant compared to Hsp90 CΔ30 that caused the signal overlap but likely other internal parts of the Hsp90 C domain.

From the initial 2D spectra of the Hsp90 C domain constructs recorded under “standard” conditions it was obvious that a backbone assignment

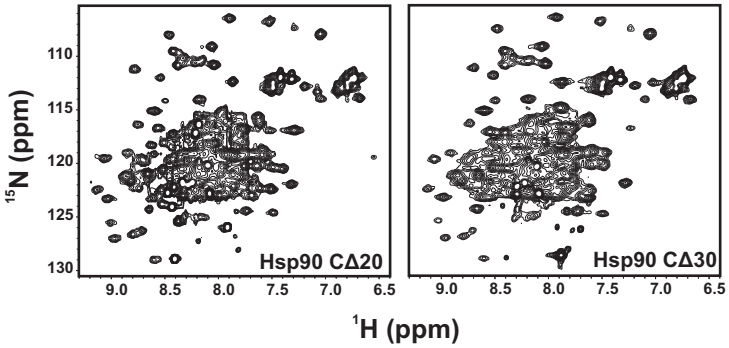

Figure 3.8: ^{15}N - HSQC spectra of Hsp90 CΔ20 (left) and Hsp90 CΔ30 (right). The spectral quality for both mutants is low at the conditions used. Therefore, an optimization of the measurement conditions was necessary to enable a backbone resonance assignment of the Hsp90 C domain. 300 μM of both mutants were measured in a buffer of 10 mM potassium phosphate, 1 mM TCEP, pH 6.8 at 303 K and 600 MHz.

would to large extent be hampered by the severe signal overlap. Therefore, prior to the measurement of the triple resonance experiments required for an NMR assignment, a major improvement of the spectral quality had to be obtained by optimizing the sample conditions. To reduce NMR signal loss caused by the fast relaxation typical for larger proteins it has become standard to apply isotope labeling with deuterium for proteins above $\sim$ 20 kDa molecular weight. This decreases the number of proton spins as a main source of unwanted relaxation by replacing them with deuterium and thus favorably influences the line width of NMR signals. A highly deuterated Hsp90 CΔ20 sample was therefore prepared by growing cells in 100 % D_2O and supplying them with $>$ 99 % deuterated ^{13}C - glucose as the only carbon source. In this way, a large portion of the side - chain protons in the protein should get replaced by deuterium.

The positive effect of high deuteration in combination with higher field strength was clearly visible in the quality of the Hsp90 CΔ20 NMR spectra. Comparing the amide regions of the 1D spectra recorded for a sample of Hsp90 CΔ30 without deuteration at 600 MHz and a sample of Hsp90 CΔ20 with high deuteration at 900 MHz shows much better line - width for the even by 20 unfolded residues larger Hsp90 CΔ20 variant (figure 3.9).

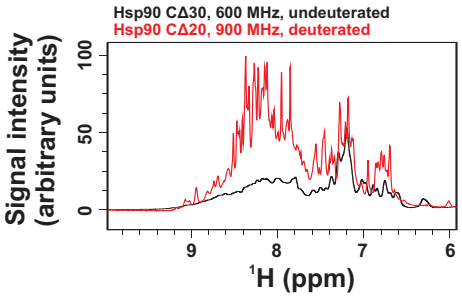

Figure 3.9: Effect of field strength and deuteration on the quality of the Hsp90 C domain NMR spectra. Overlay of the 1D NMR spectra for Hsp90 CΔ30 without deuteration recorded at 600 MHz (black) and Hsp90 CΔ20 with high deuteration recorded at 900 MHz (red). Only the amide region of the spectra is shown. Although the Hsp90 CΔ20 construct is even larger by 20 residues, the line - width is much better than for Hsp90 CΔ30. 1 mM samples of both mutants were measured in a buffer of 10 mM potassium phosphate, 1 mM TCEP, pH 6.8 at 303 K.

A further improvement of the NMR spectral quality could be achieved by using elevated temperatures. The strategy to apply high temperatures in order to increase the molecular tumbling of larger proteins and thus reduce relaxation losses and concomitant broad lines was demonstrated previously in the example of the hexameric Ph1500 [230]. This protein of 49 kDa stems from a hyperthermophilic archaeal organism and thus has intrinsically high thermal stability a priori, which suggests the usage of

high temperatures for NMR measurements. However, also in the case of the Hsp90 C domain higher temperatures seemed to be a promising approach to gain NMR signal intensity. As the CD data showed, all Hsp90 C domain variants were very stable at elevated temperatures and unfolded reversibly (figures 3.1 and 3.4). Thus, potentially a backbone resonance assignment of this domain could be obtained at a higher temperature and afterwards be transferred to a lower temperature by a series of spectra recorded at stepwise decreasing temperature. This would in particular be essential, since the binding studies that should be performed with the very thermolabile p53 DBD could not be performed beyond a temperature of ~ 298 K.

To determine the optimal measurement temperature for Hsp90 CΔ20 a series of 2D spectra was recorded. As mentioned before, one major improvement of spectral quality was already obtained by applying high deuteration which is in particular effective in combination with TROSY-type [231,232] experiments. Indeed, the 2D ^{15}N-TROSY spectrum of highly deuteratad Hsp90 CΔ20 clearly had much sharper lines than a standard ^{15}N-HSQC of an undeuterated sample at the same temperature (figure 3.10, upper panel, left; compare figure 3.8). The analysis of 2D spectra for Hsp90 CΔ20 in a temperature range from 303 to 325 K then showed that with increasing temperature the signal overlap in the middle of the spectrum was more and more reduced (figure 3.10, upper panel) whereas the peak intensities on the other hand were favorably increased. This was not that obvious from the 2D spectra directly, but when the 1D projections of the respective 2D spectra were calculated and compared, this gain in signal intensity was clearly visible (figure 3.10, lower panel). A temperature of around 318 K turned out to be a well acceptable compromise as at significantly higher temperatures even signals of folded residues then partially began to disappear due to increased exchange with water.

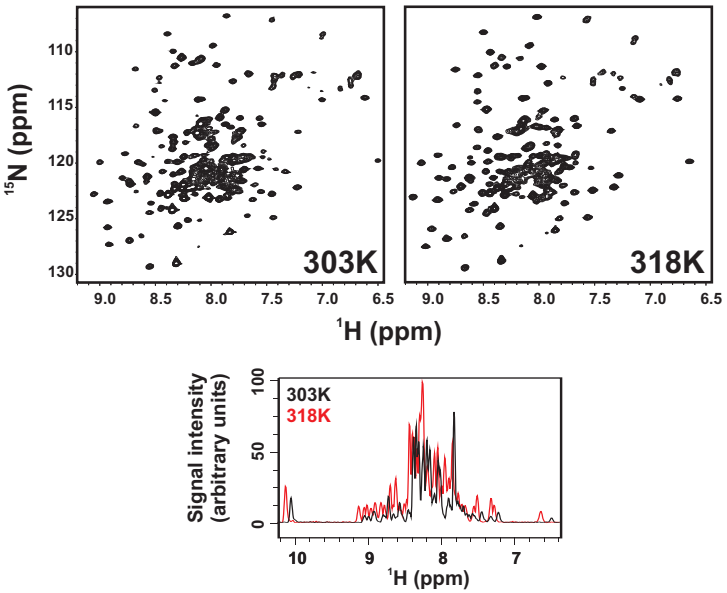

Figure 3.10: Effect of temperature on the quality of the Hsp90 C domain NMR spectra. Upper panel: ^{15}N-TROSY spectra of highly deuteratad Hsp90 CΔ20 recorded at 303 K (left) and 318 K (right). Even at the lower temperature high deuteration, TROSY-type spectra and higher field strength improved spectral quality significantly (compare figure 3.8). Higher temperatures then further contributed to a gain in signal intensity and reducing spectral overlap. Lower panel: Overlay of 1D projections calculated from the 2D spectra shown in the upper panel. In this representation the effect of elevated temperatures on NMR signal intensity becomes most obvious. A 1 mM sample of of highly deuterated Hsp90 CΔ20 was measured in a buffer of 10 mM potassium phosphate, 1 mM TCEP, pH 6.8 at 750 MHz at the temperatures indicated.

Under these optimized conditions a set of TROSY-based triple resonance experiments including trHNCO, trHN(CA)CO, trHNCACB, trHN(CO)CACB, trHNCA and trHN(CO)CA was recorded at 318 K on a 1.8 mM

highly deuterated sample of Hsp90 CΔ20. Despite its lower field strength, a 750 MHz spectrometer was preferentially chosen over an also available 900 MHz instrument since it was equipped with a room temperature probe, in contrast to the cryogenic probe of the 900 MHz magnet. Though in general cryogenic probes theoretically should have up to fourfold higher sensitivity compared to normal probes, practically also other aspects were considered here in the choice of the appropriate spectrometer. As a clear advantage, the room temperature probe provided triple axis gradients whereas the cryogenic probe had gradients only along the z axis. This difference led to markedly better water suppression of the 750 MHz instrument (especially at the higher temperatures), therefore overall more than compensating for moderate sensitivity losses due to lower magnetic field strength and its room temperature probe. Indeed, the triple resonance spectra finally obtained were of very high quality and provided sequential connectivity for the large majority of signals (figure 3.11). Overall 85 %, of all non - proline backbone NH signals could be assigned for Hsp90 CΔ20 (figure 3.12, table 11.1). For a region comprising residues ~582 to 610 an assignment was to a large extent not possible as here no more correlations were observed in the 3D spectra (see below).

As an additional validation, a TROSY - HNH NOESY was recorded of the protein. Due the the predominantly α - helical fold of the Hsp90 C domain, strong sequential HN - HN backbone connectivities could be observed for most residues and thus confirmed the assignment obtained by through - bond correlation. An evaluation of the chemical shifts for Cα and Cβ determined in the assignment process could be used for a prediction of the secondary structure content in the protein (figure 3.13). The structure elements found for Hsp90 CΔ20 in solution agreed very well with those of the Hsp90 C terminal domain as observed in the crystal structure of full - length Hsp90 (PDB: 2CG9) [52]. Furthermore, consistent

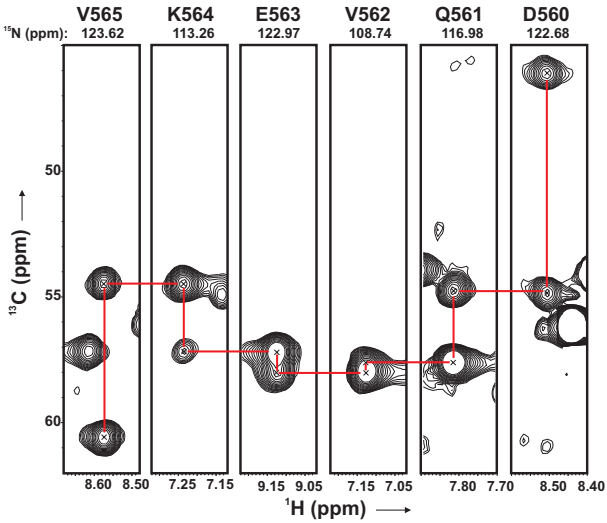

Figure 3.11: Strips from a TROSY - HNCA spectrum of Hsp90 CΔ20. Under optimized sample and measurement conditions the spectral quality of triple resonance experiments for Hsp90 CΔ20 was high, providing good sequential connectivity as shown in the example. This finally enabled the assignment of backbone NH signals for 85 % of the non - proline residues in the domain, despite its high molecular weight (~ 37.4 kDa). A 1.8 mM sample of of highly deuterated Hsp90 CΔ20 was measured in a buffer of 10 mM potassium phosphate, 1 mM TCEP, pH 6.8 at 750 MHz and 318 K.

with the previous CD data, (figure 3.4) residues 680 to 689 of Hsp90 CΔ20 which contain the putative p53 DBD binding motive seemed to be unstructured.

As mentioned, for residues ~ 582 to 610 an assignment mostly failed due to a lack of sequential connectivity in the triple resonance spectra. Likely, the signal overlap in the middle of the Hsp90 CΔ20 2D TROSY spectrum (figure 3.10, right) was caused by exactly the NH signals cor-

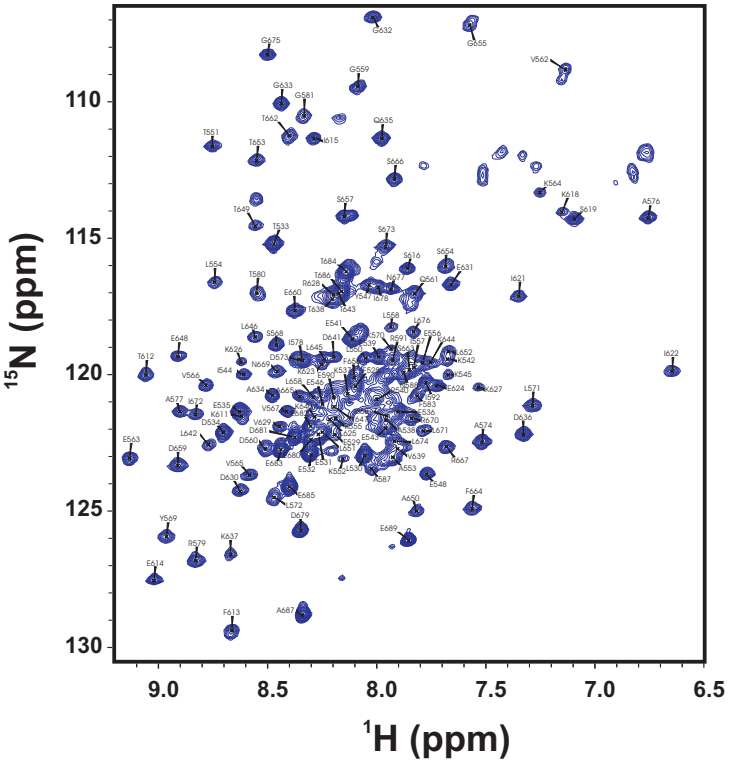

Figure 3.12: ^{15}N-TROSY spectrum of Hsp90 CΔ20 with assignment. 85 % of all non-proline backbone NH signals in the domain could be assigned. The assignment was obtained in a buffer of 10 mM potassium phosphate, 1 mM TCEP, pH 6.8 at 750 MHz and 318 K.

responding to these residues, which appeared to be unfolded. Unfavorable dynamics, as indicated by the low intensities and the shape of the peaks, might explain the loss of sequential connectivity hampering the

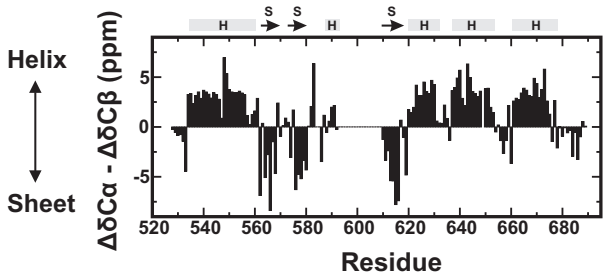

Figure 3.13: Evaluation of chemical shift data to determine the secondary structure content of Hsp90 CΔ20. Cα and Cβ carbon shifts were used to predict structure elements of Hsp90 CΔ20 in solution. The difference of the measured Cα and Cβ chemical shifts from the random coil shifts ($\Delta\delta$Cα and $\Delta\delta$Cβ) was calculated. On the y - axis the difference of $\Delta\delta$Cα and $\Delta\delta$Cβ is plotted, a sequence of four or more positive or negative bars indicates helical (H) or sheet (S) structure, respectively. The structure elements found with NMR agree well with the crystal structure of the domain (PDB: 2CG9).

assignment. To probe whether the region comprising residues 582 to 610 in Hsp90 CΔ20 indeed lacks secondary structure, another mutation was introduced into the domain deleting amino acids 583 to 607 (Hsp90 CΔ20Δ583-607). A model of Hsp90 CΔ20 obtained with Xplor - NIH [233] using NOEs back - calculated from a crystal structure of full - length Hsp90 (PDB: 2CG9) [52] and rebuilding unresolved flexible parts in the protein (598 to 610 and 678 to 689) shows that the deleted residues contain a small helix (helix 2) and a longer loop region (figure 3.14, right). In the closed conformation of Hsp90 they are protruding from the C domain, making contacts to the C - terminal part of the M domain. Without these contacts as in the isolated C domain, the helix might potentially be unfolded. A secondary structure prediction for amino acids 581 to 610 indeed indicates a significant helix propensity, thus this region of Hsp90 appears in principle to be capable of adopting structure (figure

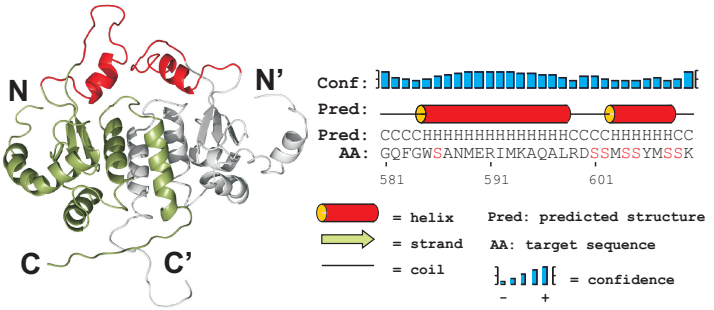

Figure 3.14: Structural model of the Hsp90 CΔ20 mutant. Left: A crystal structure of the full-length Hsp90 protein (PDB: 2CG9) [52] was used to back-calculate NOE restraints for the C domain. These were then applied in calculations with Xplor-NIH to obtain a structure model for Hsp90 CΔ20. All flexible regions not resolved in the crystal structure (residues 678 to 689 and 598 to 610) were rebuilt. The residues deleted in the Hsp90 CΔ20Δ583-607 mutant are highlighted in red. The two protomers of the dimer are colored gray and green, respectively. Right: A secondary structure prediction using PSIPRED [234] for amino acids 581 to 610 of Hsp90 C indicates helix propensity for this region. A high proportion of serine residues (colored red) in this sequence might point at a potential phosphorylation site.

3.14, right). The high content of serine residues here might furthermore point at a potential phosphorylation site involved in regulatory functions. Indeed, recently S604 was implicated as phosporylation site [235].

The additional Δ583-607 deletion mutation had obviously no effect on the expression of the Hsp90 C domain which seemed to be as soluble as the Hsp90 CΔ20 variant and could be purified with a comparable yield. However, during the purification the double mutant was much more resistant against proteolysis than Hsp90 CΔ20. This supports the assumption that the deleted residues were indeed – at least partially – unstructured. This was then also confirmed by a comparison of the 2D ^{15}N-TROSY

spectra for Hsp90 CΔ20 and the Hsp90 CΔ20Δ583-607 variant (figure 3.15). The majority of signals in the spectrum of Hsp90 CΔ20 was unaf-

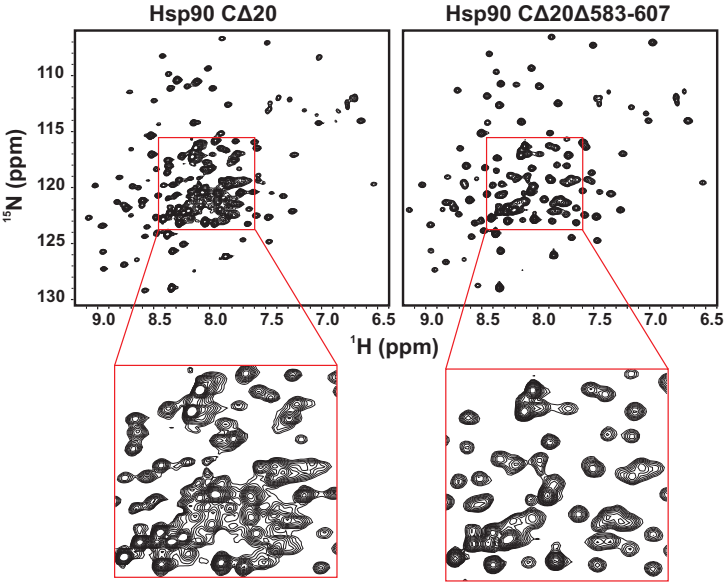

Figure 3.15: Comparison of the 2D ^{15}N - TROSY spectra for Hsp90 CΔ20 (left) and Hsp90 CΔ20Δ583-607 (right). The majority of signals in the spectrum of Hsp90 CΔ20 is unaffected by an additional deletion of residues 583 to 607 as in the Hsp90 CΔ20Δ583-607 variant (upper panel). However, the signal overlap in the center of the spectrum is significantly reduced (lower panel), indicating that the deleted region was unstructured. Both proteins were measured in a buffer of 10 mM potassium phosphate, 1 mM TCEP, pH 6.8 at 303 K at 900 MHz.

fected by the additional mutation, except for those that corresponded to amino acids located next to the deletion site. However, the strong overlap in the central region of the ^{15}N - TROSY was significantly reduced. There-

fore, the deleted residues obviously had no contacts to other parts in the protein but behaved flexibly in the isolated Hsp90 C domain. Notably, in a crystal structure of the isolated C domain of the *E. coli* Hsp90 homologue HtpG (PDB: 1SF8) the corresponding amino acids likewise adopted an unusual orientation projecting out into the solvent[49]. In this case, the small helix of this structure element was intact, however, most likely due to a stabilization by the extensive hydrophobic contacts that could be formed by crystal packing. Because of its exposed location and the amphipathic nature, in an earlier work the helix was speculated to be involved in substrate protein binding to Hsp90[49]. A certain role in direct interaction with the ligand binding domain of the human glucocorticoid receptor was indeed then demonstrated later on *in vitro*[140].

3.3 Fast Backbone Dynamics of Hsp90 CΔ20

To determine the backbone dynamics of Hsp90 CΔ20, a measurement of the $\{^1H\}$-^{15}N heteronuclear NOE (hetNOE) was carried out which reports on molecular movements on the ns- to ps-timescale (figure 3.16). An increased backbone flexibility was observed for the N-terminal part

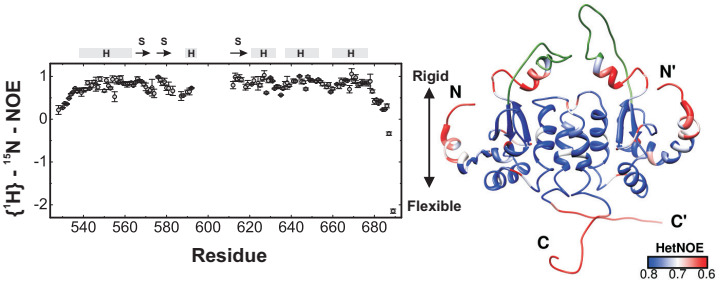

Figure 3.16: Fast backbone dynamics of Hsp90 CΔ20 determined by measurement of the $\{^1H\}$-^{15}N heteronuclear NOE (hetNOE). Left: N- and C-terminus of the domain show increased flexibility as indicated by lower NOE values. Additionally, residues next to the unfolded loop region (582 to 610) have higher backbone mobility. Secondary structure elements as determined in solution are given on top of the plot (compare figure 3.13). Right: Color coded mapping of hetNOE values onto a model of Hsp90 CΔ20 (see section 3.2 and figure 3.14). Residues from the unfolded loop for which no assignment could be obtained are colored green. The measurement was done at 900 MHz and 318 K in 10 mM potassium phosphate, 1 mM TCEP, pH 6.8 on a 1 mM highly deuterated sample of Hsp90 CΔ20.

of the protein comprising residues 528 to 540 from the first α-helix, as indicated by lower hetNOE values. Also the C-terminal 11 amino acids in the Hsp90 CΔ20 construct (residues 679 to 689) showed high flexibility, consistent with the findings from the CD experiments (figure 3.4) and the chemical shift data analysis which predicted this region in the pro-

tein to be unstructured (figure 3.13). This is of particular interest since these residues turned out to be important for the binding of p53 DBD to Hsp90 C (figure 3.5). Obviously, p53 DBD preferentially interacts with an unfolded stretch of amino acids on Hsp90.

Residues 587 to 591 likewise had increased dynamics. As a crystal structure (PDB: 2CG9) shows, these amino acids form a small helix in the closed conformation of full-length Hsp90 that has intramolecular contacts with the Hsp90 M domain. In the isolated C domain these contacts are missing, therefore the helix appears to be highly mobile or potentially even unfolded (see also section 3.2).

3.4 NMR Binding Studies With Hsp90 CΔ20 and p53 DBD

As the previous experiments indicated the Hsp90 C domain to constitute the main binding site for p53 DBD, the interaction between both proteins should be analyzed in further detail using NMR. A backbone resonance assignment for p53 DBD was available from a previous study [236], and an assignment for the fully p53 DBD binding competent Hsp90 CΔ20 variant was obtained here as described (section 3.2). Therefore, a presumable complex formation could be monitored for both proteins in a residue - wise manner, which potentially would allow to determine the exact binding surfaces on p53 DBD and Hsp90 CΔ20, respectively.

Due to the inherent instability of p53 DBD which tends to unfold and aggregate at temperatures above ∼ 298 K, it was necessary to carry out all measurements at 298 K or below. However, the resonance assignment of Hsp90 CΔ20 was obtained at 318 K as this elevated temperature favorably influenced the spectral quality (see section 3.2). Therefore, first a series of 2D ^{15}N - TROSY spectra was recored for Hsp90 CΔ20 at stepwise decreasing temperature, starting from 318 K down to 298 K. In this way, the shifting of individual NMR signals could be followed and the assignment well be transferred to the lower temperature.

Upon adding unlabeled p53 DBD, significant chemical shift perturbation (CSP) was observed in the 2D ^{15}N - TROSY spectrum of Hsp90 C Δ20 (figure 3.17, upper panel, left). The position of many peaks was altered in presence of p53 DBD, indicating a binding. Notably, the shift changes were in different directions, arguing against mere buffer effects, and therefore seemed to be specific. Additionally, although p53 DBD was added only to a ∼ 0.5 - fold molar ratio, a strong line broadening occurred

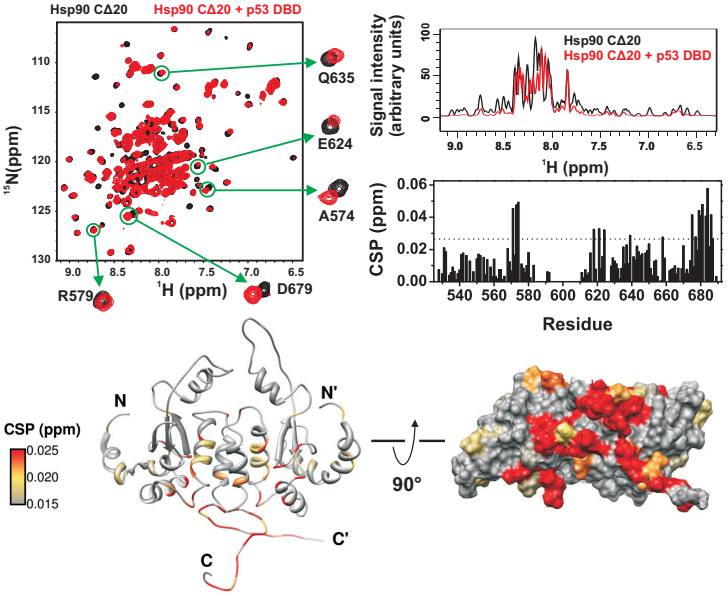

Figure 3.17: Binding of p53 DBD to Hsp90 CΔ20 monitored by NMR. Upper panel, left: Overlay of ^{15}N - TROSY spectra for Hsp90 CΔ20 alone and in complex with p53 DBD. Significant peak shifts can be observed, indicating binding between the proteins. Upper panel, right, upper plot: 1D projections calculated from the 2D spectra shown left. In presence of p53 DBD pronounced line broadening occurs, pointing at the formation of a large complex. Upper panel, right, lower plot: Calculated chemical shift perturbation for p53 DBD binding to Hsp90 CΔ20 as observed in the spectra shown left. The significance level (twofold average CSP) is indicated by a dashed line. Lower panel: Mapping of chemical perturbation upon binding of p53 DBD onto a structure model of Hsp90 CΔ20 (see section 3.2 and figure 3.14) in cartoon representation (left) and surface representation rotated by 90° (right). The measurement was done at 900 MHz and 298 K in 10 mM potassium phosphate, 1 mM TCEP, pH 6.8 on a 570 μM highly deuterated sample of Hsp90 CΔ20. p53 DBD was added in a $\sim$ 0.5 molar ratio.

for signals throughout the folded parts of Hsp90 CΔ20 (figure 3.17, upper panel, right). Thus, obviously a large complex was formed. Assuming a 1:1 binding between p53 DBD and the constitutive Hsp90 CΔ20 dimer as found in the ITC experiments (compare figure 3.7), the molecular weight of the putative complex would be around ∼ 90 kDa, explaining the pronounced line broadening.

A plot of the chemical shift perturbation and a mapping onto the structure (figure 3.17, upper panel right and lower panel) shows that mainly residues from the C - terminus of Hsp90 CΔ20 (amino acids ∼ 675 to 689) were affected by the binding of p53 DBD, likely representing a major interaction site. This is well in agreement with the previous fluorescence data which demonstrated a significant loss of p53 DBD binding upon a deletion of these residues (compare figure 3.5).

An alignment of the very C - terminal amino acid sequences for the Hsp90 isoforms Hsp82/Hsc82 from yeast and Hsp90α/Hsp90β from man indicates a rather loose conservation (figure 3.18). However, two regions seem to be highly conserved: On the one hand the last five residues that serve as interaction site for TPR domain cochaperones and on the other hand a highly charged motive of four amino acids DEDE. It seems that this small stretch of unstructured residues (compare figure 3.13 and 3.16) is of extraordinary importance for the interaction of Hsp90 C with p53: The Hsp90 CΔ20 truncation variant comprising this charge motive is capable of full p53 DBD binding whereas in contrast the Hsp90 CΔ30 variant lacking it shows much reduced p53 DBD interaction, as found previously in the fluorescence binding assays (figure 3.5). These observations could also be confirmed with NMR: Even upon adding an excess (∼ twofold) of p53 DBD to the ^{15}N - labeled Hsp90 CΔ30 variant, the line broadening was much less pronounced compared to the measurement with Hsp90 CΔ20, although there seemed to be a weak remaining binding (data not

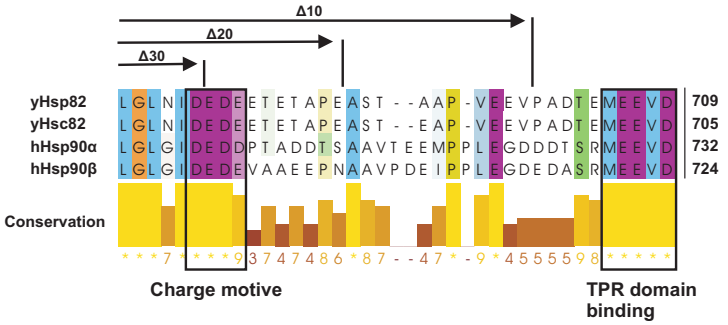

Figure 3.18: Amino acid alignment for the very C-terminal sequences of yeast (y) Hsp90 isoforms Hsp82/Hsc82 and human (h) Hsp90 isoforms Hsp90α/Hsp90β. The sequence conservation in this particular region of Hsp90 is rather low, except for the MEEVD motive serving as binding site for TPR domain cochaperones and a charged motive that seems to be implicated in p53 binding. NCBI reference codes of the sequences used for the alignment are NP_015084.1 and NP_013911.1 for yeast Hsp82 and Hsc82, respectively. The UniProt reference codes for human Hsp90α and Hsp90β are P07900-1 and P08238, respectively. The coloring scheme is according to amino acid properties and the degree of conservation of a particular position, with more intense color indicating higher conservation. The position of the different C-terminal truncations introduced into the yeast Hsp90 in this work is indicated. The alignment was generated using T-Coffee [194] and visualized with Jalview [195].

shown).

To identify the binding site of Hsp90 C on p53 DBD, the chemical shift perturbation in the 2D TROSY spectrum of ^{15}N-labeled p53 DBD upon adding Hsp90 C was monitored. As expected, also in this case specific peak shifts could be observed in the NMR spectrum of p53 DBD, accompanied by strong line broadening that indicated complex formation (figure 3.19, upper panel). A plot of the calculated chemical shift perturbation shows that mainly the C-terminal region of p53 DBD (amino acids 277 to 298) is affected by the binding of Hsp90 C. The respective residues

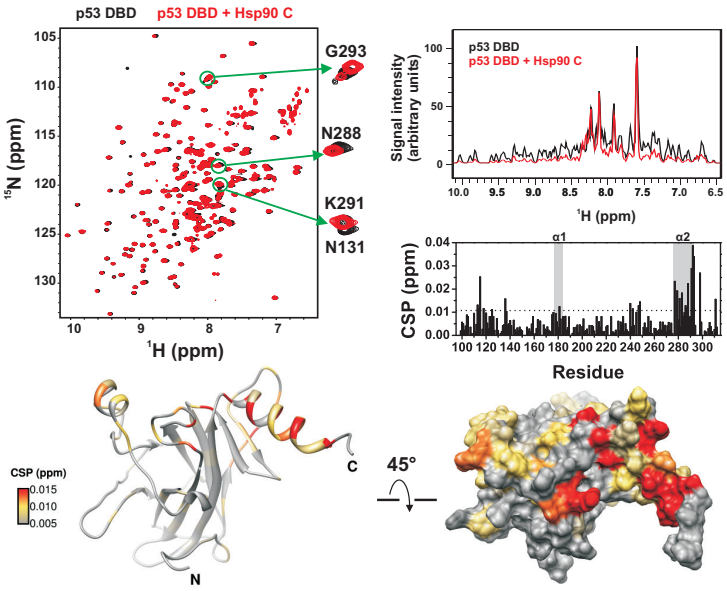

Figure 3.19: Binding of Hsp90 C to p53 DBD monitored by NMR. Upper panel, left: Overlay of ^{15}N - TROSY spectra for p53 DBD alone and in complex with Hsp90 C. Significant peak shifts can be observed, indicating binding between the proteins. Upper panel, right, upper plot: 1D projections calculated from the 2D spectra shown left. In presence of Hsp90 C, pronounced line broadening occurs, pointing at the formation of a large complex. Upper panel, right, lower plot: Calculated chemical shift perturbation for Hsp90 C binding to Hsp90 p53 DBD as observed in the spectra shown left. The significance level (twofold average CSP) is indicated by a dashed line. Lower panel: Mapping of chemical perturbation upon binding of Hsp90 C onto the structure of p53 DBD (PDB: 2FEJ) in cartoon representation (left) and surface representation rotated by 45° (right). The measurement was done at 900 MHz and 298 K in 10 mM potassium phosphate, 1 mM TCEP, pH 6.8 on a 200 μM sample of p53 DBD. Hsp90 C was added in a $\sim$ 0.5 - fold molar ratio.

form the α - helix 2 in p53 DBD which is part of its DNA binding surface (figure 3.19, lower panel). Additionally, to a lower extent, also amino

acids in the N-terminal part of p53 DBD (residues 110 to 120) as well as in some loops located within the DNA binding site experienced shift changes. Thus, the p53 residues that were found to be obviously involved in the interaction with Hsp90 C seem to cluster, which points at the formation of a specific complex.

As outlined, the C-terminal unfolded part of the Hsp90 C domain is of major importance for the binding of p53 DBD. Furthermore, the experiments with successive truncations of this region in the protein indicated that in particular residues 679 to 689 containing a highly charged and conserved peptide motive DEDE could mediate the interaction of Hsp90 C with p53 DBD (compare figures 3.18 and 3.5). To test this assumption, peptides were prepared corresponding to these amino acids of Hsp90 C and analyzed for binding to p53 DBD using NMR again. Two peptides, GLNIDEDEETETAPEAS and GLNIDEDEE, were synthesized by Dr. Oliver Demmer (Institute for Advanced Study, TUM) and kindly provided for the measurements. Indeed, significant and specific binding could be observed in the ^{15}N-TROSY spectra of p53 DBD with both peptides (figure 3.20). In contrast to the measurements with the full Hsp90 CΔ20 protein, here a larger excess of the ligand could be added to p53 DBD since the peptides due to their smaller molecular size did not markedly affect the line width of p53 signals when bound to the protein. Consequently, in this case the shifts obtained were much more pronounced.

In general, the chemical shift perturbation patterns were very similar for adding the full Hsp90 C domain or only the peptides to p53 DBD (compare figures 3.19 and 3.20). Also with the peptides shift changes were mainly found for residues within the C-terminal helix α2 of p53 DBD (275 to 292) and in an N-terminal region comprising residues 110 to 128 which form a loop located adjacent to the helix α2. Notably, even the shorter peptide GLNIDEDEE caused significant shift changes on p53 DBD.

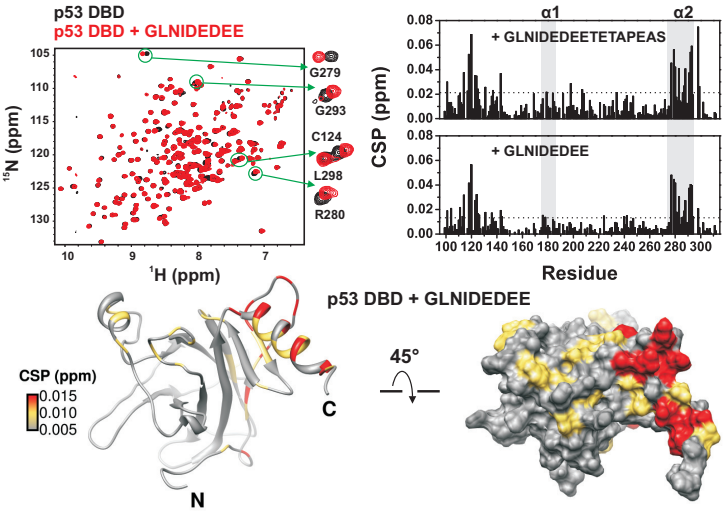

Figure 3.20: Binding of Hsp90 derived peptides to p53 DBD monitored by NMR. Upper panel, left: Overlay of ^{15}N - TROSY spectra for p53 DBD alone and in complex with the peptide GLNIDEDEE derived from the Hsp90 C domain. Significant peak shifts can be observed, indicating binding. Upper panel, right: Chemical shift perturbation plots for the binding of two peptides derived from the Hsp90 C domain to p53 DBD. The significance level (twofold average CSP) is indicated by a dashed line. Lower panel: Mapping of chemical perturbation upon binding of the Hsp90 peptide GLNIDEDEE onto the structure of p53 DBD (PDB: 2FEJ) in cartoon representation (left) and surface representation rotated by 45° (right). The measurement was done at 900 MHz and 298 K in 10 mM potassium phosphate, 1 mM TCEP, pH 6.8 on a 200 μM sample of p53 DBD. Hsp90 peptides were added in a twofold molar excess.

This strongly supports the assumption of a major role for the charge motive DEDE in the binding between Hsp90 C and p53 DBD.

The results from the binding experiments carried out here suggest that the interaction of Hsp90 and p53 DBD is to a large extent governed by

electrostatics. A calculation of the local contact potentials for p53 DBD and Hsp90 CΔ20 indeed shows charge complementarity of the respective binding sites on both proteins found with NMR (figure 3.21). The

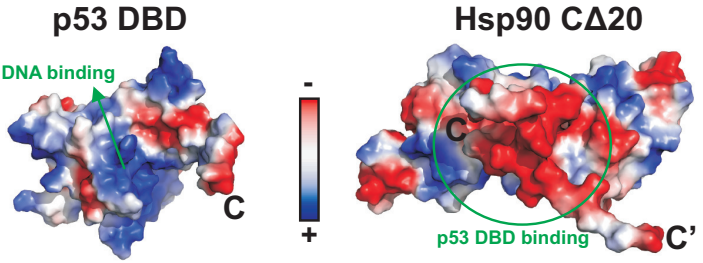

Figure 3.21: Electrostatics of corresponding binding sites on p53 DBD (left) and Hsp90 CΔ20 (right). Electrostatic potentials of p53 DBD (PDB: 2FEJ) and Hsp90 CΔ20 (PDB: 2CG9, see also figure 3.14) were determined using the program PyMOL. Blue color indicates positive, red color negative potential. The DNA binding surface on p53 DBD which is the interaction site for binding of Hsp90 C has strong positive potential whereas the binding site of p53 DBD on Hsp90 C has strong negative potential. Thus, complex formation between the two proteins seems to be largely driven by charge complementarity.

strongly positive potential of the p53 DBD DNA binding surface seems to be perfectly suited to mediate a binding of the unfolded Hsp90 C domain charge motive with its highly negative potential. A major contribution of electrostatics to the binding between Hsp90 C and p53 DBD is well in agreement with the observation that the complex formation of the two proteins is strongly salt dependent, as indicated by a significant weakening of the interaction at higher salt concentrations (data not shown).

The results from the previous fluorescence binding experiments as well as the NMR data obtained here point at an interesting aspect of the Hsp90 – p53 interaction in general: p53 obviously binds to Hsp90 even

in its native-like state because all binding studies performed here were carried out at temperatures of 25°C or below at which p53 DBD is stable and structured, as CD measurements demonstrate (the thermal melting point of p53 DBD is ~48°C, figure 3.22). Additional CD spectroscopic

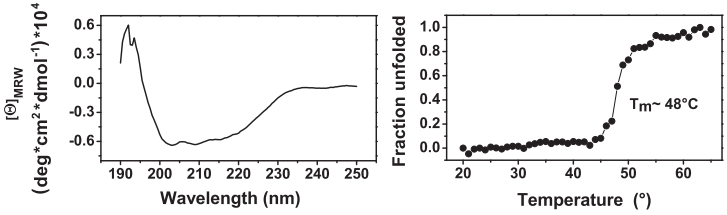

Figure 3.22: CD spectroscopic characterization of p53 DBD. Left: CD spectrum of p53 DBD recorded at 20°C. Right: Thermally induced unfolding of p53 DBD monitored by CD spectroscopy at a wavelength of 218 nm. Measurements were done in a buffer of 10 mM potassium phosphate, 1 mM TCEP, pH 6.8.

experiments further support this assumption: The calculated sum of the individual spectra for isolated Hsp90 C and p53 DBD is nearly identical to the measured spectrum for the complex of both proteins (figure 3.23). Therefore, obviously no major structural change occurs within p53 in the complex. The same applies also for p53 DBD binding to the full-length Hsp90. These findings are consistent with the NMR experiments where no indications of a significantly altered conformation were observed in the spectra of ^{15}N-labeled p53 DBD when Hsp90 C was added. The peak shifts were rather small whereas a structural rearrangement of p53 DBD in complex with Hsp90 C would have caused much larger effects.

Although the CD data indicated no global change in the structure of p53 DBD when bound to Hsp90, it still seemed possible that potentially the unfolded region of Hsp90 C which contains the charge motive mediating the binding of p53 DBD could adopt local secondary structure in the

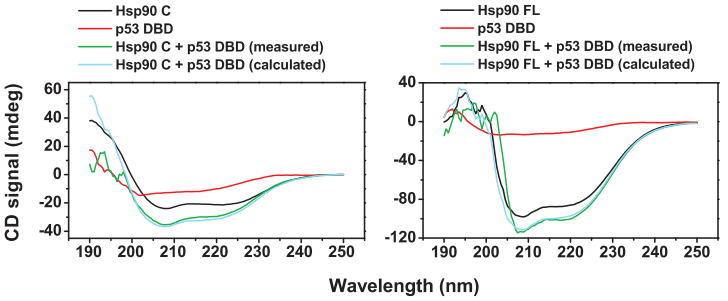

Figure 3.23: Comparison of calculated and measured CD spectra for complexes of p53 DBD with Hsp90 C (left) and full-length (FL) Hsp90 (right). The calculated sum of the individual spectra for isolated Hsp90 C/full-length Hsp90 and p53 DBD is nearly identical to the measured spectrum for the complex of both proteins, pointing at no major structural change of p53 when bound to Hsp90. Measurements were done in a buffer of 10 mM potassium phosphate, 1 mM TCEP, pH 6.8 at 20°C. All proteins were used in a 10 μM concentration.

complex of the two proteins. Such "folding-upon-binding" mechanisms have been observed previously: For example, the intrinsically disordered N-terminal region of p53 [237,238] forms a small amphiphilic helix upon binding to the N-terminal domain of Mdm2 [239,240]. Similarly, an interaction of the unfolded pKID domain from the CREB transcription factor with the KIX domain of the CREB binding protein induces helical secondary structure in pKID [241,242]. Therefore, to analyze whether also the unfolded p53 DBD binding motive of Hsp90 C might gain structure upon interaction with p53 DBD, two HNH-NOESY spectra were recorded for free Hsp90 CΔ20 and in complex with p53 DBD. In case of an induced helical conformation, significant HN-HN backbone NOE contacts should be observed for residues located in the p53 DBD binding site of Hsp90 CΔ20. Indeed, slightly stronger NOE connectivity is observed when p53 DBD is bound to Hsp90 CΔ20 (figure 3.24). However, these findings cannot def-

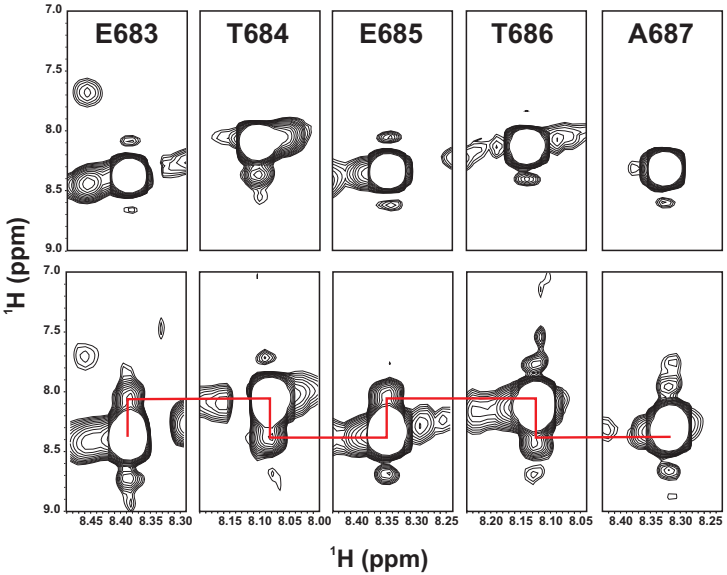

Figure 3.24: NOESY strips of Hsp90 CΔ20 residues from the unfolded p53 DBD binding site for free Hsp90 CΔ20 (upper panel) and in complex with p53 DBD (lower panel). Slightly stronger HN - HN NOE contacts are visible when p53 DBD is bound to the unfolded C - terminal region of Hsp90 CΔ20 that could indicate a gain of secondary structure. Measurements were done in a buffer of 10 mM potassium phosphate, 1 mM TCEP, pH 6.8 at 298 K and 900 MHz on a 600 μM sample of Hsp90 CΔ20. p53 DBD was added in $\sim$ 0.6 - fold molar ratio.

initely confirm a helical secondary structure because due to the large size of the complex ($\sim$ 90 kDa), spin diffusion might already play a role and thus such NOE data can potentially be misleading. Therefore, as a control additional measurements were done. The $\{^1H\}$ - ^{15}N - NOE (hetNOE) was determined for residues in the unfolded binding motive of Hsp90 CΔ20 in complex with p53 DBD (figure 3.25, left). Compared to the free state of

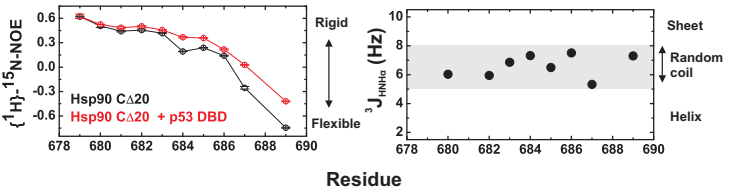

Figure 3.25: {^{1}H}-^{15}N-NOE (hetNOE, left) and $^3J_{HNH\alpha}$ coupling constants (right) of Hsp90 CΔ20 in complex with p53 DBD. In presence of p53 DBD the highly flexible residues from the unfolded C-terminal binding motive of Hsp90 CΔ20 get slightly more rigid, confirming complex formation. However, $^3J_{HNH\alpha}$ coupling constants for the respective residues are all between ~5 and 8 Hz indicative of no preferred secondary structure. Measurements were done in a buffer of 10 mM potassium phosphate, 1 mM TCEP, pH 6.8 at 298 K and 600 MHz on a 250 μM sample of Hsp90 CΔ20. p53 DBD was added in ~0.6-fold molar ratio.

Hsp90 CΔ20, these get indeed slightly more rigid, as indicated by higher hetNOE values. This confirms an involvement of amino acids ~680 to 689 in binding of p53 DBD. However, the corresponding $^3J_{HNH\alpha}$ coupling constants were found to be all between ~5 to 8 Hz which clearly points at the absence of any preferred secondary structure. Consequently, a "folding-upon-binding" model does obviously not apply for the interaction of Hsp90 C and p53 DBD.

3.5 Molecular Docking of the Hsp90 C△20 – p53 DBD Complex

The analysis of ^{1}H and ^{15}N NMR chemical shifts can be very useful in the determination of the potential binding sites in two proteins assumed to form a complex. However, such data have to be judged critically as they can also be misleading in some cases. For example, secondary effects can occur upon complex formation, causing an allosteric conformational change in the protein far off the real binding surface. As an additional validation of the interaction sites found for the complex between Hsp90 C and p53 DBD with chemical perturbation, further paramagnetic relaxation enhancement (PRE) experiments were performed here. As an advantage, this method can provide long range distance information that can potentially also be used for a molecular docking of two proteins. To this end, a site directed spin labeling of the Hsp90 C domain was done. Cysteine residues were introduced at different positions in the protein to attach a spin label. Helpfully, Hsp90 C does not contain any native cysteine. Therefore, no additional mutation was required to first remove such a residue which could lead to an unspecific labeling in the protein.

Overall, six cysteine variants of the full - length Hsp90 C domain were generated, E546C, D573C, D659C, N677C, A687C and S691C (figure 3.26, left). The mutations were located either near to the putative binding site as found with chemical shift perturbation (N677C, A687) or more distant (E546C, D573C, D659C, S691C) to serve as a control. The respective Hsp90 C mutants were labeled with 3 - (2 - Iodoacetamido) - PROXYL (2,2,5,5 - tetramethyl - 1 - pyrrolidinyloxy) and added in a 1:1 molar ratio to ^{15}N p53 DBD. Due to the size of the complexes obtained ($\sim$ 90 kDa), the spectral quality was insufficient at low salt concentrations, although

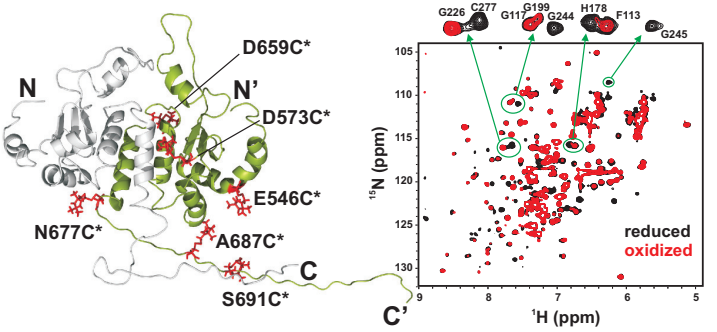

Figure 3.26: Position of cysteine residues introduced into the Hsp90 C domain for spin labeling and PRE effects in a complex of p53 DBD and a selected Hsp90 C spin labeled cysteine variant. Left: Native amino acids at 6 positions in Hsp90 C were replaced by a cysteine and modified with a spin label to probe for spatial proximity in PRE experiments with p53 DBD. Cysteines with spin label attached (indicated by "*") are highlighted in red and stick representation in a model of Hsp90 C based on a crystal structure (PDB: 2CG9). Flexible and unresolved regions in the domain were rebuilt using Xplor-NIH [233] (compare figure 3.14). For clarity, spin labels are only shown for one protomer of the dimer, individual protomers are colored gray and green, respectively. Right: Overlay of ^{15}N-HSQC spectra for p53 DBD in complex with the spin labeled Hsp90 C N677C variant before (red) and after (black) addition of ascorbic acid. Many p53 DBD signals show line broadening, indicating spatial proximity to the spin label. Measurements were done in a buffer of 10 mM potassium phosphate, 110 mM potassium chloride, 1 mM TCEP, pH 6.8 at 298 K and 900 MHz on a 150 μM sample of p53 DBD. Hsp90 C N677C* was added in a 1:1 molar ratio. For reduction, a 10-fold molar excess of ascorbic acid over p53 DBD was added and incubated for 1 h.

high field strength ((900 MHz) and a cryogenic probe were used. Massive line broadening in this case rendered PRE experiments impossible. Therefore, it was necessary to first optimize the sample conditions. The application of higher temperatures was not possible due to the tendency of p53 DBD to aggregate above ~ 298 K under the high concentrations re-

quired for NMR. However, by adding stepwise increasing amounts of salt, the complex was weakened, driving the binding to faster exchange. This led to a significant recovery of signal intensity. At a comparatively high concentration of ~ 110 mM potassium chloride, the ^{15}N - HSQC spectra of p53 DBD bound to the Hsp90 C variants were then finally of a quality suited for PRE measurements.

With the spin label attached at positions 659 and 691 of Hsp90 C, no significant line broadening was observed on p53 DBD, as expected, since these positions are farer away from the putative binding site of p53 DBD on Hsp90 C (figure 3.27). Similarly, with the PROXYL modified Hsp90 A687C variant no major relaxation enhancement could be measured, although in this case the label was placed a bit closer to the charged p53 DBD binding motive of Hsp90 C. Most likely, here increased dynamics of the position 687 played a role which led to a downscaling of the PRE effect (compare figure 3.16).

The Hsp90 C E546C and D573C mutants caused a general moderate reduction of peak intensity ratios ($I_{oxidized}/I_{reduced} \sim 0.6$) more or less throughout the folded part of p53 DBD, indicating a certain spatial proximity of the respective two position in Hsp90 C to the p53 DBD binding site. Potentially, also in this case unfavorable dynamics that might have been caused by the mutations introduced could be responsible for the rather diffuse effects observed.

However, when position 677 of Hsp90 C was modified with the spin label, a significant and pronounced line broadening of many signals in the spectrum of p53 DBD was visible (figure 3.26, right). Specifically, residues located within the DNA binding surface of p53 DBD had strongly reduced peak intensity ratios (figure 3.27, upper panel right and lower panel). This result is well in agreement with the findings from the previous chemical shift perturbation experiments and confirms the putative

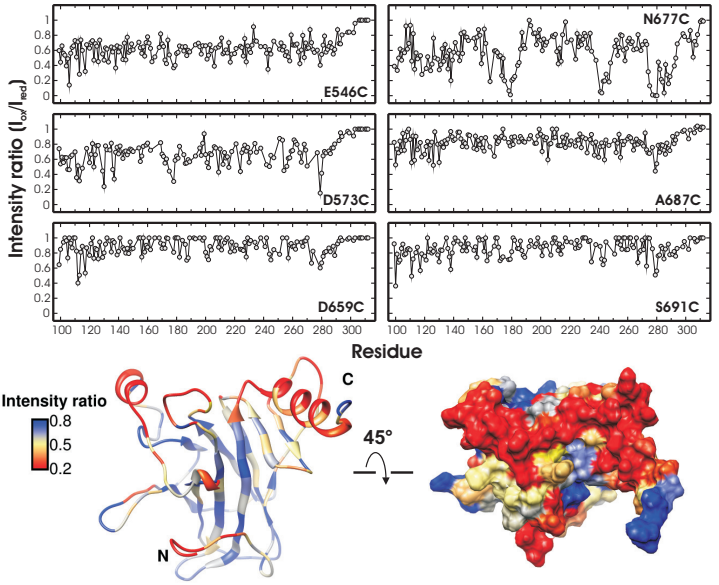

Figure 3.27: p53 DBD peak intensity ratios from PRE experiments with Hsp90 C spin label variants. Upper panel: Plot of peak intensity ratios calculated from ^{15}N - HSQC spectra for p53 DBD in complex with different PROXYL labeled Hsp90 C variants as indicated before and after addition of ascorbic acid. Most pronounced PRE effects were observed with the spin label attached at position 677 in Hsp90 C. Lower panel: Color coded mapping of PRE effects for the measurement of p53 DBD and the spin labeled Hsp90 C N677C variant (Hsp90 C N677C*) onto the NMR structure of p53 DBD (PDB: 2FEJ). Measurements were done in a buffer of 10 mM potassium phosphate, 110 mM potassium chloride, 1 mM TCEP, pH 6.8 at 298 K and 900 MHz on a 150 μM sample of p53 DBD. Hsp90 C N677C* was added in a 1:1 molar ratio. For reduction, a 10 - fold molar excess of ascorbic acid over Hsp90 C N677C* was added and incubated for 1 h.

interaction sites of Hsp90 C and p53 DBD.

With the NMR chemical shift perturbation and PRE data a molecular

docking between Hsp90 C and p53 DBD was then performed using HADDOCK[243]. To this end, first a set of ambiguous interaction restraints (AIRs) was generated using information from the chemical shift perturbation experiments. Several active and passive residues were specified for both binding partners of the complex. Active residues are residues that showed significant peak shifts upon binding and have a relative surface accessibility of ∼ 40 % or higher as determined with the program NACCESS. These amino acids should most likely be be involved in direct binding contacts between the two proteins. In contrast, passive residues are the surface accessible neighbors of the active residues but do not directly participate in the interaction. Table 3.1 summarizes active and passive residues used in the HADDOCK docking calculations.

Table 3.1: Ambiguous interaction restraints for the docking of Hsp90 C and p53 DBD. Active and passive residues as shown were defined for Hsp90 C and p53 DBD and used for NMR data driven complex docking with HADDOCK[243].

	Hsp90 C	p53 DBD
active	531 - 533, 541, 542, 544, 545, 551, 571 - 574, 579, 580, 621, 623, 624, 630, 635 - 637, 653, 670, 675, 677 - 687	114, 115, 118, 120, 123, 136, 137, 175, 178, 181, 184 - 186, 240, 242, 244, 245, 247, 248, 276, 277, 280, 281, 283 - 288, 291 - 293
passive	530, 534, 546, 570, 620, 631, 638, 674, 688	116, 117, 119, 121, 122, 138, 174, 177, 182, 241, 243, 289, 290, 294

The docking was then performed with a model of the Hsp90 C domain based on a crystal structure (PDB: 2CG9)[52] but with flexible and unresolved regions in the protein rebuilt using Xplor - NIH[233]. For p53 DBD, a crystal structure (PDB: 1TUP) was used and since the ITC data found a binding stoichiometry of approximately 1:1 for its interaction with Hsp90

(compare figure 3.7), a dimeric template was taken for the calculations with the likewise dimeric Hsp90 C domain. As further input for the docking, the C-terminal unfolded amino acids 675 to 709 of Hsp90 C were defined as a fully flexible segment. Similarly, for p53 DBD two loop regions connecting β-strands within the Hsp90 binding interface comprising residues 163 to 175 and 236 to 250 were specified to be behave flexibly.

Including concrete atomic distances between Hsp90 C and p53 DBD that were derived from the PRE experiments with the Hsp90 C N677C variant as restraints in the calculations turned out to be disadvantageous. The resulting complexes had a rather bad agreement with the experimental chemical shift data, and also the PRE intensity ratios that were back-calculated from the complex structures as a further validation were not very well consistent with the measured ratios. Even when generous upper and lower bounds were applied on the distances, the docking solutions were not satisfying. Obviously, the quality of the PRE data was not sufficient to extract reliable distance information. Maybe the comparatively high salt concentrations that had to be used in the PRE measurements to overcome the problems of strong line broadening had weakened the complex too much, so that faster exchange might have led to an averaging of different orientations of the binding partners. This would consequently transfer into erroneous distances. Therefore, finally only chemical shift perturbation data were included in the calculations. Compared to docking runs where additionally atomic distances were specified, this resulted in a higher number of complex cluster with similar quality indicators. However, the best docking model out of several equally ranked solutions could then be identified afterwards by evaluating the consistency of the different complexes with the experimental NMR shift and PRE data.

The model for the complex between Hsp90 C and p53 DBD that had the

best overall agreement with the experimental data is shown in figure 3.28, the corresponding docking statistics can be found in table 3.2. p53 DBD

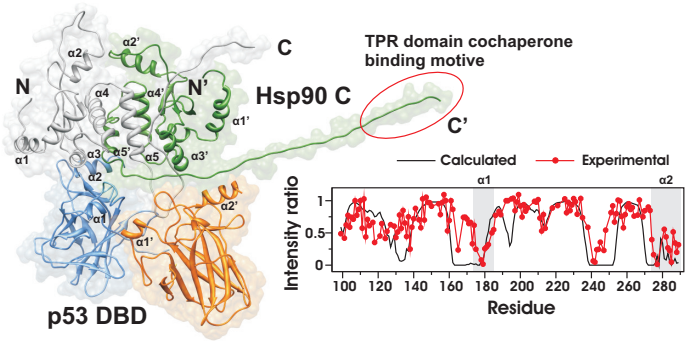

Figure 3.28: NMR data driven docking between Hsp90 C and p53 DBD using HADDOCK[243]. Left: Model for the complex between Hsp90 C and p53 DBD (PDB: 1TUP) obtained from docking with HADDOCK. N- and C-termini for the protomers of the Hsp90 C dimer are indicated. Right: Comparison of p53 DBD PRE intensity ratios determined experimentally (red dots and line) and back-calculated from the complex model shown left (black line). Measured and calculated data show a reasonable overall match.

binds in slightly twisted orientation to the Hsp90 C domain dimer at its C-terminal part where the unfolded C-terminal tails (residues 679 to 709) containing the charge motive protrude from the folded part of the protein. The helices α1 and α3 of Hsp90 C provide here a broad surface for the interaction with p53 DBD. Indeed, overall a large buried surface area of $\sim 4200\,\text{Å}^2$ is found for the complex between p53 DBD and Hsp90 C (table 3.2). p53 DBD contacts Hsp90 C with its DNA binding site involving mainly the helices α1 (residues 175 to 182) and α2 (residues 278 to 288) and a large loop (residues 236 to 250). By this interaction mode,

Table 3.2: Statistics of the best complex cluster for the docking between Hsp90 C and p53 DBD obtained with HADDOCK[243]. The complex was obtained by specifying active and passive residues according to table 3.1. 1000 initial rigid-body docking runs were performed followed by semi-flexible refinement of 200 complex structures in torsion angle space and final refinement in explicit solvent.

HADDOCK score*	-217.2 ± 6.3
Cluster size	120
RMSD from the overall lowest-energy structure (Å)	31.4 ± 0.4
Van der Waals energy (kcal/mol)	-114.7 ± 5.3
Electrostatic energy (kcal/mol)	-1242.2 ± 55.6
Desolvation energy (kcal/mol)	11.5 ± 4.1
Restraints violation energy (kcal/mol)	1344.2 ± 104.76
Buried surface area (Å^2)	4209.6 ± 138.2

*Weighted sum of van der Waals, electrostatic, desolvation and restraint violation energies together with buried surface area

the structurally labile DNA binding site of p53 DBD might get stabilized. Notably, the dimeric Hsp90 C domain allows for a binding of p53 DBD in its preferred dimeric state with an inter-subunit salt bridge formed by residues E180 and R181 from the two monomers.

PRE intensity ratios back-calculated from the complex model showed a reasonable overall match with the experimental data (figure 3.28, right). As outlined above, potential exchange processes under the conditions used that lead to an averaging of multiple orientations of the binding partners and a downscaling of the PRE effects might explain differences between the calculated and measured data. Additionally, also internal dynamics within both proteins could play a certain role.

3.6 Validation of p53 DBD Binding Sites on Hsp90 by Mutagenesis

To further evaluate the significance of the different p53 DBD binding sites on Hsp90 identified in the previous experiments (see sections 3.1 and 3.4), selected Hsp90 binding site mutants were assessed for their interaction with p53 DBD. In particular, the comparatively low affinity of p53 DBD for Hsp90 M (see figures 3.2 and 3.3) raises the question to which extent the complex observed between the two proteins was specific. In an NMR study carried out earlier by Dr. Franz Hagn (Institute for Advanced Study, TUM), the putative binding site of p53 DBD on Hsp90 M was determined. Thereby, E412 and E415 of Hsp90 M were found to be key residues implicated in the interaction with p53 DBD. Two corresponding charge reversal mutations of Hsp90 M, E412K and E415K, were generated already previously by Dr. Franz Hagn and could be used in this work here for testing their ability to bind p53 DBD. To this end, analytical ultracentrifugation experiments were performed in collaboration with Dr. Klaus Richter (Lehrstuhl für Biotechnologie, TUM) as well as fluorescence polarization assays.

First, p53 DBD was labeled with carboxyfluorescein (p53 DBD*) and analyzed for complex formation with wild - type Hsp90 M and the E415K variant in an ultracentrifugation run with fluorescence detection (figure 3.29, left). p53 DBD* alone sedimented with a S - value (S, Svedberg constant) of $\sim$ 2.7. Upon adding increasing amounts of Hsp90 M, a gradual peak shift to higher S - values could be observed, indicating complex formation. With the Hsp90 M E415K variant, however, the peak shift at the corresponding concentrations was smaller (sedimentation coefficient $\sim$ 3.1 versus 3.4 S at 20 μM concentration of Hsp90 variant added). This

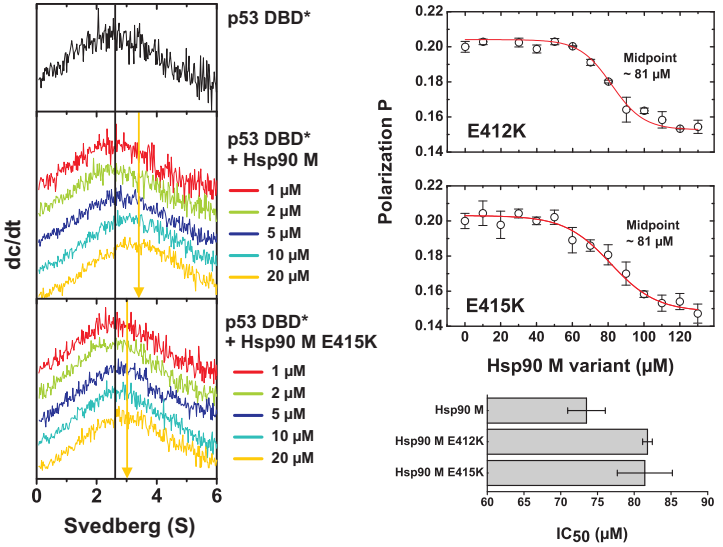

Figure 3.29: Interaction of p53 DBD and Hsp90 M binding site mutants studied with analytical ultracentrifugation (left) and fluorescence polarization (right). Left: Fluorescently labeled p53 DBD (p53 DBD*) was monitored for complex formation with Hsp90 M and a p53 DBD binding site mutant thereof, Hsp90 M E415K. Titration of p53 DBD* with Hsp90 M causes a peak shift to higher S-values, indicating complex formation. With Hsp90 M E415K the shift at comparable concentrations is lower, pointing at an impaired interaction. Right: Titration of a preformed complex between fluorescently labeled p53 DBD and full-length Hsp90 with the p53 DBD binding site mutants Hsp90 M E412K and E415K (upper panel). Compared to wild-type Hsp90 M, both mutants have reduced affinity for p53 DBD (lower panel, compare also figure 3.3). Measurements were done in a buffer of 10 mM potassium phosphate, 1 mM TCEP, pH 6.8 at 20°C. For all measurements 500 nM of labeled p53 DBD (p53 DBD*) was used. Hsp90 variants were added in increasing concentration as indicated. In the polarization experiments, 5 μM full-length Hsp90 was added to preformed a complex with p53 DBD*.

points at an impaired interaction between p53 DBD and the Hsp90 M mutant, confirming that indeed a residue important for p53 DBD binding was

substituted.

To estimate how much the E415K mutation as well as the second putative binding site mutation E412K affect the affinity of Hsp90 M for p53 DBD, additional fluorescence polarization measurements were done. Again, fluorescently labeled p53 DBD was used in a displacement binding assay as described in section 3.1. For both Hsp90 M variants binding to p53 DBD was observed, and the transition midpoints in the displacement curves were around $\sim 81\,\mu$M (figure 3.29, right, upper panel). For comparison, the transition midpoint for wild - type Hsp90 M and p53 DBD was $\sim 74\,\mu$M (figure 3.29, right, lower panel). Thus, the effect of the mutations on the binding affinity of Hsp90 M for p53 DBD is rather moderate. Nevertheless, this decrease in binding strength can be regarded as significant. Given the fact that typical protein - protein interactions usually involve large surfaces within both binding partners, it is in general unlikely that single point mutations would completely disrupt such an interaction.

Overall, the results from the analytical ultracentrifugation and fluorescence polarization measurements demonstrate that – despite the low affinity – the binding between Hsp90 M and p53 DBD observed in the previous experiments was clearly specific. Additionally, the decrease in binding strength upon mutation of E412 and E415 in Hsp90 M is a confirmation for the interaction site of p53 DBD found on Hsp90 M in previous work.

As described in section 3.4, a stretch of five amino acids, DEDEE, within the unfolded C - terminal region of Hsp90 C is essential for high affinity binding of p53 DBD. Furthermore, isolated peptides comprising this motive showed significant interaction with p53 DBD. To further analyze the importance of the respective individual charged residues for complex formation with p53 DBD, an alanine scan was done. A set of different nonapeptides (amino acids 675 to 683 of Hsp90) containing the bind-

ing motive was prepared with successive substitutions of the D and E residues. All peptides were N-terminally labeled with carboxyfluorescein and could thus be assessed for binding to p53 DBD in titrations using fluorescence polarization. The peptides were synthesized by Dr. Oliver Demmer (Institute for Advanced Study, TUM) and kindly provided for the measurements.

As a first control to evaluate the reliability of the assay, isolated carboxyfluorescein was titrated with p53 DBD (figure 3.30). No binding of

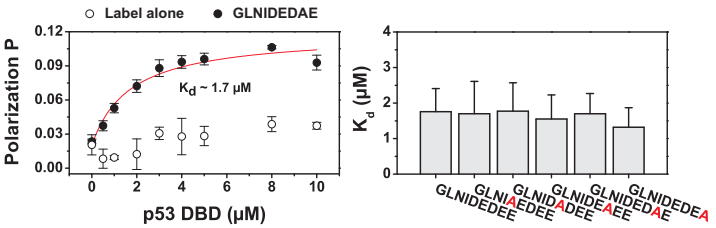

Figure 3.30: Alanine scanning of the charged p53 DBD binding motive using Hsp90 C domain peptides Left: Polarization binding curves for the titration of a fluorescein labeled Hsp90 peptide (black dots) and, as a control, isolated fluorescein (open dots) with p53 DBD. Only the peptide shows binding to the protein, thus an unspecific interaction with the label can be excluded. Right: Affinities of the different Hsp90 C domain peptides containing alanine substitutions for binding to p53 DBD. No major weakening of the interaction with p53 DBD occurs for replacing single charged residues. Measurements were done in a buffer of 10 mM potassium phosphate, 1 mM TCEP, pH 6.8 at 20°C. For all measurements 500 nM of labeled peptides were used.

the label to the protein could be observed in this case. Thus, in the following experiments an unspecific interaction of p53 DBD with the peptides caused by the presence of the label in the molecule could be ruled out. For all five peptides containing an alanine substitution as well as for the wild-type peptide that was measured as a control, typical bind-

ing curves upon adding increasing amounts of p53 DBD were obtained from which an affinity could be determined. The native peptide bound to p53 DBD with a K_d of $\sim 1.8\,\mu$M and thus with nearly identical affinity as the full - length Hsp90 protein (compare figure 3.2). This confirms the essential importance of the charge motive for the interaction of Hsp90 C with p53 DBD and is well consistent with the previous results (compare sections 3.1 and 3.4).

Interestingly, all alanine substituted peptide variants showed a binding to p53 DBD basically similar to the control peptide with affinities of K_d ~ 1.5 to $1.8\,\mu$M. Obviously, a mutation of only one charged residue is not sufficient to significantly disrupt the interaction of the peptide with p53 DBD. This might be explained by the fact that the binding between p53 DBD and the charge motive to a certain degree lacks high specificity. The CD and NMR data have demonstrated that the charge motive neither contains an inherent preferred secondary structure (compare figure 3.4) nor adopts any structure in complex with p53 DBD (compare figure 3.25). Thus, p53 DBD does likely not recognize a specific orientation of the charged side - chains from the D and E residues in the peptide as it would be found in a structured/folded peptide. Rather, the negative charge of the ligand in general seems to be important. Consequently, the loss of only a single D or E residue has less impact on the binding than in case of peptide ligand that is bound in a well defined conformation to its protein target.

The binding of the charge replacement peptides to p53 DBD was also studied using NMR. Adding the respective alanine containing peptides (without fluorescein label) to the protein, significant chemical shift perturbation could be observed, demonstrating that the mutant peptides still interacted with p53 DBD (figure 3.31). The overall chemical shift perturbation pattern of the p53 DBD residues with the alanine peptides was

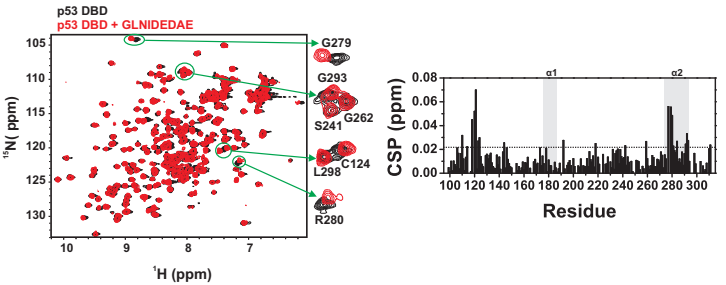

Figure 3.31: Binding of an Hsp90 peptide from an alanine scanning to p53 DBD monitored by NMR. Left: Overlay of ^{15}N - HSQC spectra for p53 DBD alone and in complex with the mutant peptide GLNIDEDAE derived from the Hsp90 C domain and containing a replacement of one charged residue by alanine. Significant peak shifts indicate a binding of the peptide despite the mutation. Right: Chemical shift perturbation (CSP) plot for binding of the GLNIDEDAE peptide to p53 DBD. The overall CSP pattern is similar to binding of the native peptide to p53 DBD (compare figure 3.20). Similar results were obtained with the other peptides from the alanine scanning (see figure 3.30). The significance level (twofold average CSP) is indicated by a dashed line. The measurement was done at 600 MHz and 298 K in 10 mM potassium phosphate, 1 mM TCEP, pH 6.8 on a 100 μM sample of p53 DBD. The peptide was added in a twofold molar excess.

basically similar as in the case of the native peptide (compare figures 3.20 and 3.31), indicating identical binding modes. Therefore, the NMR data are well in agreement with the results from the fluorescence polarization experiments.

3.7 Coupling of Client Protein Binding to the Hsp90 Chaperone Cycle

A basic question regarding Hsp90 - client protein complexes is to which extent or if at all the client protein binding is coupled to the Hsp90 ATPase cycle. As several earlier studies clearly showed, Hsp90 undergoes large structural changes upon nucleotide binding during the ATPase cycle [52,55,60,86]. Therefore, the binding of substrate proteins might be dependent on the conformation of Hsp90 (open or closed). In particular, the accessibility of potential interaction sites provided by the more inner surface of the M domain should be strongly connected to nucleotide state of Hsp90 as the M domains undergo larger movements when ATP binds to the Hsp90 N - terminal domains.

Additionally, given the fact that several Hsp90 cochaperones bind either to the Hsp90 M domain like Aha1 [48,197] or target the unfolded C - terminal region of Hsp90 for interaction as in the case of the TPR domain containing cochaperones Sti1 [66,68,70,148,151,169–172], PP5 [65], Cns1 [71] or the immunophilins FKBP51/FKBP52 [69,70], it could be assumed that the binding of cochaperones and client proteins like p53 to Hsp90 mutually exclude each other. The previous NMR data and the model for the p53 DBD – Hsp90 C complex obtained here indeed indicate that the peptide motive recognized by the TPR domain cochaperones is accessible even when p53 DBD is bound to Hsp90 C (compare figure 3.28), as it is located by ~ 22 residues more C - terminally of the charge motive important for p53 DBD binding (compare figure 3.18). Nevertheless, a simultaneous binding of p53 DBD and TPR domain cochaperones to Hsp90 C might for steric reasons be hindered.

To address these issues, analytical ultracentrifugation (aUC) runs were

performed here in collaboration with Dr. Klaus Richter (Lehrstuhl für Biotechnologie, TUM). This method allows for a qualitative analysis of even very large protein complexes and thus can provide information not available from NMR. For the ultracentrifugation measurements p53 DBD was labeled with carboxyfluorescein (p53 DBD*) and could therefore be monitored for sedimentation in a fluorescence detected experimental set-up. A potential complex formation of p53 DBD with Hsp90 was then studied in the presence of different nucleotides and cochaperones. Under the conditions used, p53 DBD* alone sedimented with a Svedberg constant S of roughly 3 (figure 3.32). Adding a molar excess (sixfold) of

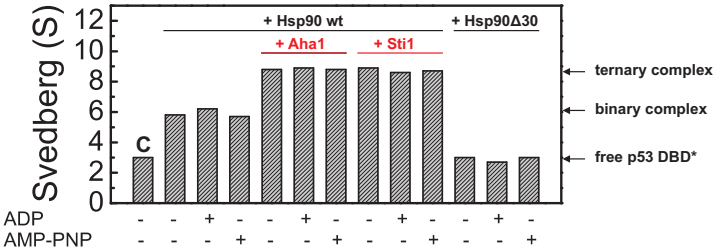

Figure 3.32: Influence of nucleotides and cochaperones on p53 DBD binding to Hsp90 monitored by analytical ultracentrifugation. Fluorescently labeled p53 DBD (p53 DBD*) was monitored for complex formation with wild-type (wt) Hsp90 or the Hsp90Δ30 deletion mutant under different nucleotide states. Additionally, formation of ternary complexes with the cochaperones Aha1 and Sti1 was assessed in case of wild-type Hsp90. p53 DBD fails to bind to the Hsp90 deletion variant and the nucleotide state has no influence on the interaction. Clearly, ternary complexes are formed between p53 DBD, Hsp90 and the cochaperones tested. For the measurements 1 μM of labeled p53 DBD was used. Hsp90 constructs were added in a 6-fold and cochaperones in a 8-fold molar excess over p53 DBD. Measurements were done in 10 mM potassium phosphate, 1 mM TCEP, 2 mM $MgCl_2$, pH 6.8 at 20°C. Nucleotides were added in a 1 mM concentration.

Hsp90, as expected a larger complex was formed, indicated by a shift in

the S - value to ~ 6. The additional presence of the nucleotides ADP and AMP - PNP (adenosine 5' - (β,γ - imido)triphosphate, a non - hydrolysable ATP analogue) had no major effect on the binding between p53 DBD and Hsp90. In both cases the 6 S complex was observed again. Likely, due the dominating binding site of p53 DBD within the Hsp90 C domain, a potential influence of nucleotides on the binding of p53 DBD to the Hsp90 M domain is not significantly reflected in these experiments. As a control, a full - length Hsp90Δ30 variant lacking the unfolded 30 residues form the C - terminus (in analogy to the Hsp90 CΔ30 variant) was also tested for complex formation with p53 DBD. However, no indications of a significant binding between this Hsp90 mutant and p53 DBD could be found, irrespective of the presence or absence of nucleotides. Obviously, the affinity of p53 DBD for the Hsp90 M domain is too weak to obtain a detectable shift in the sedimentation coefficient under the conditions used.

The formation of ternary Hsp90 – p53 DBD – cochaperone complexes was then analyzed for two Hsp90 cochaperones, Sti1 and Aha1 (purified Aha1 was kindly provided by Lars Mitschke, Lehrstuhl für Biotechnologie, TUM). Aha1 was shown to bind to the Hsp90 M and also to the N domain [48,197,198] whereas Sti1 has binding sites on Hsp90 M and additionally interacts with the unfolded C - terminus of Hsp90 C (see section 4.12). Obviously, also in presence of either of the two cochaperones p53 DBD can still bind to Hsp90. Ternary complexes containing Hsp90, p53 DBD and the respective cochaperone were well formed, as indicated by a shift of the p53 DBD sedimentation coefficient to higher values around 9 S (figure 3.32). Again, the nucleotide state of Hsp90 had no major effect. These findings are in agreement with the NMR docking model between Hsp90 C and p53 DBD obtained here, which suggested the C - terminal TPR domain binding motive of Hsp90 C to be fully acces-

sible even when p53 DBD is bound (compare figure 3.28). As outlined above, a potential blocking of the p53 DBD binding site on Hsp90 M by cochaperone binding is likely not detectable in these experiments due to the low affinity of p53 DBD for Hsp90 M (compare figures 3.2 and 3.3).

Although the ultracentrifugation experiments pointed at a nucleotide and cochaperone independent binding of p53 DBD to Hsp90, the interaction with a client protein might nevertheless have influence on the Hsp90 ATP hydrolysis and thus be coupled to its ATPase cycle. To test this assumption, ATPase assays were performed here in presence of p53 DBD and the cochaperone Aha1, known to be a potent stimulator of the Hsp90 ATP hydrolysis [193,198]. p53 DBD alone had clearly no effect on the Hsp90 ATPase activity (figure 3.33). The presence of Aha1 alone caused a sig-

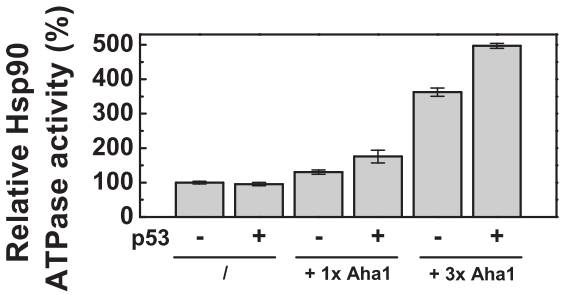

Figure 3.33: Influence of client protein binding on the Hsp90 ATPase activity. The Hsp90 ATPase activity was determined under presence of a 1:1 (1x) or 3:1 (3x) molar ratio of the cochaperone Aha1 without and with p53 DBD. p53 DBD alone has no influence on the ATP hydrolysis of Hsp90. However, the Aha1 mediated Hsp90 ATPase stimulation is higher when p53 DBD is present. Measurements were done in 10 mM potassium phosphate, 5 mM $MgCl_2$, 2 mM ATP, pH 7.5, at 20 °C. Protein concentrations were 3 μM for Hsp90 and 10 μM for p53 DBD. The ATPase activity was determined using a coupled regenerating assay [244].

nificant and concentration dependent stimulation of the Hsp90 ATPase

activity, as expected. However, when additionally p53 DBD was added to the reaction, the Aha1 mediated acceleration of the Hsp90 ATP hydrolysis was surprisingly increased. This result argues for certain cochaperone dependent coupling of the client protein binding to the Hsp90 ATPase cycle by a so far unknown mechanism.

3.8 Influence of Hsp90 C Domain Mutants on the *In Vivo* Activity of p53

To further analyze the role of Hsp90 in the activation of p53 *in vivo*, reporter assays were performed in collaboration with Dr. Julia Rohrberg (Lehrstuhl für Biotechnologie, TUM). For this purpose, mutations were introduced into the C domain of Hsp90 in the full - length protein and tested in yeast cells for supporting p53 transcriptional activity. Three different Hsp90 variants were generated: Hsp90 679-680A and Hsp90 679-682A contained alanine substitutions of residues D679/E680 and D679/E680/D681/E682 respectively, thus targeting the charged p53 DBD binding motive (compare section 3.4 and figure 3.18). Furthermore, an Hsp90Δ583-607 mutant was prepared, deleting a region comprising residues 583 to 607 in the Hsp90 C domain which was found to be to a large extent unstructured in the isolated Hsp90 C domain (see section 3.2). Although the deleted amino acids of Hsp90Δ583-607 are not involved in direct p53 interaction, they might serve regulatory functions as they have a higher content of serine residues that could be potential targets of phosphorylation by kinases. Thus, it was interesting to test also this variant for *in vivo* functionality.

All three mutations were introduced into Hsp90 in a p2HGal yeast expression vector that could be used for plasmid shuffling (see below). Additionally, the Δ583-607 deletion as well as a complete deletion of the unfolded C - terminal amino acids 680 to 709 (Hsp90Δ30 variant) were generated in full - length Hsp90 in a pET28a vector suited for expression of the respective proteins in *E. coli*. These two mutants were purified separately and tested *in vitro* for their ATPase activities as a control to later yeast cell experiments. A comparison with wild - type Hsp90 showed

that the Hsp90Δ30 mutant has similar ATPase activity as expected (figure 3.34, left). Thus, also the Hsp90 679-680A and 679-682A variants that should be analyzed *in vivo* could be assumed to be unaffected in their ATP hydrolysis by the mutations. An impaired Hsp90 ATPase function as a source of cellular effects potentially observed could hence be excluded. The Hsp90Δ583-607 variant, in contrast, had an ATPase activity that was moderately reduced to ∼ 70 % of the wild - type.

A testing of the generated yeast plasmids containing the Hsp90 679-680A, Hsp90 679-682A and Hsp90Δ583-607 variants *in vivo* was then carried out by Dr. Julia Rohrberg (Lehrstuhl für Biotechnologie, TUM). First, yeast strains expressing the respective Hsp90 mutants had to be obtained by the plasmid shuffling technique. In general, a genomic knockout of Hsp90 would cause a lethal phenotype. Therefore, a template strain is used in this approach that harbors a rescue plasmid constitutively expressing wild - type Hsp90 to complement for the genomic loss of Hsp90. The template strain is then transformed with the p2HGal vector containing the Hsp90 mutant of interest and an amino acid auxotrophy selection marker. The rescue plasmid can afterwards be counter - selected by transferring yeast cells onto selection medium containing 5' - FOA (5' - fluor orotic acid). Cells still containing the rescue plasmid with wild - type Hsp90 would not be viable on this medium since an enzyme, orotidine 5' - phosphate decarboxylase, additionally encoded on the rescue plasmid by the URA3 gene would convert 5' - FOA into the toxic product 5' - fluorouracil. This ensures that cells are devoid of any source of wild - type Hsp90.

The yeast strains with the respective mutant Hsp90 variants were first analyzed for their temperature dependent growth by spotting cells onto agar plates and applying a temperature gradient (figure 3.34, right). Yeast cells expressing Hsp90 679-680A and Hsp90 679-682A from a plas-

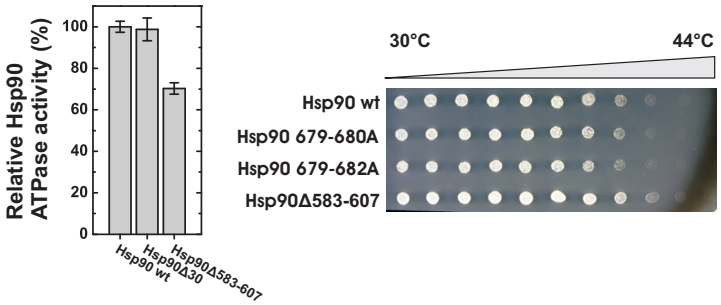

Figure 3.34: ATPase activity and temperature dependent growth of different Hsp90 C domain mutants. Left: The ATPase activity of Hsp90 is not affected by the deletion of the 30 unfolded C-terminal resides as in the Hsp90Δ30 variant. However, deletion of the loop region (residues 583 to 607) in the Hsp90Δ583-607 mutant causes a moderate reduction in ATP hydrolysis. Right: Yeast cells expressing Hsp90 containing different mutations in the C domain as indicated show similar growth as wild-type Hsp90. Growth experiments were performed by Dr. Julia Rohrberg (Lehrstuhl für Biotechnologie, TUM) who kindly provided the data for this work. ATPase measurements were done in 40 mM HEPES, 150 mM potassium chloride, 5 mM $MgCl_2$, 2 mM ATP, pH 7.5 at 30°C. Protein concentrations were 4 μM for all Hsp90 variants. The ATPase activity was determined using a coupled regenerating assay [244].

mid as the only Hsp90 source showed a growth similar to cells containing a plasmid with the wild-type Hsp90 as a control. Interestingly, cells with the Hsp90Δ583-607 mutant were even slightly more viable at elevated temperatures despite the reduced ATPase activity of this Hsp90 variant. Thus, in summary, all Hsp90 mutants tested showed a normal growth behavior.

With the yeast strains expressing the different Hsp90 C domain mutants then p53 activity assays were performed. Briefly, the cells were transformed with two additional selectable plasmids. The first encoded inducible full-length p53, the second was a reporter plasmid that had

the β - galactosidase under control of a p53 response element. Active p53 would bind to its target DNA in the response element and initiate the transcription of the β - galactosidase. In a colorimetric assay the conversion of a model substrate by the enzyme can be monitored, allowing for a relative quantification of the β - galactosidase level which is an indirect measure for the transcriptional activity of p53.

In order to test the Hsp90 679-680A, 679-682A and Δ583-607 variants for their ability to support p53 transcriptional activity, cells were grown at 30°C and p53 expression induced for 24 h. Afterwards, the relative β - galactosidase activity was determined. Compared to cells with wild - type Hsp90, the β - galactosidase activity in cells expressing Hsp90 679-680A and Hsp90 679-682A was reduced to $\sim$ 60 %, indicating a significantly lower p53 activity in these cellular backgrounds (figure 3.35). Obviously,

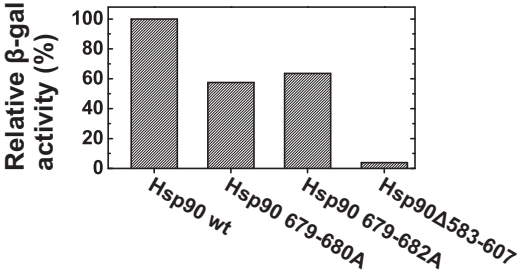

Figure 3.35: Activation of p53 *in vivo* by Hsp90 C domain mutants. The activity of β - galactosidase (β - gal) as an indirect measure for the p53 transcriptional activity was determined for yeast cells expressing different Hsp90 mutants as indicated. The mutants could support p53 activity to a much lower extent than the wild - type (wt) Hsp90. The assays were performed by Dr. Julia Rohrberg (Lehrstuhl für Biotechnologie, TUM) who kindly provided the data for this work.

the mutation of the charged p53 binding motive had strong impact on the stabilization of p53 by Hsp90. Surprisingly, in cells expressing the

Hsp90Δ583-607 variant, p53 seemed to be nearly inactive. Since in this case a region outside the p53 binding site on Hsp90 was deleted, the observed failure in p53 activation likely reflects a secondary effect as a consequence of an altered regulation of this Hsp90 mutant in general (phosphorylation, compare figure 3.14), its slightly lower ATPase activity or potentially different interactions with cochaperones.

3.9 Chaperoning of p53 DBD by Hsp90

Although the main role of Hsp90, in contrast to Hsp70, is believed to be rather a binding of substrate proteins that have nearly native - like structure and to act in the late steps of their activation, Hsp90 was demonstrated to have also a very basic chaperone function in the classical sense as it can prevent the aggregation of denatured proteins [112–114]. Exploiting this particular property of Hsp90, further assays were performed here with Hsp90 and mutants or single domains thereof, analyzing the ability of the respective proteins to suppress the thermally induced aggregation of p53 DBD *in vitro*. To this end, p53 DBD was incubated at 45°C in absence or presence of different Hsp90 variants and the formation of protein aggregates monitored by measuring light scattering at a wavelength of 360 nm. As shown, at this temperature p53 DBD already starts to slightly unfold (compare figure 3.22), concomitantly forming aggregates, whereas Hsp90 or its domains are well stable (data not shown).

First, isolated Hsp90 domains were tested for preventing p53 DBD aggregation. The constructs used comprised residues 1 to 210 for the N, residues 273 to 527 for the M and residues 528 to 709 for the C domain. Importantly, the N domain construct covered only the folded part of the domain but lacked the presumably unstructured charged linker region. Neither of the three domains could significantly reduce the p53 DBD aggregation (figure 3.36, upper panel, left). Rather, even a slightly increased aggregation was observed in these experiments under the conditions used, especially with Hsp90 C. This indicates coaggregation between the respective Hsp90 domain and p53 DBD, thus pointing at a certain interaction between the proteins, which is consistent with the binding data obtained previously (section 3.1). The comparatively higher affinity of p53 DBD for Hsp90 C might explain the moderately stronger coaggrega-

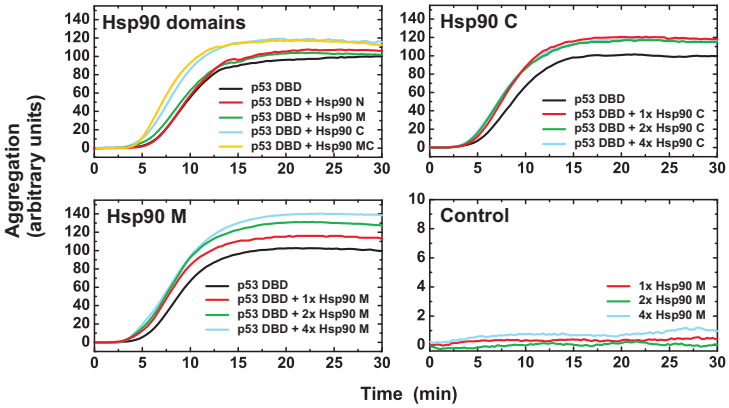

Figure 3.36: Suppression of thermally induced aggregation of p53 DBD by isolated Hsp90 domains. Upper panel, left: All isolated Hsp90 domains as well as the MC fragment are unable to suppress p53 DBD aggregation. However, slight coaggregation (in particular for Hsp90 C and MC) indicates complex formation. Upper panel, right: Even a higher molar excess of Hsp90 C over p53 DBD does not improve suppression of aggregation. Lower panel, left: Hsp90 M shows a concentration dependent increase in coaggregation with p53 DBD, indicating complex formation. Lower panel, right: Control experiment with Hsp90 M alone. The domain does not aggregate significantly under the conditions used. Measurements were done in 10 mM potassium phosphate, 1 mM TCEP, pH 7.5. 5 μM of p53 DBD was incubated at 45°C. The respective Hsp90 variants were added in an equal amount or a molar excess (2x, 4x) as indicated. Aggregation was followed by light scattering monitored at 360 nm.

tion in this case.

Additionally, an Hsp90 MC construct comprising the M and C domains was tested for its ability to stabilize p53 DBD (a plasmid for the expression/purification of this variant was kindly provided by Alina Röhl, Lehrstuhl für Biotechnologie, TUM). However, also Hsp90 MC could not prevent p53 DBD from aggregation and the light scattering profile was very similar to the measurement with Hsp90 C. These results are surprising

since the MC fragment should contain the two major p53 DBD binding sites of Hsp90 (compare section 3.1) and was thus expected to be at least partially able to suppress p53 DBD aggregation. Obviously, the Hsp90 chaperone function essentially requires regions located N - terminal of the M domain in the protein. The fact that the isolated N domain tested here lacking the charged linker, as mentioned, was not active in suppressing p53 DBD aggregation suggests that this region of Hsp90 might be of particular importance for chaperoning.

The application of a higher molar excess (up to fourfold) of Hsp90 C over p53 DBD in the assays also had no impact on p53 DBD stability. The light scattering traces for 1:1, 1:2 and 1:4 molar ratios between p53 DBD and Hsp90 C were nearly identical (figure 3.36, upper panel, right). However, in analogous experiments with Hsp90 M, a concentration dependent increase in coaggregation was visible (figure 3.36, lower panel, left), pointing at interaction of p53 DBD and Hsp90 M. Likely, due to the lower affinity, the binding between Hsp90 M and p53 DBD at a 1:1 molar ratio as used in the initial aggregation measurements was not yet saturated, in contrast to the measurements with Hsp90 C. A control experiment monitoring the aggregation behavior of Hsp90 M alone at the respective concentrations showed that the domain was substantially stable under these conditions (figure 3.36, lower panel, right). Thus, the coaggregation effects observed with p53 DBD were due to a binding between Hsp90 M and p53 DBD. The moderately higher coaggregation levels for p53 DBD and Hsp90 M compared to p53 DBD and Hsp90 C at the highest molar ratio tested might indicate an in general higher thermal stability of p53 DBD – Hsp90 C complexes due to a better solubility of Hsp90 C.

Then Hsp90 full - length variants were assessed for their ability to prevent p53 aggregation. As expected, wild - type Hsp90 could significantly

decrease thermally induced p53 DBD aggregation (figure 3.37, left). Also

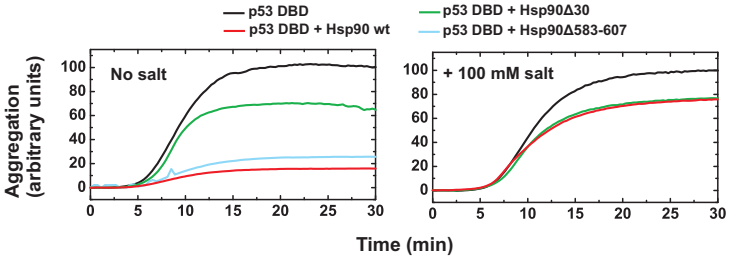

Figure 3.37: Suppression of thermally induced aggregation of p53 DBD by full-length Hsp90 variants. Left: Wild-type (wt) Hsp90 and to a slightly lower extent Hsp90Δ583-607 well suppress p53 DBD aggregation. However, deletion of the C-terminal p53 DBD binding site in the Hsp90Δ30 variant significantly reduces p53 DBD stabilization by Hsp90. Right: At higher salt concentrations, stabilization of p53 DBD by Hsp90 is reduced, wild-type Hsp90 and Hsp90Δ30 have similar ability to suppress p53 DBD aggregation under these conditions. Measurements were done in 10 mM potassium phosphate, 1 mM TCEP, pH 7.5. In the measurements shown right additionally 100 mM potassium chloride was added. 5 μM of p53 DBD was incubated at 45°C. The respective Hsp90 variants were added in a 1:1 molar ratio. Aggregation was followed by light scattering monitored at 360 nm.

the Hsp90Δ583-607 variant was well able to stabilize p53 DBD, however, to a slightly lower extent than wild-type Hsp90. Since in Hsp90Δ583-607 a region clearly not important for p53 DBD binding was deleted, here potentially secondary effects are responsible for the difference observed.

The Hsp90Δ30 mutant lacking the C-terminal p53 DBD binding site then had a strongly reduced ability to prevent p53 DBD from aggregation, supporting the high importance of this region in Hsp90 for p53 interaction. Consistently, a role of the C-terminal unfolded residues in Hsp90 for suppressing the aggregation of other Hsp90 model substrates was also reported recently[45]. Despite the deletion of the major p53 DBD site, a remaining function of Hsp90Δ30 to suppress the aggregation of p53 DBD

was found. This suggests that the chaperoning of substrate proteins involves multiple domains of Hsp90, consistent with the results from the previous binding studies (see section 3.1).

Additional aggregation assays were performed with wild-type Hsp90 and Hsp90Δ30 at higher salt concentration (100 mM potassium chloride). In this case, for both variants basically identical aggregation profiles were observed (figure 3.37, right), confirming the strong electrostatic contribution in the interaction between p53 DBD and the charged C-terminal p53 DBD binding motive. Obviously, at higher ionic strength the Hsp90 C-terminal binding site does not anymore contribute significantly to the interaction with p53 DBD under the conditions used. On the other hand, the remaining suppression of p53 DBD aggregation by Hsp90 even at increased salt concentration indicates that alternative binding sites for p53 DBD exist that are less governed by electrostatics but might rather be based on the recognition of hydrophobic regions in the substrate protein exposed upon thermal unfolding.

To analyze the importance of the M domain binding site in Hsp90 for chaperoning p53 DBD, four point mutants of full-length Hsp90 were assessed for suppressing p53 DBD aggregation. The E412K and E415K mutations were shown previously to reduce p53 DBD binding to the Hsp90 M domain (section 3.6). These two amino acid substitutions in the full-length Hsp90 were tested in aggregation assays with p53 DBD, purified proteins for the measurements were kindly provided by Dr. Marco Retzlaff, Lehrstuhl für Biotechnologie, TUM. Additional alanine replacements at the respective positions in Hsp90 were generated in this work here and likewise used in the assays. The charge reversal mutations had significant impact on the ability of Hsp90 to suppress thermally induced aggregation of p53 DBD. Hsp90 E412K, and especially Hsp90 E415K, could significantly less stabilize p53 DBD (figure 3.38, left), in agreement with a lower

p53 DBD binding of these mutants as found in fluorescence polarization and ultracentrifugation experiments (figure 3.29). In contrast, the E412A

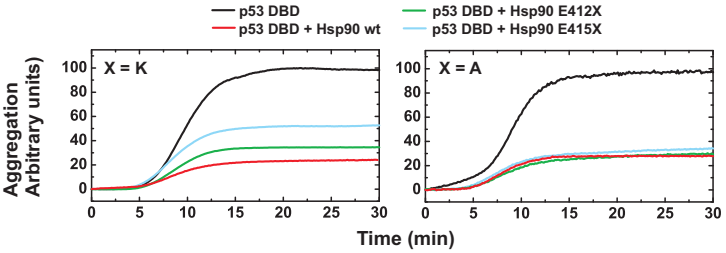

Figure 3.38: Suppression of thermally induced aggregation of p53 DBD by full-length Hsp90 M domain mutants. Left: The Hsp90 E412K and E415K charge reversal variants have impaired ability to stabilize p53 DBD under heat shock conditions compared to wild-type Hsp90, demonstrating the importance of the Hsp90 M domain for p53 DBD chaperoning. Right: Hsp90 E412A and E415A suppress the p53 DBD aggregation similar to wild-type Hsp90. Measurements were done in 10 mM potassium phosphate, 1 mM TCEP, pH 7.5. 5 μM of p53 DBD was incubated at 45°C. The respective Hsp90 variants were added in a 1:1 molar ratio. Aggregation was followed by light scattering monitored at 360 nm.

and E415A mutants were nearly as efficient in preventing p53 DBD aggregation as the wild-type Hsp90 (figure 3.38, right). Potentially, the alanine substitutions here were not sufficient to significantly reduce p53 DBD binding to the Hsp90 M. Overall, these data again show that the chaperone function is mediated by multiple domains of Hsp90 and that the M domain – despite its comparatively low affinity for the native protein – plays an important role for stabilizing p53 DBD at heat shock conditions.

Finally, the effect of nucleotides was tested to probe whether the conformational state of Hsp90 has any influence on its chaperone activity. Interestingly, when ADP and the non-hydrolysable ATP analogue AMP-PNP were added in the assays, Hsp90 was clearly less capable of prevent-

ing p53 DBD from aggregation (figure 3.39). In particular, AMP - PNP

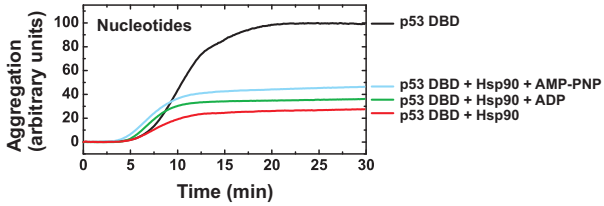

Figure 3.39: Effect of nucleotides on the suppression of thermally induced p53 DBD aggregation by Hsp90. In presence of nucleotides the suppression of p53 DBD aggregation by Hsp90 is reduced, especially fo AMP - PNP. Measurements were done in 10 mM potassium phosphate, 2 mM $MgCl_2$, 1 mM TCEP, pH 7.5. Nucleotides were added to a 1 mM concentration. 5 μM of p53 DBD and Hsp90 were incubated at 45°C. Aggregation was followed by light scattering monitored at 360 nm.

which should stabilize the closed conformation of Hsp90, decreased the Hsp90 chaperone function. Notably, in agreement with the results here, also in a previous report an ATP dependent dissociation of Hsp90 - p53 complexes was found [141]. Since the Hsp90 nucleotide state should not affect the C - terminal p53 DBD binding site but to a large extent its N and M domains, the effects observed might be due to a reduced accessibility of p53 DBD binding sites within these two domains. But also the Hsp90 linker region might play a role here.

In general, so far little knowledge exists about the structure of the charged linker located between the Hsp90 N and M domain. A secondary structure prediction for the respective Hsp90 residues from yeast (amino acids 211 to 270) at least indicates a significant helix propensity (figure 3.40). Thus, this region in principle could adopt structure, and folding/defolding transitions under certain conditions (e.g. Hsp90 nucleotide state) seem – although being speculative – possible. As outlined above,

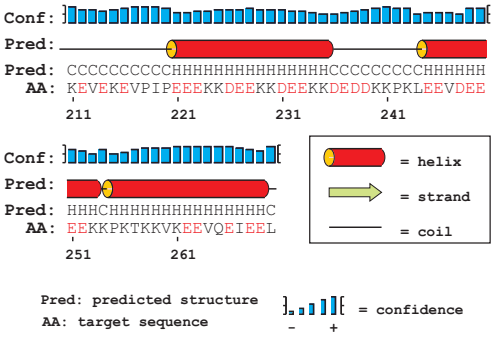

Figure 3.40: Secondary structure prediction for the yeast Hsp90 linker region using PSIPRED [234]. Residues 211 to 270 contain a high proportion of negatively charged residues (highlighted red) and show a significant propensity to form α-helical structure which might be important for the general Hsp90 chaperone activity.

neither the isolated N domain lacking the linker nor the Hsp90 MC fragment comprising the M and C domain and thus the main p53 DBD binding sites were chaperone active. This supports the assumption of the linker having a particular importance for this Hsp90 function. A similar conclusion was drawn in a recent study: A deletion of its linker region clearly reduced the ability of Hsp90 to suppress the thermally induced aggregation of two other model substrates, citric synthase and the nucleotide binding domain 1 of CFTR [45]. Additionally, in a another report it was found that yeast cells had a reduced growth under heat shock conditions when deletions within the linker region of Hsp90 were introduced, and furthermore, the *in vivo* activation of client proteins was impaired with these Hsp90 variants [44].

The Hsp90 linker sequence contains a high proportion of negatively charged residues D and E (figure 3.40), partially arranged in consecutive

amino acid stretches that resemble the charged p53 DBD binding motive found in the C domain (compare figure 3.18). In principle, these could also serve as potential p53 DBD binding sites, however, presumably only in case they lack secondary structure, as the data obtained here clearly demonstrated that p53 DBD binds such peptide motives in a random coil conformation (compare figure 3.25). At least, under non heat shock conditions the linker does obviously not play a role as a p53 DBD binding site since the Hsp90 – p53 DBD interaction can nearly fully be described by the binding between p53 DBD and the Hsp90 C domain at normal temperatures (compare figure 3.2). Assuming a role of the linker region as a p53 DBD binding site would imply the corresponding residues to loose secondary structure at heat shock conditions, thereby presenting additional negative charge motives as binding sites that are otherwise not available for p53 DBD interaction in a folded state of the linker. With nucleotide bound to Hsp90, these charge motives might by structural rearrangements then potentially be less accessible for p53 DBD binding.

3.10 Interactions of Hsp90 with α - Synuclein

A collaboration with Dr. Fabio Falsone (Institute of Chemistry, University of Graz, Austria) allowed for studying the interaction of Hsp90 with a second client protein functionally and structurally completely unrelated to p53, α - synuclein. A mutation in this small protein of $\sim$ 14 kDa was found to be involved in a hereditary form of the neuropathological Parkinson's disease [245]. Typically, so called Lewy Bodies, intracellular proteinaceous inclusions, are found in the substantia nigra of dopaminergic neurons in patients with this disease that contain α - synuclein [246]. α - synuclein belongs to the increasing number of proteins found to be natively unfolded [247]. However, it was shown to adopt α - helical structure upon interaction with acidic phospholipid membranes [248] or β - sheet structure in amyloid fibrils [249].

In vivo, α - synuclein was found to be associated with Hsp90 in filamentous inclusions of Lewy Bodies [250], therefore representing another potential Hsp90 client protein. Indeed, an interaction of α - synuclein and Hsp90 could be confirmed also *in vitro* [251]. The affinity for the binding between the two proteins was on the order of $K_d \sim 1\,\mu$M and thus, interestingly, comparable to the affinity of p53 DBD for Hsp90 as determined in this work. Obviously, Hsp90 can modulate the oligomeric state of α - synuclein in a nucleotide dependent manner: In absence of ATP, Hsp90 prevented a fibril formation of α - synuclein whereas in presence of ATP a strong acceleration of this process was observed [251]. However, so far no details are known about the interaction between Hsp90 and α - synuclein.

Here, NMR and ITC experiments were performed to identify the regions within Hsp90 that could mediate the binding of α - synuclein and to estimate the affinity of a potential complex. First, the chemical shift perturbation in the NMR spectra of isotopically labeled isolated Hsp90

domains was analyzed upon adding α-synuclein in a 1:1 molar ratio (purified unlabeled α-synuclein was kindly provided by Dr. Fabio Falsone). Neither for the Hsp90 N domain (residues 1 to 210) nor for the M domain significant peak shifts were observed in the ^{15}N-HSQC spectra (data not shown). However, in presence of α-synuclein specific chemical shift perturbation occurred for residues of the Hsp90 CΔ20 variant, indicating a binding event (figure 3.41, left). The peak shifts were into

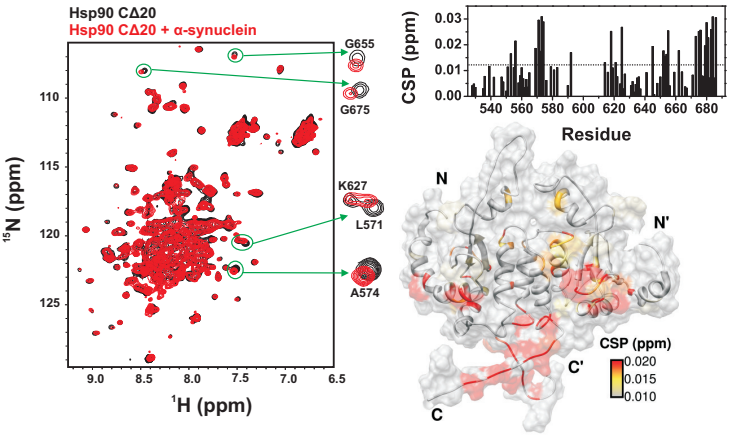

Figure 3.41: Binding between α-synuclein and Hsp90 CΔ20 monitored by NMR. Left: Overlay of ^{15}N-HSQC spectra for Hsp90 CΔ20 alone and in complex with α-synuclein. Significant peak shifts can be observed, indicating binding between the proteins. Right, upper panel: Calculated chemical shift perturbation for α-synuclein binding to Hsp90 CΔ20. The significance level (twofold average CSP) is indicated by a dashed line. Right, lower panel: Mapping of chemical perturbation upon binding of α-synuclein onto a structure model of Hsp90 CΔ20 (see section 3.2 and figure 3.14). The measurement was done at 600 MHz and 298 K in 10 mM potassium phosphate, 1 mM TCEP, pH 7.5 on a 150 μM sample of Hsp90 CΔ20. α-synuclein was added in a 1:1 molar ratio.

different directions and thus presumably not only mere buffer effects. In-

deed, residues within Hsp90 CΔ20 affected upon addition of α - synuclein seemed to cluster. Interestingly, it was again the unfolded C - terminal region of Hsp90 CΔ20 with the charge motive (amino acids ∼ 679 to 689) for which chemical shift perturbation was detected (figure 3.41, right), similar as in the case of p53 DBD binding to Hsp90 CΔ20 (compare figure 3.17). Obviously, this structure element of Hsp90 appears to have a broader relevance as a potential client protein binding site. α - synuclein was reported to preferentially interact with negatively charged lipids which leads to a stabilization of its secondary structure [248]. Thus, it could be speculated that the charge motive of Hsp90 C might possibly serve as a mimic for such lipids. Additionally, a loop region of Hsp90 CΔ20 comprising residues 568 to 574 connecting two β - strands showed stronger chemical shift perturbation when α - synuclein was added. With α - synuclein as another protein structurally and functionally unrelated to p53 targeting Hsp90 C for interaction, it might be assumed that this domain potentially plays a role for client protein binding more important than thought so far.

For comparison, also two mutant forms of α - synuclein (kindly provided as purified proteins by Dr. Fabio Falsone, University of Graz) found to be involved in the development of familial Parkinson's disease and containing the A30P [252] and E46K [253] amino acid substitutions were tested for interaction with Hsp90 CΔ20 using NMR. Also these two variants bound similarly well and at the same region to Hsp90 CΔ20 as the wild - type protein (data not shown), indicating unchanged complex formation with mutant α - synuclein.

To confirm the results obtained by NMR on the binding between α - synuclein and Hsp90 by another method and to estimate the affinity and stoichiometry of the interaction, additional ITC experiments were carried out. Surprisingly, in control experiments titrating α - synuclein from the

syringe into buffer alone, a thermogram with a sigmoidal shape similar as in case of an intermolecular binding between a protein and a ligand was observed (data not shown). This could potentially have reflected a transition in the oligomeric state of α-synuclein that was diluted from a solution with high concentration in the syringe of the instrument into the measurement cell. Indeed, α-synuclein was reported to exist as a dimer in a significant extent even at physiological pH of 7.0 [254], which is comparable to the conditions used here for ITC. Thus, effects due to a monomer – dimer equilibrium of α-synuclein might have caused the sigmoidal thermogram here. To avoid such undesired contributions in an ITC binding experiment with Hsp90 C domain constructs, α-synuclein was therefore always applied in a fixed and lower concentration in the measurement cell of the instrument whereas the respective Hsp90 C construct served as the ligand titrated from the syringe. With this setup, first Hsp90 CΔ20 was tested for binding to α-synuclein (figure 3.42). In this case, a binding between the two proteins could be detected, confirming the NMR data. A data fitting yielded an affinity of $K_d \sim 17\,\mu$M for the interaction. This is on the order of a magnitude weaker than the binding of p53 DBD to Hsp90 (compare section 3.1) but can still be regarded as significant.

The stoichiometry N found for the binding of Hsp90 CΔ20 to α-synuclein was ~ 0.5 under the conditions used, which would imply the binding of two molecules α-synuclein to one protomer of the dimeric Hsp90 C domain. This is in sharp contrast to a previous report that found a binding of one molecule α-synuclein per Hsp90 dimer [251]. A possible explanation for this discrepancy might be different buffer conditions. Also, different α-synuclein preparation conditions could be responsible. Since this protein is natively unfolded and has in general a tendency to form oligomers, it does likely not exist in a completely homogeneous structural state but

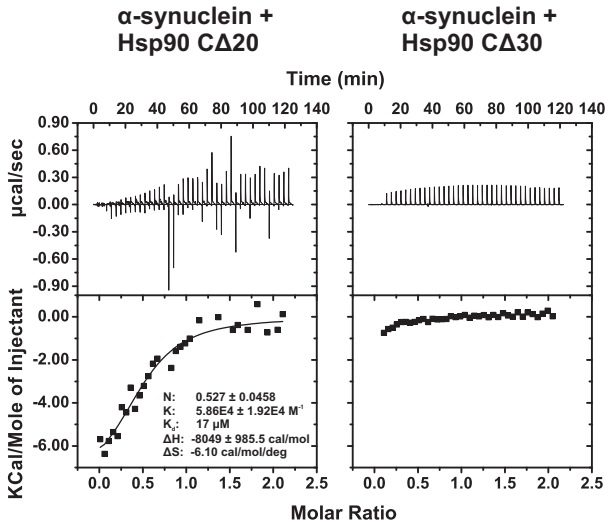

Figure 3.42: Binding of Hsp90 CΔ20 (left) and Hsp90 CΔ30 (right) to α - synuclein monitored by ITC. The upper panel shows the raw thermograms, the lower panel the integrated binding heats and the data fit for the titration with Hsp90 CΔ20. Only with Hsp90 CΔ20 a binding transition can be observed. Data fitting yields an affinity of $K_d \sim 17\,\mu$M for the interaction. 20 μM of α - synuclein in the measurement cell of the instrument was titrated with a 200 μM solution of the respective Hsp90 C domain construct at 15°C in a buffer of 10 mM potassium phosphate, 1 mM TCEP, pH 6.8.

rather in an ensemble of molecules that have potentially slightly different conformation and oligomerization properties. The unusual stoichiometry between Hsp90 CΔ20 and α - synuclein observed here with ITC could point at only a subfraction of α - synuclein being competent to bind Hsp90 CΔ20 whereas the remaining fraction – maybe due to an unfavorable structural state – might be unable to undergo complex formation. Alternatively, α - synuclein could bind as dimer to a single protomer of Hsp90

CΔ20.

As a control, α-synuclein was also titrated with the Hsp90 CΔ30 variant lacking the charged binding motive (compare sections 3.1 and 3.4). Here, no major interaction was detectable, again demonstrating the important role of the unfolded charged residues in the C domain of Hsp90 for complex formation with client proteins.

3.11 Discussion

In the past few years the knowledge about Hsp90 function has enormously increased. In particular, mechanistic aspects of the Hsp90 ATPase function have been studied intensively [46,55,60,79,81,86,88,255] as well as the regulation of Hsp90 by a large cohort of different associated cochaperones [52,71,73,87,147,167,172,185,187,193,198,256–258]. Compared to that, little data exist regarding the fundamental question of how client protein activation by Hsp90 is achieved. The number of proteins found to be potentially dependent on stabilization or activation by Hsp90 is still constantly growing, however, without knowing details about these interactions. Therefore, one aim of this work was to characterize the complex of the DNA binding domain (DBD) of the human tumor suppressor protein p53 as a model substrate with Hsp90.

Given the overall high structural and functional conservation of the Hsp90 chaperone systems from man and the yeast *Sacharomyces cerevisiae* [62,79,259], it seemed valid to perform the studies here using the well described Hsp90 homologue from yeast. Previous work carried out by Dr. Fanz Hagn (Institute for Advanced Study, TUM) could already identify binding sites for p53 DBD within the N and M domain of Hsp90 using NMR. Surprisingly, the data obtained here now indicate the existence of an additional binding site for p53 DBD located in the C domain, mediated by an unfolded stretch of negatively charged amino acids. The interaction of p53 DBD with the C domain was at least about 30 - fold stronger than with the N or M domain and thus reflects obviously the main binding site for p53 DBD on Hsp90. The identified charge motive of the C domain represents a novel client protein binding site that has not yet been described so far. This supports the assumption that the C domain might in general have more important function in the interaction of Hsp90 with

substrate proteins than previously thought. Indeed, another area within the C domain was also suggested to be involved in the binding of substrate proteins [49] which could later be confirmed for the glucocorticoid receptor ligand binding domain [140].

The region within p53 DBD that interacted with the C domain of Hsp90 was the DNA binding surface that was reported to be also involved in the binding of other proteins [260–262] and therefore seems to constitute a "promiscuous" binding site [260]. Electrostatics seem to be the main driving force in complex formation between Hsp90 C and p53 DBD, indicated by the involvement of charged residues in the binding and a strong salt dependency of the interaction. The data on the binding between p53 DBD and Hsp90 C are well in agreement with a previous report in which a small peptide, CDB3, derived from a p53 interacting protein was found to bind in a charge dependent manner and with comparable affinity to the DNA binding site of p53 DBD [263]. Potentially, the charge motive of the Hsp90 C domain might serve as a molecular mimic for the negatively charged phosphodiester backbone of the p53 target DNA.

A further analysis of the binding mode showed that the charge motive of Hsp90 C remains in its unfolded state when in complex with p53 DBD. Clearly, it is not a separate binding pocket on p53 DBD into which the Hsp90 C domain peptide would bind in a well defined conformation. Rather, mainly the negative charge of the ligand in general seems to be important for the interaction than a particular orientation of the amino acid side - chains presenting these charges. Thus, to a certain extent the binding between Hsp90 C and p53 DBD can be regarded as devoid of high specificity. However, this might possibly also apply for other Hsp90 – client protein complexes and give an explanation for the capability of Hsp90 to interact with so many different proteins structurally completely unrelated.

It seems likely that the binding site for p53 DBD in the Hsp90 C domain could potentially be targeted also by other client proteins, in particular transcription factors that have an intrinsic affinity for negatively charged ligands due to their DNA binding function. But similarly, proteins unrelated in structure and function obviously bind to this region in Hsp90, as the data obtained here with α-synuclein demonstrate. Therefore, the unfolded charge motive in the C domain might constitute a general feature of Hsp90 to mediate client protein interactions, which is supported by the high conservation of the respective residues.

The affinity of p53 DBD for the Hsp90 C domain was on the order of $\sim 2\mu$M and therefore of moderate strength. Such a rather intermediate affinity might likely be an important prerequisite for allowing complex formation of Hsp90 with the other numerous client proteins as it ensures, that these kind of interactions are more transient with comparatively faster exchange on a timescale required for cellular processes. This could potentially have hampered a structural analysis of Hsp90 – client protein complexes by crystallography so far.

Commonly, it is assumed that Hsp90 rather recognizes native-like substrates [112]. Indeed, recent binding studies with HtpG, the *E. coli* Hsp90 homologue, revealed that the chaperone selectively interacted only with the highly structured part of an otherwise unfolded staphylococcal nuclease fragment [63]. In this work, consistent with a previous report [62], also p53 DBD was found to bind in its folded state to Hsp90. This is in sharp contrast to a recent study which concluded p53 DBD to form a so called "molten globule" in complex with Hsp90 [264]. The CD and NMR data obtained here clearly demonstrated no major structural change within p53 DBD when comparing its free state and in complex with Hsp90.

In another NMR work, p53 DBD was also found to bind in an unfolded form to Hsp90 [227]. In this case, full-length Hsp90 was added to ^{15}N-

labeled p53 DBD, which led to a disappearance of NMR signals in a region of the spectrum that is typical for folded p53 DBD. Likely, in this study a simple line broadening due the large size of the complex formed was wrongly interpreted as an unfolded state of p53 DBD. Indeed, also in the NMR experiments performed here many signals in the spectrum of p53 DBD bound to the Hsp90 C domain were missing at low salt concentrations whereas signals predominantly in the middle of the spectrum and thus indicative for a lack of secondary structure content were still visible. However, upon adding more salt to the sample thus weakening the complex and driving it into faster exchange, the missing signals could all be recovered in the spectrum. This clearly points at a line broadening effect due to the molecular size causing the observed signal disappearance.

The existence of several potential p53 DBD binding sites within Hsp90 with significantly different affinities raises the question about the relevance each of them. To address this issue, chaperone assays were employed here. The fact that neither of the isolated Hsp90 domains but only the full-length protein was capable of stabilizing p53 DBD under heat shock conditions clearly indicates that multiple domains are necessary for this Hsp90 function. Interestingly, also the the Hsp90 MC fragment was inactive in preventing the thermally induced p53 DBD aggregation although it comprises both major p53 DBD binding sites of Hsp90. This points at an important role of the N-terminal parts within Hsp90 for this function, which could either be assigned to the N domain or potentially the charged linker region, whose precise function so far is not yet well understood. Notably, also in another recent study the linker was found to contribute to the chaperoning of two model substrates, citrate synthase and CFTR-NBD1 [45].

Clearly, to a large extent the interaction between Hsp90 and p53 DBD is mediated by the C-terminal binding site. A deletion of the respec-

tive residues led to a significantly reduced ability of Hsp90 to suppress p53 DBD aggregation at heat shock conditions. However, also in this case a remaining chaperone activity of Hsp90 again supports the existence and importance of alternative client protein binding sites. Indeed, mutations to targeting the presumable binding site within Hsp90 M had a pronounced effect on p53 DBD chaperoning by Hsp90. In agreement with that, previous reports likewise identified the Hsp90 M but also its N domain as being involved in substrate interactions [62,136].

There seems to be a cooperation between the different p53 DBD binding sites in Hsp90 since only the presence and integrity all of them allows for an efficient chaperoning of the substrate. The high affinity electrostatic binding site within the C domain might serve to capture p53 DBD and hold it in a native state before it binds to its target DNA. Upon heat shock, p53 DBD might by exposure of hydrophobic areas as a consequence of partial unfolding also gain increased affinity for the other potential binding sites on Hsp90 N or M and be transferred from the C domain to these alternative sites that rather interact with hydrophobic substrates.

Interestingly, the client protein binding could – at least partially – be coupled to the Hsp90 chaperone cycle. Though binding of cochaperones like Aha1 or Sti1 and p53 DBD to Hsp90 did not exclude each other, there seems to be nevertheless a certain influence of the substrate on the Hsp90 ATP hydrolysis: p53 DBD alone did not directly affect the ATP turnover of Hsp90, however, together with Aha1 its presence clearly increased the Hsp90 ATPase stimulation by this activator protein [193]. This suggests that the client protein somehow affects the rate limiting conformational transitions Hsp90 undergoes during ATP hydrolysis [86,168]. A stimulation of the Hsp90 ATPase function was also observed in two previous reports: The ligand binding domain of the human glucocorticoid receptor could enhance the weak basal ATP turnover of human Hsp90 by ~ 200 - fold [78]

and the ATPase activity of the *E. coli* Hsp90 homologue HtpG was likewise increased by a fragment of a staphylococcal nuclease substrate [63]. Therefore, it seems that the client dependent ATPase stimulation is conserved throughout the Hsp90 systems of different organisms.

A nucleotide dependence of p53 DBD chaperoning by Hsp90 additionally argues for a coupling of client protein interactions and the Hsp90 conformational state. In presence of the non - hydrolysable ATP analogue AMP - PNP which stabilizes its closed conformation, Hsp90 was less capable of suppressing the thermally induced aggregation of p53 DBD. This is in agreement with a study that reported the presence of ATP to stimulate a dissociation of Hsp90 - p53 complexes [141]. The Hsp90 nucleotide state should not affect the C - terminal p53 DBD binding site, thus these effects can likely be assigned to the N or M domain of Hsp90 or potentially the linker region connecting them.

Notably, in earlier work carried out by Dr. Franz Hagn the p53 DBD binding site on Hsp90 M was clearly found to be at the outside of the Hsp90 dimer, thus being well accessible even in the closed conformation of Hsp90 when ATP is bound. This would indeed suggest that the nucleotide effects observed in the aggregation assays performed here could be rather connected to the Hsp90 linker region or the N domain than to the M domain. But also additional binding sites for p53 DBD might exist at the inner surface of the M domain access to which is dependent on the nucleotide state of Hsp90. Such a potential binding site could be important for stabilizing of non - native p53 DBD exposing hydrophobic areas as under heat shock conditions, in contrast to the binding site at the outside of Hsp90 M which clearly interacts with p53 DBD in its native - like state and rather driven by electrostatics. Indeed, potential binding sites within Hsp90 M were identified in previous studies with other client proteins which were rather located at the inner surface of the M domain [63,134].

Chapter 4

The Hsp90 Cochaperone Sti1

4.1 Design and CD Characterization of Sti1 TPR Domains

Although crystal structures for the TPR1 and TPR2A domain from human Hop were published (see 2.1.3) [68], a more detailed structural and *in vitro* characterization of the yeast protein Sti1 is missing so far. Most data on Sti1 available in the literature currently involve mutational studies on the *in vivo* functions of the TPR domains or pull down assays to determine binding specificities of the TPR domains [147,187]. Therefore, one aim of this work was to get further insight into the properties of yeast Sti1 applying mostly *in vitro* and biophysical methods. As outlined in 2.1.2, Sti1 contains three TPR domains. Their positions within Sti1 can well be determined since TPR domains are usually very similar in size and structure and therefore a precise prediction of the TPR domain boundaries is possible. The availability of crystal structures for TPR1 and TPR2A do-

mains for the human homologue Hop [68] could be used to fix the Sti1 TPR domain boundaries according to the respective TPR domains from Hop (figure 4.1). Applying a sequence alignment between human Hop and yeast Sti1 led to Sti1 TPR domains comprising residues 1 - 129 for TPR1, which is slightly longer than the human Hop TPR1, residues 261 - 387 for TPR2A and 388 - 526 for TPR2B. Additionally, a two - domain construct TPR2A + TPR2B was designed (TPR2A - TPR2B, residues 261 - 526) and a TPR2B domain lacking the solubility helix 7 (TPR2BΔh7, residues 388 - 492). This TPR2B construct could be used to determine the influence of the solubility helix on the TPR domain properties. In principle, the helix 7 should be dispensable for the peptide binding of the TPR domain but is supposed to influence the stability of the protein (see 2.1.3). All experiments in this work involving Sti1 TPR fragments were carried out using these proteins.

The Sti1 TPR domain constructs were cloned into a pET28a expression vector fused to an N - terminal His - tag. TPR1, TPR2A, TPR2B and TPR2A - TPR2B behaved very well in isolation. They could be expressed solubly at temperatures of 25°C and purified according to standard protocols. However, TPR2BΔh7 formed inclusion bodies and had to be refolded (see section 9.9). This observation already indicated that the stability of the TPR2B domain might be affected by the deletion of helix 7. Protein yields were high with up to 80 mg pure protein per liter of cell culture for the TPR2B domain and only slightly less for TPR2A and TPR2A - TPR2B. TPR1 and TPR2BΔh7, in contrast, gave significantly lower protein amounts (~ 10 mg per liter of culture medium).

As the TPR2BΔh7 mutant formed inclusion bodies when expressed in *E.coli*, a chemical crosslink was carried out with the purified protein to determine whether this variant has a general tendency to form oligomers which could promote the formation of inclusion bodies. Adding glu-

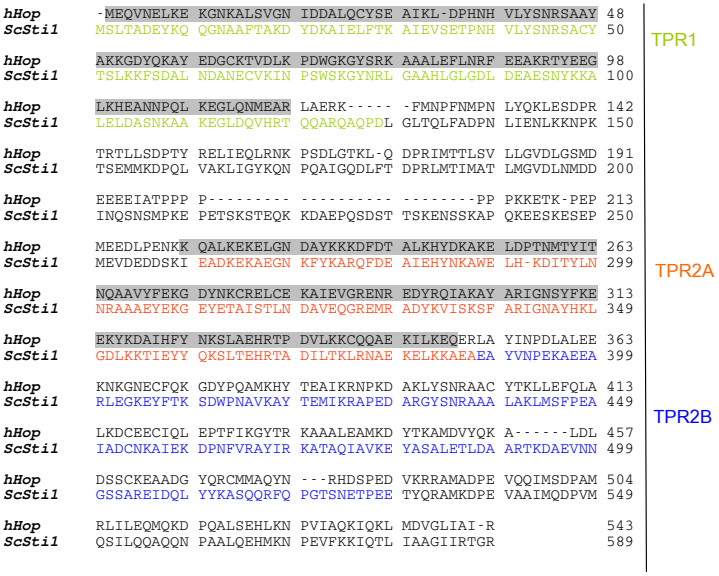

Figure 4.1: Amino acid sequence alignment for human Hop (hHop) and Sti1 from the yeast *Saccharomyces cerevisiae* (ScSti1). TPR domains of Sti1 as used in this work are marked in colors. On the right, sequence position numbers for yeast Sti1 and human Hop are given. Highlighted in gray are the location of the TPR1 and TPR2A domains in human Hop as determined by crystallographic studies [68]. NCBI reference codes of the sequences used for the alignment are NP_006810.1 for human Hop and NP_014670.1 for yeast Sti1. The alignment was generated using the program MUSCLE [265].

taraldehyde as crosslinking reagent to TPR2BΔh7 resulted in significant homo - oligomer bands (dimers, trimers, tetramers) on an sodium dodecyl sulphate (SDS) polyacrylamide gel, in contrast to a control sample with the Sti1 DP2 domain (figure 4.2). This shows that the TPR2BΔh7 mutant is clearly prone to self - association.

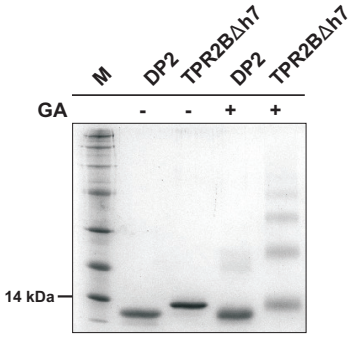

Figure 4.2: Chemical crosslink of TPR2BΔh7 to estimate oligomer forming tendency. TPR2BΔh7 and as a control the Sti1 DP2 domain were chemically crosslinked with 0.5 % glutaraldehyde. Samples were analyzed on a 12.5 % SDS-gel. The TPR2BΔh7 sample with crosslinker added shows significant oligomer formation in contrast to the control with the DP2 domain. GA = glutaraldehyde, M = marker.

The isolated purified TPR domain constructs were characterized using CD spectroscopy. All three single domains as well as the TPR2B deletion mutant and the two-domain construct showed very similar CD spectra that were typical for α-helical secondary structure as expected (figure 4.3, left). The CD thermal unfolding curves of the proteins monitored at a wavelength of 222 nm had cooperative transitions (figure 4.3, right) and the thermal melting points T_M for TPR1, TPR2A, TPR2B and TPR2A-TPR2B determined from these unfolding curves were between $\sim$ 40°C and $\sim$ 49°C as summarized in table 4.1. TPR2BΔh7 had markedly reduced thermal stability with an unfolding midpoint of $\sim$ 21°C. This explains why this mutant failed to express solubly in the temperature range between 20 and 37°C that is normally used for protein expression. Overall, the TPR

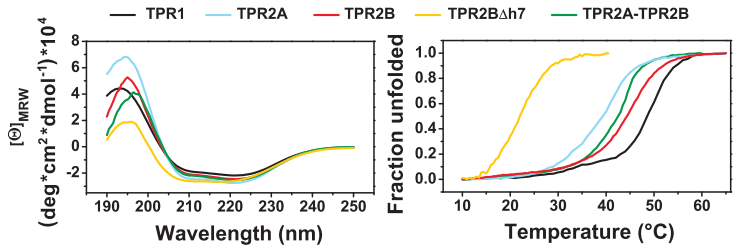

Figure 4.3: CD spectroscopic characterization of Sti1 TPR domains. Left: CD spectra for Sti1 TPR domain constructs recorded at 20°C. Right: Thermally induced unfolding of TPR domain constructs monitored by CD spectroscopy at a wavelength of 222 nm. Proteins were measured in a buffer of 10 mM potassium phosphate, 1 mM TCEP, pH 7.5.

Table 4.1: Melting temperatures (T_M) of Sti1 TPR domain constructs. Melting temperatures of Sti1 TPR domain constructs as determined from CD spectroscopy (see figure 4.3).

	TPR1	TPR2A	TPR2B	TPR2BΔh7	TPR2A-TPR2B
T_M (°C)	48.7	39.8	44.4	21.2	42.2

domain constructs seemed to be well folded and – except for TPR2BΔh7 – reasonably stable in isolation and therefore suited for further studies.

For TPR2BΔh7 additional measurements were carried out testing different buffer conditions that could potentially have a stabilizing effect on the protein because optimal sample stability would in particular be of importance for later NMR experiments with this TPR domain mutant. A variation of the buffer pH did not have any significant influence on the CD spectra and the thermal stability of the domain. Melting temperatures at all pH values tested were around 22°C (figure 4.4).

Some buffer additives were also tested on their ability to thermally sta-

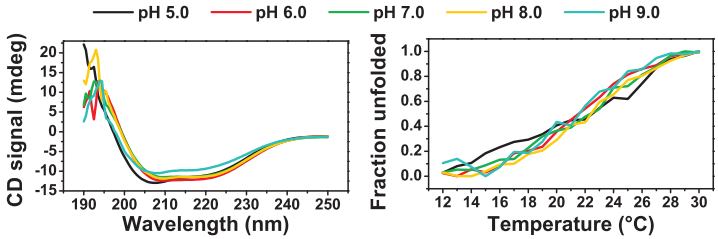

Figure 4.4: Influence of the buffer pH on the stability of the TPR2BΔh7 mutant. Left: CD spectra for TPR2BΔh7 at different buffer pH recorded at 20°C. Right: Thermally induced unfolding of TPR2BΔh7 at different buffer pH monitored by CD spectroscopy at a wavelength of 222 nm. Measurements were carried out in a buffer of 10 mM potassium phosphate, 1 mM TCEP with a pH as indicated.

bilize the TPR2BΔh7 mutant using CD spectroscopy. The results are summarized in table 4.2. The non-ionic detergent Triton X-100 (TX-100) gave some slight increase in stability at a higher concentration of 0.1 %. The zwitterionic detergent 3-[(3-cholamidopropyl)dimethylammonio]-1-propanesulfonate (CHAPS) and L-arginine had similarly a modest stabilizing effect. Trifluoroethanol (TFE) that is commonly known to induce/stabilize helical structures [266–270] was nearly ineffective. Since proteins are often stabilized by a binding of their ligand, the Hsp90 peptide MEEVD was added to the buffer in a fivefold molar excess, but also in this case the unfolding temperature was nearly unaffected. The best results could be observed with a simple addition of an increased amount of salt to the sample, shifting the melting point by ~ 5°C.

For NMR measurements not only the melting temperature of the protein is of importance but also its long term stability. Therefore, simple aggregation tests were carried out on a more concentrated sample of TPR2BΔh7 with 1 mM protein. This is a concentration on the order of a typical NMR sample used for recording triple resonance experiments.

Table 4.2: Melting temperatures (T_M) of the Sti1 TPR2BΔh7 variant under different buffer conditions. Melting temperatures were determined from CD spectroscopy at a wavelength of 222 nm. As a buffer 10 mM potassium phosphate, 1 mM TCEP, pH 7.5 was used with the respective additive. / = reference without additive, L - Arg = L - arginine, TFE = trifluoroethanol, TX - 100 = Triton X - 100, CHAPS = 3 - [(3 - cholamidopropyl)dimethylammonio] - 1 - propanesulfonate, 5x MEEVD = 5 - fold molar excess of the peptide MEEVD.

	/	1 mM L - Arg	1 % TFE	500 mM KCl	0.003 % TX - 100	0.01 % TX - 100
T_M (°C)	21.1	23.4	22.0	26.0	22.0	21.4

	0.1 % TX - 100	1 mM CHAPS	0.01 % TX - 100 1 mM CHAPS	5x MEEVD
T_M (°C)	24.9	23.5	24.7	21.5

First, again different buffer additives were tested for their ability to suppress aggregation in a short incubation assay where samples were kept at 20°C for two hours (table 4.3). At the temperature chosen, TPR2BΔh7 already starts to unfold, as determined from the CD unfolding transition (figure 4.3). Although the additives Triton X - 100 and CHAPS could slightly stabilize TPR2BΔh7 in the thermal unfolding assays (table 4.2), they could not protect the mutant from aggregation at higher concentrations used here. Also glycerol had no effect. Only the samples with the peptide ligand MEEVD (which did not significantly stabilize against thermal unfolding, table 4.2) and an increased amount of salt had no visible aggregation after two hours incubation at 20°C. Thus, adding ligand and salt were most effective in preventing aggregation.

The effect of salt and ligand was tested in another long term assay with incubation of the samples at 15°C for seven days (table 4.4). This

Table 4.3: Aggregation tendency of the Sti1 TPR2BΔh7 variant under different buffer conditions. A 1 mM solution of TPR2BΔh7 with different buffer additives was incubated at 20°C for 2 h and samples were assessed for aggregation by visual inspection afterwards. As a buffer 10 mM potassium phosphate, 1 mM TCEP, pH 7.5 was used with the respective additive. / = reference without additive, TX - 100 = Triton X - 100, CHAPS = 3 - [(3 - cholamidopropyl)dimethylammonio] - 1 - propanesulfonate, 5x MEEVD = fivefold molar excess of the peptide MEEVD.

	/	500 mM KCl	2 mM CHAPS	20 % Glycerol	0.1 % TX - 100	5x MEEVD
Aggregation	+	–	+	+	+	–

Table 4.4: Long term stability of the TPR2BΔh7 variant in the presence of salt and ligand. A 1 mM solution of TPR2BΔh7 with salt or the Hsp90 peptide ligand MEEVD was incubated at 15°C for 7 days and samples were assessed for aggregation by visual inspection afterwards. As a buffer 10 mM potassium phosphate, 1 mM TCEP, pH 7.5 was used with the respective additive. / = reference without additive.

	/	200 mM KCL	1 mM MEEVD	200 mM KCL 1 mM MEEVD
Aggregation	++	–	–	+++

temperature is slightly below the temperature at which TPR2BΔh7 starts to unfold (figure 4.3). Interestingly, ligand and salt were both able to completely suppress aggregation. However, when combined, they seem to rather enhance aggregation.

The data obtained on the TPR2BΔh7 variant show what important role the helix 7 (helix C, solubility/capping helix) plays for the stability of TPR domains in general. Including different additives in the buffer sup-

posed to stabilize proteins could not compensate for a deletion of this structure element. The conservation of residues in the solubility helix is rather loose as an alignment of respective sequences shows (figure 4.5), but commonly a high proportion of charged (Asp, Glu, Arg, Lys) and polar (Asn, Gln, Ser, Cys, Thr) residues can be found within the solubility helix, contributing to the stability of the TPR domain. The TPR2B domains of Sti1/Hop also contain Tyr residues in their solubility helices. The aromatic residue Tyr could be regarded as rather hydrophobic, but its solubility is surprisingly high and therefore it can often be found on the surface of proteins.

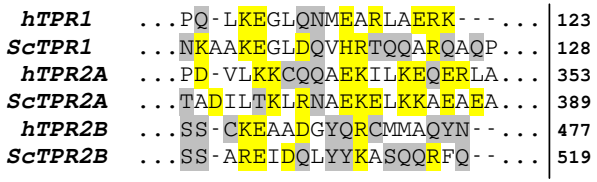

Figure 4.5: Alignment of amino acid sequences for the helix 7 (helix C, solubility/capping helix) in TPR1, TPR2A and TPR2B from yeast (*Sc*) Sti1 and human (*h*) Hop. The sequence conservation of the helix 7 is rather loose, however, a high proportion of polar (highlighted gray) and charged (highlighted yellow) residues can be found within this structure element to increase the stability of the TPR domains. NCBI reference codes of the sequences used for the alignment are NP_006810.1 for human Hop and NP_014670.1 for yeast Sti1. The alignment was generated using the program MUSCLE[265]. Sequence positions for the last residues of the respective sequences shown are given on the right.

4.2 Design and CD Characterization of Hsp70/Ssa1 Fragments

To study the interaction of Sti1 and its fragments with Hsp70, a set of single and two-domain constructs for the yeast cytosolic Hsp70 isoform Ssa1 (stress seventy-related a) were designed. This was necessary since the Ssa1 full-length protein could not be expressed in *E.coli* with reasonable yields. In addition, also NMR measurements should be performed with Sti1 and Ssa1 and therefore it was useful to have smaller fragments available for Ssa1.

Ssa1 consists of 642 residues and has a molecular weight of 69.6 kDa. It can be divided into three domains: A large N-terminal ATPase domain (~ 42 kDa), a middle/substrate binding domain (~ 18 kDa) and a C-terminal domain (~ 10 kDa) containing the peptide motive recognized by TPR domains [6]. Using structures solved for isolated domains of Hsp70 proteins from other organism and sequence alignments, the boundaries of yeast Ssa1 domains could be determined. This resulted in an ATPase domain (N) comprising residues 1-379, a substrate binding domain (M) comprising residues 380-540 and a C-terminal domain (C) comprising residues 541-642.

The single domains of Ssa1 were cloned into a pET28a expression vector fused to an N-terminal His-tag. Additionally, a two-domain fragment was prepared consisting of the middle/substrate binding and the C-terminal domain (MC, residues 380-642). All proteins could be expressed solubly in *E. coli* at 30°C, the protein yields after a standard protein purification were between 6 and 26 mg protein per liter of cell culture medium (section 9.10).

As the CD spectra showed, all Ssa1 fragments were properly folded and

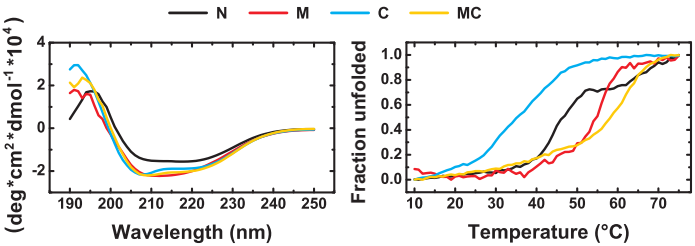

Figure 4.6: CD spectra (left) and CD thermal transitions (right) for Ssa1 fragments. All proteins are properly folded and show reasonable stability. N = N-terminal/ATPase domain, M = middle/substrate binding domain, C = C-terminal domain, MC = two-domain construct comprising middle and C-terminal domain. CD spectra were recorded at 10°C. Thermal transitions were monitored at a wavelength of 220 nm. As a buffer 10 mM potassium phosphate, 1 mM TCEP, pH 7.5 was used.

the CD thermal transitions indicated reasonable stability, with unfolding midpoints between ~ 35°C (C-terminal domain) and 62°C (two-domain construct comprising middle and C-terminal domain, figure 4.6). Therefore, all proteins could be used for further experiments.

4.3 Peptide Binding Selectivity of Sti1 TPR Domains

For the human homologue Hop a detailed analysis of the peptide binding properties of the TPR1 and TPR2A domains has been carried out in a previous study, involving calorimetric measurements and structure determination by crystallography. These experiments clearly demonstrated that TPR1 recognizes the Hsp70 and TPR2A the Hsp90 C-terminal peptide with high selectivity[68]. For the yeast homologue Sti1, however, comparable data are missing so far. Some biochemical studies indicated that the Sti1 TPR1 and TPR2A domains could have binding preferences similar to the respective domains from Hop[147,187], but these experiments gave a rather qualitative picture about the function of the Sti1 TPR domains. Especially the role of the TPR2B domain in both human Hop and yeast Sti1 could not yet be clearly determined (see 2.1.3). For Hop TPR2B only a very weak peptide binding was reported[184] and for Sti1 TPR2B biochemical data implicated this domain in binding both Hsp70 and Hsp90[147,185,187].

To get more detailed insights into the role of the individual TPR domains in organizing the Hsp70/Hsp90 complexes, a comprehensive *in vitro* study on the peptide binding behavior of Sti1 TPR domains was carried out here. Since the Sti1/Hop system is complex with three potential binding sites (TPR1, TPR2A and TPR2B) but only two ligands (Hsp70 and Hsp90), it seemed reasonable to first clarify the binding selectivities and affinities of the TPR domains in isolation. In the yeast *Saccharomyces cerevisiae* 14 different Hsp70 proteins can be found[271]. Nine of them are located in the cytosol, they can be divided into the subfamilies Ssa, Ssb, Sse and Ssz (Ss = stress seventy-related; a,b,e and z indicate the subfamiliy). The four members of the Ssa group of Hsp70 proteins are closely related to the mammalian cytosolic Hsp70s[6] and it was shown that only

the Ssa members interact with Sti1 in the cytosol[164]. They share a high sequence homology (96 % identity between Ssa1 and Ssa2, ~ 80 % identitiy between Ssa1 and Ssa3/4) and terminate with a highly conserved eight residues long peptide motive at their C-terminal ends, serving as binding site for Sti1 TPR domains (figure 4.7). For Hsp90 two isoforms exist in *Saccharomyces cerevisiae* called Hsc82 (constitutively expressed form) and Hsp82 (inducible form), as outlined in section 1.1. Similar to the Ssa members, both Hsp90 variants have a conserved peptide stretch at their C-terminus (figure 4.7).

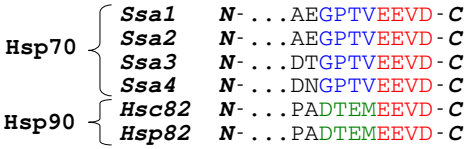

Figure 4.7: C-terminal conserved peptide motives of yeast (*Saccharomyces cerevisiae*) Hsp70 and Hsp90 members. The Hsp70 family members of yeast that interact with Sti1 called Ssa-proteins[164] have a highly conserved eight residue long peptide motive at their very C-terminal ends. Likewise, the two Hsp90 isoforms of yeast, Hsc82 and Hsp82, carry a conserved peptide stretch at their C-terminus serving as a binding site for Sti1 and other TPR cochaperones. Both, Hsp70 and Hsp90 proteins share the EEVD motive (consensus peptide, colored red). NCBI reference codes for the sequences are: Ssa1: NP_009396.2, Ssa2: NP_013076.1, Ssa3: NP_009478.1, Ssa4: NP_011029.1, Hsc82: NP_013911.1, Hsp82: NP_015084.1.

As all Sti1 interacting Hsp70 and Hsp90 proteins from yeast share the EEVD residues in their C-terminal ends, the ligand discrimination by the Sti1 TPR domains must be achieved via residues that are located upstream/N-terminally of the EEVD stretch. Therefore, a set of peptides with different length corresponding to either Hsp90 (Hsc82/Hsp82) or

Hsp70 (Ssa members) and the consensus peptide EEVD should be tested for binding to isolated Sti1 TPR domain constructs (figure 4.8). By mea-

Hsp70 peptides	**Hsp90 peptides**
N*–EEVD–*C	
N*–VEEVD–*C	***N*–MEEVD–*C***
N*–TVEEVD–*C	***N*–EMEEVD–*C***
N*–PTVEEVD–*C	***N*–TEMEEVD–*C***
N*–GPTVEEVD–*C	***N*–DTEMEEVD–*C***

Figure 4.8: Hsp70/Hsp90 peptides that were assessed for binding to Sti1 TPR domains using isothermal titration calorimetry. Eight different peptides corresponding to yeast (*Saccharomyces cerevisiae*) Hsp70 or Hsp90 C - terminal ends and the consensus peptide EEVD were tested in isothermal titration calorimetry (ITC) measurements for binding to Sti1 TPR domains.

suring peptides with consecutively increasing length, the contribution of each residue in the peptide to the binding affinity and selectivity of the respective TPR domain could be studied.

For the determination of the affinities between a peptide and a protein in principle several methods can be applied, but there are some inherent drawbacks with each of them. Fluorescence polarization has the disadvantage that the peptide ligand has to be coupled with a dye that could possibly interfere with binding. Since the TPR ligand binding grooves are rather narrow, especially the binding of the shorter peptides might be disturbed by attaching a fluorescein label. As a solution to avoid these problems, spacer residues could be introduced between the label and the real peptide. However, if the spacer is too flexible, no significant change in the polarization will be observable upon binding of the peptide.

Alternatively, an affinity for the Sti1 - peptide interactions could also be

obtained from NMR titration experiments. But this method on the other hand has some limitations with respect to the range of binding affinities that can be studied. Reliable K_d - values can only be determined from interactions on the fast NMR exchange regime, corresponding to weaker interactions in the higher μM to mM affinity range. For nM to low μM interactions the use of other methods is recommendable. The binding studies with human Hop TPR1 and TPR2A showed that the affinities of the TPR domains for their peptide ligands are in the lower μM range [68]. Therefore, it had to be assumed that also Sti1 TPR domains might bind their ligands with a comparable affinity and NMR would not be the best suited method.

Finally, isothermal titration calorimetry (ITC) seemed as most appropriate for the system to investigate as it has some major advantages compared to the two other methods. It can measure binding affinities from the higher nM up to the mM range and has the unique feature to additionally provide the thermodynamic parameters for molecular interactions. Drawbacks of ITC are the relatively high amount of protein/ligand needed for the measurement and shear forces created by the obligatory stirring in the measurement cell, which can lead to aggregation of labile proteins. As all TPR domains of Sti1 could be expressed in a sufficient amount and turned out to be reasonably stable (except for TPR2BΔh7, see section 4.1), ITC was chosen for determining binding affinities.

The amino acid composition of the conserved peptide motives, especially of Hsp90, with a higher number of acidic residues (Asp and Glu) indicated that binding of the peptides to the Sti1 TPR domains is strongly driven by electrostatic contributions. Therefore, a buffer with low salt concentration was used for all ITC measurements to obtain preferably high binding strength. All peptides used for the ITC experiments were synthesized by Dr. Oliver Demmer (Institute for Advanced Study, TUM)

and kindly provided for the measurements.

For TPR1 typical ITC binding curves could be obtained with the Hsp70 and Hsp90 peptides as shown in the two examples of figure 4.9 with octapeptides. A summary of the TPR1 binding affinities obtained by ITC

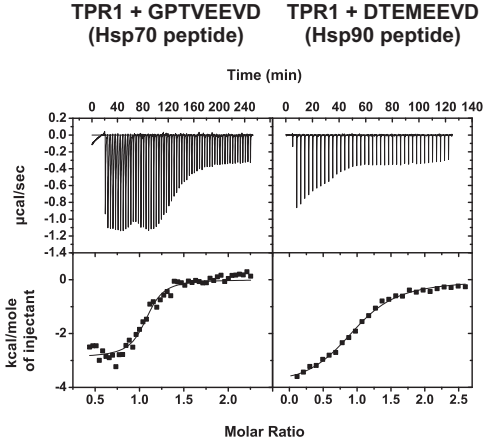

Figure 4.9: ITC measurements of TPR1 titrated with the Hsp70 octapeptide GPTVEEVD (left) and the Hsp90 octapeptide DTEMEEVD (right). 150 μM of TPR1 in the measurement cell of the instrument was titrated with a 1.5 mM solution of the respective peptide at a temperature of 20°C. As a buffer 10 mM potassium phosphate, 1 mM TCEP, pH 7.5 was used. The upper panel shows the respective thermograms with the raw data, the lower panel the integrated binding heats and fitting curves for both titrations. TPR1 shows selectivity for binding the Hsp70 peptide, the corresponding affinities for the measurements shown are 1.4 μM for the Hsp70 peptide and 13.1 μM for the Hsp90 peptide.

for the complete set of Hsp70 and Hsp90 peptides is given in figure 4.10. The Hsp70/Hsp90 consensus peptide EEVD gave only a moderate basal binding affinity with TPR1 around 18 μM. However, only one additional residue Val in the Hsp70 VEEVD pentapeptide leads to a significant in-

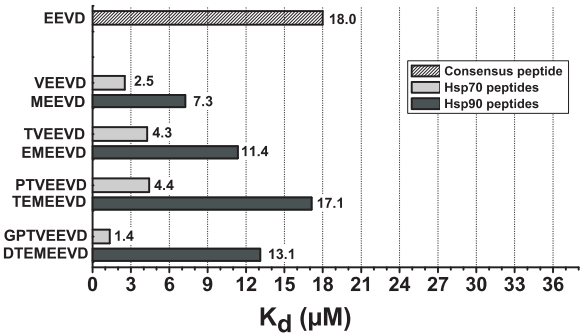

Figure 4.10: Affinities of the Sti1 TPR1 domain for a set of different Hsp70 and Hsp90 peptides as determined by ITC. 150 μM of TPR1 in the measurement cell of the instrument was titrated with a 1.5 mM solution of the respective peptide at a temperature of 20°C. As a buffer 10 mM potassium phosphate, 1 mM TCEP, pH 7.5 was used. TPR1 shows a clear selectivity for binding the Hsp70 peptides, the maximum binding affinity is obtained for the octapeptide ($K_d \sim 1.4\,\mu$M).

crease in binding strength with a drop of the K_d - value to $\sim 2.5\,\mu$M. Also the Hsp90 pentapeptide MEEVD shows stronger interaction with TPR1 compared to the EEVD consensus peptide, but the drop in the K_d here is smaller to only $\sim 7\,\mu$M. This difference between the Hsp70 and Hsp90 pentapeptide indicates a possible involvement of side - chain contacts between TPR1 and the ligand for the ligand residue position - 4 (amino acids of the ligand are numbered 0, - 1, - 2 etc. starting from the C-terminus, see also figure 2.3). Obviously, hydrophobic contacts from the - 4 Val residue in the Hsp70 peptide give a major contribution to the binding and selectivity of the TPR1 domain.

With increasing length of the Hsp70 ligand, the binding affinity is not significantly influenced, in contrast to the initial drop from the consensus peptide EEVD to the pentapeptide. There is even a slight decrease in the

binding affinity for the hexa - and heptapeptides. The maximum binding is then obtained on the octapeptide, with a further drop of the K_d from $\sim 4.4\,\mu$M for the heptapeptide to $\sim 1.4\,\mu$M for the octapeptide. Therefore, the position - 7 of the ligand together with the - 4 position seems to be of particular importance for the binding of peptides to TPR1.

In case of the Hsp90 peptides, increasing the length from penta - to heptapetides led to a reduction in the binding affinities and – compared to the Hsp70 peptides of the respective length – to a clear selectivity for the Hsp70 ligand. However, the longest Hsp90 ligand tested, the octapeptide, again binds better to TPR1 than the heptapeptide ($\sim 13\,\mu$M versus $\sim 17\,\mu$M). This observation is similar to the Hsp70 hepta - and octapeptides. In both cases the drop in the K_d is on the same order. As the Hsp70 and Hsp90 octapeptides have amino acids with significant difference in their side - chain properties at position - 7, Gly and Asp respectively, it can be assumed that the position - 7 residue is recognized via contacts to the peptide backbone by TPR1. A detailed summary of the ITC data obtained on the TPR1 domain can be found in table 4.5.

Overall, the ITC measurements show that the Sti1 TPR1 domain is clearly selective for binding the Hsp70 peptide (~ 10 - fold higher affinity for the Hsp70 octapeptide compared to the Hsp90 peptide of the same length). The maximum binding is obtained on the octapeptides and residues - 4 and - 7 of the ligand turned out to give the most significant contributions to the interaction with TPR1 additional to residues of the consensus motive EEVD.

For the TPR2A domain ITC binding curves could be obtained on the complete peptide set as well (figure 4.11). Again, as for TPR1, the consensus peptide EEVD gave only a rather weak basal binding affinity of $K_d \sim 26\,\mu$M (figure 4.12). This is on the order of TPR1 binding the respective peptide. The additional residues Val (Hsp70 peptide) and Met

Table 4.5: Summary of affinities and thermodynamical parameters for Sti1 TPR1 binding different Hsp70 and Hsp90 peptides. 150 μM of TPR1 in the measurement cell of the instrument was titrated with a 1.5 mM solution of the respective peptide at a temperature of 20°C. As a buffer 10 mM potassium phosphate, 1 mM TCEP, pH 7.5 was used. Affinity as K_a (association constant) and K_d (dissociation constant), binding enthalpy (ΔH), entropy (ΔS) and stoichiometry (N) are given for each measurement.

	N	K_a (* 10^5 M^{-1})	K_d (μM)	ΔH (cal/mol)	ΔS (cal/mol/deg)
consensus peptide					
EEVD	1.03 ± 0.08	0.55 ± 0.17	18.0	- 1757 ± 219	15.7
Hsp70 peptides					
VEEVD	0.97 ± 0.02	3.96 ± 1.06	2.5	- 5725 ± 188	6.1
TVEEVD	0.96 ± 0.04	2.34 ± 0.72	4.3	- 2121 ± 200	17.3
PTVEEVD	0.97 ± 0.01	2.26 ± 0.35	4.4	- 3170 ± 58	13.7
GPTVEEVD	1.07 ± 0.01	7.37 ± 1.94	1.4	- 2885 ± 80	17.0
Hsp90 peptides					
MEEVD	1.03 ± 0.04	1.38 ± 0.52	7.3	- 1113 ± 88	19.7
EMEEVD	1.01 ± 0.08	0.88 ± 0.22	11.4	- 2759 ± 438	13.2
TEMEEVD	1.00 ± 0.04	0.58 ± 0.10	17.1	- 2795 ± 171	12.3
DTEMEEVD	1.00 ± 0.01	0.76 ± 0.06	13.1	- 4053 ± 76	8.5

(Hsp90 peptide) in the pentapeptides led to a strong increase in the binding strength, with a drop of the K_d to 3.1 and 2.0 μM, respectively. This is similar as for TPR1, however, in the case of TPR2A the selectivity between the Hsp70 and the Hsp90 pentapeptide is only low. Increasing the length of the Hsp90 peptides from penta to heptapeptides led only to a slight drop of the K_d. In contrast to that, comparing the Hsp70 penta and hexapaptides, a significant reduction of the binding affinity could be observed (K_d 3.1 μM versus 9.3 μM). This means, starting from the hexapep-

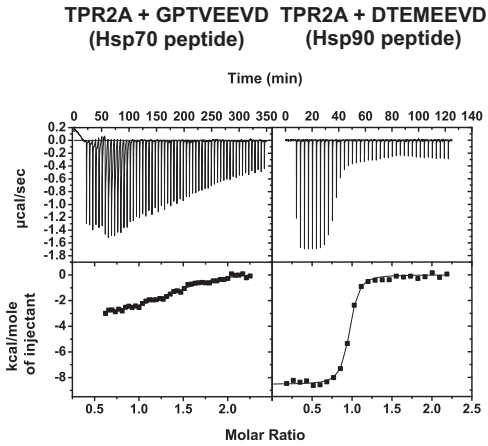

Figure 4.11: ITC measurements of TPR2A titrated with the Hsp70 octapeptide GPTVEEVD (left) and the Hsp90 octapeptide DTEMEEVD (right). 150 μM of TPR2A in the measurement cell of the instrument was titrated with a 1.5 mM solution of the respective peptide at a temperature of 20°C. As a buffer 10 mM potassium phosphate, 1 mM TCEP, pH 7.5 was used. The upper panel shows the respective thermograms with the raw data, the lower panel the integrated binding heats and fitting curves for both titrations. TPR2A shows high selectivity for binding the Hsp90 peptide, the corresponding affinities for the measurements shown are 37.0 μM for the Hsp70 peptide and 0.3 μM for the Hsp90 peptide.

tides, there is a clear selectivity of TPR2A for binding the Hsp90 peptides (9.3 μM versus 1.7 μM for the hexapeptides). The position -5 residue of the peptides therefore seems to be particularly important for the discrimination of TPR2A between Hsp70 and Hsp90. The residues at this position of the ligand (Hsp70 peptide: Thr, Hsp90 peptide: Glu) have clearly differing side-chain properties (hydrophobic versus charged), giving rise to selective recognition of the ligand by TPR2A. In both cases, for Hsp70 and Hsp90 peptides, the affinities determined for the respective hexa and

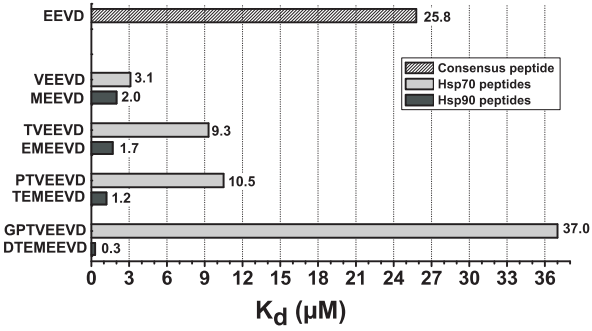

Figure 4.12: Affinities of the Sti1 TPR2A domain for a set of different Hsp70 and Hsp90 peptides as determined by ITC. 150 μM of TPR2A in the measurement cell of the instrument was titrated with a 1.5 mM solution of the respective peptide at a temperature of 20°C. As a buffer 10 mM potassium phosphate, 1 mM TCEP, pH 7.5 was used. TPR2A shows a clear selectivity for binding the Hsp90 peptides, the maximum binding affinity is obtained for the octapeptide ($K_d \sim 0.3\,\mu$M).

heptapeptides were nearly identical, which indicates that the position -6 residue does not contribute significantly to the interaction. In contrast, the -7 residue seems to be of high importance for binding and selectivity. For the Hsp70 ligand a marked decrease in the binding strength could be observed comparing the hepta and octapeptide (K_d 10.5 μM versus 37.0 μM), for the Hsp90 peptides a further increase in the affinity was obtained (K_d 1.2 μM versus 0.3 μM). This leads to an even more pronounced selectivity of TPR2A for the Hsp90 ligand. In conclusion, the ligand positions -4 and -7 seem to be most important for high affinity binding and selectivity in case of the TPR2A domain, similar as for TPR1. The data on the ITC measurements with TPR2A and the Hsp70/Hsp90 peptides are summarized in table 4.6.

Also for the TPR2B domain binding curves could be measured using

Table 4.6: Summary of affinities and thermodynamical parameters for Sti1 TPR2A binding different Hsp70 and Hsp90 peptides. 150 μM of TPR2A in the measurement cell of the instrument was titrated with a 1.5 mM solution of the respective peptide at a temperature of 20°C. As a buffer 10 mM potassium phosphate, 1 mM TCEP, pH 7.5 was used. Affinity as K_a (association constant) and K_d (dissociation constant), binding enthalpy (ΔH), entropy (ΔS) and stoichiometry (N) are given for each measurement.

	N	K_a ($*10^5$ M^{-1})	K_d (μM)	ΔH (cal/mol)	ΔS (cal/mol/deg)
consensus peptide					
EEVD	1.03 ± 0.04	0.39 ± 0.07	25.8	-2279 ± 129	13.2
Hsp70 peptides					
VEEVD	1.09 ± 0.01	3.19 ± 0.39	3.1	-5108 ± 99	7.8
TVEEVD	1.06 ± 0.01	1.07 ± 0.11	9.3	-3369 ± 52	11.5
PTVEEVD	1.05 ± 0.02	0.96 ± 0.08	10.5	-5057 ± 111	5.5
GPTVEEVD	1.04 ± 0.06	0.27 ± 0.06	37.0	-6492 ± 533	-1.8
Hsp90 peptides					
MEEVD	1.03 ± 0.01	4.97 ± 0.39	2.0	-6377 ± 44	4.3
EMEEVD	0.99 ± 0.03	5.92 ± 0.44	1.7	-8300 ± 53	-1.9
TEMEEVD	0.98 ± 0.01	8.49 ± 1.46	1.2	-6217 ± 79	5.9
DTEMEEVD	0.93 ± 0.04	35.4 ± 4.59	0.3	-8547 ± 64	0.8

ITC that indicated ligand binding with reasonable affinity (figure 4.13). This is surprising given the fact that for TPR2B from human Hop only a very weak basal peptide binding from *in vitro* experiments was reported [184]. The affinity of Sti1 TPR2B for the consensus peptide EEVD was $\sim 12\,\mu$M (figure 4.14) and thus comparable to TPR1 and TPR2A. Increasing length of the ligand from penta - to hepatpeptides led to stepwise slight increase of the binding affinity, and this applied for both Hsp70 and Hsp90 peptides. The differences in the K_d - values between the Hsp70 and

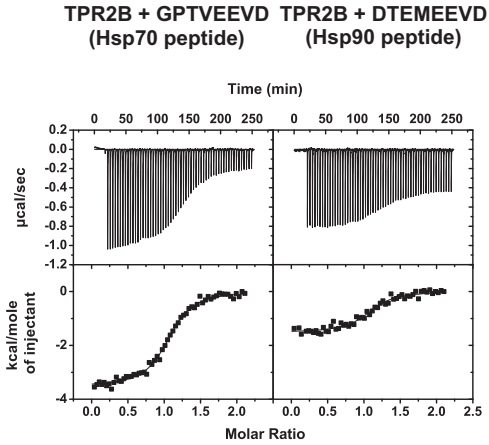

Figure 4.13: ITC measurements of TPR2B titrated with the Hsp70 octapeptide GPTVEEVD (left) and the Hsp90 octapeptide DTEMEEVD (right). 150 μM of TPR2B in the measurement cell of the instrument was titrated with a 1.5 mM solution of the respective peptide at a temperature of 20°C. As a buffer 10 mM potassium phosphate, 1 mM TCEP, pH 7.5 was used. The upper panel shows the respective thermograms with the raw data, the lower panel the integrated binding heats and fitting curves for both titrations. TPR2B shows nearly identical affinity for binding the Hsp70 and Hsp90 peptide, the corresponding K_d - values for the measurements shown are 4.2 μM for the Hsp70 peptide and 4.3 μM for the Hsp90 peptide.

Hsp90 specific peptides were rather marginal (at maximum 2.5 μM). In contrast to TPR1 and TPR2A, no significant drop in the K_d - value between the consensus peptide and the pentapeptides was observable for TPR2B. The rather moderate increase in binding affinity for increasing peptide length from the consensus peptide to the longer peptides suggests a predominant involvement of contacts only to the backbone of the ligand in the interaction between TPR2B and the peptide. This would explain the

small difference in binding affinities for the respective Hsp70 and Hsp90 peptides. Unlike for TPR1 and TPR2A, the maximum binding affinity was obtained already on the heptapeptides for both, the Hsp70 and the Hsp90 peptides. The Hsp70 and the Hsp90 heptapeptide gave nearly identical binding affinity (K_d 4.7 versus 3.8 μM), so TPR2B does not show a preferred binding selectivity. This is in sharp contrast to TPR1 and TPR2A.

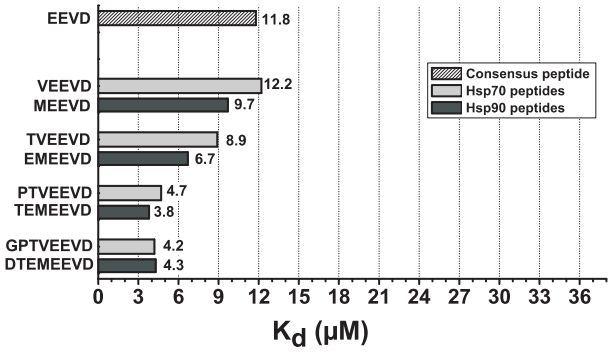

Figure 4.14: Affinity of the Sti1 TPR2B domain for a set of different Hsp70 and Hsp90 peptides as determined by ITC. 150 μM of TPR2B in the measurement cell of the instrument was titrated with a 1.5 mM solution of the respective peptide at a temperature of 20°C. As a buffer 10 mM potassium phosphate, 1 mM TCEP, pH 7.5 was used. TPR2B does not show a preferred binding selectivity, Hsp70 and Hsp90 peptides are bound with nearly identical affinity ($K_d \sim 4\,\mu$M).

Though the Hsp70 and Hsp90 peptides bound with almost similar affinity to TPR2B, the interaction mode seems to be different. As summarized in table 4.7, the enthalpy and entropy contributions to the binding of the Hsp70 and Hsp90 peptides are quite different. The Hsp70 heptapeptide (and similarly the octapeptide) has a lower entropy contribution to the binding compared to the respective Hsp90 peptide ($\Delta S = 13.5$ ver-

sus 20.4 cal/mol/deg) but the binding enthalpy term is more negative, which compensates for the more unfavorable entropy part ($\Delta H = -3173$ versus -1275 cal/mol). Thus, overall both peptides are bound with the same affinity. However, the thermodynamical parameters indicate that, compared to the Hsp90 peptide, binding of the Hsp70 peptide might be accompanied by potential larger structural changes of either TPR2B, the ligand or both.

Table 4.7: Summary of affinities and thermodynamical parameters for Sti1 TPR2B binding different Hsp70 and Hsp90 peptides. 150 μM of TPR2B in the measurement cell of the instrument was titrated with a 1.5 mM solution of the respective peptide at a temperature of 20°C. As a buffer 10 mM potassium phosphate, 1 mM TCEP, pH 7.5 was used. Affinity as K_a (association constant) and K_d (dissociation constant), binding enthalpy (ΔH), entropy (ΔS) and stoichiometry (N) are given for each measurement.

	N	K_a ($*10^5\,M^{-1}$)	K_d (μM)	ΔH (cal/mol)	ΔS (cal/mol/deg)
consensus peptide					
EEVD	1.07 ± 0.03	0.85 ± 0.17	11.8	-1225 ± 42	18.4
Hsp70 peptides					
VEEVD	1.07 ± 0.03	0.82 ± 0.19	12.2	-976 ± 38	19.2
TVEEVD	1.09 ± 0.02	1.12 ± 0.17	8.9	-944 ± 22	19.9
PTVEEVD	0.99 ± 0.01	2.11 ± 0.17	4.7	-3173 ± 30	13.5
GPTVEEVD	1.08 ± 0.01	2.38 ± 0.17	4.2	-3517 ± 29	12.6
Hsp90 peptides					
MEEVD	1.09 ± 0.03	1.03 ± 0.24	9.7	-748 ± 28	20.3
EMEEVD	1.01 ± 0.01	1.49 ± 0.17	6.7	-2239 ± 40	16.0
TEMEEVD	1.06 ± 0.02	2.62 ± 0.48	3.8	-1275 ± 26	20.4
DTEMEEVD	1.10 ± 0.02	2.35 ± 0.43	4.3	-1515 ± 32	19.4

To determine whether the Hsp70 and Hsp90 peptides in general could

adopt structure which might explain the observation of the ITC measurements on the different ligand binding modes in case of TPR2B, a secondary structure prediction was done and CD spectra were recorded. A sequence analysis for the octapeptides using the program PSIPRED[234] showed a weak tendency to form sheet structure for the Hsp70 peptide and helical structure for the Hsp90 peptide (figure 4.15, left). In both cases it were residues of the consensus motive predicted to form structure. The experimental CD spectra measured on the Hsp70 and Hsp90

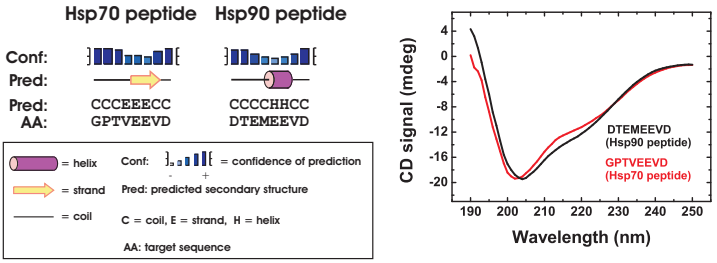

Figure 4.15: Secondary structure prediction (left) and CD spectra (right) of the Hsp70 and Hsp90 octapeptides GPTVEEVD and DTEMEEVD. A secondary structure prediction using PSIPRED[234] shows a weak tendency to form strand structure for the Hsp70 peptide and α-helix for the Hsp90 peptide. The experimental CD data show nearly identical spectra for both peptides and rather indicate low α-helical content or potentially a lack of secondary structure. CD spectra were recorded on 100 μM peptide solutions in a buffer of 10 mM potassium phosphate, 1 mM TCEP, pH 7.5 at 20°C.

octapeptides were very similar and showed curves that rather indicated a low helical content or potentially a lack of secondary structure (figure 4.15, right). Thus, in isolation the Hsp70 peptide is presumably unfolded but could in principle undergo a folding upon interaction with TPR2B, as suggested by the ITC data.

ITC measurements were also carried out with the TPR2BΔh7 mutant. The lack of the solubility helix had severe influence on its peptide binding behavior. Although binding curves could be obtained with the mutant (figure 4.16), the affinity for all peptides tested was several times lower than that of the wild-type protein (figure 4.17). The consensus

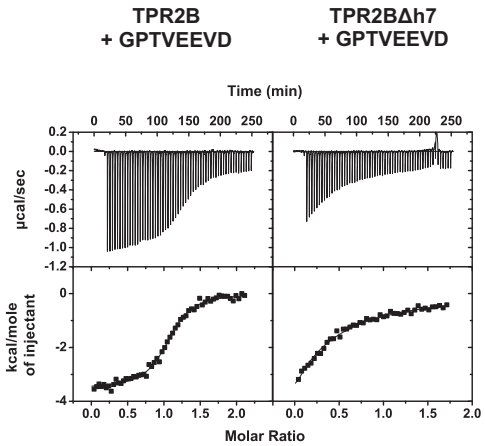

Figure 4.16: ITC measurements of TPR2B (left) and the mutant thereof, TPR2BΔh7 (right), titrated with the Hsp70 octapeptide GPTVEEVD. 150 μM of the respective protein in the measurement cell of the instrument was titrated with a 1.5 mM solution of the Hsp70 peptide at a temperature of 20°C. As a buffer 10 mM potassium phosphate, 1 mM TCEP, pH 7.5 was used. The upper panel shows the respective thermograms with the raw data, the lower panel the integrated binding heats and fitting curves for both titrations. The mutant shows a significantly lower binding of the peptide, the corresponding affinities for the measurements shown are 4.2 μM for TPR2B and 45.5 μM for the mutant TPR2BΔh7.

peptide EEVD gave a K_d of $\sim 49\,\mu$M, compared to $\sim 12\,\mu$M in case of the wild-type TPR2B domain. The Hsp70 pentapeptide then was bound weaker (K_d $\sim 83\,\mu$M) whereas the Hsp90 pentapetide was bound tighter

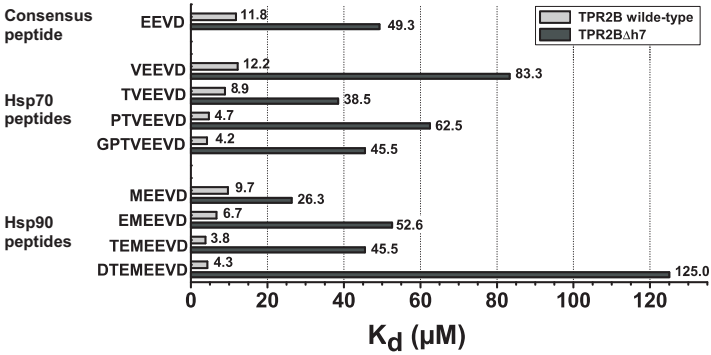

Figure 4.17: Affinities of the Sti1 TPR2BΔh7 mutant for Hsp70 and Hsp90 peptides in comparison to the wild-type domain as determined by ITC. 150 μM of TPR2B or the mutant TPR2BΔh7 in the measurement cell of the instrument was titrated with a 1.5 mM solution of the respective peptide at a temperature of 20°C. As a buffer 10 mM potassium phosphate, 1 mM TCEP, pH 7.5 was used. TPR2BΔh7 has significantly impaired peptide binding compared to the wild-type protein.

($K_d \sim 26\,\mu$M). The other Hsp70 or Hsp90 specific peptides showed an affinity that was roughly comparable to that of the consensus peptide, except for the Hsp90 octapeptide DTEMEEVD, which interacted significantly weaker ($K_d = 125\,\mu$M). The affinities and thermodynamical parameters of the ITC measurements with the TPR2BΔh7 mutant are summarized in table 4.8. Thus, contrary to expectations, the deletion of the solubility helix in the TPR2B domain has a strong impact on the peptide binding properties of the protein. Although residues that form the binding groove of the domain are not deleted by the mutation, the ligand recognition is on the order of a magnitude weaker compared to the wild-type protein. Whereas the wild-type TPR2B domain does not have a distinct selectiv-

Table 4.8: Summary of affinities and thermodynamical parameters for Sti1 TPR2BΔh7 mutant binding the different Hsp70 and Hsp90 peptides. 150 μM of TPR2BΔh7 in the measurement cell of the instrument was titrated with a 1.5 mM solution of the respective peptide at a temperature of 20°C. As a buffer 10 mM potassium phosphate, 1 mM TCEP, pH 7.5 was used. Affinity as K_a (association constant) and K_d (dissociation constant), binding enthalpy (ΔH), entropy (ΔS) and stoichiometry (N) are given for each measurement.

	N	K_a (* 10^5 M^{-1})	K_d (μM)	ΔH (cal/mol)	ΔS (cal/mol/deg)
consensus peptide					
EEVD	0.99 ± 0.11	0.20 ± 0.05	49.3	-1766 ± 274	13.7
Hsp70 peptides					
VEEVD	1.09 ± 0.10	0.12 ± 0.02	83.3	-4640 ± 517	2.9
TVEEVD	0.95 ± 0.05	0.26 ± 0.03	38.5	-3122 ± 210	9.5
PTVEEVD	0.99 ± 0.07	0.16 ± 0.02	62.5	-5709 ± 477	-0.3
GPTVEEVD	1.00 ± 0.04	0.22 ± 0.02	45.5	-3552 ± 189	7.7
Hsp90 peptides					
MEEVD	1.05 ± 0.05	0.38 ± 0.06	26.3	-3616 ± 222	8.6
EMEEVD	1.03 ± 0.08	0.19 ± 0.04	52.6	-4324 ± 511	4.8
TEMEEVD	0.98 ± 0.08	0.22 ± 0.04	45.5	-2740 ± 285	10.5
DTEMEEVD	1.05 ± 0.36	0.08 ± 0.02	125.0	-2394 ± 962	9.8

ity for the longer Hsp70 or Hsp90 peptides, the mutant binds the Hsp90 octapeptide weaker than the Hsp70 peptide of the same length. Therefore, the solubility helix seems to be not only an essential element for the stability of TPR domains but also for a proper ligand binding function.

Overall, the ITC data show that two of the Sti1 TPR domains have a clear preference for binding either the Hsp70 or the Hsp90 peptide. TPR1 binds the Hsp70 octapeptide with ∼ 10 - fold higher affinity than the Hsp90 octapeptide. TPR2A, in contrast, is selective for recognizing

Hsp90. In this case, the ligand discrimination is even more pronounced with ~ 100 - fold higher affinity of TPR2A for the Hsp90 octapeptide compared to the Hsp70 peptide of the same length. TPR1 and TPR2A seem to have ligand binding grooves that accommodate octapeptides, both domains showed the tightest binding on the eight residue long peptides. The maximum binding affinities that could be observed with TPR1 and TPR2A are quite different with 1.4 μM for TPR1 binding the Hsp70 ocatpeptide and 0.3 μM for TPR2A binding the Hsp90 octapeptide.

TPR2B seems to be largely different compared to TPR1 and TPR2A. Unlike the two other domains, TPR2B did not show a preferred ligand in the ITC measurements. The maximum affinities for the Hsp70 and Hsp90 peptides were both around 4 μM and therefore significantly lower than the affinity of TPR2A for the Hsp90 peptide and moderately lower than the affinity of TPR1 for the Hsp70 peptide. Furthermore, TPR2B appears to recognize shorter ligands, the maximum binding could be observed already with heptapeptides. Thus, Sti1 seems to have one selective Hsp90 peptide binding site with high affinity in TPR2A, one selective Hsp70 peptide binding site with moderate affinity in TPR1 and a third unselective potential Hsp70/Hsp90 peptide binding site with moderate affinity in TPR2B.

4.4 NMR Characterization of Sti1 TPR Domains

4.4.1 NMR Backbone Assignment of Sti1 TPR Domains

For further NMR studies on Sti1 TPR domains first backbone resonance assignments had to be obtained for the TPR2A and TPR2B constructs, as outlined in section 4.1. The 2D ^{15}N - TROSY spectra of TPR2A and TPR2B showed typical α - helical folds as expected for TPR domains (figure 4.18).

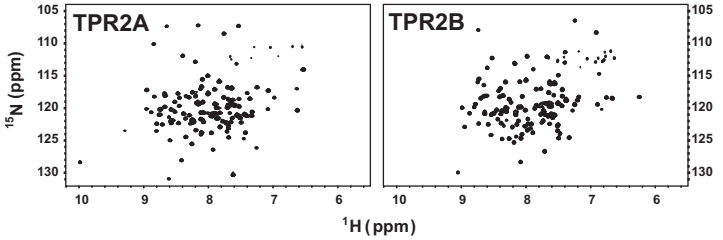

Figure 4.18: ^{15}N - TROSY spectra of Sti1 TPR2A (left) and TPR2B (right). Both domains show typical α - helical folds with excellent signal dispersion. 150 μM of TPR2A and TPR2B in a buffer of 50 mM potassium phosphate, 50 mM potassium chloride, 1 mM TCEP, pH 7.5 were measured at 293 K at 900 MHz.

The signal dispersion for both domains was surprisingly high given the fact that they consist exclusively of α - helices which normally leads to partially more overlapped spectra for proteins of comparable size. This is due to the large number of aromatic residues in both domains (13 each), likely involved in tight packing of helices within the TPR motives. As estimated from the 2D spectra, the proportion of unfolded regions in both constructs appeared to be small, which could be confirmed by chemical shift analysis and backbone dynamic measurements later. This indicated

that the domain boundaries were chosen properly and the isolated domains were well folded.

Since the 2D spectra were promising, it seemed reasonable to proceed with further experiments to obtain backbone resonance assignments. For both domains protein samples were used with a ~ 2.5 mM concentration and these were sufficiently stable to record complete data sets for the backbone assignments. As the TPR2A and TPR2B constructs had a molecular weight of ~ 15 kDa and the typical TPR domain fold with its rather open and flat molecular shape was expected to have unfavorable relaxation properties, the proteins were partially deuterated (~ 60 %) to improve the spectral quality. For both domains a set of standard triple resonance experiments was then recorded, including HNCO, HN(CA)CO, HNCA, HN(CO)CA, HNCACB and HN(CO)CACB. Additionally, also HNH - NOESY spectra were evaluated to confirm the assignments obtained by scalar coupling data.

The quality of the TPR2A and TPR2B triple resonance spectra allowed for a 100 % assignment of all non - proline backbone NH resonances for each domain (figure 4.19). Lists with the chemical shift assignments can be found under part IV (tables 11.2 and 11.3). Due to a nearly complete assignment of backbone carbon chemical shifts, a precise prediction of the secondary structure content for TPR2A and TPR2B in solution could be performed (figure 4.20). The chemical shift index (CSI) method[272] and the difference in the secondary chemical shifts of α - and β - carbons ($\Delta\delta C\alpha$ - $\Delta\delta C\beta$) agreed well and indicated the typical TPR domain fold with three TPR motives (helices A1 - B3) and a solubility helix (helix C) for TPR2A and TPR2B. Thus, the domains were well folded in solution.

For the TPR2BΔh7 mutant the ^{15}N - HSQC spectrum similarly showed a folded protein (figure 4.21). Thus, the deletion of the solubility helix did not result in a major loss of structure, confirming the CD data (figure 4.3).

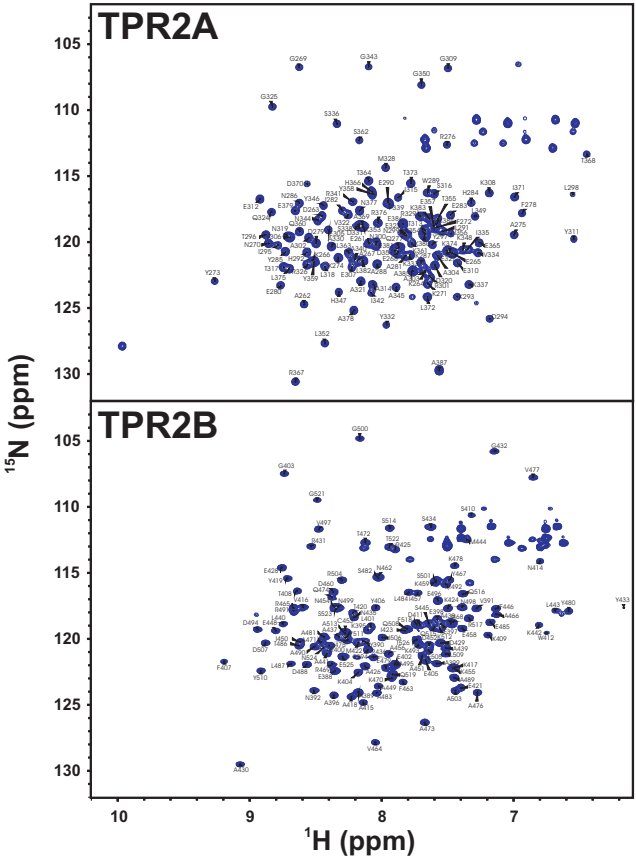

Figure 4.19: ^{15}N-HSQC spectra of the Sti1 TPR2A and TPR2B domain with backbone resonance assignment. Due to the high spectral quality, 100 % of the non-proline backbone NH resonances could be assigned for both domains. The proteins were measured in a buffer of 50 mM potassium phosphate, 50 mM potassium chloride, 1 mM TCEP, pH 7.5 at 293 K.

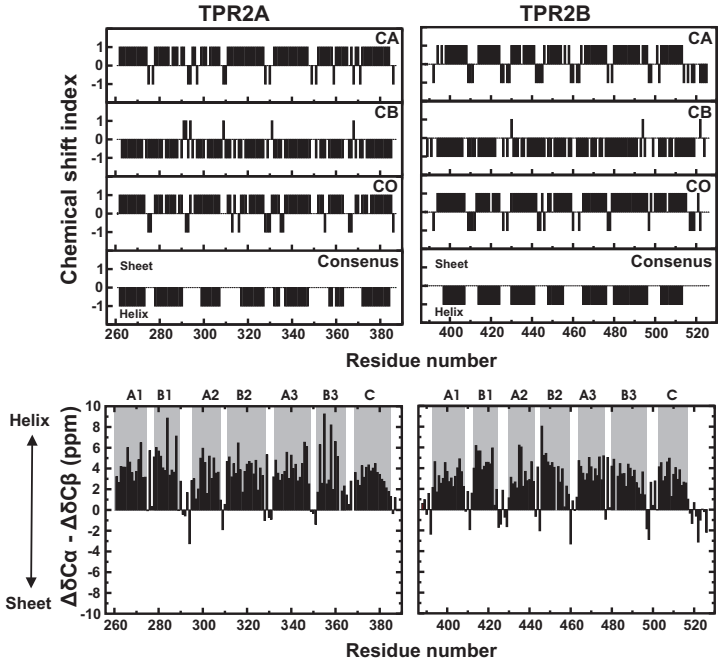

Figure 4.20: Evaluation of chemical shift data for TPR2A (left) and TPR2B (right) to determine the secondary structure content. Upper panel: Individual carbon chemical shifts for Cα (CA), Cβ (CB) and carbonyl (CO) were analyzed using the chemical shift index (CSI) method [272]. A plot for the consensus prediction combining data from the individual carbon shifts is given. In the consensus plot - 1 indicates helical structure, + 1 would be indicative of sheet structure. Lower panel: Evaluation of secondary structure content using Cα and Cβ shifts. The difference of the measured Cα and Cβ chemical shifts from the random coil shifts ($\Delta\delta$Cα and $\Delta\delta$Cβ) was calculated. On the y - axis the difference of $\Delta\delta$Cα and $\Delta\delta$Cβ is plotted, a sequence of more than five positive or negative bars indicates helical or sheet structure, respectively. The helices of the TPR motives are indicated on top of the plots.

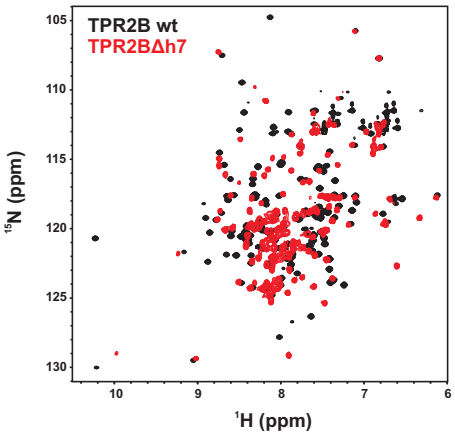

Figure 4.21: Overlay of ^{15}N-HSQC spectra for Sti1 wild-type TPR2B (black) and the mutant TPR2BΔh7 (red). Overall, the spectrum of the mutant shows a folded protein, however, many peaks are shifted significantly compared to the wild-type domain. A small portion of random coil content seems to be present in the mutant. The spectra were recorded in a buffer of 50 mM potassium phosphate, 50 mM potassium chloride, 1 mM TCEP, pH 7.5 at 293 K at 900 MHz.

However, a small portion of random coil content seemed to be present in the mutant, indicated by some peak overlap between 7.5 and 8.5 ppm, which is typical for unfolded structure, and the shape of these peaks. In general, many signals were shifted compared to the wild-type TPR2B domain. This is not surprising since the solubility helix normally tightly packs against the helices A3 and B3 in a TPR domain. Its deletion results in a significantly different chemical environment for residues in A3 and B3, leading to altered chemical shifts. A slightly changed conformation of the remaining helices in the protein could also possibly be responsible for the chemical shift differences compared to the wild-type protein.

Besides the single TPR domains, also the two-domain construct comprising TPR2A and TPR2B was characterized by NMR (see section 4.1). As this construct consists of 266 residues and has a molecular weight of 30.6 kDa, a higher protein concentration ($\sim 500\,\mu$M) in combination with TROSY-type spectra and high field strength was used to obtain reasonable spectral quality. Also measuring at moderately higher temperature (303 K) compared to the single domain constructs (293 K) was helpful to improve the signal to noise ratio. Under these conditions, however, the quality of 2D ^{15}N-TROSY spectrum of TPR2A-TPR2B even without deuteration was surprisingly high (figure 4.22). Due to the excellent sig-

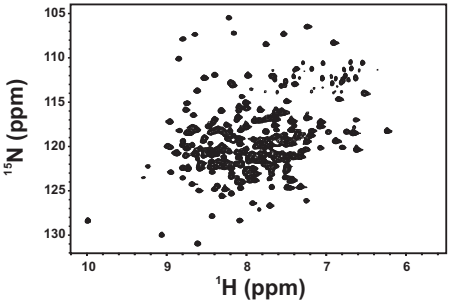

Figure 4.22: ^{15}N-TROSY spectrum of the Sti1 two-domain construct TPR2A-TPR2B. Many signals are well resolved despite the size of the protein and the exclusively α-helical fold. The spectrum was recorded on a $\sim 500\,\mu$M sample in a buffer of 50 mM potassium phosphate, 50 mM potassium chloride, 1 mM TCEP, pH 7.5 at 303 K and 900 MHz.

nal dispersion of the individual domains, many signals of the two-domain construct were well resolved despite the size of the protein and its exclusively α-helical fold (14 helices overall). The spectra of the individual TPR2A and TPR2B domains overlaid mostly very well with the spectrum of the two-domain construct (figure 4.23). This shows that TPR2A and

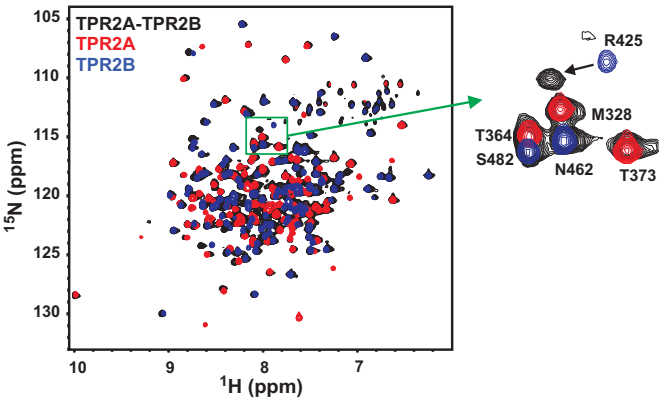

Figure 4.23: Overlay of the ^{15}N-TROSY spectra for the Sti1 TPR2A (red) and TPR2B (blue) domain with the spectrum of the TPR2A-TPR2B construct (black). Most of the signals in the spectra of the individual domains and the two-domain construct overlay very well. However, significant chemical shift differences can be observed for residues around R425 in the TPR2B domain as shown in the enlargement on the right. This indicates possible domain contacts between TPR2A and TPR2B in the two-domain construct. Proteins were measured in a buffer of 50 mM potassium phosphate, 50 mM potassium chloride, 1 mM TCEP, pH 7.5 at 303 K and 900 MHz.

TPR2B in the two-domain construct are more or less folded like in isolation. Therefore, it was possible to transfer the assignments of the individual domains nearly completely onto TPR2A-TPR2B. As expected, larger chemical shift differences between the individual domains and TPR2A-TPR2B were only observed for residues connecting TPR2A and TPR2B (residues 386-392). However, interestingly within TPR2B a few residues around R425 which are not in the region connecting the domains were also shifted significantly when comparing the spectra of isolated TPR2B and TPR2A-TPR2B (figure 4.23, enlarged region). This indicates a possi-

ble involvement of R425 in domain contacts between TPR2A and TPR2B although the rest of TPR2B seems to be largely unaffected by the presence of the second domain in TPR2A - TPR2B. In general, the lines for the two - domain construct were much broader than for the isolated domains. This is on the one hand of course due to the increased size of the two - domain construct but on the other hand could maybe also point at a rigid connection between TPR2A and TPR2B. In a case of two protein domains connected by a flexible linker and thus behaving nearly independently, the line width of both domains would be expected to be not that much different compared to the isolated domains.

4.4.2 NMR Structure Determination of the Sti1 TPR2B Domain

So far only two crystal structures for the TPR1 and TPR2A domains from the human homologue Hop have been reported [68]. The TPR2B domain from both yeast Sti1 and human Hop remains structurally uncharacterized. Therefore, a model of the Sti1 TPR2B domain based on chemical shift data, a small set of long range NOEs and residual dipolar couplings was built in this work. The analysis of the backbone chemical shift data (section 4.4.1) already indicated that TPR2B would have the typical TPR domain fold with three TPR motives and an additional solubility helix, similar to the crystal structures of TPR1 and TPR2A from human Hop. Hence, the aim here was clearly not to obtain a high resolution structure using all possible NOE information. Rather, a good model of this domain for further NMR studies should be built that provides more detailed information than a pure homology model generated without experimental data from sequence alignments and structure prediction tools.

Due to the size of the protein (139 residues) the ^{13}C - HSQC spectrum of

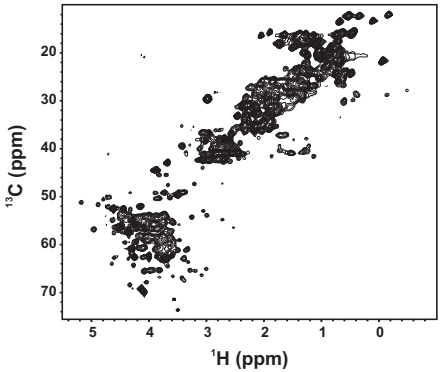

Figure 4.24: ^{13}C - HSQC spectrum of the Sti1 TPR2B domain. The spectrum is rather overlapped in some parts of the aliphatic region. The measurement was done on a $\sim$ 1 mM sample of TPR2B in a buffer of 50 mM potassium phosphate, 50 mM potassium chloride, 1 mM TCEP, pH 7.5 at 293 K and 750 MHz.

the TPR2B domain was partially rather overlapped in the aliphatic region (figure 4.24). Also methyl groups showed stronger overlap. To assign the side - chain resonances in TPR2B, a set of 3D spectra was recorded. Backbone Hα - protons were assigned from an HNHA experiment, which also provided information on the backbone ϕ - angle. $^{3}J_{HNH\alpha}$ coupling constants could be determined for 81 of 133 non - proline residues (figure 4.25) which were mostly between 2 and 6 Hz, indicating α - helical structure as expected. Overall, 74 couplings were later included in the structure calculation as some of the couplings for residues within loop regions of the protein were likely averaged due to dynamics.

Hβ - protons were assigned from an HNHB experiment. Stereospecific assignment of non - equivalent β - protons were made using information from the peak - intensity pattern in NOESY spectra and the HNHB experiment. Additionally, the HNHB experiment could be used for determining

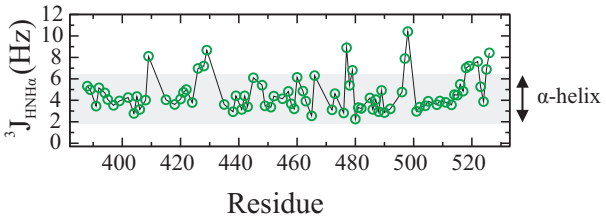

Figure 4.25: $^3J_{HNH\alpha}$ coupling constants of the Sti1 TPR2B domain. The coupling constants were mostly between 2 and 6 Hz, which is indicative of helical secondary structure.

χ_1 - side - chain torsion angles. Proton chemical shifts of longer aliphatic side - chains could be measured by running a HC(C)H - COSY experiment. Aromatic protons could be assigned using an HCH - NOESY spectrum connecting aromatic signals with Hβ - protons. The carbon shifts for the aliphatic side - chains were assigned nearly completely using information from an (H)CC(CO)NH experiment. Additional information on carbon shifts were obtained from a 3D (H)CCH - TOCSY experiment. A list with all backbone and side - chain chemical shifts can be found under part IV, table 11.3.

For structure determination, a set of 3D ^{15}N - ^{13}C - edited NOESY spectra was recorded including HNH -, NNH -, CNH -, HCH - and CCH - NOESY. Side - chain χ_1 - and χ_2 - angles were determined from the NOESY intensity pattern and using information from the HNHB experiment for the χ_1 - angle. Overall, 66 χ_1 - and 30 χ_2 - angles could be determined. For 43 β - methylene groups and the prochiral methyl groups of seven leucine and valine residues stereospecific resonance assignments were obtained. As structure calculation engine Xplor - NIH was used [233]. On the backbone ϕ - and ψ - angles TALOS [273] restraints were applied in calcula-

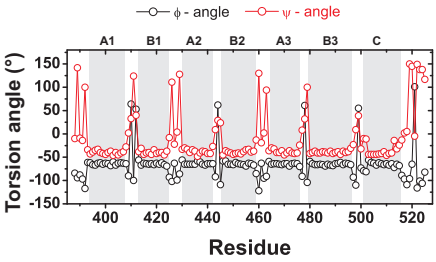

Figure 4.26: TALOS [273] prediction for ϕ - and ψ - backbone angles of the Sti1 TPR2B domain. The predicted ϕ - angles around - 60° and ψ - angles around - 40° indicate helical secondary structure. The helices of the TPR motives are given on top of the plot.

tions using the chemical shift information of Cα, Cβ, CO and Hα. For 96 residues the shift matches found by TALOS gave clustering ϕ/ψ combinations and could be included in the calculations (figure 4.26). The predicted ϕ - angles were mostly around - 60° and the ψ - angles around - 40°, indicating helical secondary structure as expected.

In the first step of the structure determination the helices of the TPR2B domain were defined by applying $^3J_{HNH\alpha}$ coupling constants, TALOS restraints and sequential HN - HN, HN - Hα and HN - Hβ NOE contacts. In further rounds of calculations then the fold of the protein was fixed by including long range NOE contacts. As crucial for the TPR structure turned out to be aromatic residues. TPR2B contains a high number of them with four phenylalanine, eight tyrosine and one tryptophan (figure 4.27, upper panel). They provided important long range contacts between the helices of the TPR motives (figure 4.27, middle and lower panel). Typically, an aromatic amino acid like tyrosine in the helix A of one TPR motive packs against a hydrophobic residue like isoleucine in the helix B of the preceding TPR motive.

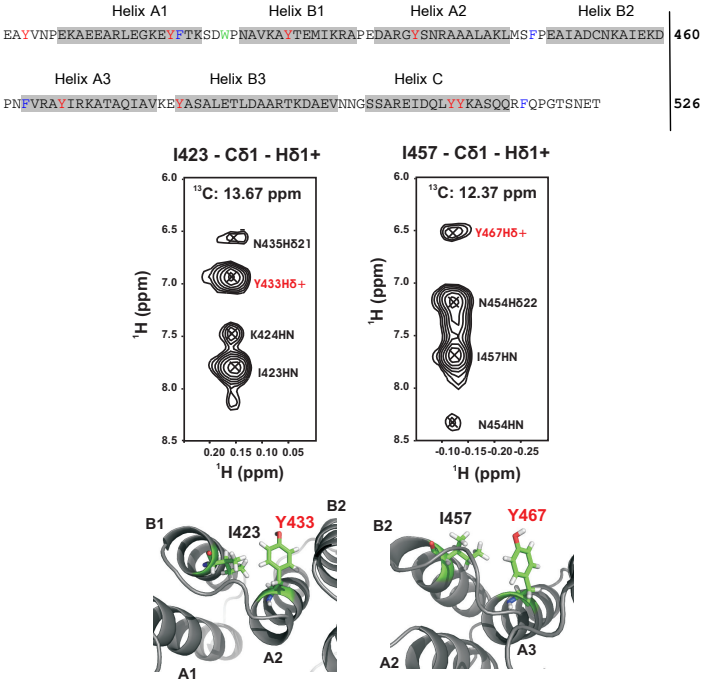

Figure 4.27: Long range contacts involving aromatic residues in the Sti1 TPR2B domain. Upper panel: TPR2B contains four phenylalanine (blue), eight tyrosine (red) and one tryptophan (green) residue. They provide important hydrophobic contacts that turned out to be crucial for the NMR structure determination. The helices of the TPR motives are indicated. Middle panel: Two strips from a HCH - NOESY spectrum are shown for the δ - methyl groups of isoleucine 423 (left) and 457 (right). Both residues are involved in hydrophobic contacts to tyrosine residues in the helix from a neighboring TPR motive as shown in the sections from the NMR structure in the lower panel. The helices of the TPR motives are indicated.

For refining the TPR2B structure, a set of backbone NH residual dipolar couplings (RDCs) was included in the last step of the calculation. To obtain partial orientation of the protein, a solution of Pf1 phages [274] was added in a final concentration of 12 mg/ml to the buffer. NH RDCs were measured by recording in - phase/antiphase J - coupled spectra [275] on a reference sample without alignment medium and on an aligned sample (figure 4.28, upper panel). Overall, 122 couplings could be determined that were ranging from - 40 to + 40 Hz. A plot of the NH RDCs against the residue number shows a typical periodicity (~ 3.6) as expected for a helical protein (figure 4.28, lower panel).

With the PALES software [276] the alignment tensor could be determined for the TPR2B RDC measurements as summarized in table 4.9, allowing for utilization of the couplings in the structure refinement. A plot for

Table 4.9: Parameters of the alignment tensor for the Sti1 TPR2B domain in Pf1 phage medium as determined by using the PALES software [276]. RDCs were back - calculated from the regularised average NMR structure (figure 4.29) and compared to the experimentally determined RDCs. The linear correlation coefficient R can have values between - 1 (no correlation) and + 1 (perfect correlation). Partial alignment of TPR2B was obtained by adding Pf1 phages in a final concentration of 12 mg/ml to the buffer (50 mM potassium phosphate, 50 mM potassium chloride, 1 mM TCEP, pH 7.5). Measurements were done at 900 MHz and 293 K.

Parameter	Value
Rhombicity	0.17
Da (HN) (Hz)	22.90
Correlation R	0.98
Q Saupe	0.12

the correlation between RDCs back - calculated from final regularised average NMR structure and the experimentally determined RDCs showed a good agreement (figure 4.32) with a high correlation coefficient R of

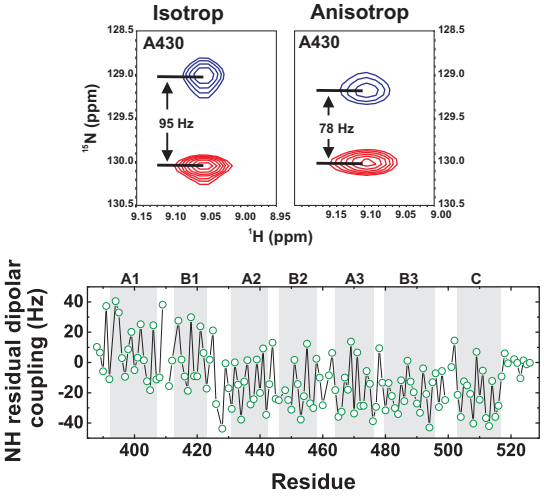

Figure 4.28: NH residual dipolar couplings of the Sti1 TPR2B domain. Upper panel: Individual upfield (blue) and downfield (red) components of the signal for residue A430 for the sample without alignment (isotropic case, left) and with partial alignment (anisotropic case, right) obtained by measuring in-phase/antiphase J-coupled spectra [275]. The dipolar coupling for A430 is -17 Hz. Lower panel: Plot of TPR2B NH residual dipolar couplings against the sequence position. A typical periodicity of ~ 3.6 can be observed due to the helical secondary structure of TPR2B. The helices of the TPR motives are indicated on top of the plot. Partial alignment of TPR2B was obtained by adding Pf1 phages in a final concentration of 12 mg/ml to the buffer (50 mM potassium phosphate, 50 mM potassium chloride, 1 mM TCEP, pH 7.5). Measurements were done at 900 MHz and 293 K.

0.98 (R can take values between -1 for no correlation and +1 for perfect correlation, table 4.9).

Due to spectral overlap caused by the size of the protein it was difficult to obtain reliable long range NOEs for the TPR2B domain. Therefore, overall a rather small number of 68 unambiguous long range NOEs was

finally used for the structure calculation (table 4.10). As in general often little long range contacts in helical proteins are found and helices have a tendency to shift easily against each other, it was difficult to fix the position of the three TPR motives relative to each other. This transferred into a higher overall backbone RMSD (root mean square deviation) of ~ 1.53 Å for the structured part of the domain (residues 393 to 499 and 507 to 516) in the final ensemble of the ten lowest energy conformers (figure 4.29, upper panel).

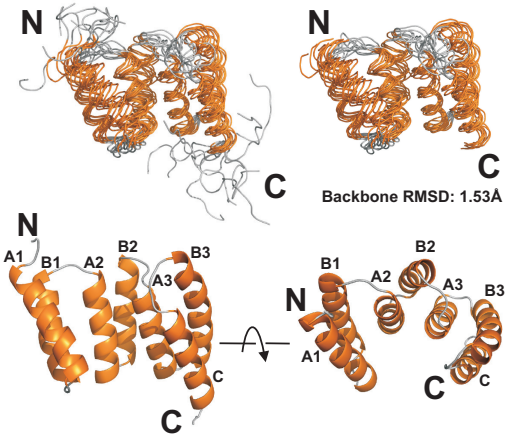

Figure 4.29: Low resolution structure of the Sti1 TPR2B domain determined by NMR spectroscopy. Upper panel: Overlay of the ten lowest energy conformers of TPR2B in ribbon representation. The left side shows all residues of the construct used for the NMR structure determination (amino acids 388 - 526), on the right side the flexible N - and C - terminal ends are hidden for clarity. The backbone RMSD within the structured parts of the domain is 1.53 Å. Lower panel: Average structure of the ten lowest energy conformers of TPR2B after energy minimization in cartoon representation. The right side shows the structure rotated by 90° around the horizontal axis. Helices of the TPR motives are labeled. The N - and C - terminus are indicated in each panel.

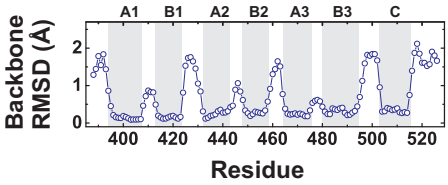

Figure 4.30: Positional backbone RMSD of the Sti1 TPR2B final structure ensemble. The average backbone RMSD for each residue of TPR2B was calculated from the ten lowest energy conformers of the final NMR structure ensemble. The structured elements of the domain have an average backbone RMSD of ~ 0.3 Å, loops between the helices and N - and C - terminus have higher RMSD, as expected.

For the structure determination a TPR2B construct was used comprising residues 388 to 526, however, residues 388 to 392 and 517 to 526 turned out to be unstructured. TPR2B showed the typical TPR domain fold: It consists of three TPR motives, each comprising two helices A and B arranged in tandem repeats, and a solubility helix C (figure 4.29, lower panel). The orientation of the TPR motives leads to a right - handed twist of the domain. All secondary structure elements in the protein were well defined. The average positional backbone RMSD for residues within the helices of TPR2B was around 0.3 Å, loops between the helices and the N - and C - terminus had higher RMSD, as expected (figure 4.30). A summary of the structural statistics for the ten lowest energy conformers of TPR2B can be found in table 4.10.

The electrostatic potential calculated for the TPR2B domain is strongly positive within the putative peptide binding groove, which is typical for Hsp70/Hsp90 binding TPR domains recognizing the negative EEVD motive (figure 4.31). By this charge complementarity, a basic anchoring of the ligand can be achieved in the TPR2B peptide binding site.

To evaluate the approach of calculating low - resolution protein struc-

Table 4.10: Structural statistics for the ten lowest energy NMR structures of the Sti1 TPR2B domain.

	SA[a]	<SA>$_r$
RMSD from distance restraints (Å)[b]		
all (462)	0.098 ± 0.080	0.042
intraresidual (220)	0.044 ± 0.008	0.042
sequential (129)	0.044 ± 0.013	0.032
medium (9)	0.051 ± 0.031	0.025
long (68)	0.212 ± 0.233	0.066
RMSD from dihedral restraints (deg) (288)	0.223 ± 0.041	0.475
RMSD from J-coupling restraints (Hz) (74)	1.211 ± 0.108	1.149
H-bond restraints (Å/deg) (76)[c]	2.14 ± 0.38 / 20.3 ± 8.9	2.25 ± 0.23 / 20.7 ± 7.9
RDC restraints (Hz) (122)	4.07 ± 0.18	4.69
Deviations from ideal covalent geometry		
Bonds (Å*10^{-3})	5.23 ± 0.15	3.90
Angles (deg)	0.67 ± 0.02	0.79
Impropers (deg)	3.65 ± 0.24	0.93
Ramachandran map regions(%)[d] **(ordered residues)**[e]	87.0/10.4/2.6/0.0	87.0/7.8/5.2/0.0

	SA versus <SA>		SA versus <SA>$_r$	
Atomic RMSD (Å)[f] **(ordered residues)**[e]	backbone	all	backbone	all
	1.53 ± 0.28	2.05 ± 0.27	1.82 ± 0.30	2.44 ± 0.27

[a] Structures are labeled as follows: SA = set of ten final simulated annealing structures; <SA> = the mean structure calculated by averaging the coordinates of SA structures after fitting over secondary structure elements; <SA>$_r$ = the structure obtained by regularising the mean structure under experimental restraints.

[b] Numbers in brackets indicate the number of restraints.

[c] H-bonds were restrained by treating them as pseudocovalent bonds. Deviations are expressed as average distance/average deviation from linearity for restrained H-bonds.

[d] Using the program PROCHECK-NMR. Percentages are for residues in allowed/additionally allowed/generously allowed/disallowed regions of the Ramachandran map.

[e] Ordered residues are defined as residues 393-499 and 507-516.

[f] Based on heavy atom superpositions.

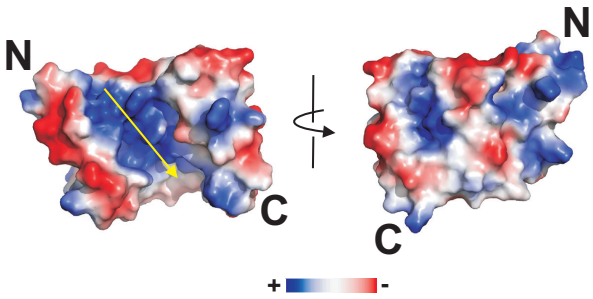

Figure 4.31: Electrostatics of the Sti1 TPR2B domain. Electrostatic potential of the TPR2B domain determined using the program PyMOL. Blue color indicates positive, red color negative potential. The left side shows a view onto the ligand binding groove, the putative orientation of the peptide ligand from its C- to N-terminus is indicated with a yellow arrow. The right side shows the domain rotated by 180° around the vertical axis. Within the ligand binding groove, a highly positive potential can be observed that mediates binding of the EEVD consensus motive via electrostatic charge complementarity. The N- and C-terminus are indicated.

tures by using only sparse NOE data combined with chemical shift analysis and RDC data, additionally a pure homology model of TPR2B was built for comparison. Based only on sequence information, a structure for the TPR2B domain was obtained using the program MODELLER [277]. The algorithm performs a search for similar amino acid sequences and generates 3D models using structures available for related sequences found in the search. Figure 4.32 (upper panel, left) shows an overlay of the experimentally determined NMR structure and the model for TPR2B. The overall fold of TPR2B was predicted correctly by the model. However, there were some differences compared to the experimental structure. In general, the orientation of the TPR motives relative to each other differed slightly from the NMR structure, especially for the terminal helix C. Also,

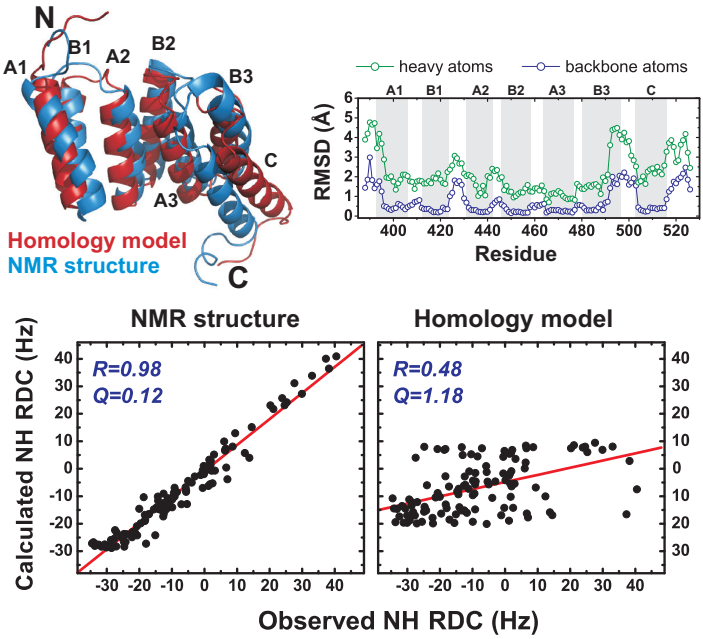

Figure 4.32: Comparison of the experimental Sti1 TPR2B NMR structure with a homology model. Upper panel left: Overlay of the TPR2B NMR structure (blue) with a model obtained using the program MODELLER [277]. Although the overall fold is predicted correctly by the model, the length of the helices and their relative orientations differ partially significantly from the NMR structure. The helices of the TPR motives are indicated. Upper panel right: Positional RMSD of backbone atoms (blue) and all heavy atoms (green) for the comparison of the experimental NMR structure and the homology model of TPR2B. Major differences can be observed for loops between the helices and for helix B3. The secondary structure elements as determined experimentally are indicated. Lower panel: Comparison of RDCs back-calculated from the TPR2B NMR structure (left) and the homology model (right) with experimentally determined RDCs. The correlation coefficient R and the quality factor Q are given for both fits. R- and Q-values are significantly better for the NMR structure, indicating higher reliability for the NMR structure despite its relatively low resolution.

the helix B3 of the domain was shorter in the model.

A residue-wise RMSD analysis showed that the model and the NMR structure disagreed most for flexible loops between the helices, as expected (figure 4.32, upper panel, right). Additionally, a higher RMSD was observed for the end of helix B3 as a consequence of its wrong length in the model. The average positional backbone RMSD between the model and the NMR structure for the secondary structure elements as determined experimentally was ~ 0.5 Å.

To further estimate the reliability of the model and the NMR structure, RDCs were analyzed (figure 4.32, lower panel). Couplings were back-calculated from the homology model and the NMR structure and compared to the measured couplings. The NMR structure had a correlation coefficient R close to 1 (0.98), which pointed at a good agreement between the calculated structure and the experimental data (R ranges from -1 for no correlation to $+1$ for perfect correlation). The model, in contrast, yielded an R-value of only 0.48. Also, the quality factor Q for the model was worse (1.18 versus 0.12 for the NMR structure). This indicated that the model was globally not extremely far off the real structure but might be wrong to some extent in a more detailed view.

In conclusion, the TPR2B model can be regarded as an acceptable structure conveying a reasonable picture of the molecule if experimental data are missing. However, the NMR structure obtained here with a smaller set of experimental data appears to be by far more reliable and provides significantly more details than the model.

4.4.3 Fast Backbone Dynamics of Sti1 TPR Domains

The backbone dynamics of the isolated TPR2A and TPR2B domains as well as of the two-domain construct TPR2A-TPR2B were analyzed by

measuring the $\{^1H\}$-^{15}N heteronuclear NOE (hetNOE). It reports on the movement of backbone NH groups on the fast NMR timescale (ns to ps range). TPR2A and TPR2B both showed rather uniform dynamics (figure 4.33). HetNOE values were mostly around 0.8 within the secondary structure elements, which indicates comparatively high rigidity of the protein backbone. Thus, all helices seem to be well structured in solution, including the small loops connecting the helices. Only the N- and C-termini of the domains showed increased flexibility. For TPR2B, the residues 388 to 392 and 518 to 526 of the construct had NOE values lower than 0.65 as they were unfolded. Overall, these data confirm that the domain boundaries were chosen correctly as both TPR2A and TPR2B contain only a small portion of unfolded residues at their termini.

4.4.4 The Oligomeric State of Sti1 TPR Domains

The literature contains contradicting reports about the oligomeric state of Sti1. Some works proposed Sti1 to be a dimer in solution [147,166] while others found it to be a monomer [278]. In particular, the TPR2A domain was suggested as a dimerization site within Sti1 [147]. To determine whether TPR2A indeed could mediate Sti1 dimerization, NMR diffusion experiments (DOSY, diffusion ordered spectroscopy) were carried out using the TPR2A and TPR2B domains. Both domains have comparable size (TPR2A: 14.8 kDa, TPR2B: 15.6 kDa) and very similar structures. Consequently, their hydrodynamic radii should also be very similar and their diffusion coefficients D should have nearly the same magnitude. However, if TPR2A should indeed behave as a dimer in solution, then it would be expected to have a significantly lower diffusion coefficient D compared to TPR2B.

Fitting exponential intensity decay curves for several selected NMR

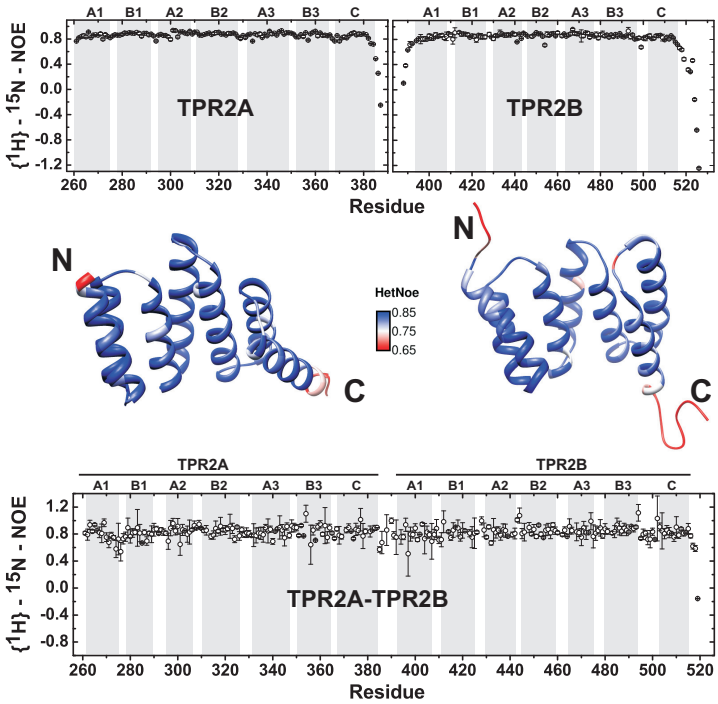

Figure 4.33: Fast backbone dynamics of the Sti1 TPR2A and TPR2B domains (upper panel) and the TPR2A-TPR2B construct (lower panel) determined by measurement of the $\{^1H\}$-^{15}N heteronuclear NOE (hetNOE). TPR2A and TPR2B show rather uniform dynamics, hetNOE values around 0.8 within the structured parts indicate comparatively high rigidity. Only N- and C-termini of the domains have increased flexibility. The measurements were done at 750 MHz and 293 K for TPR2A and TPR2B and 900 MHz and 303 K for TPR2A-TPR2B, respectively, in 50 mM potassium phosphate, 50 mM potassium chloride, 1 mM TCEP, pH 7.5. The TPR secondary structure elements as determined by NMR chemical shift data are given on top of the plots. HetNOE values were color-coded mapped onto the crystal structure of TPR2A (middle panel, left, kindly provided by Dr. Melissa Gräwert, Lehrstuhl für Biochemie, TUM) and the NMR structure of TPR2B (middle panel, right). The color code is given next to the structures.

signals of the TPR2A domain consistently gave diffusion coefficients D around $1.0*10^{-10}\,m^2/s$ (figure 4.34). For comparison, diffusion mea-

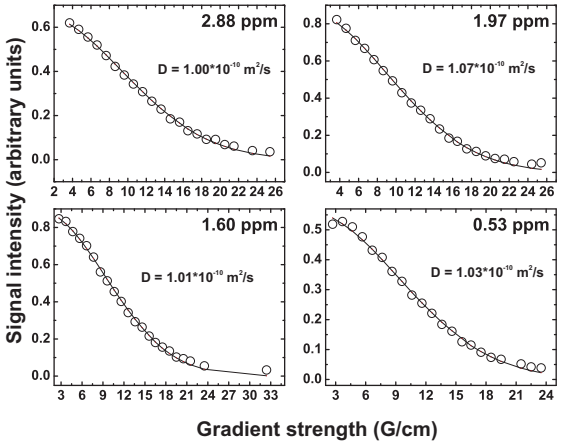

Figure 4.34: Intensity decay curves for selected NMR signals of TPR2A obtained from DOSY measurements. Fitting the data with an exponential function consistently gives diffusion coefficients around $1.0*10^{-10}\,m^2/s$. 150 μM of TPR2A was measured in 50 mM potassium phosphate, 50 mM potassium chloride, 1 mM TCEP, pH 7.5 at 293 K and 600 MHz. As gradient length (*little delta*, δ) 4 ms were used, the diffusion time (*big delta*, Δ) was set to 500 ms.

surements were then also done with TPR2B under identical conditions as they were used for TPR2A (figure 4.35). Again, the diffusion coefficients D were around $1.0*10^{-10}\,m^2/s$. This shows, that TPR2A and TPR2B behave nearly identical in solution. This could mean that either both domains behave as a dimer or both are monomeric. Evaluating intensity decay curves for five different NMR signals and averaging the obtained diffusion coefficients yielded values D of $1.02*10^{-10}\,m^2/s$ for TPR2A and likewise $1.02*10^{-10}\,m^2/s$ for TPR2B (table 4.11).

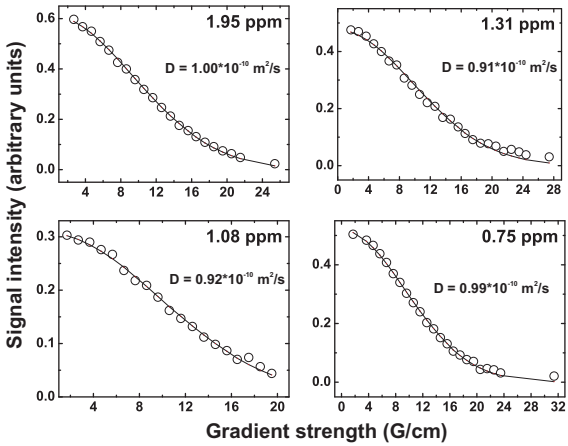

Figure 4.35: Intensity decay curves for selected NMR signals of TPR2B obtained from DOSY measurements. Fitting the data with an exponential function gives diffusion coefficients around $1.0*10^{-10}\,m^2/s$, which is comparable to the diffusion coefficients determined for TPR2A (compare figure 4.34). 150 μM of TPR2B was measured in 50 mM potassium phosphate, 50 mM potassium chloride, 1 mM TCEP, pH 7.5 at 293 K and 600 MHz. As gradient length (*little delta*, δ) 4 ms were used, the diffusion time (*big delta*, Δ) was set to 500 ms.

For comparison, the theoretical diffusion coefficients were calculated for TPR2A, TPR2B and a few additional proteins of similar or different size (table 4.12). The calculated diffusion coefficients D for monomeric TPR2A and TPR2B were 1.01 and $0.98*10^{-10}\,m^2/s$. The slightly smaller value for TPR2B reflects the moderately larger size of the TPR2B construct used with a few unfolded residues at its N - and C - terminus (compare section 4.4.2). Consequently, its hydrodynamic radius is slightly higher compared to TPR2A. The experimentally determined diffusion coefficients with $1.02*10^{-10}\,m^2/s$ for both domains agreed very well with the calculated data, especially for TPR2A. This indicates that both TPR2A

Table 4.11: Diffusion coefficients of the Sti1 TPR2A and TPR2B domains obtained from DOSY measurements. For both domains intensity decay curves of 5 different signals were fitted to determine the diffusion coefficient D. Diffusion measurements were done at 293 K and 600 MHz using 150 μM of TPR2A or TPR2B in 50 mM potassium phosphate, 50 mM potassium chloride, 1 mM TCEP, pH 7.5. As gradient length (*little delta*, δ) 4 ms were used, the diffusion time (*big delta*, Δ) was set to 500 ms.

	TPR2A		TPR2B	
	Signal (ppm)	D ($*10^{-10}$ m^2/s)	Signal (ppm)	D ($*10^{-10}$ m^2/s)
	2.88	1.00	2.10	1.26
	1.97	1.07	1.95	1.00
	1.60	1.01	1.31	0.91
	1.01	0.96	1.08	0.92
	0.53	1.03	0.75	0.99
Average D ($*10^{-10}$ m^2/s)		1.02 ± 0.04		1.02 ± 0.14

Table 4.12: Theoretical diffusion coefficients of Sti1 TPR2A and TPR2B domains and comparison proteins. Diffusion coefficients were calculated from the 3D structures using the program HYDRONMR [279] for a temperature of 293 K. PDB codes for the proteins analyzed are 2LYZ (Lysozym), 1MBN (Myoglobin), 3LR2 (spider silk N-terminal domain). For TPR2B the NMR structure obtained in this work was used for the calculations, for TPR2A a crystal structure was kindly provided by Dr. Melissa Gräwert (Lehrstuhl für Biochemie, TUM).

Protein	Residues	MW (kDa)	D ($*10^{-10}$ m^2/s)	
			Calculated	Experimental
Lysozym (hen egg)	129	14.3	1.08	/
Myoglobin	153	17.2	1.01	/
Spider silk (monomer)	146	15.2	1.04	/
Spider silk (dimer)	292	30.4	0.92	/
TPR2A (monomer)	127	14.8	1.01	1.02
TPR2B (monomer)	139	15.6	0.98	1.02

and TPR2B likely behave as monomers in solution.

The diffusion coefficients were also calculated for the monomeric N-

terminal spider silk domain from *Latrodectus hesperus* and for its dimeric state. As the results showed, there is a significant difference in the D values for the monomer and the dimer (1.04 versus $0.92*10^{-10}\,m^2/s$). Thus, if TPR2A or TPR2B indeed behaved as dimers, their experimentally determined diffusion coefficients would be expected to deviate stronger from the theoretical values calculated for the monomer, arguing against TPR2A and TPR2B being dimers.

Lysozym has a size very similar to TPR2A. The calculated D value for Lysozym, however, is higher (1.08 versus $1.01*10^{-10}\,m^2/s$). This might be due to the far more compact and globular shape of Lysozym. Myoglobin on the other hand has a larger size compared to TPR2A (17.2 versus 14.8 kDa). Nevertheless, myoglobin has a calculated D value identical to that of TPR2A as it has a very globular shape like Lysozym. This shows in general that the TPR domain fold which is rather open and flat has hydrodynamic properties that are comparable to those of significantly larger proteins but with globular shape. This might be the reason for some reports concluding Sti1 to be a dimer [147,166] because in these studies techniques like size - exclusion chromatography were used where molecular masses are deduced from calibration standards containing predominantly rather globular proteins. The NMR diffusion experiments, however, strongly support the assumption that Sti1 is a monomer.

4.4.5 Peptide Binding of Sti1 TPR Domains Monitored by NMR

The results of the ITC measurements with Sti1 TPR domains showed that TPR2A and TPR2B have very different peptide binding properties. TPR2A is highly selective for binding Hsp90 peptides, but TPR2B in principle can bind both Hsp70 and Hsp90 peptides promiscuously with nearly identical

affinity (see section 4.3). To analyze these differences in more detail, the peptide binding of TPR2A and in particular of TPR2B was further studied by NMR.

Since in the ITC measurements TPR2A was found to bind octapeptides with the highest affinity, the respective Hsp70 and Hsp90 peptides were added to ^{15}N-labeled TPR2A and the chemical shift perturbation upon complex formation between the ligand and the protein was analyzed in the ^{15}N-HSQC (figure 4.36). For both peptides shifting peaks could be

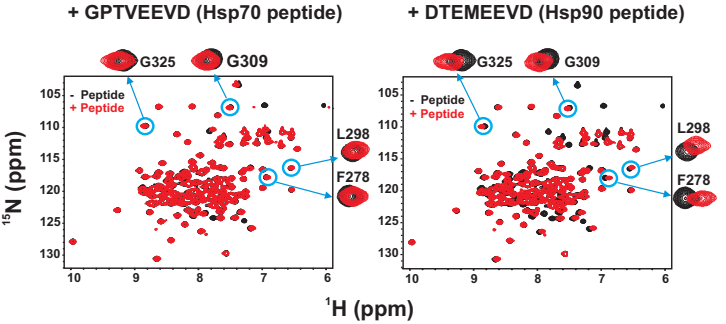

Figure 4.36: Binding of the Hsp70 and Hsp90 octapeptides GPTVEEVD (left) and DTEMEEVD (right) to the Sti1 TPR2A domain monitored by NMR. An overlay of the ^{15}N-HSQC spectra is shown for TPR2A alone (black) and with peptide bound (red). Significantly larger shift differences occur for binding of the Hsp90 peptide to TPR2A, as shown in the examples with enlarged peaks. 150 μM of TPR2A was measured in 50 mM potassium phosphate, 50 mM potassium chloride, 1 mM TCEP, pH 7.5 at 293 K and 750 MHz. Peptides were added in a 1:1 molar ratio.

found, however, for adding the Hsp90 peptide the shifts were in general much more pronounced and significantly more peaks experienced shift perturbation. Some of the signals that showed only slight shifts upon adding the Hsp70 peptide were broadened beyond detection limit in

the case of the Hsp90 peptide. Especially several side - chain resonances around a ^{15}N chemical shift of 112 ppm which typically correspond to arginine and glutamine NH_2 - groups disappeared when the Hsp90 peptide was added. Although for TPR2A only backbone resonances were assigned in this work, these resonances most likely originated from some residues that are not part of the conserved TPR carboxylate clamp but are additionally important for mediating the specific recognition of the Hsp90 peptide. The disappearance of some signals upon binding the Hsp90 peptide in contrast to only small shifts of the same signals upon binding the Hsp70 peptide indicates chemical exchange on different timescales. For the Hsp90 peptide, the respective resonances exchange on the intermediate NMR timescale whereas for the Hsp70 peptide fast exchange applies, causing only shifts instead of line broadening. This observation can be interpreted as stronger binding for the Hsp90 peptide compared to the Hsp70, thus confirming the results of the ITC measurements.

A detailed analysis of the shift data by calculating the weighted chemical shift perturbation (CSP) according to formula 10.4 for each residue showed higher CSP - values for binding of the Hsp90 peptide to TPR2A (figure 4.37). The average CSP for binding of the Hsp70 peptide to TPR2A was 0.006 ppm, for binding of the Hsp90 peptide, in contrast, 0.016 ppm. In general in both cases it were mainly the helices A1 to A3 which were affected by the ligand binding. The helices B3 and the solubility helix C did not seem to play a major role for the interaction of TPR2A with the peptide. The strongest CSP was clearly observable for the helices A2 and A3.

High CSP - values were not only found for the well conserved two - carboxylate clamp residues K266, N270, N300 and K337 but also for neighboring residues. This could point at some moderate conformational changes that might occur upon ligand binding. Residues with CSP above the

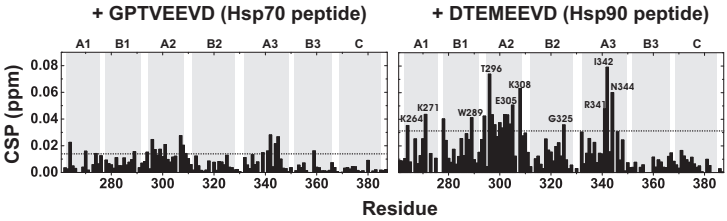

Figure 4.37: Chemical shift perturbation (CSP) plots for the binding of the Hsp70 (left) and Hsp90 (right) octapeptides to the Sti1 TPR2A domain. Much stronger chemical shift perturbation occurs for binding of the Hsp90 peptide to TPR2A, indicating a potentially tighter interaction. Significance levels (defined as twofold average chemical shift perturbation, which is 0.012 ppm for the Hsp70 peptide and 0.032 ppm for the Hsp90 peptide) are indicated in the plots by a dashed line. 150 μM of TPR2A was measured in 50 mM potassium phosphate, 50 mM potassium chloride, 1 mM TCEP, pH 7.5. Peptides were added in a 1:1 molar ratio. TPR domain secondary structure elements are given on top of the plots.

significance level (twofold average CSP, 0.012 ppm for the Hsp70 peptide and 0.032 ppm for the Hsp90 peptide) are summarized in table 4.13. Residues K264, W289, D294, T296, Y297, K308, R341, I342 and N344 were consistently found to be significantly affected by binding of both the Hsp70 and Hsp90 peptide. Shifting of their resonances likely reflects the basal TPR2A peptide binding of the conserved EEVD motive. Out of these residues, T296, R341 and N344 are conserved residues predicted to directly contact the EEVD motive, their side-chains directly point into the peptide binding groove of TPR2A. Residues N270 in the case of the Hsp70 peptide and N300 in the case of the Hsp90 peptide are conserved two-carboxylate clamp residues that should contact the carboxylate groups of the terminal Asp/D0 residue in the peptide ligand (figure 4.38).

As mentioned above, some arginine/glutamine side-chain NH_2 signals were broadened when the Hsp90 ligand was added but only shifts were found for the same signals when the Hsp70 ligand was present. The

Table 4.13: Residues in the Sti1 TPR2A domain that show significant chemical shift perturbation (CSP) upon binding of the Hsp70 and Hsp90 octapeptides. Residues listed below have CSP values above the significance level, which is defined as twofold average CSP (see also figure 4.37).

TPR helix	Hsp70 peptide	Hsp90 peptide
A1	K264,N270,K274	K264,K271
B1	W289	F278,W289
A2	D294,T296,Y297,N299,R301,E307 K308,G309	D294,T296,Y297,L298,N300,A302 A303,A304,E305,K308
B2	/	G325
A3	F339,R341,I342,N344,A345	R341,I342,N344
B3	Y359	/
C	/	/

same observation could also be made for a small number of backbone NH signals. These were K274, R276, E307 and A345. It is therefore likely that the side - chain resonances originating from the residues K274 and R276 are among those side - chain signals found to be broadened in presence of the Hsp90 ligand.

K274 and E307 are located at the end of helix A1 and A2, respectively. K276 is part of the small loop connecting helix A1 to A2 and A345 is near to the end of helix A3. All these residues therefore cluster on one edge of the TPR2A domain, the side - chains of K274, R276 and E307 point into the peptide binding groove (figure 4.38, right). As the signals of all four residues were only slightly shifted with the Hsp70 peptide but broadened beyond detection limit with the Hsp90 peptide, it might be possible that these residues play a special role for the ligand discrimination of TPR2A between Hsp70 and Hsp90 peptides. The location of these residues within TPR2A should be near to where the amino acids DTEM of the Hsp90 peptide ligand DTEMEEVD are likely positioned when bound to the TPR2A domain. The line broadening of these residues indicates special dynamics

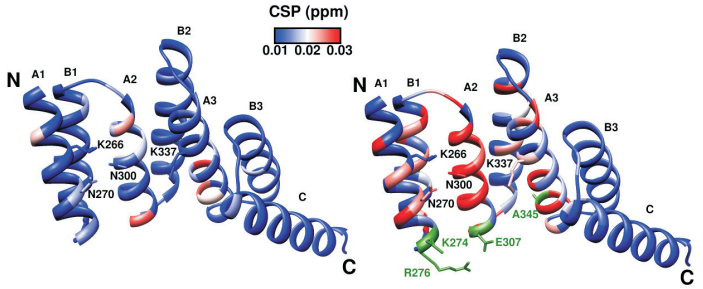

Figure 4.38: Mapping of the chemical shift perturbation upon binding of Hsp70 (left) and Hsp90 (right) octapeptides onto the Sti1 TPR2A domain. Much stronger chemical shift perturbation occurs for binding of the Hsp90 peptide to TPR2A, indicating a potentially tighter interaction. Residues showing line broadening upon ligand binding are colored green. Conserved residues from the two-carboxylate clamp are labeled. N and C-terminus and the helices of the TPR motives are indicated. 150 μM of TPR2A was measured in 50 mM potassium phosphate, 50 mM potassium chloride, 1 mM TCEP, pH 7.5. Peptides were added in a 1:1 molar ratio. The crystal structure of TPR2A was kindly provided by Dr. Melissa Gräwert (Lehrstuhl für Biochemie, TUM)

in the ligand bound state, maybe due to additional contacts of their side-chains with the Hsp90 peptide that can not be formed with the Hsp70 peptide. The small shifts that were observed for these residues when the Hsp70 peptide was bound might reflect only secondary effects caused by slight conformational changes upon binding of the unfavored Hsp70 ligand.

As outlined in section 4.3, the Sti1 TPR2B domain was found to be unselective in binding Hsp70 and Hsp90 peptides. Although the Hsp70 and Hsp90 hepta and octapeptides were bound with comparable affinity ($\sim 4\,\mu$M), the thermodynamical parameters obtained from ITC experiments indicated differences in the binding mode between the Hsp70 and Hsp90 peptides (table 4.7). Therefore, the ligand binding of TPR2B was

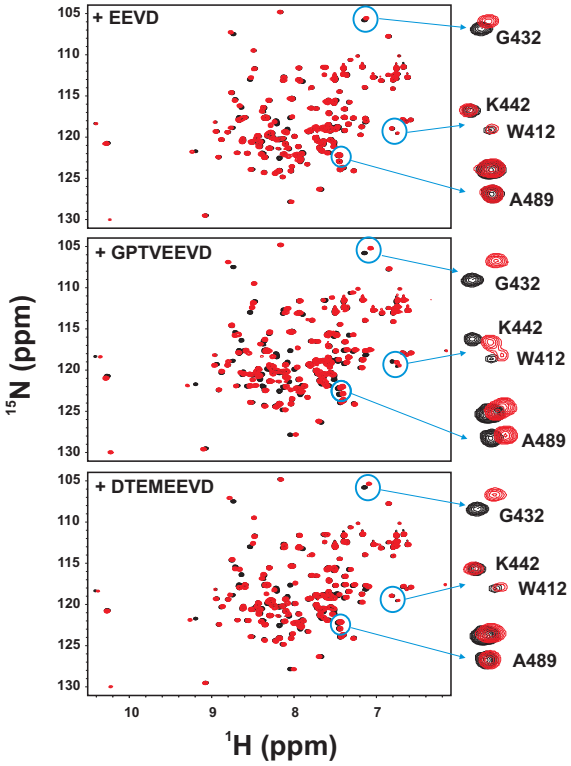

Figure 4.39: Binding of the Hsp70 and Hsp90 octapeptides GPTVEEVD (left) and DTEMEEVD (right) to the Sti1 TPR2B domain monitored by NMR. An overlay of the ^{15}N - HSQC spectra is shown for TPR2B alone (black) and with peptide bound (red). Moderately larger shift differences occur for binding of the Hsp70 peptide to TPR2B as shown in the examples with enlarged peaks. 150 μM of TPR2B was measured in 50 mM potassium phosphate, 50 mM potassium chloride, 1 mM TCEP, pH 7.5 at 293 K and 750 MHz. Peptides were added in a 1:1 molar ratio.

studied in more detail by NMR. The consensus peptide EEVD and the Hsp70 and Hsp90 specific penta to octapeptides were added to the protein and the chemical shift perturbation in the 2D NMR spectra was analyzed. In general, similar to TPR2A, also the TPR2B domain showed significant chemical shift perturbation in the ^{15}N - HSQC spectra in the presence of the different peptides (figure 4.39). In contrast to TPR2A, here only shifts were observable for all measurements but no line broadening, neither with Hsp70 nor Hsp90 peptides. This indicates a binding of the ligands on the fast NMR timescale, corresponding to a presumably weaker interaction.

The consensus peptide EEVD caused moderate but specific shifts of TPR2B signals, mainly involving conserved carboxylate - clamp residues like R400, K404, N435, R465 and neighboring residues, reflecting the basal peptide binding function of TPR2B (figure 4.40). With increasing length of the peptides, gradually more and more signals were shifted in the spectra and shifts were more pronounced for adding longer peptides. This is in line with results from the ITC experiments which demonstrated that peptides are bound tighter with increasing length (figure 4.14).

The CSP pattern were roughly similar comparing corresponding Hsp70 and Hsp90 peptides of the same length. Mainly residues from the TPR helices A1, A2 and A3 were affected by the ligand binding which contain the conserved two - carboxylate clamp residues. However, for the longest peptides with seven and eight amino acids, the binding modes for the Hsp70 and Hsp90 ligands seem to be partially different. The shifts observed upon complexation were stronger for the Hsp70 peptide (figure 4.39 and 4.40). The significance level (twofold average chemical shift perturbation) was 0.054 ppm for the Hsp70 peptide but only 0.033 ppm for the Hsp90 peptide. Furthermore, in the case of the Hsp70 peptides additionally regions in helices B3 and C within TPR2B seemed to be also

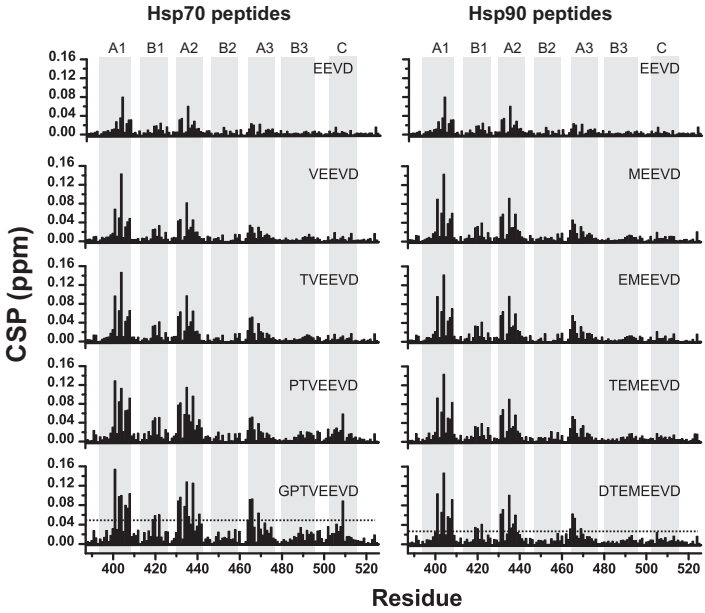

Figure 4.40: Chemical shift perturbation (CSP) plots for the binding of the Hsp70 (left) and Hsp90 (right) peptides to the Sti1 TPR2B domain. Moderately stronger chemical shift perturbation occurs for binding of the Hsp70 peptide to TPR2B. Significance levels (defined as twofold average chemical shift perturbation which is 0.054 ppm for the Hsp70 peptide and 0.033 ppm for the Hsp90 peptide) are indicated in the plots for the octapeptides by a dashed line. 150 μM of TPR2B was measured in 50 mM potassium phosphate, 50 mM potassium chloride, 1 mM TCEP, pH 7.5. Peptides were added in a 1:1 molar ratio. TPR domain secondary structure elements are indicated. For comparison plots for the consensus peptide EEVD are included.

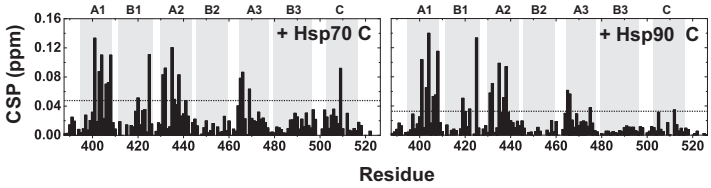

Figure 4.41: Chemical shift perturbation plots for the binding of Hsp70/Ssa1 (left) and Hsp90 (right) C-terminal fragments to the Sti1 TPR2B domain. Moderately stronger chemical shift perturbation occurs for binding of Hsp70/Ssa1 C to TPR2B. Significance levels (defined as twofold average chemical shift perturbation which is 0.047 ppm for the Hsp70 peptide and 0.035 ppm for the Hsp90 peptide) are indicated by a dashed line. 150 μM of TPR2B was measured in 50 mM potassium phosphate, 50 mM potassium chloride, 1 mM TCEP, pH 7.5. Hsp70/Ssa1 C and Hsp90 C were added in a 1:1 molar ratio. TPR domain secondary structure elements are indicated.

moderately affected by the ligand binding.

For comparison, also the Hsp70/Ssa1 and Hsp90 C-terminal domains were added to ^{15}N-labeled TPR2B. The chemical shift perturbation patterns observed with the full domains were similar to those with the respective peptides (figure 4.41). Again, the average chemical shift perturbation for binding of Hsp70/Ssa1 C was higher than for Hsp90 C and helices B3 and C were stronger affected in the case of Hsp70/Ssa1 C. Thus, the observations made for binding of the isolated peptides also seem to apply for the full domains.

Residues that were consistently found to be shifted upon binding of the Hsp70 and Hsp90 octapeptides are L401, G403, K404, Y406, F407 and T408 from helix A1, T420 and M422 from helix B1, R431, G432, N435, R436 and A438 from helix A2 and R465, A466 and R469 from helix A3 (table 4.14). K404, N435 and R465 represent conserved residues forming the two-carboxylate clamp and should contact the terminal Asp/D0

Table 4.14: Residues in the Sti1 TPR2B domain that show significant chemical shift perturbation (CSP) upon binding of the Hsp70 and Hsp90 octapeptides. Residues listed below have CSP values above the significance level, which is defined as twofold average CSP (see also figure 4.40).

TPR helix	Hsp70 peptide	Hsp90 peptide
A1	L401,G403,K404,Y406,F407,T408	L401,G403,K404,Y406,F407,T408
B1	T420,M422	Y419,T420,M422
A2	R431,G432,S434,N435,R436,A438 A441	R431,G432,N435,R436,A437,A438
B2	/	/
A3	R465,A466,R469	V464,R465,A466,R469
B3	/	/
C	L509	/

residue of the ligand. F407 and R469 are additional highly conserved residues predicted to be involved in recognizing amino acids from the consensus motive EEVD. The side - chains of all these residues directly point into the peptide binding groove of TPR2B and are likely to make direct interactions with the ligand, as a mapping of the results from the analysis of the CSP data onto the NMR structure of TPR2B shows (figure 4.42). The shifts observed for the other residues should mostly reflect secondary effects of slight conformational changes caused by binding of the ligand to a neighboring residue.

As mentioned above, in case of binding of the Hsp70 peptide to TPR2B significant shifts were also observable in helix B3 and C. The residues affected within these helices cluster at the C - terminal part of helix B3 and the N - terminal part of helix C. It might be possible that these two helices have to undergo conformational changes first in order to accommodate the Hsp70 peptide, which are not necessary for binding the Hsp90 peptide. This would explain the significantly different entropy terms found in the ITC experiments for binding the Hsp70 and Hsp90 peptides although

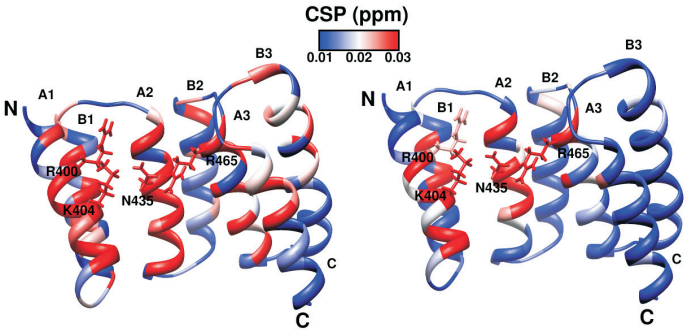

Figure 4.42: Mapping of the chemical shift perturbation upon binding of Hsp70 (left) and Hsp90 (right) octapeptides onto the NMR structure of the Sti1 TPR2B domain. Stronger chemical shift perturbation occurs for binding of the Hsp70 peptide to TPR2B, indicating potentially larger conformational changes when the Hsp70 peptide is bound. Conserved residues from the two - carboxylate clamp are labeled. N - and C - terminus and the helices of the TPR motives are indicated. 150 μM of TPR2A was measured in 50 mM potassium phosphate, 50 mM potassium chloride, 1 mM TCEP, pH 7.5. Peptides were added in a 1:1 molar ratio.

they are bound with a similar affinity to TPR2B (see table 4.7).

CSP experiments were also performed with the two - domain construct TPR2A - TPR2B. Adding the Hsp70 and Hsp90 octapeptides GPTVEEVD and DTEMEEVD, respectively, to the protein led to comparable chemical shift perturbation as observed for the isolated TPR2A and TPR2B domains (figure 4.43). The presence of the Hsp70 peptide caused exclusively shifts in the ^{15}N - TROSY spectrum of TPR2A - TPR2B whereas the Hsp90 peptide also led to the disappearance of the backbone NH signals for K274, R276, E307 and A345 as observed for the isolated TPR2A domain. As expected, for the Hsp70 peptide the most pronounced shifts occurred in the TPR2B portion of the two - domain construct, especially within helices A1, A2 and A3 (figure 4.44, upper panel). Additionally, some shifts were also

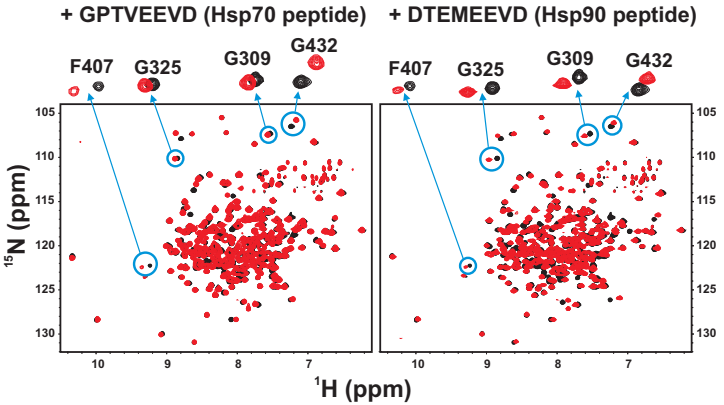

Figure 4.43: Binding of the Hsp70 and Hsp90 octapeptides GPTVEEVD (left) and DTEMEEVD (right) to the Sti1 TPR2A-TPR2B fragment monitored by NMR. An overlay of the ^{15}N-TROSY spectra is shown for TPR2A-TPR2B alone (black) and with peptide bound (red). As for the isolated TPR2A and TPR2B domains the Hsp70 peptide leads to more pronounced shifts within TPR2B and the Hsp90 peptide within TPR2A in the two-domain construct. 500 μM of TPR2A-TPR2B was measured in 50 mM potassium phosphate, 50 mM potassium chloride, 1 mM TCEP, pH 7.5 at 303 K and 900 MHz. Peptides were added in a 1:1 molar ratio.

observed in TPR2A since this domain has a certain affinity in the higher μM-range (see table 4.6) even for the non-favored Hsp70 ligand. Vice versa, presence of the Hsp90 peptide caused the most intense shifts in TPR2A due to its higher binding affinity for the Hsp90 ligand compared to TPR2B (0.3 μM versus 4.3 μM, tables 4.6 and 4.7), with some moderate shifts also occurring in TPR2B at the same time. As the peptides were added only in a 1:1 molar ratio in the measurements to a protein with two potential binding sites for the same ligand, the high affinity binding site for the Hsp90 peptide within the TPR2A domain should be occupied

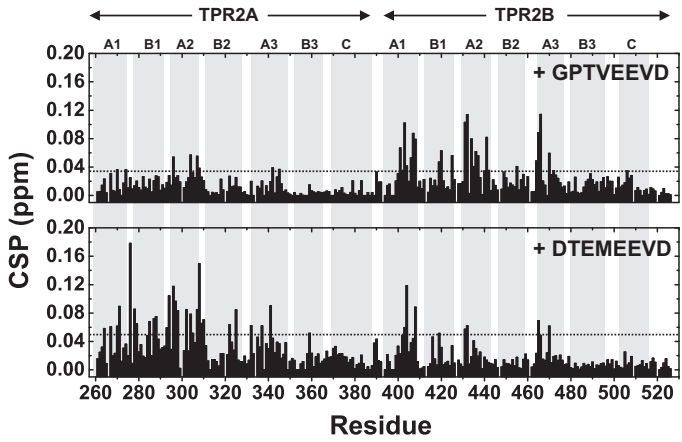

Figure 4.44: Chemical shift perturbation (CSP) plots for the binding of Hsp70 (upper panel) and Hsp90 (lower panel) octapeptides to the Sti1 TPR2A-TPR2B fragment. The Hsp70 peptide leads to more pronounced CSP within TPR2B, the Hsp90 peptide within TPR2A in the two-domain construct. Significance levels (defined as twofold average chemical shift perturbation which is 0.037 ppm for the Hsp70 peptide and 0.049 ppm for the Hsp90 peptide) are indicated in the plots by a dashed line. 500 μM of TPR2A-TPR2B was measured in 50 mM potassium phosphate, 50 mM potassium chloride, 1 mM TCEP, pH 7.5. Peptides were added in a 1:1 molar ratio. TPR domain secondary structure elements are indicated.

to a large extent under these conditions whereas only a smaller fraction of TPR2B should be bound by the ligand. Adding the Hsp90 ligand in a higher excess would mostly likely have caused more pronounced shifts also within TPR2B. Overall, the NMR studies with the TPR2A-TPR2B fragment demonstrate that both TPR2A and TPR2B behave independently in the two-domain construct, retaining the peptide binding selectivities as found for the isolated domains.

4.5 Characterization of Sti1 Peptide Binding Mutants

The peptide binding of TPR domains in general is largely mediated by a few well conserved residues in their ligand binding grooves. The Hsp70 and Hsp90 binding TPR domains in particular have highly conserved amino acids forming the two - carboxylate clamp (see section 2.1.3) and additional conserved amino acids mediating contacts to the EEVD consensus motive of the peptide ligands. To further study its function *in vitro* and *in vivo*, a set of TPR2B peptide binding mutants was designed. The conserved two - carboxylate clamp residues N435 and R465 of the protein as well as R469, which is supposed to contact residues from the EEVD motive of the peptide ligand, were targeted for point mutation. As a replacement, alanine was chosen as it is well compatible with helical conformation and therefore should be incorporated in the protein without causing major distortion of secondary structure elements.

Three single point mutations N435A, R465A and R459A as well as two combined mutations N435A/R465A and N435A/R469A were introduced into the TPR2B domain. The mutants were purified and characterized by CD and NMR spectroscopy. The CD spectra of isolated TPR2B mutants indeed indicated no major distortion of the structure, except for the double mutant N435A/R469A which showed a slightly reduced secondary structure content (figure 4.45, left). The CD thermal unfolding transitions for the mutants and the wild - type TPR2B domain gave nearly identical melting points, confirming that the mutants were not destabilized (figure 4.45, right).

The NMR spectra of the respective mutants showed some shifts compared to the spectrum of the wild - type TPR2B domain, however, none of the mutant spectra indicated a significantly increased portion of random coil content (figure 4.46). All mutants appeared to be folded nearly to the

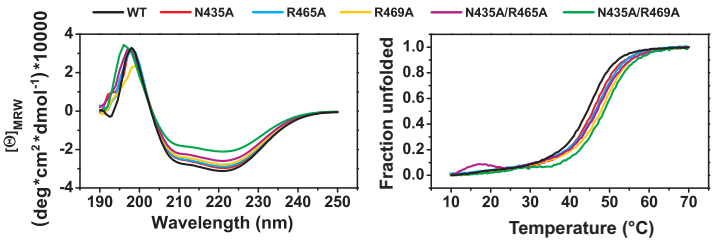

Figure 4.45: CD spectra (left) and CD thermal unfolding transitions (right) of Sti1 TPR2B domain peptide binding mutants. The CD spectra of the mutants are nearly identical with the wild - type, except for the double mutant N435A/R469A, and the thermal melting points indicate no major loss of stability by the mutations introduced. 20 μM of wild - type TPR2B or the respective mutants were measured in 50 mM potassium phosphate, 50 mM potassium chloride, 1 mM TCEP, pH 7.5. CD spectra were recorded at 20°C, thermal unfolding was monitored at a wavelength of 222 nm.

same extent as the wild - type protein. Therefore, consistent with the CD data, the NMR measurements confirmed that the mutations did not interfere much with the secondary structure of the domain, and the overall TPR fold of the domain was presumably preserved in the mutants.

The peptide binding properties of the respective TPR2B mutants were then probed by NMR spectroscopy. As the experiments with the TPR2B wild - type domain showed, binding of the Hsp70 octapeptide GPTVEEVD causes significant chemical shift perturbation (figure 4.39). Therefore, again NMR was chosen to easily assess the peptide binding behavior of the mutants. For the N435A mutant no shifts could be observed upon adding the Hsp70 peptide (figure 4.47), and consequently the same applied for the N435A/R465A and N435A/R469A double mutants. For the R465A and R469A variants only some very slight shifts occurred for a few residues like the highly conserved K404 or G432. These residues are among those which showed the largest chemical shift perturbation

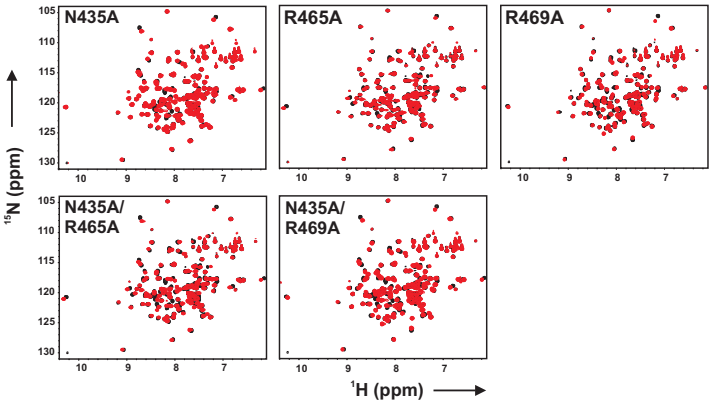

Figure 4.46: Overlay of the ^{15}N - HSQC spectra for the wild - type Sti1 TPR2B domain (black) and peptide binding mutants thereof (red). Although the mutations caused some peak shifts, none of the mutants shows an NMR spectrum with significantly increased random coil content compared to the TPR2B wild - type domain. 150 μM of wild - type TPR2B or the respective mutants were measured in 50 mM potassium phosphate, 50 mM potassium chloride, 1 mM TCEP, pH 7.5 at 293 K and 750 MHz.

in the case of binding of the Hsp70 peptide to the wild - type TPR2B domain (compare figure 4.39 and 4.40). Therefore, the peptide binding was significantly reduced for the TPR2B mutants R465A and R469A and in case of N435A and the double mutants no remaining peptide binding was found using NMR. N435 seems to be a key residue to mediate the ligand binding of TPR2B. Surprisingly, the mutation of only this residue was sufficient to reduce Hsp70 peptide binding to TPR2B down to levels not detectable with NMR under the conditions used.

Peptide binding mutations within TPR2B were also introduced into the TPR2A - TPR2B fragment and full - length Sti1 for further experiments. As already the single point mutations turned out to be very effective in re-

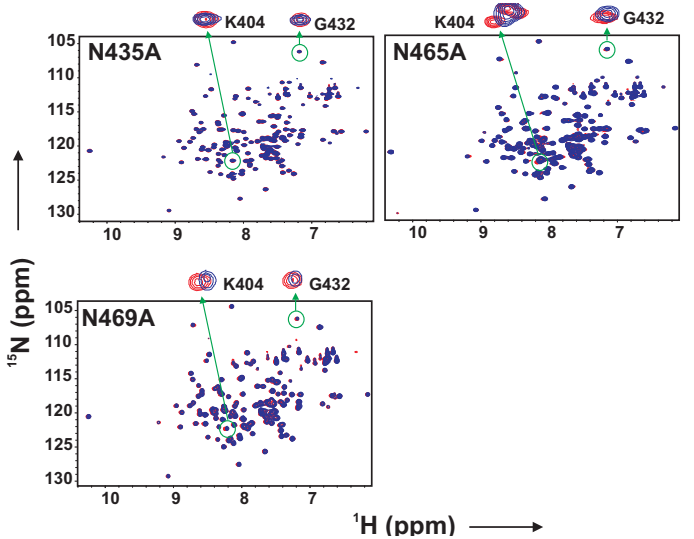

Figure 4.47: Overlay of the ^{15}N-HSQC spectra for free Sti1 TPR2B peptide binding mutants (red) and in presence of the Hsp70 octapeptide GPTVEEVD (blue). Only for the single point mutants R465A and R469A some very slight peak shifts can be observed for a few residues, indicating that the mutations had nearly completely abolished the peptide binding function of TPR2B. 150 μM of the respective TPR2B mutants were measured in 50 mM potassium phosphate, 50 mM potassium chloride, 1 mM TCEP, pH 7.5 at 293 K and 750 MHz. The peptide was added in a 1:1 molar ratio.

ducing or nearly abolishing ligand binding to TPR2B, only the N435A, R465A and R469A variants of TPR2A-TPR2B and the full-length protein were generated. Again, CD data showed that also the two-domain construct TPR2A-TPR2B was nearly unaffected by mutations within the TPR2B portion of the protein with respect to secondary structure content and thermal stability (figure 4.48). Thus, a further characterization of the respective full-length Sti1 mutants seemed not required.

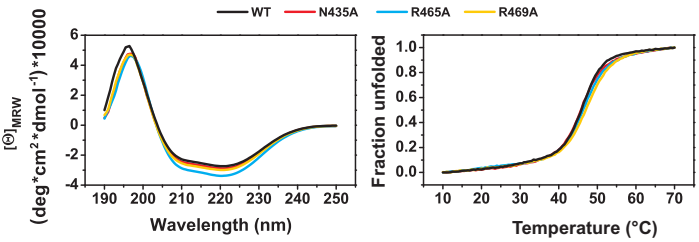

Figure 4.48: CD spectra (left) and CD thermal unfolding transitions (right) of Sti1 TPR2A - TPR2B peptide binding mutants. The CD spectra of the mutants are nearly identical with the wild - type and the thermal melting points indicate no major loss of stability by the mutations introduced. 10 μM of wild - type TPR2A - TPR2B or the respective mutants were measured in 50 mM potassium phosphate, 50 mM potassium chloride, 1 mM TCEP, pH 7.5. CD spectra were recorded at 20°C, thermal unfolding was monitored at a wavelength of 222 nm.

4.6 Influence of Sti1 on the Hsp90 ATPase Activity

Sti1 was previously shown to be a non - competitive inhibitor of the Hsp90 ATP hydrolysis [166,167]. To characterize this function of the cochaperone further, ATPase assays were performed here with different Hsp90 and Sti1 mutants. First, the importance of the Sti1 TPR domain peptide binding for the inhibition of Hsp90 was assessed. To this end, instead of mutating the individual peptide binding sites of all three TPR domains in Sti1, a deletion mutant of Hsp90 was used lacking the last 30 C - terminal residues (Hsp90Δ30 mutant, compare section 3.8). The residues deleted contain the peptide motive recognized by TPR domain proteins and, as shown, these residues are unstructured (see figure 3.4) and do not influence the ATPase activity of Hsp90 (see figure 3.34). Wild - type full - length Sti1 was added to the Hsp90Δ30 mutant in increasing concentration and the remaining ATPase activity was measured by an enzymatic

coupled regenerating assay [244] (figure 4.49). As a comparison of the in-

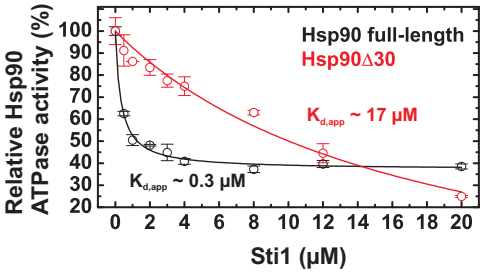

Figure 4.49: ATPase inhibition of the Hsp90Δ30 mutant (red) and for comparison wild-type Hsp90 (black) by full-length wild-type Sti1. The inhibition of its ATP hydrolysis by Sti1 is significantly lower for mutant Hsp90. Wild-type full-length Sti1 was titrated to 4 μM of wild-type or mutant Hsp90. ATPase activities were measured in 40 mM HEPES, 150 mM potassium chloride, 5 mM $MgCl_2$, 2 mM ATP, pH 7.5 at 30°C using a coupled regenerating assay [244].

hibition curves for mutant and wild-type Hsp90 showed, the deletion of the amino acids in Hsp90 recognized by the TPR domain peptide binding grooves significantly reduced the inhibition of Hsp90 by Sti1. The apparent K_d-values ($K_{d,app}$) obtained from the curves were 0.33 μM for wild-type Hsp90 and 17.28 μM for the mutant. On the one hand, this result demonstrates that the peptide-TPR interaction plays a major role for complex formation and concomitantly ATPase inhibition of Hsp90 by Sti1. On the other hand, however, the data clearly show that additional binding sites between Hsp90 and Sti1 exist which are independent from the Sti1 peptide binding function. These non-peptide binding interactions obviously mediate the ATPase inhibition of Hsp90 by Sti1. Given the fact that a relatively high salt concentration was used in the assay (150 mM potassium chloride), these interactions can be regarded as specific and significant.

In previous work Dr. Andreas Schmid (Lehrstuhl für Biotechnologie, TUM) could demonstrate that a Sti1 fragment comprising only the TPR2A and TPR2B domain shows an inhibition of the Hsp90 ATP hydrolysis comparable to the full - length Sti1 protein (figure 4.50). Therefore, the TPR1

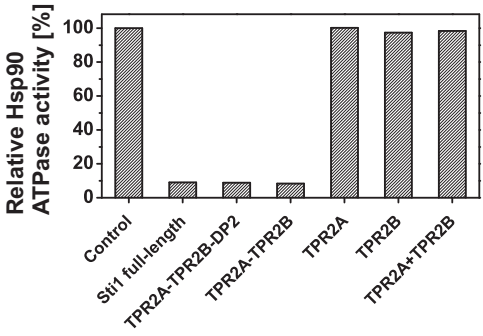

Figure 4.50: Inhibition of the Hsp90 ATPase activity by different Sti1 fragments. The TPR2A - TPR2B fragment shows inhibition of the Hsp90 ATPase activity comparable to full - length Sti1. ATPase activities were measured in 50 mM HEPES, 50 mM potassium chloride, 5 mM $MgCl_2$, 2 mM ATP, pH 7.5 at 30°C using a coupled regenerating assay [244]. The data were kindly provided by Dr. Andreas Schmid (Lehrstuhl für Biotechnologie, TUM).

as well as the DP domains of Sti1 seem to be dispensable for this particular function of Sti1. Interestingly, adding the isolated TPR2A or TPR2B domain separately to Hsp90 had no influence on the ATP hydrolysis, and likewise, adding isolated TPR2A and TPR2B at the same time showed no effect. This means that for the inhibition of Hsp90 TPR2A and TPR2B have to be within the same polypeptide chain.

Based on these observations, further experiments were carried out in this work to characterize the influence of the Sti1 TPR2A - TPR2B fragment on the Hsp90 ATPase activity. First, the findings for the ATPase

inhibition of Hsp90 by TPR2A - TPR2B could be confirmed for a higher salt concentration compared to the previous measurements by Dr. Andreas Schmid (150 mM versus 50 mM potassium chloride). The inhibition curves for full - length Sti1 and TPR2A - TPR2B were nearly identical, the respective apparent K_d - values were 0.33 μM and 0.42 μM (figure 4.51). The data also show that one molecule of Sti1 or the TPR2A - TPR2B frag-

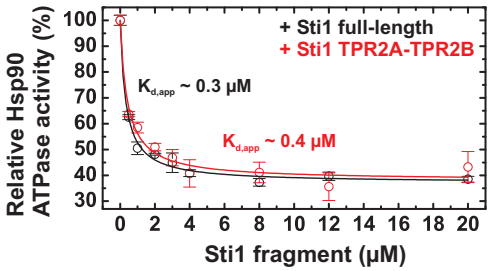

Figure 4.51: Inhibition of the Hsp90 ATPase activity by the Sti1 TPR2A - TPR2B fragment (red) in comparison to full - length Sti1 (black). The inhibition curve with the TPR2A - TPR2B fragment is nearly identical to the curve with the full - length protein. Full - length Sti1 or the TPR2A - TPR2B fragment was titrated to 4 μM of wild - type Hsp90. ATPase activities were measured in 40 mM HEPES, 150 mM potassium chloride, 5 mM $MgCl_2$, 2 mM ATP, pH 7.5 at 30°C using a coupled regenerating assay [244].

ment per Hsp90 dimer is sufficient to decrease the Hsp90 ATP hydrolysis, the maximum Hsp90 ATPase inhibition is observed already at a ratio of Sti1:Hsp90 ~1:2. This is in agreement with a previous report [278].

As the ITC and NMR experiments showed, TPR2B can bind both Hsp70 and Hsp90 peptides with similar affinities (see sections 4.3 and 4.4.5). This raises the question whether the ability of TPR2B to bind Hsp90 peptides has any functional importance for regulating the Hsp90 ATPase activity. Since the TPR2A domain has a much higher affinity for the Hsp90

peptides and is far more selective in peptide binding, it would be expected that TPR2A is the main binding site for Hsp90 and the TPR2B peptide binding function should be dispensable for inhibition of the Hsp90 ATPase activity. To test this assumption, the inhibition of the Hsp90 ATP hydrolysis was measured using a TPR2A - TPR2B N435A mutant. As demonstrated in section 4.5, the N435A mutation renders TPR2B unable to bind peptide. Comparing Hsp90 inhibition curves for wild - type TPR2A - TPR2B and the mutant, it can be seen that there is a slight reduction of the inhibitory capacity of the TPR2A - TPR2B fragment when N435 is substituted by alanine (figure 4.52). The apparent K_d - value for the mutant

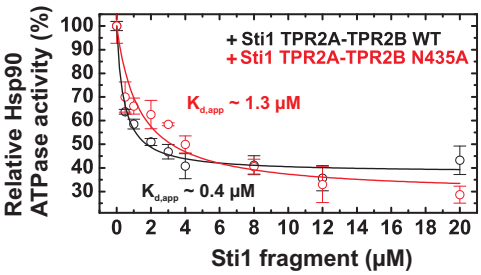

Figure 4.52: Inhibition of the Hsp90 ATPase activity by the Sti1 TPR2A - TPR2B N435A mutant (red) in comparison to wild - type TPR2A - TPR2B (black). The N435A mutation within TPR2B has a slight influence on the inhibitory capacity of the TPR2A - TPR2B fragment, indicating a small contribution of TPR2B to the binding of Hsp90. TPR2A - TPR2B or the mutant was titrated to 4 μM of wild - type Hsp90. ATPase activities were measured in 40 mM HEPES, 150 mM potassium chloride, 5 mM $MgCl_2$, 2 mM ATP, pH 7.5 at 30°C using a coupled regenerating assay [244].

is about three times higher compared to the wild - type ($\sim 0.4\,\mu$M versus $\sim 1.3\,\mu$M). Although this difference seems rather small, it can nevertheless be regarded as significant given the fact that higher salt concentra-

tions were used in the assay which should further weaken the peptide binding of TPR2B and in particular since the binding of TPR2A - TPR2B to Hsp90 should be dominated by the high affinity peptide binding of TPR2A.

4.7 Peptide Independent Binding Contacts of Sti1 with Hsp90

The results from the ATPase inhibition assays with Sti1 and Hsp90 indicated interactions between both proteins that are independent from the recognition of the peptide motive in Hsp90 by Sti1 TPR domains (compare section 4.6). To further characterize these, ITC experiments using Hsp90 or its C-terminal domain were performed, analyzing the binding of different Sti1 fragments. As the previous ITC peptide binding data showed, TPR1 should preferably bind Hsp70/Ssa1, therefore only the potentially Hsp90 interacting fragments TPR2A, TPR2B and TPR2A-TPR2B of Sti1 were tested here.

Titrating the C-terminal domain of Hsp90 with isolated TPR2A and TPR2B yielded K_d-values of 0.3 and 3.2 μM, respectively (table 4.15). This is very well in agreement with results for the binding of the Hsp90 octapeptide to TPR2A and TPR2B, which gave affinities of comparable magnitude (see table 4.6) and shows that no additional contacts between the Hsp90 C-terminal domain and the two TPR domains occur extra to the TPR-peptide interaction.

Previous NMR measurements with TPR2B further support the findings here, because the chemical shift perturbation patterns observed for binding of the Hsp90 octapeptide and the full Hsp90 C-domain were largely comparable (section 4.4.5). Additionally, in these experiments no major line broadening was observed when the Hsp90 C-domain was added to TPR2B. As the Hsp90 C-domain is a dimer of $\sim$ 40.6 kDa and should bind two molecules of TPR2B, a large complex of $\sim$ 70 kDa would be expected with concomitant broad signals. However, this was not the case. TPR2B obviously exclusively binds the Hsp90 peptide motive located at the end

Table 4.15: Summary of affinities and thermodynamical parameters for the binding of Sti1 domains to Hsp90, its C-terminal domain or the Hsp90 peptide. 20 μM of Hsp90 or its C-terminal domain in the measurement cell of the instrument was titrated with a 200 μM solution of the respective Sti1 fragment at a temperature of 20°C. In case of the Hsp90 peptide, 20 μM of the Sti1 fragment in the measurement cell was titrated with a 200 μM peptide solution. As a buffer 10 mM potassium phosphate, 1 mM TCEP, pH 7.5 was used. Affinity as K_a (association constant) and K_d (dissociation constant), binding enthalpy (ΔH), entropy (ΔS) and stoichiometry (N) are given for each measurement.

	N	K_a (10^5 M^{-1})	K_d (μM)	ΔH (cal/mol)	ΔS (cal/mol /deg)
Hsp90 peptide DTEMEEVD					
TPR2A - TPR2B	0.53 ± 0.02	12.7 ± 3.6	0.8	-6951 ± 331	4.2
Hsp90 C-terminal domain					
TPR2A	0.96 ± 0.01	34.9 ± 4.7	0.3	- 8170 ± 115	2.1
TPR2B	0.98 ± 0.04	3.1 ± 0.7	3.2	- 1818 ± 99	18.9
TPR2A - TPR2B	0.53 ± 0.01	16.8 ± 3.4	0.6	- 9375 ± 301	- 3.5
TPR2A - TPR2B N435A	1.01 ± 0.01	30.7 ± 5.6	0.3	- 7142 ± 166	5.3
Hsp90 full-length					
TPR2A	1.00 ± 0.01	60.6 ± 14.9	0.2	- 8464 ± 175	2.2
TPR2B	0.97 ± 0.05	11.1 ± 5.9	0.9	- 1153 ± 81	23.7
TPR2A - TPR2B	0.97 ± 0.02	*	*	*	*
TPR2A - TPR2B N435A	1.01 ± 0.03	51.0 ± 20.2	0.2	- 10110 ± 417	- 3.8

*Data fitting not possible because of too strong interaction

of a 20 residues stretch of unfolded amino acids in the Hsp90 C-terminal domain. Consequently, even when bound to the peptide motive, TPR2B is not significantly restricted in mobility due to the flexibility of these 20 residues, so that the line width of TPR2B remains nearly unaffected upon complex formation.

Binding of the TPR2A-TPR2B fragment to the Hsp90 C-terminal do-

main showed a stoichiometry of approximately 1:2, indicating a complex of one Hsp90 C-terminal domain dimer with one molecule of TPR2A-TPR2B. Again, this is consistent with the previous results on the TPR2B peptide binding properties which suggested that TPR2B can function as a potential Hsp90 peptide binding site (see table 4.7). The affinity for the binding between the TPR2A-TPR2B fragment and the Hsp90 C-terminal domain was slightly lower than for binding of isolated TPR2A (K_d 0.6 μM versus 0.3 μM) but significantly higher than for binding of isolated TPR2B (K_d 3.2 μM). The binding of the TPR2A-TPR2B two-domain fragment to the C-terminal domain is therefore likely dominated by the affinity of the TPR2A portion for the Hsp90 C domain.

In contrast to the binding of isolated TPR2A and TPR2B, the entropy contribution for binding of TPR2A-TPR2B to the Hsp90 C-terminal domain was unfavorable (-3.5 cal/mol/deg). This might be due to a loss of the normally high flexibility of the Hsp90 C-terminal domain peptide motive upon complex formation with the two-domain fragment, which is however compensated by the highly negative and therefore favorable enthalpy term (table 4.15). For comparison, the TPR2A-TPR2B was also titrated with the Hsp90 octapeptide DTEMEEVD. The affinity obtained here was 0.8 μM and therefore of similar magnitude as TPR2A-TPR2B binding the full Hsp90 C-terminal domain. This again supports the assumption that no major interactions occur between TPR2A, TPR2B and the Hsp90 C-terminal domain.

The TPR2A-TPR2B fragment containing the N435A mutation within TPR2B had nearly the same affinity for the Hsp90 C-terminal domain as isolated TPR2A ($\sim$ 0.3 μM), and the stoichiometry for the interaction was close to one. This confirms the results from the NMR experiments which showed that the N435A two-carboxylate clamp mutation is sufficient to abolish peptide binding to the TPR2B domain (compare section 4.5).

Then the respective Sti1 fragments were tested for binding to full-length Hsp90. In this case, the isolated TPR2A and TPR2B domains both showed higher binding affinities compared to binding of the Hsp90 peptide alone. This is in contrast to the measurements with the Hsp90 C domain before. Especially the binding of TPR2B to full-length Hsp90 was significantly stronger (K_d 0.9 μM for binding full-length Hsp90 versus K_d 4.3 μM for binding the Hsp90 peptide, compare table 4.7). Therefore, it can be assumed that TPR2A and TPR2B both have binding contacts with Hsp90 additional to the mere peptide motive recognition, and these contacts involve parts of Hsp90 that are outside its C-terminal domain.

For the complex between the TPR2A-TPR2B fragment and full-length Hsp90 no affinity could be determined since the binding was so tight that it exceeded the affinity range for which ITC can be applied to study molecular interactions. This suggests a binding with a K_d-value probably on the order below $\sim$0.02 μM. For the TPR2A-TPR2B N435A mutant, in contrast, the binding was weakened as a comparison of the raw ITC binding curves shows (figure 4.53). In this case the integrated binding heats could be fitted and a K_d-value could be determined which is $\sim$ 0.2 μM. This is comparable to isolated TPR2A binding to full-length Hsp90. The weaker binding of the TPR2A-TPR2B N435A mutant compared to the wild-type protein again shows that the TPR2B peptide binding plays a certain role for the interaction with Hsp90.

Interestingly, the stoichiometries for TPR2A-TPR2B and its mutant binding to full-length Hsp90 were close to one, in contrast to TPR2A-TPR2B binding to the Hsp90 C-terminal domain. This observation points at significant differences in the complexes between Sti1 and full-length Hsp90 or its C-terminal domain.

For comparison, the affinity between full-length Hsp90 and TPR2A-TPR2B was also determined using another method, fluorescence polar-

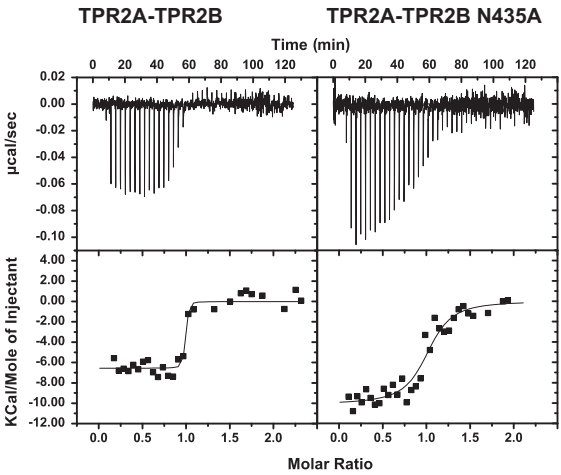

Figure 4.53: ITC curves for the interaction of TPR2A - TPR2B (left) and the TPR2A - TPR2B N435A mutant (right) with full - length Hsp90. The upper panel shows the raw binding heats, the lower panel the integrated binding heats and the data fits. The binding affinity for wild - type TPR2A - TPR2B is too strong, therefore the data fit does not give a reliable K_d - value and is only shown for comparison. 20 μM of full - length Hsp90 in the measurement cell was titrated with a 200 μM solution of the respective Sti1 fragment at 20°C. As a buffer 10 mM potassium phosphate, 1 mM TCEP, pH 7.5 was used.

ization. Here, fluorescein labeled TPR2A - TPR2B was titrated with full - length Hsp90. A binding curve could be obtained for this interaction and the corresponding K_d - value was 0.33 μM (figure 4.54). This affinity is lower compared to the estimated K_d from the ITC experiments ($< 0.02\,\mu$M) for the same binding partners, yet the value is roughly on the same order of magnitude. A possible explanation for these differences could be that the fluorescein label attached to TPR2A - TPR2B interfered with the binding. Although conditions were chosen that should favor

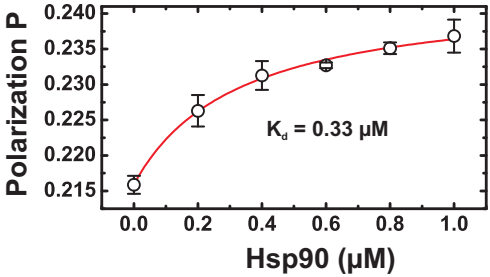

Figure 4.54: Fluorescence polarization measurement of Sti1 TPR2A - TPR2B and full - length Hsp90. The K_d - value obtained from fitting the data points is 0.33 μM. The estimated affinity from the ITC experiments for binding between TPR2A - TPR2B and full - length Hsp90, however, seems to be higher (compare table 4.15). 0.5 μM of fluorescein labeled TPR2A - TPR2B was titrated with full - length Hsp90 at 20°C. As a buffer 10 mM potassium phosphate, 1 mM TCEP, pH 7.5 was used.

the labeling of only the N - terminus of the protein and avoid attachment of the label to side - chain NH groups, the degree of labeling was determined to be ~ 190 %. This indicates that a fraction of the protein might have contained multiple labels. Since the TPR domain peptide binding is mediated strongly by side - chain residues with NH groups, a partial modification of these residues with the label could have influenced the binding of TPR2A - TPR2B to Hsp90. On the other hand, attaching the label to Hsp90 as a solution would probably not have resulted in a detectable change in the polarization as Hsp90 is significantly larger than TPR2A - TPR2B. Therefore, only a labeling of the Sti1 fragment appeared to be reasonable for obtaining binding data. In conclusion, fluorescence polarization does not seem to be an appropriate method for determining reliable K_d - values for this specific case with TPR domains.

4.8 Peptide Independent Binding Contacts of Sti1 with Hsp70

Sti1 was reported to be a potent stimulator of the yeast Hsp70/Ssa1 ATPase activity[164]. This finding suggests that, similar as for the interaction between Hsp90 and Sti1, there might also be additional binding contacts between Hsp70/Ssa1 and Sti1 besides the recognition of the Hsp70/Ssa1 C-terminal peptide via Sti1 TPR domains. To address this question, ITC and surface plasmon resonance (SPR, Biacore) experiments were performed with fragments of Hsp70/Ssa1 and Sti1. If indeed such peptide independent binding contacts exist, the affinities for Hsp70/Ssa1 fragments binding to Sti1 should be different compared to the affinities for binding of only the Hsp70/Ssa1 peptide.

As a control first the TPR2A-TPR2B fragment of Sti1 was titrated with the Hsp70/Ssa1 octapeptide GPTVEEVD. As the previous ITC experiments using isolated TPR domains showed, TPR2A should only weakly interact with the Hsp70/Ssa1 peptide whereas TPR2B should recognize it with reasonable affinity (compare section 4.3). Indeed, binding of the Hsp70/Ssa1 peptide to TPR2A-TPR2B seemed to be dominated by the TPR2B domain (table 4.16). The stoichiometry was close to one, although two binding sites were accessible. The affinity obtained for this interaction is $\sim 3.5\,\mu$M, which is nearly identical with the affinity of isolated TPR2B for the peptide ($4.2\,\mu$M), enthalpy and entropy terms had magnitudes comparable to those of the measurement with isolated TPR2B (see table 4.7). Although the TPR2A domain in the TPR2A-TPR2B fragment should display a basic peptide binding even with the unfavored Hsp70/Ssa1 peptide, this interaction does not contribute significantly to the overall binding affinity of TPR2A-TPR2B. In the ITC raw data, the

Table 4.16: Summary of affinities and thermodynamical parameters for the binding of Sti1 domains to Ssa1 fragments. 20 μM of the respective Hsp70/Ssa1 fragment in the measurement cell of the instrument was titrated with a 200 μM solution of the Sti1 fragment at a temperature of 20°C. In the case of the Hsp70/Ssa1 peptide 20 μM of the Sti1 fragment in the measurement cell was titrated with a 200 μM peptide solution. As a buffer 10 mM potassium phosphate, 1 mM TCEP, pH 7.5 was used. Affinity as K_a (association constant) and K_d (dissociation constant), binding enthalpy (ΔH), entropy (ΔS) and stoichiometry (N) are given for each measurement.

	N	K_a (10^5 M^{-1})	K_d (μM)	ΔH (cal/mol)	ΔS (cal/mol /deg)
Hsp70/Ssa1 peptide GPTVEEVD					
TPR2A - TPR2B	1.01 ± 0.05	2.86 ± 0.8	3.5	-3424 ± 240	13.3
Hsp70/Ssa1 C					
TPR2A - TPR2B	0.47 ± 0.02	18.1 ± 7.08	0.6	- 4497 ± 317	13.3
TPR2A - TPR2B N435A	1.01 ± 0.21	0.9 ± 0.5	11.2	- 6851 ± 222	- 0.7
Sti1 full - length	0.34 ± 0.03	4.7 ± 1.0	2.1	- 11590 ± 1252	- 13.6
Hsp70/Ssa1 MC					
TPR1	1.01 ± 0.06	6.6 ± 3.5	1.5	- 5484 ± 531	8.0
TPR2A - TPR2B	0.49 ± 0.01	12.6 ± 1.2	0.8	- 5994 ± 104	7.5
Sti1 full - length	0.30 ± 0.01	17.2 ± 2.0	0.6	- 10930 ± 230	- 8.7

binding contribution of TPR2A could only be guessed from the barely saturable constant decrease in binding heat following the typical binding transition for the TPR2B domain at a molar ratio of around one (figure 4.55). This binding behavior was similar as observed for isolated TPR2A and the Hsp70/Ssa1 peptide (compare figure 4.11, left). Overall, the binding of the Hsp70/Ssa1 peptide to TPR2A - TPR2B would be expected have a stoichiometry of 2:1, which can however be hardly deduced from the ITC data due to the low binding affinity of TPR2A for the peptide.

Then the Hsp70/Ssa1 C - terminal domain was analyzed for binding to

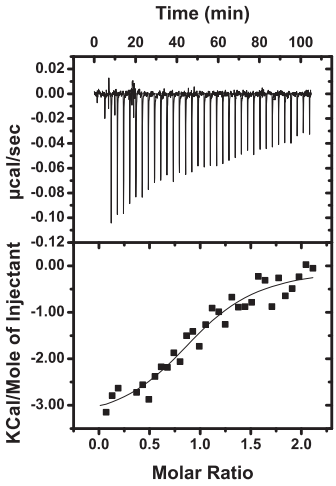

Figure 4.55: ITC raw binding heats (upper panel) and integrated binding heats with data fit (lower panel) for binding of the Hsp70/Ssa1 peptide GPTVEEVD to Sti1 TPR2A - TPR2B. The binding curve is a mixture of two binding events: The dominating binding of the peptide to TPR2B is visible as typical sigmoidal transition curve with midpoint at a molar ratio of ~ 1 whereas the underlying weak binding of the peptide to TPR2A causes the barely saturable slow decrease in binding heat following the TPR2B transition curve. 20 μM of TPR2A - TPR2B in the measurement cell was titrated with a 200 μM solution of the peptide at 20°C. As a buffer 10 mM potassium phosphate, 1 mM TCEP, pH 7.5 was used.

TPR2A - TPR2B. Here, the stoichiometry was found to be approximately 1:2. Additionally, the K_d for this interaction was significantly lower compared to TPR2A - TPR2B binding the Hsp70/Ssa1 peptide alone (0.6 μM versus 3.5 μM). This indicates potential important peptide independent binding contacts and shows that likely the interaction between TPR2A - TPR2B and Hsp70/Ssa1 cannot be fully described by a mere peptide binding. Possibly, the oligomeric state of Ssa1 has some influence on the bind-

ing because for human Hsp70 a tendency to form dimers was reported which is mediated by the C-terminal portion of the protein [280]. This might also apply for yeast Hsp70/Ssa1. The stoichiometry obtained here clearly shows that two molecules of the Hsp70/Ssa1 C-terminal domain bind to one molecule of TPR2A-TPR2B.

The TPR2A-TPR2B N435A mutant with its peptide binding deficient TPR2B domain recognized the Hsp70/Ssa1 C-terminal domain with an affinity of $\sim 11\,\mu$M, the stoichiometry was close to one for the interaction. This result is within expectation and indicates that TPR2A can also function as a low affinity Hsp70/Ssa1 binding site. Compared to binding of the Hsp70/Ssa1 peptide to isolated TPR2A, the affinity is moderately higher for TPR2A-TPR2B N435A binding the Hsp70/Ssa1 C-terminal fragment (11.2 versus 37.0 μM, compare table 4.6), again supporting the assumption of peptide independent binding contacts.

Full-length Sti1 bound the Hsp70/Ssa1 C-terminal domain with a stoichiometry of $\sim$ 1:3, reflecting the presence of three TPR domains in the protein that can all potentially bind Hsp70/Ssa1. The affinity here was moderately lower compared to the complex between TPR2A-TPR2B and the Hsp70/Ssa1 C-terminal domain (2.1 versus 0.6 μM). This difference can be explained by the different entropies because for binding of full-length Sti1 the entropy is unfavorable ($\Delta S = -13.6$ cal/mol/deg) whereas for TPR2A-TPR2B it supports binding ($\Delta S = 13.3$ cal/mol/deg).

For comparison, the Hsp70/Ssa1 two-domain construct MC comprising the middle/substrate binding domain and the C-terminal domain was also assessed for interaction with Sti1 fragments. Isolated TPR1 which is the TPR domain of Sti1 that had the highest affinity for the Hsp70/Ssa1 peptide (compare section 4.3) bound Hsp70/Ssa1 MC with a K_d of 1.5 μM. This is nearly identical with the K_d of TPR1 binding the Hsp70/Ssa1 peptide (compare table 4.5). Thus, TPR1 probably has no

additional interactions with the Hsp70/Ssa1 M and C domains.

Binding of TPR2A - TPR2B to Hsp70/Ssa1 MC gave a very similar K_d (0.8 μM) when compared to TPR2A - TPR2B binding the Hsp70/Ssa1 C fragment (0.6 μM). The binding entropy here is less favorable (7.5 versus 13.3 cal/mol/deg), however, the more negative enthalpy (- 5994 versus - 4497 cal/mol) could indicate additional binding interactions. The stoichiometry was again approximately 1:2. Therefore, the Hsp70/Ssa1 middle domain might further contribute to the interaction with the TPR2A - TPR2B fragment.

Full - length Sti1 bound the Hsp70/Ssa1 MC fragment better than the Hsp70/Ssa1 C - terminal domain alone (K_d 0.6 μM versus 2.1 μM) which is partially due to a less unfavorable entropy term ΔS (- 13.6 versus - 8.7 cal/mol/deg). The stoichiometry was again approximately 1:3. Looking only at the binding enthalpies for the interaction of Hsp70/Ssa1 MC with TPR1, TPR2A - TPR2B and full - length Sti1, it can be seen that summing up the individual enthalpies of TPR1 and TPR2A - TPR2B binding to Hsp70/Ssa1 MC yields approximately the enthalpy observed for full - length Sti1 binding to Hsp70/Ssa1 MC. This might indicate that parts of Sti1 outside the TPR1, TPR2A and TPR2B domains likely do not significantly contribute to the binding between Sti1 and Hsp70/Ssa1 M and C domain.

To estimate the significance of the binding data from the ITC measurements, additional experiments with another method were carried out for comparison using surface plasmon resonance (SPR, Biacore). The Sti1 full - length protein was immobilized on a sensor chip and Hsp70/Ssa1 C or MC fragments were added. Binding was monitored as change in response units (RU). Both Hsp70/Ssa1 fragments showed interaction with Sti1 on the chip and binding curves could be fitted to the data yielding K_d - values of $\sim 49\,\mu$M for the C - terminal domain and $\sim 11\,\mu$M for

the MC construct (figure 4.56). The difference in the binding affinity of

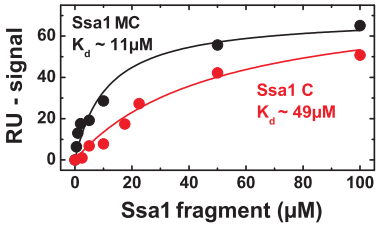

Figure 4.56: Binding curves obtained using surface plasmon resonance for the interaction of full - length Sti1 with the Hsp70/Ssa1 C - terminal domain (red) and the MC construct (black). Similar to the ITC experiments, the MC construct is found to bind stronger to Sti1 than the C - domain alone (compare table 4.16). However, the affinities obtained with surface plasmon resonance are significantly lower compared to ITC. Full - length Sti1 was immobilized on a CM5 sensor chip for the measurements. The respective Ssa1 fragments were added and the change in response units (RU) was monitored. Data fitting yielded binding curves as shown. Measurements were done at 20°C using 10 mM potassium phosphate, 1 mM TCEP, pH 7.5 as buffer.

Hsp70/Ssa1 C and MC for Sti1 was of comparable size as found with ITC (roughly a factor 4). Thus, the SPR data confirm the results from the ITC measurements. However, the affinities obtained with surface plasmon resonance were in general significantly lower than those from ITC. Possibly, immobilizing Sti1 on the sensor chip had adversely affected the TPR domains to a certain extent, maybe hindering access of the peptide to the ligand binding grooves. Therefore, the K_d - values from ITC can likely be regarded as more reliable. Nevertheless, the SPR data are an independent confirmation of the results from the ITC experiments. In conclusion, these measurements demonstrate that the Hsp70/Ssa1 M and C domains have additional binding contacts with TPR2A - TPR2B besides a mere peptide binding. In contrast to that, for TPR1 the data do not indicate any non - peptide binding interactions with Hsp70/Ssa1 M and C.

4.9 Formation of Sti1/Hsp70/Hsp90 Ternary Complexes

The binding selectivities and affinities from the ITC experiments in this work so far gave important information about how a ternary complex between Sti1, Hsp70/Ssa1 and Hsp90 could be composed. These data indicated that Hsp90 is likely bound to the central TPR2A - TPR2B unit in Sti1 whereas Hsp70/Ssa1 could bind either to TPR1, TPR2B or possibly even both at the same time. To further study the complex formation between Sti1, Hsp70/Ssa1 and Hsp90, analytical ultracentrifugation experiments (aUC) were carried out in collaboration with Alina Röhl and Dr. Klaus Richter (both Lehrstuhl für Biotechnologie, TUM). Thereby, especially the role of TPR2B for the formation of ternary complexes should be addressed.

Analytical ultracentrifugation is an ideal method to qualitatively analyze large protein complexes as found in the Sti1 - Hsp70 - Hsp90 system because other methods like ITC and NMR in general require significantly higher protein amounts/concentrations compared to ultracentrifugation. This can often be problematic with large proteins. Furthermore, NMR in particular is limited with respect to the size of proteins that can be studied. Therefore, it is rather applicable for isolated domains than for the full - length proteins of the system to analyze here, because the molecular weight of a potential ternary complex comprising Sti1, Hsp70/Ssa1 and Hsp90 is roughly 300 kDa. Ultracentrifugation, in contrast, works best with larger molecules and can thus give valuable information complementary to ITC and NMR.

For aUC experiments, full - length Hsp70/Ssa1 purified from *Pichia pastoris* (kindly provided by Lars Mitschke and Alina Röhl, Lehrstuhl für Biotechnologie, TUM) was labeled with carboxyfluorescein (Ssa1*). Thus the sedimentation behavior specifically of Hsp70/Ssa1 could be followed

in aUC runs with fluorescence detected experimental setup. First, the formation of a binary complex between Ssa1* and full-length Sti1 or the Sti1 TPR2A-TPR2B fragment was analyzed (figure 4.57, upper panel). Ssa1* alone sedimented with ~3.8 S. Addition of TPR2A-TPR2B or full-

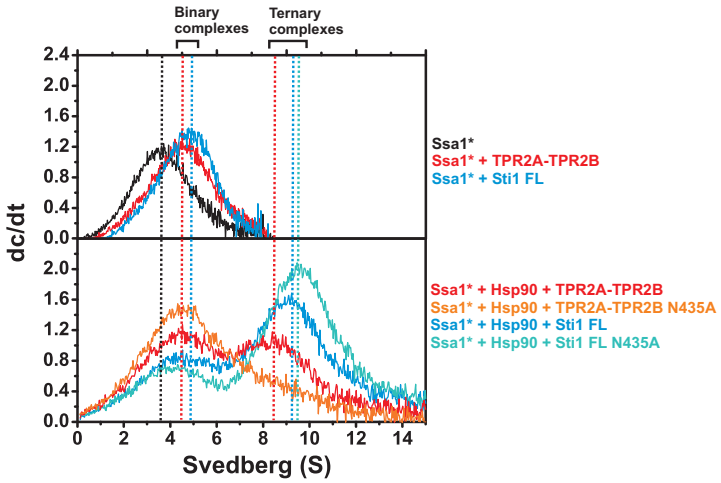

Figure 4.57: Formation of Sti1-Hsp70 binary (upper panel) and Sti1-Hsp70-Hsp90 ternary (lower panel) complexes studied by analytical ultracentrifugation. Hsp70/Ssa1 that had been labeled with carboxyfluorescein (Ssa1*) was monitored for complex formation with wild-type and mutant full-length (FL) Sti1 or the Sti1 TPR2A-TPR2B fragment. Upper panel: Ssa1 forms a binary complex with Sti1 FL and equally well with TPR2A-TPR2B. Lower panel: Sti1 FL and also TPR2A-TPR2B mediate ternary complex formation with Hsp70/Ssa1 and Hsp90. Sti1 FL containing the N435A mutation in TPR2B still supports the ternary complex, however, TPR2A-TPR2B with the respective mutation does not. This indicates that TPR2B has an important function for simultaneous binding of Hsp70/Ssa1 and Hsp90 to Sti1. For the measurements 500 nM of labeled Ssa1 were used, Sti1 variants and Hsp90 were added in excess (3 μM). Measurements were done in 10 mM potassium phosphate, 1 mM TCEP, pH 7.5 at 20°C.

length Sti1 led to a shift of the peak maximum to S-values of ~4.5 and

4.9, respectively. Therefore, both Sti1 proteins formed a complex with Ssa1 which confirms the ITC experiments that found TPR2A - TPR2B as a potential Hsp70/Ssa1 binding site (section 4.8).

Then, the ability of full - length Sti1 and TPR2A - TPR2B was tested to support the formation of ternary complexes with Hsp70/Ssa1 and Hsp90. Again labeled Ssa1 (Ssa1*) was used with both Sti1 variants, but in this case additionally Hsp90 was added in excess ($\sim$ sixfold) over Ssa1*. In presence of Hsp90, the peaks for the binary complex between Ssa1* and TPR2A - TPR2B or full - length Sti1 could be observed at 4.5 and 4.9 S as before (figure 4.57, lower panel). However, new peaks appeared at $\sim$ 8.5 (TPR2A - TPR2B) and 9.2 S (full - length Sti1), representing the ternary complexes between Sti1, Hsp70/Ssa1* and Hsp90. This result clearly confirms that TPR2A - TPR2B can act as Hsp70/Ssa1 and also Hsp90 binding site and demonstrates that TPR2A - TPR2B allows for a simultaneous binding of both proteins. Thus, TPR2A - TPR2B seems to be the minimal fragment to mediate ternary complexes between Sti1, Hsp70/Ssa1 and Hsp90. Consequently, TPR1 as additional Hsp70/Ssa1 binding site is not essential for ternary complex formation. However, more Hsp70/Ssa1* seems to be present in the ternary complex with full - length Sti1 compared to the TPR2A - TPR2B fragment, as the relative heights of the respective peaks corresponding to the binary and ternary complex indicate.

Finally, full - length Sti1 and TPR2A - TPR2B containing the N435A mutation within TPR2B were likewise analyzed for supporting ternary complex formation. For the full - length Sti1 N435A mutant the respective peak at $\sim$ 9.2 S typical for the ternary complex was still visible. However, with TPR2A - TPR2B N435A no peak for the ternary complex at $\sim$ 8.5 S could be observed anymore. Similar results were obtained using full - length Sti1 and the TPR2A - TPR2B fragment containing the R465A and R469A mutations within TPR2B (data not shown), which were likewise

found to abolish peptide binding to TPR2B (compare section 4.5). This shows again that TPR2B functions as an Hsp70/Ssa1 binding site.

Interestingly, the peak observed for the measurement with TPR2A - TPR2B N435A had its maximum at a S - value of ~ 4.5, which corresponds to the binary complex between TPR2A - TPR2B N435A and Hsp70/Ssa1*, but not ~ 3.8 S as would be expected for free Hsp70/Ssa1*. This indicates that – despite the mutation of the Hsp70/Ssa1 peptide binding site in TPR2A - TPR2B – there is still remaining binding between the two proteins. Under the conditions used with approximately equal amounts of Hsp90 and TPR2A - TPR2B N435, most of the Sti1 mutant should bind to Hsp90 because TPR2A - TPR2B with the N435A mutation can still bind Hsp90 with a high affinity ($\sim 0.2\,\mu$M, table 4.15). However, a minor fraction of unbound TPR2A - TPR2B N435A could still be available for binding to Hsp70/Ssa1*, even if the preferred Hsp70/Ssa1 peptide binding site within TPR2B is not functional due to the mutation. On the one hand, the intact TPR2A domain has a basic binding also of the unfavored Hsp70/Ssa1 peptide. On the other hand, the additional peptide independent binding interactions between Hsp70/Ssa1 and TPR2A - TPR2B as found in the ITC experiments (compare section 4.8) could further contribute to the binding between Hsp70/Ssa1 and mutant TPR2A - TPR2B. Overall, this might give sufficient binding strength to yield a visible complex between the mutant TPR2A - TPR2B and Hsp70/Ssa1, especially since the labeled Hsp70/Ssa1 was used in a comparatively low concentration of only $0.5\,\mu$M. Therefore, the fraction of the free TPR2A - TPR2B N435A available for binding Hsp70/Ssa1* might nearly saturate Hsp70/Ssa1*. Indeed, control experiments carried out to form binary complexes using Hsp70/Ssa1* and TPR2A - TPR2B containing the N435A, R465A or R469A amino acid replacements could confirm these findings, for all mutants complex formation was observed (data not shown).

4.10 Analysis of a Sti1 TPR2A - TPR2B Linker Mutant

As a comparison of the ^{15}N - TROSY spectra for isolated TPR2A and TPR2B with the spectrum of the two - domain fragment TPR2A - TPR2B indicated, there are no major inter - domain contacts between both TPR subunits in TPR2A - TPR2B (section 4.4.1). Only a few residues around R425 within TPR2B showed shifted resonances in the two - domain construct (compare figure 4.23), pointing at slight but potentially important domain interactions. Adding the unlabeled isolated TPR2A domain to the ^{15}N - labeled isolated TPR2B domain without and in presence of Hsp90 peptide ligand did not result in detectable binding between the two domains in the NMR spectra of TPR2B (data not shown). Thus, these domain contacts seem to be rather weak. To test whether these interactions play a role for

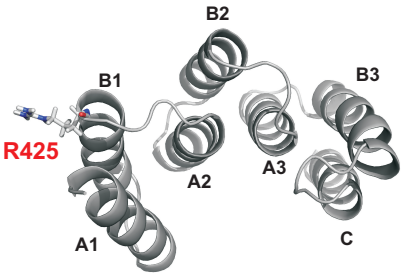

Figure 4.58: NMR structure of the Sti1 TPR2B domain showing the position of residue R425. R425 within helix B1 of TPR2B is solvent exposed and could therefore potentially undergo inter - domain contacts with residues from the TPR2A domain in the TPR2A - TPR2B fragment. The helices of the TPR motives are indicated.

the function of the two - domain construct comprising TPR2A and TPR2B, a mutation was introduced into the TPR2A - TPR2B fragment replacing R425 by alanine (termed “linker mutant”). This conservative mutation

should presumably not interfere with the secondary structure of TPR2B. As an inspection of the NMR structure shows, R425 is solvent exposed and points to the convex backside of TPR2B (figure 4.58). Therefore, in principle R425 could undergo domain contacts mediated by its long side - chain. A CD spectroscopic characterization of the TPR2A - TPR2B R425A linker variant shows that the mutation had little influence on the structure and stability of the protein, as expected (figure 4.59). The secondary

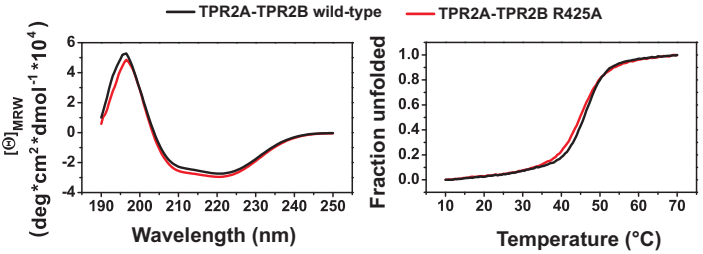

Figure 4.59: CD spectrum (left) and CD thermal transition (right) of the Sti1 TPR2A - TPR2B R425A (linker) mutant in comparison to wild - type TPR2A - TPR2B. The mutation has only very minor effect on the structure and stability of the TPR2A - TPR2B fragment. 10 μM of wild - type TPR2A - TPR2B or the mutant were measured in 50 mM potassium phosphate, 50 mM potassium chloride, 1 mM TCEP, pH 7.5. CD spectra were recorded at 20°C, thermal unfolding was monitored at a wavelength of 222 nm.

structure content and the thermal stability of the protein was nearly identical to the wild - type.

Next, the binding of the mutant to Hsp90 was analyzed using ITC. As outlined, the wild - type TPR2A - TPR2B bound Hsp90 so strong that no affinity could be obtained from ITC (section 4.7). Therefore, it was likely that the linker mutant would bind to Hsp90 with a similar affinity. Indeed, the TPR2A - TPR2B linker mutant showed very tight interaction with Hsp90, however, the shape of the ITC binding curve indicated a re-

duced affinity compared to the wild-type TPR2A-TPR2B (figure 4.60). Thus, in case of the linker mutant a data fitting was possible, yielding

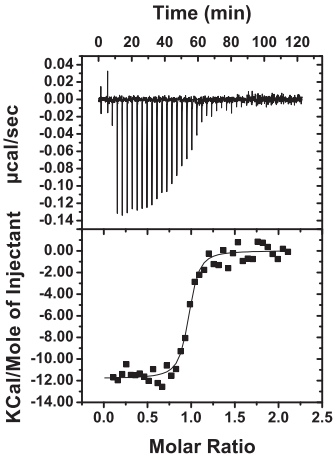

Figure 4.60: ITC binding curve for the interaction of the Sti1 TPR2A-TPR2B R425A (linker) mutant and full-length Hsp90. The upper panel shows the raw binding heats, the lower panel the integrated binding heats and the data fit. Surprisingly, the affinity of the linker mutant for Hsp90 is lower compared to wild-type TPR2A-TPR2B, as visible from the shape of the raw binding data (compare figure 4.53, left). 20 μM of full-length Hsp90 in the measurement cell was titrated with a 200 μM solution of the TPR2A-TPR2B R425A (linker) mutant at 20°C. As a buffer 10 mM potassium phosphate, 1 mM TCEP, pH 7.5 was used.

a K_d value of $\sim$ 40 nM (table 4.17). The result of a weakened binding as a consequence of the linker mutation is unexpected since the peptide binding site of TPR2B within TPR2A-TPR2B should not be affected by the R425A mutation. This could point at somewhat reduced peptide independent binding interactions between the linker mutant and Hsp90.

The TPR2A-TPR2B R425A was further analyzed for its capacity to in-

Table 4.17: Summary of affinities and thermodynamical parameters for the binding of the Sti1 TPR2A - TPR2B R425A (linker) mutant to Hsp90. 20 μM of Hsp90 in the measurement cell of the instrument was titrated with a 200 μM solution of TPR2A - TPR2B R425A at a temperature of 20°C. As a buffer 10 mM potassium phosphate, 1 mM TCEP, pH 7.5 was used. Affinity as K_a (association constant) and K_d (dissociation constant), binding enthalpy (ΔH), entropy (ΔS) and stoichiometry (N) are given for the measurement.

N	K_a (10^5 M^{-1})	K_d (μM)	ΔH (cal/mol)	ΔS (cal/mol/deg)
0.95 ± 0.01	277 ± 78.6	0.036	- 11790 ± 199	- 6.2

hibit the Hsp90 ATPase activity (figure 4.61). The linker mutant was still able to significantly reduce the ATP hydrolysis of Hsp90. But compared

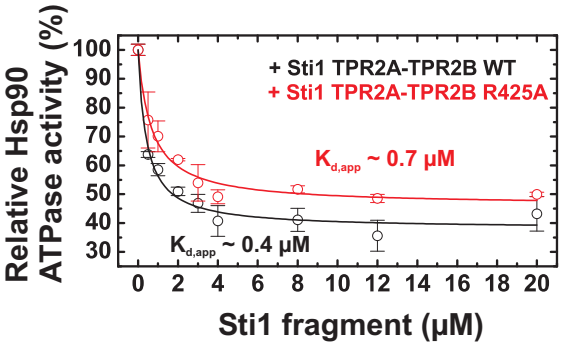

Figure 4.61: Inhibition of the Hsp90 ATPase activity by the Sti1 TPR2A - TPR2B R425A (linker) mutant compared to wild - type TPR2A - TPR2B. The mutant has a lower inhibitory capacity than the wild - type protein. TPR2A - TPR2B or the mutant was titrated to 4 μM of wild - type Hsp90. ATPase activities were measured in 40 mM HEPES, 150 mM potassium chloride, 5 mM $MgCl_2$, 2 mM ATP, pH 7.5 at 30°C using a coupled regenerating ATPase assay [244].

to wild-type TPR2A-TPR2B, the apparent K_d-value obtained from fitting the inhibition curve was higher ($\sim 0.7\,\mu$M versus $\sim 0.4\,\mu$M). This is in agreement with the ITC binding data, although the K_d-values determined from the ATPase measurements in general were higher due to the elevated salt concentrations used in the assay. The maximum inhibition of Hsp90 by the linker mutant seems to be lower compared to wild-type TPR2A-TPR2B: Under the conditions used, the wild-type protein reduced the relative ATPase activity of Hsp90 down to levels of $\sim 40\,\%$, the mutant, in contrast, only to $\sim 50\,\%$. This might indicate slight mechanistic differences in the inhibition of Hsp90 by wild-type and mutant TPR2A-TPR2B.

4.11 *In Vivo* Analysis of Sti1 TPR Domain Mutants

The *in vitro* data obtained in this work so far indicated that the TPR2B domain of Sti1 plays a certain role for the binding of Hsp90 but can also serve as an Hsp70/Ssa1 binding site. Furthermore, the analytical ultracentrifugation experiments demonstrated that the TPR2B domain in the Sti1 TPR2A - TPR2B fragment can mediate the formation of ternary complexes with Hsp70/Ssa1 and Hsp90 (section 4.9). Therefore, the importance of the second potential Hsp70/Ssa1 binding site within Sti1 provided by TPR1 remains unclear. At least it turned out that with the TPR1 domain additionally present in Sti1 more Hsp70/Ssa1 was found in ternary complexes with Hsp90. Earlier studies found that mutations within Sti1 TPR2B targeting its peptide binding site significantly reduced the activity of heterologously expressed human GR receptor in yeast cells, however, not down to control levels [187]. Previous work carried out by Dr. Andreas Schmid (Lehrstuhl für Biotechnologie, TUM) now interestingly showed that the TPR1 domain of Sti1 seems to be dispensable for the activation of the human GR in yeast cells (figure 4.62). A complete deletion of the TPR1 domain had no effect on the *in vivo* activity of the receptor. Taken together, these findings would suggest that TPR2B can functionally fully compensate for a loss of the TPR1 domain whereas TPR1 can only partially replace TPR2B.

To further investigate the role of the TPR2B domain, additional *in vivo* assays were performed with yeast cells. Point mutations within the TPR2B peptide binding groove were introduced into the Sti1 ΔTPR1 mutant and tested for supporting activation of the human GR. In the ΔTPR1 variant only one possible Hsp70/Ssa1 peptide binding site is present provided by TPR2B. Therefore, TPR2B point mutations in such a Sti1 background allow for directly assessing the importance of the TPR2B peptide binding

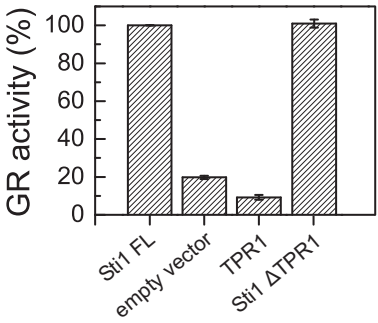

Figure 4.62: *In vivo* function of a Sti1 TPR1 deletion mutant. The plot shows the relative activity of the human glucocorticoid receptor (GR) in yeast cells expressing different Sti1 variants as indicated. The Sti1 ΔTPR1 mutant supports GR activity comparable to full-length (FL) Sti1 and therefore seems to be dispensable for *in vivo* GR activation. The data were kindly provided by Dr. Andreas Schmid (Lehrstuhl für Biotechnologie, TUM).

for the Sti1 *in vivo* functions. As mutation sites N435, R465 and R469 were chosen. Amino acid replacements at these positions were already shown to significantly reduce or abolish peptide binding to TPR2B without affecting the secondary structure of the domain too much (section 4.5). Thus, even with the peptide binding ability lost, the TPR2B domain should still retain all its other essential functions like contributing to the Hsp90 ATPase inhibition.

The single point mutants N435A, R465A and R469A as well as the double point mutants N435A/R465A and N435A/R469A of Sti1 ΔTPR1 in a p425GPD vector were generated by standard protocols. The *in vivo* testing of the mutant plasmids was then done by Alina Röhl (Lehrstuhl für Biotechnologie, TUM). Briefly, the plasmids with the different Sti1 mutants were used to transform a yeast strain lacking genomic Sti1 (Δ*sti1*). This yeast strain additionally contained a plasmid for the expression of

the human GR and a reporter plasmid which carried β - galactosidase under the control of a GR response element. Upon addition of the GR ligand deoxycorticosterone (DOC) to the cells, active GR would bind to the GR response element and induce the transcription and expression of β - galactosidase. The amount of β - galactosidase could then be assessed by a colorimetric assay in which the yeast cells are lysed and the enzyme converts the added substrate o - nitrophenyl - β - D - galactopyranosid (ONPG) to the yellowish o - nitrophenol and galactose. The rate of substrate conversion in this assay then is an indirect measure for the activity of the GR.

As shown in figure 4.63, Sti1 ΔTPR1 with a functional TPR2B domain supported GR activity similar to full - length (FL) Sti1, in agreement with the previous findings (figure 4.62). For cells transformed with an empty

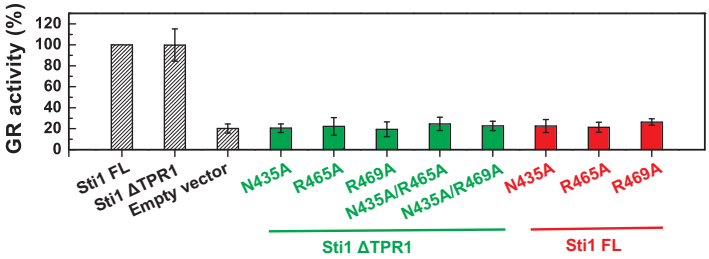

Figure 4.63: *In vivo* function of Sti1 TPR2B point mutants. The plot shows the relative activity of the human glucocorticoid receptor (GR) in yeast cells expressing full - length (FL) Sti1 or the Sti1 ΔTPR1 deletion variant containing different point mutations within TPR2B as indicated. All point mutants fail to support GR activity to a level higher than obtained with the empty vector.

p425GPD vector as a control, in contrast, only ~ 20 % relative GR activity were observed. When the Sti1 ΔTPR1 point mutants then were tested, all variants were unable to support GR activity to levels above the con-

trol. Thus, the ability of TPR2B to bind peptide seems to be an essential requirement for the *in vivo* function of Sti1.

As a control, additionally the single point mutations N435A, R465A and R469A were introduced into the full-length Sti1 and the mutant plasmids were likewise tested in yeast cells as before. If TPR1 is able to at least partially compensate for a lost peptide binding of TPR2B, then GR activity should be observed with the these mutants significantly above the control level. Surprisingly, also these mutants all completely failed to function in GR activation under the conditions used. The relative GR activity was comparable to the control. This is unexpectedly in contrast to a previous report as mentioned above [187]. Therefore, according to the data, TPR1 obviously cannot compensate for a peptide binding deficient TPR2B domain.

As described in section 4.10, a mutation of residue R425 targeting the potential inter-domain linkage of the Sti1 TPR2A and TPR2B domains had modest but significant influence on the binding and ATPase inhibition of Hsp90 by the Sti1 TPR2A-TPR2B fragment. To analyze whether

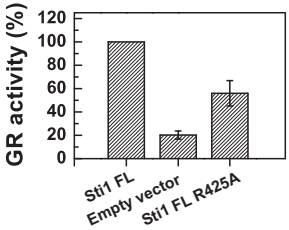

Figure 4.64: *In vivo* function of the Sti1 linker mutant. The plot shows the relative activity of the human glucocorticoid receptor (GR) in yeast cells expressing wild-type full-length (FL) Sti1 or the R425A ("linker") mutant thereof. The mutant is significantly less effective in supporting GR activation.

the biochemical *in vitro* data obtained on this mutant are likewise of relevance *in vivo*, the R425A ("linker") mutation was also introduced into the full-length Sti1 in a p425GPD yeast vector. GR activity assays were then performed with the mutant plasmid by Alina Röhl (Lehrstuhl für Biotechnologie, TUM) as described before. In good agreement with the *in vitro* data, the R425A ("linker") mutation within TPR2B had a significant impact on GR activation in yeast cells (figure 4.64). With the mutant the GR activity was reduced down to a level of only $\sim 60\,\%$ compared to wild-type Sti1. Therefore, not only the peptide binding of TPR2B seems to be important for the Sti1 *in vivo* function but also its role in the ihibition of the Hsp90 ATPase activity.

4.12 NMR Docking of Sti1 TPR2A - TPR2B and Hsp90

As the ITC binding studies and ATPase inhibition data indicated, there seem to be significant interactions between Hsp90 and Sti1 which are independent of the peptide binding by the Sti1 TPR domains. These interactions are weaker than the peptide binding contacts but essential for the inhibition of Hsp90 by Sti1. To identify the binding interfaces and to obtain a model for the complex between Sti1 and Hsp90, NMR experiments were carried out using isolated domains of both proteins. NMR is a well suited method to study the rather weak interactions as often found for protein complexes as it uses higher protein concentrations. Thus, in the case of Sti1 and Hsp90, NMR could likely provide further information on the peptide independent binding contacts between the two proteins. Since all domains of Hsp90 and Sti1 expressed in sufficient amounts and behaved well in isolation and additionally backbone resonance assignments were available for all Hsp90 domains as well as the Sti1 TPR2A and TPR2B domains, a detailed characterization of the Hsp90 - Sti1 complex could be carried out.

First, the ^{15}N - labeled Hsp90 domains were analyzed for binding Sti1 domains. Upon adding full - length Sti1, no shifts or other indications for complex formation like line broadening could be observed in the spectrum of the Hsp90 N - terminal domain (residues 1-210, data not shown). However, from these data it cannot be ruled out that there is an interaction between Sti1 and the Hsp90 N - terminal domain in the full - length Hsp90. At least under the conditions used here for NMR, the isolated Hsp90 N - terminal domain appears to be not involved in binding to Sti1.

Next, the isotopically labeled isolated Hsp90 C - terminal domain was tested for binding Sti1. To exclusively monitor peptide independent interactions with Sti1, a mutant of the Hsp90 C - terminal domain was used

lacking 20 residues from its C - terminal end (Hsp90 CΔ20 mutant, residues 528 to 689) which contain the peptide motive bound by the Sti1 TPR domains. An assignment for this mutant was obtained in this work as described (see section 3.2). As the ITC data indicated (table 4.15), there should not be major peptide independent binding contacts between the Hsp90 C - terminal domain and the Sti1 TPR2A - TPR2B fragment. Surprisingly, strong line broadening was observed when TPR2A - TPR2B was added to Hsp90 CΔ20. Only signals corresponding to flexible parts of the domain were still visible in the spectrum (figure 4.65). This indicated the formation of a large complex (molecular weight of the complex ~ 68 kDa). However, the binding observed here might most likely reflect an unspecific binding (see below).

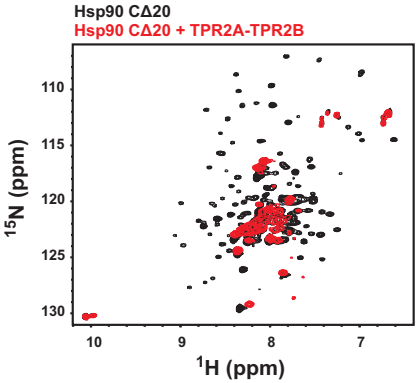

Figure 4.65: Overlay of the ^{15}N - TROSY NMR spectra for the free Hsp90 C - terminal domain mutant CΔ20 (black) and in complex with the Sti1 fragment TPR2A - TPR2B (red). The line broadening for Hsp90 CΔ20 residues observed in the presence of TPR2A - TPR2B indicates the formation of a large complex which might potentially be unspecific. 250 μM of Hsp90 CΔ20 was measured at 303 K and 750 MHz in a buffer of 10 mM potassium phosphate, 1 mM TCEP, pH 7.5. The TPR2A - TPR2B fragment was added in a 1:1 molar ratio.

Finally the binding of TPR2A, TPR2B and TPR2A - TPR2B to the Hsp90 middle domain (Hsp90 M, residues 273 to 527) was assessed. An assignment for Hsp90 M was obtained previously by Dr. Franz Hagn (bmrb accession code 16279), thus a detailed analysis of the binding to this domain could be carried out. Adding isolated TPR2A and TPR2B resulted in peak shifts in the NMR spectrum of ^{15}N - labeled Hsp90 M in both cases, however, only if a larger excess (threefold) of the respective domain over Hsp90 M was used (data not shown). This demonstrates that both TPR domains in principle can bind to Hsp90 M. Thus, the peptide independent interactions between Sti1 and Hsp90 involve the Hsp90 M domain, as the ITC data already indicated (section 4.7).

Then, the two - domain fragment TPR2A - TPR2B was tested for binding to Hsp90 M. Here – in contrast to the isolated TPR domains – adding lower a concentration of the Sti1 fragment (twofold molar excess over Hsp90 M) was sufficient to give significant peak shifts. Additionally, several signals of Hsp90 M showed severe line broadening beyond detection limit (figure 4.66, left, upper panel). In general, the chemical shift perturbation with TPR2A - TPR2B was stronger compared to the measurements with the isolated TPR2A and TPR2B domains (figure 4.66, left, lower panel) although a lower concentration of was used here. These observations indicate a stronger binding of TPR2A - TPR2B. Thus, the data confirm the assumption that both TPR2A and TPR2B have binding sites with Hsp90 M that contribute synergistically to the interaction with Hsp90 M in the TPR2A - TPR2B two - domain fragment.

A mapping of the chemical shift perturbation data for the binding between Hsp90 M and TPR2A - TPR2B onto the crystal structure of Hsp90 M shows that it is mainly a region involving residues 447 to 463 which is affected by the binding of Sti1 TPR2A - TPR2B (figure 4.66, right). In the full - length Hsp90, this part of Hsp90 M is located at the outside of the

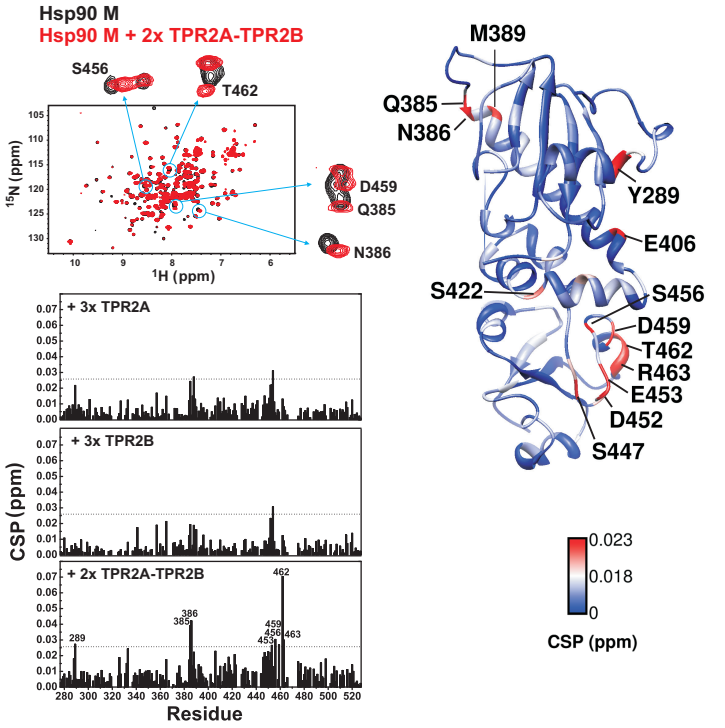

Figure 4.66: Binding of Sti1 TPR2A, TPR2B and TPR2A - TPR2B to the Hsp90 M domain monitored by NMR. Left, upper panel: Overlay of ^{15}N - TROSY spectra for free Hsp90 M (black) and in complex with TPR2A - TPR2B. Significant shifts and line broadening can be observed upon complex formation. Left, lower panel: Chemical shift perturbation (CSP) plots for binding of TPR2A, TPR2B and TPR2A - TPR2B to Hsp90 M. The significance level (average CSP + 2x SD) for the measurement with TPR2A - TPR2B is indicated in the plots by a dashed line. Right: Mapping of CSP data for binding of TPR2A - TPR2B onto a crystal structure of Hsp90 M (PDB: 1HK7). The strongest shifts occur at the outside of the M domain. 200 μM of Hsp90 M was measured at 298 K and 900 MHz in a buffer of 10 mM potassium phosphate, 20 mM potassium chloride, 1 mM TCEP, pH 7.5. The TPR2A - TPR2B fragment was added in a 1:2, TPR2A and TPR2B in a 1:3 molar ratio.

dimer and is therefore well accessible for binding interactions with other proteins.

Then, ^{15}N-labeled Sti1 fragments were analyzed for binding of Hsp90 domains. As outlined before, interestingly the Hsp90 C-terminal domain lacking the peptide motive also bound the TPR2A-TPR2B fragment. Adding the Hsp90 CΔ20 mutant to labeled isolated TPR2A led to severe line broadening, which was however abolished when additional ten residues were removed in the C domain (figure 4.67). The same could be

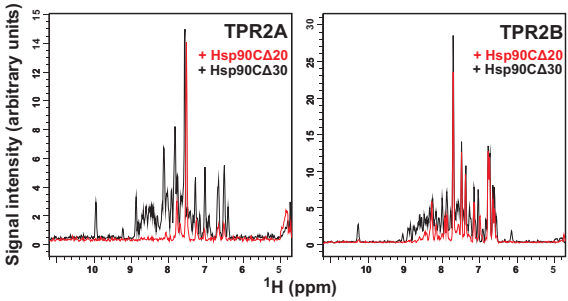

Figure 4.67: Binding of Hsp90 C-domain mutants to Sti1 TPR2A and TPR2B monitored by NMR. The plots show projections for the 2D ^{15}N-HSQC spectra of TPR2A (left) and TPR2B (right) in complex with the Hsp90 C-domain deletion mutants Hsp90 CΔ20 (red) and Hsp90 CΔ30 (black) lacking either 20 or 30 residue from the C-terminus. The strong line broadening observed for the Hsp90 CΔ20 mutant indicates complex formation which is abolished with Hsp90 CΔ30. 150 μM of TPR2A or TPR2B was measured at 293 K and 750 MHz in a buffer of 10 mM potassium phosphate, 1 mM TCEP, pH 7.5. Hsp90 mutants were added in a twofold molar excess.

found for TPR2B. The results confirm the observations made with TPR2A-TPR2B binding to ^{15}N-labeled Hsp90 CΔ20. The data point at unspecific binding mediated by a stretch of about ten unfolded residues in the Hsp90 C-terminal domain which serve as binding site for Hsp90 substrates as

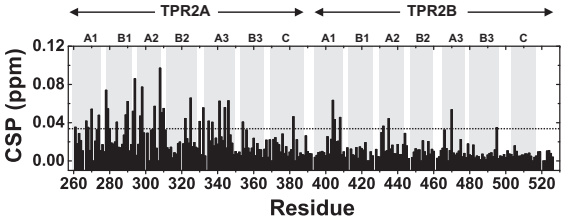

Figure 4.68: Chemical shift perturbation plot for binding of the Hsp90 C-domain to ^{15}N-labeled Sti1 TPR2A-TPR2B. The chemical shift perturbation pattern is comparable to binding of the Hsp90 octapeptide to TPR2A-TPR2B (see figure 4.44). Mainly residues within TPR2A are affected by the binding of Hsp90 C. The significance level (twofold average CSP) is indicated by a dashed line. 600 μM of TPR2A-TPR2B was measured at 303 K and 900 MHz in a buffer of 50 mM potassium phosphate, 50 mM potassium chloride, 1 mM TCEP, pH 7.5. Hsp90 C was added in a 1:1 molar ratio. TPR secondary structure elements are indicated.

shown (see section 3). This region of Hsp90 C contains predominantly charged residues (E and D) and likely these are bound unspecifically via charge complementarity here since the TPR domains both have very positive electrostatic potentials within their ligand binding grooves.

Binding of the wild-type Hsp90 C domain to TPR2A-TPR2B gave a chemical shift perturbation pattern comparable to binding of only the Hsp90 octapeptide (figure 4.68). Mainly residues within TPR2A showed peak shifts. This argues for no additional binding contacts between Hsp90 C and TPR2A-TPR2B besides the peptide binding, confirming the previous ITC data (section 4.7).

Isolated ^{15}N-labeled TPR2A and TPR2B were then tested for binding the Hsp90 M domain. In case of TPR2A, peak shifts and line broadening could be observed when Hsp90 M was added (figure 4.69, upper panel). The strongest shift perturbation occurred in the N-terminal part of helix C (residues 368 to 374, figure 4.69, middle panel). Additionally, some

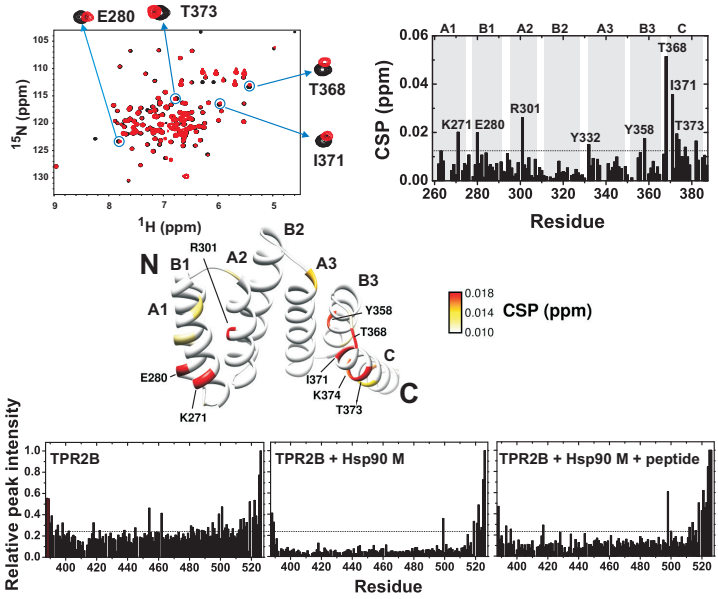

Figure 4.69: Binding of Hsp90 M to ^{15}N-labeled Sti1 TPR2A and TPR2B monitored by NMR. Upper panel, left: Overlay of the ^{15}N-HSQC spectra for TPR2A alone (black) and in complex with Hsp90 M (red). Peak shifts and line broadening are indicative of binding. Upper panel, right: Chemical shift perturbation (CSP) plot for binding of Hsp90 M to ^{15}N-labeled TPR2A. Secondary structure elements are given on top of the plot. Middle panel: Mapping of the chemical shift perturbation for binding of Hsp90 M onto the TPR2A crystal structure (kindly provided by Dr. Melissa Gräwert, Lehrstuhl Biochemie, TUM). N- and C-terminus and helices of the TPR motives are indicated. Lower panel: Plot of relative TPR2B ^{15}N-HSQC peak intensities for TPR2B (left), TPR2B + Hsp90 M (middle) and TPR2B + Hsp90 M + Hsp70/Ssa1 peptide PTVEEVD (right). Peak intensities were normalized with the last C-terminal residue of TPR2B (T526) having intensity 1.0. Significance levels (twofold average CSP or average peak intensity of free TPR2B, respectively) are indicated by a dashed line in the plots. 150 μM of TPR2A or TPR2B were measured at 293 K and 750 MHz or 600 MHz, respectively, in a buffer of 10 mM potassium phosphate, 1 mM TCEP, pH 7.5. Hsp90 M and the peptide were added in a 2:1 molar ratio.

charged residues in helices A1, B1 and A2 pointing with their side - chains to the convex backside of TPR2A showed peak shifts. However, it seems likely that these shift could reflect unspecific binding to some charge complementary regions on Hsp90 M. The binding of Hsp90 M to TPR2A was also assessed in the presence of the Hsp90 C - terminal peptide TEMEEVD (added in a twofold molar excess over TPR2A). In this case, there was still line broadening of TPR2A signals in the NMR spectrum, indicating that TPR2A can bind to Hsp90 M even with peptide bound to its ligand binding groove (data not shown).

Adding Hsp90 M to ^{15}N - labeled TPR2B did not result in significant peak shifts, although some very slight shifts for a few residues could be detected. However, signal intensities throughout the folded part of TPR2B (residues 393 to 516) were markedly decreased, indicating the formation of a larger complex (figure 4.69, lower panel). Interestingly, some of the signal intensity could be recovered when the Hsp70/Ssa1 peptide PTVEEVD was added in excess (twofold) over TPR2B to the TPR2B - Hsp90 M complex. This might indicate that TPR2B bound with the side of its peptide binding groove to Hsp90 M or – alternatively – conformational changes upon peptide binding weakened the affinity of TPR2B for Hsp90 allosterically. Also, adding increasing amounts of salt to the complex could weaken the interaction (data not shown). With only 20 mM additional potassium chloride, the intensities reached the level from the reference experiments with TPR2B alone, indicating that the complex was dissociated again. Thus, the binding between TPR2B and Hsp90 M seems to be very weak.

Overall, these data demonstrate that both TPR2A and TPR2B can bind individually to Hsp90 M and therefore potentially both contribute to the binding of Hsp90 M within the TPR2A - TPR2B fragment. However, it cannot be ruled out completely here that there is also unspecific binding in

the complexes of isolated TPR2A and TPR2B with Hsp90 M via electrostatic interactions. Both TPR domains have very positive potentials within their ligand binding grooves and Hsp90 M has a large surface providing some regions with highly negative potential that could mediate unspecific binding through charge complementarity.

Finally, ^{15}N labeled TPR2A - TPR2B was analyzed for binding Hsp90 M. As expected, the two - domain fragment showed significant peak shifts and line broadening when Hsp90 M bound to it (figure 4.70). Shifts oc-

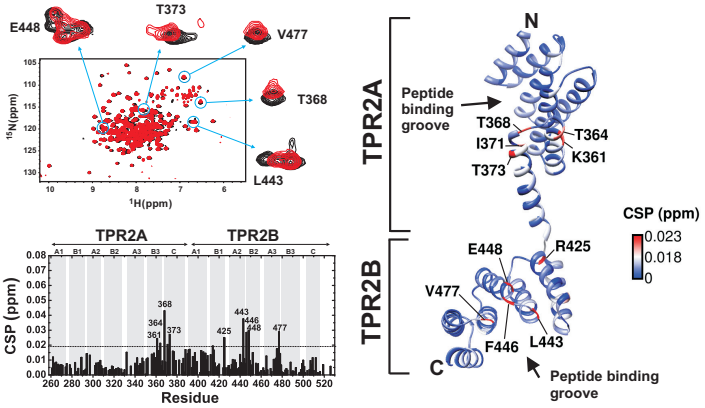

Figure 4.70: Binding of Hsp90 M to Sti1 TPR2A - TPR2B monitored by NMR. Left, upper panel: Overlay of the ^{15}N - TROSY spectra for free TPR2A - TPR2B (black) and in complex with Hsp90 M (red). Left, lower panel: Plot of the chemical shift perturbation for the binding of Hsp90 M to TPR2A - TPR2B. Both TPR2A and TPR2B subdomains experience shift perturbation upon binding of Hsp90 M. The significance level (average CSP + 2x standard deviation) is indicated by a dashed line in the plot. Right: Color coded mapping of chemical shift perturbation data for binding of Hsp90 M onto the crystal structure of TPR2A - TPR2B (PDB: 3UQ3). 150 μM of TPR2A - TPR2B was measured at 303 K and 900 MHz in a buffer of 10 mM potassium phosphate, 20 mM potassium chloride, 1 mM TCEP, pH 7.5. Hsp90 M was added in a 2:1 molar ratio.

curred within both TPR2A and TPR2B subdomains demonstrating that TPR2A and TPR2B form a joint binding site for Hsp90 M in TPR2A - TPR2B. Within TPR2A, shifts clustered involving amino acids from the C - terminal portion of helix B3 and the N - terminal part of helix C (residues 361 to 373, figure 4.70, right). This is the same region of TPR2A that was found to be affected when the binding of Hsp90 M to isolated TPR2A was monitored. For TPR2B larger shifts could be found at one edge of the domain including residues 443, 446, 448 and 477. In contrast to isolated TPR2B binding Hsp90 M, here significant shifts were observed within TPR2B instead of predominantly line broadening. As outlined before, this supports the assumption that isolated TPR2B potentially had formed a to a certain extent unspecific complex with Hsp90 M.

Information from NMR chemical shift perturbation experiments can be useful in the determination of potential binding sites. However, such data have to be evaluated carefully because allosteric rearrangement of structure elements within proteins upon binding can also lead to secondary chemical shifts. Thus, for a further confirmation of the potential binding sites found by the chemical shift perturbation experiments and for performing an NMR data driven docking, additionally paramagnetic relaxation enhancement (PRE) measurements were carried out. To this end, single cysteine mutants of Hsp90 M were generated for site - specifically attaching a spin label. Hsp90 M was preferentially chosen for the mutation because it does not contain any native cysteine, in contrast to TPR2A - TPR2B (one cysteine at position 453). Consequently, it was not necessary to carry out an additional mutation reaction to remove native cysteines prior to the actual mutation step.

Six different positions in Hsp90 M – N298, Q384, S411, S422, K469 and K484 – were chosen for a mutation. These are spread over the whole length of the molecule and covering the inner and outer side of

Hsp90 M with respect to the orientation of Hsp90 M in the dimeric full-length Hsp90. Another cysteine mutant, S456C, was already available and kindly provided by Dr. Franz Hagn (Institute for Advanced Study, TUM). Especially residues S411, S422 and S456 were supposed to be within the potential binding site of TPR2A-TPR2B on Hsp90 M (compare figure 4.66) and seemed to be well suited for a mutation since the side-chain of the native serine at these positions and the engineered cysteine are similar in size. Thus, the mutation should not disrupt any secondary structure elements.

All mutants generated behaved well and could be expressed solubly and with amounts comparable to wild-type Hsp90 M. The PROXYL-modified variants were then added to ^{15}N-labeled Sti1 TPR2A-TPR2B and a potential reduction of signal intensities in the 2D ^{15}N-TROSY NMR spectra was analyzed. For TPR2A-TPR2B in complex with the PROXYL-modified Hsp90 M mutants N298C, Q384C, K469C and K484C no significant relaxation enhancement could be observed (figure 4.71). As a control, also the isolated ^{15}N-labeled TPR2A and TPR2B domains were analyzed for PRE effects with the PROXYL-modified Hsp90 M mutants Q384C and K469C. Likewise, in this case no significant reduction in signal intensities could be observed.

The PROXYL-modified Hsp90 M variants S411C, S422 and S456C, however, gave reasonable effects. Especially S411C caused very pronounced line broadening of TPR2A-TPR2B NMR signals (figure 4.72). With the PROXYL label attached to position 411 and 456 located at the outer surface of Hsp90 M, mainly residues within TPR2A showed a reduction of the signal intensity (figure 4.73, upper panel). The strongest effects were within helix C of TPR2A (residues 360 to 380) for both Hsp90 M variants (figure 4.73, lower panel). This is well in agreement with the chemical shift perturbation data because the most pronounced shifts

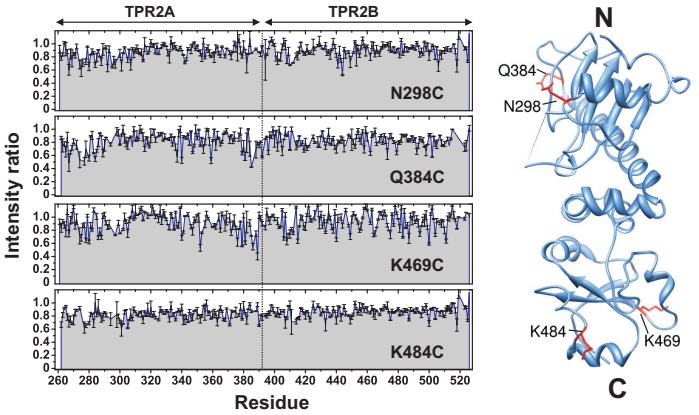

Figure 4.71: PRE experiments with Sti1 TPR2A - TPR2B and the Hsp90 M mutants N298C, Q384C, K469C and K484C. Left: Peak intensity ratios calculated from TPR2A - TPR2B ^{15}N - TROSY spectra before and after addition of ascorbic acid. No major relaxation enhancement could be observed for TPR2A - TPR2B signals in complex with the Hsp90 M mutants carrying a PROXYL spin label attached to the cysteine residue at the indicated positions. Right: Crystal structure (PDB: 1HK7) showing the position of the mutation sites within Hsp90 M to create cysteine variants for modification with a PROXYL spin label. 300 μM of ^{15}N - labeled TPR2A - TPR2B was measured at 303 K and 900 MHz in a buffer of 10 mM potassium phosphate, 20 mM potassium chloride, 1 mM TCEP, pH 7.5. The respective Hsp90 M variants with a PROXYL spin label attached to the cysteine was added in a 1:1 molar ratio. For removing the spin label a 5 - fold molar excess of ascorbic acid was added to the sample and incubated for 1 h.

upon binding of Hsp90 M to TPR2A - TPR2B were also found in this region (compare figure 4.70). Thus, it is likely that this portion of TPR2A is involved in direct contacts with Hsp90 M.

When the label was placed at position 422 which is located more at the inner side of Hsp90 M, the PRE effects were smaller compared to the two other sites (figure 4.73, upper panel, left). In this case, it were only residues in TPR2B that exhibited signal intensity reduction in com-

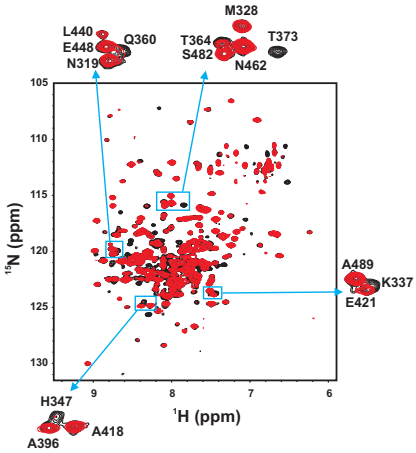

Figure 4.72: ^{15}N - TROSY NMR spectra of Sti1 TPR2A - TPR2B in complex with PROXYL - modified Hsp90 M S411C before (red) and after (black) addition of ascorbic acid. Many signals of TPR2A - TPR2B show reduced intensities when the PROXYL spin label is attached to the cysteine residue at position 411 in Hsp90 M, indicating a spatial proximity to the label. 300 μM of ^{15}N - labeled TPR2A - TPR2B was measured at 303 K and 900 MHz in a buffer of 10 mM potassium phosphate, 20 mM potassium chloride, 1 mM TCEP, pH 7.5. The Hsp90 M mutant S411C with a PROXYL spin label attached to the cysteine was added in a 1:1 molar ratio. For removing the spin label, a 5 - fold molar excess of ascorbic acid was added to the sample and incubated for 1 h.

plex with the PROXYL - modified Hsp90 M. Mainly amino acids around position 410 and 450 (consistent with chemical shift perturbation data, compare figure 4.70) showed decreased signal intensities. These positions are at the C - terminal ends of TPR helices A1 and B2 and are part of one edge of the TPR2B domain (figure 4.73, lower panel).

Overall, the PRE measurements confirm the binding sites of Hsp90 M on TPR2A - TPR2B identified with the chemical shift perturbation data.

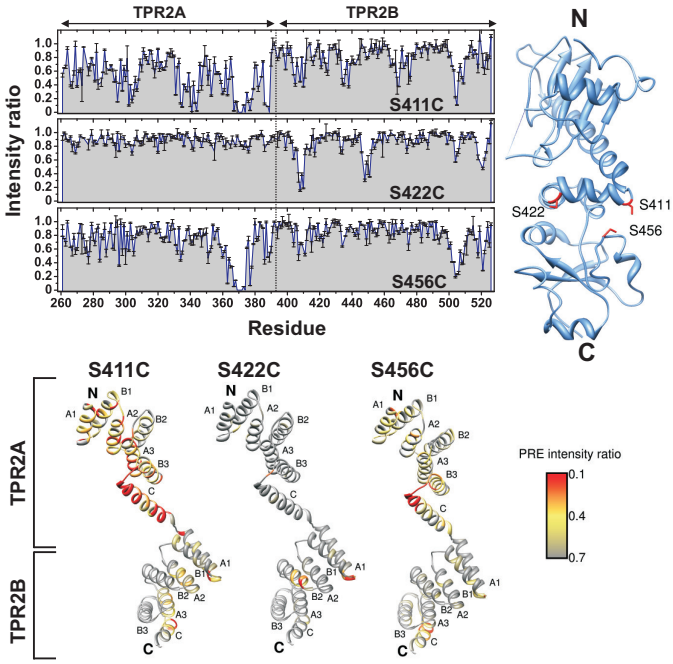

Figure 4.73: PRE experiments with Sti1 TPR2A - TPR2B and the Hsp90 M mutants S411C, S422C and S456C. Upper panel, left: Peak intensity ratios calculated from TPR2A - TPR2B ^{15}N - TROSY spectra before and after addition of ascorbic acid. Upper panel, right: Crystal structure (PDB: 1HK7) showing the position of the mutation sites within Hsp90 M to create cysteine variants for modification with a PROXYL spin label. Lower panel: Mapping of PRE effects with PROXYL - modified Hsp90 M mutants S411C, S422C and S456C onto the crystal structure of TPR2A - TPR2B (PDB: 3UQ3). 300 μM of ^{15}N - labeled TPR2A - TPR2B was measured at 303 K and 900 MHz in a buffer of 10 mM potassium phosphate, 20 mM potassium chloride, 1 mM TCEP, pH 7.5. The respective Hsp90 M variants with a PROXYL spin label attached to the cysteine was added in a 1:1 molar ratio. For removing the spin label a 5 - fold molar excess of ascorbic acid was added to the sample and incubated for 1 h.

A main contribution to the interaction seems to come from residues in helix C of TPR2A which are obviously in close proximity to the outer surface of Hsp90 M in the complex. TPR2B, in contrast, appears to be rather oriented to the inner side of Hsp90 according to the PRE data. This is an important finding with respect to the docking of Hsp90 M and TPR2A - TPR2B which could not be obtained with only information from the chemical shift perturbation experiments.

With the NMR data a molecular docking was performed using HADDOCK[243] to obtain a model for the complex between Sti1 and Hsp90 which potentially could explain the biochemical data. Considering the findings from the NMR binding measurements and also the previous ITC experiments, it seemed justified to make some basic simplifications to restrict the complexity of the docking system. This was anyway necessary since no structure of the full - length Sti1 protein was available so far that could be used for the docking. Therefore, in summary the following simplifications were made:

- As the chemical shift perturbation data showed, there was no interaction of Sti1 with the Hsp90 N - terminal domain. Thus, the docking was done with an Hsp90 fragment lacking the N - terminal domain and the highly flexible linker region connecting it to the middle (M) domain.

- The peptide independent binding between Hsp90 and Sti1 involves only the Hsp90 M domain and the Sti1 TPR2A - TPR2B fragment, as found by NMR and ITC. Thus, for Sti1 only the isolated TPR2A - TPR2B fragment could be used in the docking and restraints involving only Hsp90 M and TPR2A - TPR2B were applied in the calculations.

- Although no binding contacts additional to the peptide binding were found between Hsp90 C and TPR2A - TPR2B, this domain was nevertheless included in the docking by using a Hsp90 MC fragment (Hsp90 M + C domain). This was intended to avoid the generation of wrong/unphysiological docking solutions. The additional presence of the Hsp90 C - terminal domain should sterically further restrict the number of possible orientations of the binding partners during the docking.

- A further simplification in the docking was introduced by using only a monomeric Hsp90 MC template. The second Hsp90 MC protomer was afterwards included in the complex to yield the dimeric Hsp90 MC using molecular modeling.

The monomeric Hsp90 MC fragment for the docking was obtained from the protein data bank (PDB: 2CGE), a crystal structure of the Sti1 TPR2A - TPR2B fragment was kindly provided by Dr. Melissa Gräwert (Lehrstuhl für Biochemie, TUM). For both binding partners ambiguous interaction restraints (AIRs) were generated. A list of so called active and passive residues were defined based on the chemical shift perturbation data and the solvent accessibility determined with the program NACCESS. Active residues are residues that showed significant peak shifts upon binding and have a relative surface accessibility of $\sim 40\,\%$ or higher. These residues are supposed to be involved in direct binding contacts. Passive residues are the surface accessible neighboring residues of the active residues. Table 4.18 summarizes active and passive residue used in the HADDOCK docking calculations.

Besides the definition of active and passive residues, concrete atom distances between Hsp90 M and TPR2A - TPR2B were also used in initial docking runs. To this end, the PRE intensity ratios obtained from

Table 4.18: Ambiguous interaction restraints for the docking of Hsp90 MC and Sti1 TPR2A - TPR2B. The table summarizes active and passive residues of Hsp90 M and Sti1 TPR2A - TPR2B that were used for the NMR data driven docking with HADDOCK [243].

	Hsp90 M	TPR2A - TPR2B
active	411 - 413, 446, 449, 450, 451 - 453, 456 458, 459, 462, 463	360, 361, 364, 367, 368, 369, 370, 372 373, 374, 376, 377
passive	410, 414, 445, 447, 448, 454, 455, 457 460, 461, 464	359, 362, 363, 365, 366, 371, 375, 378

the spin labeling experiments with the Hsp90 M mutants S411C, S422C and S456C were converted into distances between NH groups of TPR2A - TPR2B and the PROXYL spin label in Hsp90 M and included as restraints in the calculations. The distances were applied with generously chosen upper and lower bounds to account for dynamic effects in the PRE measurements that potentially lead to a downscaling of the PRE intensity ratios which would consequently translate into wrong atomic distances. In the docking, 1000 initial rigid - body runs were performed with HADDOCK, followed by semi - flexible refinement of 200 complex structures in torsion angle space and a final refinement in explicit solvent. The resulting complexes from the calculations were then evaluated for agreement with the chemical shift perturbation data and, as additional control, PRE intensity ratios were back - calculated from the complexes and compared with the experimentally determined values.

Docking runs using both chemical shift perturbation data and atomic distances as input resulted in a relatively low number of highly ranked docking solutions. However, the evaluation of the complexes gave a rather bad agreement with the experimental data. Including different

sets of distance restraints was tested in the docking using either the data obtained from only one of the S411C, S422C or S456C Hsp90 M mutants or combinations of the distances from the different mutants. None of these docking runs yielded a satisfying solution for the complex. The back - calculation of the PRE effects was poorly consistent with the experimental data. Therefore, the distance restraints were finally not included in the docking. In this case, as expected, a larger number of ten complex cluster was obtained that were highly ranked by HADDOCK and had comparable quality indicators. These were then likewise evaluated as before and the docking cluster fitting the experimental data best was then selected as complex model. A statistics for this cluster is given in table 4.19. A comparison of the PRE intensity ratios back - calculated from the

Table 4.19: Statistics of the best complex cluster for the docking of Hsp90 MC and Sti1 TPR2A - TPR2B obtained with HADDOCK[243]. The complex was obtained by specifying active and passive residues according to table 4.18. 1000 initial rigid - body docking runs were performed, followed by semi - flexible refinement of 200 complex structures in torsion angle space and final refinement in explicit solvent.

HADDOCK score*	-123.5 ± 12.9
Cluster size	15
RMSD from the overall lowest - energy structure (Å)	35.8 ± 0.5
Van der Waals energy (kcal/mol)	-47.7 ± 4.2
Electrostatic energy (kcal/mol)	-487.6 ± 65.4
Desolvation energy (kcal/mol)	14.9 ± 9.2
Restraints violation energy (kcal/mol)	68.8 ± 45.85
Buried surface area (Å^2)	1972.4 ± 122.1

*Weighted sum of van der Waals, electrostatic, desolvation and restraint violation energies together with buried surface area

selected docking cluster with the experimental data showed a reasonable

agreement (figure 4.74, upper panel). The back-calculation with the spin label placed at position 411 had a good match with the measured data for residues ~330 to 390. The spin label at position 422 gave less pronounced PRE effects in the back-calculation, in agreement with the experimental data. Lower ratios were found consistently around residues 450 within TPR2B. The spin label at position 456 should give the most intense signal intensity reduction for residues ~355 to 380 according to the theoretical calculation. Indeed, also the experimental data showed the lowest PRE intensity ratios around residue 370 and therefore again an acceptable match. The differences observed between the calculated and the experimental data can either be due to dynamics that lead to reduced PRE effects (i.e. less signal intensity reduction than theoretically expected) or due to unspecific binding causing signal intensity reduction for regions of TPR2A-TPR2B not expected to be involved in binding.

In the complex obtained, TPR2A-TPR2B is bound rather at the outside of the Hsp90 dimer slightly wrapped around the Hsp90 M domain. The main binding contacts between Hsp90 and TPR2A-TPR2B involve the N-terminal part of helix 7 within TPR2A (residues around position 370). TPR2A is oriented to the C-terminal part of Hsp90 M and points to the C-terminal domain of Hsp90 without making direct contacts to it. TPR2B is oriented to the N-terminal part of the Hsp90 M domain with its backside pointing towards Hsp90 M. The peptide binding groove of TPR2A is accessible for binding the Hsp90 peptide and, importantly, the TPR2B peptide binding groove is likewise directly accessible to bind a ligand. Overall, a large buried surface area of ~2000 $Å^2$ is obtained by these binding contacts (table 4.19).

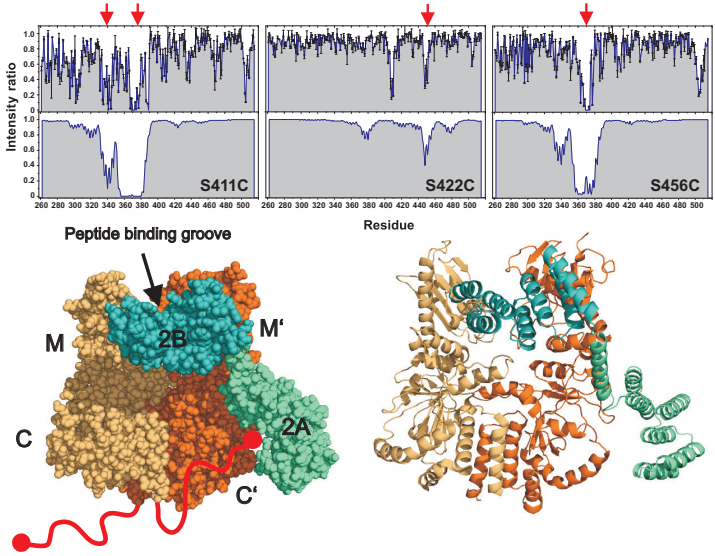

Figure 4.74: NMR docking between Hsp90 MC and Sti1 TPR2A - TPR2B using HADDOCK. Upper panel: Comparison of experimental PRE intensity ratios (upper panel) with PRE intensity ratios back - calculated from the complex between Hsp90 MC and Sti1 TPR2A - TPR2B obtained with HADDOCK (lower panel). The back - calculation was done for the spin label placed at positions 411, 422 and 456 within Hsp90 M. Positions with a reasonable match between experimental and back - calculated data are marked with red arrows on top of the plots. Lower panel: Complex between Hsp90 MC (PDB: 2CGE) and Sti1 TPR2A - TPR2B (PDB: 3UQ3) obtained from docking with HADDOCK [243]. Hsp90 domains (M and C) and Sti1 TPR domains (2A and 2B) are labeled, the peptide binding groove of TPR2B is indicated. The flexible C - terminal ends of Hsp90 that were not used in the docking are drawn schematically in red, the peptide motive of Hsp90 is represented by red dots.

4.13 Screening for Inhibitors of the Sti1 Peptide Binding

It is well known that Hsp90 is involved in the establishment of cancer by chaperoning client proteins that are essential for tumorigenesis like different kinases and receptors involved in cellular signaling. Especially in tumor cells these inherently unstable proteins are highly expressed and require Hsp90 for stabilization and promoting their maturation. Therefore, an inhibition of the Hsp90 function by small molecules seems to be a promising approach in the treatment of cancer and indeed several clinical trials are currently going on with compounds targeting Hsp90 [281]. Most of these compounds like the ansamycin antibiotics derivative 17 - N - allylamino - 17 - demethoxygeldanamycin (17 - AAG) [96,282] bind to the N - terminal ATP binding site of Hsp90 and thus block its ATPase cycle by inhibiting the ATP - driven conformational changes within Hsp90 (see section 1.3).

A different and more indirect way to modulate the function of Hsp90 for the treatment of cancer has been proposed recently [283–285]: In this approach, the interaction of Hsp90 with Sti1/Hop is targeted for inhibition. By preventing the formation of ternary complexes between Sti1, Hsp90 and Hsp70, the substrate transfer from Hsp70 onto Hsp90 could be blocked. Consequently, the strictly Hsp90 dependent client proteins responsible for the establishment of cancer would not become fully activated and finally be directed to the proteasome for degradation. This would lead to apoptosis of cancer cells.

Following this latter approach for the inhibition of Hsp90, a screening for small molecules capable of influencing the Hsp90 - Sti1 interaction was carried out in collaboration with Dr. Andreas Frank (Institute for Advanced Study, TUM). In contrast to common screening strategies which require the testing of large compound libraries to identify a small subset

of potentially protein binding ligands suited for further chemical optimization, here a virtual screening (VS) procedure was applied [286]. To this end, first a pharmacophore model of the ligand based on an available structure of the protein target (presumably in complex with its natural ligand) from experimental data (crystallography/NMR) or alternatively from a homology model is created. The pharmacophore model specifies the general structural properties that a ligand has to exhibit to potentially fit into the binding pocket of the protein.

Then, compound libraries are searched for molecules that fulfill the requirements of the ligand model. Identified matches can again be evaluated *in silico* by performing a virtual docking of the molecule to the protein target. With this strategy, a preselection of the compounds to be subjected a further experimental validation can be achieved, which drastically reduces the number of compounds that have to be tested in order to obtain a hit. Thus, in such a case often no high - throughput screening (HTS) assay is required. The comparatively small number of selected molecules can be tested easily by standard biochemical or NMR methods which are typically not suited for the evaluation of a larger number of molecules.

In particular due to the availability of an increasing number of 3D protein structures and freely accessible small molecule databases a VS approach appears very useful and promising nowadays. Additionally, improved computer power and better searching algorithms further speed up the process of screening large compound libraries. Therefore, potentially interesting ligands for a given protein receptor can be identified within reasonable time and with acceptable experimental effort.

The Sti1/Hop TPR domains with their peptide binding grooves seemed to be well suited for a VS approach to identify small organic non - peptidic molecules that could potentially inhibit the interaction of Sti1/Hop with

its native peptide ligand(s) for the following reasons:

- Crystal structures of the human Hop TPR1 and TPR2A domains in complex with their respective ligands were available [68]. Therefore, a precise pharmacophore model could be built for the screening.

- In particular the Hsp70/Hsp90 interacting TPR domains have well defined and similar ligand binding sites. They all share the highly conserved residues of the two - carboxylate clamp (section 2.1.3) that mediate the binding of the EEVD consensus peptide motive common to nearly all Hsp70/Hsp90 family members. Thus, molecules identified by VS using a pharmacophore model obtained from a crystal structure of a human Hop TPR domain would likely also bind to the yeast Sti1 TPR domains that were available for the experimental validation of the screening hits.

- Identified compounds from the VS could be easily tested for binding by NMR chemical shift mapping; a backbone resonance assignment for the yeast Sti1 TPR2B domain was available (section 4.4.1). Additionally, chemical shift perturbation data obtained previously for the binding of the natural peptide ligand to TPR2B could be used to assess the specificity of the interaction of a potential inhibitor compound with the TPR domain (section 4.4.5). For comparison, also affinity data for binding of the natural peptide ligand to TPR2B existed (table 4.7). Thus, a comprehensive evaluation of the identified compounds was possible.

On the basis of a crystal structure for the human Hop TPR2A domain in complex with the Hsp90 MEEVD pentapeptide (PDB: 1ELR) [68] Dr. Andreas Frank built a pharmacophore model for the TPR domain ligand binding pocket. Since the natural peptide ligand of TPR2A comprising

five amino acids in extended conformation occupies a rather large surface on the protein but the screening was intended to identify only small organic and non-peptidic compounds, the model for the database search had to be restricted to a smaller fragment of the natural ligand. Thus, only the terminal Asp (D0) residue of the peptide ligand that is bound to the highly conserved two-carboxylate clamp of the TPR domain and the preceding Val residue (V-1) were considered. Consequently, a potential TPR binding compound that is in agreement with the model should on the one hand carry carboxylate groups corresponding to the D0 residue and on the other hand mimic the hydrophobic methyl groups of V-1.

Dr. Andreas Frank then performed a database search to identify molecules matching the model. In summary, six different databases were screened and overall more than 380000 compounds analyzed. A small set of 36 compounds was selected in the end for a further evaluation in a virtual docking. Six out of these showed reliable binding to the human Hop TPR2A domain in the docking runs and were therefore suggested for an experimental validation by Dr. Andreas Frank. Figure 4.75 shows the structures of these compounds.

The compounds were ordered from different suppliers (table 4.20) and tested for binding to the Sti1 TPR2B domain using NMR. Since all structures contain charged functional groups, it was expected that the compounds should have reasonable solubility in aqueous buffer solution as required for the NMR measurements with TPR2B. However, most of them could unfortunately not be dissolved directly in the measurement buffer at the required higher concentrations, except for compound number 3. Two compounds (number 1 and 4) turned out to be completely insoluble in all solvents tested and were therefore not analyzed in the NMR experiments. In the other cases, deuterated DMSO (DMSO-d_6; DMSO, dimethyl sulfoxide) was used to prepare a highly concentrated stock solu-

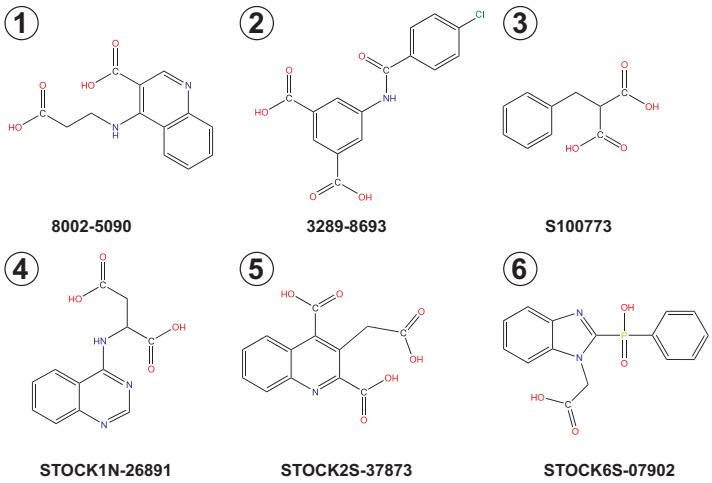

Figure 4.75: Compounds potentially binding to Sti1/Hop TPR domains identified by virtual screening. Above molecules represent the final selection of potential hits in a virtual screening of more than 380000 compounds for Sti1/Hop TPR domain binders carried out by Dr. Andreas Frank (Institute for Advanced Study, TUM). These were subjected to a further experimental validation by NMR in this work.

tion of the respective compound which was then added in a small volume to the protein sample to check for binding. Table 4.20 summarizes the observed solubilities of the compounds.

The binding of the compounds 2, 3, 5 and 6 to the Sti1 TPR2B domain was assessed by monitoring chemical shift perturbation in the ^{15}N - HSQC spectrum of the protein. The concentration of the respective compounds in the stock solutions was between $\sim$ 180 and 350 mM. As it was not absolutely clear at the beginning if the compounds would show interaction with the TPR2B domain at all and if so, how strong, in a first round

Table 4.20: Solubility of potentially Sti1 binding compounds identified in a virtual screening. Contrary to expectations, most of the compounds turned out to be insoluble in the tested buffer (50 mM potassium phosphate, 50 mM potassium chloride, 1 mM TCEP, pH 7.5) at higher concentrations, except for number 3. Compounds 1 and 4 were insoluble all solvents tested, in the other cases solubility was observed with DMSO.

Compound			Solubility						
Nr.	Name	Supplier	Buffer	DMSO	Isopropanol	Acetone	MeOH	EtOH	$CDCl_3$
1	8002-5090	Chemdiv	–	–	–	–	–	–	–
2	3289-8793	Chemdiv	–	+	*	*	*	*	*
3	S100773	Sigma	+	*	*	*	*	*	*
4	STOCK1N-26891	IBS	–	–	–	–	–	–	–
5	STOCK2S-37873	IBS	–	+	*	*	*	*	*
6	STOCK6S-07902	IBS	–	+	*	*	*	*	*

* not determined

of testing a high molar excess (~ 70 x) of each compound over the protein was added to the protein sample. This way, a maximum chemical shift perturbation should be obtained and even very weak binders should be identifiable. The NMR spectra of TPR2B with compound added were compared to a reference spectrum of the protein without compound. To avoid solvent effects in case of the compounds 2, 5 and 6 which were added from a DMSO containing stock solution, a reference spectrum of TPR2B was recorded with an equal amount of DMSO alone.

The first testings were carried out with the Δh7 variant of the TPR2B domain which has a reduced but still significant ability to bind peptide (compare section 4.3). Indeed, all four compounds caused significant shifts in the spectrum of TPR2B. These seemed to be specific since they were not unidirectional as would be expected for buffer effects (figure 4.76). The strongest shifts were observed with STOCK2S-37873 (compound 5), indicating a likely tighter interaction with the protein com-

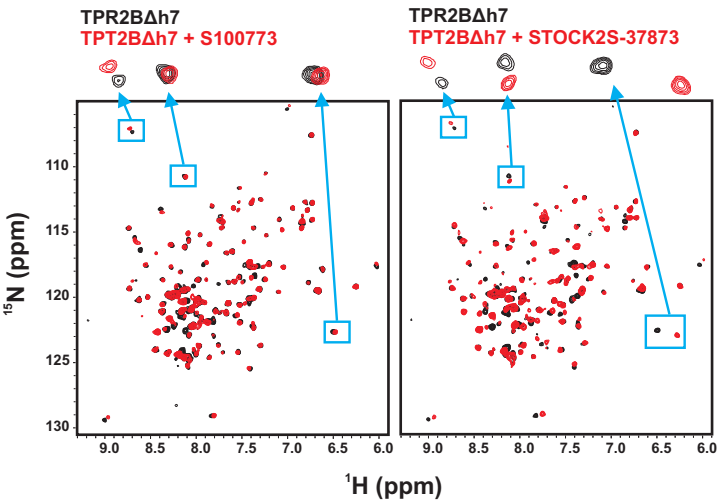

Figure 4.76: Chemical shift perturbation in the ^{15}N - HSQC NMR spectra of the Sti1 TPR2BΔh7 mutant upon binding of small molecule inhibitors identified by a virtual screening. The indicated compounds previously identified by a virtual screening as potential TPR domain binders by Dr. Andreas Frank (Institute for Advanced Study, TUM) were added in a high molar excess (~ 70 x) to the protein. In both cases binding is observed, however, likely stronger for the STOCK2S-37873 compound. 150 μM of TPR2BΔh7 was measured in 50 mM potassium phosphate, 50 mM potassium chloride, 1 mM TCEP, pH 7.5 at 900 MHz and 283 K.

pared to the other compounds. This was then confirmed by the second round of testing. Here – in contrast to the initial measurements – now a lower concentration of the ligands was added to the protein (only ~ 7 x molar excess). In this case, no more chemical shift perturbation was found in the NMR spectra for the compounds 2,3 and 6. However, with compound number 5 still significant shifts occurred (data not shown). Therefore, this molecule seemed to have much higher binding affinity

compared to the others.

To estimate the affinity of compound 5 for binding to the TPR2B domain, a full NMR titration was performed. The ligand was added successively in increasing concentration to the protein and ^{15}N - HSQC spectra were recorded again to monitor for chemical shift perturbation. For each ligand concentration in the titration a separate reference spectrum of the protein was measured with an equal amount of DMSO alone added to account for slight shifts that are inevitably caused by the DMSO. For the titration now the wild - type TPR2B domain was used. The compound caused significant and specific chemical shift perturbation in the spectrum of TPR2B already at lower molar protein:ligand ratios (figure 4.77). Importantly, only shifting peaks were observed but no broadening of signals or the appearance of a second signal set. Thus, the binding of the compound was on the fast NMR timescale, indicating a weaker interaction (mM affinity range). The ligand was titrated to the protein up to a sevenfold molar excess. At this point already saturation was visible in the spectra.

The NMR titration data could be used to determine an affinity for the binding of compound 5 to TPR2B by fitting the shifts of individual TPR2B NMR signals in dependence of the ligand concentration according to equation 10.5 (figure 4.78). Overall, 13 residues of TPR2B were evaluated, the corresponding K_d - values are summarized in table 4.21. As already indicated by the the observation of only shifting peaks in the NMR spectra of TPR2B when the ligand was added, the affinities obtained were rather weak. The average K_d found for fitting the chemical shift perturbation data of the 13 selected backbone NH signals was $\sim 360\,\mu$M. Attempts to further confirm the binding affinity obtained from NMR using ITC as another method failed. On the one hand, the DMSO in which the ligand had to be dissolved caused strong buffer effects during the titration with

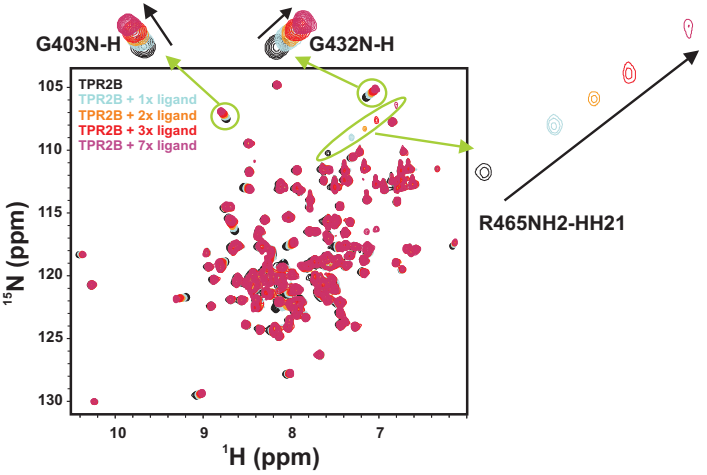

Figure 4.77: Chemical shift perturbation in the ^{15}N-HSQC NMR spectra of the Sti1 TPR2B domain upon titration of a small molecule inhibitor identified by a virtual screening. The inhibitor STOCK2S-37873 (compound 5, compare figure 4.75) titrated to the Sti1 TPR2B domain causes specific and significant chemical shift perturbation. 200 μM of TPR2B was measured in 50 mM potassium phosphate, 50 mM potassium chloride, 1 mM TCEP, pH 7.5 at 600 MHz and 293 K. The compound was added in small volumes from a DMSO-d_6 stock solution with 360 mM.

high dilution heats. On the other hand, the estimated K_d for the interaction in the higher μM range was already near to the lower limit of binding affinities for which ITC is well applicable.

For analyzing the binding mode of compound 5, the NMR data were evaluated in more detail. A plot of the chemical shift perturbation against the residue number showed that significant shifts occurred predominantly in helices A1 and A2 of the TPR2B domain and to a smaller extent in helix B1 (figure 4.79). This clearly indicated that the compound was indeed

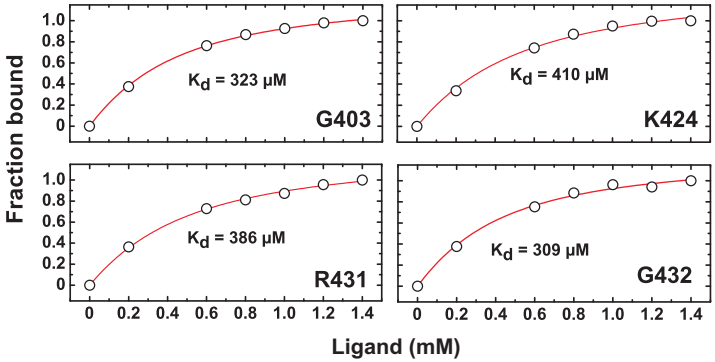

Figure 4.78: K_d fitting of NMR chemical shift perturbation data for binding of a small molecule inhibitor to the Sti1 TPR2B domain. The normalized chemical shift perturbation of selected signals of TPR2B upon binding the STOCK2S-37873 compound was plotted against the ligand concentration. The data could be used to fit binding curves as shown in the examples to determine an affinity for the interaction between TPR2B and the ligand. Similar binding curves were obtained for another 9 residues of TPR2B.

bound within the peptide binding cleft of the TPR2B domain and therefore a specific interaction was observed here. In contrast to the binding of the Hsp70 or Hsp90 peptides to TPR2B, the helices B2 to C were not affected by the binding of the compound (compare section 4.4.5). This is well in agreement with the assumed binding mode of STOCK2S-37873 because according to the pharmacophore model the screening was intended to identify only molecules mimicking the D0 and V-1 residues of the natural peptide ligand.

As expected, the backbone NH signals of conserved residues forming the two-carboxylate clamp like K404 and N435 showed strong chemical shift perturbation when the compound was added to the protein. However, backbone NH signals of the other residues R400 or R465 likewise

Table 4.21: Affinities for the binding of compound STOCK2S-37873 to the Sti1 TPR2B domain obtained from fitting NMR CSP data. The shifting of the backbone NH signals of 13 TPR2B residues upon addition of the ligand was fitted against the ligand concentration yielding binding curves (compare figure 4.78) from which the affinity for the interaction could be determined.

Residue	G403	E405	Y406	F407	T408	S410	K424	A430	R431	G432	S434	L440	V464
K_d (μM)	323	375	526	177	342	191	410	423	386	309	310	382	488
average K_d (μM)	357 ± 100												

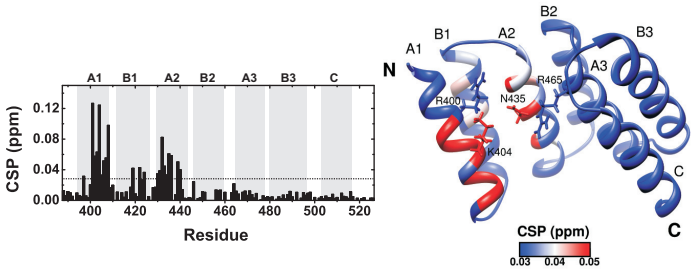

Figure 4.79: CSP plot for the binding of compound STOCK2S-37873 to Sti1 TPR2B (left) and color coded mapping of the CSP data onto the NMR structure of TPR2B (right). Significant shifts upon binding the compound occur predominantly for residues in helices A1 and A2 of TPR2B, indicating that the ligand occupies the typical region of the peptide binding cleft that is normally involved in interaction with residues D0 and V-1 of the natural peptide ligand. The significance level (2 - fold average CSP) is indicated by a dashed line in the CSP plot, helices of the TPR motives are given on top of the plot and in the structure. Conserved residues of the two - carboxylate clamp are labeled in the structure. 200 μM of TPR2B was measured in 50 mM potassium phosphate, 50 mM potassium chloride, 1 mM TCEP, pH 7.5 at 600 MHz and 293 K. The compound was added in a 3 - fold molar excess over the protein.

part of the two - carboxylate clamp seemed to be unaffected. Therefore, the compound potentially might not undergo all binding interactions with the residues from the two - carboxylate as the D0 amino acid in the natural peptide ligand does. This could explain the comparatively weak affinity of TPR2B for the compound. A main contribution to the binding of the compound to TPR2B should come from hydrophobic interactions with the aromatic ring system of STOCK2S-37873 mimicking the V-1 residue of the natural peptide ligand (compare figure 4.75). Indeed, significant shifts were observed for the conserved F407 located at the C - terminal end of helix A1 and predicted to be involved in binding contacts to the peptide ligand (compare figure 4.125).

With the chemical shift perturbation data then a docking of compound 5 to the Sti1 TPR2B domain was performed with HADDOCK[243]. Although HADDOCK is preferentially applied in the docking of protein - protein complexes, it can in principle also be used for obtaining complexes between proteins and small ligands. To this end, first a topology and parameter file of the ligand required as input for the docking was built from its coordinates with PRODRG[287]. For the TPR2B domain then ambiguous interaction restraints (AIRs) were specified by defining active and passive residues based on the chemical shift perturbation data and the solvent accessibility determined with the program NACCESS. Active residues are residues that showed significant peak shifts upon ligand binding and have a relative surface accessibility of $\sim 40\,\%$ or higher. These residues are supposed to be involved in direct binding contacts. Passive residues are the surface accessible neighboring residues of the active residues. Table 4.22 summarizes active and passive residue used in the docking calculations.

In contrast to a complex determination between two proteins, here the ligand was treated as a single active residue in the calculations. For

Table 4.22: Ambiguous interaction restraints for the Sti1 TPR2B domain applied in the NMR data driven docking with the inhibitor compound STOCK2S-37873 using HADDOCK[243]. Active and passive residues were only defined for the protein in the docking as listed here, the ligand was treated as single active residue.

active	passive
401,402,403,404,405,406,407,408,431,432,433,434 435,436,437,439,440	400,409,430,438,441

TPR2B the NMR structure (section 4.4.2) was used as template for the docking. 1000 initial rigid - body docking runs were performed followed by semi - flexible refinement of 200 complex structures in torsion angle space and a final refinement in explicit solvent. The statistics for the complex cluster that was ranked highest can be found in table 4.23.

Table 4.23: Statistics of the best complex cluster from the docking of the Sti1 TPR2B domain and the compound STOCK2S-37873. The complex was obtained by specifying active and passive residues according to table 4.22. 1000 initial rigid - body docking runs were performed followed by semi - flexible refinement of 200 complex structures in torsion angle space and final refinement in explicit solvent.

HADDOCK score*	-16.9 ± 5.1
Cluster size	198
RMSD from the overall lowest - energy structure (Å)	0.6 ± 0.3
Van der Waals energy (kcal/mol)	3.2 ± 1.5
Electrostatic energy (kcal/mol)	0.0 ± 0.0
Desolvation energy (kcal/mol)	-23.5 ± 2.0
Restraints violation energy (kcal/mol)	34.6 ± 19.27
Buried surface area (Å^2)	435.4 ± 40

*Weighted sum of van der Waals, electrostatic, desolvation and restraint violation energies together with buried surface area

Figure 4.80 shows an overlay of the four best structures from this HADDOCK cluster. Unfortunately, the position of the ligand in the binding

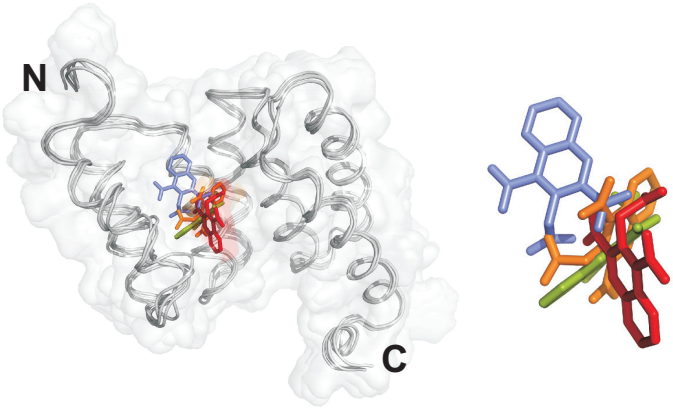

Figure 4.80: Overlay of the 4 best structures out of the complex cluster with the highest ranking for the docking between Sti1 TPR2B and the compound STOCK2S-37873. The inhibitor STOCK2S-37873 (compound 5, compare figure 4.75) was docked to the NMR structure of the Sti1 TPR2B domain using HADDOCK [243]. The left side shows the 4 best structures from the HADDOCK cluster with the highest ranking in an overlay. Unfortunately, the orientation of the ligand in the binding pocket is not very well defined (right side).

pocket was not very well defined when the complex structures were compared to each other. The compound adopted different orientations although the region where it was bound within the TPR2B peptide binding groove was roughly similar for all structures. Given the fact that no additional restraints like inter - molecular NOEs were applied in the docking besides the definition of active and passive residues, this result is not very surprising. A more detailed inspection of the docking results showed that one of the structures was in much better agreement with the experimen-

tal data than the others (figure 4.81). The binding mode of the ligand observed for this particular complex structure was consistent – however only partially – with expectations from the initial pharmacophore model that was built for the virtual screening: It is mainly the conserved two-carboxylate clamp residues K404, N435 and R465 as well as F407 predicted to contact the V-1 residue of the natural peptide ligand that are involved in binding the compound. R400, which is additionally part of the two-carboxylate clamp, is too far away from the binding interface in the model and thus – in agreement with the chemical shift data – not contributing to the complexation of the compound. With the ligand oriented as in the model, T-shaped stacking of the aromatic rings of F407 from the protein and from the ligand would be possible.

A further analysis of potential polar contacts between the protein and the carboxylate groups in the ligand shows that theoretically several H-bonds could be formed. The side-chain amides of R465 might coordinate the carboxylate group of the ligand in ortho-position to the nitrogen in the heterocyclic aromatic ring. The ligand carboxylate group in para-position, on the other hand, points directly to the backbone amide of A438 in helix A2 of TPR2B which would be within reach for an H-bond. The side-chain hydroxyl group as well as the backbone carbonyl of S434, also within helix A2, could serve to make contacts with the carboxymethyl-moiety in meta position of the ligand's heterocyclic aromatic ring. Close to this functional group is also the side-chain amide of N435 and thus likewise available for binding interactions. Furthermore, its backbone carbonyl and the aromatic hydroxyl group of Y419 from TPR2B helix B1 are located near to the para-carboxylate group of the ligand heterocyclus.

Overall, the approach of using HADDOCK[243] for the docking of a small ligand to a protein has some limitations, especially if only chemical

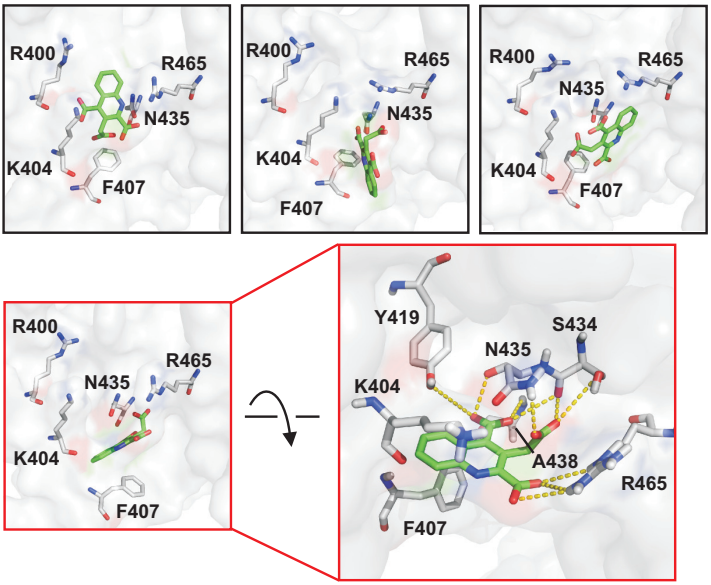

Figure 4.81: Details of the interaction between the Sti1 TPR2B domain and the STOCK2S-37873 inhibitor compound as observed in the 4 best structures of the HADDOCK complex cluster with the highest ranking. For 3 structures (upper panel) the orientation of the inhibitor STOCK2S-37873 (compound 5, compare figure 4.75) in the TPR2B binding pocket is not very well consistent with the expected binding mode of the ligand and shows rather bad agreement with the experimental data. However, in the structure 4 (lower panel, left), in contrast, a reasonable binding mode is observed that fits acceptably to the measured CSP data. The right side in the lower panel shows potential polar interactions between the ligand and the protein (indicated by yellow dashed lines) for this particular orientation of the ligand in the binding pocket. It should be noted that the contacts displayed are only theoretical and for illustration and may deviate from ideal geometry and bond-length of real H-bonds. Conserved residues of TPR2B predicted to interact with the D0 and V-1 residues of the natural peptide ligand are indicated in the small drawings. For clarity, only heavy atoms are shown.

shift data are used as input as it was done here and no other restraints like atomic distances are specified. In such a case the results of the docking have to be analyzed in particular carefully for agreement with experimental data and evaluated for reasonability. Nevertheless, the docking of the inhibitor compound to the Sti1 TPR2B domain performed here could yield an acceptable model which is to a large extent consistent with the experimental NMR data.

4.14 Structural Characterization of Sti1 DP Domains

4.14.1 Characterization of Initial DP Domain Constructs

So far the DP domains of Sti1/Hop proteins from any organism are structurally poorly characterized. Therefore, a detailed study on the DP domains from yeast Sti1 should be carried out in this work. Initial constructs for the Sti1 DP1 domain (residues 108 to 261) and DP2 domain (residues 493 to 589) cloned into a pGEX vector and fused to a GST - tag (GST, glutathione S - transferase) were kindly provided by Dr. Sebastian Wandinger (Lehrstuhl für Biotechnologie, TUM). Both proteins could be expressed solubly in *E. coli*. After affinity chromatography using a Glutathione Sepharose column, the GST - tag was cleaved off by thrombin digestion followed by gelfiltration on a Superdex 75 column as last step of the purification. The protein yields obtained were on the order of ~ 5 mg of pure protein per liter of cell culture and thus sufficient for an initial CD and NMR spectroscopic characterization of the DP domains.

The CD spectra of both the DP1 and DP2 domain indicated folded and α - helical proteins, however, with a higher random coil content, especially for DP1 (figure 4.82). CD thermal unfolding transitions recorded for DP1 and DP2 did not show cooperativity and pointed at high thermal stability of the proteins. The chemical stabilities of both proteins were comparable and relatively high, with urea unfolding midpoints at ~ 4.1 M for DP1 and 4.4 M for DP2, respectively. Thus, overall both DP domains seemed in principle suited for further NMR structural studies.

The ^{15}N - HSQC spectra of the DP1 and DP2 constructs confirmed the CD data. The lower signal dispersion for both proteins in the proton dimension pointed at exclusively α - helical folds (figure 4.83). Unfortunately, in particular the DP1 construct showed some severe signal overlap

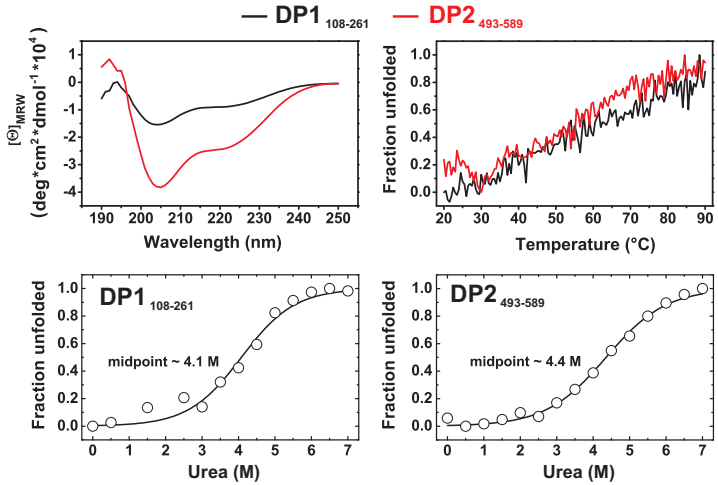

Figure 4.82: CD spectroscopic characterization of the initial Sti1 DP domain constructs. Upper panel: CD spectra for DP domain constructs recorded at 20°C (left) and thermally induced unfolding monitored by CD spectroscopy at a wavelength of 205 nm (right). Lower panel: Chemically induced unfolding transitions using urea for DP domains monitored by CD spectroscopy at a wavelength of 220 nm and 20°C. Proteins were measured in a buffer of 50 mM potassium phosphate, 50 mM potassium chloride, 1 mM TCEP, pH 7.5.

in the region between 8.0 and 8.6 ppm of proton chemical shift. Also the side - chain NH resonances of arginine, asparagine and glutamine residues between 110 and 115 ppm of nitrogen chemical shift were not well resolved. This pointed at a significant content of unfolded regions for the DP1 construct. The spectrum of DP2, in contrast, was much less overlapped and therefore clearly better amenable for NMR structural studies.

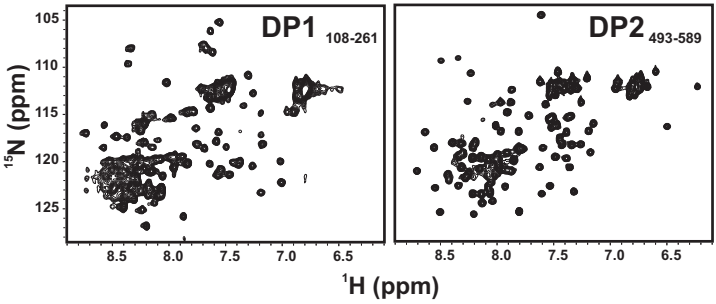

Figure 4.83: ^{15}N - HSQC spectra of the initial Sti1 DP1 (left) and DP2 (right) constructs . Both proteins appear to be exclusively α - helical. Especially for DP1 a larger content of unfolded structure seems to be present, causing significant signal overlap. Proteins were measured in a buffer of 50 mM potassium phosphate, 50 mM potassium chloride, 1 mM TCEP, pH 7.5 at 20°C and 600 MHz.

4.14.2 Construct Optimization and NMR Backbone Assignment of Sti1 DP Domains

For a later structure determination backbone assignments as a prerequisite had to be obtained for the DP1 and DP2 domain. The initial CD and 2D NMR spectra indicated that the DP2 construct had a higher structure content compared to the DP1 construct (section 4.14.1). Therefore, it seemed reasonable to first subject DP2 a further NMR characterization. Structural data for DP2 could then potentially be helpful in optimizing the domains boundaries of DP1 afterwards. However, since the protein yields using the initial expression system with pGEX vectors were rather low, which might be problematic for further isotope labeling required for advanced NMR experiments, the DP2 domain was cloned into a pET28a vector. Instead of the GST - tag, DP2 now was fused to an N - terminal His - tag. This could significantly increase the amount of protein obtained

after a standard purification (see section 9.9) and thus the construct was well suited for isotope labeling.

Using a doubly $^{15}N/^{13}C$-labeled 2 mM concentrated sample, a set of standard triple resonance experiments was recorded for DP2, including HNCO, HN(CA)CO, HNCA, HN(CO)CA, HNCACB and HN(CO)CACB to achieve a backbone resonance assignment for the domain. Additionally, an HNH-NOESY was measured to further confirm the assignment obtained by scalar coupling. As the DP2 domain was likely α-helical, strong sequential HN-HN should be visible within the secondary structure elements. Overall, backbone NH signals for 87 out of 93 non-proline residues in the construct could be assigned (figure 4.84). For the remaining unassigned residues that were all located in the N-terminal part of the DP2 construct no backbone NH signals could be observed in the ^{15}N-HSQC spectrum, likely due to flexibility and exchange processes.

Using the backbone backbone chemical shift assignments, the DP2 domain could structurally be further characterized. With the chemical shift index (CSI) method[272] evaluating the Cα, Cβ and CO carbon chemical shifts of DP2 a secondary structure prediction was done (figure 4.85, upper panel). Five helical elements were found for the DP2 construct, located between residues 527 and 582. This was well in agreement with the CD data (figure 4.82). Within the last eight amino acids a small sheet structure was predicted, which however might be wrong. The N-terminal part of the DP2 construct lacked secondary structure content up to residue 526 according to the CSI analysis. Indeed, for this region of the protein no NOE contacts could be observed in the HNH-NOESY spectrum, whereas the presence of helices for residues between 527 and 582 could be confirmed by strong sequential HN-HN NOEs. Also, the cross peaks corresponding to the N-terminal residues showed low signal intensities in the ^{15}N-HSQC spectrum, likely caused by dynamics.

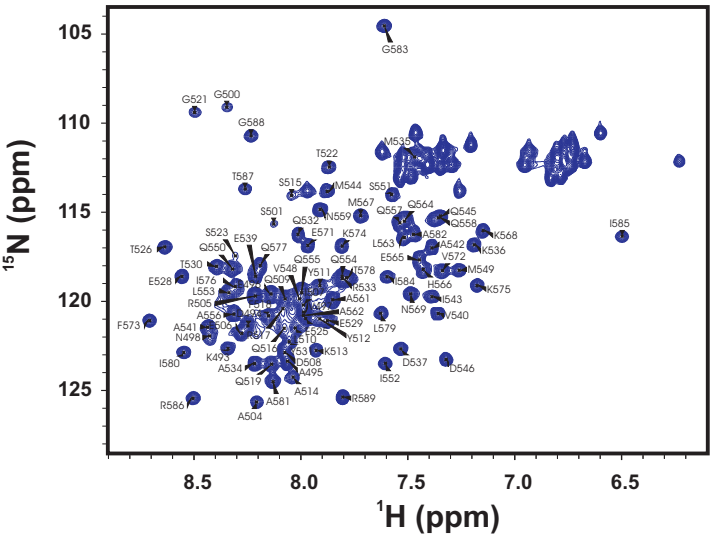

Figure 4.84: ^{15}N - HSQC spectrum of the DP2 domain with assignment. 93 % of the backbone NH signals for non - proline residues in the DP2 construct could be assigned. The assignment was obtained in a buffer of 50 mM potassium phosphate, 50 mM potassium chloride, 1 mM TCEP, pH 7.5 at 293 K and 750 MHz.

These observations were well supported by a measurement of the {^{1}H} - ^{15}N - heteronuclear NOE (figure 4.85, lower panel) to determine fast backbone dynamics of DP2 (ns - to ps - timescale movements). Consistent with the CSI data, the residues predicted to have no secondary structure also showed increased backbone mobility ({^{1}H} - ^{15}N - NOE values below ~ 0.6). Thus, in conclusion these results indicated that the folded part of the DP2 domain likely involved only the Sti1 residues 527 to 582 and that the domain boundaries of the initial DP2 (and DP1) construct could be further optimized.

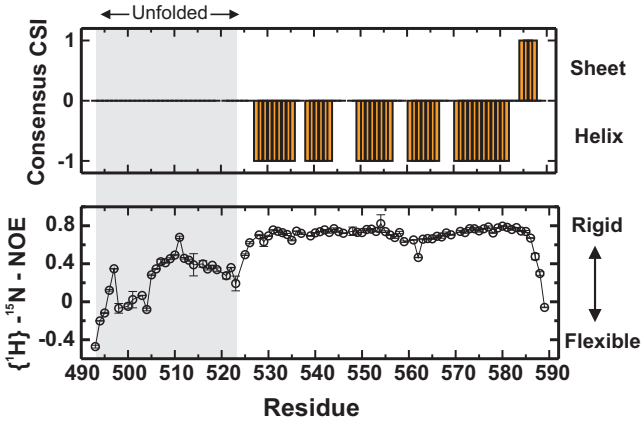

Figure 4.85: Chemical shift index (CSI) and fast backbone dynamics of the DP2 domain . The consensus CSI for Cα, Cβ and CO carbon shifts (upper panel) predicts random coil structure for the N - terminal part of the DP2 construct. Consistently, the $\{^1H\}$ - ^{15}N - heteronuclear NOE (lower panel) indicates higher backbone flexibility for the respective region. Dynamic measurements were carried out on a 1 mM ^{15}N - labeled DP2 sample in a buffer of 50 mM potassium phosphate, 50 mM potassium chloride, 1 mM TCEP, pH 7.5 at 293 K and 600 MHz.

Considering the structural data from the NMR experiments with the initial DP2 fragment so far, new DP1 and DP2 constructs were then designed to remove unstructured regions at the N - and C - termini of the domains that would hamper an NMR structure determination. This led to a new DP2 domain now comprising only residues 525 to 589 and therefore significantly shortening the initial construct by 32 residues. To optimize the DP1 construct, a secondary structure prediction using PSIPRED [234] was carried out (figure 4.86). As the NMR and CD spectra of DP1 already indicated, a large portion of random coil content was found, especially in the C - terminal region of the sequence. Residues $\sim$ 193 to 260 seemed to

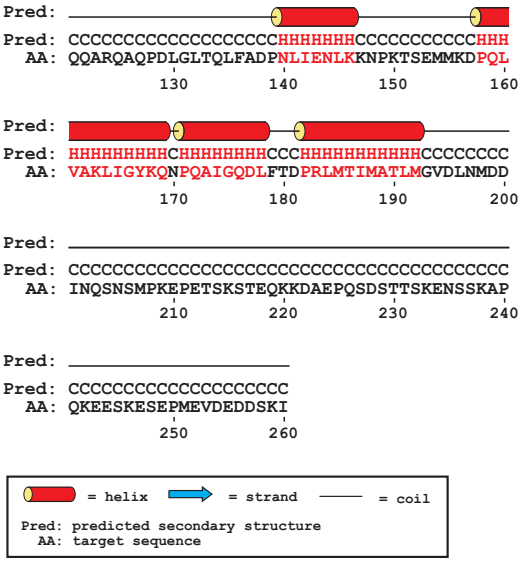

Figure 4.86: Secondary structure prediction for the DP1 domain using PSIPRED [234]. For the amino acid sequence of the initial DP1 construct (section 4.14.1) a large portion of random coil content within the C-terminal region is predicted.

lack any secondary structure and could therefore likely be cut off from the protein. The folded part of the DP1 domain obviously only involves the residues ~ 140 to 192. An additional amino acid sequence alignment between the Sti1 DP1 and DP2 domains further confirmed the results from the secondary structure prediction (figure 4.87). With these data, also a new DP1 construct could now be designed. The initial DP1 domain was shortened N- and C-terminally to finally comprise only the Sti1 residues 127 to 197, thus making the DP1 domain smaller by overall 93 residues.

```
DP1  QARQAQPDLG LTQLFADPNL IENLKKNPKT SEMMKDPQLV | 161
DP2  SQQRFQPG-- TSNET-PEET YQRAMKDPEV AAIMQDPVMQ | 550

DP1  AKLIGYKQNP QAIGQDLFTD PRLMTIMATL MGVDL----N | 197
DP2  SILQQAQQNP AAL-QEHMKN PEVFKKIQTL IAAGIIRTGR | 589
```

Figure 4.87: Amino acid sequence alignment for the Sti1 DP1 and DP2 domains. The conserved DP/NP motives are highlighted in red. The alignment was generated using T-Coffee [194]. The NCBI reference code of the sequence used for the alignment is NP_014670.1.

Both DP1 and DP2 fragments with optimized domain boundaries were again cloned into a pET28a vector fused to an N-terminal His-tag. The proteins expressed well and isotopically labeled samples suited for NMR experiments could be obtained after standard protein purification (section 9.9). The CD spectra of the optimized domains showed a drastically reduced random coil content compared to the old constructs, as expected (figure 4.88). However, the thermal stabilities of both proteins were unaffected, indicating that no structurally important residues had been deleted by the truncations.

The ^{15}N-HSQC spectra of the DP1 and DP2 domains after optimization also showed a significantly improved spectral quality (figure 4.89). Especially for DP1 the severe signal overlap between 8.0 and 8.6 ppm of proton chemical shift as observed with the previous construct was resolved, and linewidth was clearly reduced due to the decreased molecular size of the domain. These observations confirmed the results from secondary structure prediction with PSIPRED that a large portion of random coil was present in the initial DP1 construct. Thus, after the optimization both DP domains now appeared well amenable for an NMR structure determination.

The backbone resonance assignment of DP2 obtained with the initial

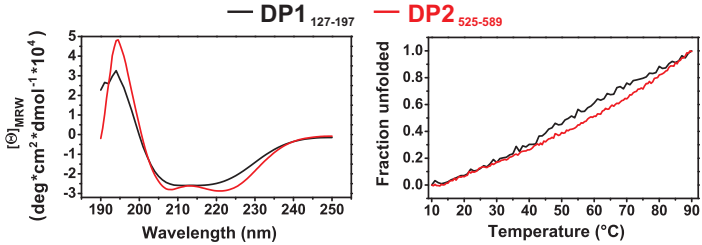

Figure 4.88: CD spectra and thermal stabilities of optimized Sti1 DP domain constructs. Left: CD spectra for DP domain constructs recorded at 20°C. Both proteins show significantly improved spectral quality compared to the initial constructs (see figure 4.82). Right: Thermally induced unfolding of DP domain constructs monitored by CD spectroscopy at a wavelength of 205 nm. Proteins were measured in a buffer of 50 mM potassium phosphate, 50 mM potassium chloride, 1 mM TCEP, pH 7.5.

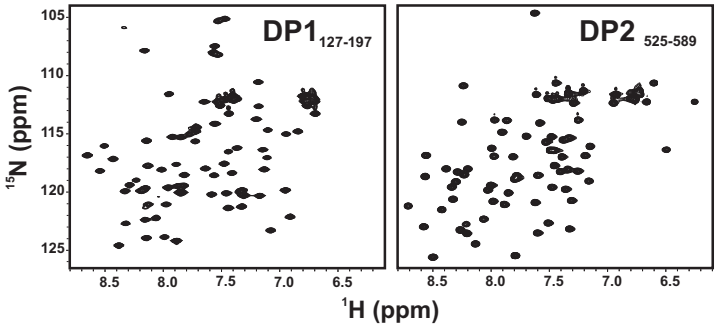

Figure 4.89: ^{15}N-HSQC spectra of optimized Sti1 DP1 and DP2 constructs. Both proteins show significantly improved spectral quality compared to the initial constructs (see figure 4.83). Proteins were measured in a buffer of 50 mM potassium phosphate, 50 mM potassium chloride, 1 mM TCEP, pH 7.5 at 293 K and 600 MHz.

construct could easily be transferred onto the spectra of the new DP2 domain. For DP1, a backbone resonance assignment was carried out using the optimized construct. Similar as described for DP2, a set of standard triple resonance experiments was recorded as well as an HNH - NOESY. Due to the high spectral quality, 100 % of all non - proline backbone NH signals of the protein could be assigned (figure 4.90).

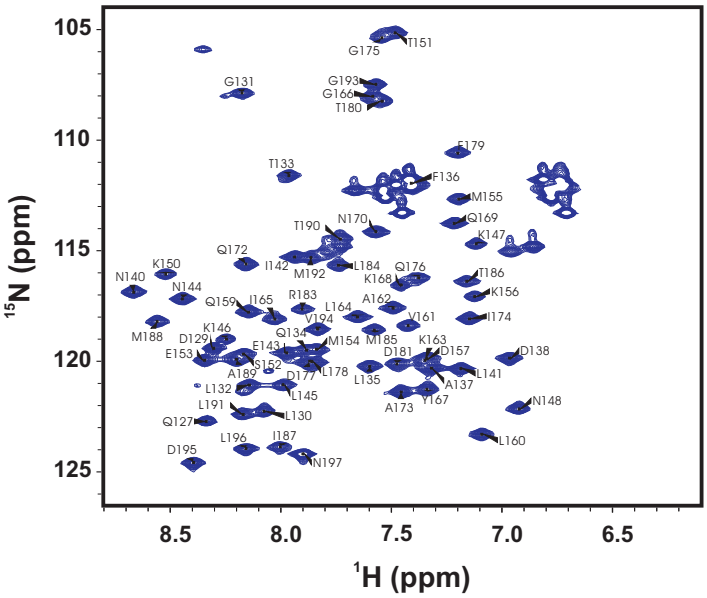

Figure 4.90: ^{15}N - HSQC spectrum of the DP1 domain with assignment. 100 % of the backbone NH signals for non - proline residues in the optimized DP1 construct (Sti1 residues 127 to 197) could be assigned. The assignment was obtained in a buffer of 50 mM potassium phosphate, 50 mM potassium chloride, 1 mM TCEP, pH 7.5 at 293 K and 750 MHz.

Similar as for DP2, again a secondary structure analysis could be performed with the DP1 backbone chemical shifts assigned for Cα, Cβ and CO. Figure 4.91 shows a comparison of the secondary structure elements found for DP1 and DP2. Using the chemical shift index method [272] as

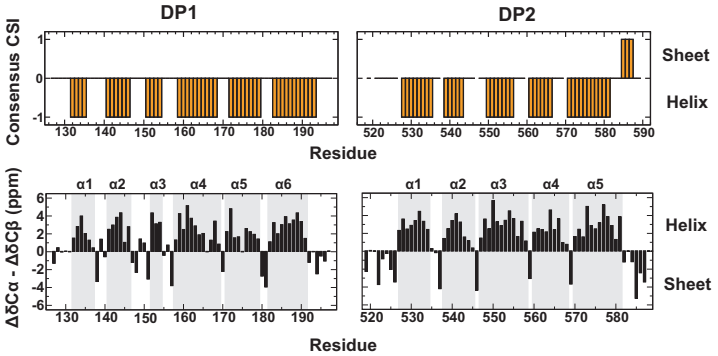

Figure 4.91: Evaluation of DP1 (left) and DP2 (right) NMR chemical shift data to determine secondary structure elements. Upper panel: Individual carbon chemical shifts for Cα, Cβ and carbonyl (CO) were analyzed using the chemical shift index (CSI) method [272]. The consensus prediction combining the data from the individual carbon shifts is given. In the consensus plot, -1 indicates helical structure, +1 would be indicative of sheet structure. Lower panel: Evaluation of secondary structure content using Cα and Cβ shifts. The difference of the measured Cα and Cβ chemical shifts from the random coil shifts ($\Delta\delta$Cα and $\Delta\delta$Cβ) was calculated. On the y-axis the difference of $\Delta\delta$Cα and $\Delta\delta$Cβ is plotted, a sequence of three or more positive or negative bars indicates helical or sheet structure, respectively.

well as an analysis of the difference between $\Delta\delta$Cα and $\Delta\delta$Cβ, five helices were identified for DP2 but surprisingly six helices for DP1. The additional helix within DP1 is located at the N-terminus comprising residues 132 to 136 and was not predicted by the PSIPRED analysis performed to optimize the DP1 construct (compare figure 4.86). The correspond-

ing region within DP2 (residues ~520 to 526, compare figure 4.87) is obviously unfolded.

Overall, the NMR data now provided valuable information helpful for exactly defining the domain boundaries within Sti1. Considering the results on the TPR domains (section 4.1) and on the DP domains, Sti1 can be divided into five structured fragments as shown in figure 4.92. Most

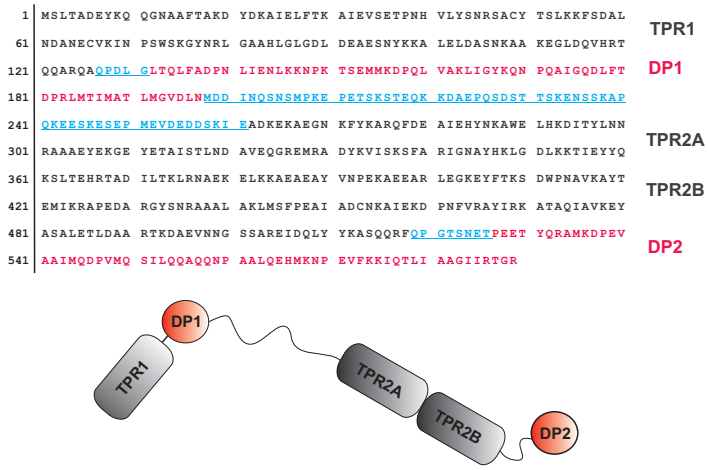

Figure 4.92: Summary of Sti1 domain boundaries as determined in this work. Upper panel: Amino acid sequence of Sti1 with individual TPR (black) and DP (red) domains indicated. Unfolded linker regions are highlighted blue and underlined. Lower panel: Schematic representation of Sti1 considering the relative domain boundaries as found in this work. A large region of more than 60 residues between DP1 and TPR2A is unfolded and likely serves as linker region connecting the TPR1 - DP1 module flexibly to the rest of the protein.

interestingly, the TPR1 - DP1 module seems to be flexibly connected to the rest of the protein by a comparatively long linker region of more than 60

likely unfolded residues between DP1 and TPR2A.

4.14.3 NMR Structure Determination of Sti1 DP Domains

So far no structure of a Sti1/Hop DP domain was described and also for the homologous DP region of the protein Hip[190] such data are not yet available. As outlined, the DP2 domain was shown to have essential functions for the activation of Hsp90 client proteins like the GR[173] (see section 2.1.4), therefore, in particular the DP2 structure is of high interest. With the optimized DP domain constructs as described in section 4.14.2 an NMR structure determination was performed here. For assigning the missing backbone and side - chain resonances of DP1 and DP2 a set of 3D NMR experiments was recorded.

The backbone Hα proton chemical shifts were assigned from an HNHA experiment which also provided information on the backbone ϕ - angle. Overall, $^{3}J_{HNH\alpha}$ coupling constants could be determined for 64 (DP1) and 67 (DP2) non - proline residues (figure 4.93), which were mostly between 2 and 6 Hz, indicating α - helical structure as expected. Most of these couplings could later be included in the structure calculations except for a few that were belonging to residues located between the secondary structure elements and seemed to be averaged due to dynamics. Hβ protons were assigned from an HNHB experiment which was also used for determining χ_1 - side - chain torsion angles. A stereospecific assignment of non - equivalent β - protons was possible from the peak - intensity patterns in NOESY spectra and the HNHB experiment. Chemical shifts for protons of longer aliphatic side - chains were obtained by a combination of HC(C)H - COSY and HC(C)H - TOCSY experiments. For assigning carbon chemical shifts, (H)CC(CO)NH, 3D (H)CCH - TOCSY and 3D (H)CCH - COSY experiments were recorded. Assignment of aromatic residues was done with

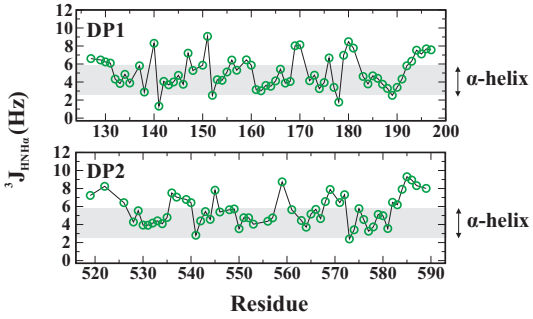

Figure 4.93: $^3J_{HNH\alpha}$ coupling constants of the Sti1 DP domains. The coupling constants were mostly between 2 and 6 Hz which is indicative of helical secondary structure.

a ^{13}C - HSQC centered to the aromatic region, a 2D NOESY and an HCH - NOESY. Important chemical shift information was furthermore provided by 2D HBCBCGCDHD and HBCBCGCDCEHE experiments connecting the spin systems of the aromatic rings with the Cβ atoms by scalar coupling. A list with all backbone and side - chain chemical shifts for DP1 and DP2 can be found under part IV, tables 11.4 and 11.5.

A set of 3D ^{15}N -, ^{13}C - edited NOESY spectra was then recorded for the structure calculation, including HNH -, NNH -, CNH -, HCH - and CCH - NOESY. Side - chain χ_1 - and χ_2 - angles were determined from the NOESY intensity pattern and using information from the HNHB experiment for the χ_1 - angle. Overall, 56/48 χ_1 - and 40/26 χ_2 - angles could be determined for DP1/DP2. For 43/30 β - methylene groups and the prochiral methyl groups of 10/1 leucine and 1/3 valine residues stereospecific resonance assignments were obtained.

As structure calculation engine Xplor - NIH was used [233]. On the backbone ϕ - and ψ - angles TALOS [273] restraints were applied in the calcu-

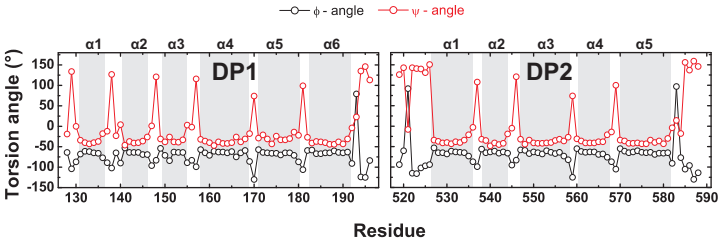

Figure 4.94: TALOS [273] prediction for ϕ - and ψ - backbone angles of the Sti1 DP1 (left) and DP2 (right) domain. The predicted ϕ - angles around - 60° and ψ - angles around - 40° indicate helical secondary structure.

lations, using the chemical shift information of Cα, Cβ, CO and Hα. For 58/43 residues of DP1/DP2 the shift matches found by TALOS gave clustering ϕ/ψ combinations and could be applied in the calculations (figure 4.94). The predicted ϕ - angles were mostly around - 60° and the ψ - angles around - 40°, which is consistent with α - helical secondary structure as expected.

In the first step of the structure determination, the helices of the DP domains were defined by applying $^{3}J_{HNH\alpha}$ coupling constants, TALOS restraints and sequential HN - HN, HN - Hα and HN - Hβ NOE contacts. In further rounds of calculations then the fold of the protein was fixed by including long range NOE contacts. For DP1 important contacts stabilizing the tertiary structure were provided by the F136 residue within the first α - helix (figure 4.95, upper panel). For DP2 significantly less long range NOEs could be found due to the lack of the respective helix. This transferred into a higher RMSD of the final DP2 NMR structure ensemble. Of major importance for hydrophobic packing of the helices in DP2 turned out to be ϵ - methyl groups of several methionine residues (figure 4.95, lower panel).

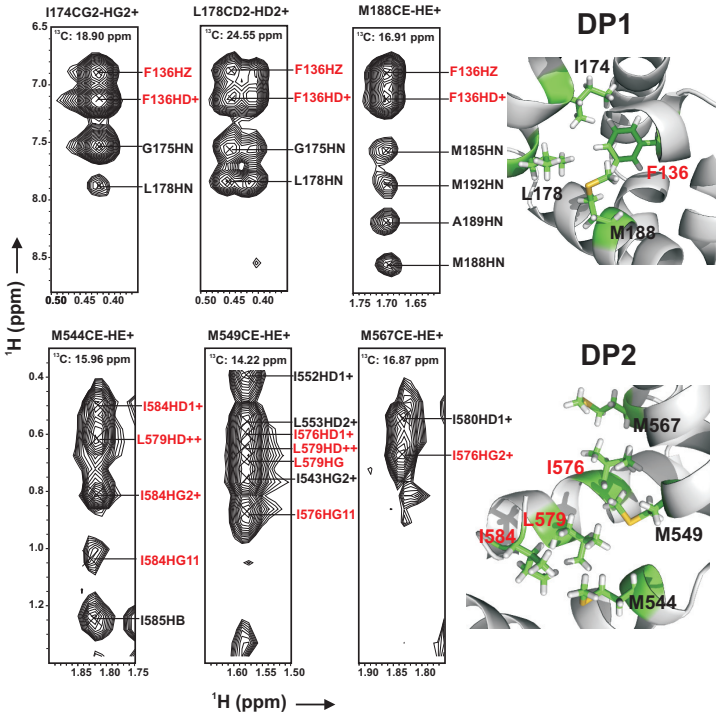

Figure 4.95: Hydrophobic packing in the structures of DP1 (upper panel) and DP2 (lower panel). Left: Strips from a HCH-NOESY spectrum of DP1 and DP2. In DP1, F136 provides important contacts for stabilizing the fold. In DP2, methyl groups of several methionine residues have major importance for the structure. Right: Sections from the NMR structures of DP1 and DP2 showing hydrophobic packing.

For refining both DP1 and DP2 structures, backbone NH residual dipolar couplings (RDCs) were measured. Partial alignment of the proteins was achieved using Pf1 phages [274] added to the proteins in a concentration of 8 mg/ml. Recording in-phase/antiphase J-coupled spectra [275] on the respective aligned and unaligned samples, NH RDCs could be measured for 63/60 residues of DP1/DP2. Couplings ranged from -23 to +23 Hz for DP1 and -6 to +6 Hz for DP2 (figure 4.96). Due to the

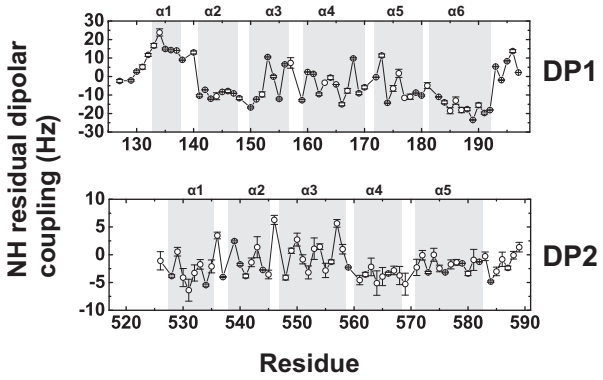

Figure 4.96: NH residual dipolar couplings of the Sti1 DP1 (upper panel) and DP2 (lower panel) domain. Plot of NH residual dipolar couplings against the sequence position. A periodicity of ~3.6 can be observed due to the helical secondary structure of the DP domains. The secondary structure elements are indicated on top of the plots. Partial alignment of the proteins was obtained by adding Pf1 phages in a final concentration of 8 mg/ml to the buffer (50 mM potassium phosphate, 50 mM potassium chloride, 1 mM TCEP, pH 7.5). Measurements were done at 750 MHz (DP1) and 900 MHz (DP2) at 293 K.

α-helical secondary structure, a typical periodicity of the couplings of ~3.6 can be observed. Using the PALES software [276], the parameters of the alignment tensor for DP1 and DP2 could be determined, allowing to include the NH RDC data in the last step of the structure calculations

(table 4.24). The structures of DP1 and DP2 after the refinement were

Table 4.24: Parameters of the alignment tensor for the Sti1 DP1 and DP2 domain in Pf1 phage medium as determined by using the PALES software [276]. RDCs were back - calculated from the regularised average NMR structures and compared to the experimentally determined RDCs. The linear correlation coefficient R can have values between - 1 (no correlation) and + 1 (perfect correlation). Partial alignment of DP domains was obtained by adding Pf1 phages in a final concentration of 8 mg/ml to the buffer (50 mM potassium phosphate, 50 mM potassium chloride, 1 mM TCEP, pH 7.5). Measurements were done at 750 MHz (DP1) and 900 MHz (DP2) at 293 K.

Parameter	DP1	DP2
Rhombicity	0.47	0.36
Da (HN) (Hz)	9.60	4.11
Correlation R	0.98	0.96
Q Saupe	0.13	0.14

then analyzed for agreement with experimentally determined NH RDCs (figure 4.97). Both proteins showed a reasonable correlation between the

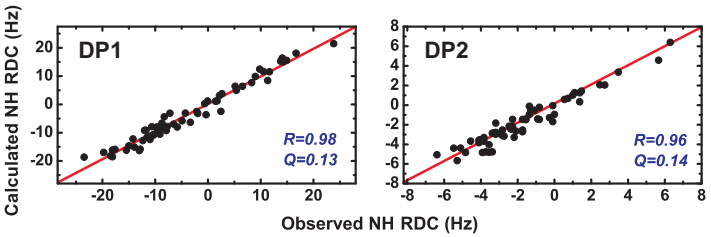

Figure 4.97: Correlation between measured and back - calculated NH RDCs for DP1 (left) and DP2 (right). RDCs were back - calculated from the DP1 and DP2 NMR structures and compared with the experimentally determined RDCs. The linear correlation coefficient R and the quality factor Q are given. R can have values between - 1 (no correlation) and + 1 (perfect correlation). Both DP domains show reasonable agreement with the experimental data.

calculated and the observed couplings, the linear correlation coefficients R were close to 1 (R can have values between - 1 indicating no correlation and + 1 for perfect correlation).

For a further structure validation, NOESY spectra strips of individual residues in DP1 and DP2 were back - calculated from the NMR structures using the program SPIRIT [288] and in house written software (figures 4.98 and 4.99). The simulated and experimental spectra showed a reasonable

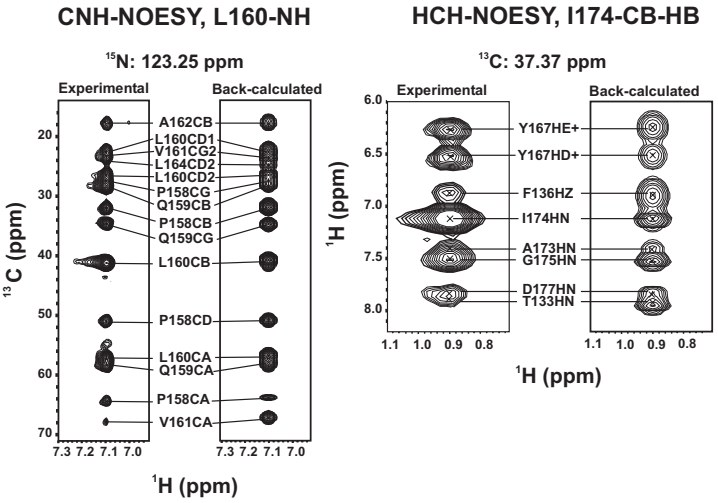

Figure 4.98: Back - calculation of CNH - and HCH - NOESY strips from the DP1 NMR structure for residues L160 (left) and I174 (right) using the program SPIRIT [288]. Despite some slight differences caused potentially by special relaxation properties of individual nuclei or dynamics, the simulated and experimental spectra show a reasonable agreement.

agreement. Some slight differences may be caused by special relaxation properties of individual nuclei or dynamics that are not considered in the

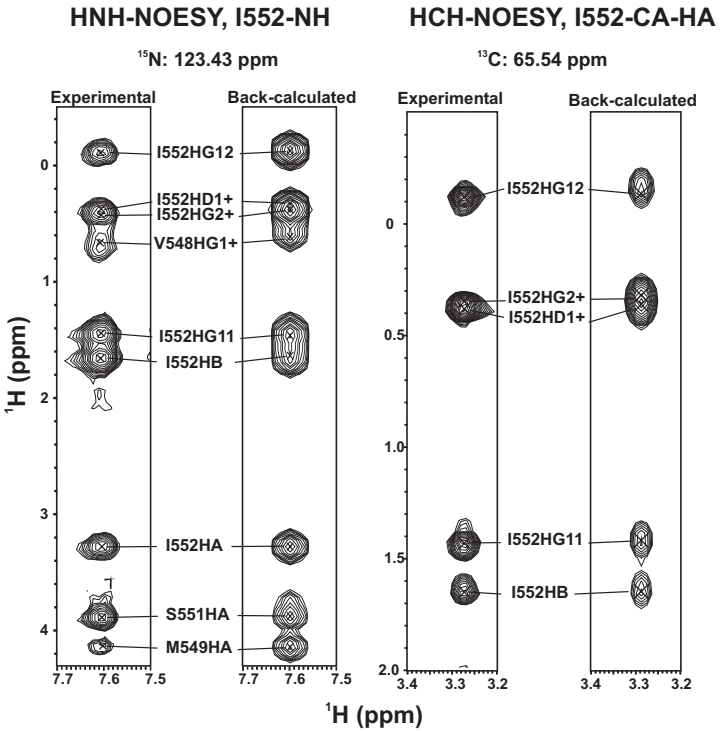

Figure 4.99: Back-calculation of HNH- and HCH-NOESY strips from the DP2 NMR structure for the residue I552 using the program SPIRIT[288]. Despite some slight differences caused potentially by special relaxation properties of individual nuclei or dynamics, the simulated and experimental spectra show a reasonable agreement.

calculations made by the SPIRIT program.

The stereochemical quality of the final DP1 and DP2 NMR structure ensembles was evaluated using the PROCHECK - NMR program [289]. The statistics for the structure determination of the DP1 and DP2 domain can be found in tables 4.25 and 4.26, respectively.

Figure 4.100 shows a comparison of the NMR structures for the DP1 and DP2 domain. As expected, both domains exhibit largely similar overall folds, however, with some slight differences. DP1 consists of six and DP2 of five α - helices located between the conserved DP/NP motives. They are arranged in a left handed twist in both domains. Helices $\alpha 3/\alpha 6$ of DP1 and $\alpha 2/\alpha 5$ of DP2 have a similar orientation. The DP1 helices $\alpha 4/\alpha 5$ and the corresponding helices in DP2, $\alpha 3/\alpha 4$, form a somehow wedge shaped structure element like a lid with an angle of $\sim 45°$ between the helix axes. The plane of these helices is nearly perpendicular to the plane of helices $\alpha 3/\alpha 6$ in DP1 and $\alpha 2/\alpha 5$ in DP2, and little contacts exist between the helices of the respective planes.

The helices $\alpha 2$ of DP1 and $\alpha 1$ of DP2 are oriented roughly parallel to the respective wedge shaped elements in the DP domains. This leaves a kind of groove in the DP2 domain theoretically accessible for the binding of a potential ligand. In DP1, in contrast, this space is occupied by the additional small N - terminal helix $\alpha 1$. It comprises only five residues and thus forms only slightly more than one helix turn. However, as outlined above (figure 4.95), this helix provides important hydrophobic contacts via F136 that stabilize the fold of DP1. Therefore, significantly more long range NOEs were found for DP1 which transferred into a lower RMSD value for final DP1 NMR structure ensemble compared to DP2 (overall backbone RMSD 0.11 Å for DP1 versus 0.66 Å for DP2, figure 4.100).

A detailed plot of the positional average backbone heavy atom RMSD from the final DP1 and DP2 NMR structure ensembles shows that the

Table 4.25: Structural statistics for the 20 lowest energy NMR structures of the Sti1 DP1 domain (PDB accession code 2LLV).

	SA[a]	<SA>$_r$
RMSD from distance restraints (Å)[b]		
all (1070)	0.025 ± 0.0005	0.025
intraresidual (168)	0.021 ± 0.0023	0.024
sequential (402)	0.023 ± 0.0017	0.021
medium (303)	0.021 ± 0.0015	0.021
long (187)	0.038 ± 0.0009	0.035
RMSD from dihedral restraints (deg) (212)	0.34 ± 0.01	0.52
RMSD from J-coupling restraints (Hz) (50)	0.87 ± 0.03	0.89
H-bond restraints (Å/deg) (35)[c]	2.05 ± 0.42 / 29.4 ± 13.69	2.20 ± 0.24 / 25.28 ± 13.41
RDC restraints (Hz) (63)	2.49 ± 0.02	3.1
Deviations from ideal covalent geometry		
Bonds (Å$*10^{-3}$)	5.29 ± 0.09	4.77
Angles (deg)	0.74 ± 0.008	0.92
Impropers (deg)	4.13 ± 0.10	1.14
Ramachandran map regions(%)[d] **(ordered residues)**[e]	94.6/5.4/0.0/0.0	92.3/7.7/0.0/0.0

	SA versus <SA>		SA versus <SA>$_r$	
Atomic RMSD (Å)[f] **(ordered residues)**[e]	backbone	all	backbone	all
	0.11 ± 0.06	0.32 ± 0.06	0.42 ± 0.03	0.65 ± 0.02

[a] Structures are labeled as follows: SA = set of 20 final simulated annealing structures; <SA> = the mean structure calculated by averaging the coordinates of SA structures after fitting over secondary structure elements; <SA>$_r$ = the structure obtained by regularising the mean structure under experimental restraints.

[b] Numbers in brackets indicate the number of restraints.

[c] H-bonds were restrained by treating them as pseudocovalent bonds. Deviations are expressed as average distance/average deviation from linearity for restrained H-bonds.

[d] Using the program PROCHECK-NMR. Percentages are for residues in allowed/additionally allowed/generously allowed/disallowed regions of the Ramachandran map.

[e] Ordered residues are defined as residues 133-193.

[f] Based on heavy atom superpositions.

Table 4.26: Structural statistics for the 20 lowest energy NMR structures of the Sti1 DP2 domain (PDB accession code 2LLW).

	SA[a]	<SA>$_r$
RMSD from distance restraints (Å)[b]		
all (539)	0.018 ± 0.0006	0.029
intraresidual (189)	0.013 ± 0.0013	0.025
sequential (168)	0.019 ± 0.0014	0.038
medium (75)	0.016 ± 0.0033	0.020
long (91)	0.025 ± 0.0012	0.027
RMSD from dihedral restraints (deg) (160)	0.07 ± 0.008	0.09
RMSD from J-coupling restraints (Hz) (67)	0.49 ± 0.04	0.72
H-bond restraints (Å/deg) (34)[c]	2.21 ± 0.17 / 18.32 ± 9.65	2.20 ± 0.18 / 19.05 ± 10.32
RDC restraints (Hz) (60)	0.78 ± 0.04	0.84
Deviations from ideal covalent geometry		
Bonds (Å*10^{-3})	4.03 ± 0.08	3.07
Angles (deg)	0.49 ± 0.008	0.52
Impropers (deg)	1.94 ± 0.14	0.40
Ramachandran map regions(%)[d] **(ordered residues)**[e]	97.9/2.1/0.0/0.0	98.0/2.0/0.0/0.0

	SA versus <SA>		SA versus <SA>$_r$	
Atomic RMSD (Å)[f] **(ordered residues)**[e]	backbone	all	backbone	all
	0.66 ± 0.36	1.04 ± 0.37	0.77 ± 0.38	1.23 ± 0.35

[a] Structures are labeled as follows: SA = set of 20 final simulated annealing structures; <SA> = the mean structure calculated by averaging the coordinates of SA structures after fitting over secondary structure elements; <SA>$_r$ = the structure obtained by regularising the mean structure under experimental restraints.

[b] Numbers in brackets indicate the number of restraints.

[c] H-bonds were restrained by treating them as pseudocovalent bonds. Deviations are expressed as average distance/average deviation from linearity for restrained H-bonds.

[d] Using the program PROCHECK-NMR. Percentages are for residues in allowed/additionally allowed/generously allowed/disallowed regions of the Ramachandran map.

[e] Ordered residues are defined as residues 527-582.

[f] Based on heavy atom superpositions.

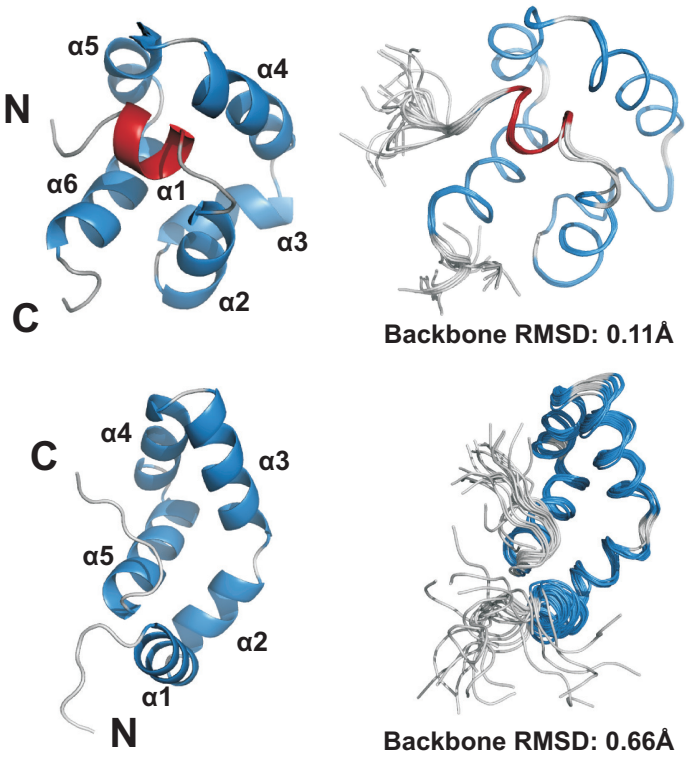

Figure 4.100: NMR structures of the Sti1 DP1 (upper panel) and DP2 (lower panel) domain. Left: Average NMR structure of the 20 lowest energy conformers after energy minimization for the Sti1 DP1 and DP2 domain in cartoon representation. Secondary structure elements, N - and C - terminus are indicated. DP1 has one additional helix at its N - terminus (colored red). Right: Overlay of the 20 lowest energy conformers of DP1 and DP2. The DP1 domain has a lower ensemble backbone RMSD for the structured parts due to the stabilization of its fold by the additional small N - terminal helix.

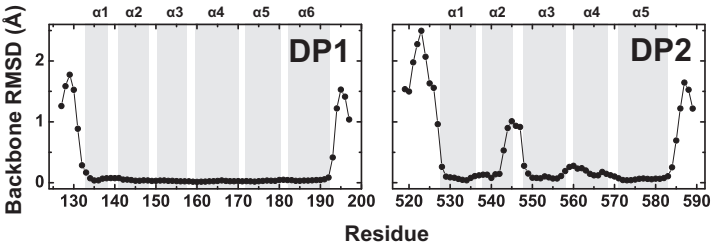

Figure 4.101: Backbone RMSD of Sti1 DP domain final structure ensembles. Positional average backbone RMSD of the 20 lowest energy structures from the NMR structure ensembles of DP1 (left) and DP2 (right). Only backbone heavy atoms were analyzed. DP1 has a lower overall backbone RMSD compared to DP2.

unstructured N- and C-termini of both DP domains have higher RMSD values, as expected (figure 4.101). The folded part of DP1 (residues 133 to 193) has a uniformly low RMSD. In contrast to that, within DP2 a region at the end of helix α2 and the beginning of helix α3 (residues 543 to 548) is structurally less well defined, indicated by an increased RMSD. Thus, in general the DP2 domain appears to be more flexible than the DP1 domain, which might be of functional importance.

The arrangement of the secondary structure elements in the DP domains (in particular in DP2) is rather loose and predominantly achieved by hydrophobic packing, as mentioned (figure 4.95), potentially explaining the non-cooperative thermal unfolding of both proteins as observed with CD spectroscopy (figure 4.88). Only the side-chains of E153 (helix α3) and R183 (helix α6) in DP1 are within a distance that would allow for the formation of a salt bridge that could contribute to a stabilization of the structure (figure 4.102).

The calculated electrostatic potentials for DP1 and DP2 show regions with predominantly positive and negative charge on the surface of the

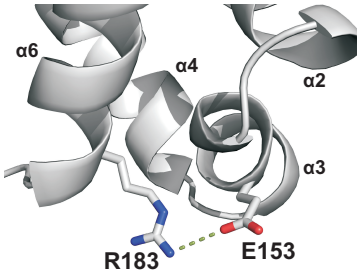

Figure 4.102: Potential salt bridge in the structure of the Sti1 DP1 domain. The side-chains of residues E153 from helix α3 and R183 from helix α6 are close enough to potentially form a salt bridge.

proteins, conferring high solubility to the domains (figure 4.103). Within the central groove of DP2, a slightly positive to neutral potential can be found (figure 4.103, lower panel, left). In contrast to that, in DP1 this area is occupied by the additional small helix with a highly negative potential dominating here.

The importance of the conserved DP motives in the DP domains becomes obvious from the structures now: They are part of the loops connecting individual helices and serve as helix caps to saturate hydrogen bond donor and acceptor groups at the beginning and the end of helices. Figure 4.104 shows two examples from the NMR structures of the DP1 and DP2 domain. The backbone NH moiety of the respective D or N residue of a DP motive provides contacts to saturate the backbone carbonyl oxygen of the i-4 and i-3 residues within the preceding helix. This is commonly known as helix C capping [290]. In some cases, a D/N residue additionally can function in capping also the N-terminal end of the following helix at the same time. The backbone and side-chain carbonyls then act as hydrogen bond acceptors contacting backbone NH groups of

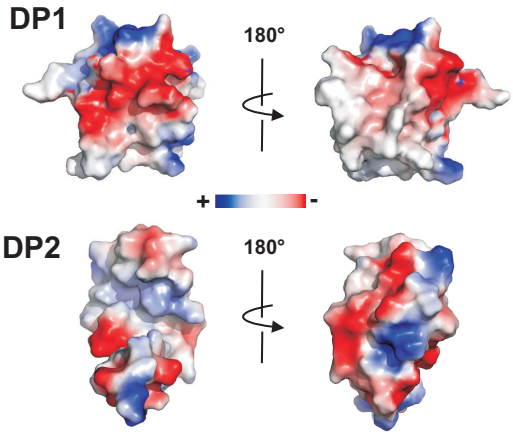

Figure 4.103: Electrostatics of the Sti1 DP1 (upper panel) and DP2 (lower panel) domain. Electrostatic potential of the DP domains were determined using the program PyMOL. Blue color indicates positive, red color negative potential. The left side shows the domains in a front view (similar orientation as in figure 4.100), the right side rotated by 180° around the vertical axis.

the i+2, i+3 or i+4 residues (figure 4.104, right).

Helix N and C capping in general has an important function for the stability of helices. Hydrogen bond donor and acceptor groups in the first/last helical turn cannot be saturated by intrahelical contacts, which would lead to an unfavorable energy loss if these groups were left unsaturated. It was found that helix capping is in most cases also accompanied by hydrophobic interactions [291] that shield polar groups at the end of helices. In case of the DP domains, hydrophobic residues located in position i-3 to the D/N in the preceding helix and i+3 or i+4 in the following helix can be found. These residues fix the orientation of the helices by hydrophobic packing and shield helix ends from forming hydrogen bonds

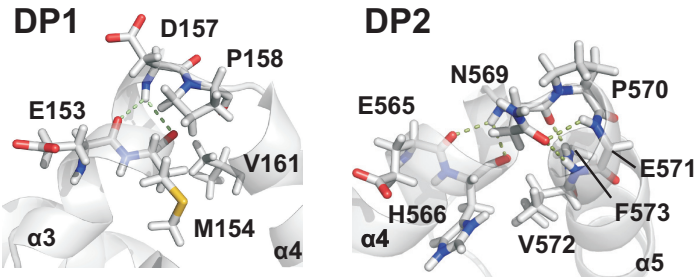

Figure 4.104: Helix capping by the conserved DP/NP motives in the Sti1 DP1 (left) and DP2 (right) domains. The conserved D/N residues in the loops connecting helices act as hydrogen bond donors that saturate the backbone carbonyls of the i-4 and i-3 residues in the preceding helix by providing backbone NH contacts. Additionally, as observed in DP2, the side - chain and backbone carbonyls of D/N can in some cases at the same time function as hydrogen bond acceptor to saturate backbone NH groups of the following helix. For clarity, the side - chains of E571 and F573 in DP2 are not shown.

with water molecules. As shown in the example of figure 4.104, right, the side - chain of the D/N can can participate in these hydrophobic interactions in some cases.

The proline residue in DP motives functions either as “helix breaker” terminating helices and/or initiates the beginning of a new helix. Proline is very frequently found as first residue of helices due its special properties: Its is surprisingly well water soluble and therefore suited for being incorporated at the solvent exposed N - terminal ends of helices. Its backbone ϕ - angle is constrained to values around - 70° which allows proline to be part of helical secondary structure. However, its bulky side - chain forces the preceding residue to adopt a non - helical conformation [290]. This is very well compatible with loop regions as found in case of the DP domains where the N/D in the DP motive functions as capping for the

preceding and following helix that can perfectly provide hydrogen bond donors and acceptors when present in a such loop conformation.

Since no DP structures were reported so far, a search in the PDB database was performed to find out whether the DP structures determined here represent a novel folding type. To this end, two algorithms were applied that compare an input template structure against the protein structures in the PDB and report on potential 3D similarities. First, the Dali analysis tool was used [292]. However, the results obtained here indicated only little structural homology with already known protein folds. The structures from the PDB found by Dali to have the highest 3D similarity with DP1 and DP2 had only poor Z-scores with values slightly above 2 (Z-scores below 2 are regarded as spurious, table 4.27). The sequence

Table 4.27: PDB search for structural similarities of Sti1 DP domains with other proteins using Dali [292]. The five best matches between the Sti1 DP1 and DP2 template structures and existing structures from the PDB are listed. The low Z-scores indicate low 3D similarity.

	Dali search						
	No	PDB-chain	Z[a]	RMSD (Å)	lali[b]	id (%)[c]	Molecule
DP1	1	2GGZ-B	2.9	3.9	65	6	Guanylyl cyclase activating protein 3
	2	2PEM-E	2.7	3.3	50	4	ORF134
	3	2GGZ-A	2.6	3.7	63	6	Guanylyl cyclase activating protein 3
	4	3KJ6-A	2.5	3.5	54	7	Beta-2 adrenergic receptor
	5	2HQA-A	2.5	2.7	50	4	DNA polymerase III alpha subunit
DP2	1	2OEE-B	2.8	4.0	64	0	UPF0342 PROTEIN YHEA
	2	2OEE-A	2.7	4.0	61	2	UPF0342 PROTEIN YHEA
	3	1FIY-A	2.6	16.1	79	11	Phosphoenolpyruvate carboxylase
	4	1JQN-A	2.4	13.4	68	12	Phosphoenolpyruvate carboxylase
	5	2ZZE-A	2.4	7.2	69	9	Alanyl-tRNA synthetase

[a] Z-score. Similarities with a Z-score lower than 2 are spurious.
[b] Alignment length (residues).
[c] Relative identity.

identities for the five best matches found were around 10 % or lower. Functionally, the proteins were completely unrelated to the DP domains.

A visual inspection of an overlay between DP1/DP2 and the respective highest scored structural neighbor showed some similarity of the DP domain templates with the identified PDB entries, especially for DP2 (figure 4.105). But overall the DP domains had a rather poor agreement with

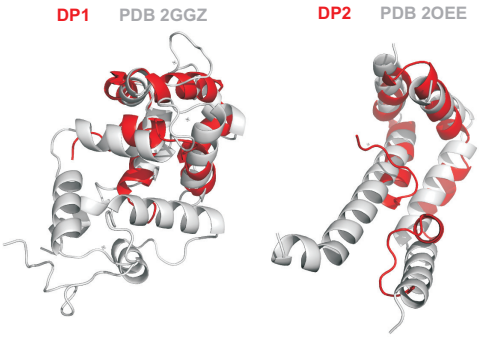

Figure 4.105: Overlay of the Sti1 DP1 (left) and DP2 (right) domains with the highest scored matches from a structure similarity search using Dali [292]. Although some structural similarity is found between the two DP domain structure templates and the PDB entries 2GGZ/2OEE, especially for DP2, the match is overall rather poor.

these proteins. Notably, the structural matches found by Dali comprised only a small portion of an otherwise much larger protein domain but did not represent a full individual domain. Thus, taken together, with Dali no structurally related protein domain with a fold similar to the Sti1 DP domains could be identified.

For comparison, also another structure similarity search algorithm was used, FATCAT [293–295], which in contrast to the rigid-body search per-

formed by Dali additionally considers conformational flexibility of proteins. To optimize structural alignments, so called twists are introduced into protein structures at positions where flexibility is detected. This can in some cases reveal significant structural similarities that are not found by rigid-body searches. Indeed, with the FATCAT algorithm different hits were obtained compared to the Dali (table 4.28). For both DP1 and DP2 the hit with the lowest P-value (which reports on the probability of finding a hit with a higher score and therefore is a measure for the significance of a hit) was consistently the PDB entry 3L4H. It is the crystal structure of a fragment comprising the tandem helical box and second WW domains of human HECW1, an E3 ubiquitin-protein ligase.

A visual inspection showed that the N-terminal helical box of the protein has high similarity with the Sti1 DP domains, especially with DP1 (figure 4.106). Although the respective sequence of HECW1 and the se-

Figure 4.106: Overlay of Sti1 DP domains with the best matches from a FATCAT [293–295] structure similarity search. Left: Crystal structure of the tandem helical box and second WW domain of human HECW1, an E3 ubiquitin-protein ligase which was identified as closest structural neighbor of the Sti1 DP domains by FATCAT. Middle and right: Overlay of the Sti1 DP domains with the helical box of HECW1.

quences of the Sti1 DP domains have little identity (DP1 vs. HECW1:

Table 4.28: PDB search for structural similarities of Sti1 DP domains with other proteins using FATCAT [293–295]. The five best matches between the Sti1 DP1 and DP2 template structures and existing structures from the PDB are listed. Results are ranked by the P-value.

	FATCAT search								
	No	PDB-chain	Score	P-value[a]	T[b]	Opt/chain RMSD(Å)[c]	lali[d]	id[e]	Molecule
DP1	1	3L4H-A	104.28	6.56e-04	0	3.03/2.98	64	6.25	*H. sapiens* ubiquitin-protein ligase HECW1
	2	2JVW-A	79.00	9.85e-03	0	3.17/3.44	78	3.85	*V. fischeri* protein Q5E7H1
	3	1PVE-A	74.30	1.03e-02	0	3.02/2.90	53	7.55	*H. sapiens* DNA repair protein hHR23B
	4	2P98-P	75.30	1.09e-02	1	1.60/8.18	39	7.69	*E. coli* methionine aminopeptidase
	5	3HE5-B	61.45	1.40e-02	1	0.86/12.13	37	10.81	Synthetic coiled-coil pair SYNZIP2:SYNZIP1
DP2	1	3L4H-A	112.23	2.05e-03	0	1.60/8.70	58	3.45	*H. sapiens* ubiquitin-protein ligase HECW1
	2	1TUW-A	108.87	2.67e-03	0	3.17/3.07	74	5.41	*S. glaucescens* tetracenomycin F2 cyclase
	3	2KKO-A	105.86	4.25e-03	0	3.13/4.35	67	8.96	*M. bovis* DNA-binding domain Mb0332
	4	2OQG-A	96.40	6.54e-03	1	3.18/3.93	63	14.29	*R. sp. RHA1* ArsR-like transcript. regulator
	5	1N1J-B	85.32	7.79e-03	1	0.95/12.84	61	8.20	*H. sapiens* NF-YB/NF-YC histone pair

[a] Significance of structural similarity: The probability of observing a greater score.
[b] Number of structural rearrangements/twists T necessary for obtaining optimal alignment.
[c] RMSD of Cα atoms for alignment with/without twist.
[d] Alignment length (residues).
[e] Relative identity (%).

$\sim 6\,\%$, DP2 vs. HECW1: $\sim 4\,\%$, table 4.28), the structures are surprisingly well conserved. Functionally, the helical box of HECW1 remains uncharacterized so far. However, it seems likely that here a particular protein fold might have been adapted for rather different functions.

4.14.4 Fast Backbone Dynamics of Sti1 DP Domains

Fast backbone dynamics of the Sti1 DP1 and DP2 domains in the ns to ps timescale were determined by measurements of the $\{^1H\}$-^{15}N heteronuclear NOE (hetNOE). As expected, the unfolded N- and C-termini of the proteins had increased flexibility, indicated by lower hetNOE values (figure 4.107). Within the folded parts, DP1 and DP2 showed a hetNOE around ~ 0.8.

In general, on average DP2 seems to have moderately higher flexibility, hetNOE values for its structured residues (527 to 582) were slightly below 0.8. In contrast, hetNOE values of residues in the corresponding region of DP1 (133 to 193) were mostly above 0.8. In particular, DP2 residues at the end of helix $\alpha 3$, the beginning of helix $\alpha 4$ and the connecting residues in between displayed increased backbone mobility. These residues form the tip of the wedge shaped arrangement of helices $\alpha 3$ and $\alpha 4$, and a higher flexibility of this element might be of functional importance.

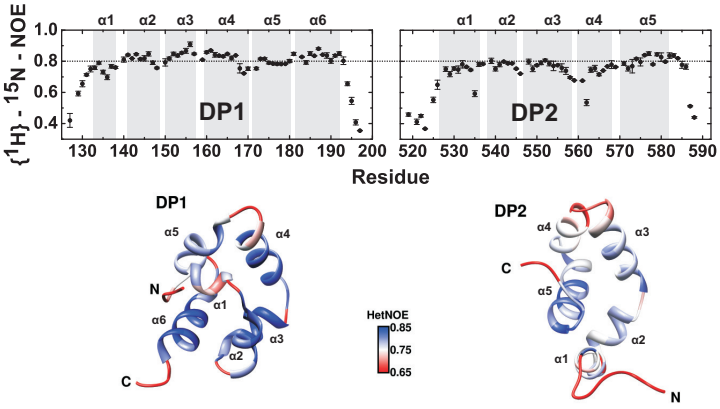

Figure 4.107: Fast backbone dynamics of the Sti1 DP1 (left) and DP2 (right) domains determined by measurement of the $\{^1H\}$-^{15}N heteronuclear NOE (hetNOE). hetNOE values around 0.8 within the structured parts indicate comparatively high rigidity. Only N- and C-termini of the domains have increased flexibility. The measurements were done at 750 MHz and 293 K in 50 mM potassium phosphate, 50 mM potassium chloride, 1 mM TCEP, pH 7.5. The secondary structure elements are given on top of the plots. HetNOE values were color-coded mapped onto the NMR structures. The color code is given next to the structures.

4.15 *In Vivo* Function of Sti1 DP Domains

Previous reports demonstrated the essential importance in particular of the DP2 domain for the *in vivo* function of Sti1/Hop. A deletion of the Sti1 DP2 domain led to lethal phenotype in yeast cells when combined with a knockout of YDJ1 [187]. But likewise, even smaller truncations or a simple V540E point mutation of DP2 had the same effect. Furthermore, in a system expressing the human GR heterologously in yeast cells, the activity of the receptor was reduced down to control levels by truncation or only point mutation of DP2.

Except for the mentioned V540E variant, no other point mutants of DP2 have been analyzed so far which could reveal functionally important regions within the domain. Using the NMR structure obtained here, now a directed design of DP2 domain mutants was possible and a more detailed study about its structure - function relation could be carried out. To this end, a set of six different DP2 point mutants was generated targeting residues for amino acid substitution with different properties (hydrophobic or polar) and spread over the protein as summarized in figure 4.108. As a sequence alignment with the human Hop DP2 domain and Hip DP

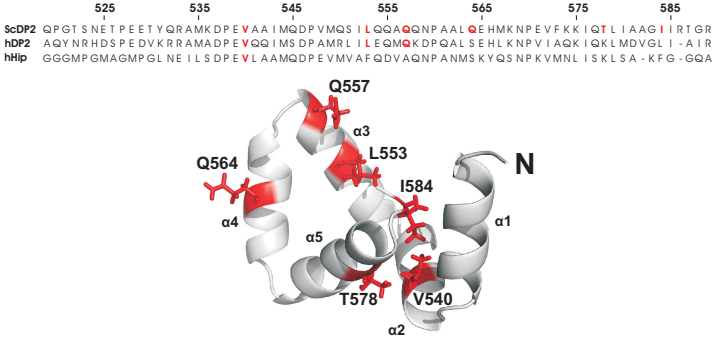

Figure 4.108: Design of Sti1 DP2 points mutants. Upper panel: Amino acid sequence alignment for the yeast (*Saccharomyces cerevisiae*, Sc) Sti1 DP2 domain, the human (h) Hop DP2 domain and the human Hip DP domain. Residues of Sti1 DP2 selected for mutation are colored red. V540, L553 and Q557 seem to be partially conserved. The alignment was generated using T - Coffee [194]. NCBI reference codes of the sequences are NP_006810.1 for human Hop and NP_014670.1 for yeast Sti1. The UniProt reference code for the human Hip sequence is P50502. Lower panel: NMR structure of Sti1 DP2 showing the position of the residues chosen for mutation.

domain shows, the residues V540 from helix α2 and L553/Q557 from helix α3 seem to be partially conserved. Q564 (helix α4) and T578/I584

(helix α5), in contrast, show no conservation. The residues at all six positions were replaced by alanine as this amino acid is well compatible with helical structure and should not disturb the overall fold of the domain too much. Although a V540E mutant was described earlier, as mentioned [187], this position was again chosen for mutation to address the question whether a more conservative substitution of this residue with A still has a significant effect on the function of DP2.

Prior to the *in vivo* analysis in yeast cells, all mutants were characterized by CD and NMR spectroscopy. To this end, the respective mutations were first introduced into the DP2 domain in an *E. coli* pET28a expression vector. All variants expressed equally well and comparable to wild - type DP2. A first CD spectroscopic characterization showed that the mutations did not significantly affect the structure and stability of the DP2 domain (figure 4.109).

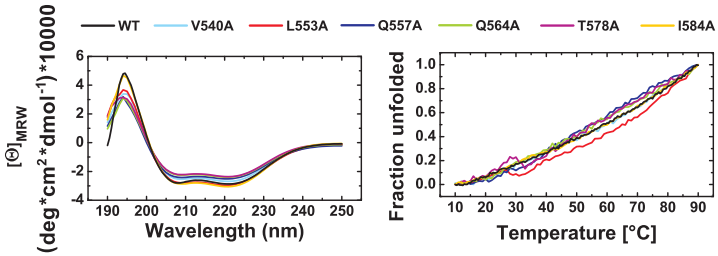

Figure 4.109: CD spectra (left) and CD thermal unfolding transitions (right) of Sti1 DP2 domain point mutants. The CD spectra of the mutants are very similar to the wild - type. The thermal unfolding transitions indicate no major loss of stability by the mutations introduced. 20 μM of wild - type DP2 or the respective mutants were measured in 50 mM potassium phosphate, 50 mM potassium chloride, 1 mM TCEP, pH 7.5. CD spectra were recorded at 20°C. Thermal unfolding was monitored at a wavelength of 222 nm.

Comparing the ^{15}N - HSQC spectra for the wild - type DP2 domain and

the mutants thereof, peak shifts could be observed (figure 4.110). These

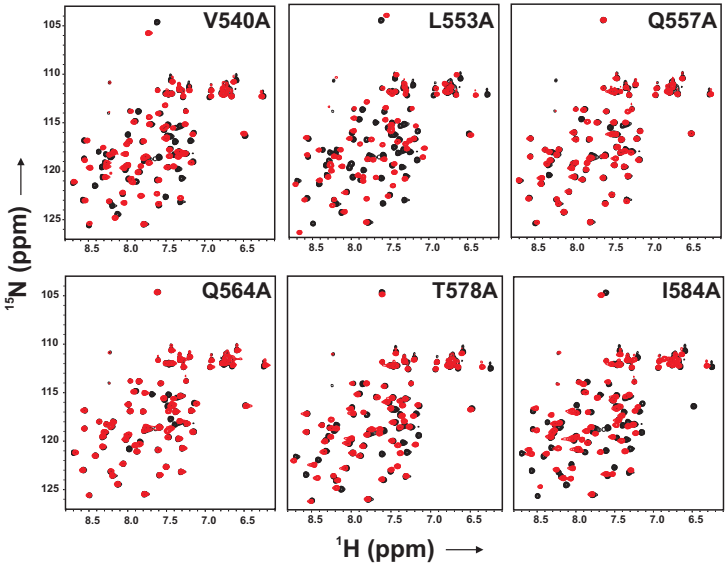

Figure 4.110: Overlay of ^{15}N-HSQC spectra for wild-type Sti1 DP2 (black) and point mutants thereof (red). Although peak shifts are observed upon mutation, the spectra for the DP2 variants indicate a folded protein in each case. 150 μM of wild-type DP2 or the respective mutant was measured in 50 mM potassium phosphate, 50 mM potassium chloride, 1 mM TCEP, pH 7.5 at 70 MHz and 293 K.

were more pronounced for the mutation of hydrophobic residues like V540 or L553, as expected. Nevertheless, the NMR spectra of all DP2 variants indicated folded proteins in agreement with the CD data. Thus, the amino acid substitutions did not cause a major distortion of the DP2 structure and its overall fold was preserved in the mutants. Also the line width of signals in the NMR spectra of the mutants was not markedly

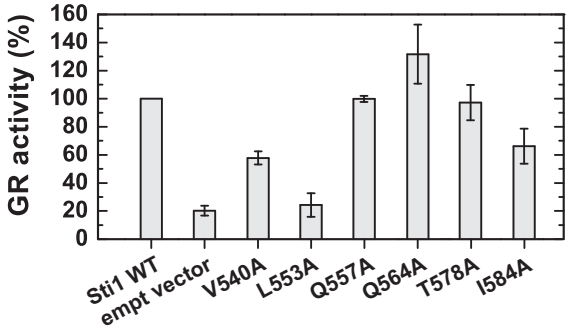

Figure 4.111: *In vivo* function of Sti1 DP2 point mutants. The plot shows the relative activity of the human glucocorticoid receptor (GR) in yeast cells expressing wild - type (WT) Sti1 or Sti1 containing different point mutations within DP2 as indicated. A mutation of hydrophobic residues has stronger impact on the ability of Sti1 to support GR activation.

higher than for the wild - type DP2 domain, which shows that none of the mutations resulted in the formation of higher order oligomeric DP2 species.

Since the *in vitro* characterization proved the DP2 mutants to be structurally comparable to the wild - type protein, all six mutants were suited for a functional testing in yeast cells. The respective DP2 mutations were therefore introduced into the full - length Sti1 protein in a p425GPD plasmid for expression in yeast cells. The mutants were then assessed for their ability to support the activation of the heterologously expressed human GR, similar as described already in section 4.11. The *in vivo* testing of the respective plasmids was done by Alina Röhl (Lehrstuhl für Biotechnologie, TUM).

The Sti1 mutants Q557A and T578A supported GR activity comparable to the wild - type protein (figure 4.111). With the Sti1 V540A and I584

variants, the receptor was only active on a level around 60 % whereas Sti1 L553A completely failed to act on the GR. The receptor activity in this case was on the level of the control. Surprsingly, the Q564A mutant seemed to have an even higher capacity to promote GR functionality than wild - type Sti1, with an activity of GR around ~ 130 %. Thus, overall these data show that also rather conservative point mutations within DP2 that affect the structure of this domain only to a small extent significantly impact the *in vivo* function of Sti1, demonstrating the essential importance of DP2.

The structural similarity of the Sti1 DP1 and DP2 domains as found by NMR (section 4.14.3) raises the question whether DP1 might be able to functionally substitute for DP2. For addressing this issue, a Sti1 DP domain swap was constructed replacing DP2 by DP1. Thereby, some modifications of the original pGPD425 yeast plasmid containing the full - length Sti1 gene were required (figure 4.112). A region suited for a DP domain exchange seemed to be a stretch comprising amino acids 517 to 525 of Sti1 as the NMR data obtained in this work indicated that these residues do not have any secondary structure. Inserting the DP1 domain here should leave the rest of the Sti1 protein unaffected.

First, a new restriction site had to be introduced into this region of the Sti1 gene located C - terminal of the TPR2B domain in order to specifically cut out the DP2 domain. As a good choice appeared to be a *PstI* restriction site as the recognition sequence of this enzyme was neither present in the Sti1 gene nor in the backbone of the p425GPD template vector available for the mutation. Furthermore, this recognition site could be obtained by a mutation of only three bases from the codons of G521 and T522 which are located exactly within the region favored for the domain exchange.

Concomitant with introducing the *PstI* site, T522 was unfortunately exchanged to an artificial C. Using the C - terminal *HindIII* and the new N - terminal *PstI* sites, the DP2 domain was cut out of the vector. The DP1

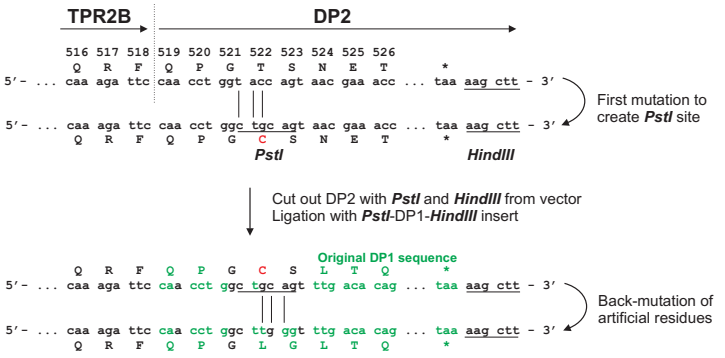

Figure 4.112: Strategy to generate a Sti1 DP domain swap. For replacing the DP2 with the DP1 domain, first a *PstI* restriction site was generated C-terminally of the TPR2B domain. The native DP2 domain was then cut out of the vector and the DP1 domain ligated into the vector instead. Afterwards, artificial amino acids were replaced again in a back-mutation, leaving overall only 1 artificial residue G in the sequence of DP1 instead of a native D. Restriction sites are underlined.

domain flanked with the respective restriction sites could then afterwards be ligated into the vector instead. Overall, at this step three artificial amino acids G, C and S at the N-terminal part of the DP1 domain were present due to the *PstI* site required for the construction of the domain swap. To avoid any effects caused by these non-native amino acids, a final back-mutation was done replacing two of them, C and S, again with the native L and G. The only remaining artificial residue G instead of the native D seemed to be acceptable as it should not interfere with the DP1 structure and was therefore kept.

The mutant plasmid was then tested again in yeast cells for supporting GR activity by Alina Röhl (Lehrstuhl für Biotechnologie, TUM). Surprisingly, the DP1 domain was nearly unable to substitute for the DP2 domain. The GR activity with the Sti1 DP swap plasmid was only slightly

above the control level (figure 4.113). Thus, the slight structural differ-

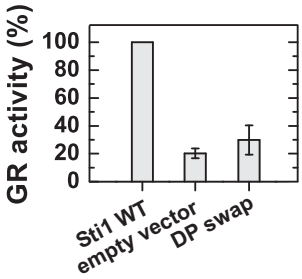

Figure 4.113: *In vivo* function of a Sti1 DP domain swap mutant. The DP2 domain of Sti1 was replaced with the Sti1 DP1 domain and tested for supporting GR activation in yeast cells. The mutant fails to support GR activity to a level significantly above the control.

ences of DP2 compared to DP1 and its specific properties as found in the experiments with the point mutants obviously seem to play an important role for its function in the process of GR activation *in vivo*.

4.16 Binding Studies with Sti1 DP Domains

Although the previous *in vivo* experiments demonstrated the essential importance in particular of the DP2 domain for the Sti1 function, the precise role of its DP domains in the process of steroid hormone receptor (SHR) activation remains unclear. In principle, it seems possible that the DP domains could serve as an interaction partner for a component in the Hsp70/Hsp90/SHR heterocomplex. The assumption of Sti1 DP2 constituting a binding site for an unknown ligand is supported by the fact that the DP1 domain was unable to substitute for the DP2 domain in promoting GR activation in yeast cells, as observed with the domain swap experiment (section 4.15). This finding is surprising given the largely similar overall folds of Sti1 DP1 and DP2. The most significant difference between the two domains is the presence of an additional small N-terminal helix in DP1 (compare figure 4.100). It might potentially be responsible for the failure of DP1 in the GR activation assays by preventing access to a binding site available in DP2.

Indeed, for the DP2 domain of human Hop a role in Hsp70 binding was found in a previous study[66,171], which does obviously not apply for the DP2 domain from yeast according to another work that furthermore could not detect any contribution of yeast DP2 to the binding of Hsp90[147]. However, in general these observations can not completely exclude an interaction of yeast DP2 with one of the two chaperones since the pull down assays performed in the mentioned study would likely not be able to detect a very weak but potentially important binding. With NMR, in contrast, weak complexes might still be visible. Therefore, the Sti1 DP1 and DP2 domain were again assessed for binding of Hsp70/Ssa1 fragments (see section 4.2) and the full-length Hsp90 here.

^{15}N-HSQC spectra of the isotopically labeled DP domains were recor-

ded and analyzed for chemical shift perturbation upon adding the different potential binding partners in a 1:1 (full-length Hsp90) to 1:4 (Ssa1 fragments) molar ratio. With full-length Hsp90, no indications of binding like peak shifts could be observed in the NMR spectra of DP1 and DP2, even in presence of an excess of the non-hydrolyzable nucleotide AMP-PNP (data not shown). Also in case of only a very weak complex, the high molecular weight of the dimeric Hsp90 ($\sim$ 162 kDa) should have caused line broadening of DP domain signals if an interaction occurred, but line width was unaffected here.

Likewise, the addition of the Hsp70/Ssa1 fragments N and MC to the ^{15}N-labeled Sti1 DP1 and DP2 domains did not result in any sign of binding in the NMR spectra, and again the presence of the nucleotide had no effect (data not shown). Thus, overall these experiments indicate that the Sti1 DP domains do not – even weakly – interact with Hsp70 (Ssa1) fragments and full-length Hsp90. The full-length Ssa1 protein could not be tested for binding to Sti1 DP domains as it did not express in *E. coli*. Therefore, an interaction with full-length Ssa1 cannot be ruled out completely at this point.

Another possibility of a potential interaction partner for the Sti1 DP domains could be the steroid hormone receptor substrate itself. Though Sti1 was found to have no chaperone activity[149], the function of the DP domains does not necessarily need to be related to a basic influence on the receptor folding. This role in client protein maturation is most likely anyway accomplished to a large extent by Hsp70. However, the DP domains could act on conformational transitions of the steroid hormone receptor in later steps of the activation process. A crystal structure of the ligand binding domain (LBD) of the human GR[296] revealed interesting details about the hormone binding and the oligomeric state of this receptor: The ligand is bound in a small hydrophobic pocket and seems to be trapped

by a kind of lid, formed by two small β - strands comprising residues 620 to 629 of the GR (figure 4.114). It is located directly within the dimeriza-

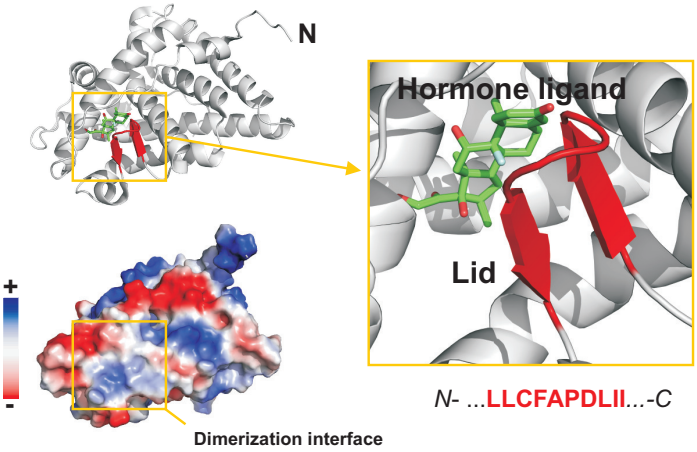

Figure 4.114: Crystal structure of the ligand binding domain (LBD) of the human GR in complex with the steroid drug dexamethasone (PDB: 1M2Z). Left, upper panel: LBD of the GR in cartoon representation. For clarity, only one protomer of the dimer is shown. Right: Enlarged view of the GR ligand binding site. The steroid drug bound in the hydrophobic pocket is depicted in sticks and colored green. It is trapped in the binding pocket by a kind of lid formed by two small β - strands (residues 620 to 629, colored red) which have rather hydrophobic amino acid composition. This lid element is located within the LBD dimerization site. Left, lower panel: Electrostatics of the GR LBD. Only one protomer of the dimer is shown. In the indicated dimerization site, neutral to slightly positive potential is found.

tion site of the GR LBD. It has rather hydrophobic amino acid composition with several L and I residues. These are required to provide a hydrophobic environment for the steroid ligand in the binding pocket, allowing for optimal trapping of the ligand when the lid is closed. In this state, the

hydrophobic side - chain of I628 would unfavorably point out to the solvent which could lead to a destabilization of the protein. However, it is well protected by contacts to the second protomer in the GR LBD dimer. A major driving force for the GR LBD dimerization thus seems to come from the lid element, and indeed a mutation of I628 significantly reduced the dimerization of the domain [296]. These observations show that the lid of the GR LBD in particular seems to have an important role for GR function.

Very early experiments to determine binding stoichiometries in Hsp90 - GR heterocomplexes indicated that only a monomeric GR is bound to the Hsp90 dimer [297]. This would imply that the GR LBD lid is not protected from solevent by dimerization as in the GR LBD dimer, and therefore this hydrophobic region of the GR might require additional stabilization. Such a function could potentially be exerted by Hsp90. This would be in agreement with the current model of Hsp90's role in steroid receptor maturation which is believed to keep the ligand binding cleft of the receptor open [298]. However, so far no evidence exists that Hsp90 directly interacts with the lid - element of the GR LBD. In contrast, it was reported that a different small region within the GR located more N - terminal to the lid - element should mediate binding between Hsp90 and steroid hormone receptors [126]. This observation leaves the possibility that maybe the DP domains of Hop/Sti1 could serve in stabilizing the hydrophobic steroid hormone receptor lid. Since Sti1/Hop can interact with both Hsp70 and Hsp90, the DP domains, in particular DP2, could bind and protect the lid from solvent either in the Hsp70 or Hsp90 bound state of the receptor.

To test this hypothesis, a peptide was prepared comprising residues 619 to 630 of the GR LBD corresponding to the lid segment. The peptide was synthesized by Dr. Oliver Demmer (Institute for Advanced Study, TUM) and kindly provided for the measurements. The peptide dissolved and

dialyzed excessively against measurement buffer was added to the ^{15}N-labeled Sti1 DP2 domain and binding was studied by analyzing chemical shift perturbation in the NMR spectra of the protein. The peptide indeed caused a slight shifting of several backbone resonances in DP2 (figure 4.115). The peak shifts occurred into different directions, indicating that

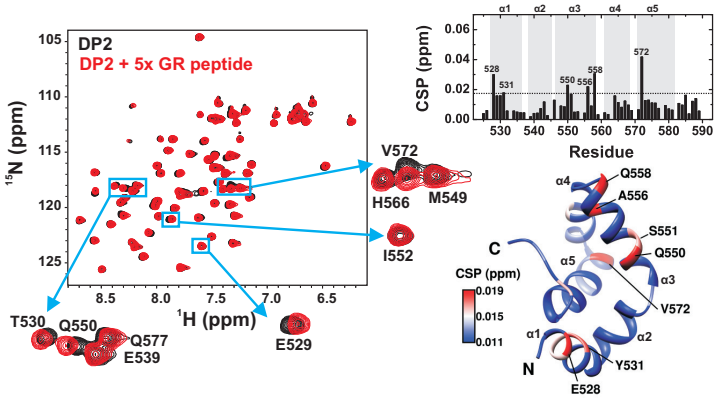

Figure 4.115: Binding of a model peptide corresponding to the lid element from the human GR ligand binding domain to the Sti1 DP2 domain. Left: ^{15}N-HSQC spectra without (black) and with (red) the GR peptide. Some slight shifts can be observed for a number of residues, indicating binding. Right, upper panel: Chemical shift perturbation (CSP) plot for the binding of the GR peptide to DP2. Mainly helices α1 and α3 seem to be affected by the binding of the peptide. Right, lower panel: Mapping of the CSP data onto the NMR structure of DP2. 150 μM of DP2 was measured in an buffer of 50 mM potassium phosphate, 50 mM potassium chloride, 1mM TCEP, pH 7.5 at 750 MHz and 293 K. The peptide was added in a 5-fold molar excess to DP2.

likely not only mere buffer effects were observed. Mainly helices α1 and α3 seemed to be involved in binding. The shifts were rather small, arguing for a very weak interaction. Given this obviously low affinity, a partially unspecific contribution in the binding between DP2 and the pep-

tide cannot be ruled out completely here. Therefore, this result has to be judged critically. Nevertheless, the data might indicate that the DP2 domain in principle could function as a potential binding site for structure elements from the GR substrate in a Sti1/chaperone/GR heterocomplex.

4.17 Analysis of Sti1 TPR - DP Fragments

From the experiments so far it has become obvious that both the TPR2B and the DP2 domain have essential importance for GR activation *in vivo* by Sti1. Thus, it seems that key functions of Sti1 are mediated by the TPR2B - DP2 fragment. Interestingly, this combination of a TPR domain with a C - terminal DP domain is found twice in the domain structure of Sti1 with the N - terminal TPR1 - DP1 and the C - terminal TPR2B - DP2 modules (figure 4.92). Indeed, it was speculated from sequence analyses that a TPR - DP fragment represents a basic functional unit and that the Sti1/Hop proteins evolved from a successive recombination of an early TPR - DP ancestor found in bacteria [175]. Therefore, the functional and structural properties of Sti1 TPR - DP fragments were analyzed in more detail here by different methods that might reveal potential differences to the behavior of the respective isolated TPR and DP domains.

The Sti1 fragments TPR1 - DP1 (Sti1 residues 1 to 197) and TPR2B - DP2 (Sti1 residues 388 to 589) were cloned into a pET28a vector and expressed in *E. coli*. The proteins were soluble and could be purified with yields of ~ 10 mg per liter of cell culture medium. As expected, both fragments were well structured and had reasonable thermal stabilities that were comparable to those of the isolated TPR1 and TPR2B domains (figure 4.116).

Then the peptide binding properties of the TPR2B - DP2 fragment were assessed to analyze whether the presence of the DP2 domain within the same polypeptide chain had any influence on the ligand binding of the TPR2B domain. The two - domain construct seemed to recognize the peptides similarly well as the isolated TPR2B domain (figure 4.117). The ITC raw curves for the titration with the Hsp70 and Hsp90 octapeptides looked very similar to the curves obtained with the isolated TPR2B do-

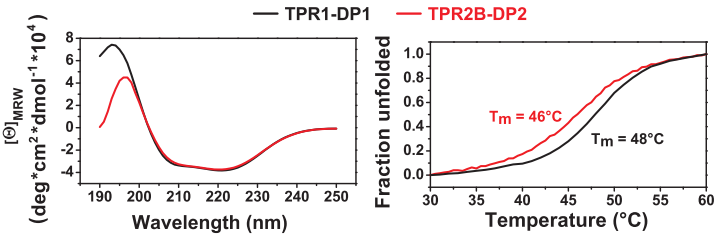

Figure 4.116: CD spectroscopic characterization of Sti1 TPR - DP fragments. Left: CD spectra for Sti1 TPR - DP constructs recorded at 20°C. Right: Thermally induced unfolding of TPR - DP fragments monitored by CD spectroscopy at a wavelength of 222 nm. The two - domain constructs have thermal stabilities comparable to the isolated TPR1 and TPR2B domains (see table 4.1). Proteins were measured in a buffer of 10 mM potassium phosphate, 1 mM TCEP, pH 7.5.

main. However, fitting the data showed that the TPR2B - DP2 fragment had a slight preference for binding of the Hsp70 peptide. The affinity for the Hsp90 hepta - and octapeptides is ~ 2.5 - fold lower than for the respective Hsp70 peptides (figure 4.118). This is somewhat in contrast to the isolated TPR2B domain (section 4.3), although the influence of the DP2 domain on the peptide binding to the neighboring TPR2B domain is not very pronounced. The affinities and thermodynamical parameters for binding of Hsp70 and Hsp90 peptides to the TPR2B - DP2 fragment are summarized in table 4.29.

To further characterize the properties of Sti1 TPR - DP fragments, analytical gel filtration experiments were performed. These could give an estimation about the relative apparent size of the two - domain constructs in solution. The TPR1 - DP1 and TPR2B - DP2 fragments, the isolated TPR1 and TPR2B domains and the Hsp90 M domain for comparison were applied onto an analytical S75 column and the elution profile of the proteins was monitored by UV (ultraviolet) detection. The TPR1 and

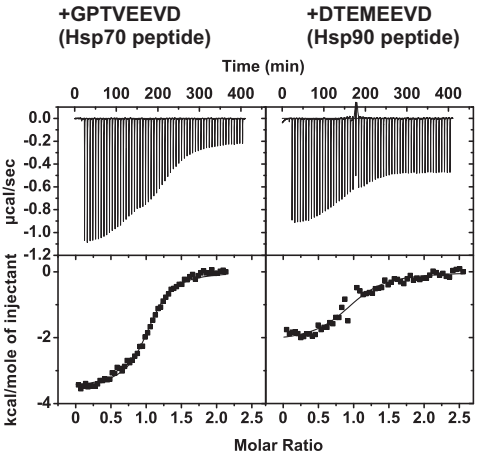

Figure 4.117: ITC measurements of the TPR2B - DP2 fragment titrated with the Hsp70 octapeptide GPTVEEVD (left) and the Hsp90 octapeptide DTEMEEVD (right). 150 μM of TPR2B - DP2 in the measurement cell of the instrument was titrated with a 1.5 mM solution of the respective peptide at a temperature of 20°C. As a buffer 10 mM potassium phosphate, 1 mM TCEP, pH 7.5 was used. The upper panel shows the respective thermograms with the raw data, the lower panel the integrated binding heats and fitting curves for both titrations. TPR2B - DP2 shows slight preference for binding the Hsp70 peptide, the corresponding K_d - values for the measurements shown are 4.2 μM for the Hsp70 peptide and 11.2 μM for the Hsp90 peptide.

TPR2B domains that have a comparable molecular weight (14.3 versus 15.6 kDa) and presumably also comparable molecular shapes eluted from the column with nearly identical volumes, as expected (figure 4.119). The Hsp90 M domain representing the protein with the highest molecular weight (33.8 kDa) tested in the gel filtration experiments with rather elongated shape had an elution volume of $\sim$ 11.9 ml. Surprisingly, although TPR1 - DP1 and TPR2 - DP2 both have much lower calculated masses with 21.8 and 22.6 kDa, respectively, which is only $\sim$ 65 % of the

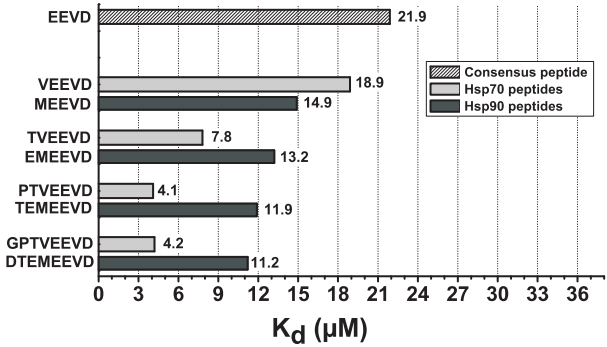

Figure 4.118: Affinities of the Sti1 TPR2B - DP2 fragment for a set of different Hsp70 and Hsp90 peptides as determined by ITC. 150 μM of TPR2B - DP2 in the measurement cell of the instrument was titrated with a 1.5 mM solution of the respective peptide at a temperature of 20°C. As a buffer 10 mM potassium phosphate, 1 mM TCEP, pH 7.5 was used. TPR2B - DP2 shows a slight selectivity for binding the Hsp70 peptides. This is in contrast to the isolated TPR2B domain (compare figure 4.14).

calculated mass for Hsp90 M, the proteins passed through the column equally fast or even faster than Hsp90 M. Especially TPR1 - DP1 eluted after a volume of only $\sim$ 11.2 ml and therefore significatly earlier than Hsp90 M.

In general, these observations indicate that the TPR - DP fragments behave in solution like proteins with a much higher molecular weight than their theoretical masses. The hydrodynamic radii of the TPR - DP fragments seem to be rather large, which could point at the TPR and DP domains not being packed together very compactly in the two - domain constructs but behaving to a certain extent independent from each other. This might in particular apply in the case of TPR1 - DP1: Although TPR1 - DP1 and TPR2B - DP2 have nearly equal calculated masses and number

Table 4.29: Summary of affinities and thermodynamical parameters for Sti1 TPR2B - DP2 fragment binding the different Hsp70 and Hsp90 peptides. 150 μM of TPR2B - DP2 in the measurement cell of the instrument was titrated with a 1.5 mM solution of the respective peptide at a temperature of 20°C. As a buffer 10 mM potassium phosphate, 1 mM TCEP, pH 7.5 was used. Affinity as K_a (association constant) and K_d (dissociation constant), binding enthalpy (ΔH), entropy (ΔS) and stoichiometry (N) are given for each measurement.

	N	K_a ($*10^5$ M^{-1})	K_d (μM)	ΔH (cal/mol)	ΔS (cal/mol/deg)
consensus peptide					
EEVD	1.09 ± 0.04	0.46 ± 0.10	21.9	- 1121 ± 56	17.5
Hsp70 peptides					
VEEVD	1.05 ± 0.06	0.53 ± 0.19	18.9	- 1725 ± 138	15.7
TVEEVD	0.98 ± 0.02	1.29 ± 0.26	7.8	- 1176 ± 36	19.4
PTVEEVD	1.07 ± 0.01	2.44 ± 0.39	4.1	- 2124 ± 39	17.4
GPTVEEVD	1.05 ± 0.01	2.39 ± 0.18	4.2	- 3513 ± 29	12.6
Hsp90 peptides					
MEEVD	0.96 ± 0.04	0.67 ± 0.18	14.9	- 1479 ± 88	17.0
EMEEVD	0.97 ± 0.02	0.76 ± 0.87	13.2	- 2556 ± 60	13.6
TEMEEVD	1.02 ± 0.03	0.84 ± 0.15	11.9	- 1647 ± 51	16.9
DTEMEEVD	1.00 ± 0.03	0.89 ± 0.17	11.2	- 2131 ± 72	15.4

of residues and furthermore should have comparable molecular shapes, a larger difference was observed with gel filtration experiments between the two fragments.

As the ITC data showed, the peptide binding selectivity of the TPR2B domain in the TPR2B - DP2 fragment seems to be slightly influenced by the DP2 domain towards a moderate preference for binding the Hsp70 peptide. This might indicate that potentially inter - domain contacts exist between TPR2B and DP2 in the two - domain construct. Although the re-

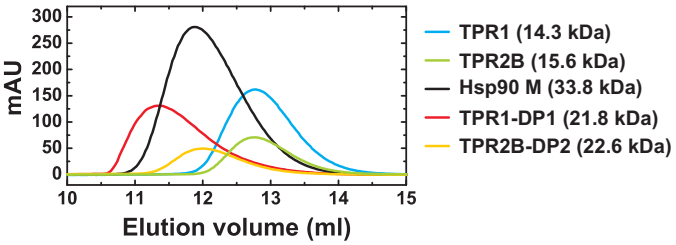

Figure 4.119: Analytical gel filtration experiments with Sti1 TPR - DP fragments. For an estimation of their relative apparent size in solution, Sti1 TPR - DP fragments and other proteins for comparison were applied onto an analytical gel filtration column to monitor their elution behavior. TPR2B - DP2 and in particular TPR1 - DP1 appear much larger in solution than expected from their calculated molecular weight. The respective protein (50 μM concentration for the injected sample) was passed over a S75 10/300 column in a buffer of 50 mM potassium phosphate, 300 mM potassium chloride, 1 mM TCEP, pH 7.5. Protein elution profiles were recorded by monitoring UV absorption (mAU; mAU = milliabsorbance units) at 280 nm. The calculated molecular weights of the proteins analyzed are given on the right.

sults from the analytical gel filtration experiments rather argue for TPR2B and DP2 not packing together very tightly, even weak domain contacts between the domains could be sufficient to have a certain impact on the ligand binding to TPR2B. To address the question whether TPR2B and DP2 behave completely independent in the two - domain fragment or indeed contacts exist between the domains, the NMR spectra of the isolated TPR2B and DP2 were compared to the spectrum of TPR2B - DP2 and analyzed for chemical shift differences. As expected, residues from the linker region connecting the TPR2B and the DP2 domains (amino acids 519 to 525) were shifted in the spectrum of the two - domain fragment (figure 4.120). However, interestingly also other residues in particular from the DP2 domain displayed significantly different chemical shifts in

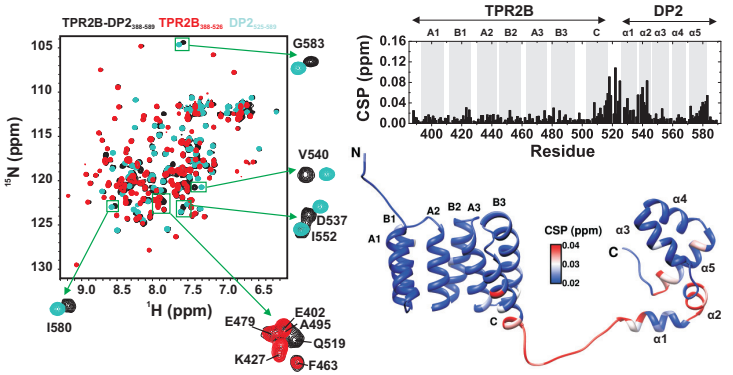

Figure 4.120: Chemical shift analysis to identify domain contacts in the Sti1 TPR2B - DP2 fragment. Left: Overlay of ^{15}N - HSQC spectra for isolated TPR2B (residues 388 - 526), isolated DP2 (residues (525 - 589) and TPR2B - DP2 (residues 388 - 589). Especially signals corresponding to DP2 are shifted in the spectrum of the two - domain fragment. Right, upper panel: Plot of chemical shift differences observed in the comparison of the NMR spectra shown left. Right, lower panel: Mapping of the chemical shift differences from the plot shown above onto a model of the TPR2B - DP2 fragment generated from the NMR structures obtained in this work for isolated TPR2B and DP2 using Xplor-NIH. Residues from the end of TPR2B helix C, the linker region between TPR2B and DP2 and the DP2 helix α2 show significant shift differences.

TPR2B - DP2 and isolated DP2. These are located at the N - terminal end of helix α1 and mainly in helix α2 of DP2. Additionally, likewise some residues from the C - terminal end of helix C in TPR2B had moderately altered chemical shifts in the two - domain fragment. The fact that not only residues from the unstructured linker region but also within secondary structure elements showed chemical shift changes argues for domain contacts that might potentially be of functional relevance. Overall – despite the spectral differences found – the resonance assignments of the individual TPR2B and DP2 domains could well be transferred onto the spectrum

of the TPR2B - DP2 fragment.

The chemical shifts of protein amides in general are very sensitive to their chemical environment and thus can report on potential molecular interactions. However, chemical shift data can be error - prone in some cases and have to be judged critically. Therefore, further intramolecular PRE NMR experiments were conducted to confirm the results on potential domain contacts between TPR2B and DP2 as obtained from chemical shift analysis. To this end, cysteine residues were introduced at five different positions in DP2 within the TPR2B - DP2 fragment and modified with a spin label. Since the TPR2B domain contains one native cysteine (C453), an additional mutation of this amino acid to serine was carried out prior to the actual mutagenesis to avoid unspecific attachment of the cysteine reactive spin label at this site. The conservative cysteine to serine replacement should not interfere with the overall structure of the TPR2B domain. In the TPR2B - DP2 C453S template then the other residues targeted for modification with the spin label could be replaced by cysteines.

E525, K536, Q545, N559 and N569 were chosen for the mutation, covering different regions in the structure of DP2. All mutants expressed well and were soluble, indicating that the amino acid substitutions did not affect the stability of the TPR2B and DP2 domains significantly. Also a CD spectroscopic characterization showed that the TPR2B - DP2 variants were structured (figure 4.121). Their thermal stabilities were slightly reduced compared to the wild - type TPR2B - DP2 fragment. Nevertheless, all mutants were reasonably stable and appeared to be suited for further experiments. Indeed, none of the HSQC spectra for the ^{15}N - labeled mutants pointed at an unfolded protein (data not shown), confirming the results from the CD measurements. Therefore, a labeling of the cysteine mutants with PROXYL and a detailed analysis of PRE data seemed promising.

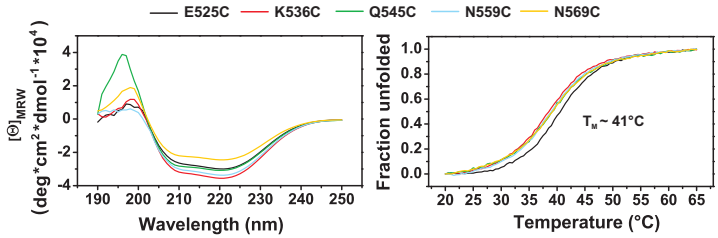

Figure 4.121: CD spectroscopic characterization of Sti1 TPR2B - DP2 cysteine mutants. Left: CD spectra for Sti1 TPR2B - DP2 cysteine mutants in a TPR2B - DP2 C435S background recorded at 20°C. Right: Thermally induced unfolding of TPR2B - DP2 cysteine mutants monitored by CD spectroscopy at a wavelength of 222 nm. The mutants have thermal unfolding midpoints that are slightly lower compared to the wild - type TPR2B - DP2 fragment (compare figure 4.116) but are nevertheless reasonably stable. All proteins were measured in a buffer of 10 mM potassium phosphate, 1 mM TCEP, pH 7.5.

For all TPR2B - DP2 variants pronounced relaxation enhancement effects could be observed, as expected mainly for signals corresponding to DP2 (figure 4.122). However, also for signals outside the DP2 domain line broadening was visible. In particular when the spin label was attached at the C - terminal end of the linker region connecting the TPR2B and DP2 domains (amino acids 519 to 524), as in case of the E525C variant, the C terminal helix C of TPR2B experienced stronger relaxation enhancement (figure 4.123). With the spin label placed N - or C - terminally of the DP2 helix α2 (mutants K536C and Q545C, respectively) likewise PRE effects were observed for the TPR2B helix C and also the TPR2B - DP2 linker region. This indicates a substantial spatial proximity of the two domains in the TPR2B - DP2 fragment. Notably, the data obtained with the K536C and Q545C variants agree well with the previous findings from the chemical shift analysis which also pointed at DP2 helix α2 potentially being involved in domain contacts (compare figure 4.120). With TPR2B

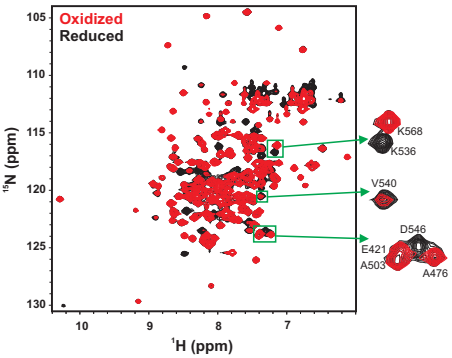

Figure 4.122: ^{15}N - HSQC NMR spectra of PROXYL - modified Sti1 TPR2B - DP2 Q545C before (red) and after (black) addition of ascorbic acid. Many signals of TPR2B - DP2 Q545C show reduced intensities when the PROXYL spin label is attached to the cysteine residue, indicating a spatial proximity to the label. Similar spectra were obtained with the other TPR2B - DP2 mutants E525C, K536C, N559C and N569C. 1 mM of ^{15}N - labeled TPR2B - DP2 Q545C was measured at 293 K and 600 MHz in a buffer of 50 mM potassium phosphate, 50 mM potassium chloride, 1 mM TCEP, pH 7.5. For removing the spin label a 5 - fold molar excess of ascorbic acid was added to the sample and incubated for 1 h.

and DP2 behaving highly dynamic and completely independent from each other in the two - domain fragment, likely no significant PRE effects would have been observable on the TPR2B portion of the protein in these experiments. Therefore, it can be concluded that a certain – probably transient – association of the TPR2B and the DP2 domains seems to occur. This interaction is presumably rather weak but might have functional relevance, as the ITC peptide binding measurements indicated.

Finally, also the ligand binding of the TPR2B - DP2 two - domain fragment was analyzed with NMR. The chemical shift perturbation plots for binding of the Hsp70/Ssa1 C and Hsp90 C fragments to ^{15}N - labeled TPR2B - DP2 showed basically patterns similar as observed with the iso-

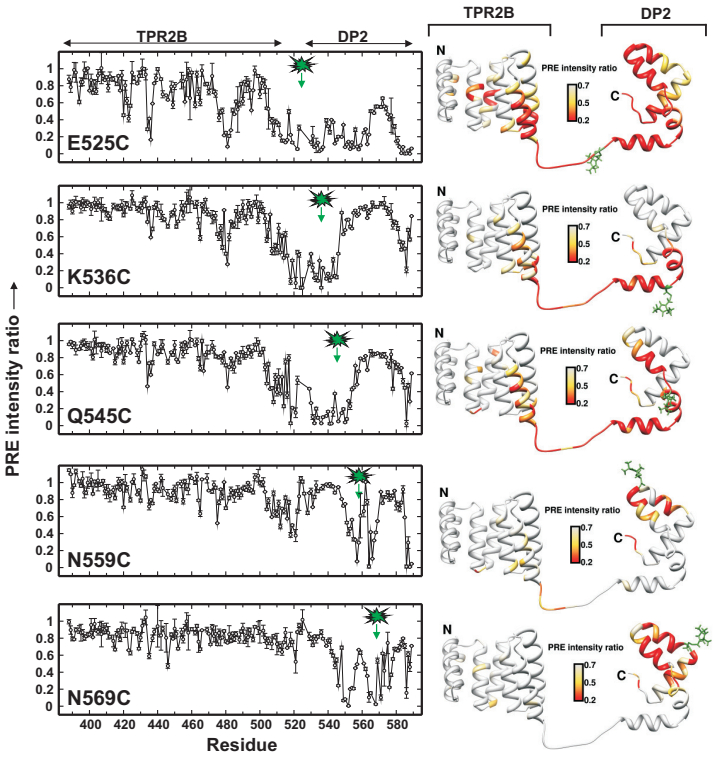

Figure 4.123: Intramolecular PRE experiments to identify domain contacts in the Sti1 TPR2B - DP2 fragment. Left: Plot of PRE intensity ratios for different TPR2B - DP2 variants obtained by comparing peak intensities from the spectra with spin label attached to the protein to peak intensities from the spectra after removal of the label. The position of the spin label is indicated by a green star. Right: Color coded mapping of the PRE effects onto a model of TPR2B - DP2 generated from the NMR structures of the isolated TPR2B and DP2 domains using Xplor - NIH. Spin labels are shown in the structure models in stick representation and colored green. In particular with the spin label attached at one side of DP2 (E525C, K536C and Q545C variants), significant PRE effects are observed on TPR2B, arguing for inter - domain contacts.

lated TPR2B domain (figure 4.124). Therefore, these data indicate that

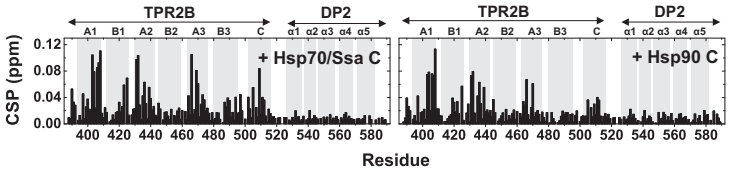

Figure 4.124: Chemical shift perturbation plots for the Sti1 TPR2B - DP2 fragment binding the Hsp70/Ssa1 C (left) and Hsp90 C (right) domains. The chemical shift perturbation patterns for binding of Hsp70/Ssa1 C and Hsp90 C to TPR2B - DP2 are comparable to the binding of the respective fragments to isolated TPR2B (see figure 4.41). The DP2 domain seems to be unaffected by the complex formation in the two - domain fragment. 150 μM of ^{15}N - labeled TPR2B - DP2 was measured at 293 K and 600 MHz in a buffer of 50 mM potassium phosphate, 50 mM potassium chloride, 1 mM TCEP, pH 7.5. Hsp70/Ssa1 C and Hsp90 C were added in a 1:1 molar ratio.

DP2 is not significantly affected by complex formation or contributes to the binding, respectively. However, even a very weak and transient association of DP2 with TPR2B might be sufficient to slightly modify the ligand binding of TPR2B by occupying regions in or near to the TPR peptide binding groove, thus influencing access of ligands to the binding site.

4.18 Discussion

4.18.1 The Role of the TPR Solubility Helix

It was speculated already earlier that the helix 7 (helix C, solubility/capping helix) might contribute to the stability of TPR domains [299,300]. But so far no detailed analysis existed about the influence of this structure element on the properties of these domains. The data on the TPR2BΔh7 mutant obtained in this work now clearly demonstrate the high importance of the solubility helix. As CD spectra showed, the secondary structure of this mutant lacking the solubility helix is not severely affected by the deletion. However, it has a thermal melting point of only ~21°C, which is by more than 20°C lower than the melting point of the wild-type protein. Although also the helices A1 to B3 forming the TPR motives contain many charged residues pointing to the solvent exposed surface, the solubility of the TPR2BΔh7 mutant is nevertheless not high enough to provide reasonable stability even at moderate physiological temperatures. Therefore, the solubility helix of the TPR domains appears to be essential for appropriate thermal stability of the proteins.

A lack of the solubility helix obviously gives rise to increased oligomerization of the TPR2BΔh7 mutant *in vivo* and *in vitro*, resulting in inclusion body formation when expressed in *E. coli* and strong aggregation tendency of the purified protein. In a recent report it was shown that the trimerization of a TPR domain was accompanied by the displacement of the C-terminal solubility helix [301]. The oligomerization interface was formed by the B3 helices which normally the solubility helix packs against. Thus, a deletion of helix 7 should enhance oligomerization as it was indeed observed here for the TPR2BΔh7 mutant. It seems that helix 7 serves as a kind of “intrinsic oligomerization inhibitor” or “intrin-

sic chaperone element". This might explain its widespread occurrence in TPR domain proteins although it does not contain residues directly involved in ligand binding functions and could therefore be assumed to be dispensable. In fact, nearly all structures of TPR domains solved so far comprise a solubility helix.

Interestingly, the solubility helix might at least for Sti1 TPR2B also contribute to the peptide binding. The ITC experiments carried out here with the TPR2BΔh7 mutant show that, compared to the wild-type protein, the peptide binding affinity is significantly reduced upon a deletion of helix 7. From the crystal structures available so far for human Hop TPR1 and TPR2A[68] it is evident that all residues of the TPR domain contacting the peptide ligand are provided by the helices A1 to B3. The solubility helix does not seem to play a role for direct interactions with the ligand. But possibly, a deletion of the solubility helix results in a slightly altered conformation of the remaining helices so that residues essential for ligand binding are not properly oriented anymore for this function. Alternatively, the increased oligomerization tendency of the deletion mutant could also render the peptide binding groove of the TPR domain partially inaccessible for the ligand. Thus, overall the solubility helix seems to have an essential role not only for the stability of TPR domains but furthermore even for their specific ligand binding.

4.18.2 Peptide Binding Selectivities of Sti1 TPR Domains

The function of Sti1/Hop as adapter protein bridging Hsp70 and Hsp90 is connected to the peptide binding properties of its TPR domains. The selectivity and binding affinity of each TPR domain in the protein is crucial for a proper organization of ternary chaperone complexes with Hsp70 and Hsp90. Therefore, a detailed analysis of the peptide binding behavior of all three TPR domains from yeast Sti1 was carried out here.

The TPR1 domain of Sti1 turned out to be clearly selective for binding the Hsp70 peptide with ~ ninefold higher affinity for the Hsp70 octapeptide than for the Hsp90 octapeptide. This is in line with studies using the TPR1 domain from human Hop[68]. The position -4 of the Hsp70 ligand seems to be of special importance for the interaction with TPR1. The additional valine residue in the VEEVD peptide leads to a significant gain in binding strength compared to the consensus peptide EEVD. The maximum binding and highest selectivity of TPR1 is obtained with the octameric peptide, however, the gain in binding affinity with the octameric ligand is rather small compared to the initial drop in the K_d from the consensus to the pentapeptide. These observations suggest contacts of the TPR1 domain to the ligand side-chain at position -4 and a major contribution of a hydrophobic interaction to the binding.

TPR2A shows similar to TPR1 a high degree of ligand discrimination, but here the preferred ligand is the Hsp90 peptide. The selectivity is even more pronounced, the affinity for the Hsp90 ocatpeptide is more than hundredfold higher compared to the Hsp70 peptide of the same length. As for TPR1, the position -4 residue of the ligand gives the most important contribution to the binding affinity. The ligand selectivity of TPR2A increases stepwise with the length of the peptides and – like TPR1 – this domain shows the maximum binding for the octapeptide. The affinity

of TPR2A for its preferred ligand is markedly higher than that of TPR1 (K_d 0.3 μM versus 1.4 μM). TPR2A from human Hop was found to have the same ligand selectivity but interestingly, in this case it was a pentapeptide that gave the maximum binding [68]. This might possibly reflect some species - specific differences in the function of the TPR2A domains. As an alignment shows, residues forming the two - carboxylate clamp and residues involved in binding the peptide consensus motive EEVD are highly conserved between yeast Sti1 and human Hop (figure 4.125). However, the differences in the peptide binding properties of the

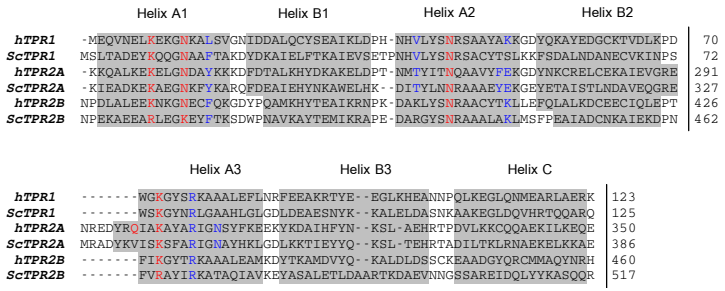

Figure 4.125: Alignment of TPR1, TPR2A and TPR2B domains from human (h) Hop and yeast (*Saccharomyces cerevisiae*, Sc) Sti1. Conserved residues forming the two - carboxylate clamp are marked in red, additional conserved residues involved in binding the EEVD consensus peptide motive are marked in blue. The position of the helices forming the TPR motives is highlighted in gray. NCBI reference codes of the sequences used for the alignment are NP_006810.1 for human Hop and NP_014670.1 for yeast Sti1. The alignment was generated using the program MUSCLE [265]. Sequence position numbers are given on the right. Residues from the two - carboxylate clamp are highly conserved between all Sti1/Hop TPR domains, additional residues contributing to the binding of the EEVD motive seem to be less conserved.

TPR2A domains for yeast Sti1 and human Hop might be due to a binding of the ligand in slightly different conformations. Usually the peptides

are bound to the TPR domains in an extended conformation, allowing for a higher degree of freedom in the backbone and side-chain torsion angles. Furthermore, the Hsp90 peptide sequences upstream/N-terminal of the MEEVD motive which both human and yeast Hsp90 have in common are significantly different (human Hsp90 octapeptide: TSRMEEVD, yeast Hsp90 octapeptide: DTEMEEVD). This suggests that these regions of the human and the yeast peptide would be contacted in a rather different manner in TPR domain-ligand interactions.

Surprisingly, also for the Sti1 TPR2B domain a significant peptide binding could be measured. This observation disagrees with studies on the human Hop TPR2B domain for which binding affinities on the order of 130 and 290 μM were reported with Hsp70 and Hsp90 octapeptides, respectively[184]. Obviously, there are species-specific differences in the function of the TPR2B domain. TPR2B of Sti1 has very unusual peptide binding properties compared to TPR1 and TPR2A. In contrast to the latter, TPR2B shows nearly identical affinities for Hsp70 and Hsp90 peptides. This finding supports the somehow confusing studies that implicated TPR2B in binding of either Hsp70 or Hsp90[147,185,187].

The basal peptide binding of the EEVD consensus motive by TPR2B is slightly higher than for TPR1 and TPR2A. This might be due to the fact that the key residues of TPR2B predicted to contact the EEVD residues are different: Instead of the two-carboxylate clamp residues K and N in the helix A1 of TPR1 and TPR2A, TPR2B has R and K, respectively, at these positions. In helix A3 of TPR2B R instead of K can be found (figure 4.125). On the other hand, increasing length of the peptides results only in a very modest gain of binding affinity for both, Hsp70 and Hsp90 peptides, different to TPR1 and TPR2A. Unlike TPR1 and TPR2A, TPR2B shows the maximum binding affinity already on the heptapeptides. The low selectivity in the binding of Hsp70 and Hsp90 peptides and the small increase

in binding affinity with increasing ligand length beyond the consensus motive EEVD indicates a predominant involvement of contacts only to the ligand backbone in the interaction with TPR2B. Thus, although the structures of all three TPR domains in Sti1 are likely quite similar, their peptide binding properties are very different. For TPR1 and TPR2A a ligand discrimination is achieved mainly by specific contacts to side - chain residues at position - 4 and - 7 of the peptide additional to backbone contacts. TPR2B, in contrast, seems to recognize mainly the backbone of the residues beyond the EEVD consensus motive in the peptides and therefore shows no preferred binding of either Hsp70 or Hsp90 peptides.

Overall, Sti1 has a selective high affinity Hsp90 binding site in TPR2A, a selective Hsp70 binding site in TPR1 with an intermediate affinity and a third unselective potential binding site for both Hsp70 and Hsp90 with lower affinity compared to TPR1 and TPR2A. With respect to the function of Sti1 in organizing Hsp70/Hsp90 complexes it might be important to have Hsp90 bound only at a well defined position in the molecule, which requires a binding site with high selectivity as it is the case for TPR2A. The rather high Hsp90 peptide binding affinity of TPR2A compared to the two other TPR domains of Sti1 could – together with the typically high abundance of Hsp90 in cells – serve to ensure that Sti1 preferentially binds Hsp90 in the first place. This might constitute the first crucial step in the organization of Hsp70/Hsp90 chaperone complexes by Sti1. Afterwards, Hsp70 could be recruited by the Hsp70 specific binding sites with lower affinities in TPR1 and potentially in TPR2B. The different selectivities and affinities of the TPR domains might thus be essential for an ordered arrangement of Sti1/Hsp70/Hsp90 ternary complexes which might be required for processes like the postulated substrate transfer from Hsp70 to Hsp90 [162].

Potentially, the lower affinity of TPR1 for its preferred ligand compared

to TPR2A (K_d TPR1 for Hsp70 ocatpeptide: 1.4 μM, K_d TPR2A for Hsp90 ocatpeptide: 0.3 μM) is compensated by the existence of a second Hsp70 binding site in TPR2B. TPR1 could serve as a selective Hsp70 binding site to enrich Hsp70 which then could also be transferred onto TPR2B under certain conditions. The difference in affinities for the Hsp70 peptide between TPR1 and TPR2B is rather small (K_d TPR1 for Hsp70 ocatpeptide: 1.4 μM, K_d TPR2B for Hsp70 ocatpeptide: 4.2 μM), which would in principle allow for such a transfer.

On the other hand, it seems likely that the TPR2B peptide binding groove could also be occupied by Hsp90. As Hsp90 is a dimer, the peptide end of one Hsp90 subunit could bind to TPR2A of a Sti1 molecule and the peptide end of the second Hsp90 subunit could bind to TPR2B. In that way, TPR2B could support binding of Hsp90 to Sti1 in a first step. Indeed, biochemical data with pull down assays implicated TPR2B in binding of Hsp90 previously: A stable interaction of Sti1 with Hsp90 was only found, when TPR2A was combined with the TPR2B domain [147]. As the affinity of TPR2B for Hsp70 and Hsp90 peptide ends is on the same order, Hsp70 could also displace Hsp90 again from the TPR2B peptide binding groove later on under certain conditions. Thus, TPRR2B would serve as a kind of flexible docking site for both chaperones.

4.18.3 TPR2B Structure Determination

Using sparse NOE data, chemical shift analysis and RDCs, a low resolution NMR structure for the Sti1 TPR2B domain was obtained in this work. A chemical shift evaluation prior to the structure determination already indicated a typical TPR domain fold for TPR2B with three TPR motives composed of two antiparallel helices and a terminal solubility helix. This was confirmed during the structure determination.

A comparison of the NMR structure with a homology model that was built only based on sequence similarity showed some significant differences between the structures in a more detailed view as for example the length of individual helices. RDCs as a quality indicator demonstrated that – despite its rather low resolution – the experimental structure was still significantly more reliable than the model. Nevertheless, also the model was not extremely far off and correctly predicted the typical TPR domain structure. This is due to the in general high overall conservation of the TPR fold and the comparatively precise predictability of helical secondary structure.

The NMR structure of TPR2B is very similar to the structures of the TPR1 and TPR2A domains from human Hop (figure 4.126). The helices A1 to A3 of the TPR motives overlay very well for Sti1 TPR2B and the Hop TPR domains. However, the helix B3 in TPR2B is significantly longer compared to the other structures by about one helix turn and its orientation is slightly different. The loop connecting the C-terminal solubility helix C to the helix B3 is also longer by about two residues.

Larger differences between the structures can be observed in the orientation of the respective solubility helix C. For TPR2B, the tilt angle of helix C is smaller compared to TPR1 and TPR2A from Hop. As a consequence, the peptide binding groove of TPR2B is more narrow. One the one hand,

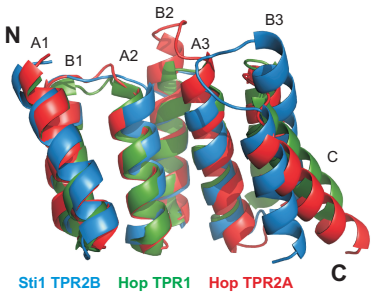

Figure 4.126: Overlay of the yeast Sti1 TPR2B domain with the human Hop TPR1 (PDB: 1ELW) and TPR2A (PDB: 1ELR) domains. All three domains have very similar folds. The helices A1 to A3 of the TPR motives overlay very well. However, in Sti1 TPR2B the helix B3 is longer compared to the two other domains. Larger differences between the structures can also be observed in the orientation of the helix B3 and especially the solubility helix C. The N - and C - terminal ends and the helices of the TPR motives are indicated.

this can be due to the rather small number of long range NOE contacts that could be found for TPR2B. This leads to difficulties in clearly defining the relative orientation of the helix. On the other hand, the position of this structure element might in general be less conserved between different TPR domains and to a certain extent variable. Even comparing the TPR domains from only Hop itself, different arrangement of the solubility helix can be observed in TPR1 and TPR2A, whereas in contrast the respective TPR motives nearly perfectly overlay. This might be a consequence of the fact that the helices A1 to B3 of the TPR motives provide the highly conserved residues that mediate the binding of the peptide ligand. Thus, it is likely important that these helices adopt a strictly defined relative orientation to each other to ensure an alignment of the peptide binding resides in a way that supports optimal ligand interactions. The solubility helix, in contrast, does not contribute at all or only partially to the

ligand binding, allowing for a higher flexibility in its orientation without affecting the biological function of the TPR domain.

Another aspect that could explain the different orientation of the helix C observed for TPR2B is that the comparison structures TPR1 and TPR2A from Hop were solved with ligand bound. TPR2B in this work, in contrast, was determined in a peptide free state. As helices in general can easily shift against each other, conformational changes upon ligand binding also seem possible.

4.18.4 Peptide Binding Properties of the Sti1 TPR2A and TPR2B Domains in Solution

NMR is a well suited method to study the weak to intermediate affinity interactions as observed between the Hsp70/Hsp90 peptide ligands and the Sti1 TPR domains. The NMR binding data obtained on the TPR2A and TPR2B domains with Hsp70 and Hsp90 peptides agree well with the affinity data from the ITC experiments. For TPR2A, the chemical shift perturbation data indicate only a basal binding of the Hsp70 peptide involving conserved residues from the two - carboxylate clamp and few additional residues mediating contacts to the consensus residues EEVD of the peptide. Overall, the shifts observed in the NMR spectrum of TPR2A upon adding the Hsp70 peptide were small. In contrast to that, when the Hsp90 peptide was bound to TPR2A, larger shifts were observed and additionally several side - chain resonances together with some backbone resonances showed line broadening, indicating intermediate timescale exchange. This points at a tighter interaction between the Hsp90 peptide and TPR2A compared to the Hsp70 peptide. The CSP data show that in general the peptide binding of the Sti1 TPR2A domain is mainly mediated by residues from the helices A1, A2 and A3. This is consistent with findings for the TPR2A domain from human Hop [68].

For the binding of both Hsp70 and Hsp90 peptides to the TPR2B domain, only shifts were observed but no line broadening as it was the case for the binding between TPR2A and its preferred ligand, the Hsp90 peptide. This is consistent with the fact that the maximum affinity of TPR2B for peptides is only around 4 μM whereas the maximum affinity of TPR2A for the Hsp90 peptide is $\sim$ tenfold higher (0.3 μM, tables 4.6 and 4.7). Although the ITC data showed that TPR2B can bind both Hsp70 and Hsp90 peptides with nearly identical affinity, the Hsp70 peptide caused larger

shifts upon binding to TPR2B compared to the Hsp90 peptide. Furthermore, with the Hsp70 peptide also regions within helix B3 and C of TPR2B showed chemical shift perturbation which was not the case for the Hsp90 peptide. This points at different binding modes for the Hsp70 and Hsp90 peptides and confirms the results from the ITC measurements.

The entropy contribution obtained with ITC for binding of the Hsp70 hepta and octapeptides to TPR2B is significantly less favorable compared to the binding of the respective Hsp90 peptides. However, this is compensated by a more favorable enthalpy term in case of the Hsp70 peptides (table 4.7). Considering both the NMR data and the findings from the ITC experiments it seems possible that in order to accommodate the Hsp70 peptide, TPR2B has to undergo some additional conformational changes involving helices B3 and C that are not required for binding the Hsp90 ligand. On the one hand, these structural rearrangements would lead to an unfavorable entropy loss but on the other hand would concomitantly enable new binding interactions which positively influence the binding enthalpy. This would explain the results from the NMR and ITC experiments. Alternatively, also the Hsp70 ligand might potentially have to undergo structural changes in order to bind to TPR2B or even both, protein and ligand.

In either case, the mode of binding of the Hsp70 peptide to TPR2B seems to be special, in particular when compared to the binding of the Hsp90 peptide to TPR2B but also in general: The findings for the interaction between TPR2B and the Hsp70 peptide are likewise unusual when compared to the binding of peptides to the other TPR domains from Sti1 or from Hop. In contrast to TPR2B, for none of these TPR domains the helix C seems to play an important role for the peptide binding. The essential function of the helix C for proper ligand binding is also reflected by the ITC measurements performed in this work using the TPR2BΔh7

mutant: These demonstrated that a deletion of this structure element significantly impairs peptide binding of the TPR2B domain.

The NMR peptide binding experiments with the two - domain construct TPR2A - TPR2B finally show that both TPR subdomains in this fragment behave independently with respect to their peptide binding properties. The chemical shift perturbation patterns within the TPR2A and TPR2B portion of the protein upon adding Hsp70 and Hsp90 peptides were comparable to those of the isolated domains. Therefore, the peptide binding grooves of TPR2A and TPR2B can occupied with different ligands at the same time in the TPR2A - TPR2B fragment. This is a prerequisite to allow for a simultaneous binding of both chaperones, Hsp70 and Hsp90, to arrange the heterocomplexes required for the activation of client proteins like the steroid hormone receptors.

4.18.5 Influence of Sti1 on the Hsp90 ATPase Activity

The results of the ATPase assays demonstrate the importance of the peptide binding by Sti1 TPR domains for proper Hsp90 inhibition. A deletion of the Hsp90 C - terminal peptide motive recognized by the TPR domains significantly reduced the ATPase inhibition of Hsp90 by Sti1. The apparent K_d - values obtained from ATPase inhibition curves for the interaction between Sti1 and wild - type Hsp90 or its deletion mutant differ by a factor of > 50 (0.33 μM versus 17.28 μM). This shows that Hsp90 - Sti1 complex formation is largely mediated through a recognition of the Hsp90 C - terminal peptide motive by the TPR domains. However, the fact that also for the Hsp90 deletion mutant an inhibition could be observed although in this case no TPR - peptide interaction was possible clearly indicates that additional contacts between Sti1 and Hsp90 exist, independent from TPR peptide binding. These contacts are likely essential for the function of Sti1 because a mere TPR - Hsp90 peptide interaction could not explain the inhibitory effect of Sti1 on the Hsp90 ATPase activity.

The Hsp90 peptide motive bound by the TPR domains is located at the end of a ~ 30 residues long stretch of unfolded amino acids. As shown, a complete deletion of these residues has no effect on the ATP hydrolysis of Hsp90 (section 3.8) and likewise a Sti1 - Hsp90 interaction involving only these residues would not have any effect on ATP hydrolysis. Sti1 was found to be a non - competitive inhibitor of Hsp90 which does not alter the binding of nucleotide to Hsp90 [167]. Therefore, more likely Sti1 could act by influencing the conformational changes within Hsp90 that were shown to be essential for its ATP hydrolysis [52,55,167]. This would require Sti1 to additionally bind to the folded part of Hsp90, which is supported by the results from the ATPase measurements carried out here.

The data from the Hsp90 ATPase inhibition measurements with the Sti1

TPR2A - TPR2B fragment containing the N435A mutation indicate a possible role of TPR2B for proper Hsp90 inhibition. The N435A mutation is located in the TPR2B domain and renders TPR2B unable to bind peptide (section 4.5). Dr. Andreas Schmid (Lehrstuhl für Biotechnologie, TUM) could show in previous work that a wild - type Sti1 TPR2A - TPR2B fragment inhibits Hsp90 similar to full - length Sti1. The TPR2A - TPR2B N435A mutant tested in this work now had a reduced ability to inhibit Hsp90. The apparent K_d - value derived from the ATPase inhibition curve was about three times higher compared to the wild - type TPR2A - TPR2B fragment (1.3 μM versus 0.4 μM).

Considering the fact that the TPR2A domain has a much higher affinity for binding the Hsp90 C - terminal peptide motive than TPR2B (K_d 0.3 μM versus 4.3 μM, section 4.3) and furthermore that rather high salt concentrations were used in the assay additionally weakening the interaction between TPR2B and Hsp90, the function of TPR2B as an Hsp90 peptide binding site appears to be of biological relevance. ITC and NMR data also support the possibility of TPR2B as a potential Hsp90 binding site (section 4.3 and 4.4.5). Although the influence of the TPR2B mutation on the Hsp90 ATPase inhibition by the TPR2A - TPR2B fragment seems to be small, it might nevertheless significantly affect *in vivo* processes like the client maturation by Hsp90 because ATP turnover of Hsp90 has to be fine - tuned very precisely for its proper biological function.

4.18.6 Peptide Independent Binding Contacts of Sti1 with Hsp70 and Hsp90

The functional ATPase assays measuring the inhibition of Hsp90 by Sti1 demonstrated that even without the C-terminal peptide motive present in Hsp90, Sti1 is still able to decrease the ATP hydrolysis of the chaperone (section 4.6). This strongly suggests additional binding contacts between Sti1 and the folded parts of Hsp90. A mere interaction of Sti1 TPR domains with the peptide motive located at the end of the $\sim$30 residues long stretch of unfolded amino acids in the Hsp90 C-terminal domain could not explain the inhibitory effect of Sti1 on the Hsp90 ATPase activity.

As ITC binding data using Sti1 fragments and full-length Hsp90 or its C-terminal domain instead of peptides show, there is indeed a contribution to the interaction with Sti1 from parts of Hsp90 outside the region containing the peptide motive. Interestingly, these parts are obviously not within the C-terminal domain of Hsp90 which provides the peptide motive because TPR2A, TPR2B and the TPR2A-TPR2B fragment bound the Hsp90 peptide and its full C-terminal domain with comparable affinities. However, the respective Sti1 proteins bound full-length Hsp90 with significantly higher affinity than the peptide. Especially the two-domain fragment TPR2A-TPR2B showed a binding which was so strong that no reliable K_d could be determined using ITC. Potentially, the peptide independent binding contacts of TPR2A and TPR2B synergistically contribute to the complex formation between TPR2A-TPR2B and Hsp90 to give such a high affinity.

The additional binding site on Hsp90 might be provided either by its N or M domain. As mentioned, the Hsp90 C-terminal domain contains a stretch of approximately 30 unfolded residues at its C-terminus with the

TPR peptide motive as the last eight residues. These 30 residues would in principle be sufficient to span a distance long enough to allow for a binding of TPR2A - TPR2B to the Hsp90 M domain while at the same time the C - terminal peptide motive is bound to TPR2A or TPR2B.

An interesting observation regards the binding stoichiometries of the complexes analyzed. TPR2A - TPR2B bound the Hsp90 C - terminal domain with a 1:2 ratio and as expected, mutation of the TPR2B peptide binding site in the TPR2A - TPR2B N435A variant led to a binding of the Hsp90 C - terminal domain with a 1:1 stoichiometry. This result again shows that TPR2B can function as a potential Hsp90 peptide binding site. However, in contrast to that, TPR2A - TPR2B bound the full - length Hsp90 with a 1:1 stoichiometry even with the TPR2B peptide binding site being functional. This implies that in the complex formed one of the two peptide binding sites in TPR2A - TPR2B is likely not occupied with ligand, which would presumably be that of TPR2B as it has a lower affinity for binding the Hsp90 peptide. The difference in the stoichiometries raises the question whether the complex observed between TPR2A - TPR2B and the isolated Hsp90 C - terminal domain is physiologically relevant. From the stoichiometry of 1:1 for full - length Hsp90 binding TPR2A - TPR2B, it could be assumed that the TPR2B peptide binding function is unimportant for complex formation with Hsp90. However, this seems to be wrong because the N435A carboxylate - clamp mutation of TPR2B had indeed influence on the affinity of the interaction and weakened the complex. This is in agreement with the ATPase data that demonstrated a reduced inhibition of Hsp90 by the TPR2A - TPR2B N435A variant.

Thus, overall the findings from the ITC experiments again indicate that a ligand binding competent TPR2B domain is important for proper biological activity of Sti1. TPR2B might possibly serve to generally enhance the affinity between TPR2A - TPR2B and Hsp90. It could provide addi-

tional electrostatic interactions with one of the two peptide motives from the Hsp90 dimer in a first encounter complex besides the high affinity binding of the other peptide motive by TPR2A. Afterwards, the functional complex could be formed by orienting TPR2A - TPR2B on Hsp90 in a way that allows for inhibition of Hsp90. This would require an unfavorable dissociation of the peptide from TPR2B but this might however be compensated by the additional peptide independent binding interactions in the final complex.

ITC binding data also indicate peptide independent interactions between Sti1 and Hsp70/Ssa1 fragments. Similar as in case of Hsp90, Sti1 was reported to influence the ATPase activity of Hsp70/Ssa1 [164], which supports the assumption of further contacts between Hsp70 and Sti1 besides the peptide based recognition. As for Hsp90, again the Sti1 TPR2A - TPR2B fragment seems to be important for providing interaction sites for binding Hsp70/Ssa1 domains. The Hsp70/Ssa1 C - terminal domain bound significantly better to TPR2A - TPR2B than the Hsp70/Ssa1 peptide, which shows that the interaction of Sti1 with Hsp70/Ssa1 cannot be fully described by mere peptide - TPR domain contacts. The stoichiometry was found to be close to 1:2. This is surprising given the fact that isolated TPR2A displayed only a very weak binding of the Hsp70/Ssa1 peptide in the previous ITC experiments ($K_d \sim 37\,\mu M$) whereas TPR2B was clearly able to bind the peptide with reasonable affinity ($K_d \sim 4\,\mu M$). Thus, the stoichiometry would be expected to be rather around 1 reflecting a dominating binding contribution of the TPR2B domain as it was indeed observed for binding of the Hsp70/Ssa1 peptide to TPR2A - TPR2B. A possible explanation could be the oligomeric status of Hsp70/Ssa1. For the C - terminal domain of human Hsp70 a tendency to form dimers was reported [280] which might possibly also apply for yeast Ssa1.

The Hsp70/Ssa1 middle/substrate binding domain might further con-

tribute to the binding of Sti1 as ITC and also SPR experiments showed. Full-length Sti1 bound the Hsp70/Ssa1 MC fragment better than the Hsp70/Ssa1 C domain alone. It seems possible that these peptide independent interactions between Sti1 and the Hsp70/Ssa1 M and C domain could be responsible for the ATPase stimulating effect of Sti1 [164]. As it was found that the binding of substrate peptides to the Hsp70 M domain stimulates the ATPase activity [302], in particular the interaction of Sti1 with Hsp70/Ssa1 M might increase the ATP turnover via an allosteric mechanism. However, it can not be ruled out that Sti1 also directly contacts the Hsp70/Ssa1 ATPase domain since the full-length Hsp70/Ssa1 could not be expressed in *E. coli* and therefore no binding measurements were performed with the full protein.

Interestingly, TPR2A-TPR2B bound Hsp70/Ssa1 MC slightly (~ twofold) better than TPR1, although TPR1 was found to have the highest affinity for binding the Hsp70/Ssa1 peptide comparing the three TRR domains in Sti1. Therefore, it seems possible that Hsp70/Ssa1 initially bound to TPR1 could be transferred onto TPR2A-TPR2B. TPR1 might serve as additional Hsp70/Ssa1 binding site to enrich the client loaded Hsp70/Ssa1 which is then passed on to TPR2A-TPR2B to allow for the client transfer from Hsp70 onto Hsp90. This might explain the existence of two Hsp70/Ssa1 binding sites in Sti1.

Similar as for Hsp90, the TPR2A-TPR2B fragment of Sti1 seems to play a key role for the interaction with Hsp70/Ssa1. The ITC data indicate that neither TPR1 nor other parts of Sti1 outside TPR2A-TPR2B like the DP domains are involved in peptide independent binding contacts. Therefore, in general TPR2A-TPR2B appears to be the central element for binding and furthermore regulating Hsp70 and Hsp90. TPR2A-TPR2B comprises the TPR modules capable of binding both chaperones and provides additional peptide independent binding sites that are impor-

tant for regulating the ATPase activities of Hsp70 and Hsp90. Its essential importance is also reflected by the fact that the TPR2A - TPR2B unit is highly conserved in different organisms while in contrast the TPR1 or DP1 domains are absent in some Sti1/Hop proteins from organisms like *Caenorhabditis elegans*.

As the ITC measurements demonstrate, the affinity of Sti1 TPR2A - TPR2B for Hsp90 seems to be markedly higher than for Hsp70/Ssa1. This is in agreement with a previous report that likewise found full - length Sti1 binding Hsp90 better than Hsp70/Ssa1 [164]. A weaker interaction with Hsp70/Ssa1 might be required to enable a faster exchange of Hsp70/Ssa1 in the ternary complex with Sti1 and Hsp90. Thus, Hsp70/Ssa1 could function to deliver partially folded substrate proteins to a preformed and longer - lived complex of Sti1 and Hsp90.

4.18.7 Ternary Complexes Between Sti1, Hsp70 and Hsp90

The results from analytical ultracentrifugation experiments with Sti1 or fragments thereof and the full-length Hsp70/Ssa1 and Hsp90 proteins are well in agreement with ITC data obtained in this work. As expected, full-length Sti1 supported the formation of ternary complexes between Sti1, Hsp70/Ssa1 and Hsp90. The ITC binding experiments with isolated Sti1 TPR domains suggested that TPR1 functions as selective Hsp70/Ssa1 and TPR2A as selective Hsp90 binding site (section 4.3). Consequently, the TPR1 and TPR2A domains of Sti1 would in general be sufficient to mediate a ternary Sti1-chaperone complex. However, TPR2B was found to recognize both the Hsp70/Ssa1 and the Hsp90 peptide with reasonable affinity (section 4.3) and therefore also the TPR2A-TPR2B fragment might in principle serve to arrange a ternary complex with Hsp70/Ssa1 and Hsp90.

As the previous experiments showed, a mutation of the TPR2B peptide binding site reduced the binding of the TPR2A-TPR2B fragment to Hsp90 (section 4.7) and functional ATPase assays further demonstrated that TPR2B might play a role for proper inhibition of Hsp90 (section 4.6). Thus, on the one hand TPR2B obviously seems to be required for binding and regulation of Hsp90. On the other hand, in the ITC experiments the binding of the TPR2A-TPR2B fragment to Hsp90 was found to have a stoichiometry of 1:1, suggesting that in the complex between the two proteins the peptide binding site of TPR2B should be unoccupied and hence available for interaction with Hsp70/Ssa1 (section 4.7). This would be an important prerequisite for the specific and stable formation of a ternary complex between TPR2A-TPR2B, Hsp70/Ssa1 and Hsp90. The ultracentrifugation data confirmed these assumptions. Wild-type TPR2A-TPR2B formed the ternary complex with Hsp70/Ssa1 and Hsp90 whereas a mu-

tant thereof rendering TPR2B unable to bind peptide did not. In general, TPR2A - TPR2B appears to be a central platform within Sti1 as it on the one hand provides a simple binding of Hsp70/Ssa1 and Hsp90 and on the other hand also seems to serve in their functional regulation.

4.18.8 The Role of the Linker Between the Sti1 TPR2A and TPR2B Domain

NMR chemical shift data demonstrated that in the Sti1 TPR2A - TPR2B fragment both TPR2A and TPR2B are structurally identical when compared to their isolated form with nearly no physical contacts between each other except for the regions connecting both domains (section 4.4.1). However, within TPR2B the residue R425 was identified to be potentially involved in domain contacts between TPR2A and TPR2B in the two - domain fragment comprising both domains. As a sequence alignment shows, this arginine residue seems to be conserved in different organisms (figure 4.127). Therefore, it might be of general importance

```
C. elegans          …YNEAVKRDPENAI… | 175
D. melanogaster     …YTEAIKRNPDDPK… | 344
H. sapiens          …YTEAIKRNPKDAK… | 395
S. cerevisiae       …YTEMIKRAPEDAR… | 431
                      *.* :** *.:.
```

Figure 4.127: Comparison of an amino acid stretch from the yeast Sti1 TPR2B domain containing the linker residue with corresponding sequences from other organisms. The linker residue (R425 of the yeast *Saccharomyces cerevisiae* TPR2B domain) seems to be highly conserved in different organisms. NCBI reference codes of the sequences used for the alignment are NP_503322.1 for *Caenorhabditis elegans* Hop, NP_477354.1 for *Drosophila melanogaster* Hop, NP_006810.1 for *Homo sapiens* Hop and NP_014670.1 for *Saccharomyces cerevisiae* Sti1. The alignment was generated using T-Coffee [194].

for the function of Sti1/Hop proteins. Indeed, a mutation of this amino acid to alanine had effects on the binding and inhibition of Hsp90 by TPR2A - TPR2B. These were not due to an altered structure of the mutant because a CD spectroscopic characterization demonstrated that the secondary structure content and the stability of the protein were com-

parable to the wild - type. As ITC measurements showed, the mutant has a reduced binding to Hsp90. This is unexpected since the mutated amino acid R425 within helix B1 of TPR2B is not involved in binding of the peptide ligand but points to the convex backside of TPR2B. A mutation of this solvent exposed residue should not have influence on the peptide mediated binding between Hsp90 and TPR2A - TPR2B. Thus, the amino acid exchange likely had impacted peptide independent binding contacts. However, it is probably not a simple disruption of these binding contacts because the exchange of only a single residue would not be expected to have such significant influence on the binding affinity as observed here. Rather, the mutation might have changed a larger binding interface within TPR2A - TPR2B. As the previous ITC data indicated (section 4.7), it seems possible that TPR2A and TPR2B form a joint peptide independent binding site for Hsp90 in the TPR2A - TPR2B fragment. To this end, it could be important that TPR2A and TPR2B have a defined orientation relative to each other to provide this binding site. The mutation of the linker residue potentially caused an increased flexibility between the TPR2A and TPR2B domains or changed their orientation relative to each other.

The inhibition of Hsp90 in the ATPase was also impaired with the TPR2A - TPR2B R425A variant. This is on the one hand due to the lower binding affinity of the mutant compared to the wild - type protein. In agreement with the ITC data, the apparent K_d - value obtained from fitting the ATPase inhibition curve was higher compared to wild - type TPR2A - TPR2B. On the other hand, the ATPase data also indicate a mechanistic difference between the linker mutant and wild - type TPR2A - TPR2B: the maximum inhibition of Hsp90 that could be obtained with the mutant was lower than for wild - type TPR2A - TPR2B. If only the binding affinity of the mutant was reduced, then the same maximum level of Hsp90 inhibi-

tion would be expected for both proteins, which was not the case, the mutant reduced the Hsp90 ATPase function to a lower extent than wild - type TPR2A - TPR2B. This supports the assumption that the linker mutation had not directly influenced the binding affinity between TPR2A - TPR2B and Hsp90 by changing a residue that is within a binding site. Rather, it might have weakened the interaction by causing secondary conformational changes.

4.18.9 *In Vivo* Function of Sti1 TPR Domain Mutants

It was shown previously that the activity of human GR expressed heterologously in yeast cells is strongly dependent on the function of Sti1 [146]. Therefore, this system is well suited to analyze potential *in vivo* effects of Sti1 mutations and was used to further assess the role of the TPR2B domain. As the GR activity assays with yeast cells now demonstrate, the ability of the TPR2B domain to bind peptide is an essential requirement for the cellular functions of Sti1. Sti1 lacking the TPR1 domain and containing mutations that eliminate peptide binding to TPR2B turned out to completely fail in supporting the activation of the GR. This might most likely be due to the lost binding of Hsp70/Ssa1 because TPR2B serves as a potential Hsp70/Ssa1 interaction site, as the previous ITC data demonstrated (section 4.3). However, also an impaired regulation of Hsp90 might additionally contribute to the observed *in vivo* defects of the Sti1 mutants since TPR2B mutations also moderately affect the ATPase inhibition of Hsp90 by Sti1 (section 4.6).

Most surprisingly, even with a functional TPR1 domain present in Sti1 that could serve as an alternative Hsp70/Ssa1 binding site (section 4.3) Sti1 mutants with a peptide binding deficient TPR2B domain were unable to activate the GR. Thus, TPR1 can obviously not compensate for a lost peptide binding of TPR2B. This is somewhat in contrast to a previous report which likewise found a significant reduction of GR activity in yeast cells when the TPR2B peptide binding site was mutated. However, in this case still remaining GR activity was observed at a level clearly above the control [187]. Despite these discrepancies, the data clearly show that the ability of TPR2B to bind peptide is important for the *in vivo* functions of Sti1.

Considering the previous results from the analytical ultracentrifuga-

tion experiments, it seems possible that the defects of the Sti1 TPR2B mutants in supporting GR activation are caused by a failure to properly arrange ternary complexes with Hsp70/Ssa1 and Hsp90. These data showed that a minimal Sti1 fragment comprising TPR2A and TPR2B is able to mediate the formation of a ternary complex with Hsp70/Ssa1 and Hsp90. A mutation of the TPR2B peptide binding site in this fragment disrupted the formation of the ternary complex (section 4.9). Furthermore, the full-length Sti1 with a TPR2B domain deficient in peptide binding in principle still supported the formation of the ternary complex. Together with the findings from the *in vivo* experiments now these observations indicate that a biologically functional ternary complex is only obtained when Hsp70/Ssa1 can bind to TPR2B. A substrate transfer from Hsp70/Ssa1 onto Hsp90 as it was postulated [162] might require a spatial proximity of the two chaperones that can potentially only be achieved when Hsp70/Ssa1 is bound to TPR2B.

The results obtained here on Sti1 from yeast might possibly not apply in the same way for the Sti1/Hop systems from other species. For the TPR2B domain from human Hop for example only a very weak peptide binding activity was found [184]. However, in this case additional Hsp70 binding sites seem to be present provided by the DP2 domain [66,171], which could compensate for a weaker Hsp70 binding to TPR2B. Therefore, in general some significant species-specific differences seem to exist in the function of Sti1/Hop proteins.

4.18.10 The Complex Between Hsp90 and Sti1

The NMR measurements carried out in this work with Sti1 fragments and the isolated Hsp90 domains could reveal further details about the interaction between both proteins. For the N domain of Hsp90 no interaction with full - length Sti1 was found under the conditions used. This observation can not directly exclude binding contacts involving this Hsp90 domain when present within the full - length Hsp90. Previous reports indeed found a role of the first 24 amino acids within the N domain of Hsp90 for the binding of Sti1 [167]. However, in contrast to that, another study neither found an effect of Hsp90 N domain mutations on the interaction between yeast Sti1 and Hsp90 nor a different ATPase arrest of the respective Hsp90 mutants by Sti1 [258]. Likewise, for the human system it was shown that the Hsp90 N domains are not required for full binding of the Sti1 homologue Hop [303]. Considering the high conservation of the Hsp90 chaperone machineries from different organisms, it therefore seems possible that also in yeast the Hsp90 N domains are at least not the major peptide independent Sti1 binding site.

According to the NMR data and consistent with the previous ITC data obtained in this work (section 4.7), the C domain of Hsp90 seems to contribute only with the residues of the C - terminal peptide motive to the binding of Sti1. No major additional peptide - TPR domain independent binding contacts were detected here. However, a weak but specific complex formation was observed when Hsp90 M and the Sti1 TPR2A - TPR2B fragment were assessed for binding using NMR. Thus, the essential interactions between Sti1 and Hsp90 independent from the peptide binding seem to involve predominantly the Hsp90 M domain. Binding contacts between Hsp90 M and the TPR2A - TPR2B fragment as determined by NMR are consistent with the previous ITC data and ATPase measurements

carried out in this work. These found the isolated TPR2A - TPR2B fragment capable and sufficient for high affinity Hsp90 binding (section 4.7) and Hsp90 ATPase inhibition comparable to full - length Sti1 (section 4.6).

The isolated TPR2A and TPR2B domains also clearly showed binding to Hsp90 M in the NMR spectra but these interactions were weaker compared to binding of the two - domain fragment TPR2A - TPR2B to Hsp90 M. Obviously, the full binding affinity is obtained only when both domains are linked as in the TPR2A - TPR2B fragment. When Hsp90 M was added to ^{15}N - labeled TPR2A - TPR2B, chemical shift perturbation was indeed observed within both TPR2A and TPR2B subdomains. This supports the assumption that TPR2A and TPR2B form a joint binding site for Hsp90 M in TPR2A - TPR2B.

Within Hsp90 M, chemical shift perturbation upon binding of TPR2A - TPR2B was found mainly at its outer surface. PRE measurements using site directed spin labeling of Hsp90 M cysteine variants further confirmed this binding site. When the spin label was attached in or near this region in Hsp90 M, significant PRE effects were observed on the ^{15}N - labeled TPR2A - TPR2B. The binding site of Hsp90 M on TPR2A - TPR2B involved in particular the C - terminal end of helix B3 and the N - terminal part of helix C in TPR2A. Within TPR2B, shifts were found at one narrow edge of the domain formed by residues from helices A2, B2 and A3.

The binding site of TPR2A - TPR2B on Hsp90 M potentially overlaps with the binding site of certain Hsp90 client proteins. The p53 DNA binding domain for example was found to interact with a similar region on Hsp90 M as Sti1 TPR2A - TPR2B [304]. This might be of functional importance for the activation of these client proteins. This region of Hsp90 M would not be available for an interaction with client proteins as long as Sti1 is bound. Sti1 is thought to be one of the first cochaperones that binds to Hsp90 during the ATPase cycle. Therefore, it could prevent an

uncontrolled binding of client proteins to Hsp90 M at the beginning of the ATPase cycle until Hsp70/Ssa1 is recruited into the complex. The potential binding of Hsp70/Ssa1 to TPR2B within Sti1 would potentially trigger conformational changes that lead to a displacement of Sti1 from its binding site on Hsp90 M, making this region again available for the transfer of the client protein from Hsp70/Ssa1 onto Hsp90. In this way, Sti1 would ensure a controlled loading of Hsp90 with client proteins. Additionally, Sti1 could also function in displacing an activated client protein from its binding site on Hsp90 M in the last step of the ATPase cycle to start another round of the cycle.

With the NMR data obtained here, a docking could be performed between Hsp90 and Sti1 using HADDOCK[243]. Due to its complex structure comprising multiple domains, unfolded regions and conformational dynamics, it seemed reasonable to use a smaller fragment of Hsp90 for the docking. Thus, the calculations were carried with a monomeric Hsp90 MC template, which should nevertheless contain the full peptide independent Sti1 binding site. For Sti1 likewise not the full-length protein was used in the docking. On the one hand, a structure is not available so far for the full protein and on the other hand, as outlined, the data anyway indicated that the TPR2A-TPR2B fragment behaves similar to full-length Sti1 with respect to Hsp90 binding and ATPase inhibition.

In principle, the PRE data sets of the Hsp90 M variants S411C, S422 and S456C seemed to be suited for extracting atomic distances that could be included as restraints in the docking. However, it turned out that the complexes obtained by HADDOCK using distance restraints derived from PRE measurements with these mutants did not agree well with the experimental data. One possible explanation could be the fact that the PRE measurements had to be carried out with the isolated Hsp90 M domain instead of the MC fragment that was used in the docking. This was nec-

essary because a complex between Sti1 TPR2A - TPR2B and the Hsp90 MC fragment would have been way too large for the PRE experiments (molecular weight of the dimeric Hsp90 MC ~ 108 kDa). However, it seems likely that for isolated Hsp90 M and TPR2A - TPR2B the binding partners have a higher degree of freedom with respect to the orientations the two proteins can adopt in a potential complex. This could have caused some "unphysiological" complex orientations in the PRE measurements that might not have been observed between TPR2A - TPR2B and the larger Hsp90 MC fragment for simple steric reasons. Due to the generally rather weak interaction between Hsp90 M and the Sti1 TPR2A - TPR2B fragment (estimated K_d in the micromolar range, compare section 4.6, figure 4.49) then likely exchange processes on the fast NMR timescale caused an averaging of the different orientations of the binding partners and consequently also an averaging/downscaling of the PRE effects. The obtained PRE distance restraints therefore were probably erroneous and could not yield a satisfying docking solution even when applied with generous upper and lower bounds in the calculations.

The application of PRE derived distance restraints in a protein docking has some limitations and seems to be not very well suited for weaker complexes as observed for Hsp90 M and Sti1 TPR2A - TPR2B. Despite the mentioned drawbacks, the PRE data nevertheless provided useful information for the docking. They could confirm the binding sites on Hsp90 M and TPR2A - TPR2B identified by the chemical shift perturbation experiments, additionally yielded insights into the overall orientation of TPR2A - TPR2B and Hsp90 M in the complex and finally could be used in a more qualitative way to select one complex cluster out of several comparably high ranked HADDOCK docking solutions which agreed best with the experimental data.

The complex between Hsp90 MC and Sti1 TPR2A - TPR2B that was fi-

nally obtained from only chemical shift perturbation data as restraints showed reasonable agreement between the back-calculated and measured PRE effects. The differences observed thereby might be due to reasons as outlined above. However, the complex model is well consistent with the previous biochemical data of this work. The TPR2A-TPR2B fragment is bound in a way to Hsp90 which orients TPR2A to the C-terminal part of Hsp90 M and near to the C-terminal domain of Hsp90. TPR2A contacts the outer surface of Hsp90 M (with respect to its placement in the Hsp90 MC dimer) but does not directly interact with the Hsp90 C-terminal domain itself, consistent with ITC and NMR binding data. The position of TPR2A nevertheless still allows for a binding of the preferred Hsp90 C-terminal peptide ligand: the Hsp90 peptide motive recognized by TPR cochaperones is located at the end of a ~ 30 residues long stretch of unfolded amino acids. These are sufficient to span a distance that enables an interaction of the peptide motive with TPR2A, even when TPR2A is bound to the Hsp90 M domain and does not directly contact to the folded part of the Hsp90 C domain. The TPR2B domain in the TPR2A-TPR2B fragment is oriented to the N-terminal part and more inner surface of Hsp90 M in the complex. Importantly, the backside of TPR2B points to Hsp90 M and therefore the peptide binding groove of TPR2B is well accessible for binding a ligand, which could be the Hsp70/Ssa1 C-terminal peptide.

In a recent cryo-EM study a low resolution structure for the complex between human Hop and Hsp90 was reported [305]. It was found that Hop binds in an elongated arrangement to Hsp90 and that the TPR2A domain most likely contacts Hsp90 in a region near to the M and C domain junction. Furthermore, the authors also observed electron density located between the two Hsp90 subunits for the Hop-Hsp90 complex. However, from the EM data it was not possible to deduce whether it cor-

responded to either the TPR1 or the TPR2B domain of Hop. All these data are in good agreement with the results obtained here for Sti1. Interestingly, in this study complexes between Hsp90 and Hop suited for EM structural analysis were stabilized by chemical crosslinking of the Hsp90 C-terminal peptide motive to TPR2A via an engineered disulfide bridge and additionally by slight unspecific crosslinking applying low concentrations of glutaraldehyde. This indicates that also the human Hop-Hsp90 interaction is rather weak and the inherent conformational flexibility in the system hampers a structural analysis.

The complex between Hsp90 MC and Sti1 TPR2A-TPR2B determined here gives an explanation for the previous findings of Dr. Andreas Schmid (Lehrstuhl für Biotechnologie, TUM) that only the TPR2A-TPR2B fragment could inhibit the Hsp90 ATPase activity but not the isolated TPR2A or TPR2B domains. This is obvious from the model: TPR2A seems to be mainly important for contacting Hsp90 M and orienting the TPR2A-TPR2B fragment properly on Hsp90 by making direct binding contacts with Hsp90 M. TPR2B, on the other hand, appears to be essential as its position more at the inner surface of Hsp90 M between the two subunits of the Hsp90 dimer might function to sterically block conformational changes in Hsp90 that are necessary for ATP hydrolysis. Without covalent linkage to TPR2A, the TPR2B domain most likely could not adopt a position on Hsp90 that would allow for an efficient inhibition of ATP hydrolysis since its capacity to bind Hsp90 M is rather weak. Isolated TPR2A bound to the outer surface of Hsp90 M on the other hand would not have any influence on the conformational changes in Hsp90. On this basis, the results of the experiments with the TPR2A-TPR2B linker mutant (section 4.10) appear meaningful. A changed orientation of the TPR2A and TPR2B domains relative to each other in the TPR2A-TPR2B fragment as caused by the R425A mutation could partially impair a proper positioning

of TPR2B on Hsp90 M required for optimal Hsp90 ATPase inhibition.

The crystal structure of full-length Hsp90 demonstrated that besides the N domain dimerization and strand swapping also the M domains undergo larger conformational rearrangements during ATP hydrolysis, moving by about 20 Å compared to the nucleotide free state [52]. The HADDOCK model now indicates that the mechanism underlying Hsp90 ATPase inhibition by Sti1 might possibly be to block Hsp90 M domain rearrangements rather than to directly inhibit Hsp90 N domain dimerization. However, blocking the M domain rearrangements concomitantly would also inhibit N-terminal dimerization. Such an inhibition mechanism would not require a direct interaction of Sti1 with the Hsp90 N domains which is in agreement with the NMR data.

The complex structure further points at an interesting aspect of the Hsp90-TPR cochaperone interactions in general: With TPR2B functioning in sterically blocking the Hsp90 M domain rearrangement by its placement between the two Hsp90 subunits, only one TPR2A-TPR2B molecule per Hsp90 dimer would be required for an efficient Hsp90 ATPase inhibition. This assumption is consistent with previous biochemical studies [278]. Therefore, the second peptide motive of Hsp90 would be available for binding another TPR cochaperone. Either a second molecule of Sti1 could bind to an existing complex of Sti1 and Hsp90 (as binding stoichiometries from ITC experiments indicate, section 4.7) or a different TPR cochaperone. Indeed, a significant formation of such asymmetric complexes between Hsp90, Sti1 and other TPR cochaperones like Cpr6 was observed previously in analytical ultracentrifugation experiments [278]. Even when displaced from its binding site on Hsp90 M during the progression of the Hsp90 ATPase cycle, Sti1 could still be anchored to Hsp90 via the TPR peptide binding of TPR2A. Thus, it would immediately be available for binding again to Hsp90 M at the beginning of a new round of the ATPase

cycle.

In conclusion, the complex structure determined here between the Hsp90 MC and the Sti1 TPR2A - TPR2B fragments is well in agreement with biochemical data and and a previous EM study on the human Hsp90 - Hop complex [305]. It provides new insights into the potential mechanism of the Hsp90 ATPase inhibition by Sti1. Due to the limitations of the docking approach used here, it should be regarded rather as a good model which cannot be compared to the quality of a real crystal structure. However, so far no high resolution crystal structure of a complex between Sti1 and Hsp90 or fragments thereof has been reported, probably for the same reasons that impeded the NMR data driven docking carried out in this work.

4.18.11 Screening for TPR Domain Inhibitors

Targeting protein - protein interactions for inhibition appears to become a more and more attractive approach in the treatment of diseases like cancer. A prominent example for the successful disruption of protein - protein interactions is the humanized monoclonal antibody Trastuzumab (*Herceptin*®) used in the treatment of breast cancer [306]. Trastuzumab binds to the HER2 receptor overexpressed on the cell surface of cancer cells in ∼ 30 % of the breast cancer patients [307] and thus likely prevents ligand binding to the receptor and also its binding to other receptors to form heterodimers [308].

Unfortunately, the strategy to inhibit protein - protein interactions with an antibody has some unfavorable drawbacks like the lack of cell permeability/bioavailability and is therefore rather limited to targets on the cell surface. On the other hand, the inhibition of protein - protein interactions with small molecules that could be administered orally is much more challenging for some reasons: Typical protein - protein interaction sites cover large surface areas with ∼ 750 to 1500 Å^2 [309]. Often, complex formation involves many different residues within both proteins that contribute only with weak individual binding contacts to the interaction but add up to give a reasonable overall binding affinity. A classical binding pocket into which a ligand would fit like in the case of many well druggable enzymes is usually not found [309]. Hence, disrupting such an interface with a small organic and non - peptidic molecule is very difficult. Nevertheless, some rather recent reports from the last decade exist where this approach was successful, especially in cases with a smaller and better defined binding site between the two proteins. For example, complex formation between p53 and MDM2 was shown to be effectively disrupted by a class of compounds called Nutlins with affinities in the higher nM

range [310].

The screening for TPR domain inhibitors carried out in this work in collaboration with Dr. Andreas Frank (Institute for Advanced Study, TUM) also targets a protein - protein interaction and was intended to disrupt complex formation between Hsp90 and Sti1/Hop. However, in contrast to many other cases in which significant problems have to be overcome to inhibit a protein - protein interaction, as mentioned above, this system seemed to be well suited for a screening. Here, the binding of the proteins is mediated by the recognition of only a small peptide stretch (at maximum eight residues long) by the TPR domain. Additionally, all TPR domains have comparable folds with a well defined ligand binding groove, and in particular for all TPR domains known to interact with Hsp90 key residues important for ligand binding are highly conserved (two - carboxylate clamp) [68].

A virtual screening performed by Dr. Andreas Frank could identify several potential Sti1/Hop TPR domain peptide binding site inhibitors. Unfortunately, from a set of six finally selected highly interesting compounds that should be subjected to an experimental validation only four could be tested as the others suffered from poor solubility. Out of these, all were found to bind to the yeast Sti1 TPR2B domain when added in a high molar excess to the protein, but only one, STOCK2S-37873, showed binding activity also at a lower concentration. The affinity for the complex between this compound and the Sti1 TPR2B domain was on the order of $\sim 360\mu$M and therefore the interaction can be regarded as rather weak. The other three compounds likely had affinities roughly estimated in the mM range. For comparison, the affinity of Sti1 TPR2B for its natural peptide ligand is around $4\,\mu$M K_d, the conserved consensus peptide motive EEVD is still bound with $\sim 12\,\mu$M (compare section 4.3, table 4.7).

The best compound identified in the screening here interacts signifi-

cantly weaker with the protein target than the natural peptide. This can be due to several reasons: First of all the pharmacophore model built by Dr. Andreas Frank for the virtual screening was restricted to mimic only the two residues D0 and V-1 of the peptide. Consequently, it was anyway unlikely that a potential small molecule binder would show a tighter interaction with the protein than the full peptide ligand. Second, the pharmacophore model was obtained on the basis of a crystal structure from the human Hop TPR2A domain in complex with its preferred ligand, the Hsp90 peptide MEEVD[68]. However, for the experimental validation of the compounds only the Sti1 TPR2B domain from yeast was available. Although TPR2B also shows conserved two - carboxylate clamp residues within its ligand binding groove (compare figure 4.125), several differences can be found in the type of amino acids when corresponding residues from yeast TPR2B and human Hop TPR2A are compared (figure 4.128). Identical residues are are only found at the corresponding positions 435 of Sti1 TPR2B and 264 of Hop TPR2A with an asparagine. TPR2B additionally lacks an equivalent for residue Q298 present in the two - carboxylate clamp of human Hop TPR2A. The two potential hydrogen bond donor groups provided by the amide moiety of Q298 and the amino moiety of K301 in Hop TPR2A are substituted by a single residue R465 in Sti1 TPR2B. These differences might be responsible for the rather weak binding of the STOCK2S-37873 inhibitor to the TPR2B domain from yeast.

Indeed, the potential binding mode of the molecule with Sti1 TPR2B found by HADDOCK docking shows that the side - chains of the two - carboxylate clamp residues R400 and K404 probably are not directly involved in binding contacts with the compound. This is contrary to the assumptions made by the pharmacophore model. Binding of the compound to human Hop TPR2A is possibly better in agreement with the

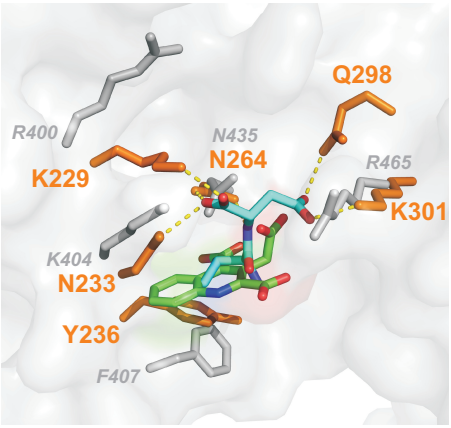

Figure 4.128: Comparison of the yeast Sti1 TPR2B - inhibitor complex obtained with HADDOCK [243] and the crystal structure of human Hop TPR2A with the MEEVD peptide bound (PDB: 1ELR) [68]. Yeast Sti1 TPR2B shows several different two - carboxylate clamp residues in the binding pocket compared to human Hop TPR2A. Two - carboxylate clamp residues are shown as sticks and colored gray for Sti1 TPR2B. Corresponding residues within human TPR2A are colored orange. The inhibitor bound to TPR2B is depicted in green, the MEEVD ligand of TPR2A in blue. Only the residues D0 and V-1 of the MEEVD peptide that are mimicked by the inhibitor compound are shown for clarity. Hydrogen bonds formed by D0 and V-1 are indicated by yellow dashed lines.

pharmacophore model and therefore a significantly higher affinity might be observed than for the Sti1 TPR2B domain.

In an earlier study, a conventional HTS was carried out for inhibitors of the human Hop TPR2A domain [284]. In this work, compounds were identified that had a binding affinity roughly in the μM range. One of them was tested in further ITC experiments that yielded a precise K_d - value of 16 μM for binding to the target. As mentioned above, it seems possible that the STOCK2S-37873 compound identified here by virtual screening

might bind to the human Hop TPR2A domain much better than to the Sti1 TPR2B domain from yeast that was used for the experimental validation. In this case, the affinity could even be on the same order as the affinity of the previously reported compound. Interestingly, all binders found in the HTS study had a common structure motive roughly similar to the compound identified here: A bicyclic heteroaromatic 7 - azapteridine ring system with different additional functional groups. These were all uncharged, conferring higher lipophilicity and making these molecules likely better bioavailable than the STOCK2S-37873 inhibitor. This is supported by the cytotoxicity of the compounds in *in vivo* experiments with cancer cell lines. However, this disadvantage of STOCK2S-37873 could be overcome easily by an esterification of the carboxy groups in a prodrug, increasing the cell permeability. The ester bonds then would be rapidly cleaved again after cellular uptake of the prodrug by esterases to yield the active compound.

Overall, the virtual screening approach turned out to be a promising strategy in the particular case of searching for TPR domain inhibitors. It is fast and resulted in the identification of the binding active compound STOCK2S-37873, which could now serve as a template for a further chemical optimization to improve its affinity for the protein target. Alternatively, an additional second site screening for small molecules mimicking the E-2 an E-3 residues of the EEVD peptide motive in the natural TPR domain ligand could also be performed. A possible hit might be chemically linked to the first inhibitor fragment, potentially yielding a new inhibitor with strongly increased affinity. This so called “fragment based approach” was already successfully applied in a number of cases and reviewed [311–316].

4.18.12 The DP Domain Structures

So far no structure of a DP domain was solved, neither from a Sti1/Hop protein nor from a related protein like Hip. The NMR structures of the Sti1 DP1 and DP2 domains from the yeast *Saccharomyces cerevisiae* determined here therefore represent the first detailed analysis of these important components in Sti1/Hop/Hip proteins. The fold of the DP domains appears to be related to a domain from the human E3 ubiquitin - protein ligase HECW1, as a database search for proteins similar in 3D structure revealed. However, the function of this structurally similar domain has not yet been described and likely the particular DP domain fold was adapted for a rather different biological task in HECW1. In general, a possible functional feature common to both the DP domains and the corresponding domain from human HECW1 could consist in mediating a particular protein - protein interaction.

Crucial for obtaining structural information turned out to be the optimization of the DP domain boundaries, in particular in the case of DP1. As the NMR data demonstrated, the TPR1 - DP1 module is connected to the other domains in yeast Sti1 by an unusually long unfolded and flexible linker of ~ 60 residues. This might be of functional importance for the yeast Sti1 protein. As a sequence alignment shows, the corresponding linker region in the human homologue Hop is significantly shorter by nearly 30 residues (compare figure 4.1). The linker region of yeast Sti1 contains a high proportion of Ser and Thr residues that could serve as potential phosphorylation sites. Therefore, the linker region might be implicated in regulatory processes.

Inaccurately chosen domain boundaries of DP domains might have hindered a crystallization of these proteins so far. But also the inherent flexibility of DP domains could play a role. Especially for the Sti1 DP2 domain

it was difficult to obtain long range NOE contacts for the NMR structure determination: for exclusively α - helical proteins like in case of the DP domains in general less long range NOEs are observed compared to β - sheet proteins. But in DP2 the helices additionally appear to be only loosely packed. This goes along with increased flexibility of the protein, indicated by the higher RMSD of the DP2 final NMR structure ensemble.

The structures of the yeast Sti1 DP1 and DP2 domains turned out to be quite similar, as expected. But surprisingly, in the DP1 structure a small N - terminal helix not present in DP2 was found, which secondary structure analysis tools could not predict. This structure element packs into a kind of groove formed by the other helices, thus stabilizing the overall fold of DP1. Consequently, a lower RMSD for the NMR structure ensemble of DP1 was found compared to DP2. In the DP2 domain this groove is well accessible, which could have functional implications.

The NMR structures of the yeast Sti1 DP1 and DP2 domains furthermore explain the role of the highly conserved DP/NP motives. It was shown previously that a mutation of the D residue in the DP motives of the human Hop DP2 domain to A causes an increased sensitivity to proteolytic digestion [189]. This is obvious now since the D/N residues of the DP motives act as helix caps that stabilize the C - and N - terminal ends of helices in the DP domains, as demonstrated by the NMR structures obtained here (figure 4.104). Earlier studies about the preferential incorporation of certain amino acid types at the capping positions of helices analyzing crystal structures of more than 1000 proteins showed that an A residue as introduced in the studies with the human Hop DP domain is highly disfavored in N - terminal helix caps [290]. It is likely that these mutations significantly destabilized the DP domain and potentially led to a partial unfolding of helices, explaining the hypersensitivity to proteolysis. Thus, the main function of the DP motives seems to be conferring structural

stability to the helices at their N- and C-terminal ends.

4.18.13 Potential Functions of Sti1/Hop DP domains

A previous study carried out with Sti1 from yeast could assign the DP2 domain an essential role in the activation of heterologously expressed human GR in yeast cells [187]. DP2 domain deletion/truncation mutants and a single amino acid substitution V540E led to a complete loss of Sti1 function in the cellular test system. However, considering the DP2 NMR structure obtained here, it seems likely that the V540E variant was structurally significantly distorted since this residue is involved in multiple hydrophobic contacts between the DP2 helices $\alpha 2$ and $\alpha 5$. Introducing a charged residue at this position is presumably not compatible with the overall fold of the domain. Consequently, from the mentioned findings with the V540E mutant no direct conclusions can be drawn about the functional importance of a particular residue or structure element in DP2. To address this issue in more detail, therefore further point mutants of this domain were designed here and tested for supporting the activation of human GR in yeast cells. With the DP2 NMR structure at hand, a more directed selection of residues that should be targeted for mutation was possible compared to earlier studies.

As expected, all Sti1 DP2 domain mutants generated turned out to be fully structured as rather conservative alanine amino acid substitutions were chosen. Thus, all effects observed in the cellular assays were not caused by a globally unfolded DP2 domain but can be regarded to reflect a specific functional impairment of the protein due to altered properties of a structure element. Two Sti1 DP2 mutants, Q557A and T578A behaved comparable to the wild - type protein, although Q557 in helix $\alpha 3$ seems to be a residue conserved between human and yeast DP2 domains (figure 4.129). The Sti1 I584A variant, in contrast, was significantly impaired in its function, here the GR activity was reduced to $\sim 65\,\%$. This is surpris-

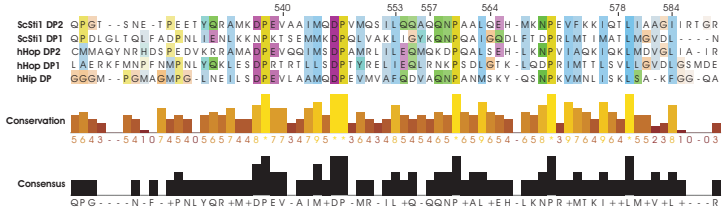

Figure 4.129: Amino acid sequence alignment for DP domains from yeast (*Saccharomyces cerevisiae*, Sc) Sti1, human (h) Hop and human Hip. The sequence conservation of the DP domains does not seem to be extremely high, except for the DP/NP motives. The alignment was generated using T-Coffee [194] and visualized with Jalview [195]. NCBI reference codes of the sequences used for the alignment are NP_006810.1 for human Hop and NP_014670.1 for yeast Sti1. The Uniprot reference code for the human Hip sequence is P50502. Residues of the Sti1 DP2 domain targeted for mutation are indicated. The coloring scheme is according to amino acid properties and the degree of conservation of a particular position with more intense color indicating higher conservation.

ing given the fact that I584 is located C-terminally of helix α5 and not part of a secondary structure element (figure 4.108). Backbone dynamics show that this residue is still within a rigid region of the protein (figure 4.107), and a sequence alignment indicates that at this particular position of DP domains in general only hydrophobic amino acids are found (figure 4.129). The mutation of this position could have affected the dynamics of the protein towards an increased mobility of helix α5 or affected the properties of a potential binding site.

Another highly conserved residue is L553 in helix α3 of Sti1 DP2. Upon L553 mutation to alanine, Sti1 nearly completely lost its ability to support GR activation. Interestingly, despite its hydrophobic properties, the side-chain of L553 is not buried deeply in a hydrophobic core engaged in packing contacts with other residues, as expected, but points rather well solvent accessible into the presumable DP2 ligand binding groove (fig-

ure 4.108). This could point at L553 being potentially involved in ligand binding contacts and in general this residue seems to play a key role for the function of Sti1.

A mutant with an amino acid replacement at the position 540 that was previously described to be important for DP2 function [187], as mentioned, was also tested here in the yeast cellular assays. In contrast to the earlier study, a V540A instead of a V540E mutant was prepared. Unlike the V540E variant, Sti1 V540A had clearly remaining *in vivo* activity ($\sim 60\,\%$ of the wild - type). This supports the assumption outlined above that the V540E mutation likely had affected the DP2 domain structure severely. The *in vitro* characterization of DP2 V540A domain showed a secondary structure content of the mutant similar to the wild - type protein. Thus, V540 does not seem to be essential for the formation of helix $\alpha 2$ but could be a key residue for stabilizing the overall fold of DP2. It obviously provides important hydrophobic side - chain contacts in the packing of DP2 helices $\alpha 2$ and $\alpha 5$. Indeed, this particular valine residue is strictly conserved in the DP2 domains from yeast Sti1 and human Hop as well as in the DP domain of human Hip (figure 4.129).

Surprisingly, also a Sti1 mutant was identified that had increasd activity (130 %) in the yeast GR assay, Q564A. Q564 is located in helix $\alpha 4$ of DP2, pointing rather to the solvent accessible outside of the domain (figure 4.108). Therefore, this residue is structurally not of major importance except for the fact that it contributes to the solubility of the protein with its polar side - chain. However, the assay data demonstrate the position 564 to have some functional relevance. This is supported by the observation that the residue at the respective position in other DP domains seems to be partially conserved, with differences between DP1 and DP2 domains of the Sti1/Hop/Hip proteins: DP2 from human Hop and the C - terminal DP domain of human Hip, which corresponds to the DP2

domains of the Sti1/Hop proteins, both contain a serine at this position. The DP1 domains from yeast Sti1 and human Hop have a glycine, instead (figure 4.129). In this respect the DP2 domain from yeast seems to be somewhat exceptional with its glutamine residue. It could be speculated that the alanine introduced at position 564 of DP2 is more similar in its properties to the serine residue found in the Hop DP2 and Hip DP domains than the native glutamine, thus causing increased activity of the mutant. An amino acid with a smaller side - chain at position 564 might sterically better fit into the binding site of a potential interaction partner.

Overall, the mutagenesis data indicate that the helices α3 and α4 might have major importance for the function of the Sti1 DP2 domain. A mutation of residues that are not essential for the global fold of DP2 (L553 from α3 and Q564 from helix α4) had significant influence on the ability of Sti1 to support GR activation. Especially hydrophobic residues seem to play a major role, replacing L553 in DP2 by A led nearly to a complete loss of function.

Interestingly, the DP domain swap experiment replacing the yeast Sti1 DP2 with the DP1 domain showed that DP1 – despite its similar fold – can not substitute for DP2 in GR activation experiments. This raises the question about the general requirement of the DP1 domain for the function of Sti1. The most striking difference in the structures of DP1 and DP2 is the small additional N - terminal helix of DP1 which packs against the helicesα4 and α5 and thus occupies the cleft accessible in the DP2 domain. Together with the observation that a mutation of the hydrophobic DP2 residue L553 pointing into this cleft causes a significant impairment of the domain's function, the result of the DP domain swap experiment supports the assumption of a ligand binding site present in DP2.

For the the human homologue Hop indeed the binding of Hsp70 was reported to be dependent on the DP2 domain [66,171], which could not be

confirmed for the DP2 domain from yeast Sti1, however[147]. A potential binding of yeast Sti1 DP domains to either Hsp70/Ssa1 or Hsp90 was assessed again here using NMR. NMR in general is one of the best methods to identify even very weak but biologically important interactions between proteins. Therefore, despite the earlier reports that DP domains of Sti1 would not be involved in Hsp70/Hsp90 binding, it seemed in principle possible that a DP domain - chaperone binding could be detected with NMR. A very weak complex formation might likely not have been observed previously with other methods like pull down assays which – in contrast to NMR – shift the binding equilibrium rather towards dissociation of protein complexes during washing steps. However, also the NMR data now indicate that the DP domains of yeast Sti1 are not involved in binding of Hsp70/Ssa1 domains or Hsp90. But still a DP domain - chaperone interaction can not be ruled out completely as DP domains might recognize a very specific conformation of the chaperones observed potentially only in larger chaperone/Sti1/receptor heterocomplexes. On the other hand, also some species - specific differences in the function of the Sti1/Hop proteins from yeast and man seem to exist. Previous reports found only a very weak peptide binding for the TPR2B domain of human Hop[184], which is in sharp contrast to the TPR2B domain from yeast Sti1. Possibly, the failure of the TPR2B domain to serve as an interaction site for the essential Hsp70 binding is compensated by Hsp70 binding to DP2 in the human Hop system.

In principle, a role of DP domains in binding another chaperone component from steroid hormone receptor containing heterocomplexes or alternatively an interaction with the receptor client itself also seems possible. To test the latter assumption, a peptide corresponding to the lid of the human GR ligand binding domain was tested for binding to the Sti1 DP2 domain. This structure element can be assumed to require particular

stabilization due to its hydrophobic nature, which might be a function of the DP2 domain. Some slight binding of the peptide to the Sti1 DP domain could indeed be observed which shows that DP2 in general can function as a binding site. However, since the interaction appeared to be very weak, it is unclear to which extent it was really specific.

As the PRE experiments performed with the Sti1 TPR2B - DP2 fragment showed, moderate domain contacts seem to exist between the DP2 and TPR2B domains. Although DP2 is connected flexibly to TPR2B by a linker region of ~ six unstructured residues, both domains do not behave completely independent but seem to associate transiently. This is also reflected by a slight influence of the DP2 domain on the peptide binding properties of TPR2B found here. Interestingly, a domain architecture combining a TPR domain with a C - terminally located DP domain is a feature common to actually all Sti1/Hop proteins. Thus, the TPR - DP modules indeed seem to represent a functional unit as it was speculated earlier from sequence analyses [175].

Chapter 5

The Hsp90 Cochaperone Hch1

5.1 Expression and Purification of Hch1

As outlined in section 2.2, the Hsp90 cochaperone Hch1 shares a high sequence homology with the N-terminal domain of Aha1 [193]. Interestingly, Hch1 seems to exist only in lower eukaryotes [193,196]. The fact that the yeast *Saccharomyces cerevisiae* harbors both, Hch1 and Aha1, raises the question to which extent the two proteins have overlapping function. Hch1 and Aha1 were shown to stimulate the Hsp90 ATPase activity, however, Hch1 is obviously less efficient in this respect [193]. To gain further insights into the properties and function of the so far rather poorly characterized Hch1, a more detailed *in vitro* analysis of this Hsp90 cochaperone was carried out here.

A plasmid encoding wild-type Hch1 for expression in *E. coli* was kindly provided by Dr. Klaus Richter (Lehrstuhl für Biotechnologie, TUM). Unfortunately, Hch1 turned out to be largely insoluble when expressed in

E. coli. Even when the protein expression was done at low temperatures (18°C), Hch1 was exclusively found only in the pellet. Thus, an inclusion body preparation had to be performed to obtain Hch1 suited for further processing. A refolding protocol was then established (see section 9.11) which allowed for purification of Hch1 with a final yield of ~ 5 mg homogeneous protein per liter of cell culture, even under conditions of isotope labeling using M9 minimal medium. These protein amounts – although comparatively low – were sufficient for performing NMR experiments with Hch1.

The formation of inclusion bodies by Hch1 upon bacterial expression is somewhat surprising given its similarity to the Aha1 N domain, which obviously behaves much better in this respect and can be produced solubly in *E. coli* [79]. To analyze whether maybe different surface properties might be responsible for this observation, a homology model for Hch1 was built using the program MODELLER [277] and the crystal structure of Aha1 N (PDB: 1USV) as a template. Taking into account the high conservation between Hch1 and the Aha1 N domain, a molecular modeling approach should yield an acceptable result in this case. The N-terminus (residues 1 to 11) and a loop region (residues 105 to 108) of Hch1 were missing in the homology model obtained due to a lack of structural information in the Aha1 N template. These parts of the protein were therefore rebuilt with Xplor-NIH [233]. Figure 5.1 shows a comparison of the Hch1 model structure with the Aha1 N domain.

The electrostatic potentials calculated for both molecules are overall roughly similar, despite some differences as expected. Aha1 N as well as Hch1 have highly charged surfaces that should render the proteins well soluble. The pI-values (pI, isoelectric point) calculated from the primary sequences are 6.34 for Aha1 N and 4.77 for Hch1, respectively. Thus, in principle Hch1 should be even more charged and better soluble

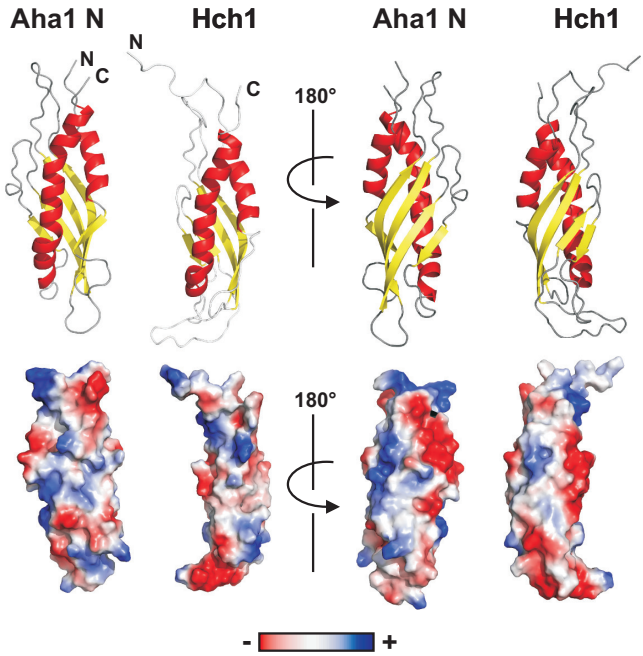

Figure 5.1: Electrostatic potentials of Aha1 N and Hch1. Upper panel: Comparison of the crystal structure for the Aha1 N domain (PDB: 2USV) with a homology model of Hch1 generated using the program MODELLER [277]. The N-terminus and a loop region of Hch1 missing in the homology model due to a lack of structural information in the Aha1 N template were rebuilt with Xplor-NIH [233]. Lower panel: The electrostatic potentials for Aha1 N and Hch1 determined with PyMOL are roughly similar.

at a physiological pH around 7 compared to Aha1 N. In conclusion, the surface properties of Hch1 cannot explain its unfavorable behavior when expressed in bacterial cells.

5.2 Structural Characterization of Hch1

Given the overall high sequence similarity between the Aha1 N domain and Hch1 [193] (compare figure 2.4), it can be assumed that the structures of the two proteins would be similar. As crystallographic data showed, the Aha1 N domain comprises a mixture of α - helical and β - sheet structure [197]. Indeed, a first CD spectroscopic characterization of purified Hch1 pointed at a predominant content of β - sheet also for this protein, as indicated by a typical minimum at 218 nm (figure 5.2, left). This con-

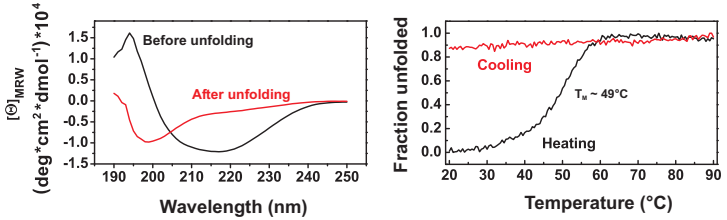

Figure 5.2: CD spectra and thermal stabilities of Hch1. Left: CD spectra of Hch1 before and after the thermal unfolding transition recorded at 20°C. Hch1 does not unfold reversibly. Right: Thermally induced unfolding of Hch1 monitored by CD spectroscopy at a wavelength of 218 nm. Measurements were done in a buffer of 50 mM potassium phosphate, 50 mM potassium chloride, 1 mM TCEP, pH 7.5 using a 10 μM concentrated sample of Hch1.

firmed that Hch1 was structured after the refolding procedure that had to be applied to obtain the purified protein.

The thermal unfolding transition for Hch1 monitored by CD demonstrated a reasonable stability of the protein, with an unfolding midpoint of $\sim$ 49°C (figure 5.2, right). Therefore, Hch1 in principle seemed to be well suited for further NMR experiments. Notably, the CD data indicate that the failure of Hch1 to express solubly in *E. coli* is likely not due to a

low temperature stability of the protein. Potentially, Hch1 might experience posttranslational modifications in yeast, contributing to an increased stability and not provided by the bacterial host organism used here for the expression.

The 2D HSQC spectrum of the $^{15]}$N - labeled Hch1 was well consistent with the CD data (figure 5.3). The signal dispersion in general clearly

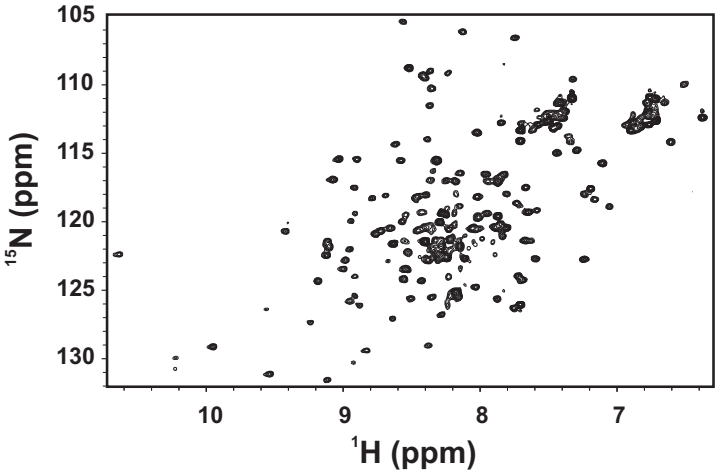

Figure 5.3: ^{15}N - HSQC spectrum of Hch1. The spectrum is clearly indicative of a folded protein. The good signal dispersion points at a higher content of β - sheet structure as expected from the similarity between the Aha1 N domain and Hch1. The measurement was done in a buffer of 50 mM potassium phosphate, 50 mM potassium phosphate chloride, 1 mM TCEP, pH 7.5 at 900 MHz and 303 K using a 200 μM concentrated sample of Hch1.

shows that the purified protein was well structured and contained presumably β - sheet. However, to some extent rather non - uniform peak intensities also point at possible exchange processes occurring within some

parts of the protein that might likely be assigned to mobile loop regions.

Since the first NMR spectra were promising and also the temperature stability of Hch1 was high, attempts were made to obtain a backbone resonance assignment for the protein. However, at the higher sample concentrations (0.5 to 1 mM) required for recording triple resonance spectra, Hch1 turned out to behave rather unfavorably and displayed very limited long term stability. In particular, an unexplainable loss of signal intensity was observed in the NMR spectra of Hch1 within only ∼ 24 h, rendering the measurement of advanced NMR experiments impossible (figure 5.4). Interestingly, no major changes like peak shifts or the appearance of new

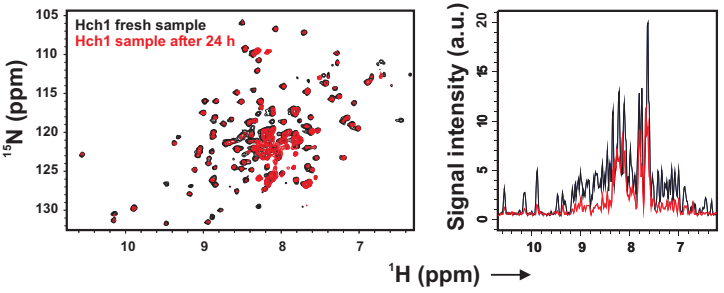

Figure 5.4: Hch1 long term sample stability. Overlay of ^{15}N - TROSY spectra (left) of a freshly prepared Hch1 NMR sample (black) and after 24 h in the magnet (red) recorded with identical parameters. The right side shows 1D projections of the respective spectra from the right as overlay. A severe loss of signal intensity is observed in the spectra of Hch1 after a comparatively short time, rendering the measurement of advanced triple resonance spectra for Hch1 impossible. Measurements were done in a buffer of 50 mM potassium phosphate, 1 mM TCEP, pH 7.5 at 750 MHz and 303 K using a 1.2 mM concentrated sample of Hch1.

signal could be found in the 2D spectra of Hch1 which would point at an unfolding of the protein. Also, no visible protein precipitates in the NMR tube or a turbidity indicative of an aggregation process was observed.

Thus, possibly well soluble higher order oligomers of Hch1 might have formed, adversely affecting the relaxation properties of the protein and causing a line broadening. These findings are to a certain extent consistent with the fact that Hch1 could only be expressed as inclusion bodies (see section 5.1). Obviously, Hch1 seems to have a general tendency to form oligomers. Potentially, the elongated shape of the molecule with the long β-sheet on on side (see figure 5.1) might contribute to such a process.

To improve the behavior of Hch1 in the NMR experiments, a screening for buffer conditions that might support the stability of the protein was carried out. Since the presence of L-arginine was found to improve the refolding yields during the Hch1 purification, the effect of this additive on the Hch1 stability was analyzed using CD spectroscopy (figure 5.5). Indeed, the amino acid could moderately stabilize Hch1. The thermal

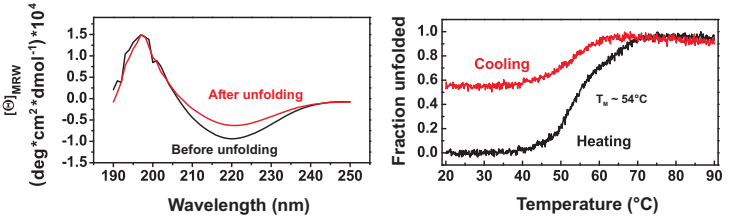

Figure 5.5: Effect of L-arginine on the stability of Hch1 . Left: CD spectra of Hch1 before and after the thermal unfolding transition in presence of L-arginine recorded at 20°C. L-arginine seems to have a stabilizing effect on Hch1, rendering its thermal unfolding partially reversible (compare figure 5.2, left). Right: Thermally induced unfolding of Hch1 in presence of L-arginine monitored by CD spectroscopy at a wavelength of 218 nm. The temperature stability of Hch1 is slightly increased with L-arginine (compare figure 5.2, right). Measurements were done in a buffer of 50 mM potassium phosphate, 50 mM potassium chloride, 1 mM TCEP, 1 mM L-arginine, pH 7.5 using a 10 μM concentrated sample of Hch1.

unfolding of the protein seemed to be partially reversible in presence of L-arginine and also the thermal melting point was slightly shifted from ~49 to 54°C (compare figures 5.2 and 5.5).

For testing additional buffer conditions in a more convenient way, a ThermoFluor stability assay was performed with Hch1 that allows for simultaneous analysis of multiple samples in 96-well plates. A dye, SYPRO Orange, is added to the protein of interest which specifically binds to hydrophobic patches of a protein exposed under unfolding. In this case, the fluorescence is increased and typical sigmoidal shaped denaturing transitions can be observed (figure 5.6). The results of the ThermoFluor

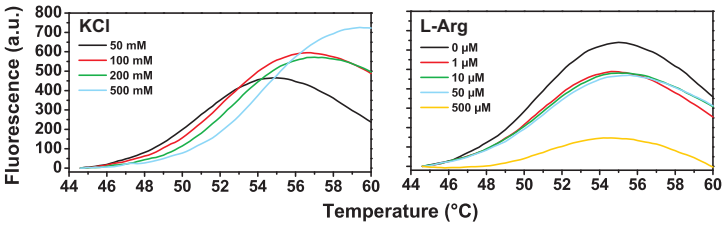

Figure 5.6: ThermoFluor stability assay with Hch1. ThermoFluor melting curves of Hch1 for different concentrations of salt (KCl, left) and L-arginine (L-Arg, right). Salt has a moderately stabilizing effect on Hch1. Measurements were done in a buffer of 50 mM potassium phosphate, 50 mM potassium chloride, 1 mM TCEP, pH 7.5 using a 5 μM concentrated sample of Hch1.

measurements are summarized in table 5.1. The pH value had a stronger influence on the Hch1 thermal stability. Whereas the protein was well stable at neutral and moderately basic pH up to 9.0, a strongly decreased melting temperature even at only slightly acidic pH of 6.0 was found. This sensitivity of Hch1 for solvent pH might potentially explain the observed failure to express solubly in bacterial cells. L-arginine as an additive in the buffer had a stabilizing effect, which was however rather small, with

Table 5.1: Melting temperatures (T_M) of Hch1 under different buffer conditions as determined in a ThermoFluor stability assay. The strongest stabilizing effect is obtained with the addition of a higher amount of salt. Measurements were done in a buffer of 50 mM potassium phosphate, 50 mM potassium chloride, 1 mM TCEP, pH 7.5 using a 5 μM concentrated sample of Hch1. L - Arg, L - arginine; L - Gly, L - glycine.

pH	**5**	**6**	**7**	**8**	**9**
T_M (°C)	38.6	38.6	49.9	49.9	49.2
L - Arg (μM)	**1**	**10**	**50**	**500**	
T_M (°C)	49.9	50.1	50.2	50.4	
L - Gly (μM)	**1**	**10**	**50**	**500**	
T_M (°C)	50.1	49.5	50.1	50.0	
KCl (mM)	**50**	**100**	**200**	**500**	
T_M (°C)	49.9	51.5	52.1	54.1	
25 μM L - Arg + KCl (mM)	**100**	**200**	**500**		
T_M (°C)	51.6	52.4	54.5		
25 μM L - Gly + KCl (mM)	**100**	**200**	**500**		
T_M (°C)	51.7	52.1	54.4		

an increase in T_M of at maximum 0.5°C at a concentration of 0.5 mM applied. In the previous CD experiments the increase in Hch1 thermal stability was more pronounced with L - arginine (figure 5.5), but in this case 1 mM of the amino acid was used. Therefore, this additive seems to be effective only in a higher concentration. The same might apply for L - glycine that was likewise tested but could not significantly influence the Hch1 melting point.

The strongest shift in the Hch1 thermal unfolding curve was obtained with the addition of a higher amount of salt. With 500 mM potassium chloride, the stability of Hch1 was increased by $\sim$4°C. A combined addition of salt together with L - arginine or L - glycine could not further increase the stability of Hch1. Thus, overall the additives tested had small

to moderate effects, with salt clearly causing the most pronounced shift of the Hch1 melting point.

Considering the results from the buffer screening, NMR measurements with Hch1 were then performed in presence of an elevated concentration of salt (150 mM), however, this could unfortunately not prevent the problems with the signal loss in longer measurements as mentioned above. The addition of even higher amounts of salt above $\sim$200 mM, which might potentially improve Hch1 long term stability, is in general not feasible for NMR due to a strongly increased sample heating and pulse length under such conditions. Therefore, the attempts to obtain a backbone resonance assignment for Hch1 unfortunately failed here.

5.3 Complex Formation of Hch1 and Hsp90

To analyze whether differences might exist in the interaction of Hch1 with Hsp90 compared to Aha1 N, binding studies were performed here using fluorescence polarization and NMR. First, the affinity of Hch1 for Hsp90 was determined. To this end, a fluorescein label was attached to Hch1 which was then titrated with full-length Hsp90. As expected, complex formation was observed between Hch1 and Hsp90, indicated by a significant increase in the polarization (figure 5.7). Interestingly, the

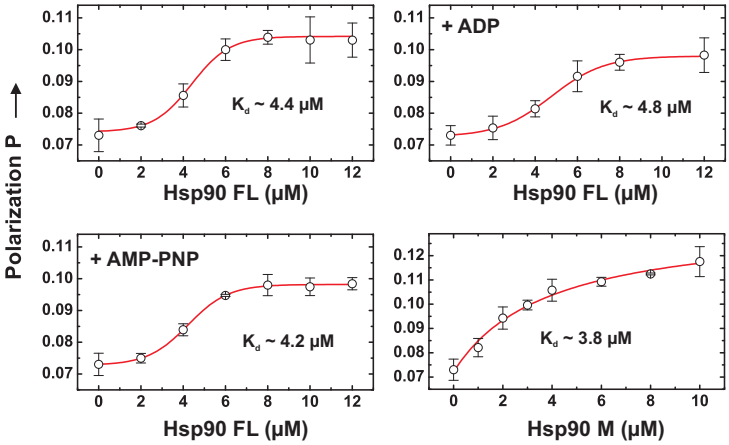

Figure 5.7: Binding between Hch1 and Hsp90 monitored by fluorescence polarization. Sigmoidal curves are observed for the binding between Hch1 and full-length (FL) Hsp90, indicating a cooperative interaction, in contrast to binding of Hsp90 M to Hch1. No major difference in the affinity of Hch1 for Hsp90 seems to exist for different nucleotides states of Hsp90. The measurements were done at 20°C in a buffer of 10 mM potassium phosphate, 2 mM $MgCl_2$, 1 mM TCEP, pH 7.5 with no nucleotide or 1 mM ADP or AMP-PNP, respectively, added. 500 nM of fluorescein labeled Hch1 was titrated with full-length Hsp90.

binding curve had a sigmoidal shape, suggesting a cooperative interaction between Hsp90 and Hch1. This clearly shows that Hch1 has influence on the structure of Hsp90. Binding of the first Hch1 molecule to the Hsp90 dimer obviously shifts the Hsp90 conformational equilibrium towards a state that is preferentially recognized by Hch1, thus allowing for easier binding of the second Hch1 molecule. Such an interaction mode cannot not be explained by a mere binding of Hch1 only to the Hsp90 M domain, as would be expected in analogy to the crystal structure between Aha1 N and Hsp90 M (PDB: 2USV) [197]. Instead, the binding data obtained here strongly argue for a second binding site for Hch1 within the Hsp90 N domain and most likely, Hch1 stabilizes the closed conformation of Hsp90. The affinity for the complex between Hsp90 and Hch1 determined from the binding curve is $K_d \sim 4.4\,\mu$M, which is in reasonable agreement with a previous work [193].

In additional experiments the nucleotide dependence of the interaction between Hch1 and Hsp90 was assessed. Neither in presence of ADP nor the non - hydrolysable ATP analogue AMP - PNP a significantly altered binding constant was observed, in both cases the K_d was again around $\sim 4\,\mu$M.

Since the sigmoidal shape of the binding isotherm argues for an involvement of the Hsp90 N domains in the interaction between Hch1 and Hsp90, the isolated N and M domains were also tested for binding to Hch1. However, for titration of Hch1 with Hsp90 N no significant complex formation could be observed, even when high concentrations of Hsp90 N (up to $100\,\mu$M) were used (data not shown). This could be due to the much lower molecular size of isolated Hsp90 N compared to the full - length Hsp90 protein, which even in case of binding to Hch1 would cause a much lower increase in the polarization. Therefore, as a control also a displacement titration was done adding increasing amounts of Hsp90 N

to a preformed complex of labeled Hch1 and full-length Hsp90. Upon significant binding of Hsp90 N to Hch1, a decrease in the polarization should be visible. But also using this indirect approach no interaction was detected (data not shown). Thus, in conclusion these results demonstrate that the binding between Hsp90 N and Hch1 must be rather weak but might nevertheless be of biological importance.

For comparison then complex formation between isolated Hsp90 M and Hch1 was monitored by fluorescence polarization (figure 5.7, lower panel, right). Here, again a significant interaction was detected and, as expected, in this case a "normal" hyperbolic binding curve was found. The affinity obtained from fitting the binding data was $K_d \sim 4\,\mu$M and therefore had a magnitude comparable to the affinity observed for binding of Hch1 to full-length Hsp90. This clearly demonstrates that the main interaction site for Hch1 on Hsp90 is the M domain.

To characterize the binding of Hch1 to the Hsp90 M and in particular to the N domain in more detail, further NMR experiments were performed. First, unlabeled Hch1 was added to the ^{15}N-labeled Hsp90 M domain and the resulting chemical shift perturbation analyzed. A strong line broadening was observed in the HSQC spectrum of Hsp90 M, indicative of complex formation, even in presence of a higher amount of salt (60 mM potassium chloride, figure 5.8, left). Many signals had intensities reduced nearly beyond detection limit whereas others remained unaffected. This argues for a highly specific interaction. At lower salt concentrations, the line broadening was so pronounced that an extraction of site specific binding information was not possible since most of the Hsp90 M signals were not visible anymore in the spectrum.

Additionally, peak shifts were observed when Hch1 was added to the Hsp90 M domain which were rather small but clustered, thus again supporting the assumption that a specific binding event was monitored. Ma-

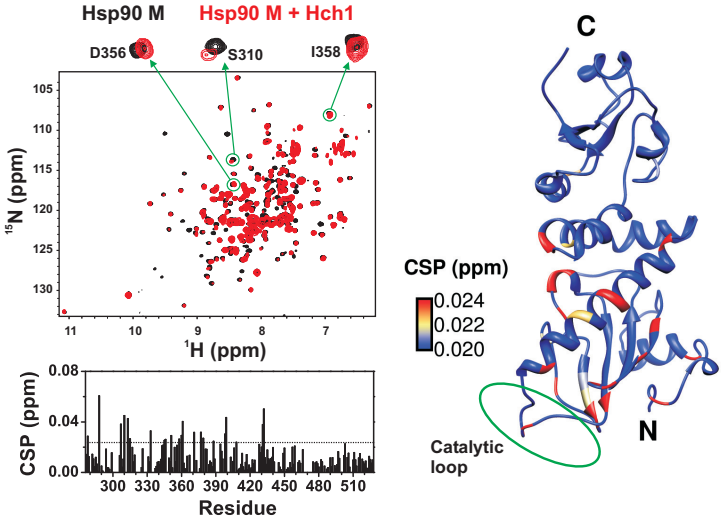

Figure 5.8: Binding between Hsp90 M and Hch1 monitored by NMR. Left, upper panel: Overlay of ^{15}N-HSQC spectra for Hsp90 M alone (black) and in presence of Hch1 (red). Strong line broadening and specific peak shifts point at complex formation. Left, lower panel: CSP plot for the binding of Hch1 to Hsp90 M. The significance level (2-fold average CSP) is indicated by a dashed line. Right: Color coded mapping of the chemical shift perturbation upon binding of Hch1 onto the crystal structure of Hsp90 M (PDB: 2CG9). The measurements were done at 298 K in a buffer of 10 mM potassium phosphate, 60 mM potassium chloride, 1 mM TCEP, pH 7.5 at 900 MHz using 200 μM of Hsp90 M. Unlabeled Hch1 was added in a $\sim$1:1 molar ratio.

jor chemical shift perturbation was visible for residues in the N-terminal part of Hsp90 M at its outer surface, involving one edge of the large β-sheet as well as the long α-helix packing against it (figure 5.8, right). The binding site of Hch1 on Hsp90 is near to the catalytic loop (residues $\sim$370 to 386) and basically identical with the binding site of the Aha1 N domain on Hsp90 as found in a crystal structure [197]. Thus, Hch1 and

Aha1 N clearly have similar interactions with Hsp90 M.

Then the binding of unlabeled Hch1 to the isolated ^{15}N - labeled Hsp90 N domain was studied. Consistent with the assumption of a weaker interaction between Hch1 and Hsp90 N compared to Hsp90 M as indicated by the results from the previous fluorescence measurements, here a higher molar excess of Hch1 ($\sim$ threefold) had to be added to obtain complex formation with Hsp90 N. Furthermore, a lower salt concentration was used in this case. However, under these conditions then a clear and highly specific binding could be observed. The peak shifts on the order of half a line width were rather small but typical for protein - protein interactions and occurred into different directions, thus arguing against buffer effects (figure 5.9, upper panel, left). Additionally, as for Hch1 binding to Hsp90 M, a highly specific broadening of individual Hsp90 N signals nearly beyond detection limit was visible whereas others remained unaffected.

The strongest chemical shift perturbation occurred for amino acids 186 to 197 constituting a helix in the very C - terminal region of Hsp90 N (figure 5.9, upper panel, right and lower panel). But also N - terminal regions in the protein were affected by binding of Hch1: amino acids 27 to 51 from the long N - terminal helix forming the wall at one side of the nucleotide binding pocket showed peak shifts in presence of Hch1 as well as amino acids 74 to 79 that are part of a strand from the β - sheet representing the bottom of the binding pocket. The site of interaction for Hch1 on Hsp90 N is consistent with a previous report analyzing the binding of Aha 1 N to Hsp90 N [198].

An evaluation of line broadening effects by comparison of internally referenced relative signal intensities of free Hsp90 and in complex with Hch1 agreed well with the shift data. Furthermore, additional to the shift data, the line broadening analysis also identified the very C - terminal residues 198 to 210 of Hsp90 N comprising the last strand from the β -

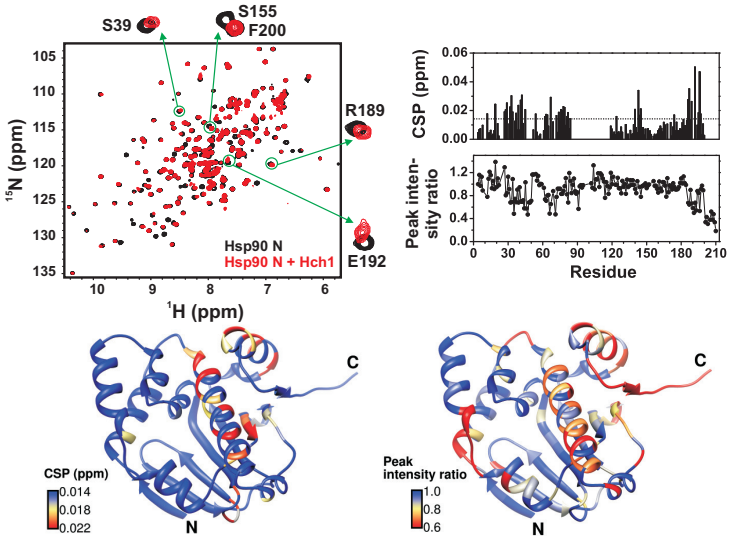

Figure 5.9: Binding between Hsp90 N and Hch1 monitored by NMR. Upper panel, left: Overlay of ^{15}N - HSQC spectra for Hsp90 N alone and in presence of Hch1. Strong line broadening and specific peak shifts point at complex formation. Upper panel, right: Plots for CSP and line broadening upon binding of Hch1 to Hsp90 N. The CSP significance level (2 - fold average CSP) is indicated by a dashed line. Line broadening is given as ratio of the relative (internally referenced) peak intensities for signals in the spectra of free Hsp90 N and in complex with Hch1. Lower panel: Color coded mapping of CSP (left) and line broadening (right) upon binding of Hch1 onto the crystal structure of Hsp90 N (PDB: 1AMW). The measurements were done at 298 K in a buffer of 10 mM potassium phosphate, 1 mM TCEP, pH 7.5 at 900 MHz using 200 μM of Hsp90 N. Unlabeled Hch1 was added in a 3 - fold molar excess.

sheet in the domain as strongly involved in the interaction with Hch1.

Mapping of the MNR binding data on a crystal structure of the Hsp90 N domain demonstrated the high specificity of the complex observed. Residues identified to potentially represent the Hch1 binding site nicely

clustered in the protein structure. In particular, the results from the line broadening analysis were very conclusive (figure 5.9, lower panel).

Although the attempts to obtain a backbone resonance assignment for Hch1 failed due to problems as outlined in section 5.2, the binding of Hsp90 N an M to ^{15}N - labeled Hch1 could also be analyzed in a more qualitative way. When unlabeled Hsp90 M was added to Hch1, a severe line broadening and peak shifts were observed in the HSQC spectrum of Hch1, consistent with a comparatively high affinity of the binding between the proteins, as expected (figure 5.10, upper panel, right).

In presence of the Hsp90 N domain, the line broadening of Hch1 signals was much less pronounced, and nearly no chemical shift perturbation was visible (5.10, upper panel, left). However, similar as in the corresponding experiments with ^{15}N - labeled Hsp90 N and unlabeled Hch1 (see figure 5.9), the line broadening seemed to be highly specific. Although no chemical shift assignment was available for Hch1, the NMR data allow for a rough localization of the Hsp90 N binding site within Hch1. The ϵ - NH side - chain signals for tryptophan residues are due to aromatic ring currents typically strongly downfield shifted in the ^{15}N - HSQC spectra, with ~ 130 ppm for nitrogen and ~ 10 ppm for proton chemical shift. Thus, they can easily be distinguished from other backbone NH signals. Hch1 contains overall three tryptophan residues, W9, W11 and W19, and in the spectrum of Hch1 in complex with Hsp90 N the corresponding ϵ - NH side - chain signals were specifically broadened (5.10, upper panel, left, inset), clearly pointing at an involvement of these amino acids in binding interactions. Therefore, the N - terminal region of Hch1 comprising residues 1 to 17 might be of particular importance for the complex formation with Hsp90 N. This is supported by the high sequence conservation of this amino acid stretch (compare figure 2.4).

A prediction of the secondary structure propensity for amino acids 1 to

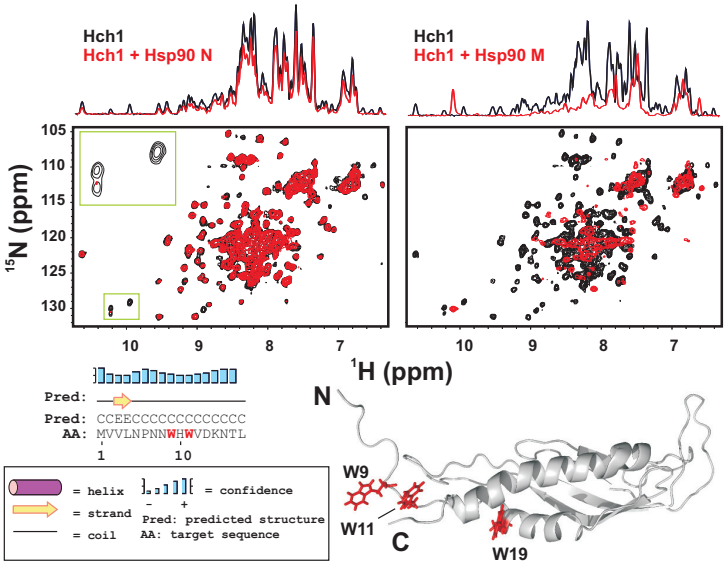

Figure 5.10: Binding between Hch1 and Hsp90 domains monitored by NMR. Upper: Overlay of ^{15}N - HSQC spectra for Hch1 alone and in presence of Hsp90 N (left) or Hsp90 M (right). Strong line broadening, in particular with Hsp90 M, and peak shifts point at complex formation. For addition of Hsp90 N, side - chain NH groups of tryptophan residues are broadened (inset in the NMR spectrum), pointing at an involvement of Hch1 N - terminal regions in the binding. On top of the plots 1D projections of the respective HSQC spectra are given. Lower panel: Secondary structure prediction for Hch1 N - terminal residues using PSIPRED (left) and homology model of Hch1 (right) highlighting the W9 and W11 residues potentially involved in Hsp90 N binding. The measurements were done at 298 K in a buffer of 10 mM potassium phosphate, 1 mM TCEP, pH 7.5 at 500 MHz using a 200 μM sample of Hch1. Unlabeled Hsp90 N and M were added in a 3:1 and 1:1 molar ratio, respectively. In case of Hsp90 M, additionally 60 mM potassium chloride was added.

17 using PSIPRED [234] revealed a slight tendency to form β - sheet structure, but overall this part of Hch1 seemed to be largely unstructured.

Indeed, in a crystal structure of Aha1 N (PDB: 2USV) the corresponding region is not resolved.

5.4 Discussion

Within the group of Hsp90 cochaperones, Hch1 is somewhat special in the respect that it is found obviously only in lower eukaryotes like the yeasts *Saccharomyces cerevisae* and *Candida albicans*[193] whereas most other cochaperones are highly conserved throughout different species. Most strikingly, in *Saccharomyces cerevisae* Hch1 is found together with its homologue Aha1 at the same time, which raises the question about the extent of functional overlap between both proteins. Hch1 shares a high sequence identity with the N-terminal domain of Aha1 (compare figure 2.4), suggesting related structures and function. Indeed, biochemical studies demonstrated an ATPase stimulating effect of Hch1 on Hsp90 comparable to that of the Aha1 N fragment[193]. So far and in contrast to Aha1, Hch1 has structurally not yet been characterized in more detail, despite the availability of some biochemical data for this protein. Therefore, one aim of this work was to assess this issue by *in vitro* methods which could potentially reveal differences in the mode of action between Aha1 and Hch1.

Given the high similarity between Aha1 N and Hch1, the unfavorable behavior of Hch1 in contrast to Aha1 N found here when expressed recombinantly in bacterial cells or under NMR conditions is surprising. As the application of homology modeling showed, largely different surface properties that could explain the inherent instability of Hch1 compared to Aha1 N do not exist. Potentially, posttranslational modifications of Hch1 not available in bacterial host organisms contribute to the *in vivo* stability of Hch1 in yeast cells. In particular, Hch1 contains a significantly higher number of threonine residues compared to Aha1 N (eight versus three) that might be involved in phosphorylation.

The fluorescence binding studies with Hsp90 and Hch1 could clearly

demonstrate a cooperative binding mechanism for the interaction between thee two proteins that has not been described so far. This indicates that Hch1 has influence on the Hsp90 conformational state and likely shifts its equilibrium towards the closed form that is capable of ATP hydrolysis [52]. Together with other cochaperones like Sba1/p23, Hch1 seems to be highly specific for a particular conformation of Hsp90, which is a prerequisite for a well-defined regulation of Hsp90 during its chaperone cycle.

Although a crystal structure (PDB: 2USV) identified the Hsp90 M domain as binding site for Aha1 N [197], suggesting that also Hch1 should bind there, the cooperativity observed here for the Hch1-Hsp90 complex formation pointed at an additional involvement of the Hsp90 N domain in binding contacts. Indeed, basically full binding affinity could be observed when only the isolated Hsp90 M domain was titrated to Hch1, confirming that this fragment of Hsp90 provides the major binding site and indicating similar mechanisms in the Hsp90 ATPase simulation by Hch1 and Aha1. However, an interaction of Hch1 only with Hsp90 M could not explain the cooperative binding mode observed for full-length Hsp90 and Hch1.

The affinity determined here for the Hsp90-Hch1 complex using fluorescence polarization experiments was around $K_d \sim 4\,\mu$M and therefore slightly lower than previously reported for the Aha1 N-Hsp90 complex ($1.75\,\mu$M) [197]. This might explain the lower Hsp90 ATPase stimulation observed for Hch1 compared to Aha1 N [193]. With the Hsp90 N domain, no detectable interaction was found, thus the binding of Hch1 to this domain seems to be rather weak.

The NMR measurements then could indeed confirm the previous fluorescence affinity data. A major binding of Hch1 was observed with the Hsp90 M domain, and the interaction site was similar to Aha1 N binding to Hsp90 M [197]. However, the NMR data furthermore clearly demon-

strated a significant complex formation between Hch1 and the Hsp90 N domain, explaining the cooperative interaction mode of Hch1 and Hsp90. Consistent with the results from the fluorescence binding assays, the complex of Hch1 with Hsp90 N was weaker than with Hsp90 M since higher concentrations of the unlabeled part had to be added in the NMR experiments to observe shifts and line broadening. Nevertheless, considering the high specificity found, this interaction can be regarded as biologically important.

Within Hsp90 N, it was clearly one side of the nucleotide binding pocket that was involved in binding of Hch1. For Hch1 the NMR data strongly pointed at its N-terminal region comprising the presumably unfolded residues 1 to 17 mediating the interaction with Hsp90 N. Indeed, the N-termini of Hch1 and Aha1 N seem to be highly conserved (figure 2.4), thus it can be assumed that the corresponding residues of Aha1 N have a similar role in Hsp90 N binding. Previously, it was reported that a deletion of the respective residues in Aha1 had basically no influence on its Hsp90 ATPase stimulating effect[197]. However, in this case the deletion was introduced in the full-length Aha1 molecule with its C-terminal domain present, which essentially contributes to the maximum ATPase stimulation of Hsp90 by Aha1[193,198]. This might explain the only minor effect observed here. Likely, a lack of the N-terminus in the background of the isolated Aha1 N domain would have caused a more pronounced impact on the Hsp90 ATPase stimulation.

Overall, the data obtained in this work suggest that the Hsp90 ATPase acceleration by Hch1 is not only due to a conformational rearrangement of the catalytic loop within the Hsp90 M domain, as found in the analysis of a crystal structure for Hsp90 M in complex with Aha1 N[197]. Additionally, a shifting of the Hsp90 conformational equilibrium towards its closed state capable of ATP hydrolysis by second site interactions with the N do-

main seems to importantly contribute to the Hsp90 activation process, in agreement with the proposed Hsp90 activation mechanism for Aha1 [198].

Using the crystal structure of Hsp90 in its closed conformation (PDB: 2CG9) and the crystal structure of the Hsp90 M - Aha1 N complex (PDB: 2USV) as templates, a model for the binding between Hch1 and Hsp90 was built here. From this complex it can be seen that the important Hch1 N - terminal region is in close proximity to both of the Hsp90 N domains (figure 5.11). However, considering the contact region for Hch1 within Hsp90 N as found by NMR (α - helix 7 and β - strand 8), it is obvious that only the N' domain from the other Hsp90 protomer would be within reach to allow for an interaction between the identified Hsp90 N domain binding site residues and the Hch1 N - terminus. Thus, most likely, Hch1 targets the trans Hsp90 N' domain for complex formation. Although speculative, in principle it seems possible that the Hch1 N - terminal residues could due to their extended nature undergo intermolecular β - strand contacts with the β - strand 8 from the Hsp90 N' domain, potentially explaining the significant binding observed between Hch1 and the isolated Hsp90 N domain.

In summary, the results here indicate very similar Hsp90 stimulation mechanisms for Hch1 and Aha1 N, thus the reason for the simultaneous existence of Hch1 and Aha1 in yeast cells remains unclear. Different regulation or interaction with Hsp90 for Hch1 and Aha1 *in vivo* not detectable by *in vitro* studies might play a role. Notably, initially Hch1 and Aha1 were identified during a screen for proteins that could suppress the temperature sensitive growth phenotypes of certain Hsp90 mutants [192]. In this screen, only Hch1 was found to effectively suppress cellular growth defects but not Aha1. This supports the assumption of to some extent different *in vivo* functions for Hch1 and Aha1, despite the obviously very similar mechanism by which the two proteins act on Hsp90.

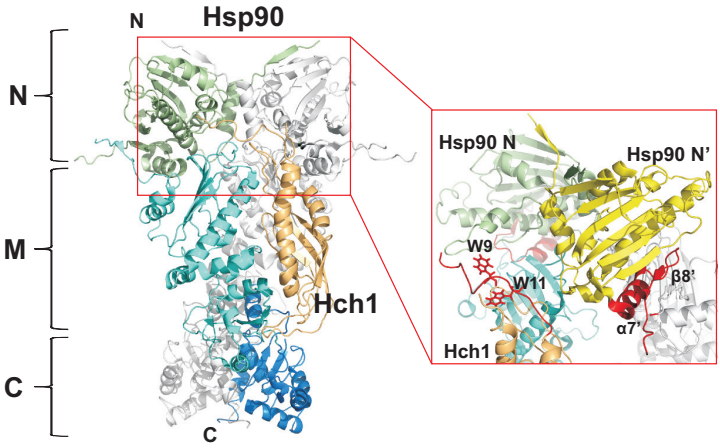

Figure 5.11: Modeling of the Hsp90-Hch1 complex. Left: Using crystal structures of full-length Hsp90 (PDB: 2CG9) and the complex between Hsp90 M and Aha1 N (PDB: 1USV) as templates, a model for the Hsp90-Hch1 complex was built. The N- and C-terminus of Hch1 are oriented towards the N domain of Hsp90. Right: Details of the complex between Hch1 and Hsp90. The N-terminus of Hch1 involved in binding of the Hsp90 N domain is highlighted in red as well as the main binding site of Hch1 on Hsp90 N. The two trypthophan residues W9 and W11 of Hch1 experiencing line broadening in complex with Hsp90 N (compare figure 5.10) are shown in stick representation. In the closed complex of Hsp90, the Hch1 N-terminal region is in proximity to both N domains of the Hsp90 dimer. However, Hch1 mediated Hsp90 ATPase stimulation is likely achieved by binding of the trans Hsp90 N' domain as only the important β-strand 8' and helix $\alpha 7$' of this domain are within reach to be contacted by the Hch1 N-terminal region.

Chapter 6

The Hsp90 Cochaperone Sba1

6.1 Initial Structural Characterization of Sba1 Variants

As outlined under section 2.3, the Hsp90 cochaperone Sba1 consists of two domains. The N-terminal part of the protein adopts a typical β-sandwich structure that is related to the structure of the small heat shock proteins and overall resembles the immunoglobulin fold [52,217]. Its C-terminal domain, in contrast, was shown to be unstructured [216]. The lack of a preferred secondary structure in general largely hampers a crystallographic analysis of this region in Sba1. However, NMR is a method well suited to obtain information also on such unfolded elements in proteins. Therefore, Sba1 was characterized in more detail here by NMR, in particular with respect to possible functions of its C-terminal region.

Initial constructs for the expression of wild-type Sba1 and a Sba1Δ69 construct lacking 69 residues from its unfolded C-terminus were obtained from Dr. Martin Hessling (Lehrstuhl für Biotechnologie, TUM).

Both variants expressed well and solubly in *E. coli* and could be obtained with yields up to 40 mg of protein per liter of cell culture, even in M9 minimal medium required for NMR isotope labeling. In agreement with the presence of a large unfolded region, wild-type Sba1 was strongly prone to proteolytic degradation during the purification, different to the Sba1Δ69 mutant, and required additional purification steps to obtain a homogeneous protein sample (section 9.12).

An initial CD spectroscopic characterization showed well folded proteins with β-sheet structure with a typical minimum at $\sim$218 nm (figure 6.1). However, as expected, wild-type Sba1 had a higher relative content of random coil structure, indicated by a significantly lower minimum around 200 nm. Both variants were reasonably stable against thermal unfolding and thus in principle well suited for NMR spectroscopy. In contrast to wild-type Sba1, the Sba1Δ69 mutant did not unfold reversibly. The CD spectrum recorded after the unfolding transition clearly showed a protein lacking secondary structure whereas wild-type Sba1 was nearly similarly well structured as before the transition. Thus, the C-terminal unfolded domain seems to confer structural stability to Sba1. Nevertheless, the midpoint of the thermal unfolding curve for Sba1Δ69 was $\sim$63°C and therefore also pointed at a protein with comparably high resistance to temperature induced melting.

For wild-type Sba1 and the Sba1Δ69 mutant then 2D NMR spectra were recorded on ^{15}N-labeled samples (figure 6.2). As expected, for both Sba1 constructs the signal dispersion in the respective HSQC was high, indicating folded proteins and β-sheet content, in agreement with the CD data. However, in the case of wild-type Sba1, the region between 7.5 and 8.5 ppm proton chemical shift in the spectrum showed a substantial signal overlap, pointing at a higher random coil content in the protein. For the Sba1Δ69 variant the signal overlap was much less pronounced,

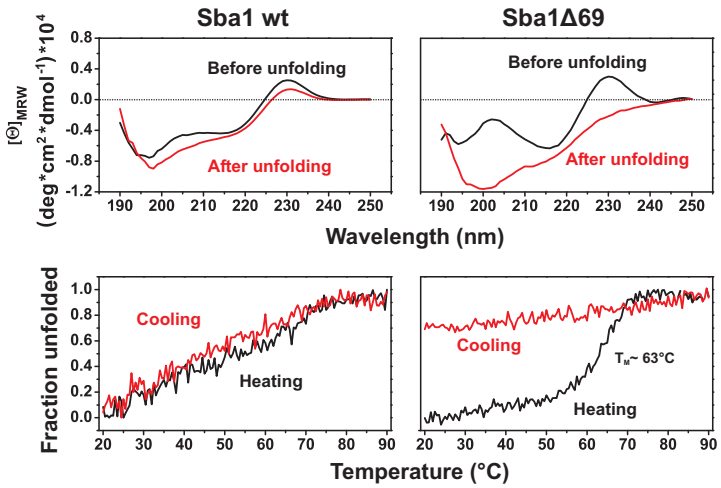

Figure 6.1: CD spectra and thermal stabilities of wild-type Sba1 (left) and Sba1Δ69 (right). Upper panel: CD spectra before and after thermal unfolding transitions recorded at 20°C. In contrast to wild-type Sba1, the deletion mutant Sba1Δ69 remains unfolded after heat denaturation. Lower panel: Thermally induced unfolding of the Sba1 variants monitored by CD spectroscopy at a wavelength of 218 nm. The deletion of the unfolded C-terminal domain as in the Sba1Δ69 mutant renders the protein less temperature stable as indicated by irreversible unfolding. The proteins were measured in a buffer of 40 mM potassium phosphate, 1 mM TCEP, pH 7.5 using 10 μM concentrated samples.

confirming the unfolded nature of the Sba1 C-terminal domain.

Despite the to a large extent presumable lack of a preferred secondary structure within the Sba1 C-terminal region as indicated by the NMR data, a certain structure content for this part of the protein cannot be ruled out completely. Repetitive sequence elements with concomitant chemical shift degeneracy and additionally a low number of aromatic residues (only two phenylalanine) that would contribute to a higher sig-

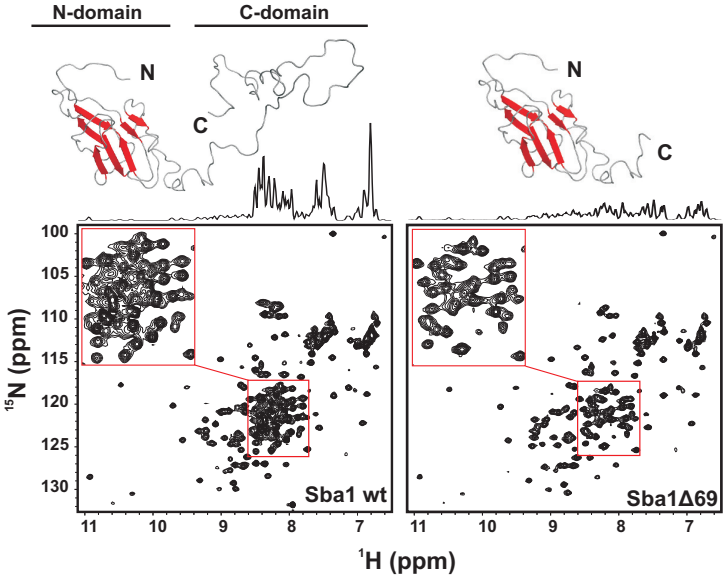

Figure 6.2: ^{15}N-HSQC spectra of wild-type Sba1 (left) and Sba1Δ69 (right). Upper panel: Structure models of wild-type Sba1 and Sba1Δ69 obtained with Xplor-NIH using NOEs back-calculated from a crystal structure (PDB: 2CG9) and rebuilding the unfolded C domain. Lower panel: A comparison of the ^{15}N-HSQC spectra for wild-type Sba1 and Sba1Δ69 indicates that the C domain is largely unfolded in solution. 1D projections of the respective 2D spectra are given on top of the plots. 200 μM concentrated Sba1 variants were measured in a buffer of 40 mM potassium phosphate, 1 mM TCEP, pH 7.5 at 303 K and 600 MHz .

nal dispersion render the NMR spectra of the Sba1 C-tail inherently rather overlapped. Thus, the existence of small secondary structure elements in this region of the protein might well be overlooked by only judging the signal dispersion of the 2D spectra. Furthermore, unfavorable dynamics might by exchange processes cause some potentially structured

parts of the Sba1 C domain to be invisible in the 2D HSQC spectrum.

6.2 Structure Propensity of the Sba1 C Domain

Although the initial CD and NMR data indicated the Sba1 C-terminal region – at least to a larger extent – as being devoid of secondary structure, a folding of the respective residues under certain conditions seems possible. Examples of natively unfolded proteins that can adopt structure have been described with Hsp12 that forms α-helices upon contact with membranes[317] or α-synuclein that likewise undergoes helix formation in presence of acidic phospholipids[248]. To test whether this might also apply for Sba1, the effect of different buffer conditions and additives on its structure content was analyzed here.

Indeed, interestingly a secondary structure prediction using the program PSIPRED[234] suggested a propensity of the Sba1 C domain to form helices with a higher confidence (figure 6.3, left). Overall, five rather short helices were identified, only the presumable helix 4 is significantly longer comprising 11 amino acids according to the prediction.

Assuming a membrane binding function for the helices in the Sba1 C-terminal region in analogy to other proteins like Hsp12, as mentioned, would require an amphiphilic character of the structure elements. Therefore, all helices identified were subjected a further helical wheel analysis to estimate their membrane binding potential (figure 6.3, right). The theoretical helices 1 and in particular 5 appear to be highly charged with a predominant content of acidic residues D and E. The predicted short helix 2 with only four residues would comprise only one helix turn, however, with a hydrophilic and a rather hydrophobic side. Helices 3 and especially 4, in contrast, seem to have indeed a more pronounced amphiphatic character. Within helix 3, two methionine and an in principle membrane compatible phenylalanine cluster at one side of the helix. In case of helix 4, three leucine and a methionine residue form a hydrophobic face suited

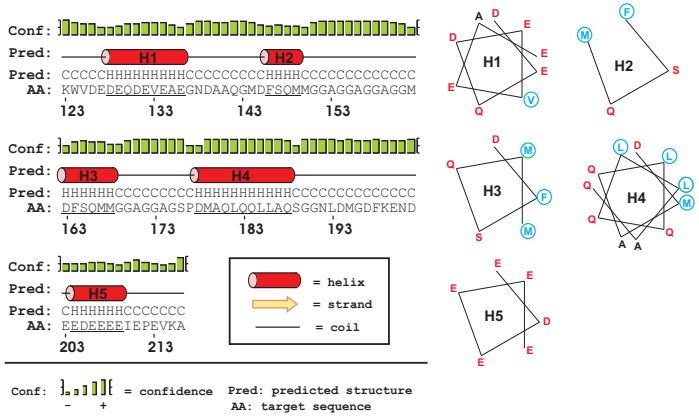

Figure 6.3: Secondary structure prediction for the Sba1 C domain (left) and helical wheel analysis for potential α-helices (right). Left: A secondary structure prediction for residues 123 to 216 of Sba1 using PSIPRED [234] indicates helical propensity with comparatively high confidence. Right: Helical wheel analysis for the 5 potential helices predicted by PSIPRED. Red color highlights charged/hydrophilic and blue color hydrophobic residues. H3 and H4 appear to have more pronounced amphipathic character and might be involved in membrane interaction.

for membrane interactions.

To assess the predicted propensity of the Sba1 C-terminal region for adopting helical structure, CD titrations of the protein were done with TFE that is commonly known to induce/stabilize helices in peptides and proteins [266–270]. Indeed, a significant change in the CD spectra of wild-type Sba1 was observed when TFE was added to the protein (figure 6.4, right). A pronounced minimum at a wavelength of 208 nm typical for α-helical secondary structure evolved with increasing amount of TFE. At a content of $\sim$ 40 % TFE, the structural change process seemed to be saturated with no further gain in ellipticity at 208 nm.

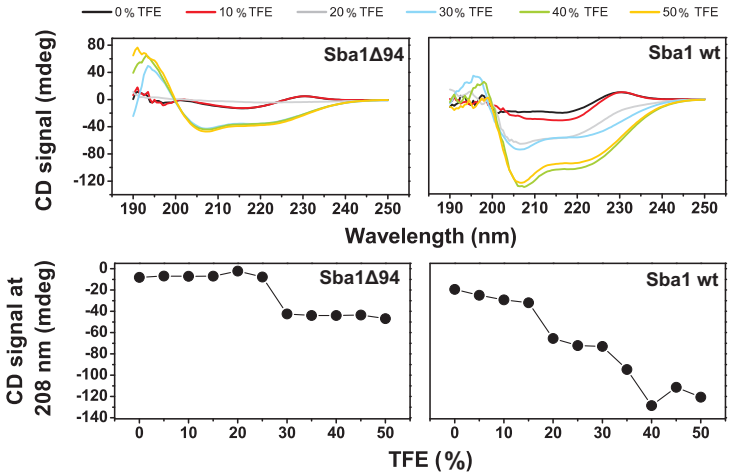

Figure 6.4: Effect of TFE on the structure of Sba1 monitored by CD spectroscopy. Upper panel: CD spectra of Sba1Δ94 (left) and wild-type (wt) Sba1 (right) recorded at different TFE concentration. A significant structure change can be observed from β-sheet to helical structure with increasing amount of TFE, however, clearly more pronounced for wild-type Sba1. Lower panel: Plot of the CD signal at 208 nm (indicative of helix structure) against TFE concentration. For Sba1Δ94 a structure transition seems to occur between 20 and 30 % TFE. Proteins were measured in a buffer of 40 mM potassium phosphate, 1 mM TCEP, pH 7.5 using 10 μM concentrated samples at 20°C.

For comparison, a Sba1Δ94 variant that will be described in section 6.3 and lacks the complete unfolded C-terminal region of Sba1 was likewise titrated with TFE (figure 6.4, left). Also in this case a significant change in the CD spectrum of the protein was found with a minimum evolving at 208 nm. This might indicate that even in the folded part of Sba1 some (potentially unstructured) regions exists capable of adopting helical conformation. However, in contrast to wild-type Sba1, the gain in structure

was much lower and saturated already at ~ 30 % TFE.

A plot of the CD signal at 208 nm versus the TFE content for both Sba1 variants tested showed that for Sba1Δ94 an apparently cooperative structural change occurs between 20 and 30 % TFE. For wild - type Sba1 this process does either not exist or is potentially underlying the dominating structural change of the C - terminal region. Here, the dependence of the CD signal on the TFE content is rather linear. Overall, these data clearly demonstrate the ability of the Sba1 C domain to adopt helical structure in agreement with the previous secondary structure prediction.

The effect of TFE on the Sba1 C - terminal domain was also monitored by NMR. At a higher concentration of TFE around 20 %, signals in the middle of the HSQC spectrum corresponding to residues from the unfolded region were sharper and also side - chain NH signals between ^{15}N 110 to 115 ppm and ^{1}H 6.5 to 7.5 ppm were better resolved, which might point at a potential gain of structure (figure 6.5).

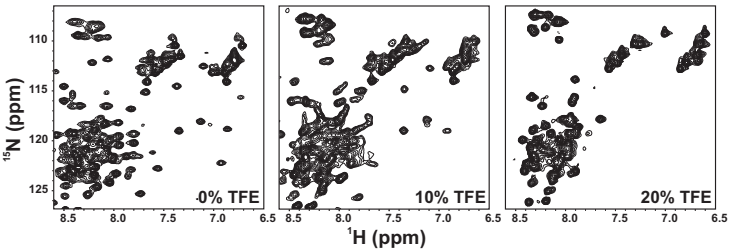

Figure 6.5: Effect of TFE on the structure of Sba1 monitored by NMR. ^{15}N - HSQC spectra of wild - type Sba1 were recorded at different TFE concentrations. Signals of unfolded residues in the middle region of the Sba1 spectrum and side - chain resonances are affected at higher concentration of TFE and might indicate a partial gain in secondary structure within the Sba1 C domain. 200 μM of Sba1 was measured in a buffer of 40 mM potassium phosphate, 1 mM TCEP, pH 7.5 at 303 K and 600 MHz.

For testing a potential membrane binding ability, Sba1 was titrated with SDS. Interestingly, also the detergent had a strong effect on the CD spectrum of Sba1 and again a minimum around 208 nm typical for helical secondary structure was induced in a concentration dependent manner (figure 6.6, left). This observation might point at a folding into heli-

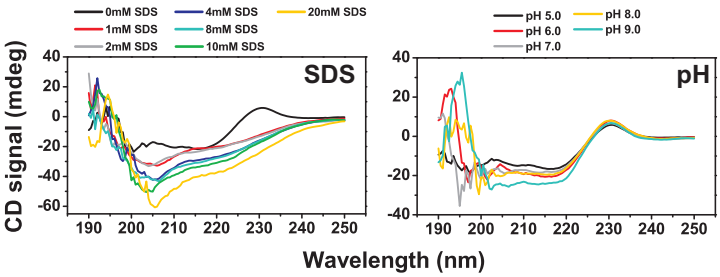

Figure 6.6: Effect of SDS and pH on the structure of Sba1 monitored by CD. Left: CD spectra of Sba1 wild-type recorded at different concentration of SDS. A significant structure change can be observed with increasing amount of SDS. Right: CD spectra of Sba1 wild-type recorded at different pH. The pH does not seem to have a major influence on the Sba1 structure between 5.0 and 8.0. 10 μM of Sba1 was measured in a buffer of 40 mM potassium phosphate, 1 mM TCEP, pH 7.5 at 20°C.

cal structure of the Sba1 C-terminal region upon interaction with lipids. Performing control titration with the shorter Sba1Δ94 variant lacking the unfolded residues (see above and section 6.3) failed due to instability of the protein in presence of SDS.

Finally, also the effect of the buffer pH on the structure content in Sba1 was assessed (figure 6.6, right). However, no particular gain or loss of structure in Sba1 was observed in a pH range between 5.0 and 9.0, despite some slight differences in the respective CD spectra. Thus, the pH does obviously not have a major impact on the folding state of Sba1.

6.3 NMR Backbone Assignment of the Sba1 N Domain

For a further study of its interaction with Hsp90 using NMR, a backbone resonance assignment had to be obtained for Sba1. To this end, only the N-terminal domain of Sba1 should be used since its C-terminal domain would to a larger extent be anyway unstructured under normal buffer conditions, likely rendering an assignment for this region in the protein impossible (see section 6.1 and 6.2). In initial attempts therefore the Sba1Δ69 variant was measured. However, it turned out that the quality of the triple resonance spectra for this construct was partially rather poor, hampering the assignment process. In particular, for the C-terminal part of the protein (residues $\sim$ 110 to 147) a reliable assignment was not possible due to chemical shift degeneracy and a lack of connectivity, potentially caused by unfavorable dynamics. Overall, it appeared that a larger portion of the C-terminus even in the Sba1Δ69 protein was unstructured and rather flexible.

Therefore, it seemed reasonable to further optimize the domain boundaries before proceeding with the assignment. Using information from the crystal structure of Sba1 in complex with Hsp90 (PDB: 2CG9), a new Sba1 construct, Sba1Δ94, was designed that should comprise only the folded part of the protein. The C-terminal shortening of Sba1Δ94 by another 25 amino acids compared to Sba1Δ69 had a marked impact on the CD and NMR spectral quality. Figure 6.7 shows the CD spectra for wild-type Sba1, Sba1Δ69 and Sba1Δ94. Clearly, the relative structure content of Sba1Δ94 was significantly increased compared to Sba1Δ69, whereas the thermal unfolding midpoint in contrast was not dramatically reduced (61 vs. 63°C). Therefore, the Sba1Δ94 construct appeared to be still well suited for NMR studies.

Using a $^{15}N/^{13}C$-labeled sample of Sba1Δ94 with additional partial

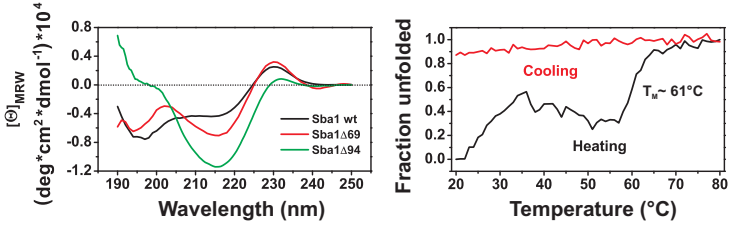

Figure 6.7: CD characterization of the Sba1Δ94 variant. Left: CD spectrum of the Sba1Δ94 variant at 20°C compared to the spectra of Sba1Δ69 and wild-type Sba1. Sba1Δ94 has a much higher relative secondary structure content. Left: Thermally induced unfolding of Sba1Δ94. The temperature stability is not significantly reduced compared to Sba1Δ69 (see figure 6.1). The proteins were measured in a buffer of 40 mM potassium phosphate, 1 mM TCEP, pH 7.5 using 10 μM concentrated samples.

deuteration (~ 50 %), a set of triple resonance specta was recored including HNCO, HN(CA)CO, HNCA, HN(CO)CA, HNCACB and HN(CO)CACB. Compared to Sba1Δ69, the NMR spectral quality in the 3D experiments was strongly improved, the deletion of 25 presumably unfolded residues had obviously favorable impact on the hydrodynamic behavior and the relaxation properties of the protein. Therefore, now it was possible to obtain a reliable assignment of backbone resonances for the Sba1Δ94 variant.

Overall, the NH backbone signals for 85 % of all non-proline residues could be assigned. For the remaining residues an assignment could not be obtained since the respective NH signals were missing in the 2D HSQC spectrum or no connectivities were found in the triple resonance spectra. This applied in particular for I28 to V30 and a larger region at the C-terminal end of the construct, R106 to T119. Most likely, these residues of the protein had unfavorable dynamics and were not part of regular secondary structure elements. The HSQC spectrum of Sba1Δ94 with res-

onance assignment is shown in figure 6.8, the chemial shifts can be found in table 11.6.

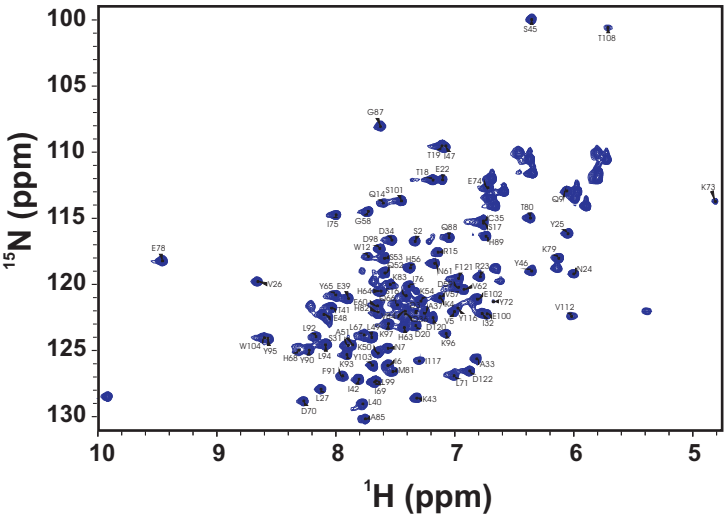

Figure 6.8: ^{15}N-HSQC spectrum of Sba1Δ94 with backbone assignment. Backbone NH signals for about 85 % of the non-proline residues could be assigned. For the remaining residues an assignment was hampered by exchange processes. The assignment was obtained at 600 MHz at 303 K in a buffer of 40 mM potassium phosphate, 1 mM TCEP, pH 7.5 using a 1.3 mM concentrated sample of Sba1Δ94.

The assigned chemical shifts could be used for a prediction of the secondary structure elements of the protein in solution. Evaluating Cα, Cβ and CO carbon shifts by the chemical shift index method [272] indicated an all β-sheet fold with overall seven strands (figure 6.9, upper panel). As mentioned, for the C-terminal region of Sba1Δ94 a secondary structure prediction was partially not possible due to missing shift information. A plot of the difference in secondary chemical shifts, $\Delta\delta$Cα - $\Delta\delta$Cβ, yielded

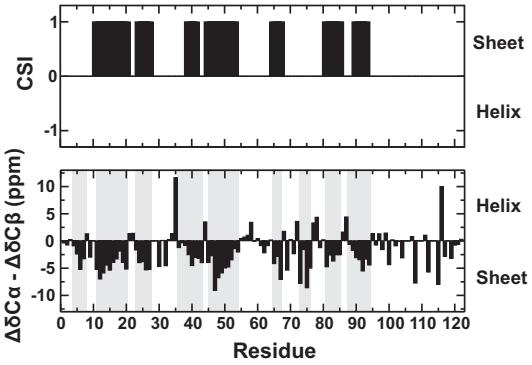

Figure 6.9: Secondary structure content of the Sba1Δ94 variant in solution. Upper panel: Evaluation of Cα, Cβ and CO carbon shifts by the chemical shift index method [272]. The plot shows the consensus prediction of the individual nuclei. Lower panel: Plot of the difference in secondary chemical shifts of Cα and Cβ. Both methods give a comparable prediction of secondary structure elements in Sba1Δ94.

an overall comparable result, despite some slight differences. Thus, the protein seemed to be well folded in solution and likely no major structure elements had been deleted in the truncation variants Sba1Δ69 and Sba1Δ94.

6.4 Model Building for the Sba1 N Domain in Solution

So far only a crystal structure of Sba1 in complex with Hsp90 in its closed conformation is available (PDB: 2CG9) [52]. To analyze whether a conformational flexibility exists and the protein potentially has a different structure in its unbound state, a model was built for Sba1Δ94 using chemical shift information, NH residual dipolar couplings and backbone coupling constants. The chemical shifts for Cα, Hα, Cβ and CO of the Sba1 N-terminal domain were analyzed with TALOS [318] to predict the backbone conformation of the protein. The Φ and Ψ angles obtained were well consistent with β-sheet structure (figure 6.10, upper panel).

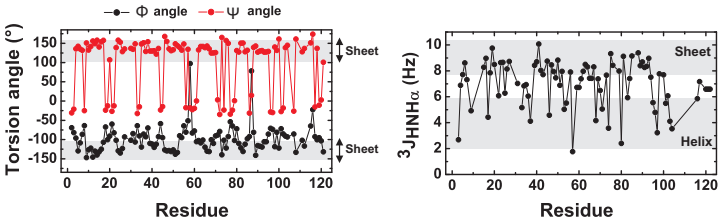

Figure 6.10: TALOS torsion angle prediction (left) and $^3J_{HNH\alpha}$ coupling constants (right) of the Sba1 N domain. Chemical shifts for Cα, Hα, Cβ and CO were analyzed with TALOS [318] and used for predicting Φ and Ψ torsion angles. Additionally, $^3J_{HNH\alpha}$ coupling constants were determined from an HNHA experiment. As expected, consistently high β-sheet content is indicated by the data for the Sba1 N domain.

Additionally, $^3J_{HNH\alpha}$ coupling constants were determined from a HNHA experiment, allowing for a determination of the backbone Φ-angle. The coupling constants observed were mostly between 8 and 10 Hz, pointing at sheet structure, or between 6 and 8 Hz, indicative of random coil.

To assess the similarity of the Sba1 structure in complex with Hsp90

as determined from crystallographic data [52] to the Sba1 structure in its unbound form and in solution, a set of NH RDCs was measured for Sba1Δ94. Using Pf1 phages as alignment medium [274], couplings between ∼ - 40 to + 40 Hz could be obtained by recording in - phase/antiphase J - coupled spectra [275] on a reference sample without alignment medium and on an aligned sample (figure 6.11). The parameters of the

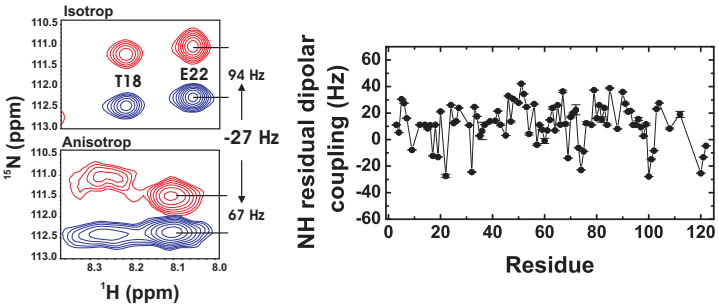

Figure 6.11: NH RDCs of the Sba1 N domain. Left: Individual upfield (red) and downfield (blue) components of the signal for residue E22 for the sample without alignment (isotropic case, upper panel) and with partial alignment (anisotropic case, lower panel) obtained by measuring in - phase/antiphase J - coupled spectra [275]. The dipolar coupling for E22 is - 27 Hz. Right: NH RDCs between ∼ 40 Hz and - 40 Hz could be measured for Sba1Δ94.

alignment tensor for Sba1Δ94 in Pf1 phage medium are summarized in table 6.1.

The information from the TALOS analysis, the $^{3}J_{HNH\alpha}$ coupling constants and most of the NH residual dipolar couplings could then be included in structure calculations with Xplor - NIH [233] to build a model of the Sba1 N domain in solution. To this end, NOEs were back - calculated from the Sba1 crystal structure (PDB: 2CG9) [52] and used as restraints to obtain an initial Sba1 template. In further refinement steps then the ex-

perimental data as mentioned were applied as additional restraints. This led to a model structure of the folded Sba1 N domain in solution and in its free state, as shown in figure 6.12. Clearly, the correlation of the experi-

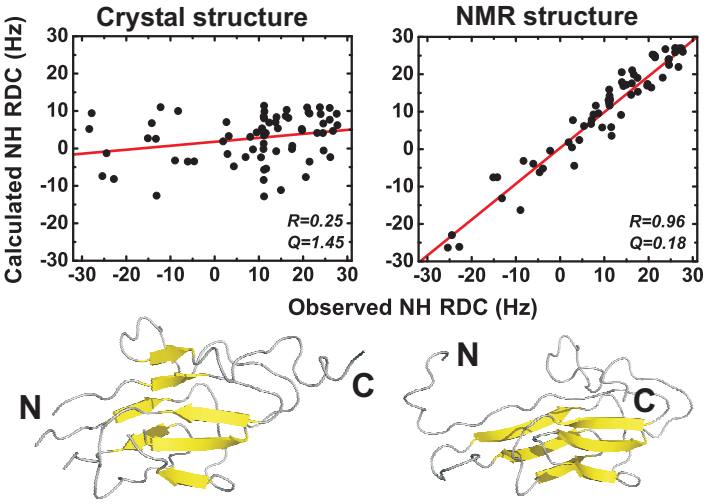

Figure 6.12: Correlation of calculated and measured RDCs for the crystal structure (left) and an NMR model (right) of the Sba1 N domain. Upper panel: Plots for the correlation of NH RDCs back - calculated from a Sba1 crystal structure (PDB: 2CG9) or an NMR model structure with experimentally observed couplings. The NMR structure has a significantly better correlation coefficient R. Lower panel: Comparison of the Sba1 structure as found in a crystal in complex with Hsp90 (left, PDB: 2CG9) with a Sba1 N domain model structure in solution as obtained by NMR data.

mentally determined NH RDCs with the couplings back - calculated from the Sba1 crystal structure is significantly worse than the correlation with the couplings back - calculated from the NMR data derived model (figure 6.12, upper panel). The correlation coefficient R is much lower for the

crystal structure than for the NMR model (0.25 vs.0.96). This indicates that Sba1 obviously undergoes some moderate conformational changes upon binding to Hsp90, consistent with previous speculations [319].

A comparison of the NMR model and the crystal structure gave an overall RMSD of ~ 1.0 Å (figure 6.13, left). Some parts of the protein were

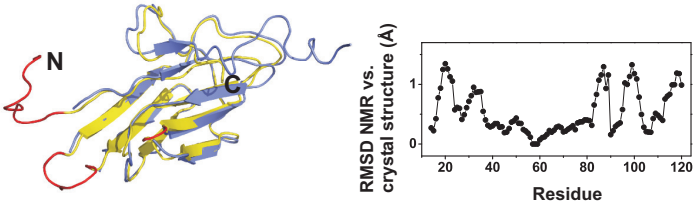

Figure 6.13: Comparison of the crystal structure and the NMR model for the Sba1 N domain. Left: Overlay of the Sba1 structure as found in complex with Hsp90 from crystallographic data (blue, PDB: 2CG9) with the NMR data derived model (yellow). Parts of the protein not resolved in the crystal and rebuilt with Xplor - NIH are colored red. Right: Positional backbone RMSD for comparing the Sba1 crystal structure and the NMR model. Especially for a region comprising residues ~ 20 to 40 and for the C - terminal part of the protein larger differences are found.

rebuilt in the structure calculations with Xplor - NIH [233] as they were not resolved in the crystal. In particular, for a region comprising residues ~ 20 to 40 and for the C - terminal part of the protein larger differences were found between the NMR model and the crystal structure of Sba1, likely pointing at some conformational rearrangements here upon complex formation with Hsp90.

Table 6.1: Parameters of the alignment tensor for Sba1Δ94 in Pf1 phage medium as determined by using the PALES software [276]. RDCs were back-calculated from the NMR model structure and compared to the experimentally determined RDCs. The linear correlation coefficient R can have values between -1 (no correlation) and +1 (perfect correlation). Partial alignment of Sba1Δ94 was obtained by adding Pf1 phages in a final concentration of 12 mg/ml to the buffer (40 mM potassium phosphate, 1 mM TCEP, pH 7.5). Measurements were done at 750 MHz and 298 K.

Parameter	**Value**
Rhombicity	0.64
Da (HN) (Hz)	-12.79
Correlation R	0.96
Q Saupe	0.18

6.5 Fast Backbone Dynamics of the Sba1 N Domain

With a resonance assignment available (section 6.3), the backbone mobility in the Sba1 N domain could be analyzed. A measurement of the $\{^1H\}$ - ^{15}N heteronuclear NOE (hetNOE) was carried out which reports on fast molecular movements on the ns - to ps - timescale (figure 6.14). As

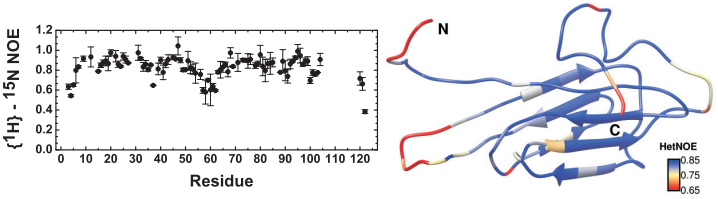

Figure 6.14: Fast backbone dynamics of the Sba1 N domain determined by measurement of the $\{^1H\}$ - ^{15}N NOE. In particular, the loop region (residues ~ 53 to 63) as well as the termini show increased backbone mobility. The measurement was done at 750 MHz and 303 K in a buffer of 40 mM potassium phosphate, 1 mM TCEP, pH 7.5 using a 1.0 mM concentrated sample of Sba1Δ94.

expected, the N - and C - termini of the protein had increased backbone mobility, indicated by lower NOE values below ~ 0.7. Within the well structured β - sheet, most residues displayed comparatively high rigidity.

A significantly increased mobility was found for a loop region comprising residues ~ 55 to 65 connecting two β - strands. Consistently, this part of the protein was not resolved in the crystal structure (PDB: 2CG9) of the protein.

6.6 Complex Formation of Sba1 and Hsp90

Sba1 was shown previously to interact with Hsp90 in a highly specific manner by recognizing and stabilizing its nucleotide bound closed conformation [52,84,85,211,217,320–322]. To analyze whether the C-terminal region of Sba1 has any influence on complex formation with Hsp90, further binding studies were carried out here using fluorescence based assays and NMR.

Wild-type Sba1 as well as the two truncation mutants Sba1Δ69 and Sba1Δ94 were labeled with fluorescein and titrated with Hsp90 to assess whether the unfolded C-domain of Sba1 contributes to its affinity for Hsp90. In the absence of nucleotide, no detectable interaction could be observed between the Sba1 variants tested and Hsp90 (data not shown). However, when the non-hydrolysable ATP analogue AMP-PNP was added, all Sba1 constructs bound Hsp90, as expected (figure 6.15).

The binding isotherms had all sigmoidal shape, clearly indicating a cooperative binding mode. This shows that Sba1 preferentially interacts with a specific structural state of Hsp90 and is able to shift its conformational equilibrium towards this state. Fitting the data yielded an affinity of $K_d \sim 0.6\,\mu$M for the interaction of wild-type Sba1 with Hsp90, which compares to results from previous reports [87,258]. For the truncation mutants Sba1Δ69 and Sba1Δ94, no significantly reduced Hsp90 binding was observed, the K_d-values were largely similar to wild-type Sba1 (~ 0.7 and $0.8\,\mu$M, respectively). Therefore, the unfolded region of Sba1 does obviously not contribute much to the interaction with Hsp90.

To gain more insights into the complex formation between Hsp90 and Sba1 in a residue-wise manner, NMR binding studies were performed. First, the interaction of Hsp90 and fragments thereof with ^{15}N-labeled Sba1 was analyzed. Surprisingly, adding full-length Hsp90 to Sba1 even

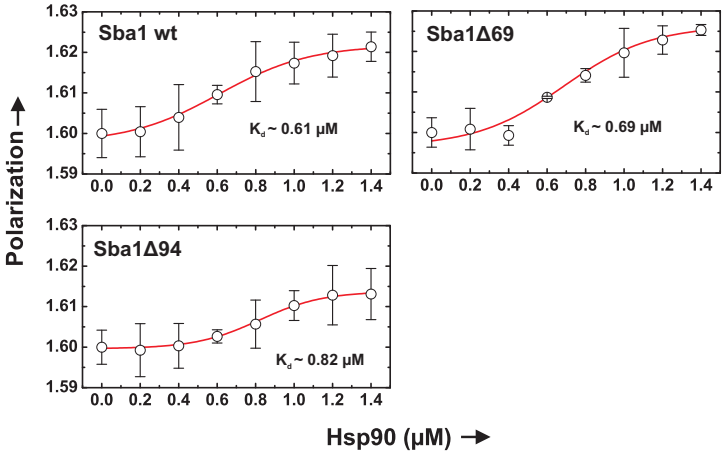

Figure 6.15: Binding between Sba1 variants and Hsp90 monitored by fluorescence polarization. For all Sba1 variants sigmoidal titration curves are observed, indicating cooperative binding. No major difference in the affinity for Hsp90 seems to exist for the Sba1 wild-type (wt), Sba1Δ69 and Sba1Δ94 constructs. The measurements were done at 20°C in a buffer of 10 mM potassium phosphate, 2 mM $MgCl_2$, 1 mM TCEP, pH 7.5 with 1 mM AMP-PNP added. 500 nM of the respective fluorescein labeled Sba1 variant was titrated with full-length Hsp90.

without the presence of nucleotide led to strong line broadening in the HSQC spectrum of Sba1, indicating a binding event (figure 6.16, left). This is somewhat in contrast to the results from the fluorescence assays where no complex formation was observed without nucleotide added. However, for NMR much higher protein concentrations are used in general, thus also rather weak interactions can be detected with this method, which might probably explain the different results. Indeed, also a previous study found a comparably weak binding of Sba1 to Hsp90 in absence of nucleotide[258]. As Hsp90 exists in a conformational equilibrium, it

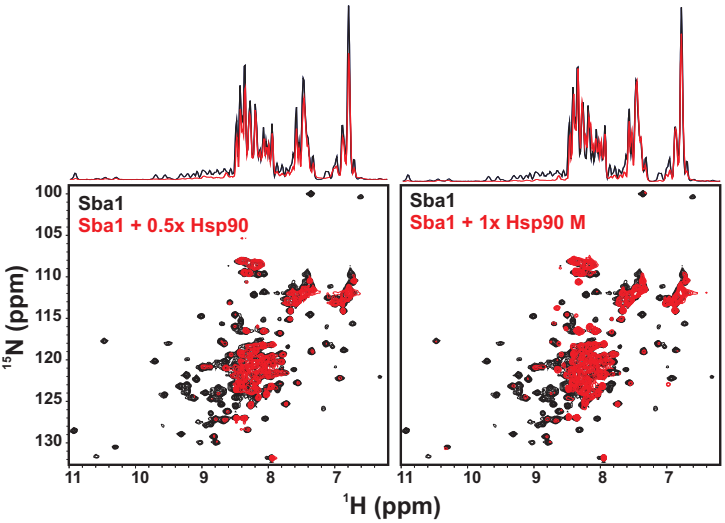

Figure 6.16: Binding between Sba1 and Hsp90 monitored by NMR. Overlay of ^{15}N-HSQC spectra for free Sba1 and in presence of full-length Hsp90 (left) or Hsp90 M (right). On top the 1D projections from the respective 2D spectra are shown. Strong line broadening points at complex formation in both cases. Only residues from the unfolded C domain are still visible in the bound state of Sba1, indicating no major participation of these residues in binding. The measurements were done at 303 K in a buffer of 40 mM potassium phosphate, 1 mM TCEP, pH 7.5 at 600 MHz using 250 μM of Sba1. Unlabeled full-length Hsp90 was added in 0.5-fold and Hsp90 M in a 1:1 molar ratio.

might well be that even without nucleotide added a certain fraction of the protein adopts the closed structure that can be bound by Sba1. Alternatively, additional binding sites for Sba1 might exist on Hsp90 that are independent from the N-terminal domain that drives the conformational rearrangements in the molecule upon nucleotide interaction.

To test the latter possibility, the isolated Hsp90 N and M domain were

assessed for binding to Sba1. Interestingly, the Hsp90 N domain did not show any detectable interaction with Sba1, irrespective of the nucleotide state (data not shown). Obviously, the N domain can only contribute to the binding of Sba1 in the context of full-length Hsp90, probably since in the isolated domain conformational changes that favor Sba1 binding like dimerization and ATP lid-closure cannot be achieved.

In contrast, when the isolated Hsp90 M domain was added to the ^{15}N-labeled Sba1, the effects on the NMR spectrum of Sba1 were basically identical as in the case of full-length Hsp90 (figure 6.16, right). Again, a strong line broadening was visible, pointing at complex formation. This demonstrates that the Hsp90 M domain represents a second important nucleotide independent binding site for Sba1. These findings seem to be in agreement with a previous study that reported the human Sba1 homologue p23 likewise interacting with the Hsp90 M domain [73].

In general, the NMR data are in support of the conclusion drawn from the fluorescence assays that the C-terminal unfolded residues of Sba1 do likely not at all are at least not significantly contribute to the interaction between Sba1 and Hsp90. Upon binding of either the isolated Hsp90 M domain or the full-length protein to Sba1, mostly only signals in the middle of the ^{15}N-HSQC spectrum and some side-chain resonances corresponding to the unfolded C-terminal region of Sba1 were still visible, whereas signals of the folded N-terminal part were broadened beyond detection limit.

To identify the binding site for Hsp90 M, the chemical shift perturbation in the NMR spectrum of the C-terminally truncated Sba1Δ94 mutant upon adding Hsp90 M was analyzed. As mentioned, the NMR spectral quality of this Sba1 variant was much improved compared to wild-type Sba1 or Sba1Δ69 (see section 6.3), therefore allowing for a more precise determination of residues involved in interaction. The Hsp90 M domain

caused significant and specific peak shifts within the folded N-terminal domain of Sba1 represented by the Sba1Δ94 variant (figure 6.17). Peak

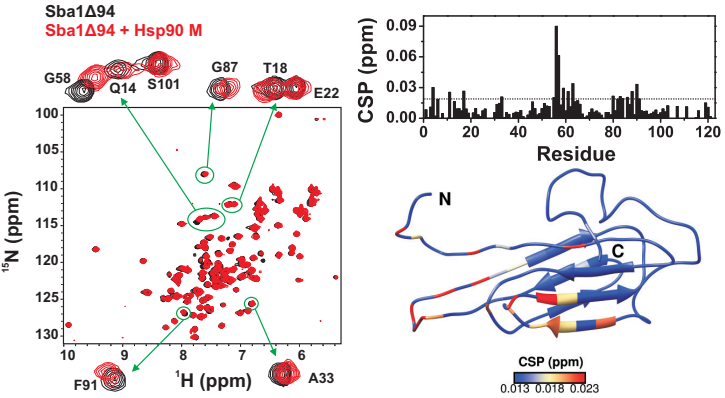

Figure 6.17: Binding between Sba1Δ94 and Hsp90 M monitored by NMR. Left: Overlay of ^{15}N-HSQC spectra for free Sba1Δ94 and in presence of Hsp90 M. Specific peak shifts point at complex formation. Right, upper panel: CSP plot for the binding of Hsp90 M to Sba1Δ94. The significance level (2-fold average CSP) is indicated by a dashed line. Right, lower panel: Color coded mapping of the chemical shift perturbation upon binding of Hsp90 M onto an NMR model of Sba1Δ94. The measurements were done at 303 K in a buffer of 10 mM potassium phosphate, 1 mM TCEP, pH 7.5 at 600 MHz using 200 μM of Sba1Δ94. Unlabeled Hsp90 M was added in a 2-fold molar excess.

shifts were into different directions, excluding mere buffer effects. The strongest chemical shift perturbation was found for a loop region comprising residues ∼ 55 to 65, which was found previously to be rather dynamic (see section 6.5). Additionally, two strands forming one edge of the β-sheet were affected by complex formation (residues ∼ 81 to 92).

Then, unlabeled Sba1 was added to the ^{15}N-labeled Hsp90 M domain and likewise a potential chemical shift perturbation analyzed as before.

Again, peak shifts and line broadening indicated complex formation, as

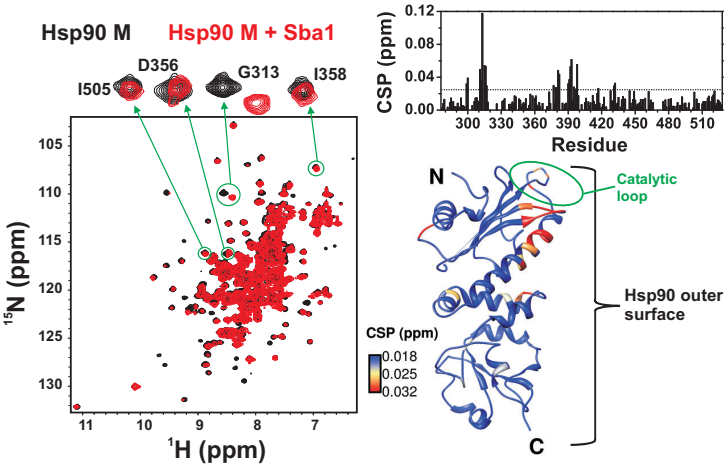

Figure 6.18: Binding between Hsp90 M and Sba1 monitored by NMR. Left: Overlay of ^{15}N - HSQC spectra for Hsp90 M alone and in presence of Sba1. Specific peak shifts point at complex formation. Right, upper panel: CSP plot for the binding of Sba1 to Hsp90 M. The significance level (2 - fold average CSP) is indicated by a dashed line. Right, lower panel: Color coded mapping of the chemical shift perturbation upon binding of Sba1 onto the crystal structure of Hsp90 M (PDB: 2CG9). The measurements were done at 303 K in a buffer of 10 mM potassium phosphate, 1 mM TCEP, pH 7.5 at 500 MHz using 200 μM of Hsp90 M. Unlabeled Sba1 was added in a $\sim$ 1:1 molar ratio.

expected. Residues that displayed significant signal shifts seemed to cluster at the more outer surface of the Hsp90 M domain with respect to the closed conformation of the Hsp90 dimer. Specifically, the N - terminal part of the Hsp90 M domain was affected that would get in close contact to the N domains upon nucleotide induced dimerization. Chemical shift perturbation was found for amino acids within the long α - helix formed

by residues 386 to 409 and for a small loop connecting two strands part of the large β-sheet (residues 310 to 318). Thus, it seems that Sba1 binds to Hsp90 M in a way that orients it in close proximity to the Hsp90 N domains with respect to the closed Hsp90 conformation. This would allow for an easy reorientation of Sba1 upon nucleotide driven Hsp90 N domain dimerization and concomitant docking to the M domains to form the high affinity Hsp90-Sba1 complex in which Sba1 interacts to a large extent with the Hsp90 N domains as found in a crystal structure [52].

In summary, the binding data show that Sba1 has obviously two distinct binding sites on Hsp90. High affinity binding of Sba1 involves the N domains of Hsp90 and nucleotide binding. Additional to that, a weaker nucleotide independent interaction of Sba1 with the Hsp90 M domain seems to exist which might serve to pre-orient Sba1 on Hsp90 to allow for a subsequent binding also to the N domains upon nucleotide driven N domain dimerization and docking to the M domain. The presumably unstructured C-terminal region of Sba1 does obviously not contribute significantly to complex formation with Hsp90.

6.7 Chaperone Activity of Sba1

Previously, p23/Sba1 was found to have chaperone activity on its own as it can suppress the aggregation of proteins under stress conditions like elevated temperatures [149,150]. Furthermore, this function clearly maps to the unfolded C-terminal region of p23/Sba1 [216,217]. To analyze whether this feature of Sba1 is also of relevance in complex with Hsp90, aggregation assays were performed here with the p53 DBD as a prototype client protein known to bind to Hsp90 (see section 3). The results from the interaction studies with Hsp90 and Sba1 carried out here suggested that the C-terminal unfolded part of Sba1 does to a large extent not participate in binding of Hsp90 (see section 6.6) and would thus be available for contributing to chaperone functions.

First, the ability of Sba1 variants alone to suppress the thermally induced aggregation of p53 DBD was tested. At the temperature (45°C) and buffer conditions used in the assay, both wild-type Sba1 and Sba1Δ94 were stable and did not aggregate (figure 6.19). However, neither wild-

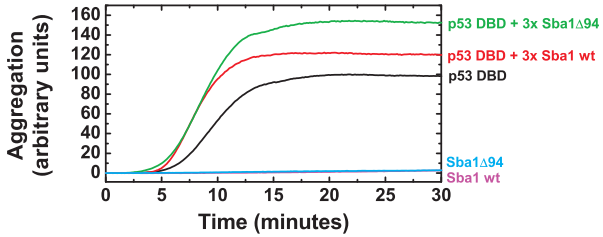

Figure 6.19: Suppression of thermally induced aggregation of p53 DBD by Sba1 variants. Neither Sba1Δ94 lacking the unfolded C domain nor wild-type (wt) Sba1 can suppress p53 DBD aggregation. Measurements were done in 10 mM potassium phosphate, 1 mM TCEP, pH 7.5. 5μM of p53 DBD was incubated at 45°C. The respective Sba1 variant was added in a 3-fold molar excess. Aggregation was followed by light scattering monitored at 360 nm.

type Sba1 nor Sba1Δ94 had the potential to suppress the aggregation of p53 DBD when incubated together, even when a larger molar excess (threefold) of the respective Sba1 construct was applied. Yet, an increased light scattering observed in presence of wild - type Sba1 and more pronounced with Sba1Δ94 pointed at coaggregation between Sba1 and p53 DBD, thus indicating a certain binding between the proteins. Likely, a higher solubility compared to Sba1Δ94 explains the lower degree of coaggregation in case of the measurement with wild - type Sba1. These findings demonstrate a certain potential of Sba1 to capture aggregation - prone substrates, partially consistent with the previous reports about the chaperone function of p23/Sba1 [149,150], as mentioned. In contrast to these earlier studies, a suppression of the aggregation process was clearly not found here. Obviously, there seems to be a difference in the stabilizing effect Sba1 exerts under stress conditions depending on the individual substrate protein.

Then the aggregation behavior of p53 DBD in presence of Hsp90 and Sba1 variants was analyzed. To ensure a proper complex formation between Hsp90 and Sba1, the non - hydrolysable ATP analogue AMP - PNP was added during the assay. As expected, Hsp90 alone could significantly stabilize p53 DBD under heat shock conditions (figure 6.20, compare also section 3.9). The additional presence of Sba1Δ94 lacking the unfolded C - terminal region had basically no effect on the Hsp90 mediated suppression of p53 DBD thermally induced aggregation. However, when a complex between wild - type Sba1 and Hsp90 was formed, a different kinetic profile of the aggregation process was observable. In an earlier phase up to $\sim$ 15 minutes Sba1 obviously contributes to maintaining the substrate protein in a native - like state whereas afterwards an even increased aggregation is found compared to Hsp90 being added alone. This demonstrates a certain role of the Sba1 C domain in the chaperoning of client

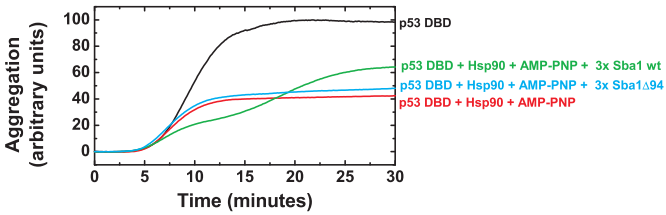

Figure 6.20: Suppression of thermally induced aggregation of p53 DBD by Sba1 variants in complex with Hsp90. The Sba1Δ94 variant lacking the unfolded C domain has no major impact on the suppression of p53 DBD aggregation by Hsp90. However, in presence of Sba1 wild - type (wt), a different kinetics of the aggregation process is observed. Measurements were done in 10 mM potassium phosphate, 2 mM $MgCl_2$, 1 mM AMP - PNP, 1 mM TCEP, pH 7.5. 5 μM of p53 DBD and full - length Hsp90 were incubated at 45°C. The respective Sba1 variant was added in a 3 - fold molar excess. Aggregation was followed by light scattering monitored at 360 nm.

proteins by bound to Hsp90. Nevertheless, this might reflect only one particular and rather specific function. Considering the structure propensity analysis (see section 6.2), it seems possible that the unfolded region of Sba1 could also serve in membrane association under certain conditions, which could be an even more important cellular function.

6.8 Discussion

The Hsp90 cochaperone Sba1/p23 seems to serve different functions. On the one hand, it was shown to have a general chaperone activity on its own, independent from Hsp90 [149,150]. On the other hand, it has obviously a role in the activation of Hsp90 dependent client proteins like the steroid hormone receptors [154,209]. The importance of the presumably unfolded C-terminal region within Sba1/p23 is not yet fully understood, although it is clearly involved in the Sba1/p23 chaperone activity. The results obtained here indicate a new potential role for this part of the protein: a secondary structure prediction found a significant propensity for the C-terminal domain of Sba1 to form α-helices which had partially amphipathic character. This could point at a function in membrane association. Indeed, it was possible to induce α-helical structure in Sba1 with TFE and furthermore with SDS, which supports the assumption of Sba1 localizing to membranes under certain conditions. However, this might not apply to the same extent for other homologues of Sba1 like human p23, as a sequence alignment shows only a partial conservation of the respective C-terminal regions (figure 6.21). Interestingly, and in support

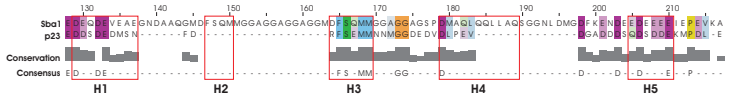

Figure 6.21: Amino acid sequence alignment of yeast Sba1 and human p23 C-terminal regions. The C-terminal regions of Sba1 and p23 seem to be only partially conserved. UniProt reference codes of the sequences used for the alignment are Q15185 for human p23 and P28707 for yeast Sba1. The alignment was generated using T-Coffee [194] and visualized with Jalview [195]. The coloring scheme is according to amino acid properties and the degree of conservation of a particular position with more intense color indicating higher conservation. The position of the predicted helices in Sba1 is marked by red boxes (compare 6.3).

of the structural *in vitro* data obtained here, a recent study suggested a requirement of Sba1 for proper golgi function in yest cells and also a nuclear role[225]. It seems that Sba1/p23 could have much more cellular tasks than thought previously that might be independent from Hsp90 and involve its natively unfolded C-terminal domain.

Under normal conditions, the Sba1 C domain seems to be largely unfolded, as indicated by NMR data obtained here. Consistent with previous reports[216,217,319,323], it was found to be dispensable for the binding of Hsp90, deletion of the respective residues had no major influence on the affinity of Sba1 for Hsp90. Upon complex formation with Hsp90, signals corresponding to the unfolded region in the HSQC spectrum of Sba1 were mostly unaffected, supporting the assumption of no major role for Hsp90 interaction.

For a particular Hsp90 client protein, the DNA binding domain of p53, a certain function of the unfolded residues in Sba1 could be found for suppressing a thermally induced unfolding, however, only when Sba1 was bound to Hsp90. This is somewhat different to earlier reports that found a pronounced chaperone effect of isolated p23 on the model substrate citrate synthase[149,324] and might reflect a certain client-specific chaperone activity of Sba1/p23. Supporting the assumption of a role for its C-terminal domain in chaperoning client proteins when bound to Hsp90, it was found that Sba1 truncations of the unfolded region led to a reduced activity of the estrogen receptor expressed in yeast cells[325].

High affinity complex formation between Sba1 and Hsp90 was clearly cooperative and dependent on the presence of nucleotide, pointing at the involvement of the Hsp90 N domains, in agreement with several previous reports[52,82,85,87,211,321,322,326]. However, a weaker but still significant binding to Hsp90 was observed also in absence of nucleotide that maps to the M domain of Hsp90, which seems to be consistent with the human

p23 [73,327]. These additional binding contacts may serve to pre-orient Sba1 on Hsp90 to allow for a subsequent binding also to its N domains upon nucleotide driven N domain dimerization and docking to the M domain. Thus, to a certain extent the Hsp90-Sba1 interaction is nucleotide independent.

In summary, the results obtained here indicate that the C-terminal domain of Sba1 is likely involved in so far unknown functions that might – at least partially – be independent from the Hsp90 chaperone system. Indeed, one such Hsp90 independent Sba1 function was shown to be its influence on the activity of telomerase *in vitro*, and this effect was connected to the presence of the protein's C-terminal region [328].

Part III

Experimental Section

Chapter 7

Molecular Biology

Chemicals were obtained from Carl Roth GmbH + Ko.KG, Merck KGaA and Sigma - Aldrich, if not otherwise stated.

7.1 Polymerase Chain Reaction

Amplification of DNA fragments was achieved by polymerase chain reaction (PCR) [329–331]. A standard reaction mixture contained the components as given in table 7.1. For cloning purposes, two polymerases with proofreading function were used, *Pfu* DNA Polymerase (Promega, Madison, WI, USA) and Herculase II Fusion DNA Polymerase (Agilent Technologies, Waldbronn, Germany), with the corresponding buffers provided by the supplier. For control PCR reactions, normal *Taq* polymerase (New England Biolabs, Ipswich, MA, USA) lacking proofreading was applied. Polymerases with proofreading function were added to the PCR reaction mixture at a temperature of 95°C ("hot start").

Table 7.1: Components of a PCR reaction mixture. Buffers were used as provided by the supplier of the respective polymerase. For cloning purposes, *Pfu* DNA Polymerase and Herculase II Fusion DNA Polymerase were applied with hot start adding the enzyme at 95°C, in contrast to control PCR reactions with *Taq*.

5 μl	10 x reaction buffer
1.5 μl	dNTP mixture (25 mM each nucleotide)
2 μl	forward primer (10 μM)
2 μl	backward primer (10 μM)
1 μl	template DNA (50 - 100 ng/μl)
1 μl	DNA polymerase (3 U/μl)
ad 50 μl	ddH_2O

The general cycling scheme for PCR reactions is given in table 7.2. Annealing temperatures were set to values $\sim$ 5 - 10°C below the calcu-

Table 7.2: PCR cycling scheme.

2 min	95°C	Initial melting	
30 s	95°C	Melting	
30 - 45 s	52 - 70°C[a]	Annealing	Cycling, 20 - 30 x
0.5 - 10 min[b]	68/72°C[c]	Extension	
10 min	68/72°C[c]	Final extension	
∞	4°C	Storage	

[a] Annealing temperature was chosen to be $\sim$ 5 -10°C below calculated primer T_M.
[b] Extension time depending on the polymerase and length of DNA to be amplified.
[c] 68°C for *Pfu* polymerase, 72°C for Herculase II Fusion and *Taq* polymerase.

lated melting temperature of the primers. *Taq* and Herculase II Fusion polymerase provide a synthesis rate of $\sim$ 2000 bp (base pairs), *Pfu* and $\sim$ 500 bp. Extension times during PCR reactions were set appropriately considering the synthesis rate of the polymerase used and the length of

the DNA fragment to be amplified.

7.2 Plasmid DNA Isolation and DNA Fragment Purification

Isolation of plasmid DNA from *E. coli* cells was done using the Wizard® *Plus* SV Minipreps DNA Purification System (Promega, WI, USA). DNA fragments were purified by loading PCR reaction mixtures onto agarose gels (see section 7.6). The fragment of interest was cut out of the gel, afterwards performing a gel extraction with the Wizard® DNA Clean-Up System (Promega, WI, USA).

7.3 Oligonucleotides

Oligonucleotides were purchased from Biomers GmbH (Ulm, Germany). Lyophilized oligonucleotides were dissolved in an appropriate volume ddH_2O to a concentration of 100 μM according to the supplier's recommendation and further 1:10 diluted to obtain solutions suited for PCR reactions.

Table 7.3: Oligonucleotides for introducing point mutations into the Hsp90 M domain.

Construct	Primer	Sequence
Hsp90 M N298C	sense	ctataagtctatttcatgcgactgggaagaccc
	anti	gggtcttcccagtcgcatgaaatagacttatag
Hsp90 M Q384C	sense	ttgtccagagaaatgttatgccaaaataagatcatgaagg
	anti	ccttcatgatcttattttggcataacatttctctggacaa
Hsp90 M S411C	sense	gaaattgctgaagactgtgaacaatttgaaaag
	anti	cttttcaaattgttcacagtcttcagcaatttc
Hsp90 M E412A	sense	gaaattgctgaagactctgcacaatttgaaaagttctac
	anti	gtagaacttttcaaattgtgcagagtcttcagcaatttc
Hsp90 M E415A	sense	gaagactctgaacaatttgcaaagttctactcggctttc
	anti	gaaagccgagtagaacttttgcaaattgttcagagtcttc
Hsp90 M S422C	sense	gttctactcggctttctgcaaaaatatcaagttgg
	anti	ccaacttgatatttttgcagaaagccgagtagaac
Hsp90 M K469C	sense	ccagaatgccagaacaccaatgcaacatctactacatcactgg
	anti	ccagtgatgtagtagatgttgcattggtgttctggcattctgg
Hsp90 M K484C	sense	ctctaaaggctgtcgaatgctctccatttttggatgc
	anti	gcatccaaaaatggagagcattcgacagcctttagag

Table 7.4: Oligonucleotides for the Hsp90 C domain and truncation variants thereof. C - terminal truncations of the domain were obtained by introducing a stop codon at the respective position in a plasmid encoding the wild - type protein.

Construct	Primer	Sequence
Hsp90 C	*NdeI*_sense	ggaattccatatgttcgaattggaagaaactgacg
	*BamHI*_anti	ctagggatcccttaatctacctcttccatttcggtgt
Hsp90 CΔ10	sense	ccggttgaagaggtttaagctgacaccgaaatg
	anti	catttcggtgtcagcttaaacctcttcaaccgg
Hsp90 CΔ20	sense	gagactgctccagaataatccaccgcagctccg
	anti	cggagctgcggtggattattctggagcagtctc
Hsp90 CΔ30	sense	ctttgggtttgaacattgattaggatgaagaaacagagactgc
	anti	gcagtctctgtttcttcatcctaatcaatgttcaaacccaaag
Hsp90 CΔ583-607	sense	tcttccaagaagactttcgaaatttctccaaaatctcc
	anti	ttgaccagttctgatagcagctggggc

Table 7.5: Oligonucleotides for introducing point mutations into the Hsp90 C domain. The Hsp90 679-682A quadruple mutant (compare section 3.8) was obtained in two steps first introducing the 679A/680A substitutions into Hsp90 and then performing a second mutagenesis on an Hsp90 679A/680A template to additionally introduce the 681A/682A substitution.

Construct	Primer	Sequence
Hsp90 C E546C	sense	gagaaggagatcaaatgctatgaaccattgacc
	anti	ggtcaatggttcatagcatttgatctccttctc
Hsp90 C D573C	sense	cttacaaattgttgtgtgccccagctgctatc
	anti	gatagcagctggggcacacaacaatttgtaag
Hsp90 C D659C	sense	ccggcttcagtttgtgcgaaccaacttcc
	anti	ggaagttggttcgcacaaactgaagccgg
Hsp90 C N677C	sense	gatctctttgggtttgtgcattgatgaggatgaag
	anti	cttcatcctcatcaatgcacaaacccaaagagatc
Hsp90 C A687C	sense	gaagaaacagagacttgtccagaagcatccacc
	anti	ggtggatgcttctggacaagtctctgtttcttc
Hsp90 C S691C	sense	gctccagaagcatgcaccgcagctccg
	anti	cggagctgcggtgcatgcttctggagc
Hsp90 D679A/E680A	sense	gggtttgaacattgctgcggatgaagaaacagagactgctcc
	anti	ggagcagtctctgtttcttcatccgcagcaatgttcaaaccc
Hsp90 D681A/E682A	sense	gggtttgaacattgctgcggctgcagaaacagagactgctcc
	anti	ggagcagtctctgtttctgcagccgcagcaatgttcaaaccc

Table 7.6: Oligonucleotides for Ssa1 constructs.

Construct	Primer	Sequence
Ssa1 N	*NdeI*_sense	ggaattccatatgagcaaagctgtcggtattgatttagg
	*BamHI*_anti	ctagggatccttaaccagtcaaaatagcagcttgaacagc
Ssa1 M	*NdeI*_sense	ggaattccatatggacgaatcttccaagactcaagatc
	*BamHI*_anti	ctagggatccttattccaattggttcttggaagcaattc
Ssa1 C	*NdeI*_sense	ggaattccatatgtccattgcttactctttgaagaacacc
	*BamHI*_anti	ctagggatccttaatcaacttcttcaacggttggacc

Table 7.7: Oligonucleotides for Sti1 constructs. The TPR1 and TPR1 - DP1 fragments were obtained by introducing a stop codon into a plasmid containing full - length Sti1. Other Sti1 two - domain constructs were generated by combining the appropriate oligonucleotides used for single - domain constructs.

Construct	Primer	Sequence
TPR1	sense	gcaagacaggcacagcctgattaagggttgacacagttgtttg
	anti	caaacaactgtgtcaacccttaatcaggctgtgcctgtcttgc
$DP1_{127-197}$	*NdeI*_sense	ggaattccatatgcagcctgatttagggttgacacagttgtttgc
	*BamHI*_anti	ctagggatccttagtttaaatcaacccccatcaatgtagccatgatgg
TPR1 - DP1	sense	cattgatgggggttgatttaaactaggatgatataaaccaatcaaac
	anti	gtttgattggtttatatcatcctagtttaaatcaacccccatcaatg
TPR2A	*NdeI*_sense	ggaattccatatggaggccgacaaggaaaaggccg
	*BamHI*_anti	ctagggatccttacgcctcagctttcttcaattctttttcagc
TPR2B	*NdeI*_sense	ggaattccatatggaggcgtatgttaaccctgaaaagg
	*BamHI*_anti	ctagggatccttaggtttcgttactggtaccagg
TPR2BΔh7	*NdeI*_sense	ggaattccatatggaggcgtatgttaaccctgaaaagg
	*BamHI*_anti	ctagggatccttaggttctggccgcatctagtgtttc
$DP2_{493-589}$	*NdeI*_sense	ggaattccatatgaaagatgctgaagtgaataatggttc
	*BamHI*_anti	ctagggatccttagcggccagtccggatgat
$DP2_{525-589}$	*NdeI*_sense	ggaattccatatggaaaccccagaagaaacctatc
	*BamHI*_anti	ctagggatccttagcggccagtccggatgat

Table 7.8: Oligonucleotides for Sti1 TPR2B peptide binding mutants and the linker variant.

Construct	Primer	Sequence
TPR2B N435A	sense	gctagaggatattctgctagagctgctgcactagc
	anti	gctagtgcagcagctctagcagaatatcctctagc
TPR2B N465A	sense	gatccaaatttcgtggcagcttatatcagaaaagg
	anti	cctttctgatataagctgccacgaaatttggatc
TPR2B N469A	sense	gtgagagcttatatcgcaaaggccaccgcac
	anti	gtgcggtggcctttgcgatataagctctctac
TPR2B R425A	sense	gcttacactgaaatgatcaaagcggcacctgaagatgctagagg
	anti	cctctagcatcttcaggtgccgctttgatcatttcagtgtaagc

Table 7.9: Oligonucleotides for Sti1 DP2 point mutants.

Construct	Primer	Sequence
DP2 V540A	sense	gccatgaaagatcctgaagcggctgcgatcatgcaagatcc
	anti	ggatcttgcatgatcgcagccgcttcaggatctttcatggc
DP2 L553A	sense	gatcctgttatgcaaagtattgcgcagcaggcccaacagaatccc
	anti	gggattctgttgggcctgctgcgcaatactttgcataacaggatc
DP2 Q557A	sense	gcaaagtattttgcagcaggccgcacagaatcccgctgctttacaag
	anti	cttgtaaagcagcgggattctgtgcggcctgctgcaaaatactttgc
DP2 Q564A	sense	cagaatcccgctgctttagcagaacacatgaaaaatcc
	anti	ggatttttcatgtgttctgctaaagcagcgggattctg
DP2 T578A	sense	gaagtattcaaaaagattcaggcgttgatcgctgctggtatc
	anti	gataccagcagcgatcaacgcctgaatctttttgaatacttc
DP2 I584A	sense	cgttgatcgctgctggtgccatccggactggccgc
	anti	gcggccagtccggatggcaccagcagcgatcaacg

Table 7.10: Oligonucleotides for Sti1 TPR2B - DP2 point mutants. To obtain TPR2B - DP2 cysteine variants suited for spin labeling, first the native cysteine at position 453 was substituted for serine. Using the C453S variant as a template, the desired cysteine variants were generated then.

Construct	Primer	Sequence
TPR2B - DP2 C453S	sense	gctatcgcagatagtaacaaagcc
	anti	ggctttgttactatctgcgatagc
TPR2B - DP2 E525C	sense	gattccaacctggtaccagtaactgcaccccagaagaaacctatcaaa
	anti	tttgataggtttcttctggggtgcagttactggtaccaggttggaatc
TPR2B - DP2 K536C	sense	gaaacctatcaaagggccatgtgcgatcctgaagtggctgcgatc
	anti	gatcgcagccacttcaggatcgcacatggccctttgataggtttc
TPR2B - DP2 Q545C	sense	gatcctgaagtggctgcgatcatgtgcgatcctgttatgcaaagtattttg
	anti	caaaatactttgcataacaggatcgcacatgatcgcagccacttcaggatc
TPR2B - DP2 N559C	sense	gcagcaggcccaacagtgtcccgctgctttacaa
	anti	ttgtaaagcagcgggacactgttgggcctgctgc
TPR2B - DP2 N569C	sense	aatcccgctgctttacaagaacacatgaaatgtccagaagtattcaaaaag
	anti	ctttttgaatacttctggacatttcatgtgttcttgtaaagcagcgggatt

Table 7.11: Oligonucleotides for generating a Sti1 DP1 domain swap mutant. The details about the construction of the DP1 domain swap mutant are described in section 4.15.

Construct	Primer	Sequence
Sti1 vector_*PstI*	sense	caaagattccaacctggctgcagtaacgaaacccc
	anti	ggggtttcgttactgcagccaggttggaatctttg
DP1_swap	*PstI*_sense	ggaattcctgcagtttgacacagttgtttgctgaccc
	*HindIII*_anti	ctagaagcttttagtttaaatcaacccccatcaatgtagccatgatgg
Sti1 vector_back	sense	caaagattccaacctggcttgggtttgacacagttgtttgc
	anti	gcaaacaactgtgtcaaacccaagccaggttggaatctttg

Table 7.12: Oligonucleotides for generating the Sba1Δ94 mutant. The C-terminal truncation variant was generated by introducing a stop codon into a template plasmid containing wild-type Sba1.

Construct	Primer	Sequence
Sba1Δ94	sense	catcaaaactgatttcgattaatgggttgatgaagatg
	anti	catcttcatcaacccattaatcgaaatcagttttgatg

Table 7.13: Oligonucleotides for sequencing plasmids.

Primer	Sequence
T7_upstream	gatgcgtccggcgtagag
T7_downstream	ccggatatagttcctcctttcagc
T7_promotor	taatacgactcactataggg
T7_terminator	gctagttattgctcagcgg

7.4 DNA Manipulation

For cutting DNA, restrictions enzymes were used obtained from New England Biolabs (Ipswich, MA, USA) or Promega (Madison, WI, USA). Digestions were done according to the recommendations of the respective supplier. After digestion, DNA restriction enzymes were heat inactivated, if possible. Digested DNA fragments were purified from restriction enzymes as described in section 7.2.

Digested plasmid DNA was further additionally treated with calf intestinal phosphatase (CIP, New England Biolabs, Ipswich, USA) for dephosphorylation before purification to prevent recircularization in subsequent ligation reactions and false positive clones.

Ligation of DNA fragments was done with T4 DNA Ligase (New England Biolabs, Ipswich, USA) according to recommendations of the supplier. After the reaction, the enzyme was heat inactivated and ligated DNA used for transformation of cells.

7.5 Mutagenesis of DNA

For site directed mutagenesis of DNA, a whole plasmid mutagenesis strategy was applied using double stranded circular DNA as template[332]. To this end, PCR reactions as described in section 7.1 were performed with a proofreading polymerase and primers containing the desired base pair substitution. Unmutated template DNA was removed by adding 1 μl *DpnI* restriction enzyme (10 U/μl, Promega, Madison, WI, USA) directly to the reaction mix after PCR and incubation at 37°C over night, taking advantage of *DpnI* selectively cutting only methylated parental DNA.

For introducing deletions into a protein coding DNA sequence, an oligonucleotide pair was designed annealing with the template DNA such that

the region to be deleted was not amplified in a PCR reaction performed similarly as for single base pair substitutions. After *DpnI* digestion as described above, T4 polynucleotide kinase (Promega, WI, USA) was added according to the supplier's recommendation to phosphorylate DNA ends as required for ligation since 5' - unmodified primers were used for all PCR reactions. Subsequently, a blunt end ligation of the linear DNA was done (see section 7.4) to obtain circular DNA suited for transformation of cells.

7.6 Agarose Gel Electrophoresis

1 % or 1.5 % agarose gels for analytical and preparative purposes were prepared by solving 0.5 or 0.7 g agarose in 50 ml hot 1x TAE buffer (table 7.14). 8 μl ethidiumbromide stock solution (1 % w/v) was added directly before casting the gel at a temperature of $\sim$ 50°C. Typical samples consisted of 1 μl 10x DNA sample buffer (table 7.14) and 9 μl PCR product. The electrophoresis was performed applying a constant voltage of 80 V. DNA was visualized by fluorescence excited at 254 nm using a gel documentation system (Bio - Rad Laboratories GmbH, Munich, Germany).

Table 7.14: Buffer for DNA gel electrophoresis. The pH of the 10x TAE buffer stock was adjusted to 8.0. EDTA, ethylenediaminetetraacetate.

10x TAE buffer		**10x DNA loading buffer**	
48.4 g	Tris base	4 % (w/v)	Bromophenol blue
11.4 ml	Acetic acid	50 % (v/v)	Glycerine
2.92 g	EDTA disodium salt		
ad 1000 ml	H_2O		

7.7 DNA Sequencing

DNA sequencing was provided by the SeqLab GmbH (Göttingen, Germany). For sequencing reactions, a 7 μl solution was prepared containing purified plasmid DNA in a concentration > 200 ng/μl, mixed with an appropriate sequencing primer (table 7.13) in a buffer of 10 mM Tris/HCl (2 - amino - 2 - hydroxymethyl - propane - 1,3 - diol), pH 8.5.

Chapter 8

Cell Culture

8.1 Cell Strains

For cloning purposes, the *E. coli* strains XL1 - Blue (Stratagene, Cedar Creek, TX, USA) and DH10B (Invitrogen, Carlsbad, CA, USA) were used, for protein expression the *E. coli* BL21(DE3) strain (Merck KGaA).

Table 8.1: Genotypes of *E. coli* strain.

Strain	Genotype
DH10B	F^- endA1 recA1 galE15 galK16 nupG rpsL ΔlacX74 Δ Φ80lacZΔM15 araD139 Δ(ara,leu)7697 mcrAΔ(mrr-hsdRMS-mcrBC)λ^-
XL1 - Blue	endA1 gyrA96(nal^R) thi-1 recA1 relA1 lac glnV44 F'[::Tn10 proAB$^+$ lacI^q Δ(lacZ)M15] hsdR17($r_K{}^-$ $m_K{}^+$)
BL21(DE3)	F^- ompT gal dcm lon hsdS_B($r_B{}^-$ $m_B{}^-$) λ(DE3 [lacI lacUV5-T7 gene 1 ind1 sam7 nin5])

8.2 Media for Growing Cells

For liquid cell cultures, autoclaved LB or M9 minimal medium was used according to table 8.2, supplemented with 1 ml per liter of an appropriate antibiotics 1000x stock solution. 1000x ampicillin and kanamycin stocks in water had a concentration of 100 mg/ml and 35 mg/ml, respectively, and were applied only after sterile filtration. For preparing plates, 15 g/l agar was added to liquid LB medium and autoclaved. At a temperature of $\sim 40°C$, 1 ml per liter of an appropriate antibiotics 1000x stock solution was added to the still liquid solution and poured into petri plates. For isotope labeling of proteins with deuterium, all components required for M9 medium were prepared with deuterium instead of water.

Table 8.2: LB_0 and M9 minimal medium. LB medium was autoclaved before use. For M9 medium, water, basic salts, $MgSO_4$, $CaCl_2$ and trace elements were autoclaved before use, all other components were applied after sterile filtration.

LB_0 medium		**M9 minimal medium**	
5 g	Yeast extract	100 ml	M9 basic salts (10x)
5 g	NaCl	10 ml	U-^{13}C/U-$^{13}C^2$H glucose solution (0.2 g/l)
10 g	Tryptone	10 ml	$^{15}NH_4Cl$ solution (0.1 g/l)
ad 1000 ml	ddH_2O	2 ml	1M $MgSO_4$
		0.1 ml	1M $CaCl_2$
		2 ml	Thiamine solution (2 mg/ml)
		1 ml	Biotin solution (2 mg/ml)
		10 ml	Trace element solution (100x)
		1 ml	Kanamycin/ampicillin (1000x)
		ad 1000 ml	ddH_2O

Table 8.3: M9 basic salts and trace element solutions. After adjustment of the pH to 7.5, the solutions were autoclaved.

M9 basic salts (10x)		**M9 trace element solution (100x)**	
60 g	Na_2HPO_4	5 g	EDTA
30 g	KH_2PO_4	0.83 g	$FeCL_3 * 6 H_2O$
5 g	NaCl	84 mg	$ZnCl_2$
ad 1000 ml	ddH_2O	13 mg	$CuCl_2 * 2 H_2O$
		10 mg	$CoCl_2 * 6 H_2O$
		10 mg	H_3BO_3
		1.6 mg	$MnCl_2 * 6 H_2O$
		ad 1000 ml	ddH_2O

8.3 Preparation of Competent Cells

Chemically competent *E. coli* cells were prepared as follows: 2 ml of 1 M $MgCl_2$ were added to an exponentially growing cell culture (100 ml) with an OD_{600} (optical density at 600 nm) ~ 0.5 - 1.0 and further incubated for 10 minutes at 37°C. Afterwards, the culture was chilled on ice for 60 minutes, the cells pelleted (5 minutes, 4°C, 5000 rpm; rpm: rotations per minute), resuspended in 20 ml of buffer A (table 8.4) and incubated another 60 minutes on ice. Following pelletation (5 minutes, 4°C, 5000 rpm), cells were again resuspended in 2 ml of buffer B (table 8.4) and aliquots prepared (200 μl each). These were then snap frozen in liquid nitrogen and stored at - 80°C.

8.4 Transformation of Cells

200 μl of chemically competent *E. coli* cells (see section 8.3) were mixed with 1 - 5 μl of purified plasmid DNA (in water) and incubated on ice for 1 - 15 minutes. Then, a heat shock was applied (45 s, 42°C), followed by

Table 8.4: Buffer for the preparation of chemically competent *E. coli* cells. Both buffers were only applied after sterile filtration.

Buffer A		**Buffer B**	
13 ml	3 M NaAc (pH 5.5)	69 ml	Glycerine (87 %)
100 ml	1 M $CaCl_2$	331 ml	Buffer A
25 ml	2.8 M $MnCl_2$		
862 ml	H_2O		

further incubation on ice for 5 minutes. Afterwards, 800 μl of LB - medium without antibiotics was added to the cells, which were subsequently incubated under gentle shaking at 37°C for 45 minutes. Cells were pelleted (5 minutes, 3000 rpm) and 900 μl of the supernatant discarded. Finally, cells were resuspended in the remaining volume and streaked on LB - plates supplemented with the appropriate antibiotics. Plates were incubated overnight at 37°C.

8.5 Long Term Storage of Cells

For long term storage of cells strains, cryocultures were prepared. 200 μl of an exponentially growing cell culture were mixed with 800 μl of 75 % sterile glycerine solution and incubated on ice for 1 h. Afterward, cells were snap frozen in cryo vials with liquid nitrogen and stored at - 80°C.

8.6 Preparation of *E. coli* Protein Expression Cultures

For protein expression, small overnight precultures were prepared in LB medium supplemented with the appropriate antibiotic (see section 8.2). These were inoculated from cryocultures of the respective *E. coli* strain (see section 8.5) and incubated under shaking at 37°C. With the precul-

tures, larger scale cultures in Erlenmeyer flasks with 1 or 5 L volume were inoculated 1:20, which were grown at 37°C to an OD_{600} of ~ 0.6 to 0.8. Depending on the protein, either expression was induced by adding ITPG (isopropyl - β - D - thiogalactopyranosid) in a final concentration of 1 mM to the culture or the culture was first chilled down to a lower temperature and then expression induced similarly. For isotope labeling of proteins with deuterium, the LB medium of the preculture was prepared with D_2O instead of water to adapt cells for growing in deuterium containing environment, thus preventing a long lag phase when inoculating the large scale culture for protein expression.

Chapter 9

Protein Expression and Purification

Chemicals were obtained from Carl Roth GmbH + Ko.KG, Merck KGaA and Sigma - Aldrich, if not otherwise stated.

9.1 Preparation of Cell Extracts

Following protein expression (see section 8.6 and sections within this chapter for individual protein expression procedures), cells were harvested by centrifugation at 4°C and 6000 g (standard gravity) for 20 minutes. Cell pellets were washed in a smaller volume of buffer (50 to 200 ml, 50 mM potassium phosphate, 300 mM potassium chloride, pH 7.5) and centrifuged again as before. The supernatant was discarded and cells pellets snap frozen in liquid nitrogen, which were then either stored at - 20°C or directly processed further.

Cell pellets of protein expression cultures were thawed on ice and cells resuspended carefully in the respective buffer as used for the first step

of the individual purification procedure. After adding protease inhibitor mix (SERVA GmbH, Heidelberg, Germany) and DNase (SERVA GmbH, Heidelberg, Germany) according to the supplier's recommendation, cell disruption was done using a Basic Z cell disruption apparatus (Constant Systems LTD, Warwick, UK) applying a pressure of 1.8 kbar. The extract was then centrifuged at 4°C and 40000 g for 60 minutes. The supernatant could then be applied to the respective column for fast protein liquid chromatography purification.

9.2 Preparation of Inclusion Bodies

Following protein expression (see section 8.6 and sections within this chapter for individual protein expression procedures), cells were harvested by centrifugation at 4°C and 6000 g for 20 minutes. Cell pellets were resuspended in buffer A (~ 5 ml added per gram of cell pellet, table 9.1), DNase (SERVA GmbH, Heidelberg, Germany) added according to the supplier's recommendation and cell disruption performed as described under 9.1. Then, 1 volume of buffer B (table 9.1) was added to the extract and mixed for 30 minutes at 4°C. After centrifugation (15000 rpm, 4°C, 20 minutes), the pellet obtained was washed twice with buffer A. The inclusion body pellet obtained was stored at - 20°C until use or directly processed further: 1 ml of 6 M guanidinium chloride or for proteins with cysteine residues 6 M guanidinium chloride/50 mM 2 - mercaptoethanole was added per 100 mg inclusion body material and resuspended. After centrifugation (15000 rpm, 4°C, 20 minutes) the supernatant could be used for protein refolding procedures (section 9.3).

Table 9.1: Buffer for inclusion body preparation. The pH of both buffers was adjusted to 7.5 before use.

Buffer A		**Buffer B**	
100 mM	Tris/HCl	100 mM	Tris/HCl
100 mM	NaCl	100 mM	NaCl
10 mM	EDTA	10 mM	EDTA
		5 % (V/V)	Triton X - 100

9.3 Refolding of Proteins

Proteins dissolved in guanidinium chloride after inclusion body preparation (see section 9.2) were refolded by dialysis against 5 L buffer 1 (table 9.2) at 4°C over night in a first step. The supernatant obtained after centrifugation (60 minutes, 4°C, 40000 g) of the protein solution was subjected a second dialysis step using 5 L buffer 2 (table 9.2) over night at 4°C. Following further centrifugation (60 minutes, 4°C, 40000 g), the protein solution could be applied to the first column in an appropriate fast protein liquid chromatography purification procedure.

Table 9.2: Buffer for refolding of proteins after inclusion body preparation. The pH of both buffers was adjusted to 7.5 before use.

Buffer 1		**Buffer 2**	
50 mM	KH_2PO_4	50 mM	KH_2PO_4
300 mM	KCl	300 mM	KCl
3 M	Guanidinium chloride	500 mM	Guanidinium chloride
500 mM	L - arginine	500 mM	L - arginine
5 mM	2 - mercaptoethanole	5 mM	2 - mercaptoethanole

9.4 Fast Protein Liquid Chromatography

Purification of proteins was done using an ÄKTA^{TM}FPLC (FPLC, fast protein liquid chromatography) system equipped with conductivity and UV detection (GE Healthcare, Munich, Germany).

9.4.1 Affinity Chromatography

For purification of His_6-tagged proteins, immobilized metal ion affinity chromatography (IMAC) was used as first step. To this end, self-packed columns (XK 16/20 column body, GE Healthcare, Munich, Germany) with a bed volume of 30 ml were prepared containing Chelating Sepharose Fast Flow carrier material (GE Healthcare, Munich, Germany) loaded with Ni^{2+} according to the supplier's recommendation. Crude protein extracts (see sections 9.1 and 9.3) were applied to the column at a flow rate of 2 ml/min to allow for binding. After a washing step with $\sim$5 to 10 column volumes (CV) of buffer A (table 9.3), proteins were eluted by a linear gradient applied over $\sim$5 column volumes to 100 % buffer B (table 9.3). During the elution step, protein fractions of 5 ml were collected and afterwards analyzed by SDS-PAGE (sodium dodecyl sulfate polyacrylamide gel electrophoresis). Fractions containing the protein of interest were pooled and the solution subjected Thrombin cleavage to remove the affinity tag (see section 9.6).

For purification of proteins carrying a GST affinity tag, self-packed columns (XK 16/20 column body, GE Healthcare, Munich, Germany) containing Glutathione Sepharose 4 Fast Flow material (GE Healthcare, Munich, Germany) with a bed volume of 30 ml were used. Columns were prepared according to the supplier's recommendation. Crude proteins extracts (see sections 9.1) were applied to the column at a flow rate of not

Table 9.3: Buffer for IMAC affinity chromatography of proteins . The pH of both buffers was adjusted to 7.5 before use.

Buffer A		**Buffer B**	
50 mM	KH_2PO_4	50 mM	KH_2PO_4
300 mM	KCl	300 mM	KCl
10 mM	Imidazole	500 mM	Imidazole
5 mM	2 - mercaptoethanole*	5 mM	2 - mercaptoethanole*

*Only added for proteins with cysteine

higher than 0.5 ml/min to account for the comparatively slow binding kinetics of the GST tag. After a washing step with ∼ 5 to 10 CV of buffer A (table 9.4), proteins were eluted with 5 CV of 100 % buffer B (table 9.4). During the elution step, protein fractions of 5 ml were collected and afterwards analyzed by SDS - PAGE. Fractions containing the protein of interest were pooled and the solution subjected Thrombin cleavage to remove the affinity tag (see section 9.6).

Table 9.4: Buffer for GST affinity chromatography of proteins . The pH of buffer A was adjusted to 7.3 before use, the pH of buffer B to 8.0.

Buffer A		**Buffer B**	
10 mM	NaH_2PO_4	50 mM	Tis/HCL
1.8 mM	KH_2PO_4	10 mM	reduced glutathione
140 mM	NaCl		
2.7 mM	KCl		

9.4.2 Anion Exchange Chromatography

For proteins purified with an anion exchange chromatography as first step, self-packed columns (XK 16/20 column body, GE Healthcare, Munich, Germany) with a bed volume of 40 ml were prepared containing Q-Sepharose Fast Flow carrier material (GE Healthcare, Munich, Germany). Crude proteins extracts (see sections 9.1) were applied to the column equilibrated with buffer A (table 9.5) at a flow rate of 2 ml/min to allow for binding. After a washing step with 10 column volumes of buffer A , proteins were eluted by a linear gradient applied over ∼ 5 CV to 100 % buffer B (table 9.5). Protein fractions of 8 ml were collected during the whole run and afterwards analyzed by SDS-PAGE. Fractions containing the protein of interest were pooled.

In some cases, anion exchange chromatography was also used as last step of a purification to remove presumably degradation products of proteins that due to their small difference in molecular size compared to the native protein could not be removed otherwise by gelfiltration. Here, a prepacked Resource Q column (5 ml, GE Healthcare, Munich, Germany) was used similarly as described above. However, typically smaller fractions of 2 to 5 ml were collected and the gradient for elution was applied over ∼ 10 CV, in contrast.

Table 9.5: Buffer for anion exchange chromatography of proteins . The pH of both buffers was adjusted with HCl to 8.5 before use.

Buffer A		**Buffer B**	
40 mM	Tris	40 mM	Tris
20 mM	KCl	1 M	KCl

9.4.3 Cation Exchange Chromatography

For purifying p53 DBD, a heparin column was used. This column can be applied for affinity chromatography of coagulation factors that specifically bind heparin. However, it can also serve as cation exchange material due to its anionic sulfate groups, as in case of p53 DBD. For this purpose, a prepacked 5 ml HiTrap Heparin HP Column (GE Healthcare, Munich, Germany) was used. p53 DBD was applied to the column equilibrated with buffer A (table 9.6) at a flow rate of 2 ml/min to allow for binding. After a washing step with 10 column volumes of buffer A, the protein was eluted by a linear gradient applied over ~ 10 CV to 100 % buffer B (table 9.6). Protein fractions of 5 ml were collected during the protein elution step and afterwards analyzed by SDS - PAGE. Fractions containing the protein of interest were pooled.

Table 9.6: Buffer for heparin column chromatography of proteins. The pH of both buffers was adjusted with KOH to 6.8 before use.

Buffer A		**Buffer B**	
20 mM	NaH_2PO_4	20 mM	NaH_2PO_4
50 mM	NaCl	1 M	NaCl
5 mM	2 - Mercaptoethanole	5 mM	2 - Mercaptoethanole

9.4.4 Hydroxylapatite Chromatography

For purification of the Hsp90 N domain, a hydroxylapatite column was used. A self - packed column (XK 50/20 column body, GE Healthcare, Munich, Germany) with a bed volume of 80 ml was prepared containing hydroxylapatite carrier material (Bio - Rad Laboratories GmbH, Munich, Germany). The protein in buffer A was applied to the column equilibrated

with buffer A (table 9.7) at a flow rate of 2 ml/min. Hsp90 N bound only weakly to the column and was therefore already eluted during washing with 5 CV buffer A. Proteins bound to the column were eluted afterwards simply by applying buffer B (5 CV) (table 9.7). Protein fractions of 8 ml were collected during the whole run and afterwards analyzed by SDS - PAGE. Fractions containing the protein of interest were pooled.

Table 9.7: Buffer for hydroxylapatite chromatography of proteins. The pH of both buffers was adjusted with KOH to 6.8 before use.

Buffer A		**Buffer B**	
20 mM	NaH_2PO_4	200 mM	NaH_2PO_4

9.4.5 Gelfiltration Chromatography

As final step of most purifications, gelfiltration was performed. Depending on the size of the protein, a HiLoad 26/60 Superdex 75 pg or a HiLoad 26/60 Superdex 200 pg (GE Healthcare, Munich, Germany). Columns were equilibrated with an appropriate buffer (table 9.8) and proteins applied to the column in a maximum volume of 10 ml. Proteins were passed over the column at a constant flow of 2.5 ml/min. Protein fractions of 5 ml were collected after the void volume ($\sim$ 100 ml) had been eluted and afterwards analyzed by SDS - PAGE. Fractions containing the protein of interest were pooled.

9.4.6 Desalting/Buffer Exchange

For buffer exchange, a prepacked HiPrep 26/10 Desalting column (GE Healthcare, Munich, Germany) was used according to the recommenda-

Table 9.8: Buffer for gelfiltration chromatography of proteins. The pH of both buffers was adjusted with KOH to 7.5 before use.

Buffer 1		**Buffer 2**	
50 mM	KH_2PO_4	40 mM	HEPES
300 mM	KCL	300 mM	KCl
1 mM	TCEP*	1 mM	TCEP*

*Only added for proteins with cysteine

tions given by the supplier.

9.5 Concentration of Proteins

Concentration of protein solutions was done using Amicon Ultra - 4 and - 15 Centrifugal Filter Units (Merck Millipore, Billerica, MA, USA) with membranes of NMWL (nominal molecular weight limit) 3000, 10000 and 30000 Da in a swinging bucket rotor.

9.6 Protein Digest with Thrombin

Cleavage of affinity tags was achieved by digestion with thrombin (Merck KGaA, Darmstadt, Germany). Typically, fractions of affinity chromatography containing the protein of interest were pooled and concentrated to a volume of 10 ml (see section 9.5). 100 μl of thrombin (1 U/μl) were added and the mixture dialyzed over night at 4°C against 2 L of the respective buffer that was used in the next purification step.

9.7 Expression and Purification of Hsp90 Constructs

A construct of the yeast Hsp90 N domain (residues 1 to 210) in a pET11a plasmid (Novagen, Madison, WI, USA) was already available and could be used for expression. *E. coli* BL21(DE3) cells transformed with the plasmid were grown at 37°C to an OD_{600} of ~0.8. Then, protein expression induced with 1 mM IPTG was done for 3 h at 37°C. Cells were harvested, disrupted and a crude extract prepared as described under section 9.1. As a first step of the purification, an anion exchange chromatography was performed using a Q-Sepharose column (section 9.4.2). Protein fractions containing Hsp90 N were pooled and a buffer exchange (see section 9.4.6) was done with buffer A used for hydroxylapatite chromatography (table 9.7). Then a hydroxylapatite column run was performed as described in section 9.4.4. Hsp90 N was found only in the flow-through. The respective fractions were pooled again, concentrated to a volume of 10 ml (see section 9.5) and subjected gelfiltration using buffer 1 (table 9.8) as described in section 9.4.5. Fractions of the gelfiltration chromatography with Hsp90 N were pooled, concentrated to a volume of ~10 ml and again a buffer exchange done with a buffer as required for respective purpose. After concentration of the protein to an appropriate volume, aliquots were prepared, snap frozen in liquid nitrogen and stored at -80°C until use.

A construct of the yeast Hsp90 M domain (residues 273 to 527) in a pET28a plasmid (Novagen, Madison, WI, USA) carrying an N-terminal His_6-tag was available for expression and kindly provided by Dr. Franz Hagn (Institute for Advanced Study, TUM). A construct for the Hsp90 C domain (residues 528 to 709) was obtained here: The domain was cloned into a pET28a plasmid (Novagen, Madison, WI, USA) using the *NdeI*/*BamHI* restriction sites, adding an N-terminal His_6-tag to the pro-

tein. For expression of Hsp90 M and C, *E. coli* BL21(DE3) cells transformed with the respective plasmids were grown at 37°C to an OD_{600} of ~ 0.8. Then, protein expression was induced with 1 mM IPTG. Expression was done for 3 h at 37°C. Only in case of isotope labeling of Hsp90 C with deuterium, expression was done overnight at 30°C due the slower growth of cells in D_2O containing medium. Cells were harvested, disrupted and a crude extract prepared as described under section 9.1. As a first step of the purification, an IMAC affinity chromatography was performed as described in section 9.4.1. Fractions containing the protein of interest were pooled and subjected Thrombin cleavage to remove the affinity tag (see section 9.6). Afterwards, proteins were applied onto a Superdex 75 gelfiltration column using buffer 1 (table 9.8) as described in section 9.4.5. In case of Hsp90 M, gelfiltration fractions containing the protein were pooled, concentrated to 10 ml and subjected buffer exchange using an appropriate buffer. The protein was concentrated again, aliquots prepared, snap frozen in liquid nitrogen and stored at - 80°C until use.

In case of Hsp90 C, in contrast, after gelfiltration still degradation products were observed because of a higher protease sensitivity of the domain caused by the presence of larger unfolded regions in the protein. Due to the small difference in molecular size, degradation products could not be separated efficiently anymore from native protein by gelfiltration. Therefore, here additionally an anion exchange chromatography step was included using a Resource Q column as described in section 9.4.2: After gelfiltration, fractions containing Hsp90 C were pooled, concentrated to 10 ml and a buffer exchange done with anion exchange buffer A (table 9.5). The solution was then applied to the Resource Q column. Finally, fractions containing the protein were pooled, concentrated to 10 ml and subjected buffer exchange using an appropriate buffer. The protein was concentrated again, aliquots prepared, snap frozen in liquid nitrogen and

stored at - 80°C until use.

The Hsp90 C domain variants Δ10, Δ20 and Δ30 were purified like the wild - type protein. The Hsp90CΔ20Δ583-607 variant could be purified similar as described for the Hsp90 M domain due to its improved protease resistance.

A construct of full - length Hsp90 in a pET28a plasmid (Novagen, Madison, WI, USA) with N - terminal His_6 - tag was kindly provided by Dr. Marco Retzlaff (Lehrstuhl für Biotechnologie, TUM). The Hsp90 full - length mutants Hsp90Δ30 and Hsp90Δ583-607 were generated using this initial plasmid as template for mutagenesis. For expression of Hsp90 full - length variants, *E. coli* BL21(DE3) cells transformed with the respective plasmids were grown at 37°C to an OD_{600} of ~ 0.8. Then, protein expression induced with 1 mM IPTG was done for 3 h at 37°C. Cells were harvested, disrupted and a crude extract prepared as described under section 9.1. The purification procedure was basically similar as described for the wild - type Hsp90 C domain. However, following IMAC affinity chromatography, no Thrombin cleavage was done and a Superdex 200 column was used instead of the Superdex 75 variant for gelfiltration with the buffer 2 (table 9.8).

9.8 Expression and Purification of p53 DBD

A construct of p53 DBD (residues 99 to 312) in a pET28a plasmid (Novagen, Madison, WI, USA) with N - terminal His_6 - tag was kindly provided by Dr. Franz Hagn (Institute fo Advanced Study, TUM). For protein expression, *E. coli* BL21(DE3) cells transformed with the respective plasmid were grown at 37°C to an OD_{600} of ~ 0.8. Then, 100 μM $ZnSO_4$ was added to the cell culture, the temperature shifted down to 20°C and further incubated for one hour. By adding 1 mM IPTG, protein expres-

sion was induced for ~ 15 hours. Cells were harvested, disrupted and a crude extract prepared as described under section 9.1. As a first step in the purification, an IMAC affinity chromatography was used as described in section 9.4.1. Following Thrombin cleavage (section 9.6), p53 DBD was applied to a heparin column for cation exchange as described in section 9.4.3. p53 DBD was eluted as highly pure protein from the heparin column, therefore here no further purification was required. Fractions of the heparin column containing p53 DBD were pooled, concentrated to 10 ml and subjected buffer exchange (see section 9.4.6) with 50 mM potassium phosphate, 100 mM potassium chloride, 1 mM TCEP, pH 6.8. Finally, p53 DBD was concentrated, however not beyond ~ 400 μM since p53 DBD had a strong tendency to aggregate at higher concentrations. Aliquots were prepared from the solution, snap frozen in liquid nitrogen and stored at - 80°C until use.

9.9 Expression and Purification of Sti1 Constructs

A plasmid encoding the full - length wild - type Sti1 in a pET28a vector (Novagen, Madison, WI, USA) was already available. All other Sti1 TPR domain constructs used in this work were cloned into a pET28a plasmid (Novagen, Madison, WI, USA) using the *NdeI*/*BamHI* restriction sites, adding an N - terminal His_6 - tag to the proteins. For protein fermentation of all Sti1 full - length variants and TPR domain constructs except the TPR2BΔh7 variant, *E. coli* BL21(DE3) cells transformed with the respective plasmid were grown at 37°C to an OD_{600} of ~ 0.8. Expression was induced with 1 mM IPTG and performed over night at 25°C. Cells were harvested, disrupted and a crude extract prepared as described under section 9.1. The purification procedure was similar as described for the Hsp90 M domain (see section 9.7) using an IMAC affinity chromatography as first

step, followed by Thrombin cleavage, Superdex 75 gelfiltration and final buffer exchange.

In case of TPR2BΔh7, *E. coli* BL21(DE3) cells transformed with the respective plasmid were grown at 37°C to an OD_{600} of ~ 0.8. Expression was induced with 1 mM IPTG and performed for three hours at 37°C. Then, an inclusion body preparation was carried out (see section 9.2), followed by refolding of the protein (see section 9.3). All other steps of the purification were similar as described for the Hsp90 M domain (see section 9.7).

Initial Sti1 $DP1_{108-261}$ and $DP2_{493-589}$ constructs in a pGEX-4T vector (GE Healthcare, Munich, Germany) fused to a Thrombin cleavable GST tag were kindly provided by Dr. Sebastian Wandinger (Lehrstuhl für Biotechnologie, TUM). *E. coli* BL21(DE3) cells transformed with the respective plasmids were grown at 37°C to an OD_{600} of ~ 0.8. Expression was induced with 1 mM IPTG and performed for three hours at 37°C. Then, cells were harvested, disrupted and a crude extract prepared as described under section 9.1. As a first step of the purification, an GST affinity chromatography was done as described under section 9.4.1. Protein fractions containing the protein of interest were subjected Thrombin cleavage to remove the GST tag (see section 9.6). Afterwards, proteins were applied to a Superdex 75 gelfiltration column using buffer 1 (table 9.8) for the run (see section 9.4.5). Fractions containing DP domains were pooled, concentrated to 10 ml and a buffer exchange done with 50 mM potassium phosphate, 50 mM potassium chloride, pH 7.5. Following protein concentration, aliquots were prepared, snap frozen in liquid nitrogen and stored at -80°C until use.

Additional DP domain constructs were prepared in this work optimized for expression yield and domain boundaries. The $DP1_{127-197}$, $DP2_{493-589}$ and $DP2_{525-589}$ constructs were cloned into a pET28a plasmid (Novagen,

Madison, WI, USA) using the *NdeI*/*BamHI* restriction sites, adding an N-terminal His_6-tag to the proteins. For protein fermentation of these DP domain constructs as well as for all DP2 point mutants, *E. coli* BL21(DE3) cells transformed with the respective plasmids were grown at 37°C to an OD_{600} of ~ 0.8. Expression was induced with 1 mM IPTG and performed at 30°C for four hours. Cells were harvested, disrupted and a crude extract prepared as described under section 9.1. The purification was similar as described for the Hsp90 M domain (see section 9.7) using an IMAC affinity chromatography as a first step, followed by Thrombin cleavage, Superdex 75 gelfiltration and final buffer exchange.

9.10 Expression and Purification of Hsp70/Ssa1 Fragments

All Hsp70/Ssa1 constructs used in this work were cloned into a pET28a plasmid (Novagen, Madison, WI, USA) using the *NdeI*/*BamHI* restriction sites, adding an N-terminal His_6-tag to the proteins. Protein fermentation was done in *E. coli* BL21(DE3) cells transformed with the respective plasmids. Cells were grown at 37°C to an OD_{600} of ~ 0.8. Expression was induced with 1 mM IPTG and performed for four hours at 30°C. Cells were harvested, disrupted and a crude extract prepared as described under section 9.1. The purification procedure was similar as described for the Hsp90 M domain (see section 9.7) using an IMAC affinity chromatography as first step, followed by Thrombin cleavage, Superdex 75 gelfiltration and final buffer exchange.

9.11 Expression and Purification of Hch1

A plasmid encoding wild-type Hch1 in a pET28b vector (Novagen, Madison, WI, USA) fused with a His_6-tag to the protein was kindly provided by Dr. Klaus Richter (Lehrstuhl für Biotechnologie, TUM). For Hch1 protein expression, *E. coli* BL21(DE3) cells transformed with the plasmid were grown at 37°C to an OD_{600} of ~ 0.8. Expression was induced with 1 mM IPTG and performed at 37°C for four hours. Cells were harvested, disrupted and a crude extract prepared as described under section 9.1. Then, an inclusion body preparation was done (section 9.2), followed by refolding of the protein (section 9.3). The further protein purification procedure was similar as described for the Hsp90 M domain (see section 9.7), using an IMAC affinity chromatography as first step, followed by Thrombin cleavage, Superdex 75 gelfiltration and final buffer exchange.

9.12 Expression and Purification of Sba1 Constructs

A plasmid encoding wild-type Sba1 and Sba1Δ69 in a pET28b vector (Novagen, Madison, WI, USA) fused with a His_6-tag to the proteins was kindly provided by Dr. Martin Hessling (Lehrstuhl für Biotechnologie, TUM). The Sba1Δ94 truncation mutant was prepared in this work. For expression of all Sba1 variants, *E. coli* BL21(DE3) cells transformed with the respective plasmids were grown at 37°C to an OD_{600} of ~ 0.8. Expression was induced with 1 mM IPTG and performed at 37°C for four hours. Cells were harvested, disrupted and a crude extract prepared as described under section 9.1.

For Sba1Δ69 and Sba1Δ94, the further protein purification procedure was similar as described for the Hsp90 M domain (see section 9.7), using an IMAC affinity chromatography as first step, followed by Thrombin

cleavage, Superdex 75 gelfiltration and final buffer exchange. In case of wild - type Sba1, an additional anion exchange chromatography was performed after gelfiltration using a Resource Q column (see section 9.4.2) since the construct was highly sensitive to proteolytic digestion due to its unfolded C - domain.

Chapter 10

Protein Analysis

Chemicals were obtained from Carl Roth GmbH + Ko.KG, Merck KGaA and Sigma - Aldrich, if not otherwise stated.

10.1 SDS - PAGE

Sodium dodecylsulfate polyacrylamide gel electrophoresis (SDS - PAGE) for protein analysis was performed using the Hoefer system (Hoefer Inc., Holliston, MA, USA). For SDS - PAGE gels, buffers as shown in table 10.1 were prepared.

Separation and stacking gels contained the components as shown in table 10.2, which were mixed directly before casting gels. To start polymerization, 65 μl APS (ammoniumpersulfate) solution (10 %) and 4 μl TEMED (N,N,N',N' - tetramethylethylendiamine) were added.

For running SDS - PAGE gels, a buffer given in table 10.3 was used. Typically, 8 μl of a protein sample were mixed with 2 μl of 5x sample

Table 10.1: Buffer for casting SDS - PAGE gels.

2x stacking gel buffer		**4x separation gel buffer**	
0.4 % (w/v)	SDS	0.8 % (w/v)	SDS
0.25 M	Tris/HCL (pH 6.8)	1.5 M	Tris (pH 8.8)

Table 10.2: Components for polymerization of SDS gels.

12.5 % separation gel		**3 % stacking gel**	
3.125 ml	AA/bisAA* (40 % w/v)	0.625 ml	AA/bisAA* (40 % w/v)
2.5 ml	Separation gel buffer (4x)	2.5 ml	Stacking gel buffer (2x)
0.2 ml	SDS (10 % w/v)	0.1 ml	SDS (10 % w/v)
4.175 ml	H_2O	1.175 ml	H_2O

*AA, acrylamide; AA/bisAA used as 37.5:1

buffer (table 10.3) and incubated at 95°C for five to ten minutes before loading on a gel. Gels were developed applying a constant current of

Table 10.3: Buffer for running SDS - PAGE gels.

10x running buffer		**5x sample buffer**	
0.25 M	Tis/HCl	10 % (w/v)	SDS
2 M	Glycine	50 % (v/v)	Glycerine
1 % (w/v)	SDS	300 mM	Tis/HCl (pH 6.8)
		0.05 % (w/v)	Bromophenol blue
		5 % (v/v)	2 - mercaptoethanole

35 mA per gel for ∼ 45 minutes.

For staining gels, the solutions given in table 10.4 were used. Gels were first incubated in staining solution for ∼ one hour. Afterwards, they were

transferred into destaining solution. The destaining step was repeated twice.

Table 10.4: Solutions for staining SDS - PAGE gels.

Staining solution		**Destaining solution**	
25 % (v/v)	Ethanole	25 % (v/v)	Ethanole
10 % (v/v)	Acetic acid	10 % (v/v)	Acetic acid
0.04 % (w/v)	Coomassie Brilliant Blue R250		

10.2 Determination of Protein Concentration

Protein concentration was determined photometrically by measurement of the absorption at 280 nm. Theoretical extinction coefficients of proteins at 280 nm were calculated via the ExPASy ProtParam online tool at `http://web.expasy.org/protparam/`.

10.3 Chemical Crosslinking

For chemical crosslinking, 20 μM concentrated proteins were incubated in presence of 0.5% glutaraldehyde for 10 minutes at room temperature. To quench the reaction, Tris was added in excess over glutaraldehyde. Protein samples were analyzed by SDS - PAGE afterwards (see section 10.1).

10.4 UV/Vis Spectroscopy

UV/Vis spectra were recorded on a Cary-100 UV/Vis spectrophotometer (Varian, Palo Alto, CA, USA) or a Nanodrop-1000 UV/Vis spectrophotometer (PEQLab, Erlangen, Germany).

10.5 CD Spectroscopy

CD spectra and thermal transitions were recorded on a Jasco J-715 spectropolarimeter (Jasco, Groß-Umstadt, Germany). Typically, five scans were recorded and averaged for obtaining spectra, with a scanning speed of 100 nm/min, 5 nm bandwidth and 2 s response time. 300 μl of a protein sample in phosphate buffer with a concentration of 10 to 20 μM were measured in a 1 mm path length quartz cuvette (Hellma GmbH & Co. KG, Müllheim, Germany). For thermal transitions at a fixed wavelength, a heating rate of 50°C/h was applied.

10.6 ATPase Activity Assay

For determining the ATPase activity of Hsp90, a coupled regenerating enzymatic assay was performed as described earlier [244]. Full - length Hsp90 variants were used in a concentration of 4 μM. A typical reaction mixture contained the components as given in table 10.6. A mixture of PK (pyruvate kinase) and LDH (lactate dehydrogenase) as well as NADH (nicotinamide adenine dinucleotide) and PEP (phosphoenol pyruvate) were obtained from Sigma - Aldrich. Measurements were done in thermostatable quartz cuvettes with 10 mm path length. ATP solution was added as last component to start the reaction. The hydrolysis reaction could be followed by monitoring the decrease in absorption at 340 nm by UV/Vis spectrometry (see section 10.4).

10.7 ThermoFluor Stability Assay

ThermoFluor stability assays were done with a LightCycler iQ5 real time PCR machine (Bio - Rad, Munich, Germany). SYPRO®Orange stock in

Table 10.5: Reaction mixture of the coupled regenerating ATPase assay. NADH/PEP and ATP stock solutions were prepared with reaction buffer. ATP solution was added as last component to start the reaction.

Reaction buffer		**Reaction mixture**	
40 mM	HEPES	10 μL	NADH/PEP (16 mM/200 mM)
150 mM	KCl	8 .5 μL	PK/LDH enzyme mixture
5 mM	$MgCl_2$	X μL	Hsp90 variant*
		5 μL	ATP (400 mM)
		ad 1000 μL	Reaction buffer

*Hsp90 variants were added in a volume to obtain a final concentration of 4 μM

DMSO (5000x, Invitrogen, Carlsbad, CA, USA) was diluted in buffer to a 10x solution. Measurements were done in 96 well plates with sample volumes of 50 μl. 5 μl of 10x SYPRO®Orange were added to 45 μl of a protein sample with 5 μM concentration. A linear temperature ramp was applied from 25 to 95°C with a heating rate of 0.4°C/min. Excitation and emission filters were set to 490 and 575 nm, respectively. Melting curves were fitted with a sigmoidal function to determine the unfolding midpoint.

10.8 Isothermal Titration Calorimetry

Isothermal titration calorimetry (ITC) measurements were done on a VP-ITC and ITC_{200} instrument (GE Healthcare, Munich, Germany). The ligand was injected in 5 μl aliquots into the measurements cell with a spacing of 240 s between individual injections and 300 rpm stirring for the VP-ITC. In case of the ITC_{200} instrument, 1 μl aliquots were injected with 180 s spacing and 1000 rpm stirring. Raw binding data were corrected for dilution heats and fitted to a one - site binding model using the software

provided by the manufacturer.

10.9 Surface Plasmon Resonance

Surface plasmon resonance measurements were done on a Biacore® X instrument (GE Healthcare, Freiburg, Germany). Full - length Sti1 was immobilized to the surface of a CM5 sensor chip (GE Healthcare, Freiburg, Germany) using amine coupling. The chip was activated with a 1:1 mixture of 0.4 M EDC (1 - ethyl - 3 - (3 - dimethylaminopropyl) - carbodiimide) and 0.1 M NHS (N - hydroxysuccinimide). 10 μM Sti1 was coupled to the activated surface at a pH of 4.6. Afterwards, the chip was blocked with 1 M ethanolamine - HCl pH 8.5. For interaction measurements, ligand was injected at a flow - rate of 20 μl/min and 20°C.

Binding isotherms were fitted as described previously[333] with *OriginPro7.5* software (OriginLab Corporation, Northampton, MA, USA) according to

$$RU = RU_{max} \times \frac{c}{c + K_d} \tag{10.1}$$

with RU = resonance signal, RU_{max} = maximum signal at which all Sti1 molecules on the chip are saturated with the interaction partner and c = concentration of the ligand.

10.10 Chaperone Assay

Chaperone assays were performed in thermostatable 10 mm path length quartz cuvettes. Aggregation kinetics were recorded monitoring light scattering photometrically at a wavelength of 360 nm. All protein components in chaperone assays were centrifuged extensively (1 h, 15000 rpm, 4°C) before use.

10.11 Fluorescence Polarization Binding Assays

Fluorescence polarization binding assays were performed in a 384 - well plate format using a BMG Polarstar plate reader (BMG Labtech GmbH, Offenburg, Germany). Filters were set to 495 nm for excitation and 520 nm for emission. The labeled partner in the assay was applied in a fixed concentration of ~ 500 nM.

For labeling of proteins, an amine reactive active ester, 5' - 6' - carboxyfluorescein succinimidyl ester (FAM - SE, Invitrogen, Carlsbad, CA, USA), was used. A stock solution of the dye in DMSO was prepared and added to the protein in a ~ fivefold molar excess. Labeling was done in a buffer with a pH around 6.5 to favor attachment of the dye rather to the N - terminal end of the protein than to amino acid side - chains. Typically, the reaction was done for ~ 12 h at a temperature of 10°C. Labeling was quenched by adding Tris buffer pH 8.0 in molar excess over FAM - SE to the reaction and incubating for 1 h. Afterwards, labeled protein and free dye were separated by gelfiltration in a small scale using NAP^{TM} - 5 gravity columns (GE Healthcare, Munich, Germany), passing the protein twice over the column. The labeling efficiency L was calculated according to formula

$$L\,(\%) = \frac{A_{495}/\epsilon_{495,FAM-SE}}{(A_{280} - 0.3 \times A_{495})/\epsilon_{280,protein}} \times 100 \qquad (10.2)$$

with A = absorption at the specified wavelength in a 10 mm path length cuvette, ϵ = molar extinction coefficient. For $\epsilon_{495,FAM-SE}$, 68000 $M^{-1}cm^{-1}$ was used to calculate L. Applying the labeling procedure as described above, L was found to be in most cases close to 100 % or slightly below. Raw binding data were fitted to a one - site binding model with the *OriginPro7.5* software (OriginLab Corporation, Northampton, MA, USA)

using the equation

$$P = P_0 + \frac{P_a \times c_{ligand}}{K_d + c_{ligand}} \tag{10.3}$$

P is the measured polarization, P_a the amplitude of the polarization, P_0 the polarization at ligand concentration = 0 and c_{ligand} the concentration of the ligand added.

10.12 Analytical Gelfiltration

For analytical gelfiltration, a Tricorn 10/300 GL Superdex 75 column (GE Healthcare, Munich, Germnay) was used. Samples of 250 μl volume for proteins (50 μM) in an appropriate buffer were applied to the column. Elution behavior was monitored by following UV absorption at 280 nm at a constant flow rate of 0.5 ml/ml.

10.13 NMR Spectroscopy

NMR measurements were all done on Bruker AMX, DMX, Avance or AvanceIII instruments (Bruker Biospin, Rheinstetten, Germany) operating at 500, 600, 750 and 900 MHz proton resonance frequency. NMR data acquisition and processing was performed with the Topspin software as supplied by the manufacturer. For data evaluation, Sparky (T. D. Goddard and D. G. Kneller, SPARKY 3, University of California, San Francisco) was used.

10.13.1 Protein Resonance Assignment

Protein resonance assignment was done using the program PASTA [334] as well as in house written software.

10.13.2 NMR Chemical Shift Perturbation Experiments

For monitoring complex formation between proteins, care was taken to avoid buffer effects. To this end, two samples were prepared: One contained only the isotope labeled binding partner alone as a reference. The second contained the labeled protein in the same amount as the reference sample and additionally the unlabeled partner added in the desired molar ratio. Before the measurement, both samples were subjected to gelfiltration in a small scale using NAP^{TM} - 5 gravity columns (GE Healthcare, Munich, Germany) and the same buffer, thus ensuring identical pH and salt concentration in reference and complex sample. Spectra were then recorded with similar parameters on the two samples.

The chemical shift perturbation was calculated as described earlier [335] according to formula

$$\Delta\delta_{NH}(CSP) = \sqrt{\frac{(\Delta\delta_H)^2 + (\Delta\delta_N/5)^2}{2}} \tag{10.4}$$

where $\Delta\delta_{NH}$ is the averaged weighted chemical shift perturbation (CSP), $\Delta\delta_H$ is the observed chemical shift difference in the proton dimension and $\Delta\delta_N$ the observed chemical shift difference in the nitrogen dimension.

10.13.3 Extraction of Binding Affinities from NMR data

NMR chemical shift perturbation data obtained in protein - ligand titrations could be used to estimate binding affinities, however, only in case of lower affinity complexes. To account for the comparatively high concentration of the protein target, chemical shift data were fitted according

to the equation

$$\Delta\delta_{NH} = \Delta\delta_{NH,max} \frac{L_T + P_T + K_d - \sqrt{(L_T + P_T + K_d)^2 - 4\,L_T P_T}}{2\,P_T} \tag{10.5}$$

where $\Delta\delta_{NH}$ is the the averaged weighted chemical shift perturbation (see section 10.13.2), $\Delta\delta_{NH,max}$ the maximum chemical shift perturbation at saturating concentration of the ligand, P_T the total protein concentration and L_T the total ligand concentration.

10.13.4 PRE Experiments

Site directed spin labeling of proteins was done with the cysteine reactive compound 3 - (2 - Iodoacetamido) - PROXYL (2,2,5,5 - tetramethyl - 1 - pyrrolidinyloxy, Sigma - Aldrich). A 100 mM stock solution of the label in acetonitrile was prepared and a 10 - fold molar excess added to the protein. The labeling reaction was done for 2 h at room temperature. Afterwards, free label and protein were separated by gelfiltration in a small scale using NAP^{TM} - 5 gravity columns (GE Healthcare, Munich, Germany), passing the protein - label mixture twice over the column.

Paramagnetic relaxation enhancement (PRE) measurements were done adding an appropriate molar ratio of the spin labeled binding partner to the protein of interest and recording 2D ^{15}N - HSQC/TROSY spectra applying a longer d1 relaxation delay of $\sim$ 4 s. Afterwards, a 5 - to 10 - fold molar excess of ascorbic acid in pH adjusted buffer over the spin labeled binding partner was added to the sample and incubated at room temperature for 1 h to reduce off the spin label from the cysteine residue. Then, a second reference experiment of the sample was recorded applying identical measurement parameters. PRE intensity ratios were calculated by comparing peak intensities from the respective spectra.

Chapter 11

Software

For preparing this work the following software was used:

- **Data fitting and plotting:**

  OriginPro7.5 (OriginLab Corporation, Northampton, MA, USA)

  Xmgrace (Grace Development Team, Weizman Institute, Rechovot, Israel)

- **Protein primary sequence analysis:**

  ExPASy Proteomics Server (`http://expasy.org/proteomics`)

  PSIPRED (`http://bioinf.cs.ucl.ac.uk/psipred/`)

- **Sequence alignment:**

  T-Coffee (`http://www.ebi.ac.uk/Tools/msa/tcoffee/`)

  MUSCLE (`http://www.ebi.ac.uk/Tools/msa/muscle/`)

  Jalview (`http://www.jalview.org/`)

- **NMR data processing:**

  Topsin 1.3 (Bruker Biospin, Rheinstetten, Germany)

- **NMR spectra analysis:**

  Sparky (UCSF, San Francisco, CA, USA)

- **NMR structure calculation:**

  Xplor-NIH (NIH, Bethesda, MD, USA)

- **Structure validation:**

  PROCHECK-NMR (R. Laskowski, University College London, London, UK)

- **Molecular Docking:**

  HADDOCK (A. Bonvin, Utrecht University, NL)

- **Protein hydrodynamic calculations:**

  HYDRONMR (J. Garcia de la Torre, Universidad de Murcia, Spain)

- **RDC analysis:**

  PALES (M. Zweckstetter, MPI Göttingen, Germany)

- **Structure visualization:**

  PyMOL (DeLano Scientific, Palo Alto, CA, USA)

  CHIMERA (UCSF, San Francisco, CA, USA)

- **Figure Preparation:**

  CorelDRAW X4 (Corel Corporation, Unterschleißheim, Germany)

Part IV

Appendix

Chemical Shift Lists

Table 11.1: Chemical shift assignment of Hsp90 CΔ20 . The assignment was obtained in a buffer of 10 mM potassium phosphate, 1 mM TCEP, pH 6.8 at 318 K.

Residue	N (HN)	CO	C^{α}	C^{β}
F528	120.48 (8.09)	175.55	57.18	38.79
E529	122.27 (8.18)	175.92	56.12	29.67
L530	123.03 (8.05)	177.06	54.67	41.72
E531	122.13 (8.26)	176.14	55.97	29.73
E532	122.94 (8.30)	176.75	55.92	30.34
T533	115.22 (8.48)	175.11	60.91	70.34
D534	122.12 (8.70)	179.23	56.42	39.86
E535	121.35 (8.62)	178.53	59.09	28.75
E536	121.40 (7.89)	178.74	58.30	28.96
K537	120.75 (8.14)	178.59	59.13	31.58
A538	121.78 (7.95)	180.64	54.44	17.43
E539	119.36 (7.98)	179.04	58.48	28.62
R540	120.93 (7.99)	178.01	58.56	28.89
E541	118.69 (8.11)	179.25	59.15	28.64
K542	119.45 (7.67)	178.55	59.20	31.52
E543	121.98 (7.95)	178.51	59.39	29.49
I544	120.00 (8.61)	179.38	65.82	37.30
K545	119.99 (7.66)	180.39	58.77	31.14
E546	121.12 (8.24)	178.13	58.45	28.68
Y547	116.70 (8.03)	175.80	59.77	39.00
E548	123.64 (7.76)	175.75	60.66	26.71
P549	.	.	66.16	29.62
L550	119.39 (8.05)	178.48	57.80	40.28
T551	111.63 (8.75)	177.61	66.10	67.59
K552	123.11 (8.15)	179.06	59.42	31.59
A553	123.12 (7.92)	180.22	54.64	17.69
L554	116.61 (8.74)	178.68	57.86	40.48
K555	121.52 (8.21)	178.16	58.39	30.59
E556	119.56 (7.79)	179.34	58.67	28.45
I557	119.72 (7.83)	177.69	64.38	38.16
L558	118.25 (7.93)	178.37	55.25	41.23
G559	109.47 (8.08)	176.49	46.25	
D560	122.72 (8.51)	176.81	54.86	39.96
Q561	117.03 (7.82)	176.11	57.73	28.77
V562	108.79 (7.13)	174.29	58.04	33.61
E563	123.02 (9.12)	176.74	57.27	29.91
K564	113.31 (7.24)	173.33	54.59	35.26
V565	123.67 (8.57)	174.84	60.69	32.16
V566	120.40 (8.77)	174.34	58.20	35.28
V567	121.34 (8.41)	175.88	61.14	31.32
S568	118.92 (8.45)	174.40	55.30	64.37
Y569	125.93 (8.95)	175.84	59.45	37.15
K570	119.14 (7.93)	175.93	55.25	31.77
L571	121.14 (7.28)	176.05	54.47	40.57
L572	124.54 (8.47)	177.24	55.45	40.77
D573	119.50 (8.35)	175.08	54.03	40.26
A574	122.50 (7.51)	175.88	49.92	19.48
P575	.	.	63.82	30.92
A576	114.23 (6.75)	175.76	49.98	22.76
A577	121.37 (8.89)	174.91	51.47	22.73
I578	119.47 (8.33)	175.12	57.95	38.04
R579	126.82 (8.82)	175.88	54.09	31.41
T580	116.97 (8.54)	174.92	60.67	79.99
G581	110.40 (8.33)	300.00	45.07	
Q582	.	177.81	57.54	29.39
F583	120.90 (7.83)	177.64	62.55	37.60
G584	.	.	.	
W585	.	.	.	.
S586	.	176.39	56.45	64.32
A587	123.42 (8.01)	178.33	52.80	18.13
N588	120.13 (7.88)	178.37	55.40	41.35
M589	.	176.95	56.07	31.70

Residue	N (HN)	CO	C^{α}	C^{β}
E590	120.84 (8.19)	177.46	58.02	29.04
R591	119.44 (7.92)	177.62	57.44	29.30
I592	120.32 (7.77)	177.32	62.33	37.47
M593	.	.	.	.
K594	.	.	.	.
A595	.	.	.	.
Q596	.	.	.	.
A597	.	.	.	.
L598	.	.	.	.
R599	.	.	.	.
D600	.	.	.	.
S601	.	.	.	.
S602	.	.	.	.
M603	.	.	.	.
S604	.	.	.	.
S605	.	.	.	.
Y606	.	.	.	.
M607	.	.	.	.
S608	.	.	.	.
S609	.	.	.	.
K610	.	176.80	55.54	32.39
K611	121.38 (8.60)	176.08	55.67	34.59
T612	119.98 (9.05)	172.42	62.67	70.06
F613	129.36 (8.66)	172.52	54.20	40.99
E614	127.54 (9.01)	175.49	53.49	31.91
I615	111.32 (8.28)	174.69	57.91	40.59
S616	116.08 (7.85)	174.49	52.60	64.40
P617	.	.	62.94	31.06
K618	114.04 (7.14)	176.97	55.04	31.66
S619	114.30 (7.09)	175.07	54.44	63.65
P620	.	.	64.85	31.93
I621	117.11 (7.34)	176.59	64.84	38.31
I622	119.87 (6.64)	178.31	60.69	33.63

Residue	N (HN)	CO	C^{α}	C^{β}
L658	120.86 (8.29)	177.50	53.70	41.26
D659	123.35 (8.91)	88.61	56.22	40.77
E660	117.63 (8.38)	174.70	53.17	29.82
P661	.	.	65.29	31.49
T662	111.14 (8.39)	177.50	65.57	67.69
S663	119.82 (7.85)	88.36	60.52	62.19
F664	124.93 (7.55)	176.73	60.73	38.73
A665	120.80 (8.35)	179.22	54.95	17.56
S666	112.83 (7.91)	88.59	61.76	62.48
R667	122.68 (7.68)	179.22	59.42	30.30
I668	121.55 (7.93)	177.93	63.23	35.08
N669	119.90 (8.44)	178.86	56.11	36.63
R670	121.57 (7.83)	178.71	59.37	29.02
L671	122.08 (7.78)	179.47	57.33	40.58
I672	121.47 (8.83)	177.62	65.89	37.05
S673	115.31 (7.95)	88.05	62.81	61.42
L674	122.42 (7.91)	180.99	57.67	41.27
G675	108.21 (8.50)	174.41	46.28	
L676	118.40 (7.83)	175.56	53.91	41.57
N677	116.85 (7.93)	174.33	54.02	36.77
I678	116.83 (7.98)	175.86	60.84	37.84
D679	125.81 (8.35)	175.90	54.12	40.92
E680	122.38 (8.30)	176.09	56.04	29.95
D681	122.30 (8.37)	176.12	54.14	40.92
E682	121.93 (8.30)	176.50	56.30	29.88
E683	122.82 (8.44)	176.61	56.19	29.54
T684	116.29 (8.14)	174.51	61.62	69.55
E685	124.17 (8.40)	176.43	56.20	29.72
T686	117.02 (8.17)	173.88	61.33	69.59
A687	128.84 (8.34)	175.62	50.16	17.64
P688	.	.	62.87	31.13
E689	126.11 (7.85)	181.18	57.71	30.64

Table 11.2: Chemical shift assignment of the Sti1 TPR2A domain. The assignment was obtained in a buffer of 50 mM potassium phosphate, 50 mM potassium chloride, 1 mM TCEP, pH 7.5 at 293 K.

Residue	N (HN)	CO	C^{α}	C^{β}
E261	119.67 (8.04)	179.26	58.57	28.37
A262	124.30 (8.54)	179.32	55.03	18.92
D263	117.62 (8.40)	179.61	56.81	39.33
K264	121.86 (7.62)	179.86	59.19	30.67
E265	120.43 (7.41)	179.12	58.47	27.36
K266	120.96 (8.47)	177.65	59.67	29.27
A267	121.01 (8.14)	181.09	54.78	16.68
E268	120.31 (7.83)	178.82	58.32	27.74
G269	106.34 (8.57)	174.75	47.78	
N270	119.70 (8.81)	177.41	54.77	36.47
K271	122.73 (7.60)	179.73	59.34	30.11
F272	118.36 (7.54)	177.56	62.02	36.95
Y273	122.55 (9.22)	179.59	61.70	38.71
K274	120.77 (8.28)	176.88	58.52	30.97
A275	119.04 (6.95)	175.60	51.11	17.67
R276	112.20 (7.45)	174.53	56.16	24.45
Q277	120.12 (7.83)	176.41	52.91	26.50
F278	117.40 (6.89)	177.26	61.70	38.00
D279	119.68 (8.45)	178.81	57.88	38.57
E280	122.86 (8.72)	178.76	59.30	26.63
A281	120.63 (7.77)	177.88	55.47	16.80
I282	117.19 (8.25)	176.74	66.59	37.44
E283	117.54 (7.43)	179.78	58.91	28.12
H284	116.60 (7.27)	176.89	59.46	26.81
Y285	120.32 (8.68)	178.19	58.84	35.60
N286	116.63 (8.57)	178.18	55.63	37.20
K287	121.12 (7.65)	178.66	58.58	30.55
A288	121.27 (7.99)	176.76	55.73	15.12
W289	115.84 (7.60)	176.72	58.33	28.88
E290	116.55 (7.91)	178.54	58.27	28.51
L291	118.76 (7.49)	177.38	56.42	43.02
H292	120.37 (8.52)	172.30	56.05	32.81
K293	123.74 (7.38)	174.28	53.93	27.87
D294	125.40 (7.13)	177.89	51.62	41.56
I295	119.82 (8.74)	177.12	64.53	36.61
T296	119.03 (8.83)	176.66	66.06	68.07
Y297	119.79 (7.57)	178.79	57.78	36.83
L298	115.98 (6.50)	178.21	56.11	40.30
N299	119.07 (7.76)	178.84	55.27	35.69
N300	119.76 (7.99)	176.34	55.50	34.96
R301	122.25 (7.58)	177.65	60.22	29.66
A302	119.25 (8.50)	180.53	52.91	17.84
A303	121.78 (7.62)	179.53	54.80	16.12
A304	120.63 (7.53)	178.12	54.77	18.24
E305	118.66 (8.36)	178.11	59.38	27.38
Y306	119.22 (8.64)	179.41	61.14	37.70
E307	121.52 (8.18)	178.37	57.95	27.32
K308	115.86 (7.14)	176.31	56.79	31.45
G309	106.42 (7.45)	173.74	43.11	
E310	121.18 (7.38)	176.37	52.71	25.18
Y311	119.35 (6.49)	177.19	61.25	36.69
E312	116.32 (8.87)	179.57	59.83	27.73
T313	118.68 (7.62)	174.38	65.84	67.66
A314	122.81 (8.02)	179.43	54.25	16.30
I315	116.20 (7.82)	177.30	65.95	37.37
S316	115.92 (7.55)	88.69	61.75	59.70
T317	121.49 (8.69)	177.07	65.36	66.50
L318	121.46 (8.38)	178.57	56.92	41.41
N319	119.17 (8.65)	178.61	55.92	37.62
D320	121.36 (7.55)	177.66	56.78	39.08
A321	122.55 (8.11)	179.66	54.78	16.61
V322	117.52 (8.20)	177.62	66.65	30.86
E323	118.92 (7.77)	180.53	59.27	28.81
Q324	117.31 (8.78)	178.60	58.00	27.13
G325	109.33 (8.78)	175.88	46.90	
R326	121.30 (8.51)	180.25	58.52	28.49
E327	120.21 (7.45)	177.95	58.69	28.39
M328	113.95 (7.92)	175.00	55.09	32.29
R329	117.64 (7.66)	175.80	56.42	25.11
A330	119.92 (8.33)	175.95	51.39	18.61
D331	118.36 (8.13)	177.91	54.30	41.88
Y332	125.86 (7.91)	177.06	59.41	36.33
K333	120.55 (7.74)	179.81	59.19	30.00
V334	120.40 (7.22)	177.74	65.17	30.34
I335	120.15 (7.30)	88.92	63.75	35.80
S336	110.62 (8.29)	89.40	62.00	63.02
K337	122.80 (7.29)	178.76	58.63	30.53
S338	118.19 (8.12)	176.43	62.95	61.80
F339	116.67 (7.90)	178.00	59.25	37.64
A340	120.86 (8.16)	179.08	55.48	16.71
R341	116.52 (8.17)	179.44	58.32	28.34
I342	123.44 (8.03)	177.92	66.16	36.67
G343	106.30 (8.05)	174.58	47.79	
N344	117.91 (8.43)	177.80	55.12	37.38
A345	123.01 (7.84)	178.66	55.18	17.22
Y346	116.82 (8.39)	178.49	62.87	36.45
H347	123.37 (8.28)	180.74	59.56	29.67
K348	120.17 (7.33)	179.17	56.35	29.45
L349	117.64 (7.24)	177.27	54.97	41.30
G350	107.68 (7.65)	173.47	44.68	

Residue	N (HN)	CO	C^{α}	C^{β}
D351	120.21 (7.86)	176.76	51.42	39.48
L352	127.25 (8.38)	178.33	56.79	41.29
K353	118.36 (8.11)	180.31	59.73	29.05
K354	118.91 (7.62)	178.18	57.70	30.74
T355	117.84 (7.53)	174.59	67.67	63.42
I356	118.93 (7.43)	176.99	65.35	37.75
E357	118.27 (7.56)	179.53	58.41	28.54
Y358	115.99 (8.02)	178.76	63.78	35.69
Y359	121.07 (8.47)	178.71	57.42	35.59
Q360	118.78 (8.57)	179.50	59.02	26.34
K361	119.69 (7.72)	179.23	59.50	29.96
S362	111.88 (8.12)	177.75	61.99	.
L363	120.38 (8.20)	178.37	56.69	41.08
T364	114.94 (8.05)	175.48	65.53	68.23
E365	119.64 (7.21)	176.59	57.77	29.34
H366	115.83 (8.03)	172.28	55.56	31.26
R367	130.16 (8.60)	175.01	57.47	28.70
T368	112.92 (6.40)	174.84	58.53	71.93
A369	118.19 (8.12)	180.24	54.28	17.18
D370	115.18 (8.52)	178.00	56.46	40.31
I371	116.17 (6.94)	177.21	59.83	32.38
L372	123.73 (7.60)	179.10	58.37	40.32
T373	115.13 (7.73)	176.07	66.11	67.97
K374	120.35 (7.43)	179.51	59.44	30.94
L375	121.61 (8.65)	177.27	58.33	40.20
R376	118.13 (7.98)	180.09	58.23	28.48
N377	117.21 (8.12)	177.53	55.47	36.85
A378	124.76 (8.16)	179.25	54.84	16.88
E379	117.21 (8.60)	179.91	59.59	28.98
K380	119.05 (7.62)	179.03	58.98	31.16
E381	120.11 (7.86)	179.13	58.75	28.80
L382	121.00 (8.09)	178.02	57.16	40.63
K383	117.81 (7.59)	178.44	57.57	31.05
K384	118.16 (7.55)	177.28	57.44	31.28
A385	121.78 (7.71)	178.18	52.70	17.92
E386	118.20 (7.79)	175.20	55.97	29.31
A387	129.30 (7.51)	182.53	53.55	18.87

Table 11.3: Chemical shift assignment of the Sti1 TPR2B domain. The assignment was obtained in a buffer of 50 mM potassium phosphate, 50 mM potassium chloride, 1 mM TCEP, pH 7.5 at 293 K.

Residue	N (HN)	CO	C^{α} (H^{α})	C^{β} (H^{β})	other
E388	122.18 (8.32)	176.67	56.17 (4.08)	28.58 (1.92, 1.84)	C^{γ}, 35.37 (2.15, 2.09); C^{δ}, . ;
A389	123.89 (8.16)	177.21	52.04 (4.15)	17.58 (1.30)	
Y390	120.01 (8.12)	176.11	58.32 (4.08)	38.87 (2.87, 2.79)	$C^{\delta1}$, . (7.24); $C^{\delta2}$, . (7.24); $C^{\epsilon1}$, . (6.87); $C^{\epsilon2}$, . (6.87); C^{ζ}, . ;
V391	117.47 (7.26)	176.81	63.15 (3.77)	30.30 (1.92)	$C^{\gamma1}$, 20.26 (0.90); $C^{\gamma2}$, 20.68 (0.94);
N392	123.66 (8.49)	172.63	51.56 (4.88)	39.32 (2.80, 2.50)	$N^{\delta2}$, 113.87 (7.13, 7.77);
P393	.	.	64.25 (4.27)	30.92 (2.29, 1.91)	C^{γ}, 25.70 (2.02, 2.02); C^{δ}, 50.29 (3.83, 3.63);
E394	120.58 (8.08)	179.84	59.13 (4.02)	27.51 (1.97, 2.08)	C^{γ}, 36.10 (2.32, 2.03); C^{δ}, . ;
K395	119.12 (8.10)	180.03	56.49 (3.91)	30.40 (1.50, 1.50)	C^{γ}, 24.00 (1.21, 1.21); C^{δ}, 26.94 (1.32, 1.32); C^{ϵ}, 40.82 (2.85, 2.85); N^{ζ}, . (*);
A396	124.03 (8.35)	178.30	54.87 (3.79)	18.10 (1.44)	
E397	118.68 (7.53)	177.97	56.83 (4.47)	27.30 (1.95, 1.95)	C^{γ}, 35.44 (. , .); C^{δ}, . ;
E398	118.35 (7.55)	179.28	58.58 (3.80)	28.58 (2.03, 2.03)	C^{γ}, 35.25 (2.32, 1.90); C^{δ}, . ;
A399	121.65 (7.56)	178.64	53.98 (4.02)	15.95 (1.43)	
R400	120.29 (8.36)	179.28	59.09 (3.79)	29.42 (1.98, 1.98)	C^{γ}, 25.88 (. , .); C^{δ}, 42.30 (2.96, 2.96); C^{ζ}, . ; N^{ϵ}, . (.); $N^{\eta1}$, . (*, *); $N^{\eta2}$, . (*, *);
L401	118.79 (8.06)	180.09	56.62 (3.80)	40.13 (1.67, 1.25)	C^{γ}, . (.); $C^{\delta1}$, 21.43(0.67); $C^{\delta2}$, 24.13 (0.74);
E402	121.55 (7.87)	178.80	58.30 (3.73)	28.26 (1.88, 1.88)	C^{γ}, 35.49 (2.18, 1.92); C^{δ}, .;
G403	107.31 (8.71)	174.56	47.21 (3.21, 2.72)		
K404	122.34 (8.16)	179.41	58.23 (3.91)	30.63 (1.90, 1.90)	C^{γ}, 23.21 (1.32, 1.32); C^{δ}, 28.14 (. , .); C^{ϵ}, 40.55 (2.75, 2.75); N^{ζ}, .(*);
E405	121.38 (7.64)	179.47	58.27 (3.93)	27.25 (1.69, 1.69)	C^{γ}, 34.37 (1.97, 1.97); C^{δ}, .;
Y406	117.46 (8.02)	178.15	60.73 (4.15)	35.94 (3.28, 2.51)	$C^{\delta1}$, . (7.18); $C^{\delta2}$, . (7.18); $C^{\epsilon1}$, . (6.73); $C^{\epsilon2}$, . (6.73); C^{ζ}, . ;
F407	121.48 (9.17)	179.73	61.15 (3.82)	38.90 (3.43, 3.29)	$C^{\delta1}$, . (7.18); $C^{\delta2}$, . (7.18); $C^{\epsilon1}$, . (.); $C^{\epsilon2}$, . (.); C^{ζ}, . (.);
T408	116.16 (8.62)	175.18	65.43 (4.00)	68.21 (4.33)	$C^{\gamma2}$, 20.61(1.24);
K409	119.44 (7.17)	175.18	55.15 (4.12)	30.90 (1.87, 1.87)	C^{γ}, 23.67 (1.87, 1.42); C^{δ}, 27.81 (1.54, 1.54); C^{ϵ}, 41.00 (2.81, 2.81); N^{ζ}, . (*);
S410	110.53 (7.30)	171.77	56.31 (4.19)	58.97 (3.23, 3.72)	
D411	118.8 (7.69)	176.06	48.98 (4.33)	37.60 (2.11, 2.78)	
W412	119.30 (6.72)	175.26	57.57 (4.61)	26.49 (2.89, 3.34)	$C^{\delta1}$, . (.); $C^{\delta2}$, . $C^{\epsilon2}$, . $C^{\epsilon3}$, . (.); $C^{\eta2}$, . (.); $C^{\zeta2}$, . (.); $C^{\zeta3}$, . (.); $N^{\epsilon1}$, 129.69 (10.22);
P413	.	.	65.28 (4.08)	30.09 (2.16, 2.16)	C^{γ}, 27.43 (1.23, 1.23); C^{δ}, 50.36 (3.88, 3.88);
N414	113.79 (6.79)	177.22	54.35 (4.24)	33.58 (1.31, 0.25)	$N^{\delta2}$, . (. , .);
A415	124.61 (8.12)	178.36	55.18 (4.02)	16.03 (1.65)	
V416	117.38 (8.57)	179.31	67.35 (3.39)	30.40 (2.13)	$C^{\gamma1}$, 22.83 (0.92); $C^{\gamma2}$, 19.98 (0.69);
K417	121.95 (7.43)	178.87	59.39 (3.79)	31.15 (1.81, 1.81)	C^{γ}, 24.08 (1.22, 1.22); C^{δ}, 28.04 (1.50, 1.50); C^{ϵ}, 40.80 (2.80, 2.80); N^{ζ}, . (*);
A418	124.14 (8.21)	180.12	54.17 (4.21)	16.50 (1.31)	
Y419	115.23 (8.69)	177.66	59.61 (4.42)	35.16 (3.24, 2.50)	$C^{\delta1}$, . (7.38); $C^{\delta2}$, . (7.38); $C^{\epsilon1}$, . (6.82); $C^{\epsilon2}$, . (6.82); C^{ζ}, . ;
T420	117.83 (8.19)	175.15	66.93 (3.82)	67.38 (4.45)	$C^{\gamma2}$, 19.30 (1.03);
E421	123.47 (7.38)	177.62	57.75 (4.19)	26.35 (., .)	C^{γ}, 33.68 (2.32, 2.00); C^{δ}, . ;
M422	120.12 (8.15)	176.40	60.23 (4.14)	30.49 (1.80, 1.80)	C^{γ}, 31.44 (2.65, 2.46); C^{ϵ}, 15.58 (1.90);
I423	119.25 (7.80)	177.54	63.55 (3.32)	38.04 (1.49)	$C^{\gamma1}$, 27.94 (-0.49, -0.49); $C^{\gamma2}$, 15.94 (0.49); $C^{\delta1}$, 13.31 (0.11);
K424	117.46 (7.47)	178.57	58.16 (3.80)	31.82 (1.82, 1.82)	C^{γ}, 24.33 (1.42, 1.10); C^{δ}, 28.60 (1.77, 1.77); C^{ϵ}, 41.15 (2.47, 2.47); N^{ζ}, . (*);
R425	113.00 (7.88)	176.31	54.52 (4.17)	30.22 (., .)	C^{γ}, 24.55 (. , .); C^{δ}, 42.87 (2.60, 2.60); C^{ζ}, . N^{ϵ}, . (.); $N^{\eta1}$, . (*, *); $N^{\eta2}$, . (*, *);
A426	121.89 (8.12)	173.83	49.98 (4.67)	17.87 (1.15)	
P427	.	.	63.93 (4.65)	30.87 (2.34, 1.89)	C^{γ}, 25.96 (1.96, 1.96); C^{δ}, 49.00 (3.47, 3.47)
E428	114.29 (8.74)	175.37	53.43 (4.47)	27.15 (2.24, 2.24)	C^{γ}, 34.14 (2.26, 2.26); C^{δ}, . ;
D429	120.11 (7.53)	177.16	52.16 (4.55)	40.49 (2.28, 3.34)	
A430	129.21 (9.05)	178.51	54.41 (3.88)	19.78 (1.30)	
R431	112.70 (8.51)	179.20	57.94 (3.74)	28.83 (1.48, 1.48)	C^{γ}, 26.00 (1.56, 1.56); C^{δ}, 42.40 (3.07, 3.07); C^{ζ}, . ; N^{ϵ}, . (.); $N^{\eta1}$, . (*, *); $N^{\eta2}$, . (*, *);
G432	105.60 (7.12)	174.69	47.48 (4.01, 3.67)		
Y433	117.40 (6.13)	177.61	59.65 (3.77)	37.09 (2.36, 3.44)	$C^{\delta1}$, . (6.95); $C^{\delta2}$, . (6.95); $C^{\epsilon1}$, . (6.11); $C^{\epsilon2}$, . (6.11); C^{ζ}, . ;
S434	111.36 (7.61)	176.88	60.09 (3.72)	62.41 (3.37, 3.69)	
N435	118.05 (8.19)	176.75	54.19 (3.74)	33.38 (1.63, 0.67)	$N^{\delta2}$, 118.10 (6.61, 8.95);
R436	121.19 (8.03)	178.39	61.18 (3.73)	29.15 (1.47, 1.47)	C^{γ}, 26.92 (., .); C^{δ}, 40.16 (., .); C^{ζ}, . N^{ϵ}, 111.28 (6.33); $N^{\eta1}$, .(*, *); $N^{\eta2}$, . (*, *);
A437	119.65 (8.29)	179.26	54.53 (3.86)	18.79 (1.53)	
A438	118.66 (7.46)	180.32	53.83 (3.87)	16.65 (1.32)	
A439	120.52 (7.49)	177.86	54.24 (3.97)	17.96 (1.78)	

Residue	N (HN)	CO	C^{α} (H^{α})	C^{β} (H^{β})	other
L440	118.69 (8.73)	179.68	56.81 (3.82)	40.12 (1.63, 1.29)	C^{γ}, 26.04 (1.71); $C^{\delta1}$, 25.55 (0.63); $C^{\delta2}$, 21.54 (0.67);
A441	120.81 (8.40)	181.70	54.14 (3.25)	16.02 (1.29)	
K442	118.72 (6.78)	178.06	55.73 (3.47)	28.62 (-0.57, 0.94)	C^{γ}, 21.20 (1.30, 1.24); C^{δ}, 26.59 (. , .); C^{ϵ}, 41.08 (2.54, 2.54); N^{ζ}, . (*);
L443	117.61 (6.66)	175.50	53.71 (4.03)	40.55 (1.51, 1.61)	C^{γ}, . (.); $C^{\delta1}$, 24.42 (0.62); $C^{\delta2}$, 22.53 (0.89);
M444	112.34 (7.33)	175.16	54.62 (2.72)	26.72 (2.23, 2.23)	C^{γ}, 31.24 (2.37, 2.37); C^{ϵ}, 16.16 (2.05);
S445	118.57 (7.63)	175.27	54.34 (4.46)	60.77 (3.89, 3.32)	
F446	117.51 (7.11)	174.15	62.59 (4.05)	35.95 (2.86, 2.77)	$C^{\delta1}$, . (7.01); $C^{\delta2}$, . (7.01); $C^{\epsilon1}$, . (.); $C^{\epsilon2}$, . (.); C^{ζ}, . (.);
P447	.	.	65.68 (4.08)	29.26 (2.21, 1.84)	C^{γ}, 27.50 (. , .); C^{δ}, 49.19 (3.89, 3.89);
E448	119.09 (8.77)	178.76	59.54 (3.85)	27.13 (1.87, 1.87)	C^{γ}, 36.38 (2.17, 2.17); C^{δ}, . ;
A449	123.32 (8.00)	179.78	54.58 (3.87)	16.50 (1.33)	
I450	120.03 (8.59)	176.78	66.24 (3.08)	36.90 (1.71)	$C^{\gamma1}$, 30.45 (0.62, 0.62); $C^{\gamma2}$, 15.71 (0.63); $C^{\delta1}$, 12.03 (0.55);
A451	120.99 (7.67)	181.09	54.44 (3.85)	16.41 (1.37)	
D452	120.23 (7.62)	179.46	56.55 (4.50)	39.18 (2.54, 3.10)	
C453	119.18 (8.26)	176.23	64.30 (3.67)	25.69 (2.90, 2.35)	
N454	117.37 (8.34)	178.53	54.35 (4.27)	35.61 (2.72, 2.48)	$N^{\delta2}$, 110.07 (6.72, 7.21);
K455	122.10 (7.45)	177.59	56.94 (3.66)	29.90 (0.63, 1.45)	C^{γ}, 23.04 (0.92, 0.92); C^{δ}, 27.00 (1.36, 1.24); C^{ϵ}, 40.53 (2.62, 2.62); N^{ζ}, . (*);
A456	120.90 (7.93)	178.06	54.73 (3.65)	17.30 (1.37)	
I457	116.33 (7.70)	177.52	62.98 (3.39)	37.62 (1.27)	$C^{\gamma1}$, 28.75 (-0.14, -0.14); $C^{\gamma2}$, 16.00 (0.45); $C^{\delta1}$, 12.00 (-0.15);
E458	118.93 (7.36)	178.83	57.83 (3.72)	28.57 (1.93, 1.93)	C^{γ}, 35.22 (1.89, 1.89); C^{δ}, . ;
K459	115.56 (7.57)	177.80	55.54 (3.78)	29.67 (1.87, 1.87)	C^{γ}, 23.03 (1.39, 1.39); C^{δ}, 26.38 (. , .); C^{ϵ}, 41.00 (2.64, 2.36); N^{ζ}, . (*);
D460	116.17 (8.35)	172.74	50.43 (4.76)	40.43 (2.70, 2.44)	
P461	.	.	62.75 (4.01)	30.71 (. , .)	C^{γ}, 25.77 (. , .); C^{δ}, 48.89 (3.73, 3.39)
N462	114.95 (8.00)	175.02	51.72 (4.70)	37.18 (2.94, 2.94)	$N^{\delta2}$, 110.10 (5.45, 7.54);
F463	123.08 (7.82)	174.95	54.86 (4.63)	35.07 (3.43, 3.01)	$C^{\delta1}$, . (.); $C^{\delta2}$, . (.); $C^{\epsilon1}$, . (.); $C^{\epsilon2}$, . (.); C^{ζ}, . (.);
V464	127.60 (8.02)	177.45	66.74 (3.42)	30.72 (1.82)	$C^{\gamma1}$, 19.67(0.69); $C^{\gamma2}$, 21.42(0.76);
R465	117.44 (8.64)	177.40	56.87 (3.59)	26.71 (. , .)	C^{γ}, 23.07 (1.62, 1.62); C^{δ}, 39.90 (3.12, 2.91); C^{ζ}, .; N^{ϵ}, . (.); $N^{\eta1}$, . (*, *); $N^{\eta2}$, . (*, *);
A466	117.88 (7.10)	179.57	54.30 (3.73)	17.30 (1.06)	
Y467	115.32 (7.47)	178.01	60.68 (3.78)	37.94 (3.15, 2.62)	$C^{\delta1}$, . (.); $C^{\delta2}$, . (.); $C^{\epsilon1}$, . (6.56); $C^{\epsilon2}$, . (6.56); C^{ζ}, . ;
I468	118.51 (7.45)	178.99	65.36 (3.18)	36.81 (1.63)	$C^{\gamma1}$, 28.37 (0.39, 0.39); $C^{\gamma2}$, 15.86(0.62); $C^{\delta1}$, 12.25(0.53);
R469	121.66 (8.36)	178.09	59.15 (3.73)	28.13 (1.54, 1.54)	C^{γ}, 26.91 (. , .); C^{δ}, 42.16 (2.81, 2.81); C^{ζ}, . N^{ϵ}, . (.); $N^{\eta1}$, . (*, *); $N^{\eta2}$, . (*, *);
K470	122.73 (7.90)	177.16	59.48 (3.74)	30.96 (. , .)	C^{γ}, 24.47 (. , .); C^{δ}, 28.93 (. , .); C^{ϵ}, . (. , .); N^{ζ}, . (*);
A471	119.94 (8.44)	179.56	53.65 (3.73)	17.39 (1.33)	
T472	112.63 (8.10)	176.65	66.44 (3.58)	67.51 (4.19)	$C^{\gamma2}$, 20.25 (1.09);
A473	126.07 (7.65)	177.91	53.96 (3.75)	17.19 (1.42)	
Q474	116.55 (8.36)	178.48	58.26 (3.61)	27.09 (1.71, 1.71)	C^{γ}, 34.58 (2.33, 2.33); C^{δ}, . $N^{\epsilon2}$, . (. , .);
I475	119.91 (8.24)	178.94	64.96 (3.00)	36.99 (1.74)	$C^{\gamma1}$, 30.00 (0.45, 0.45); $C^{\gamma2}$, 16.34 (0.73); $C^{\delta1}$, 13.49 (0.69);
A476	123.83 (7.25)	179.13	54.01 (3.63)	15.33 (0.46)	
V477	107.65 (6.83)	174.46	59.43 (4.21)	29.05 (2.37)	$C^{\gamma1}$, 21.30 (0.70); $C^{\gamma2}$, 17.48 (0.72);
K478	114.31 (7.42)	175.58	56.24 (2.53)	26.82 (1.59, 1.91)	C^{γ}, 23.85 (1.04, 0.71); C^{δ}, 27.10 (. , .); C^{ϵ}, 44.19 (3.07, 2.55); N^{ζ}, 115.96 (*);
E479	121.96 (7.94)	176.98	52.57 (4.33)	25.39 (1.84, 1.84)	C^{γ}, 34.15 (2.00, 1.88); C^{δ}, . ;
Y480	117.68 (6.55)	177.04	60.51 (3.67)	36.43 (3.06, 2.53)	$C^{\delta1}$, . (6.77); $C^{\delta2}$, . (6.77); $C^{\epsilon1}$, . (6.21); $C^{\epsilon2}$, . (6.21); C^{ζ}, . ;
A481	119.62 (8.42)	181.39	54.50 (3.77)	16.15 (1.31)	
S482	115.17 (8.01)	175.51	60.71 (4.10)	. (3.71, 3.71)	
A483	123.90 (8.01)	179.55	54.06 (4.35)	17.35 (1.20)	
L484	116.18 (7.77)	178.54	57.44 (3.65)	39.21 (1.22, 1.73)	C^{γ}, 26.00 (1.65); $C^{\delta1}$, 24.20 (0.47); $C^{\delta2}$, 21.65 (-0.07);
E485	118.47 (7.15)	180.47	58.64 (4.05)	28.20 (2.12, 2.12)	C^{γ}, 35.42 (2.35, 2.06); C^{δ}, . ;
T486	120.37 (8.61)	176.69	64.94 (3.94)	66.47 (4.38)	$C^{\gamma2}$, 24.24 (1.22);
L487	121.61 (8.66)	178.34	56.60 (3.84)	40.57 (1.27, 2.02)	C^{γ}, 26.13 (1.74); $C^{\delta1}$, 23.84 (0.56); $C^{\delta2}$, 21.55 (0.72);
D488	121.67 (8.55)	179.04	56.65 (4.38)	38.98 (2.79, 2.55)	
A489	122.66 (7.43)	179.94	53.96 (3.99)	16.48 (1.46)	
A490	120.36 (8.49)	178.28	53.94 (3.00)	17.26 (1.26)	
R491	117.70 (8.64)	179.16	58.82 (3.59)	29.03 (1.87, 1.87)	C^{γ}, 26.29 (. , .); C^{δ}, 42.16 (3.03, 3.03); C^{ζ}, . ; N^{ϵ}, . (.); $N^{\eta1}$, . (*, *); $N^{\eta2}$, . (*, *);
T492	115.67 (7.50)	176.66	65.21 (3.82)	67.61 (4.04)	$C^{\gamma2}$, 20.76(1.07);
K493	120.18 (7.70)	177.98	56.09 (3.79)	29.61 (1.82, 1.8)	C^{γ}, 21.00 (1.35, 1.35); C^{δ}, 30.10 (. , .); C^{ϵ}, 42.52 (2.73, 2.73); N^{ζ}, . (*);
D494	118.99 (8.91)	180.12	56.59 (4.08)	41.81 (2.44, 2.36)	

Residue	N (HN)	CO	C^{α} (H^{α})	C^{β} (H^{β})	other
E496	116.87 (7.54)	178.76	57.94 (3.98)	29.52 (2.00, 2.00)	C^{γ}, 34.84 (2.03, 2.03); C^{δ}, . ;
V497	111.49 (8.45)	176.31	61.70 (4.28)	32.24 (2.13)	$C^{\gamma 1}$, 20.03 (0.83); $C^{\gamma 2}$, 18.88 (0.85);
N498	117.35 (7.37)	176.26	51.08 (5.15)	39.35 (3.43, 2.70)	$N^{\delta 2}$, 113.11 (6.94, 8.13);
N499	117.38 (8.30)	175.36	53.70 (4.41)	36.47 (2.54, 3.00)	$N^{\delta 2}$, 112.58 (6.76, 7.49);
G500	104.56 (8.14)	177.45	45.40 (3.82, 3.71)		
S501	115.31 (7.56)	176.36	60.60 (4.08)	62.24 (3.86, 4.02)	
S502	120.46 (10.24)	174.32	56.77 (4.98)	61.19 (3.85, 3.33)	
A503	123.68 (7.41)	178.52	55.37 (3.58)	17.75 (1.33)	
R504	115.35 (8.28)	178.91	58.44 (3.95)	27.92 (1.65, 1.65)	C^{γ}, 25.85 (1.47, 1.47); C^{δ}, 42.03 (3.09, 3.09); C^{ζ}, . ; N^{ε}, . (.); $N^{\eta 1}$, . (*, *); $N^{\eta 2}$, . (*, *);
E505	120.57 (7.63)	179.25	58.21 (3.89)	28.44 (1.91, 1.59)	C^{γ}, 35.00 (1.88, 1.88); C^{δ}, . ;
I506	119.69 (7.97)	177.33	65.24 (3.29)	36.96 (1.61)	$C^{\gamma 1}$, 28.76 (0.38, 0.38); $C^{\gamma 2}$, 16.23 (0.76); $C^{\delta 1}$, 12.28 (0.34);
D507	119.96 (8.86)	179.08	56.54 (4.21)	38.65 (2.71, 2.41)	
Q508	119.06 (7.79)	179.27	58.06 (3.98)	27.01 (2.09, 2.00)	C^{γ}, 33.08 (2.45, 2.29); C^{δ}, . ; $N^{\varepsilon 2}$, 111.70 (6.74, 7.39);
L509	120.82 (7.48)	177.64	56.57 (3.90)	41.51 (1.87, 1.14)	C^{γ}, . (.); $C^{\delta 1}$, 25.70 (0.69); $C^{\delta 2}$, 22.09 (0.71);
Y510	122.21 (8.89)	178.90	61.13 (3.50)	37.84 (2.88, 3.06)	$C^{\delta 1}$, . (6.72); $C^{\delta 2}$, . (6.72); $C^{\varepsilon 1}$, . (.); $C^{\varepsilon 2}$, . (.); C^{ζ}, . ;
Y511	119.65 (8.26)	177.74	60.61 (4.08)	36.66 (3.08, 3.03)	$C^{\delta 1}$, . (.); $C^{\delta 2}$, . (.); $C^{\varepsilon 1}$, . (6.98); $C^{\varepsilon 2}$, . (6.98); C^{ζ}, . ;
K512	119.03 (7.54)	178.68	58.38 (3.81)	31.07 (1.78, 1.78)	C^{γ}, 24.22 (1.25, 1.25); C^{δ}, 28.26 (1.33, 1.33); C^{ε}, 41.10 (3.04, 3.04); N^{ζ}, . (*);
A513	119.31 (8.26)	177.78	53.48 (3.76)	16.15 (1.15)	
S514	111.37 (7.91)	175.50	59.78 (3.77)	61.86 (3.59, 3.74)	
Q515	118.86 (7.57)	176.91	56.09 (3.78)	27.35 (1.81, 1.81)	C^{γ}, 32.45 (1.85, 1.85); C^{δ}, . $N^{\varepsilon 2}$, 112.68 (6.61, 7.02);
Q516	116.39 (7.36)	175.94	55.39 (3.74)	26.73 (1.12, 1.42)	C^{γ}, 32.48 (1.94, 1.94); C^{δ}, . $N^{\varepsilon 2}$, 111.43 (6.67, 7.16);
R517	118.25 (7.32)	175.82	55.94 (3.76)	28.94 (1.42, 1.33)	C^{γ}, 25.21 (1.03, 1.03); C^{δ}, 42.20 (2.72, 2.72); C^{ζ}, . ; N^{ε}, . (.); $N^{\eta 1}$, . (*, *); $N^{\eta 2}$, . (*, *);
F518	118.65 (7.72)	175.09	56.37 (4.50)	38.10 (2.78, 3.03)	$C^{\delta 1}$, . (7.10); $C^{\delta 2}$, . (7.10); $C^{\varepsilon 1}$, . (.); $C^{\varepsilon 2}$, . (.); C^{ζ}, . (.);
Q519	122.44 (7.88)	173.37	52.40 (4.42)	27.62 (1.74, 1.88)	C^{γ}, 32.32 (2.17, 2.17); C^{δ}, . $N^{\varepsilon 2}$, 112.37 (6.74, 7.38),
P520	.	.	62.61 (4.25)	30.74 (1.82, 2.16)	C^{γ}, 26.10 (1.87, 1.87); C^{δ}, 49.56 (3.49, 3.49);
G521	109.29 (8.47)	174.32	44.38 (3.88, 3.88)		
T522	112.94 (7.92)	174.47	60.93 (4.28)	69.05 (4.15)	$C^{\gamma 2}$, 20.46 (1.04);
S523	117.55 (8.32)	174.05	57.24 (4.37)	62.64 (4.56, 4.36)	
N524	120.67 (8.41)	174.8	52.43 (4.61)	37.79 (2.69, 2.58)	$N^{\delta 2}$, 112.41 (6.85, 7.62);
E525	121.12 (8.27)	175.72	55.83 (4.20)	29.01 (1.94, 1.77)	C^{γ}, 35.02 (2.12, 2.12); C^{δ}, . ;
T526	119.94 (7.72)	179.07	62.50 (3.99)	69.68 (4.08)	$C^{\gamma 2}$, 20.89 (1.00);

Table 11.4: Chemical shift assignment of the Sti1 DP1 domain. The assignment was obtained in a buffer of 50 mM potassium phosphate, 50 mM potassium chloride, 1 mM TCEP, pH 7.5 at 293 K. The chemical shifts were deposited in the BMRB database under accession code 18090.

Residue	N (HN)	CO	C^{α} (H^{α})	C^{β} (H^{β})	other
Q127	122.72 (8.34)	173.99	53.41 (4.47)	28.60 (1.80, 1.97)	C^{γ}, 33.47 (2.23, 2.23); C^{δ}, . ;$N^{\varepsilon 2}$, 112.59 (7.53, 6.78);
P128	.	.	63.32 (4.22)	31.68 (1.74, 2.10)	C^{γ}, 27.32 (1.84, 1.84); C^{δ}, 50.49 (3.62, 3.56);
D129	119.32 (8.31)	176.12	54.05 (4.40)	40.77 (2.52, 2.52)	
L130	122.28 (8.08)	177.28	55.35 (4.13)	41.49 (1.52, 1.44)	C^{γ}, 26.87 (1.45); $C^{\delta 1}$, 25.10 (0.74); $C^{\delta 2}$, 23.40 (0.68);
G131	107.83 (8.18)	175.12	45.30 (3.74, 3.74)		
L132	121.08 (8.15)	178.00	57.18 (3.87)	41.87 (1.48, 1.37)	C^{γ}, 26.81 (1.41); $C^{\delta 1}$, 24.12 (0.62); $C^{\delta 2}$, 23.92 (0.55);
T133	111.58 (7.97)	176.53	65.94 (3.73)	68.13 (4.03)	$C^{\gamma 2}$, 21.92 (1.08);
Q134	119.49 (7.89)	178.19	57.93 (3.99)	27.85 (1.93, 1.93)	C^{γ}, 33.97 (2.26, 2.26); C^{δ}, . ; $N^{\varepsilon 2}$, 112.15 (7.41, 6.75);
L135	120.17 (7.60)	177.81	57.47 (3.82)	41.64 (1.40, 1.03)	C^{γ}, 26.40 (1.40); $C^{\delta 1}$, 23.92 (0.54); $C^{\delta 2}$, 25.65 (0.62);
F136	111.95 (7.41)	174.99	58.45 (4.38)	38.57 (3.15, 2.62)	$C^{\delta 1}$, 131.50 (7.13); $C^{\delta 2}$, 131.50 (7.13); $C^{\varepsilon 1}$, 130.44 (6.94); $C^{\varepsilon 2}$, 130.44 (6.94); C^{ζ}, 129.08 (6.89);
A137	120.23 (7.33)	177.09	52.58 (4.13)	18.66 (1.36)	
D138	119.83 (6.98)	176.37	51.96 (4.51)	41.99 (2.55, 2.61)	
P139	.	.	64.35 (4.26)	31.76 (2.25, 1.80)	C^{γ}, 27.20 (1.85, 1.85); C^{δ}, 51.28 (3.86, 3.86);
N140	116.84 (8.67)	173.84	52.38 (4.84)	38.33 (2.49, 2.79)	$N^{\delta 2}$, 114.82 (7.73, 6.86);
L141	120.29 (7.20)	177.12	59.28 (3.79)	42.98 (1.82, 1.61)	C^{γ}, 27.00 (1.35); $C^{\delta 1}$, 25.16 (0.83); $C^{\delta 2}$, 27.01 (0.86);
I142	115.29 (7.94)	177.99	62.69 (3.48)	34.62 (1.93)	$C^{\gamma 1}$, 27.41 (1.48, 1.31); $C^{\gamma 2}$, 17.65 (0.68); $C^{\delta 1}$, 10.89 (0.63);
E143	119.60 (7.97)	179.17	59.36 (3.70)	28.52 (1.81, 1.81)	C^{γ}, 36.19 (2.14, 2.14); C^{δ}, .;
N144	117.17 (8.45)	179.12	55.49 (4.27)	36.55 (2.81, 2.53)	$N^{\delta 2}$, 112.26 (7.66, 6.71);
L145	121.06 (7.99)	180.26	56.62 (4.02)	41.78 (2.00, 1.20)	C^{γ}, 27.02 (1.88); $C^{\delta 1}$, 26.95 (0.77); $C^{\delta 2}$, 22.68 (0.75);
K146	118.96 (8.25)	177.39	59.64 (3.61)	32.45 (1.77, 1.66)	C^{γ}, 26.55 (1.14, 1.51); C^{δ}, 29.87 (1.43, 1.38); C^{ε}, 41.45 (2.71, 2.57); N^{ζ}, . (*);
K147	114.72 (7.13)	175.88	56.21 (4.11)	33.00 (1.69, 1.72)	C^{γ}, 24.80 (1.41, 1.37); C^{δ}, 29.23 (1.55, 1.52); C^{ε}, 41.89 (2.82, 2.82); N^{ζ}, . (*);
N148	122.18 (6.93)	174.00	50.97 (4.74)	38.67 (2.49, 3.30)	$N^{\delta 2}$, 115.03 (7.79, 6.96);
P149	.	.	64.61 (4.30)	32.00 (2.26, 2.26)	C^{γ}, 27.47 (1.92, 1.92); C^{δ}, 50.87 (3.89, 3.62);
K150	116.06 (8.52)	178.24	57.95 (4.07)	32.59 (1.66, 1.57)	C^{γ}, 25.34 (1.41, 1.32); C^{δ}, 28.76 (1.56, 1.56); C^{ε}, 41.90 (2.84, 2.84); N^{ζ}, . (*);
T151	105.19 (7.49)	176.09	61.40 (4.39)	69.44 (4.12)	$C^{\gamma 2}$, 22.71 (0.84);
S152	119.70 (8.19)	177.47	62.45 (3.77)	62.52 (3.66, 3.54)	
E153	119.87 (8.35)	180.04	58.70 (3.89)	28.59 (1.84, 1.84)	C^{γ}, 35.67 (2.16, 2.16); C^{δ}, .;
M154	119.43 (7.85)	177.11	58.51 (4.04)	31.43 (1.89, 1.94)	C^{γ}, 31.56 (2.36, 2.57); C^{ε}, 16.83 (2.06);
M155	112.64 (7.20)	175.53	53.79 (4.34)	30.38 (1.90, 1.86)	C^{γ}, 32.10 (2.38, 2.47); C^{ε}, 18.46 (1.77);
K156	117.05 (7.13)	176.12	57.09 (3.96)	31.96 (1.66, 1.85)	C^{γ}, 25.88 (1.22, 1.52); C^{δ}, 29.50 (2.03, 1.92); C^{ε}, 42.17 (2.82, 2.72); N^{ζ}, . (*);
D157	119.81 (7.34)	174.89	50.52 (4.86)	41.01 (2.61, 3.14)	
P158	.	.	64.27 (4.13)	31.77 (2.22, 1.84)	C^{γ}, 27.24 (1.93, 1.93); C^{δ}, 51.04 (4.24, 3.93);
Q159	117.76 (8.15)	178.74	58.22 (4.00)	27.87 (2.12, 1.95)	C^{γ}, 34.64 (2.18, 2.33); C^{δ}, . ; $N^{\varepsilon 2}$, 111.95 (6.73, 7.41);
L160	123.30 (7.11)	177.98	57.05 (3.97)	40.76 (1.29, 1.96)	C^{γ}, 26.64 (1.26); $C^{\delta 1}$, 22.26 (0.67); $C^{\delta 2}$, 26.08 (0.67);
V161	118.39 (7.43)	176.84	67.70 (3.11)	31.26 (1.84)	$C^{\gamma 1}$, 21.56 (0.78); $C^{\gamma 2}$, 23.31 (0.94);
A162	117.60 (7.50)	180.62	54.72 (3.81)	17.49 (1.24)	
K163	119.88 (7.35)	177.80	58.88 (3.57)	31.61 (1.68, 1.63)	C^{γ}, 24.52 (1.25, 1.09); C^{δ}, 29.78 (1.48, 1.48); C^{ε}, 41.35 (2.72, 2.69); N^{ζ}, . (*);
L164	118.02 (7.66)	179.38	57.34 (3.67)	41.66 (1.84, 1.16)	C^{γ}, 26.90 (1.68); $C^{\delta 1}$, 26.90 (0.68); $C^{\delta 2}$, 23.38 (0.79);
I165	118.07 (8.03)	179.57	64.45 (3.51)	37.31 (1.69)	$C^{\gamma 1}$, 29.00 (1.03, 1.52); $C^{\gamma 2}$, 17.27 (0.74); $C^{\delta 1}$, 13.25 (0.66);
G166	107.97 (7.59)	176.47	46.41 (3.73, 3.63)		
Y167	121.27 (7.35)	176.47	57.13 (4.19)	35.95 (2.52, 2.41)	$C^{\delta 1}$, 131.27 (6.54); $C^{\delta 2}$, 131.27 (6.54); $C^{\varepsilon 1}$, 116.94 (6.27); $C^{\varepsilon 2}$, 116.94 (6.27); C^{ζ}, .
K168	116.52 (7.46)	177.81	59.39 (3.82)	31.58 (1.86, 1.80)	C^{γ}, 25.05 (1.52, 1.40); C^{δ}, 29.50 (1.69, 1.60); C^{ε}, 41.97 (2.96, 2.89); N^{ζ}, . (*);
Q169	113.75 (7.22)	175.84	56.23 (4.22)	29.29 (1.92, 2.00)	C^{γ}, 33.97 (2.27, 2.27); C^{δ}, .; $N^{\varepsilon 2}$, 111.77 (7.51, 6.74);
N170	114.13 (7.58)	172.20	50.78 (5.05)	38.38 (2.52, 2.72)	$N^{\delta 2}$, 112.31 (7.53, 6.78);
P171	.	.	64.80 (4.13)	31.36 (2.14, 1.69)	C^{γ}, 27.16 (1.79, 1.94); C^{δ}, 50.18 (3.64, 3.27);
Q172	115.57 (8.16)	177.36	57.95 (3.77)	27.05 (1.93, 1.91)	C^{γ}, 33.90 (2.21, 2.28); C^{δ}, . ; $N^{\varepsilon 2}$, 111.77 (7.42, 6.81);
A173	121.42 (7.47)	178.09	53.49 (4.05)	18.45 (1.44)	
I174	118.05 (7.15)	176.25	64.03 (3.18)	37.28 (0.90)	$C^{\gamma 1}$, 28.96 (0.89, 0.23); $C^{\gamma 2}$, 17.38 (0.46); $C^{\delta 1}$, 14.78 (0.41);
G175	105.39 (7.55)	174.22	46.70 (3.47, 3.72)		
Q176	116.23 (7.39)	178.12	57.32 (4.21)	28.63 (1.99, 1.99)	C^{γ}, 33.95 (2.27, 2.27); C^{δ}, . ; $N^{\varepsilon 2}$, 112.04 (7.50, 6.71);
D177	120.00 (7.87)	177.95	55.84 (4.42)	40.31 (2.59, 2.51)	
L178	120.01 (7.86)	175.81	57.62 (3.65)	41.88 (1.26, 0.94)	C^{γ}, 26.21 (1.26); $C^{\delta 1}$, 25.00 (0.40); $C^{\delta 2}$, 24.70 (0.44);

Residue	N (HN)	CO	C^{α} (H^{α})	C^{β} (H^{β})	other
F179	110.58 (7.21)	176.37	58.73 (4.23)	38.72 (2.79, 3.16)	$C^{\delta1}$, 131.76 (7.20); $C^{\delta2}$, 131.76 (7.20); $C^{\varepsilon1}$, 131.08 (7.08); $C^{\varepsilon2}$, 131.08 (7.08); C^{ζ}, 128.72 (6.85);
T180	108.19 (7.55)	174.40	62.02 (4.30)	69.73 (4.25)	$C^{\gamma2}$, 22.00 (1.11);
D181	120.06 (7.48)	174.12	50.56 (5.02)	41.19 (2.37, 2.85)	
P182	.	.	64.28 (4.32)	31.98 (2.25, 1.84)	C^{γ}, 27.14 (1.94, 1.90); C^{δ}, 51.05 (3.85, 3.64);
R183	117.66 (7.92)	179.03	59.00 (3.96)	29.75 (1.71, 2.05)	C^{γ}, 26.00 (1.72, 1.72); C^{δ}, 43.42 (3.32, 2.85); C^{ζ}, . ;N^{ε}, . (.); $N^{\eta1}$, . (*, *); $N^{\eta2}$, . (*, *);
L184	115.67 (7.75)	178.77	57.11 (3.85)	41.31 (1.90, 1.30)	C^{γ}, 27.58 (1.56); $C^{\delta1}$, 25.78 (0.88); $C^{\delta2}$, 23.32 (0.74);
M185	118.57 (7.59)	177.54	58.09 (4.06)	31.27 (2.02, 1.93)	C^{γ}, 32.44 (2.38, 2.38); C^{ε}, 16.82 (1.77);
T186	116.39 (7.18)	177.44	66.94 (3.68)	68.03 (4.06)	$C^{\gamma2}$, 21.76 (0.97);
I187	123.84 (8.01)	176.66	65.85 (3.29)	37.64 (1.90)	$C^{\gamma1}$, 30.21 (1.71, 1.00); $C^{\gamma2}$, 17.51 (0.82); $C^{\delta1}$, 14.60 (0.76);
M188	118.21 (8.56)	177.54	58.53 (3.91)	31.20 (2.02, 1.86)	C^{γ}, 32.42 (2.39, 2.39); C^{ε}, 17.06 (1.68);
A189	119.85 (8.21)	179.55	55.47 (3.73)	17.64 (1.30)	
T190	114.57 (7.74)	177.64	66.69 (3.79)	68.31 (4.09)	$C^{\gamma2}$, 20.88 (0.99);
L191	122.41 (8.18)	178.47	57.12 (3.93)	41.83 (1.72, 1.21)	C^{γ}, 26.20 (1.73); $C^{\delta1}$, 25.60 (0.42); $C^{\delta2}$, 22.16 (0.64);
M192	115.32 (7.88)	176.09	56.39 (4.09)	33.77 (1.85, 2.07)	C^{γ}, 32.76 (2.28, 2.51); C^{ε}, 17.41 (1.78);
G193	107.49 (7.58)	174.39	45.88 (3.83, 3.75)		
V194	118.52 (7.84)	174.76	61.51 (3.94)	32.67 (1.80)	$C^{\gamma1}$, 21.05 (0.68); $C^{\gamma2}$, 20.70 (0.72);
D195	124.55 (8.40)	175.14	53.76 (4.43)	40.92 (2.38, 2.54)	
L196	123.93 (8.16)	175.95	54.38 (4.20)	41.61 (1.52, 1.42)	C^{γ}, 26.26 (1.41); $C^{\delta1}$, 25.50 (0.69); $C^{\delta2}$, 23.26 (0.61);
N197	124.19 (7.90)	179.34	54.63 (4.25)	39.96 (2.52, 2.59)	$N^{\delta2}$, 113.30 (7.45, 6.71);

Table 11.5: Chemical shift assignment of the Sti1 DP2 domain. The assignment was obtained in a buffer of 50 mM potassium phosphate, 50 mM potassium chloride, 1 mM TCEP, pH 7.5 at 293 K. The chemical shifts were deposited in the BMRB database under accession code 18091.

Residue	N (HN)	CO	C^{α} (H^{α})	C^{β} (H^{β})	other
Q519	123.53 (8.13)	173.26	53.02 (4.45)	29.17 (1.88, 1.88)	C^{γ}, 33.38 (2.63, 2.20); C^{δ}, . ; $N^{\varepsilon 2}$, 112.34 (7.40, 6.75);
P520	.	.	63.25 (4.23)	31.96 (2.18, 1.82)	C^{γ}, 27.09 (1.87, 1.87); C^{δ}, 50.56 (3.51, 3.51);
G521	109.40 (8.49)	174.30	45.18 (3.87, 3.87)		
T522	112.48 (7.86)	174.69	61.24 (4.30)	69.96 (4.16)	$C^{\gamma 2}$, 21.31 (1.05);
S523	117.45 (8.30)	173.32	58.46 (3.89)	63.69 (3.72, 3.72)	
N524	. (.)	174.67	53.06 (4.35)	38.71 (., .)	$N^{\delta 2}$, 112.92 (7.48, 6.78);
E525	120.97 (7.97)	176.90	56.04 (4.34)	31.07 (1.95, 1.95)	C^{γ}, 36.43 (2.14, 2.14); C^{δ}, . ;
T526	116.96 (8.63)	173.41	60.08 (4.54)	68.50 (4.51)	$C^{\gamma 2}$, 21.76 (1.21);
P527	.	.	65.11 (4.19)	31.58 (1.79, 2.23)	C^{γ}, 27.97 (2.05, 2.05); C^{δ}, 50.26 (3.78, 3.74);
E528	118.61 (8.55)	178.55	59.58 (3.98)	28.99 (1.85, 1.85)	C^{γ}, 36.49 (2.12, 2.12); C^{δ}, . ;
E529	121.09 (7.87)	179.47	58.95 (3.93)	29.48 (1.87, 2.20)	C^{γ}, 37.03 (2.22, 2.15); C^{δ}, . ;
T530	118.05 (8.39)	175.77	66.32 (3.75)	68.43 (3.98)	$C^{\gamma 2}$, 22.34 (1.07);
Y531	122.28 (8.05)	176.42	61.44 (3.82)	38.11 (2.97, 2.97)	$C^{\delta 1}$, 132.70 (6.89); $C^{\delta 2}$, 132.70 (6.89); $C^{\varepsilon 1}$, 118.01 (6.64); $C^{\varepsilon 2}$, 118.01 (6.64); C^{ζ}, . ;
Q532	116.25 (8.01)	178.80	58.62 (3.69)	28.06 (1.98, 1.98)	C^{γ}, 33.69 (2.38, 2.24); C^{δ}, . ; $N^{\varepsilon 2}$, 111.92 (7.52, 6.79);
R533	118.73 (7.80)	179.03	59.14 (3.92)	29.80 (1.85, 1.85)	C^{γ}, 27.06 (1.58, 1.58); C^{δ}, 42.97 (3.15, 3.15); C^{ζ}, . N^{ε}, . (.); $N^{\eta 1}$, . (*, *); $N^{\eta 2}$, . (*, *);
A534	123.50 (8.21)	178.86	54.67 (3.96)	18.73 (1.28)	
M535	111.91 (7.48)	176.89	55.20 (4.02)	31.11 (1.77, 1.77)	C^{γ}, 32.56 (2.06, 2.06); C^{ε}, 16.61 (1.75);
K536	116.84 (7.18)	176.69	56.59 (3.99)	32.34 (1.70, 1.81)	C^{γ}, 25.06 (1.53, 1.53); C^{δ}, 28.92 (1.55, 1.55); C^{ε}, 42.00 (2.85, 2.85); N^{ζ}, . (*);
D537	122.68 (7.53)	174.72	51.09 (4.80)	41.97 (2.54, 3.00)	
P538	.	.	64.75 (4.14)	32.12 (1.88, 2.23)	C^{γ}, 27.38 (1.94, 1.94); C^{δ}, 50.95 (3.98, 3.77);
E539	118.59 (8.20)	179.01	58.85 (4.01)	29.34 (1.94, 1.91)	C^{γ}, 36.46 (2.23, 2.05); C^{δ}, . ;
V540	120.69 (7.35)	177.74	66.09 (3.23)	31.35 (2.28)	$C^{\gamma 1}$, 22.05 (0.52); $C^{\gamma 2}$, 23.00 (0.72);
A541	121.46 (8.43)	179.66	55.39 (3.77)	17.71 (1.28)	
A542	117.00 (7.38)	180.88	54.70 (3.94)	17.95 (1.36)	
I543	119.75 (7.38)	177.45	64.96 (3.69)	38.28 (1.86)	$C^{\gamma 1}$, 29.64 (1.93, 0.76); $C^{\gamma 2}$, 19.43 (0.78); $C^{\delta 1}$, 14.03 (0.86);
M544	113.83 (7.87)	177.68	55.66 (4.14)	30.69 (1.87, 1.95)	C^{γ}, 32.07 (2.46, 2.31); C^{ε}, 16.10 (1.83);
Q545	115.21 (7.34)	175.17	55.44 (4.08)	28.99 (2.09, 1.95)	C^{γ}, 33.79 (2.33, 2.33); C^{δ}, . ; $N^{\varepsilon 2}$, 111.41 (7.20, 6.72);
D546	123.27 (7.32)	175.22	51.34 (4.72)	42.38 (2.66, 3.06)	
P547	.	.	64.92 (4.12)	32.26 (2.27, 1.87)	C^{γ}, 27.48 (2.04, 2.04); C^{δ}, 51.12 (3.88, 3.88);
V548	119.87 (8.00)	179.01	66.00 (3.58)	31.11 (2.07)	$C^{\gamma 1}$, 20.23 (0.73); $C^{\gamma 2}$, 22.40 (0.89);
M549	118.27 (7.25)	178.83	55.14 (4.34)	28.84 (2.38, 1.72)	C^{γ}, 31.39 (2.65, 2.40); C^{ε}, 14.21 (1.58);
Q550	118.19 (8.31)	178.84	59.42 (3.74)	27.66 (1.95, 1.95)	C^{γ}, 33.61 (2.39, 2.39); C^{δ}, . ; $N^{\varepsilon 2}$, 110.56 (7.46, 6.59);
S551	114.01 (7.57)	176.84	61.33 (4.14)	62.45 (3.88, 3.88)	
I552	123.49 (7.60)	177.63	65.68 (3.28)	37.72 (1.68)	$C^{\gamma 1}$, 28.67 (-0.13, 1.45); $C^{\gamma 2}$, 15.72 (0.37); $C^{\delta 1}$, 13.94 (0.42);
L553	119.52 (8.33)	179.44	57.95 (3.75)	40.70 (1.59, 1.36)	C^{γ}, 27.10 (1.57); $C^{\delta 1}$, 24.92 (0.62); $C^{\delta 2}$, 22.84 (0.57);
Q554	118.59 (7.80)	178.56	58.66 (3.92)	28.06 (1.82, 1.82)	C^{γ}, 33.72 (2.28, 2.28); C^{δ}, . ; $N^{\varepsilon 2}$, 111.54 (7.33, 6.76);
Q555	119.52 (7.99)	178.40	58.53 (3.93)	28.79 (2.06, 2.06)	C^{γ}, 34.11 (2.50, 2.50); C^{δ}, . ; $N^{\varepsilon 2}$, 112.34 (7.29, 6.95);
A556	120.73 (8.31)	178.31	53.50 (4.11)	18.37 (1.34)	
Q557	115.60 (7.53)	177.26	57.92 (3.96)	28.48 (2.04, 2.04)	C^{γ}, 33.76 (2.35, 2.35); C^{δ}, . ; $N^{\varepsilon 2}$, . (. , .);
Q558	115.31 (7.35)	176.03	56.55 (4.18)	29.32 (2.09, 1.94)	C^{γ}, 33.69 (2.34, 2.34); C^{δ}, . ; $N^{\varepsilon 2}$, 111.99 (7.44, 6.77);
N559	114.85 (7.90)	172.42	50.43 (4.95)	38.88 (2.68, 2.88)	$N^{\delta 2}$, 111.59 (7.62, 6.93);
P560	.	.	65.00 (4.33)	31.68 (1.89, 2.31)	C^{γ}, 27.05 (1.99, 1.99); C^{δ}, 50.25 (3.78, 3.48);
A561	119.92 (7.85)	179.51	54.05 (4.13)	18.05 (1.33)	
A562	120.79 (7.98)	179.57	54.12 (4.02)	18.20 (1.37)	
L563	116.42 (7.51)	178.22	57.64 (3.98)	41.69 (1.67, 1.60)	C^{γ}, 26.93 (1.44); $C^{\delta 1}$, 24.39 (0.69); $C^{\delta 2}$, 23.97 (0.73);
Q564	115.51 (7.51)	178.30	58.72 (3.86)	28.02 (2.04, 2.04)	C^{γ}, 33.67 (2.31, 2.31); C^{δ}, . ; $N^{\varepsilon 2}$, 111.56 (7.32, 6.73);
E565	117.68 (7.44)	179.07	58.38 (3.90)	28.99 (1.66, 1.75)	C^{γ}, 35.19 (1.96, 1.96); C^{δ}, . ;
H566	118.22 (7.42)	177.28	58.86 (4.38)	31.44 (2.81, 3.01)	$C^{\delta 2}$, 118.37 (6.83); $C^{\varepsilon 1}$, 139.13 (7.60); $N^{\delta 1}$, . (6.85); $N^{\varepsilon 2}$, . (.);
M567	115.20 (7.71)	175.26	57.84 (3.84)	33.08 (2.14, 1.98)	C^{γ}, 33.27 (2.16, 2.63); C^{ε}, 17.00 (1.84);
K568	116.04 (7.14)	176.22	57.39 (3.96)	32.22 (1.68, 1.83)	C^{γ}, 25.19 (1.48, 1.27); C^{δ}, 29.19 (1.53, 1.53); C^{ε}, 42.01 (2.83, 2.83); N^{ζ}, . (*);
N569	119.60 (7.48)	173.92	49.95 (5.02)	39.00 (2.81, 3.24)	$N^{\delta 2}$, 113.80 (7.96, 7.25);
P570	.	.	65.11 (4.26)	32.27 (1.94, 2.30)	C^{γ}, 27.34 (1.94, 1.94); C^{δ}, 51.11 (4.07, 3.85);
E571	116.87 (7.96)	178.83	58.88 (4.07)	29.43 (1.96, 2.00)	C^{γ}, 36.47 (2.26, 2.17); C^{δ}, . ;
V572	118.29 (7.33)	177.62	65.10 (3.66)	32.21 (2.20)	$C^{\gamma 1}$, 21.93 (0.72); $C^{\gamma 2}$, 21.93 (0.88);
F573	121.09 (8.70)	176.76	62.23 (3.89)	38.62 (3.47, 2.98)	$C^{\delta 1}$, 131.55 (7.15); $C^{\delta 2}$, 131.55 (7.15); $C^{\varepsilon 1}$, 131.52 (7.21); $C^{\varepsilon 2}$, 131.52 (7.21); C^{ζ}, 130.03 (7.16);

Residue	N (HN)	CO	C^{α} (H^{α})	C^{β} (H^{β})	other
K574	116.91 (7.80)	178.98	59.48 (3.79)	32.20 (1.80, 1.80)	C^{γ}, 25.16 (1.51, 1.35); C^{δ}, 29.16 (1.60, 1.60); C^{ϵ}, 41.89 (2.89, 2.89); N^{ζ}, . (*);
K575	119.12 (7.17)	178.52	59.95 (3.91)	33.06 (1.98, 1.61)	C^{γ}, 26.51 (1.68, 1.29); C^{δ}, 30.17 (1.80, 1.80); C^{ϵ}, 42.12 (2.87, 2.87); N^{ζ}, . (*);
I576	119.18 (8.30)	177.82	64.53 (3.32)	36.25 (1.85)	$C^{\gamma 1}$, 29.07 (1.49, 0.91); $C^{\gamma 2}$, 16.92 (0.67); $C^{\delta 1}$, 12.78 (0.57);
Q577	118.00 (8.18)	179.25	59.12 (3.67)	27.84 (1.87, 1.80)	C^{γ}, 33.69 (1.85, 1.73); C^{δ}, . ; $N^{\epsilon 2}$, 112.17 (6.66, 6.22);
T578	118.67 (7.78)	176.06	66.89 (3.76)	68.03 (4.18)	$C^{\gamma 2}$, 21.86 (0.94);
L579	120.68 (7.62)	179.59	57.65 (3.85)	40.98 (2.04, 1.06)	C^{γ}, 26.30 (0.68); $C^{\delta 1}$, 22.20 (0.62); $C^{\delta 2}$, 22.20 (0.62);
I580	122.88 (8.54)	180.26	64.73 (4.03)	38.31 (1.67)	$C^{\gamma 1}$, 29.22 (1.56, 0.59); $C^{\gamma 2}$, 16.71 (0.75); $C^{\delta 1}$, 14.03 (0.55);
A581	124.51 (8.12)	179.00	54.84 (3.97)	17.50 (1.38)	
A582	116.25 (7.47)	177.04	52.18 (4.14)	19.86 (1.29)	
G583	104.54 (7.60)	174.18	44.79 (3.97, 3.64)		
I584	118.63 (7.59)	175.66	61.55 (3.76)	37.61 (1.72)	$C^{\gamma 1}$, 27.77 (1.20, 1.03); $C^{\gamma 2}$, 16.95 (0.82); $C^{\delta 1}$, 11.47 (0.49);
I585	116.36 (6.49)	174.37	59.48 (4.17)	39.63 (1.26)	$C^{\gamma 1}$, 27.46 (1.12, 0.80); $C^{\gamma 2}$, 17.19 (0.59); $C^{\delta 1}$, 13.86 (0.64);
R586	125.45 (8.50)	175.72	54.92 (4.38)	31.32 (1.56, 1.74)	C^{γ}, 26.85 (1.42, 1.42); C^{δ}, 43.19 (3.06, 3.06); C^{ζ}, . ; N^{ϵ}, . (.); $N^{\eta 1}$, . (*, *); $N^{\eta 2}$, . (*, *);
T587	113.71 (8.25)	174.76	61.30 (4.30)	69.72 (4.08)	$C^{\gamma 2}$, 21.27 (0.99);
G588	110.72 (8.23)	172.82	45.16 (3.85, 3.85)		
R589	125.39 (7.80)	180.91	57.21 (4.04)	31.23 (1.69, 1.63)	C^{γ}, 26.96 (1.44, 1.44); C^{δ}, 43.28 (3.05, 3.05); C^{ζ}, . ; N^{ϵ}, . (.); $N^{\eta 1}$, . (*, *); $N^{\eta 2}$, . (*, *);

Table 11.6: Chemical shift assignment of the Sba1Δ94 construct. The assignment was obtained in a buffer of 40 mM potassium phosphate, 1 mM TCEP, pH 7.5 at 303 K.

residue	N(HN)	CO	C^{α}	C^{β}
M1	. (.)	176.11	58.91 (.)	35.48
S2	116.53 (8.30)	174.18	61.75 (.)	66.90
D3	121.93 (8.27)	175.90	57.66 (4.57)	44.11
K4	120.61 (8.12)	175.84	59.26 (4.30)	35.77
V5	121.58 (7.91)	175.38	64.91 (4.33)	36.01
I6	125.93 (8.58)	175.36	63.03 (4.18)	43.14
N7	124.34 (8.53)	175.38	53.47 (5.40)	42.15
P8	.	.	66.90 (.)	34.36
Q9	112.66 (7.03)	172.27	57.12 (4.69)	34.01
V10	. (.)	.	. (.)	.
A11	. (.)	176.05	53.41 (.)	25.11
W12	117.48 (8.70)	172.58	58.29 (.)	35.79
A13	. (.)	175.71	53.82 (.)	26.20
Q14	113.57 (8.58)	172.31	57.77 (.)	36.12
R15	117.38 (8.14)	175.88	57.56 (4.30)	36.93
S16	120.66 (8.40)	172.68	60.95 (5.41)	69.29
S17	115.17 (7.75)	173.05	60.32 (4.53)	68.04
T18	112.09 (8.23)	175.44	65.68 (4.10)	72.55
T19	109.48 (8.11)	174.27	65.48 (4.51)	74.41
D20	122.97 (8.33)	174.93	53.53 (5.21)	45.41
P21	.	.	68.18 (.)	35.62
E22	111.89 (8.10)	177.63	60.08 (4.42)	31.66
R23	119.15 (7.77)	171.82	57.49 (4.41)	33.15
N24	118.95 (6.99)	173.69	54.97 (5.03)	44.36
Y25	116.00 (7.07)	172.76	59.26 (5.27)	43.16
V26	119.54 (9.65)	173.19	64.13 (4.55)	38.15
L27	127.59 (9.10)	175.98	56.14 (5.27)	47.59
I28	. (.)	.	. (.)	.
T29	. (.)	.	. (.)	.
V30	. (.)	175.97	63.66 (.)	37.06
S31	124.12 (8.84)	173.66	61.59 (4.87)	65.88
I32	121.84 (7.81)	174.10	62.93 (4.10)	42.39
A33	125.35 (7.79)	177.44	56.17 (4.20)	22.37
D34	116.10 (8.48)	174.85	58.02 (4.46)	43.36
C35	115.02 (7.74)	174.35	61.38 (4.76)	33.55
D36	122.04 (8.42)	175.07	57.17 (4.69)	45.09
A37	121.70 (8.24)	175.19	54.22 (4.37)	21.07
P38	.	.	65.66 (.)	35.28
E39	120.75 (8.89)	175.69	58.71 (4.51)	34.24
L40	128.84 (8.77)	176.35	56.88 (5.16)	47.61
T41	121.75 (9.05)	172.48	65.78 (4.40)	73.81
I42	126.91 (8.79)	173.60	63.44 (4.35)	41.53
K43	128.32 (8.32)	173.04	55.61 (4.60)	35.20
P44	.	.	69.19 (.)	34.48
S45	99.83 (7.36)	175.30	60.28 (4.81)	68.65
Y46	118.77 (7.33)	171.17	60.52 (5.41)	43.35
I47	109.73 (8.07)	174.71	60.96 (5.09)	44.96
E48	121.98 (9.06)	173.67	57.61 (5.30)	37.38
L49	123.88 (8.70)	174.50	57.36 (5.24)	49.44
K50	124.92 (8.63)	174.44	58.51 (5.18)	39.08
A51	124.07 (8.74)	174.93	54.48 (4.88)	25.77
Q52	119.09 (8.56)	174.92	57.47 (5.26)	34.85
S53	117.86 (8.64)	173.46	61.79 (4.70)	67.60
K54	121.25 (8.27)	174.91	57.61 (4.51)	35.24
P55	.	.	66.47 (.)	34.79
H56	118.99 (8.34)	175.19	58.66 (4.70)	34.13
V57	120.43 (8.12)	176.91	67.05 (3.94)	34.69
G58	113.22 (8.61)	173.90	48.44 (4.15, 3.74)	
D59	120.12 (7.92)	175.94	57.67 (4.58)	44.42
E60	120.87 (8.63)	176.13	60.10 (4.21)	32.65
N61	118.20 (8.19)	174.05	56.37 (4.64)	42.63
V62	120.04 (7.84)	174.91	65.18 (3.73)	36.06
H63	123.50 (8.41)	173.56	57.79 (4.74)	34.85
H64	120.46 (8.51)	173.69	59.10 (4.89)	35.11
Y65	120.59 (8.96)	175.98	59.66 (5.43)	43.93
Q66	121.09 (8.44)	173.44	58.41 (5.14)	35.17
L67	123.58 (8.74)	174.86	56.82 (4.78)	50.11
H68	124.56 (9.06)	173.56	59.03 (5.18)	33.45
I69	127.17 (8.67)	174.67	62.94 (4.33)	43.21
D70	128.35 (9.24)	175.63	57.48 (5.11)	43.91
L71	126.46 (7.99)	177.47	58.30 (4.41)	46.85
Y72	121.08 (7.68)	174.18	65.21 (.)	41.69
K73	113.42 (5.77)	173.31	57.51 (3.89)	40.90
E74	112.38 (7.70)	178.47	60.22 (4.61)	34.80
I75	114.68 (9.02)	176.28	61.87 (5.19)	45.38
I76	120.00 (8.38)	176.22	61.86 (4.52)	41.76
P77	.	.	70.06 (.)	35.53
E78	117.9 (10.42)	176.74	62.43 (.)	31.06
K79	117.78 (7.12)	174.82	59.24 (4.29)	36.07
T80	114.80 (7.35)	174.16	68.38 (4.51)	73.15
M81	126.17 (8.50)	173.99	57.41 (4.98)	38.36
H82	122.34 (8.66)	174.23	57.99 (.)	36.79
K83	120.08 (8.56)	173.54	58.97 (4.47)	38.26
V84	122.00 (8.41)	175.17	64.86 (4.43)	36.10
A85	129.87 (8.79)	176.64	54.53 (4.66)	23.57
N86	. (.)	175.22	57.43 (.)	41.18
G87	107.98 (8.59)	173.80	49.43 (., .)	
Q88	116.33 (8.02)	174.29	59.65 (4.40)	34.19
H89	116.54 (7.74)	173.02	58.79 (5.25)	36.71
Y90	124.63 (9.22)	174.08	60.99 (4.77)	44.16
F91	126.42 (8.98)	174.08	59.58 (5.47)	44.43
L92	123.74 (9.18)	173.74	56.99 (4.97)	48.71
K93	124.97 (8.88)	173.57	58.68 (4.74)	37.62
L94	124.28 (9.07)	175.88	54.78 (4.81)	45.40
Y95	123.58 (9.60)	175.82	62.49 (4.34)	41.24
K96	123.44 (8.07)	175.87	60.23 (4.20)	36.58
K97	122.72 (8.55)	176.54	62.43 (3.91)	36.69
D98	117.00 (8.61)	175.98	56.97 (4.76)	45.27
L99	127.01 (8.66)	175.62	58.83 (.)	43.57
E100	121.99 (7.72)	174.63	57.87 (4.64)	35.22
S101	113.48 (8.43)	175.47	62.52 (4.07)	66.70
E102	120.79 (7.80)	176.61	59.51 (4.27)	33.41
Y103	125.77 (8.66)	176.79	60.02 (4.16)	40.24
W104	123.81 (9.56)	177.05	57.95 (4.79)	31.56
P105	.	.	. (.)	.
R106	. (.)	.	. (.)	.
L107	. (.)	176.93	59.29 (.)	44.68
T108	100.56 (6.71)	175.03	62.10 (.)	74.85
K109	. (.)	.	. (.)	.
E110	. (.)	.	. (.)	.
K111	. (.)	174.81	59.22 (.)	33.75
V112	122.39 (7.04)	173.99	63.82 (.)	38.24
K113	. (.)	.	. (.)	.
Y114	. (.)	.	. (.)	.
P115	.	.	59.26 (.)	36.03
Y116	121.88 (8.02)	175.59	65.58 (4.04)	35.68
I117	125.63 (8.17)	.	63.87 (4.10)	41.60
K118	. (.)	.	. (.)	.
T119	. (.)	173.76	64.83 (.)	73.03
D120	122.17 (8.16)	175.26	57.15 (4.52)	44.63
F121	119.39 (7.97)	174.47	60.47 (4.52)	42.52
D122	126.33 (7.86)	180.67	59.11 (4.33)	45.49

Summary

In this work the interaction of Hsp90 with substrate proteins and cochaperones was studied using biochemical and NMR spectroscopic methods. A novel binding site for the DNA binding domain of the tumor suppressor protein p53 within the C-terminal domain of Hsp90 could be identified here. Applying NMR methods, furthermore a model for the complex between the two proteins was obtained that gives new insights into the substrate protein recognition by Hsp90.

Sti1/Hop, an important Hsp90 cochaperone, was previously shown to be a potent inhibitor of the Hsp90 ATPase activity, however, the mechanisms underlying this inhibition remained elusive so far. The binding site of Sti1/Hop within Hsp90 could be determined here by NMR and a model for the complex between the two proteins was derived from experimental data, explaining the inhibitory effect Sti1/Hop exerts on Hsp90. Additionally, structure and function of the isolated TPR2B, DP1 and DP2 domains of Sti1/Hop were characterized *in vitro* and *in vivo*. The TPR2B domain could be demonstrated to have essential functions in organizing Hsp90-Hsp70 chaperone complexes and to be involved in decreasing the Hsp90 ATP hydrolysis. NMR structures of the highly important DP1 and DP2 domains of Sti1/Hop playing critical roles in the activation of steroid hormone receptors by Hsp90 were also obtained in this work. These might contribute to a better understanding of the functional maturation process of these particular Hsp90 substrate proteins.

In the context of Sti1/Hop - Hsp90 complex formation, a screening was carried out for small molecule inhibitors that could potentially disrupt binding of the cochaperone to Hsp90. Targeting the Sti1/Hop - Hsp90 binding for inhibition was proposed recently to represent a promising approach in the treatment of cancer. One ligand was identified here interacting very specifically with Sti1/Hop which might serve as template structure for further chemical optimization.

The Hsp90 cochaperone Hch1, related to the Aha1 protein and known as Hsp90 ATPase activator, was characterized with respect to its structural properties and binding to Hsp90. The results of these studies give an explanation for the Hsp90 ATP hydrolysis stimulation by this protein.

p23/Sba1 is another cochaperone influencing the Hsp90 activity. It was shown to decrease the chaperone's ATP hydrolysis. This protein has an interesting structural feature, a larger presumably natively unfolded C - terminal domain. The experiments performed here with p23/Sba1 therefore in particular focused on the structure and function of this element in the protein. The data obtained on that issue indicate a significant structure propensity of the p23/Sba1 C - terminal domain and a potential role in membrane binding that might be of importance for certain p23/Sba1 functions independent from the Hsp90 chaperone system.

Zusammenfassung

In vorliegender Arbeit wurde die Wechselwirkung von Hsp90 mit Substratproteinen und Cochaperonen mit Hilfe von biochemischen und NMR spektroskopischen Methoden untersucht. Dabei wurde eine neuartige Bindestelle für die DNA bindende Domäne des Tumorsuppressorproteins p53 innerhalb der C-terminalen Domäne von Hsp90 identifiziert. Darüber hinaus konnte mittels NMR basierter Methoden ein Modell für den Komplex beider Proteine erstellt werden, welches neue Einblicke gibt, wie Hsp90 Substratproteine erkennt.

Für Sti1/Hop, ein wichtiges Hsp90 Cochaperon, wurde bereits früher gezeigt, dass es als starker Inhibitor der Hsp90 ATPase Aktivität fungiert, jedoch war der Mechansimus dieser Inhibition bisher unklar. Hier konnnte nun die Bindestelle von Sti1/Hop an Hsp90 mittels NMR bestimmmt werden und ein Modell für den Komplex beider Proteine aus experimentellen Daten abgeleitet werden, das die inhibierende Wirkung von Sti1/Hop auf Hsp90 erklärt. Zusätzlich wurden Struktur und Funktion der einzelnen Domänen TPR2B, DP1 und DP2 *in vitro* und *in vivo* charakterisiert. Für die TPR2B Domäne konnten entscheidende Funktionen für den Bildung von Hsp90-Hsp70 Chaperon Komplexen sowie eine Beteiligung an der Herabsetzung der Hsp90 ATP Hydrolyse nachgewiesen werden. Zusätzlich wurden auch NMR Strukturen bestimmt für die äußerst wichtigen Sti1/Hop DP1 und DP2 Domänen, die eine Schlüsselrolle bei der Aktivierung von Steroid Hormonrezeptoren spielen. Diese

könnten möglicherweise zu einem besseren Verständnis der funktionalen Reifung dieser speziellen Hsp90 Substratproteine beitragen.

Im Zusammenhang mit der Komplexbildung zwischen Sti1/Hop und Hsp90 wurde ein screening nach niedermolekularen Inhibitoren durchgeführt, die möglicherweise die Bindung des Cochaperons an Hsp90 aufheben könnten. Die Inhibierung der Sti1/Hop - Hsp90 Bindung wurde kürzlich als vielversprechender Ansatz in der Behandlung von Krebs vorgeschlagen. Dabei wurde ein Ligand identifiziert, der sehr spezifisch mit Sti1/Hop wechselwirkt und möglicherweise als Ausgangsstruktur für eine weitere chemische Optimierung dienen könnte.

Das Hsp90 Cochaperon Hch1, verwandt mit Aha1 und bekannt als Hsp90 ATPase Aktivator, wurde hinsichtlich seiner strukturellen Eigenschaften und Bindung an Hsp90 charakterisiert. Die Ergebnisse dieser Untersuchungen liefern eine Erklärung für die Stimulation der Hsp90 ATP Hydrolyse durch diese Protein.

p23/Sba1 stellt ein weiteres Cochaperon dar, das die Hsp90 Aktivität beeinflußt. Es wurde gezeigt, dass es die ATP Hydrolyse des Chaperons verlangsamt. Diese Protein besitzt ein interessantes Strukturmerkmal, eine größere, wahrscheinlich nativ ungefaltete C - terminale Domäne. Die hier mit p23/Sba1 durchgeführten Experimente zielten daher speziell auf die Struktur und Funktion dieses Elements innerhalb des Proteins ab. Die in diesem Zusammenhang erzielten Ergebnisse deuten auf erhebliche Neigung der p23/Sba1 C - terminalen Domäne zur Faltung hin und auf eine mögliche Rolle bei Membranbindung, die bedeutsam sein könnte für bestimmte p23/Sba1 Funktionen unahängig vom Hsp90 Chaperon System.

Bibliography

[1] Anfinsen, C. B., *Biochem J* **128** (1972), 737–749.

[2] Anfinsen, C. B., *Science* **181** (1973), 223–230.

[3] Ellis, R. J., *Adv Exp Med Biol* **594** (2007), 1–13.

[4] Lee, C. & Yu, M.-H., *J Biochem Mol Biol* **38** (2005), 275–280.

[5] Balch, W. E., Morimoto, R. I., Dillin, A. & Kelly, J. W., *Science* **319** (2008), 916–919.

[6] Wegele, H., Müller, L. & Buchner, J., *Rev Physiol Biochem Pharmacol* **151** (2004), 1–44.

[7] Chen, B., Zhong, D. & Monteiro, A., *BMC Genomics* **7** (2006), 156.

[8] Taipale, M., Jarosz, D. F. & Lindquist, S., *Nat Rev Mol Cell Biol* **11** (2010), 515–528.

[9] Welch, W. J. & Feramisco, J. R., *J Biol Chem* **257** (1982), 14.949–14.959.

[10] Lai, B. T. *et al.*, *Mol Cell Biol* **4** (1984), 2802–2810.

[11] Borkovich, K. A. *et al.*, *Mol Cell Biol* **9** (1989), 3919–3930.

[12] Cutforth, T. & Rubin, G. M., *Cell* **77** (1994), 1027–1036.

[13] Bardwell, J. C. & Craig, E. A., *J Bacteriol* **170** (1988), 2977–2983.

[14] Spence, J., Cegielska, A. & Georgopoulos, C., *J Bacteriol* **172** (1990), 7157–7166.

[15] Tanaka, N. & Nakamoto, H., *FEBS Lett* **458** (1999), 117–123.

[16] Rebbe, N. F. *et al.*, *Gene* **53** (1987), 235–245.

[17] Hickey, E. *et al.*, *Mol Cell Biol* **9** (1989), 2615–2626.

[18] Shiu, R. P., Pouyssegur, J. & Pastan, I., *Proc Natl Acad Sci U S A* **74** (1977), 3840–3844.

[19] Sorger, P. K. & Pelham, H. R., *J Mol Biol* **194** (1987), 341–344.

[20] Navarro, D., Qadri, I. & Pereira, L., *Virology* **184** (1991), 253–264.

[21] Melnick, J., Aviel, S. & Argon, Y., *J Biol Chem* **267** (1992), 21.303–21.306.

[22] Schaiff, W. T. *et al.*, *J Exp Med* **176** (1992), 657–666.

[23] Little, E. *et al.*, *Crit Rev Eukaryot Gene Expr* **4** (1994), 1–18.

[24] Melnick, J., Dul, J. L. & Argon, Y., *Nature* **370** (1994), 373–375.

[25] Ferreira, L. R. *et al.*, *J Cell Biochem* **56** (1994), 518–526.

[26] Kuznetsov, G., Chen, L. B. & Nigam, S. K., *J Biol Chem* **269** (1994), 22.990–22.995.

[27] Nicchitta, C. V., *Curr Opin Immunol* **10** (1998), 103–109.

[28] Yang, Y. & Li, Z., *Mol Cells* **20** (2005), 173–182.

[29] Song, H. Y. *et al.*, *J Biol Chem* **270** (1995), 3574–3581.

[30] Felts, S. J. *et al.*, *J Biol Chem* **275** (2000), 3305–3312.

[31] Pridgeon, J. W., Olzmann, J. A., Chin, L.-S. & Li, L., *PLoS Biol* **5** (2007), e172.

[32] Kang, B. H., *BMB Rep* **45** (2012), 1–6.

[33] Krishna, P. & Gloor, G., *Cell Stress Chaperones* **6** (2001), 238–246.

[34] Cao, D., Froehlich, J. E., Zhang, H. & Cheng, C.-L., *Plant J* **33** (2003), 107–118.

[35] Grammatikakis, N. *et al.*, *J Biol Chem* **277** (2002), 8312–8320.

[36] Stechmann, A. & Cavalier-Smith, T., *J Eukaryot Microbiol* **51** (2004), 364–373.

[37] Akner, G. *et al.*, *Eur J Cell Biol* **58** (1992), 356–364.

[38] Pratt, W. B. & Toft, D. O., *Endocr Rev* **18** (1997), 306–360.

[39] Biggiogera, M. *et al.*, *Exp Cell Res* **229** (1996), 77–85.

[40] Langer, T., Rosmus, S. & Fasold, H., *Cell Biol Int* **27** (2003), 47–52.

[41] Tsutsumi, S. & Neckers, L., *Cancer Sci* **98** (2007), 1536–1539.

[42] Bardwell, J. C. & Craig, E. A., *Proc Natl Acad Sci U S A* **84** (1987), 5177–5181.

[43] Louvion, J. F., Warth, R. & Picard, D., *Proc Natl Acad Sci U S A* **93** (1996), 13.937–13.942.

[44] Hainzl, O., Lapina, M. C., Buchner, J. & Richter, K., *J Biol Chem* **284** (2009), 22.559–22.567.

[45] Wayne, N. & Bolon, D. N., *J Mol Biol* **401** (2010), 931–939.

[46] Prodromou, C. *et al.*, *Cell* **90** (1997), 65–75.

[47] Stebbins, C. E. *et al.*, *Cell* **89** (1997), 239–250.

[48] Meyer, P. *et al.*, *Mol Cell* **11** (2003), 647–658.

[49] Harris, S. F., Shiau, A. K. & Agard, D. A., *Structure* **12** (2004), 1087–1097.

[50] Dollins, D. E., Immormino, R. M. & Gewirth, D. T., *J Biol Chem* **280** (2005), 30.438–30.447.

[51] Shiau, A. K., Harris, S. F., Southworth, D. R. & Agard, D. A., *Cell* **127** (2006), 329–340.

[52] Ali, M. M. U. *et al.*, *Nature* **440** (2006), 1013–1017.

[53] Dollins, D. E., Warren, J. J., Immormino, R. M. & Gewirth, D. T., *Mol Cell* **28** (2007), 41–56.

[54] Minami, Y. *et al.*, *Mol Cell Biol* **14** (1994), 1459–1464.

[55] Richter, K., Muschler, P., Hainzl, O. & Buchner, J., *J Biol Chem* **276** (2001), 33.689–33.696.

[56] Wegele, H. *et al.*, *J Biol Chem* **278** (2003), 39.303–39.310.

[57] Wayne, N. & Bolon, D. N., *J Biol Chem* **282** (2007), 35.386–35.395.

[58] Bergerat, A. *et al.*, *Nature* **386** (1997), 414–417.

[59] Dutta, R. & Inouye, M., *Trends Biochem Sci* **25** (2000), 24–28.

[60] Richter, K. *et al.*, *J Biol Chem* **281** (2006), 11.301–11.311.

[61] Sato, S., Fujita, N. & Tsuruo, T., *Proc Natl Acad Sci U S A* **97** (2000), 10.832–10.837.

[62] Müller, L. *et al.*, *J Biol Chem* **279** (2004), 48.846–48.854.

[63] Street, T. O., Lavery, L. A. & Agard, D. A., *Mol Cell* **42** (2011), 96–105.

[64] Chen, S. *et al.*, *Mol Endocrinol* **10** (1996), 682–693.

[65] Das, A. K., Cohen, P. W. & Barford, D., *EMBO J* **17** (1998), 1192–1199.

[66] Chen, S. & Smith, D. F., *J Biol Chem* **273** (1998), 35.194–35.200.

[67] Young, J. C., Obermann, W. M. & Hartl, F. U., *J Biol Chem* **273** (1998), 18.007–18.010.

[68] Scheufler, C. *et al.*, *Cell* **101** (2000), 199–210.

[69] Sinars, C. R. *et al.*, *Proc Natl Acad Sci U S A* **100** (2003), 868–873.

[70] Smith, D. F., *Cell Stress Chaperones* **9** (2004), 109–121.

[71] Hainzl, O., Wegele, H., Richter, K. & Buchner, J., *J Biol Chem* **279** (2004), 23.267–23.273.

[72] Wandinger, S. K., Suhre, M. H., Wegele, H. & Buchner, J., *EMBO J* **25** (2006), 367–376.

[73] Martinez-Yamout, M. A. *et al.*, *J Biol Chem* **281** (2006), 14.457–14.464.

[74] Jorge, I. *et al.*, *J Mass Spectrom* **42** (2007), 1391–1403.

[75] Retzlaff, M. *et al.*, *EMBO Rep* **10** (2009), 1147–1153.

[76] Obermann, W. M. *et al.*, *J Cell Biol* **143** (1998), 901–910.

[77] Panaretou, B. *et al.*, *EMBO J* **17** (1998), 4829–4836.

[78] McLaughlin, S. H., Smith, H. W. & Jackson, S. E., *J Mol Biol* **315** (2002), 787–798.

[79] Richter, K. *et al.*, *J Biol Chem* **283** (2008), 17.757–17.765.

[80] Scheibel, T. & Buchner, J., *Biochem Pharmacol* **56** (1998), 675–682.

[81] Weikl, T. *et al.*, *J Mol Biol* **303** (2000), 583–592.

[82] Prodromou, C. *et al.*, *EMBO J* **19** (2000), 4383–4392.

[83] Csermely, P. *et al.*, *J Biol Chem* **268** (1993), 1901–1907.

[84] Grenert, J. P. *et al.*, *J Biol Chem* **272** (1997), 23.843–23.850.

[85] Sullivan, W. *et al.*, *J Biol Chem* **272** (1997), 8007–8012.

[86] Richter, K., Reinstein, J. & Buchner, J., *J Biol Chem* **277** (2002), 44.905–44.910.

[87] Richter, K., Walter, S. & Buchner, J., *J Mol Biol* **342** (2004), 1403–1413.

[88] Hessling, M., Richter, K. & Buchner, J., *Nat Struct Mol Biol* **16** (2009), 287–293.

[89] Southworth, D. R. & Agard, D. A., *Mol Cell* **32** (2008), 631–640.

[90] Whitesell, L., Shifrin, S. D., Schwab, G. & Neckers, L. M., *Cancer Res* **52** (1992), 1721–1728.

[91] Fukazawa, H. *et al.*, *Biochem Pharmacol* **42** (1991), 1661–1671.

[92] Taniguchi, M., Uehara, Y., Matsuyama, M. & Takahashi, M., *Biochem Biophys Res Commun* **195** (1993), 208–214.

[93] Schnur, R. C. *et al.*, *J Med Chem* **38** (1995), 3813–3820.

[94] Roe, S. M. *et al.*, *J Med Chem* **42** (1999), 260–266.

[95] Dehner, A. *et al.*, *Chembiochem* **4** (2003), 870–877.

[96] Whitesell, L. *et al.*, *Proc Natl Acad Sci U S A* **91** (1994), 8324–8328.

[97] Miller, P. *et al.*, *Biochem Biophys Res Commun* **201** (1994), 1313–1319.

[98] Chavany, C. *et al.*, *J Biol Chem* **271** (1996), 4974–4977.

[99] Mimnaugh, E. G., Chavany, C. & Neckers, L., *J Biol Chem* **271** (1996), 22.796–22.801.

[100] Schulte, T. W., Blagosklonny, M. V., Ingui, C. & Neckers, L., *J Biol Chem* **270** (1995), 24.585–24.588.

[101] Schneider, C. *et al.*, *Proc Natl Acad Sci U S A* **93** (1996), 14.536–14.541.

[102] Clarke, P. A. *et al.*, *Oncogene* **19** (2000), 4125–4133.

[103] Chiosis, G. *et al.*, *Mol Cancer Ther* **2** (2003), 123–129.

[104] Chiosis, G., *Expert Opin Ther Targets* **10** (2006), 37–50.

[105] Chiosis, G., Rosen, N. & Sepp-Lorenzino, L., *Bioorg Med Chem Lett* **11** (2001), 909–913.

[106] Chiosis, G. & Tao, H., *IDrugs* **9** (2006), 778–782.

[107] Chiosis, G., *Curr Top Med Chem* **6** (2006), 1183–1191.

[108] Winssinger, N., Fontaine, J.-G. & Barluenga, S., *Curr Top Med Chem* **9** (2009), 1419–1435.

[109] Jhaveri, K., Taldone, T., Modi, S. & Chiosis, G., *Biochim Biophys Acta* **1823** (2012), 742–755.

[110] Oppermann, H., Levinson, W. & Bishop, J. M., *Proc Natl Acad Sci U S A* **78** (1981), 1067–1071.

[111] Farrelly, F. W. & Finkelstein, D. B., *J Biol Chem* **259** (1984), 5745–5751.

[112] Jakob, U., Lilie, H., Meyer, I. & Buchner, J., *J Biol Chem* **270** (1995), 7288–7294.

[113] Miyata, Y. & Yahara, I., *J Biol Chem* **267** (1992), 7042–7047.

[114] Freeman, B. C. & Morimoto, R. I., *EMBO J* **15** (1996), 2969–2979.

[115] Falsone, S. F. *et al.*, *FEBS Lett* **579** (2005), 6350–6354.

[116] Falsone, S. F., Gesslbauer, B., Rek, A. & Kungl, A. J., *Proteomics* **7** (2007), 2375–2383.

[117] Echeverría, P. C. *et al.*, *PLoS One* **6** (2011), e26.044.

[118] Pratt, W. B. & Toft, D. O., *Exp Biol Med (Maywood)* **228** (2003), 111–133.

[119] Queitsch, C., Sangster, T. A. & Lindquist, S., *Nature* **417** (2002), 618–624.

[120] Cowen, L. E. & Lindquist, S., *Science* **309** (2005), 2185–2189.

[121] Breitkreutz, B.-J. *et al.*, *Nucleic Acids Res* **36** (2008), D637–D640.

[122] Stark, C. *et al.*, *Nucleic Acids Res* **39** (2011), D698–D704.

[123] Ziemiecki, A., Catelli, M. G., Joab, I. & Moncharmont, B., *Biochem Biophys Res Commun* **138** (1986), 1298–1307.

[124] Joab, I. *et al.*, *Nature* **308** (1984), 850–853.

[125] Howard, K. J., Holley, S. J., Yamamoto, K. R. & Distelhorst, C. W., *J Biol Chem* **265** (1990), 11.928–11.935.

[126] Xu, M. *et al.*, *J Biol Chem* **273** (1998), 13.918–13.924.

[127] Giannoukos, G., Silverstein, A. M., Pratt, W. B. & Simons, S., Jr, *J Biol Chem* **274** (1999), 36.527–36.536.

[128] Steinmetz, A. C., Renaud, J. P. & Moras, D., *Annu Rev Biophys Biomol Struct* **30** (2001), 329–359.

[129] Nathan, D. F., Vos, M. H. & Lindquist, S., *Proc Natl Acad Sci U S A* **94** (1997), 12.949–12.956.

[130] Brugge, J. S., Purchio, A. F. & Erikson, R. L., *Virology* **83** (1977), 27–33.

[131] Xu, Y. & Lindquist, S., *Proc Natl Acad Sci U S A* **90** (1993), 7074–7078.

[132] Brugge, J. S., *Curr Top Microbiol Immunol* **123** (1986), 1–22.

[133] Xu, Y., Singer, M. A. & Lindquist, S., *Proc Natl Acad Sci U S A* **96** (1999), 109–114.

[134] Vaughan, C. K. *et al.*, *Mol Cell* **23** (2006), 697–707.

[135] Pearl, L. H., *Curr Opin Genet Dev* **15** (2005), 55–61.

[136] Park, S. J., Kostic, M. & Dyson, H. J., *J Mol Biol* **411** (2011), 158–173.

[137] Hawle, P. *et al.*, *Mol Cell Biol* **26** (2006), 8385–8395.

[138] Scheibel, T., Weikl, T. & Buchner, J., *Proc Natl Acad Sci U S A* **95** (1998), 1495–1499.

[139] Johnson, B. D. *et al.*, *J Biol Chem* **275** (2000), 32.499–32.507.

[140] Fang, L., Ricketson, D., Getubig, L. & Darimont, B., *Proc Natl Acad Sci U S A* **103** (2006), 18.487–18.492.

[141] Walerych, D. *et al.*, *J Biol Chem* **285** (2010), 32.020–32.028.

[142] Smith, D. F. *et al.*, *Mol Cell Biol* **15** (1995), 6804–6812.

[143] Sepp-Lorenzino, L. *et al.*, *J Biol Chem* **270** (1995), 16.580–16.587.

[144] Segnitz, B. & Gehring, U., *J Biol Chem* **272** (1997), 18.694–18.701.

[145] Nicolet, C. M. & Craig, E. A., *Mol Cell Biol* **9** (1989), 3638–3646.

[146] Chang, H. C., Nathan, D. F. & Lindquist, S., *Mol Cell Biol* **17** (1997), 318–325.

[147] Flom, G. *et al.*, *Biochem J* **404** (2007), 159–167.

[148] Honoré, B. *et al.*, *J Biol Chem* **267** (1992), 8485–8491.

[149] Bose, S., Weikl, T., Bügl, H. & Buchner, J., *Science* **274** (1996), 1715–1717.

[150] Freeman, B. C., Toft, D. O. & Morimoto, R. I., *Science* **274** (1996), 1718–1720.

[151] Smith, D. F. *et al.*, *Mol Cell Biol* **13** (1993), 869–876.

[152] Chang, H. C. & Lindquist, S., *J Biol Chem* **269** (1994), 24.983–24.988.

[153] Smith, D. F., *Mol Endocrinol* **7** (1993), 1418–1429.

[154] Dittmar, K. D., Hutchison, K. A., Owens-Grillo, J. K. & Pratt, W. B., *J Biol Chem* **271** (1996), 12.833–12.839.

[155] Pratt, W. B., Dalman, F. C., Meshinchi, S. & Scherrer, L. C., *Nihon Naibunpi Gakkai Zasshi* **66** (1990), 1185–1197.

[156] Picard, D. *et al.*, *Nature* **348** (1990), 166–168.

[157] Kosano, H. *et al.*, *J Biol Chem* **273** (1998), 32.973–32.979.

[158] Pratt, W. B. & Dittmar, K. D., *Trends Endocrinol Metab* **9** (1998), 244–252.

[159] Morishima, Y. *et al.*, *Biochemistry* **40** (2001), 1109–1116.

[160] Hernández, M. P., Chadli, A. & Toft, D. O., *J Biol Chem* **277** (2002), 11.873–11.881.

[161] Hernández, M. P., Sullivan, W. P. & Toft, D. O., *J Biol Chem* **277** (2002), 38.294–38.304.

[162] Wegele, H. *et al.*, *J Mol Biol* **356** (2006), 802–811.

[163] Dittmar, K. D. *et al.*, *J Biol Chem* **272** (1997), 21.213–21.220.

[164] Wegele, H., Haslbeck, M., Reinstein, J. & Buchner, J., *J Biol Chem* **278** (2003), 25.970–25.976.

[165] Johnson, B. D., Schumacher, R. J., Ross, E. D. & Toft, D. O., *J Biol Chem* **273** (1998), 3679–3686.

[166] Prodromou, C. *et al.*, *EMBO J* **18** (1999), 754–762.

[167] Richter, K. *et al.*, *J Biol Chem* **278** (2003), 10.328–10.333.

[168] Richter, K. & Buchner, J., *J Cell Physiol* **188** (2001), 281–290.

[169] Prapapanich, V., Chen, S. & Smith, D. F., *Mol Cell Biol* **18** (1998), 944–952.

[170] Smith, D. F., *Biol Chem* **379** (1998), 283–288.

[171] Carrigan, P. E. *et al.*, *J Biol Chem* **279** (2004), 16.185–16.193.

[172] Odunuga, O. O., Longshaw, V. M. & Blatch, G. L., *Bioessays* **26** (2004), 1058–1068.

[173] Carrigan, P. E., Riggs, D. L., Chinkers, M. & Smith, D. F., *J Biol Chem* **280** (2005), 8906–8911.

[174] Gaiser, A. M., Brandt, F. & Richter, K., *J Mol Biol* **391** (2009), 621–634.

[175] Hernández Torres, J., Papandreou, N. & Chomilier, J., *Cell Stress Chaperones* **14** (2009), 281–289.

[176] Blatch, G. L. & Lässle, M., *Bioessays* **21** (1999), 932–939.

[177] Hirano, T., Kinoshita, N., Morikawa, K. & Yanagida, M., *Cell* **60** (1990), 319–328.

[178] Sikorski, R. S., Boguski, M. S., Goebl, M. & Hieter, P., *Cell* **60** (1990), 307–317.

[179] Lamb, J. R., Tugendreich, S. & Hieter, P., *Trends Biochem Sci* **20** (1995), 257–259.

[180] Lässle, M. *et al.*, *J Biol Chem* **272** (1997), 1876–1884.

[181] Demand, J., Lüders, J. & Höhfeld, J., *Mol Cell Biol* **18** (1998), 2023–2028.

[182] Carrello, A. *et al.*, *J Biol Chem* **274** (1999), 2682–2689.

[183] Chen, S., Sullivan, W. P., Toft, D. O. & Smith, D. F., *Cell Stress Chaperones* **3** (1998), 118–129.

[184] Brinker, A. *et al.*, *J Biol Chem* **277** (2002), 19.265–19.275.

[185] Song, Y. & Masison, D. C., *J Biol Chem* **280** (2005), 34.178–34.185.

[186] Flom, G., Weekes, J. & Johnson, J. L., *Curr Genet* **47** (2005), 368–380.

[187] Flom, G., Weekes, J., Williams, J. J. & Johnson, J. L., *Genetics* **172** (2006), 41–51.

[188] Gross, M., Hessefort, S., Olin, A. & Reddy, G., *J Biol Chem* **271** (1996), 16.842–16.849.

[189] Nelson, G. M., Huffman, H. & Smith, D. F., *Cell Stress Chaperones* **8** (2003), 125–133.

[190] Höhfeld, J., Minami, Y. & Hartl, F. U., *Cell* **83** (1995), 589–598.

[191] Nathan, D. F., Vos, M. H. & Lindquist, S., *Proc Natl Acad Sci U S A* **96** (1999), 1409–1414.

[192] Nathan, D. F. & Lindquist, S., *Mol Cell Biol* **15** (1995), 3917–3925.

[193] Panaretou, B. *et al.*, *Mol Cell* **10** (2002), 1307–1318.

[194] Di Tommaso, P. *et al.*, *Nucleic Acids Res* **39** (2011), W13–W17.

[195] Waterhouse, A. M. *et al.*, *Bioinformatics* **25** (2009), 1189–1191.

[196] Lotz, G. P., Lin, H., Harst, A. & Obermann, W. M. J., *J Biol Chem* **278** (2003), 17.228–17.235.

[197] Meyer, P. *et al.*, *EMBO J* **23** (2004), 1402–1410.

[198] Retzlaff, M. *et al.*, *Mol Cell* **37** (2010), 344–354.

[199] Koulov, A. V. *et al.*, *Mol Biol Cell* **21** (2010), 871–884.

[200] Wang, X. *et al.*, *Cell* **127** (2006), 803–815.

[201] Holmes, J. L., Sharp, S. Y., Hobbs, S. & Workman, P., *Cancer Res* **68** (2008), 1188–1197.

[202] Smith, D. F., Faber, L. E. & Toft, D. O., *J Biol Chem* **265** (1990), 3996–4003.

[203] Johnson, J. L., Beito, T. G., Krco, C. J. & Toft, D. O., *Mol Cell Biol* **14** (1994), 1956–1963.

[204] Felts, S. J. & Toft, D. O., *Cell Stress Chaperones* **8** (2003), 108–113.

[205] Nair, S. C. *et al.*, *Cell Stress Chaperones* **1** (1996), 237–250.

[206] Xu, Z. *et al.*, *Eur J Biochem* **246** (1997), 461–470.

[207] Holt, S. E. *et al.*, *Genes Dev* **13** (1999), 817–826.

[208] Hu, J., Toft, D., Anselmo, D. & Wang, X., *J Virol* **76** (2002), 269–279.

[209] Hutchison, K. A. *et al.*, *J Biol Chem* **270** (1995), 18.841–18.847.

[210] Young, J. C., Moarefi, I. & Hartl, F. U., *J Cell Biol* **154** (2001), 267–273.

[211] Johnson, J. L. & Toft, D. O., *Mol Endocrinol* **9** (1995), 670–678.

[212] Freeman, B. C., Felts, S. J., Toft, D. O. & Yamamoto, K. R., *Genes Dev* **14** (2000), 422–434.

[213] Garcia-Ranea, J. A., Mirey, G., Camonis, J. & Valencia, A., *FEBS Lett* **529** (2002), 162–167.

[214] Fang, Y., Fliss, A. E., Rao, J. & Caplan, A. J., *Mol Cell Biol* **18** (1998), 3727–3734.

[215] Grad, I. *et al.*, *Mol Cell Biol* **26** (2006), 8976–8983.

[216] Weikl, T., Abelmann, K. & Buchner, J., *J Mol Biol* **293** (1999), 685–691.

[217] Weaver, A. J. *et al.*, *J Biol Chem* **275** (2000), 23.045–23.052.

[218] Kim, K. K., Kim, R. & Kim, S. H., *Nature* **394** (1998), 595–599.

[219] van Montfort, R. L. *et al.*, *Nat Struct Biol* **8** (2001), 1025–1030.

[220] Pasta, S. Y., Raman, B., Ramakrishna, T. & Rao, C. M., *J Biol Chem* **277** (2002), 45.821–45.828.

[221] Kovacs, J. J. *et al.*, *Mol Cell* **18** (2005), 601–607.

[222] Kekatpure, V. D., Dannenberg, A. J. & Subbaramaiah, K., *J Biol Chem* **284** (2009), 7436–7445.

[223] Harst, A., Lin, H. & Obermann, W. M. J., *Biochem J* **387** (2005), 789–796.

[224] Tanioka, T. *et al.*, *J Biol Chem* **275** (2000), 32.775–32.782.

[225] Echtenkamp, F. J. *et al.*, *Mol Cell* **43** (2011), 229–241.

[226] Peng, Y. *et al.*, *J Biol Chem* **276** (2001), 40.583–40.590.

[227] Rudiger, S., Freund, S. M. V., Veprintsev, D. B. & Fersht, A. R., *Proc Natl Acad Sci U S A* **99** (2002), 11.085–11.090.

[228] Wang, C. & Chen, J., *J Biol Chem* **278** (2003), 2066–2071.

[229] Walerych, D. *et al.*, *J Biol Chem* **279** (2004), 48.836–48.845.

[230] Varnay, I. *et al.*, *J Am Chem Soc* **132** (2010), 15.692–15.698.

[231] Pervushin, K., Riek, R., Wider, G. & Wüthrich, K., *Proc Natl Acad Sci U S A* **94** (1997), 12.366–12.371.

[232] Salzmann, M. *et al.*, *Proc Natl Acad Sci U S A* **95** (1998), 13.585–13.590.

[233] Schwieters, C. D., Kuszewski, J. J., Tjandra, N. & Clore, G. M., *J Magn Reson* **160** (2003), 65–73.

[234] Bryson, K. *et al.*, *Nucleic Acids Res* **33** (2005), W36–W38.

[235] Soroka, J. *et al.*, *Mol Cell* **45** (2012), 517–528.

[236] Wong, K. B. *et al.*, *Proc Natl Acad Sci U S A* **96** (1999), 8438–8442.

[237] Lee, H. *et al.*, *J Biol Chem* **275** (2000), 29.426–29.432.

[238] Dawson, R. *et al.*, *J Mol Biol* **332** (2003), 1131–1141.

[239] Kussie, P. H. *et al.*, *Science* **274** (1996), 948–953.

[240] Chen, H.-F. & Luo, R., *J Am Chem Soc* **129** (2007), 2930–2937.

[241] Radhakrishnan, I. *et al.*, *Cell* **91** (1997), 741–752.

[242] Sugase, K., Dyson, H. J. & Wright, P. E., *Nature* **447** (2007), 1021–1025.

[243] de Vries, S. J., van Dijk, M. & Bonvin, A. M. J. J., *Nat Protoc* **5** (2010), 883–897.

[244] Ali, J. A., Jackson, A. P., Howells, A. J. & Maxwell, A., *Biochemistry* **32** (1993), 2717–2724.

[245] Polymeropoulos, M. H. *et al.*, *Science* **276** (1997), 2045–2047.

[246] Spillantini, M. G. *et al.*, *Nature* **388** (1997), 839–840.

[247] Weinreb, P. H. *et al.*, *Biochemistry* **35** (1996), 13.709–13.715.

[248] Davidson, W. S., Jonas, A., Clayton, D. F. & George, J. M., *J Biol Chem* **273** (1998), 9443–9449.

[249] Vilar, M. *et al.*, *Proc Natl Acad Sci U S A* **105** (2008), 8637–8642.

[250] Uryu, K. *et al.*, *Am J Pathol* **168** (2006), 947–961.

[251] Falsone, S. F. *et al.*, *J Biol Chem* **284** (2009), 31.190–31.199.

[252] Krüger, R. *et al.*, *Nat Genet* **18** (1998), 106–108.

[253] Zarranz, J. J. *et al.*, *Ann Neurol* **55** (2004), 164–173.

[254] Bernstein, S. L. *et al.*, *J Am Soc Mass Spectrom* **15** (2004), 1435–1443.

[255] Prodromou, C., Roe, S. M., Piper, P. W. & Pearl, L. H., *Nat Struct Biol* **4** (1997), 477–482.

[256] Siligardi, G. *et al.*, *J Biol Chem* **277** (2002), 20.151–20.159.

[257] Meyer, P. *et al.*, *EMBO J* **23** (2004), 511–519.

[258] Siligardi, G. *et al.*, *J Biol Chem* **279** (2004), 51.989–51.998.

[259] Piper, P. W. *et al.*, *Gene* **302** (2003), 165–170.

[260] Friedler, A. *et al.*, *J Biol Chem* **280** (2005), 8051–8059.

[261] Tomita, Y. *et al.*, *J Biol Chem* **281** (2006), 8600–8606.

[262] Hagn, F. *et al.*, *J Biol Chem* **285** (2010), 3439–3450.

[263] Friedler, A. *et al.*, *Proc Natl Acad Sci U S A* **99** (2002), 937–942.

[264] Park, S. J., Borin, B. N., Martinez-Yamout, M. A. & Dyson, H. J., *Nat Struct Mol Biol* **18** (2011), 537–541.

[265] Edgar, R. C., *Nucleic Acids Res* **32** (2004), 1792–1797.

[266] Nelson, J. W. & Kallenbach, N. R., *Proteins* **1** (1986), 211–217.

[267] Nelson, J. W. & Kallenbach, N. R., *Biochemistry* **28** (1989), 5256–5261.

[268] Lehrman, S. R., Tuls, J. L. & Lund, M., *Biochemistry* **29** (1990), 5590–5596.

[269] Segawa, S., Fukuno, T., Fujiwara, K. & Noda, Y., *Biopolymers* **31** (1991), 497–509.

[270] Shiraki, K., Nishikawa, K. & Goto, Y., *J Mol Biol* **245** (1995), 180–194.

[271] Werner-Washburne, M. & Craig, E. A., *Genome* **31** (1989), 684–689.

[272] Wishart, D. S. & Sykes, B. D., *J Biomol NMR* **4** (1994), 171–180.

[273] Shen, Y., Delaglio, F., Cornilescu, G. & Bax, A., *J Biomol NMR* **44** (2009), 213–223.

[274] Hansen, M. R., Hanson, P. & Pardi, A., *Methods Enzymol* **317** (2000), 220–240.

[275] Ottiger, M., Delaglio, F. & Bax, A., *J Magn Reson* **131** (1998), 373–378.

[276] Zweckstetter, M. & Bax, A., *Journal of the American Chemical Society* **122** (2000), 3791–3792.

[277] Sali, A. *et al.*, *Proteins* **23** (1995), 318–326.

[278] Li, J., Richter, K. & Buchner, J., *Nat Struct Mol Biol* **18** (2011), 61–66.

[279] García de la Torre, J., Huertas, M. L. & Carrasco, B., *J Magn Reson* **147** (2000), 138–146.

[280] Nemoto, T. K. *et al.*, *J Biochem* **139** (2006), 677–687.

[281] Stravopodis, D. J., Margaritis, L. H. & Voutsinas, G. E., *Curr Med Chem* **14** (2007), 3122–3138.

[282] Powers, M. V. & Workman, P., *FEBS Lett* **581** (2007), 3758–3769.

[283] Cortajarena, A. L., Yi, F. & Regan, L., *ACS Chem Biol* **3** (2008), 161–166.

[284] Yi, F. & Regan, L., *ACS Chem Biol* **3** (2008), 645–654.

[285] Yi, F. *et al.*, *J Biomol Screen* **14** (2009), 273–281.

[286] Sun, H., *Curr Med Chem* **15** (2008), 1018–1024.

[287] Schüttelkopf, A. W. & van Aalten, D. M. F., *Acta Crystallogr D Biol Crystallogr* **60** (2004), 1355–1363.

[288] Zhu, L., Dyson, H. J. & Wright, P. E., *J Biomol NMR* **11** (1998), 17–29.

[289] Laskowski, R. A. *et al.*, *J Biomol NMR* **8** (1996), 477–486.

[290] Aurora, R. & Rose, G. D., *Protein Sci* **7** (1998), 21–38.

[291] Aurora, R., Srinivasan, R. & Rose, G. D., *Science* **264** (1994), 1126–1130.

[292] Holm, L. & Rosenström, P., *Nucleic Acids Res* **38** (2010), W545–W549.

[293] Ye, Y. & Godzik, A., *Bioinformatics* **19 Suppl 2** (2003), ii246–ii255.

[294] Ye, Y. & Godzik, A., *Protein Sci* **13** (2004), 1841–1850.

[295] Ye, Y. & Godzik, A., *Nucleic Acids Res* **32** (2004), W582–W585.

[296] Bledsoe, R. K. *et al.*, *Cell* **110** (2002), 93–105.

[297] Mendel, D. B. & Ortí, E., *J Biol Chem* **263** (1988), 6695–6702.

[298] Grad, I. & Picard, D., *Mol Cell Endocrinol* **275** (2007), 2–12.

[299] Main, E. R. G. *et al.*, *Structure* **11** (2003), 497–508.

[300] D'Andrea, L. D. & Regan, L., *Trends Biochem Sci* **28** (2003), 655–662.

[301] Krachler, A. M., Sharma, A. & Kleanthous, C., *Proteins* **78** (2010), 2131–2143.

[302] Flynn, G. C., Chappell, T. G. & Rothman, J. E., *Science* **245** (1989), 385–390.

[303] Onuoha, S. C., Coulstock, E. T., Grossmann, J. G. & Jackson, S. E., *J Mol Biol* **379** (2008), 732–744.

[304] Hagn, F. *et al.*, *Nat Struct Mol Biol* **18** (2011), 1086–1093.

[305] Southworth, D. R. & Agard, D. A., *Mol Cell* **42** (2011), 771–781.

[306] Vogel, C. L. *et al.*, *J Clin Oncol* **20** (2002), 719–726.

[307] Slamon, D. J. *et al.*, *Science* **235** (1987), 177–182.

[308] Baselga, J., Albanell, J., Molina, M. A. & Arribas, J., *Semin Oncol* **28** (2001), 4–11.

[309] Arkin, M. R. & Wells, J. A., *Nat Rev Drug Discov* **3** (2004), 301–317.

[310] Vassilev, L. T. *et al.*, *Science* **303** (2004), 844–848.

[311] Shuker, S. B., Hajduk, P. J., Meadows, R. P. & Fesik, S. W., *Science* **274** (1996), 1531–1534.

[312] Hajduk, P. J., Meadows, R. P. & Fesik, S. W., *Q Rev Biophys* **32** (1999), 211–240.

[313] Hajduk, P. J. *et al.*, *J Med Chem* **43** (2000), 4781–4786.

[314] Braisted, A. C. *et al.*, *J Am Chem Soc* **125** (2003), 3714–3715.

[315] Jahnke, W. *et al.*, *Curr Top Med Chem* **3** (2003), 69–80.

[316] Erlanson, D. A., McDowell, R. S. & O'Brien, T., *J Med Chem* **47** (2004), 3463–3482.

[317] Welker, S. *et al.*, *Mol Cell* **39** (2010), 507–520.

[318] Cornilescu, G., Delaglio, F. & Bax, A., *J Biomol NMR* **13** (1999), 289–302.

[319] Forafonov, F. *et al.*, *Mol Cell Biol* **28** (2008), 3446–3456.

[320] Johnson, J., Corbisier, R., Stensgard, B. & Toft, D., *J Steroid Biochem Mol Biol* **56** (1996), 31–37.

[321] Chadli, A. *et al.*, *Proc Natl Acad Sci U S A* **97** (2000), 12.524–12.529.

[322] McLaughlin, S. H. *et al.*, *J Mol Biol* **356** (2006), 746–758.

[323] Woo, S. H. *et al.*, *J Biol Chem* **284** (2009), 30.871–30.880.

[324] Mollerup, J. & Berchtold, M. W., *FEBS Lett* **579** (2005), 4187–4192.

[325] Oxelmark, E. *et al.*, *J Biol Chem* **278** (2003), 36.547–36.555.

[326] Grenert, J. P., Johnson, B. D. & Toft, D. O., *J Biol Chem* **274** (1999), 17.525–17.533.

[327] Karagöz, G. E. *et al.*, *Proc Natl Acad Sci U S A* **108** (2011), 580–585.

[328] Toogun, O. A., Zeiger, W. & Freeman, B. C., *Proc Natl Acad Sci U S A* **104** (2007), 5765–5770.

[329] Saiki, R. K. *et al.*, *Science* **230** (1985), 1350–1354.

[330] Mullis, K. *et al.*, *Cold Spring Harb Symp Quant Biol* **51 Pt 1** (1986), 263–273.

[331] Mullis, K. B. & Faloona, F. A., *Methods Enzymol* **155** (1987), 335–350.

[332] Braman, J., Papworth, C. & Greener, A., *Methods Mol Biol* **57** (1996), 31–44.

[333] Mayr, C., Richter, K., Lilie, H. & Buchner, J., *J Biol Chem* **275** (2000), 34.140–34.146.

[334] Leutner, M. *et al.*, *J Biomol NMR* **11** (1998), 31–43.

[335] Lüttgen, H. *et al.*, *J Mol Biol* **316** (2002), 875–885.